Role of nuclear lamins in the regulation of nucleolar structure and function

A thesis

submitted in partial fulfillment of the requirements

for the degree of

Doctor of Philosophy

By

Ayantika Sen Gupta

20113121

Under the guidance of

Dr. Kundan Sengupta

INDIAN INSTITUTE OF SCIENCE EDUCATION AND RESEARCH, PUNE

2018

DSO 13

DSO 13

भारतीय विज्ञान शिक्षा एवं अनुसंधान संस्थान, पुणे
INDIAN INSTITUTE OF SCIENCE EDUCATION AND RESEARCH (IISER), PUNE
(An Autonomous Institution, Ministry of Human Resource Development, Govt. of India)
Dr. Homi Bhabha Road, Pashan, Pune – 411 008

IISER PUNE

DOCTORAL STUDIES OFFICE

Form for submission of Ph.D. Thesis

Declaration by student

Name of Student: AYANTIKA SEN GUPTA Reg. No.: 20113121

Thesis Supervisor(s): DR. KUNDAN SENGUPTA Department: BIOLOGY

Date of joining : 1.08.2011 Date of Pre-Synopsis Seminar : 24/12/2018

Title of Thesis : Role of nuclear lamins in the regulation of nucleolar structure and function

I declare that this written submission represents my idea in my own words and where others' ideas have been included; I have adequately cited and referenced the original sources. I also declare that I have adhered to all principles of academic honesty and integrity and have not misrepresented or fabricated or falsified any idea/data/fact/source in my submission. I understand that violation of the above will be cause for disciplinary action by the Institute and can also evoke penal action from the sources which have thus not been properly cited or from whom proper permission has not been taken when needed.

The work reported in this thesis is the original work done by me under the guidance of DR. KUNDAN SENGUPTA

Date: 11th May, 2019

Signature of the student

IISER PUNE

भारतीय विज्ञान शिक्षा एवं अनुसंधान संस्थान, पुणे
INDIAN INSTITUTE OF SCIENCE EDUCATION AND RESEARCH (IISER), PUNE
(An Autonomous Institution, Ministry of Human Resource Development, Govt. of India)
Dr. Homi Bhabha Road, Pashan, Pune – 411 008

DOCTORAL STUDIES OFFICE

Form for submission of Ph.D. Thesis

Certificate by Supervisor

I certify that the thesis entitled Role of Lamins in the Regulation of nucleolar Structure & function presented by ~~Mr~~/Ms AYANTIKA SEN GUPTA represents ~~his~~/her original work which was carried out by ~~him~~/her at IISER, Pune under my guidance and supervision during the period from 1st AUG. 2011 to 11.05.2018.

The work presented here or any part of it has not been included in any other thesis submitted previously for the award of any degree or diploma from any other University or institutions. I further certify that the above statements made by him/her in regard to ~~his~~/her thesis are correct to the best of my knowledge.

Date: 11.05.2018

Kundan Sengupta
(Supervisor)

Recommended and Forwarded

Date: 11.5.2018.

Head of the Discipline

Dedicated to my beloved grandmother ~
Late Smt. Susama Sengupta

Acknowledgements

I would like to begin by thanking my supervisor Dr. Kundan Sengupta for giving me the opportunity to pursue my PhD thesis in the Chromosome Biology Lab. Throughout the course of my PhD, he has inculcated the habit of being an independent thinker, in me, but also guided me when I failed to do so. I also thank him for pushing me hard to achieve things that I did not think were possible. He has always been supportive of my work and has never lost hope in me. I thank him for his help with planning and execution of my experiments, and also for carefully reading this thesis.

I would like to thank my Research Advisory Committee (RAC) members Dr. Thomas Pucadyil (IISER, Pune) and Dr. Jomon Joseph (NCCS, Pune) for critically evaluating my work and their timely suggestions during my RAC meetings. I would also like to thank Dr. Richa Rikhy (IISER, Pune) for helping me with live-imaging experiments and providing critical inputs on my work. Suggestions from Dr. M. S. Madhusudhan, Dr. Gayathri Pananghat, Dr. Girish Ratnaparkhi (IISER, Pune) and Dr. Girish Deshpande (Princeton University) have positively impacted this work. I thank Bionivid, Bangalore for microarray hybridization and data analysis.

I am extremely grateful to IISER, Pune for extending all its support in the form of equipments, infrastructure, management (Mrinalini Virkar, Kalpesh Thakare, Piyush Gadekar, Rupali Jadhav, Shabnam Patil and Mahesh Rote) and intra-mural grants, which were all necessary for the execution of my thesis work. I thank the open lab policy of IISER, Pune, which allows uninhibited sharing of equipments, reagents and even ideas, between the labs, and all the faculty and students of IISER, Pune, that abide by this. I also thank the IISER Pune Microscopy facility (Vijay Vitthal), on which my work heavily relied. I thank the hardworking Dinesh Dada, who provided help with lab chores. I thank the funding agencies – CSIR for a Junior and Senior Research Fellowship, DBT for an extended Senior Research Fellowship and Wellcome-DBT India Alliance for funding the work.

I would especially like to thank CBL members, present and past for keeping up the lively environment in the lab. Devika, Sumit, Shivsmriti and Aishwarya have helped the lab since its inception. I would thank Sumit for commencing the project on Histone 2B dynamics that I later carried forward. I would further like to thank Gaurav Joshi, who helped me with the completion of the same project. I would thank Sumit and Gaurav, for the numerous thought-provoking discussions that we have had on the function of the nucleolus. I thank the students that I mentored – Haresh Shankar who helped me with generation of deletion constructs of Lamin B2 and Niharika Sane who helped me establish protocols for nucleolar isolation. Devika, Roopali, Ajay, Maithilee, Shalaka, Apoorva, Neelima, Sishil and Trupti have been

constant sources of support and inspiration for me. Our discussions resplendent with positive criticisms and inputs have really helped in improving my work.

I would like to end by thanking my ever so supportive family, without whom I could not have completed this thesis. I thank my parents Mousumi and Siddhartha Sengupta, for being understanding when I have gone for days without talking to or meeting them, due to my work. It was due to their dream that I pursued my PhD. I would especially thank my husband Avishek who has unfailingly supported and motivated me throughout my PhD and shared all my highs and lows, without losing trust in me. I thank my parents-in-law Subhra and Asoke Saha, for being supportive and wishing me well.

Contents

Abstract

The nucleolus is a nuclear sub-organelle that lacks a membrane. It is the site of ribosome biogenesis within the nucleus bearing RNA Polymerase I and associated transcription factors. In addition to its role in ribosome biogenesis, the "multifunctional" nucleolus is involved in cellular stress sensing, cell cycle regulation, DNA damage repair, senescence and apoptosis. Nucleoli assemble on ribosomal DNA (rDNA) present on the p-arms of human chromosomes 13, 14, 15, 21 and 22, at the end of mitosis. Cancer cells show an increase in nucleolar numbers required for protein synthesis. However, the factors that regulate nucleolar numbers and morphology in cancer cells, is unclear. Here, we have assessed the role of nuclear Lamins in regulating nucleolar morphology. Lamins are type V intermediate filament proteins that maintain the mechanical integrity of the nucleus. We show a prominent role of Lamin B2 in modulating nucleolar structure in colon cancer cells. We found that in addition to its association with the nuclear envelope, a subpopulation of Lamin B2 localizes to the border of the nucleolus. The nucleolar subpool of Lamin B2 associates with the nucleolar proteins Nucleolin and Nucleophosmin (B23). Furthermore, we found that the head domain of Lamin B2 is essential for maintaining nucleolar morphology, whereas the tail domain is required to maintain an intact nuclear morphology. Interestingly, Lamin B2 depletion is accompanied by the upregulation of pre-rRNA and intergenic RNAs. Nucleolin speckles formed upon inhibition of RNA Pol I, persisted for a much longer duration upon Lamin B2 depletion. We found that localization of non-coding IGS RNA is enhanced in Nucleolin speckles in Lamin B2 depleted cells. Thus, Lamin B2 impinges on structure and function of the nucleolus. We also found a regulatory feedback between Lamins and the nucleolar rRNA methyltransferase - Fibrillarin. Fibrillarin depletion showed invaginated nuclei with decrease in Lamin A/C and B2 expression levels. Furthermore, Fibrillarin depleted cells showed Actin accumulation adjacent to the nucleus. We surmise that a combined effect of a weakening of the nuclear lamina and altered cytoskeletal arrangement impinges on nuclear morphology in Fibrillarin depleted cells. Finally, we investigated mechanisms by which proteins are shuttled and retained in the nucleolus. We found a predominant role for Nucleolin in mediating nucleolar localization of H2B. The N-terminal and the RNA binding domains of Nucleolin are required for the compartmentalization of H2B into the nucleolus in an RNA dependent manner. Taken together, we have investigated into the mechanisms that regulate morphology, function and dynamics of the nucleolus.

Synopsis

Introduction

The nucleus is a highly organized structure with spatially separated functional sub-domains (Spector, 2001). Most nuclear proteins, although in dynamic equilibrium with the nucleoplasm, self-organize into distinct nuclear bodies like the nucleolus, RNA Pol II transcription factories, PML bodies, nuclear speckles, to name a few (Handwerger and Gall, 2006; Lallemand-Breitenbach and de Thé, 2010; Rieder et al., 2012; Sirri et al., 2008; Sleeman and Trinkle-Mulcahy, 2014; Spector and Lamond, 2011). This compartmentalization is a mechanism by which the nucleus attains maximum efficiency by locally concentrating molecules required for functions like - transcription and splicing (Dundr and Misteli, 2010).

The nucleolus is the largest sub-organelle present within the nucleus and is the hub of RNA polymerase I mediated rDNA transcription, processing and ribosome assembly (Scheer and Hock, 1999; Sirri et al., 2008). The nucleolus appears as a distinct intra-nuclear entity in cells during interphase, when active rRNA synthesis and processing occur (Klein and Grummt, 1999). Electron microscopy revealed that the nucleolus is further compartmentalized into the Fibrillar centres (FC), Dense Fibrillar compartment (DFC) and Granular component (GC) (Cheutin et al., 2002). Ribosomal DNA (rDNA) transcription occurs at the border of FC and DFC, pre-rRNA processing occurs at the DFC, while final steps of rRNA processing and ribosome assembly occurs at the GC. During mitosis, rDNA transcription is inhibited due to phosphorylation of TIF-IB/SL1 (RNA Pol I transcription factor) and TTF-1 by cdc2/Cyclin B (Heix et al., 1998; Sirri et al., 1999). At the end of mitosis, CDK1 is inactivated and rDNA transcription resumes while pre-rRNA processing machinery (DFC and GC proteins) form multiple **p**re-**n**ucleolar **b**odies (PNBs) in the nucleoplasm (Carron et al., 2012). Shortly after telophase, DFC and GC proteins are sequentially recruited from PNBs to sites of rDNA transcription and the nucleolus re-assembles on **N**ucleolus **O**rganizer **R**egions (NORs) present on the p-arms of acrocentric human chromosomes 13, 14, 15, 21 and 22 (Henderson et al., 1972). Thus, for the rest of the interphase, the nucleolus exists as an entity that is phase-separated from the nucleoplasm (Hult et al., 2017). What is intriguing is that the nucleolus is devoid of a bounding membrane and nucleolar proteins can freely diffuse in and out of the nucleolus, into the nucleoplasm. In fact, several photobleaching experiments show that the mean residence time of nucleolar proteins – UBF, Fibrillarin and NPM1 is only of the order of tens of seconds (Chen and Huang, 2001; Shav-Tal et al., 2005). How then is structure of the nucleolus maintained? What are the consequences if nucleolar structure is altered? The consequences of a disrupted nucleolar structure has been extensively studied with respect to inhibition of active rDNA transcription and nucleolar stress response. Inhibition of RNA Polymerase I by Actinomycin D disrupts nucleolar structure, induces formation of nucleolar caps and dispersal of nucleolar proteins into the nucleoplasm, suggesting that ongoing rDNA transcription is essential for maintaining the tripartite organization of FC, DFC and GC of the

nucleolus (Shav-Tal et al., 2005). Thus nucleolar structure is integrally connected to its function. This response of nucleolar disruption is useful as a sensor for cellular stress. Under stress free conditions, the nucleolus confines p14Arf and Nucleophosmin which are negative regulators of hDM2 (Kurki et al., 2004; Llanos et al., 2001), hDM2 binds to p53 and targets it for proteasome mediated degradation. During cellular stress, rDNA transcription is abolished and the nucleolus disintegrates releasing p14Arf and Nucleophosmin into the nucleoplasm where it degrades hDM2 (James et al., 2014; Kurki et al., 2004). Thus, p53 levels in the cell increases leading to cell cycle arrest and apoptosis.

However, how nucleolar structure is maintained in the absence of a bounding membrane remained poorly understood. Brangwynne et. al. showed that nucleoli displayed properties of liquid droplets in the nucleoplasm, which determined their shape and size (Brangwynne et al., 2011). Thus the nucleolus separates out from the surrounding nucleoplasm due to liquid-liquid phase separation, much like oil-water interfaces (Feric et al., 2016). Phase separation of nucleoli results from interactions between nucleolar proteins such as Nucleophosmin with ribonucleoprotein complexes (Mitrea et al., 2016). Inside the liquid-like nucleolus, DFC and GC compartments do not merge due to immiscibility of proteins like the DFC protein Fibrillarin and GC protein Nucleophosmin and differences in their surface tension (Feric et al., 2016).

Although the biophysical principles guiding nucleolar assembly and structure are being actively investigated, much of these studies rely on in vitro reconstitution of nucleolar proteins and their interactions. However within the nucleus, the nucleolus does not exist as an isolated system but is surrounded by a complex milieu of chromosomes, nucleoproteins, other nuclear bodies like Cajal bodies that constantly exchange material with the nucleolus, and also the nuclear matrix. In addition, various signaling pathways and cellular cues of growth, differentiation and cell death also affect nucleolar structure (Baker, 2013; Malatesta et al., 2000; Tsang et al., 2003). The nucleolus is likely to have co-evolved with the nuclear envelope (Lo et al., 2006). Prokaryotes lack both the nuclear envelope and the nucleolus. In yeast, a single crescent shaped nucleolus contacts the nuclear envelope (Taddei and Gasser, 2012). Yeast cells undergo closed mitosis (without nuclear envelope breakdown) and their nucleolus remains intact during the process (Granot and Snyder, 1991), unlike higher eukaryotes where nucleolus disperses during open mitosis. It is therefore likely that nuclear envelope proteins may impact nucleolar structure.

The nuclear envelope in higher eukaryotes is a double layered membrane encapsulating the nucleus. LINC (Linker of Nucleoskeleton and Cytoskeleton) complex Sun proteins and Nesprins span the nuclear envelope and connect the cellular actin cytoskeleton with the nuclear lamina that underlies the nuclear envelope, on the nucleoplasmic side (Aebi et al., 1986; Kim et al., 2015). The nuclear lamina is a filamentous meshwork composed of interdigitating

networks of A type (Lamin A and Lamin C) and B-type (Lamin B1 and Lamin B2) lamins (Aebi et al., 1986; Höger et al., 1990; Lin and Worman, 1997). B-type lamins are expressed in most vertebrate cells, whereas Lamin A/C is expressed predominantly in differentiated cells (Constantinescu et al., 2006; Eckersley-Maslin et al., 2013). The nuclear lamina provides mechanical strength to maintain nuclear shape and integrity. Although Lamins primarily localize to the nuclear envelope, intranuclear pools of Lamins are required for chromatin dynamics, splicing and DNA damage repair (Bronshtein et al., 2015; Camps et al., 2014; Mahen et al., 2013; Moir et al., 1994). Mutations in lamins result in the accelerated ageing syndrome Hutchinson Gilford Progeria Syndrome (HGPS) characterized by massive changes in nuclear structure (Mounkes and Stewart, 2004). Cultured fibroblast derived from HGPS patients with mutations in Lamin A, also show redistribution of nucleolar proteins (Mehta et al., 2010) and nucleolar expansion (Buchwalter and Hetzer, 2017). Similar effects of enlarged nucleoli observed upon depletion of the LINC complex protein Sun1, a Lamin A interactor (Matsumoto et al., 2016). Although, Lamin B1 depletion in HeLa cells disrupts the nucleolus, the role of Lamin B2 in nucleolar organization has not been investigated (Martin et al., 2009). Moreover, in the absence of a mechanistic understanding of how nuclear envelope proteins and lamins affect nucleolar structure, these observations remains correlative.

Consistent with the membrane-less and dynamic constitution of the nucleolus, nearly ~4,500 proteins have been identified by mass-spectrometric studies, to either stably or transiently localize inside the nucleolus (Ahmad et al., 2009). Majority of these proteins serve roles unrelated to ribosome biogenesis. An outstanding question in the field is how proteins localize to or are retained in the nucleolus. Unlike the presence of well-defined nuclear localization signals (NLS) that are required for nucleoporin mediated import of proteins into the nucleus, the localization of proteins inside the nucleolus is potentially mediated through interactions with nucleolar proteins Nucleophosmin and Nucleolin, or through binding to nucleolar RNA.

Several questions remain to be answered – (i) how do nuclear envelope proteins regulate nucleolar structure (ii) do lamins affect nucleolar function? (iii) do lamins regulate phase separation of nucleolar proteins? (iv) do nuclear and nucleolar proteins show regulatory cross-talk to maintain nuclear and nucleolar structure? (v) how are proteins targeted and retained in the nucleolus?

Here, I have attempted to answer these questions under the following sub sections of the thesis.

I. Role of lamins in regulating nucleolar structure
II. Role of lamins in regulating nucleolar function and the dynamics of nucleolar proteins
III. Regulatory cross-talk of nucleolar proteins with lamins

IV. Targeting and retention of proteins in the nucleolus

Aims

I. To investigate the role of lamins in regulating nucleolar structure

We assessed nucleolar morphologies across cancer cell lines of varied tissue origins and normal colon cells by immunostaining for Nucleolin. Nucleolin staining revealed two categories of nucleolar morphologies in cells – (1) discrete and (2) aggregated. DLD1 colorectal cancer cells showed the highest sub-population of round and discrete nucleoli, amongst cancer cells. DLD1 cells also showed comparable levels of all three nuclear lamins, i.e., Lamins A/C, B1, and B2, which vary considerably in most other cell types. To assess impact of lamins on nucleolar morphology, we performed siRNA mediated knockdowns of Lamin A/C, B1 and B2 in DLD1 cells and performed immunostaining for Nucleolin. Lamin B2 knockdown disrupted nucleolar morphology in DLD1 cells. In contrast, Lamin A and B1 knockdowns, did not affect nucleolar morphology. This showed differential roles of Lamins B2, A/C and B1 in modulating nucleolar morphology.

Although Lamin B2 is primarily localized at the nuclear envelope, removal of soluble nuclear proteins and digestion of chromatin revealed the presence of intranuclear pools of Lamin B2, proximal to the nucleolus. Isolated nucleoli showed enrichment of Lamin B2 as punctae at the border of granular component (GC) of the nucleolus, while Lamin A was localized in the nucleolar interior. Co-immunoprecipitation assays showed that Lamin B2 forms a sub-complex with nucleolar GC proteins – Nucleophosmin and Nucleolin. Essentially, Lamin B2 forms two distinct sub-complexes – at the nuclear periphery and at the nucleolar periphery respectively.

We sought to examine if Lamin B2 protein showed separation of function at the nuclear periphery and the nucleolar periphery. Two separate deletion mutants of Lamin B2 showed distinct functions in maintaining the nucleolar and the nuclear structure. We found that the N-terminal head domain of Lamin B2 is important to maintain discrete, spherical nucleolar morphology while a stretch of amino acids in the C-terminal tail domain of Lamin B2 was important to maintain bleb-free nuclear morphology.

II. To investigate the role of lamins in regulating rDNA transcription

Since the primary function of the nucleolus is rDNA transcription and ribosome biogenesis, we sought to examine if structural aberrations seen upon Lamin B2 depletion were accompanied by altered rRNA expression levels. The rDNA is transcribed as a 47S/45S precursor which is further processed into 28S, 5.8S, and 18S rRNAs. Semi-quantitative RT-PCR showed a ~2.7 fold increase in 45S rRNA levels, while 28S and 18S levels were not

affected. This showed that rRNA transcription but not processing is affected upon Lamin B2 depletion. Lamin B2 depletion also showed increase in expression levels of non-coding RNAs transcribed from intergenic sequences of rDNA.

To address possible mechanisms by which Lamin B2 affects 45S expression, we assessed known regulators of rDNA transcription. Immunofluorescence and western blotting showed a ~40% decline in DNMT1 levels. Dnmt1 methylates rDNA and represses rDNA transcription (Espada et al., 2007). Thus, loss of Dnmt1 upon Lamin B2 knockdown is a potential mechanism by which rDNA transcription is deregulated. Consistent with derepression of rDNA, HP1α - a marker of perinucleolar heterochromatin, showed enhanced nuclear mobility.

We also assessed the impact of Lamin B2 depletion on global transcription with a focus on genes involved in rDNA transcription, processing and assembly, using whole genome expression profiling microarray. We found that chromatin modifiers – *EHMT1* and *JARID2* were downregulated upon Lamin B2 knockdown, while the positive regulator of rDNA transcription – the oncogene *MYC* was upregulated. At least 8 out of 80 ribosomal protein coding genes were affected upon Lamin B2 depletion, which includes *RPL27A*, knockdown of which affects nucleolar structure.

Ongoing rDNA transcription and processing is an important factor in regulating nucleolar structure and dynamics of nucleolar proteins (Chen and Huang, 2001; Shav-Tal et al., 2005). Thus, we assessed dynamics of the nucleolar protein Nucleolin in Lamin B2 depleted cells where transcription from ribosomal DNA locus is upregulated. Nucleolin is an RNA binding protein and its sequestration in the nucleolus is dependent on its binding to ribosomal DNA, ribosomal RNA and nucleolar non-coding RNAs (Caudron-Herger et al., 2015; Ghisolfi-Nieto et al., 1996; Tajrishi et al., 2011). Ribosomal DNA (rDNA) transcription was inhibited in cells using the RNA Pol I transcription inhibitor Actinomycin D (0.05μg/ml). This showed the formation of nucleoplasmic aggregates of Nucleolin that dispersed into the nucleoplasm over time. Lamin B2 depleted cells showed much larger aggregates of Nucleolin that persisted in the nucleoplasm. We found that intergenic RNA transcripts that were upregulated upon Lamin B2 depletion, co-localized with nucleoplasmic Nucleolin aggregates. We thus surmise, that Lamin B2 regulates dynamics and potentially phase separation of Nucleolin, in an RNA dependent manner.

III. Investigating the role of nucleolar DFC protein Fibrillarin in regulating nucleolar and nuclear structure

Fibrillarin is a DFC protein responsible for 2-O'-methylation of rRNA and translational fidelity (Tollervey et al., 1993). Downregulation of Fibrillarin shows severely distorted

nucleolar morphology but does not affect nuclear morphology. We therefore investigated if Fibrillarin and nuclear lamins show regulatory feedback in expression. Whole genome expression analysis of Fibrillarin depleted cells showed dysregulation of 1118 genes. Genes that were upregulated upon Fibrillarin knockdown clustered under the following categories – (i) Nucleosome core, (ii) innate immune response in mucosa, (iii) methylation, (iv) TNF signaling pathway, (v) cell chemotaxis and so on (Fig. 6.5A). Genes that were downregulated upon Fibrillarin knockdown clustered under the following categories – (i) Transferase, (ii) Transcription factor activity, (iii) Golgi cisterna membrane, (iv) regulation of cell shape, (v) developmental pathways, (vi) Methylation.

Expression profiling using a custom Taqman array showed dysregulation of nuclear architectural genes upon Fibrillarin knockdown. Downregulated genes included (i) nuclear envelope encoding genes – *BANF1*, *TMEM48*, *EMD*, *TMPO* and *LMNA*; (ii) nucleoporin encloding genes – *NUP93*, *SEC13*; (iii) transcription factor encoding genes – *E2F1*, *SREBF1*, *POU5F1* and (iv) DNA modifier – *DNMT1*. Upregulated genes included histone binding protein – *CBX5*, transcription factor – *FOS* and cell-cell junction protein – *CDH1*.

Immunofluorescence assay, western blotting and qRT-PCR independently revealed that Lamin A/C and Lamin B2 were indeed downregulated upon Fibrillarin knockdown, however Lamin B1 levels were unaltered. Fibrillarin depletion also showed massive reorganization of the actin cytoskeleton as assessed by immunofluorescence. Fibrillarin depleted cells showed significantly higher surface area compared to control cells. These cells also showed an accumulation of actin aggregates near the nuclear envelope. Fibrillarin depleted cells were also more resistant to actin depolymerisation using Latrunculin A. This suggests that actin cytoskeleton is more stabilized in Fibrillarin depleted cells. This could be due to dysregulation of actin organizers *CORO1A*, *PLXNB2*, *ARAP3* genes upon Fibrillarin knockdown. We also found that cell migration was enhanced in Fibrillarin depleted cells.

We surmise that changes in nuclear morphologies upon Fibrillarin depletion is potentially a combined manifestation of a weak nuclear envelope and increase in extra nuclear actin accumulation.

IV. Investigating the role of nucleolar GC protein Nucleolin in regulating histone 2B compartmentation and dynamics in the nucleolus

A previous study showed that histone 2B (H2B) localizes into the nucleolus when overexpressed (Musinova et al., 2011). In order to investigate the role of nuclear factors that regulate targeting and retention of proteins in the nucleolus, we studied nuclear and nucleolar localization of histone 2B as a useful paradigm. Fluorescently tagged H2B (H2B-ECFP) localized in the nucleus of all transfected DLD1 cells, however in ~40% of H2B-ECFP also showed nucleolar localization. We assessed if lamins and nucleolar proteins affected the

localization of H2B-ECFP in the nucleolus. To this end we performed siRNA mediated knockdowns of lamins A/C, B1, B2 and nucleolar proteins Fibrillarin, Nucleostemin and Nucleolin and found that Nucleolin depletion significantly affects H2B-ECFP localization in the nucleolus, which was reduced to ~10%. By 72h of transfection, nucleolar H2B-ECFP redistributed into the nucleoplasm, however, overexpression of Nucleolin-GFP (NCL-GFP) retained H2B-ECFP in the nucleolus for a longer duration. We screened several cancer cell lines and normal colon cells, and found that H2B-ECFP localization in the nucleolus increased with an increase in endogenous Nucleolin expression level. Furthermore, cells expressing higher levels of Nucleolin also showed greater mobility of H2B-ECFP in the nucleolus, as assessed by FRAP.

Co-immunoprecipitation assays show that H2B-ECFP associates with Nucleolin. Further, deletion mutants of Nucleolin, lacking the N-terminal domain and RNA binding domain (RBD), hardly retain H2B-ECFP in the nucleolus. Thus, we show that binding to the GC protein Nucleolin is a possible mechanism by which proteins get retained in the nucleolus.

Summary

Taken together, here we show a novel role for nuclear Lamin B2 as a modulator of nucleolar structure, function and dynamics. We show that Lamin B2 forms a sub-complex with nucleolar GC proteins – Nucleolin and Nucleophosmin and localizes at the nucleolar boundary. Distinct domains of Lamin B2 regulate nucleolar and nuclear structure. Lamin B2 potentially regulates phase separation of the Nucleolin, in an RNA dependent manner. Furthermore, we have identified a regulatory cross-talk between lamins and the nucleolar DFC protein Fibrillarin. We have uncovered that Fibrillarin is essential for maintaining normal nuclear and cell morphology. We also studied the mechanisms of protein targeting and retention into the nucleolus, and identified the overarching role of Nucleolin in protein sequestration within the nucleolus. In this thesis, we have attempted to answer three important aspects of nucleolar biology (i) its structure-function relationship (ii) relationship of nuclear and nucleolar proteins and (iii) principles of nucleolar protein retention. This study aims to form the foundation for understanding the significance of dysregulated nucleolar structure and signaling – hallmarks of diseases such as ribosomopathies, cancers and neurodegenerative disorders.

References

Aebi, U., Cohn, J., Buhle, L., and Gerace, L. (1986). The nuclear lamina is a meshwork of intermediate-type filaments. Nature *323*, 560–564.

Ahmad, Y., Boisvert, F.M., Gregor, P., Cobley, A., and Lamond, A.I. (2009). NOPdb: Nucleolar Proteome Database--2008 update. Nucleic Acids Res *37*, D181–4.

Baker, N.E. (2013). Developmental regulation of nucleolus size during Drosophila eye differentiation. PLoS ONE *8*, e58266.

Brangwynne, C.P., Mitchison, T.J., and Hyman, A.A. (2011). Active liquid-like behavior of nucleoli determines their size and shape in Xenopus laevis oocytes. Proc Natl Acad Sci USA *108*, 4334–4339.

Bronshtein, I., Kepten, E., Kanter, I., Berezin, S., Lindner, M., Redwood, A.B., Mai, S., Gonzalo, S., Foisner, R., Shav-Tal, Y., et al. (2015). Loss of lamin A function increases chromatin dynamics in the nuclear interior. Nat Commun *6*, 8044.

Buchwalter, A., and Hetzer, M.W. (2017). Nucleolar expansion and elevated protein translation in premature aging. Nat Commun *8*, 328.

Camps, J., Wangsa, D., Falke, M., Brown, M., Case, C.M., Erdos, M.R., and Ried, T. (2014). Loss of lamin B1 results in prolongation of S phase and decondensation of chromosome territories. FASEB J *28*, 3423–3434.

Carron, C., Balor, S., Delavoie, F., Plisson-Chastang, C., Faubladier, M., Gleizes, P.E., and O'Donohue, M.F. (2012). Post-mitotic dynamics of pre-nucleolar bodies is driven by pre-rRNA processing. J Cell Sci *125*, 4532–4542.

Caudron-Herger, M., Pankert, T., Seiler, J., Németh, A., Voit, R., Grummt, I., and Rippe, K. (2015). Alu element-containing RNAs maintain nucleolar structure and function. EMBO J *34*, 2758–2774.

Chen, D., and Huang, S. (2001). Nucleolar components involved in ribosome biogenesis cycle between the nucleolus and nucleoplasm in interphase cells. J Cell Biol *153*, 169–176.

Cheutin, T., O'Donohue, M.F., Beorchia, A., Vandelaer, M., Kaplan, H., Defever, B., Ploton, D., and Thiry, M. (2002). Three-dimensional organization of active rRNA genes within the nucleolus. J Cell Sci *115*, 3297–3307.

Constantinescu, D., Gray, H.L., Sammak, P.J., Schatten, G.P., and Csoka, A.B. (2006). Lamin A/C expression is a marker of mouse and human embryonic stem cell differentiation. Stem Cells *24*, 177–185.

Dundr, M., and Misteli, T. (2010). Biogenesis of nuclear bodies. Cold Spring Harb Perspect Biol *2*, a000711.

Eckersley-Maslin, M.A., Bergmann, J.H., Lazar, Z., and Spector, D.L. (2013). Lamin A/C is expressed in pluripotent mouse embryonic stem cells. Nucleus *4*, 53–60.

Espada, J., Ballestar, E., Santoro, R., Fraga, M.F., Villar-Garea, A., Németh, A., Lopez-Serra, L., Ropero, S., Aranda, A., Orozco, H., et al. (2007). Epigenetic disruption of ribosomal RNA genes and nucleolar architecture in DNA methyltransferase 1 (Dnmt1) deficient cells. Nucleic Acids Res *35*, 2191–2198.

Feric, M., Vaidya, N., Harmon, T.S., Mitrea, D.M., Zhu, L., Richardson, T.M., Kriwacki, R.W., Pappu, R.V., and Brangwynne, C.P. (2016). Coexisting liquid phases underlie nucleolar subcompartments. Cell *165*, 1686–1697.

Ghisolfi-Nieto, L., Joseph, G., Puvion-Dutilleul, F., Amalric, F., and Bouvet, P. (1996). Nucleolin is a sequence-specific RNA-binding protein: characterization of targets on pre-ribosomal RNA. J Mol Biol *260*, 34–53.

Granot, D., and Snyder, M. (1991). Segregation of the nucleolus during mitosis in budding and fission yeast. Cell Motil Cytoskeleton *20*, 47–54.

Handwerger, K.E., and Gall, J.G. (2006). Subnuclear organelles: new insights into form and function. Trends Cell Biol *16*, 19–26.

Heix, J., Vente, A., Voit, R., Budde, A., Michaelidis, T.M., and Grummt, I. (1998). Mitotic silencing of human rRNA synthesis: inactivation of the promoter selectivity factor SL1 by cdc2/cyclin B-mediated phosphorylation. EMBO J *17*, 7373–7381.

Henderson, A.S., Warburton, D., and Atwood, K.C. (1972). Location of ribosomal DNA in the human chromosome complement. Proc Natl Acad Sci USA *69*, 3394–3398.

Höger, T.H., Zatloukal, K., Waizenegger, I., and Krohne, G. (1990). Characterization of a second highly conserved B-type lamin present in cells previously thought to contain only a single B-type lamin. Chromosoma *100*, 67–69.

Hult, C., Adalsteinsson, D., Vasquez, P.A., Lawrimore, J., Bennett, M., York, A., Cook, D., Yeh, E., Forest, M.G., and Bloom, K. (2017). Enrichment of dynamic chromosomal crosslinks drive phase separation of the nucleolus. Nucleic Acids Res *45*, 11159–11173.

James, A., Wang, Y., Raje, H., Rosby, R., and DiMario, P. (2014). Nucleolar stress with and without p53. Nucleus *5*, 402–426.

Kim, D.I., Birendra, K.C., and Roux, K.J. (2015). Making the LINC: SUN and KASH protein interactions. Biol Chem *396*, 295–310.

Klein, J., and Grummt, I. (1999). Cell cycle-dependent regulation of RNA polymerase I transcription: the nucleolar transcription factor UBF is inactive in mitosis and early G1. Proc Natl Acad Sci USA *96*, 6096–6101.

Kurki, S., Peltonen, K., Latonen, L., Kiviharju, T.M., Ojala, P.M., Meek, D., and Laiho, M. (2004). Nucleolar protein NPM interacts with HDM2 and protects tumor suppressor protein p53 from HDM2-mediated degradation. Cancer Cell *5*, 465–475.

Lallemand-Breitenbach, V., and de Thé, H. (2010). PML nuclear bodies. Cold Spring Harb Perspect Biol *2*, a000661.

Lin, F., and Worman, H.J. (1997). Expression of nuclear lamins in human tissues and cancer cell lines and transcription from the promoters of the lamin A/C and B1 genes. Exp Cell Res *236*, 378–384.

Llanos, S., Clark, P.A., Rowe, J., and Peters, G. (2001). Stabilization of p53 by p14ARF without relocation of MDM2 to the nucleolus. Nat Cell Biol *3*, 445–452.

Lo, S.J., Lee, C.C., and Lai, H.J. (2006). The nucleolus: reviewing oldies to have new understandings. Cell Res *16*, 530–538.

Mahen, R., Hattori, H., Lee, M., Sharma, P., Jeyasekharan, A.D., and Venkitaraman, A.R. (2013). A-type lamins maintain the positional stability of DNA damage repair foci in mammalian nuclei. PLoS ONE *8*, e61893.

Malatesta, M., Gazzanelli, G., Battistelli, S., Martin, T.E., Amalric, F., and Fakan, S. (2000). Nucleoli undergo structural and molecular modifications during hibernation. Chromosoma *109*, 506–513.

Martin, C., Chen, S., Maya-Mendoza, A., Lovric, J., Sims, P.F., and Jackson, D.A. (2009). Lamin B1 maintains the functional plasticity of nucleoli. J Cell Sci *122*, 1551–1562.

Matsumoto, A., Sakamoto, C., Matsumori, H., Katahira, J., Yasuda, Y., Yoshidome, K., Tsujimoto, M., Goldberg, I.G., Matsuura, N., Nakao, M., et al. (2016). Loss of the integral nuclear envelope protein SUN1 induces alteration of nucleoli. Nucleus *7*, 68–83.

Mehta, I.S., Bridger, J.M., and Kill, I.R. (2010). Progeria, the nucleolus and farnesyltransferase inhibitors. Biochem Soc Trans *38*, 287–291.

Mitrea, D.M., Cika, J.A., Guy, C.S., Ban, D., Banerjee, P.R., Stanley, C.B., Nourse, A., Deniz, A.A., and Kriwacki, R.W. (2016). Nucleophosmin integrates within the nucleolus via multi-modal interactions with proteins displaying R-rich linear motifs and rRNA. Elife *5*.

Moir, R.D., Montag-Lowy, M., and Goldman, R.D. (1994). Dynamic properties of nuclear lamins: lamin B is associated with sites of DNA replication. J Cell Biol *125*, 1201–1212.

Mounkes, L.C., and Stewart, C.L. (2004). Aging and nuclear organization: lamins and progeria. Curr Opin Cell Biol *16*, 322–327.

Musinova, Y.R., Lisitsyna, O.M., Golyshev, S.A., Tuzhikov, A.I., Polyakov, V.Y., and Sheval, E.V. (2011). Nucleolar localization/retention signal is responsible for transient accumulation of histone H2B in the nucleolus through electrostatic interactions. Biochim Biophys Acta *1813*, 27–38.

Rieder, D., Trajanoski, Z., and McNally, J.G. (2012). Transcription factories. Front Genet *3*, 221.

Scheer, U., and Hock, R. (1999). Structure and function of the nucleolus. Curr Opin Cell Biol *11*, 385–390.

Shav-Tal, Y., Blechman, J., Darzacq, X., Montagna, C., Dye, B.T., Patton, J.G., Singer, R.H., and Zipori, D. (2005). Dynamic sorting of nuclear components into distinct nucleolar caps during transcriptional inhibition. Mol Biol Cell *16*, 2395–2413.

Sirri, V., Roussel, P., and Hernandez-Verdun, D. (1999). The mitotically phosphorylated form of the transcription termination factor TTF-1 is associated with the repressed rDNA transcription machinery. J Cell Sci *112 (Pt 19)*, 3259–3268.

Sirri, V., Urcuqui-Inchima, S., Roussel, P., and Hernandez-Verdun, D. (2008). Nucleolus: the fascinating nuclear body. Histochem Cell Biol *129*, 13–31.

Sleeman, J.E., and Trinkle-Mulcahy, L. (2014). Nuclear bodies: new insights into assembly/dynamics and disease relevance. Curr Opin Cell Biol *28*, 76–83.

Spector, D.L. (2001). Nuclear domains. J Cell Sci *114*, 2891–2893.

Spector, D.L., and Lamond, A.I. (2011). Nuclear speckles. Cold Spring Harb Perspect Biol *3*.

Taddei, A., and Gasser, S.M. (2012). Structure and function in the budding yeast nucleus. Genetics *192*, 107–129.

Tajrishi, M.M., Tuteja, R., and Tuteja, N. (2011). Nucleolin: The most abundant multifunctional phosphoprotein of nucleolus. Commun Integr Biol *4*, 267–275.

Tollervey, D., Lehtonen, H., Jansen, R., Kern, H., and Hurt, E.C. (1993). Temperature-sensitive mutations demonstrate roles for yeast fibrillarin in pre-rRNA processing, pre-rRNA methylation, and ribosome assembly. Cell *72*, 443–457.

Tsang, C.K., Bertram, P.G., Ai, W., Drenan, R., and Zheng, X.F. (2003). Chromatin-mediated regulation of nucleolar structure and RNA Pol I localization by TOR. EMBO J *22*, 6045–6056.

List of publications

1. Sen Gupta, A., and Sengupta, K. (2017). Lamin B2 modulates nucleolar morphology, dynamics, and function. Mol. Cell. Biol. *37*, e00274-17.
2. Sen Gupta, A., Joshi, G., Pawar, S. and Sengupta, K. (2018). Nucleolin modulates compartmentalization and dynamics of histone 2B-ECFP in the nucleolus. Nucleus. 1-18.

Essential Abbreviations

rDNA	Ribosomal DNA
rRNA	Ribosomal RNA
FC	Fibrillar compartment
DFC	Dense Fibrillar compartment
GC	Granular component
NOR	Nucleolar organizer region
UBF	Upsteam binding factor
NPM1/B23	Nucleophosmin
FBL	Fibrillarin
GNL3	Nucleostemin
LINC	Linker of Nucleoskeleton and Cytoskeleton
RBD	RNA binding domain
GAR	Glycine Arginine Rich
ChIP	Chromatin immunoprecipitation
IGS	Intergenic sequence
FISH	Fluorescence in-situ hybridization
NLS	Nuclear localization signal
NoLS	Nucleolar localization signal
Act D	Actinomycin D
Kbp	Kilobase pair
TF	Trancription factor
Kd	Knockdown

Chapter 1:

Introduction and Review of Literature

1.1. The Nucleolus

Nucleolus is the most prominent nuclear sub-structure that can be detected by light microscopy. It is the site of rDNA transcription and ribosome biogenesis. Nucleolus was first discovered in eel cells by Fontana in 1774. This was much before the cell nucleus was discovered by Robert Brown in 1831. However the first documentation of nucleolus, were independently made by Wagner and Valentin (Valentin, 1836; Wagner, 1834). The term nucleolus was coined by Valentin which meant "a nucleus within a nucleus". The important function of the nucleolus in rRNA synthesis was first discovered by Brown and Gurdon, when they found that anucleolate (without nucleolus) mutants of Xenopus embryos failed to develop (Brown and Gurdon, 1964). Barbara McClintock then discovered the nucleolar organizing-elements on the satellite chromosome in *Zea mays*, on which nucleoli assemble at telophase (McClintock, 1934).

Nucleolus organizer regions in the interphase nucleus, containing ribosomal genes, were initially visualized by silver staining (AgNOR staining), that bound to argyrophilic proteins of the nucleolus (Goodpasture and Bloom, 1975). This methodology was useful for histopathologists to distinguish malignant cells that showed greater silver staining from benign cells (Derenzini and Ploton, 1991). Further, electron microscopy revealed three ultrastructural regions of the nucleolus – the fibrillar compartment (FC), the dense fibrillar compartment (DFC) and the granular component (GC), containing the machinery for rDNA transcription, processing and ribosome assembly, respectively (Hernandez-Verdun et al., 2010).

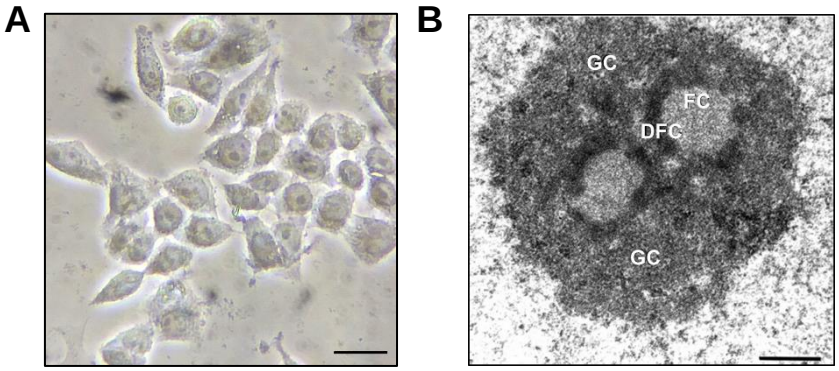

Figure 1.1. Nucleolar structure in human cells.
A. Monolayer cultures of DLD1 cells imaged with phase contrast microscopy showing prominent nucleoli in the nucleus. Scale bar ~ 10 μm. **B.** Ultrastructure of the HeLa nucleolus by electron microscopy showing fibrillar (FC), dense fibrillar (DFC) and granular component (GC). Scale bar: 1 μm. Reprinted with permission from (Sirri et. al., 2002).

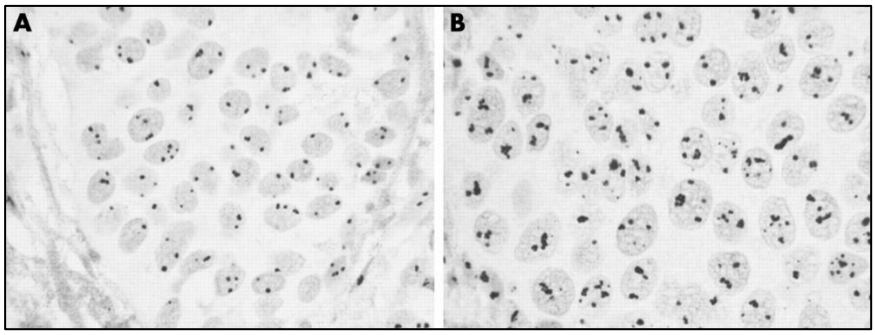

Figure 1.2. Silver stained histological sections of two breast carcinomas. A. Case with low numbers of argyrophilic nucleolar organizer regions (AgNORs) **B.** case with higher numbers of AgNORs. Reprinted with permission from (Derenzini et al., 2004)

1.2. Nucleolus during cell cycle

The nucleolar structure is highly dynamic during different stages of cell cycle and is intimately linked to the process of ribosome biogenesis. Ribosome biogenesis begins at the end of telophase, gradually rises during G1, peaks at G2 and ceases at prophase (Gébrane-Younès et al., 1997; Sirri et al., 2000). Nucleolus during interphase are nearly spherical ribonucleoprotein rich structures present in the nucleus. During mitosis, the nucleolus dismantles and releases its components into the nucleoplasm (Gavet and Pines, 2010). During prophase the nucleolus disassembles as the rDNA transcription, processing machinery are phosphorylated by Cdk1-Cyclin B and inhibited (Heix et al., 1998; Negi and Olson, 2006). While the rDNA transcription machinery (UBF, RNA Pol I) is still bound to NORs, the rRNA processing machinery is released and relocalizes to the periphery of condensing mitotic chromosomes, by mechanisms that are not very well investigated (Gautier et al., 1992; Gébrane-Younès et al., 1997). Breakthrough experiments from McStay lab show that introduction of arrays of *Xenopus* Upstream Binding factor (UBF) binding sequences at ectopic sites on human chromosomes (pseudoNORs) are sufficient to sequester RNA Polymerase I transcription machinery, even in the absence of active transcription at the during mitosis (Mais et al., 2005). During telophase, cdc14B mediated dephosphorylation of the transcription machinery induce rDNA transcription forming primitive FC and DFC (Voit et al., 2015). During the same time the processing machinery forms pre-nucleolar bodies (PNBs) at periphery of chromosomes (Carron et al., 2012; Savino et al., 2001). At the end of mitosis, the rRNA machinery progressively transfers from the PNBs to the newly generating rRNA transcripts from active NORs, forming primitive GC (Savino et al., 2001). Multiple nucleolar domains then fuse during early G1 to form nucleoli (Anastassova-Kristeva, 1977).

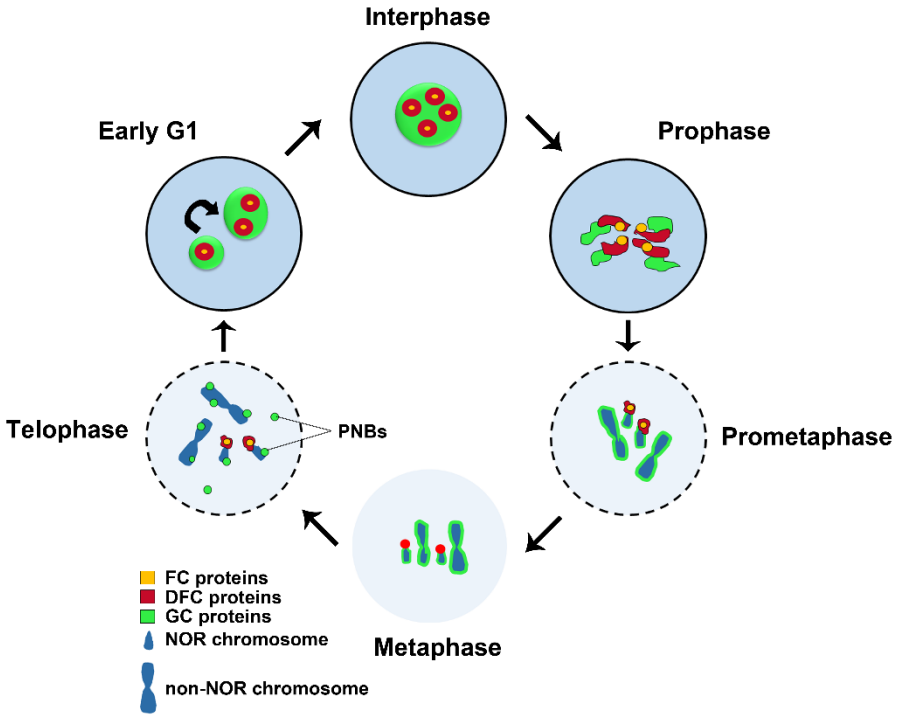

Figure 1.3. Nucleolar structure during mitosis

1.3. Nucleolar formation by phase-separation

Although the steps of nucleolar formation during cell cycle progression were worked out, how nucleolar structure is maintained and why nucleoli fuse is unclear. Biophysical experiments on isolated *Xenopus* germinal vesicle nucleolus showed that nucleoli have properties of a liquid droplet and adjacent droplets can fuse to form a larger nucleolus, when brought in close proximity (Brangwynne et al., 2011). These droplet like nucleoli attain spherical structures due to liquid-liquid phase separation from the nucleoplasm (Feric et al., 2016). Inside the nucleolus, DFC and GC compartments do not intermingle due to distinct surface tensions of DFC and GC marker proteins – Fibrillarin and NPM1, respectively (Feric et al., 2016).

1.4. Functions of the nucleolus

Recent advances in fluorescence microscopy and proteomics have helped in understanding the structure and functions of the nucleolus (Andersen et al., 2005; Chen and Huang, 2001). Although the primary function of the nucleolus is ribosome biogenesis (described in detail in section 3.1), nearly 30% of the nucleolar proteome consist of proteins that do not have a role in this process and are associated with cell cycle and proliferation, cell death, telomere metabolism, RNA post-translational modification, energy production, and DNA replication, recombination or repair (Ahmad et al., 2009; Andersen et al., 2002, 2005; Scherl et al., 2002). Nucleolus also has "stress sensing" functions, whereby a large plethora of cellular stresses like DNA damage, nutrient deprivation, heat shock, cause its disintegration, causing stabilization of p53 protein, ultimately leading to cell cycle arrest and apoptosis (Boulon et al., 2010; Daniely et al., 2002; Kurki et al., 2004; Rubbi and Milner, 2003). However nucleolar stress can also be mediated independent of p53 induction (Al-Baker et al., 2004; James et al., 2014).

1.4.1. Ribosomal DNA (rDNA) transcription – canonical function of the nucleolus

Human cells have ~200-400 copies of rDNA genes distributed on the p-arms of Nucleolus organizer region (NOR)-bearing chromosomes 13, 14, 15, 21 and 22 (Henderson et al., 1972). Molecular combing approaches have revealed that two thirds of rDNA genes are oriented in a telomere to centromere orientation (canonical repeats) while the rest are present as palindromic (non-canonical) repeats (Caburet et al., 2005). Further, rDNA genes are present in three distinct transcriptional states – active, poised and silent (Srivastava et al., 2016). Active rDNA genes can be visualized as a typical "christmas tree" structure in Miller spreads. Active NORs are embedded into the nucleolus during interphase and appear as secondary constrictions on the p-arms of NOR-bearing chromosomes during interphase (Mais et al., 2005).

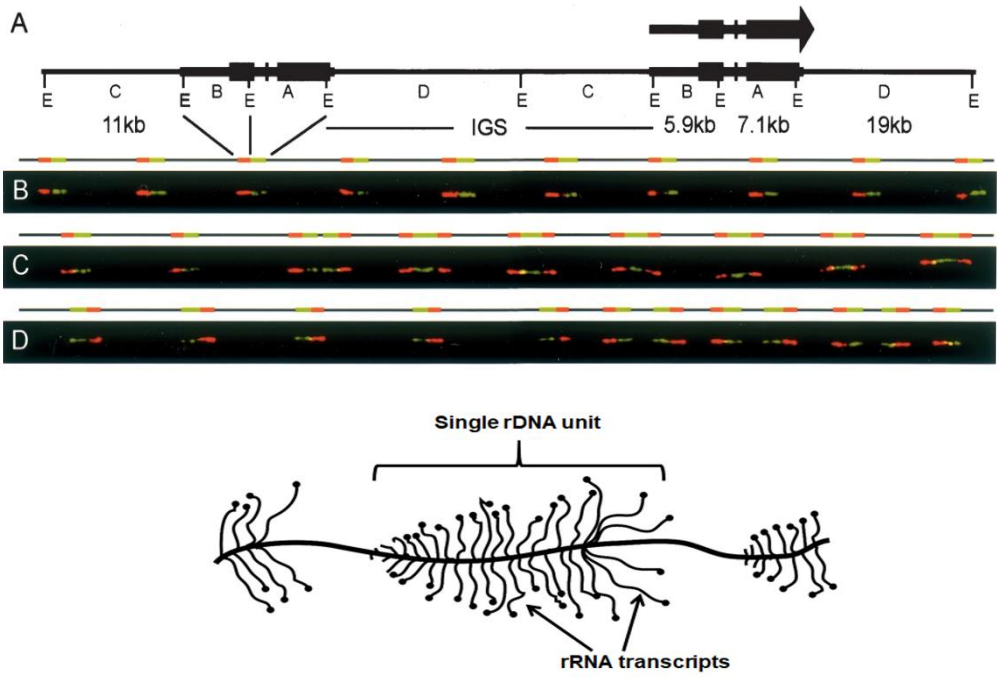

Figure 1.4. Structural analysis of the human rDNA locus by molecular combing.
A. Schematic of human rDNA repeats with positions of fluorescent in-situ hybridization (FISH) probes used for rDNA repeat visualization are indicated. Red – 5'-probe, Green – 3'-probe. **B.** Two-color hybridization on combed human DNA showing 10 canonical rDNA repeats in tandem with red probes proximal to telomeres and green probes proximal to centromeres. **C-D.** Hybridizations of the probes on human DNA that illustrate noncanonical palindromic units. Image from (Caburet et al., 2005). **E.** Cartoon of Miller spreads of rDNA showing "christmas tree" structure of emanating rRNA transcripts from rDNA repeats.

1.4.1.1. Transcription initiation of RNA Polymerase I

A single unit of ribosomal DNA (rDNA) consists of an upstream control element (UCE), a core promoter (CP), the rDNA coding region and termination elements (Haltiner et al., 1986; Maden et al., 1987). rDNA transcription begins with the assembly of the pre-initiation complex (PIC) at the rDNA promoter. The pre-initiation complex comprises of the upstream binding factor (UBF) and the promoter selectivity factor SL1 in humans (TIF-IB in mouse) (Clos et al., 1986; Jantzen et al., 1990; Learned et al., 1986). There is very little sequence similarity in the UCE and PE across species, making Pol I transcription highly species specific. This is because the promoter elements from one species cannot be recognized by the SL1 factors of other species (Grummt et al., 1982; Heix and Grummt, 1995; Miller et al., 1976). However, the structural features of ribosomal promoter DNA are conserved across evolution and important for assembly of pre-initiation factors (Marilley and Pasero, 1996). UBF protein can dimerize and mediate DNA bending via its HMG box to form a scaffold for the assembly of PIC (Bazett-Jones et al., 1994; Jantzen et al., 1990; Stefanovsky et al., 2001). Transcription of rDNA requires the sequential events of binding of SL1 to the promoter followed by the

recruitment of RNA Polymerase I (RNA Pol I) at these sites. The SL1 complex is composed of TATA binding protein (TBP), and Pol I transcription associated factors (TAF_I110, TAF_I68, TAF_I48, TAF_I41, and TAF_I12) (Comai et al., 1992; Denissov et al., 2007; Eberhard et al., 1993; Gorski et al., 2007; Heix et al., 1997). UBF stabilizes the binding of the SL1 complex at the rDNA promoter (Kuhn and Grummt, 1992). C-terminal phosphorylation of UBF by CK2 increases its ability to bind TIF-IB/SL1, while interaction of UBF with pRB, p130 and p53 inhibits its interaction with TIF-IB/SL1. Next UBF interacts with Pol I subunit PAF53 (mammalian homolog of yeast A49) and recruits it to the rDNA promoter (Hanada et al., 1996), and TIF-IB/ SL1 interacts and recruits the regulatory factor TIF-IA (mammalian homolog of yeast Rrn3p) (Miller et al., 2001). Acetylation of UBF and TAF_I68 of TIF-IB/SL1 by pCAF and p300 enhance binding to rDNA and increase transcription.

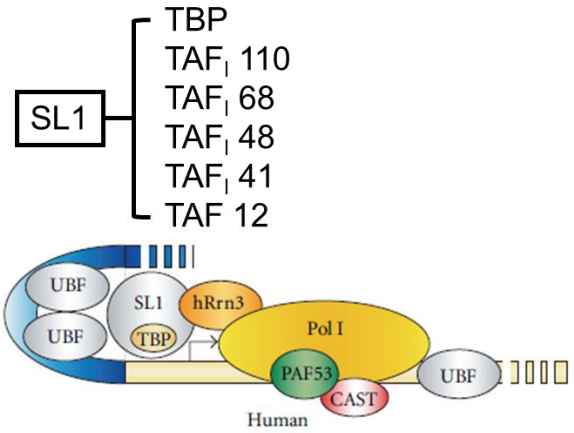

Figure 1.5. RNA polymerase I pre-initiation complex.
Adapted from (Albert et al., 2012)

1.4.1.2. Promoter escape and elongation

RNA Pol I has to detach from its promoter bound transcription initiation factors for rRNA synthesis to commence (Panov et al., 2001, 2006). This event is known as promoter escape initiated by the detachment of the elongating RNA Pol I from TIF-IA or Rrn3 (Hirschler-Laszkiewicz et al., 2003). Casein kinase 2 mediates phosphorylation of TIF-IA at Ser 170 and 172 which releases RNA Pol I (Bierhoff et al., 2008). While unphosphorylated UBF inhibits elongation of rRNA, phosphorylation at threonines 117 and 201, promotes RNA Pol I elongation by release of the UCE and CP enhanceosome (Stefanovsky et al., 2006). RNA pol I elongation is mediated by nuclear actin and nuclear myosin I via their interaction with WSTF-Snf2h chromatin remodelling complex (Percipalle et al., 2006; Ye et al., 2008). Further, considerable topological stress is generated due to the high rate of transcription by RNA Pol I.

Thus, topoisomerases assist in transcriptional elongation of RNA Pol I by releasing positive and negative supercoiling (French et al., 2011).

Pre-rRNA association with ribosomal proteins occurs co-transcriptionally during RNA Pol I elongation phase. Thus pre-rRNA transcription, processing and assembly of ribosomal particles are tightly coupled and show feedback. Decrease and defects in rRNA transcription affects its processing and packaging into pre-ribosomes and likewise improper processing or assembly of ribosomal particles negatively affects pre-rRNA transcription (Kopp et al., 2007; Schneider et al., 2007). In yeast, this coupling between transcription elongation and rRNA processing is carried out by the Spt4 and Spt5 proteins (Anderson et al., 2011; Leporé and Lafontaine, 2011; Schneider et al., 2006).

1.4.1.3. RNA Polymerase I transcription termination

The rRNA coding unit is succeeded by upto ten transcription termination sites (T1-T10) (Grummt et al., 1985). These transcription termination sites are bound by the transcription termination factor TTF-I. TTF-I causes pausing of RNA Pol I while PTRF (Pol I and transcript release factor) dissociates Pol I from the termination site (Bartsch et al., 1988; Jansa and Grummt, 1999). When transcription does not terminate at termination site T1, RNA Pol I proceeds to the downstream "fail safe" termination sites and the "torpedo" mechanism of transcription termination comes to play (Reeder et al., 1999). During this time the nascent rRNA is cleaved by the endonuclease Rnt1 and the residual RNA Pol I associated RNA is cleaved by Rat1 (mammalian Xrn2) that chases the elongating RNA Pol I (El Hage et al., 2008; Kawauchi et al., 2008; Mason et al., 1997; West et al., 2004). Upon reaching the paused RNA Pol I, Rat1 destabilizes the binding of RNA Pol I to rDNA and causes it to disassemble (El Hage et al., 2008).

1.4.1.4. Re-initiation

Re-initiation of RNA Pol I transcription requires interaction of RNA Pol I with TIF-IA protein. Thus, at this point, TIF-IA previously phosphorylated by CK2 Ser 170/172 to dissociate from RNA Pol I, is dephosphorylated by the phosphatase FCP1 (Bierhoff et al., 2008). Thereafter RNA Pol I can re-associate with TIF-IA. Moreover, rDNA terminator sequences form a loop with the promoter and UCE, which is mediated by TTF-I (Denissov et al., 2011; Németh et al., 2008). This may facilitate transfer of terminated RNA Pol I to the promoter for re-initiation of transcription.

1.5. Orchestrators of nucleolar structure and function

1.5.1. Nucleolar proteins

Although mass-spectrometric studies have identified ~4500 proteins that dynamically associate with the nucleolus, the functions of a large number of nucleolar proteins remain uncharacterized (Ahmad et al., 2009; Leung et al., 2006). This chapter reviews few key nucleolar proteins that maintain nucleolar structure and functions, and whose roles have been extensively investigated in this study.

1.5.1.1. Nucleolin

Nucleolin (C23) is one of the most abundant non-ribosomal proteins present in the nucleolus representing ~10% of total nucleolar proteins (Bugler et al., 1982). Nucleolin localizes in the DFC and GC of the nucleolus and functions in multiple steps of rDNA transcription, processing and ribosome biogenesis (Biggiogera et al., 1990; Cong et al., 2012; Ghisolfi-Nieto et al., 1996; Ginisty et al., 1998). It was first identified as the C23 protein in nucleolar extracts of normal liver and liver cancer cells from rat, and subsequently detected in Chinese hamster ovary (CHO) cells, human cells and many other eukaryotic cells (Bugler et al., 1982; Orrick et al., 1973; Prestayko et al., 1974; Srivastava et al., 1989). It is encoded by the *NCL* gene located on Chr 2q12-qter in humans and shows characteristics of "housekeeping genes" e.g. high GC content in first intron and 5' flanking sequences (Srivastava et al., 1990). Nucleolin in CHO cells is 713 amino acid in length, with a predicted molecular weight of 77kDa (Lapeyre et al., 1987). However, due to its highly charged and phosphorylated N-terminal region, Nucleolin shows an apparent molecular weight of 100-110 kDa (Mamrack et al., 1979; Olson et al., 1975).

1.5.1.1.1. Structure of Nucleolin

Nucleolin structure in eukaryotes is highly conserved across evolution. Nucleolin protein sequence comprises of (i) an N-terminal domain, (ii) central RNA binding domains, (iii) a C-terminal GAR domain. The N-terminal domain of Nucleolin is variable in length across species and contains multiple acidic stretches interspersed with basic stretches of amino acids. Human Nucleolin contains four acidic stretches in the N-terminus composed of glutamate and aspartate repeats. These acidic stretches mediate the interaction of Nucleolin with histone H1 and induce chromatin de-condensation (Erard et al., 1988). Nucleolin in most higher eukaryotes including human, mouse, rat, hamster and *Xenopus*, have four RNA binding domains, through which it can bind to pre-RNA and mRNA (Ghisolfi-Nieto et al., 1996; Sengupta et al., 2004; Serin et al., 1996). The Glycine Arginine Rich (GAR) domain of Nucleolin as the name suggests, comprises of glycine, arginine and phenylalanine repeats, and mediates protein-

protein interaction with multiple ribosomal and non-ribosomal proteins (Bhatt et al., 2012; Bouvet et al., 1998).

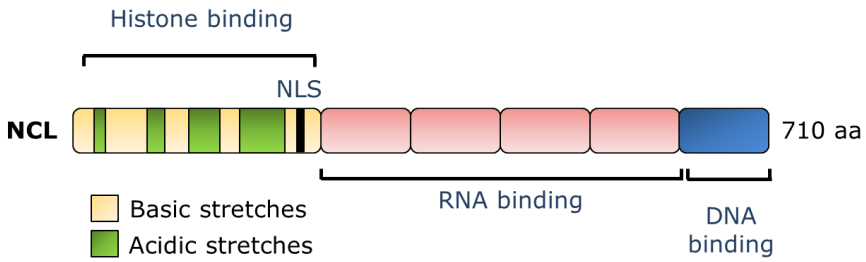

Figure 1.6. Domain structure of Nucleolin

1.5.1.1.2. Nucleolin post-translational modifications (PTMs)

Post-translational modifications of Nucleolin regulate its stability, functions and localization (Table 1.1). Nucleolin is a highly phosphorylated and methylated protein (Lischwe et al., 1982; Mamrack et al., 1979; Rao et al., 1982). Besides these PTMs, it also undergoes acetylation (Das et al., 2013), ADP-ribosylation (Leitinger and Wesierska-Gadek, 1993), glycosylation (Carpentier et al., 2005) and SUMOylation (Zhang et al., 2015). Nucleolin is a target for many kinases viz. cell division control protein 2 homolog (cdc2), casein kinase 2 (CK2), protein kinase C (PKC) and cyclin dependent kinase 1 (CDK1) (Table 1.1). Nucleolin is phosphorylated by casein kinase II (CK2) and cdc2 during interphase and M-phase, respectively, at threonines within the TPXK motif. CK2 phosphorylates nucleolin in actively growing cells at serine with the consensus SEDE motifs that are present in the N-terminus of the protein.

Nucleolin ADP-ribosylation is mediated by PRMT1 and PRMT5 (Cimato et al., 2002; Teng et al., 2007). Inhibition of PRMT5 mediated ADP-ribosylation using AS1411 is a major therapeutic intervention used in cancers showing Nucleolin upregulation (Teng et al., 2007).

Table. 1.1. Selected post-translational modifications of Nucleolin and their function

Post translational modification	Residue	Functional significance
Phosphorylation	CK2 kinase TPXK motif – T76, T84, T92, T99, T106, T113, T121, T214	Phosphorylated during interphase (Belenguer et al., 1990; Caizergues-Ferrer et al., 1987)
	SEDE motif – S28, S34, S145, S153, S184, S206	Positively co-relates with rDNA transcription (Belenguer et al., 1989) Important for nucleolar localization, cell proliferation, p53 stability (Xiao et al., 2014)
	cdc2 kinase TPXK motif – T76, T84, T92, T99, T106, T113, T121, T214	• Phosphorylated in M-phase (Belenguer et al., 1990; Peter et al., 1990) • Cytoplasmic localization upon phosphorylation (Schwab and Dreyer, 1997) • Spindle pole and chromosomal periphery localization during mitosis, chromosome congression (Ma et al., 2007) • May cause mitotic re-organization of nucleoli and inhibition of rRNA transcription during mitosis (Peter et al., 1990) • Implicated in Alzheimer's disease (Dranovsky et al., 2001)
	PKC Unknown	Competes with REST and transcriptional activation of gene (Tediose et al., 2010)
Acetylation	K88	Colocalizes with pre-mRNA splicing factors (Das et al., 2013)
Methylation	N^G, N^G-dimethylarginine – R656, R660, R666, R670, R673, R679, R681, R687, R691, R694	• Largely unknown. Methylation in concentrated in GAR domain (Lischwe et al., 1982). • May be important for regulation of Nucleolin interactions, protein stability or localization (Ginisty et al., 1999)
	Nω-monomethylarginine – K694	Modulates binding to nucleic acids (Raman, 2001)
ADP-ribosylation	Unknown	Unknown (Leitinger and Wesierska-Gadek, 1993)
Glycosylation	N317, N492	Important for cell surface localization (Carpentier et al., 2005; Losfeld et al., 2009)
SUMOylation	K294	Nuclear sequestration, GADD45α mRNA binding (Zhang et al., 2015)

1.5.1.1.3. Ribosomal function of Nucleolin

Nucleolin is involved in multiple steps of ribosome biogenesis. There are contrasting reports of positive and negative regulation of rDNA transcription by Nucleolin in *in vitro* systems and *in vivo* models (Bouche et al., 1984; Cong et al., 2012; Egyhazi et al., 1988). In this section, we focus on the regulation of rDNA by Nucleolin in *in vivo* systems. Most recent ChIP-sequencing experiments have revealed that Nucleolin binds to ribosomal DNA (Cong et al., 2012). It is most enriched in the coding and promoter region of rDNA and depleted from the intergenic regions (Fig. 1.7). Nucleolin knockdown and knockout in human and chicken cells, respectively, result in reduction of pre-rRNA (Cong et al., 2012; Ma et al., 2007; Rickards et al., 2007; Storck et al., 2009; Ugrinova et al., 2007). It is hypothesized that Nucleolin depletion inhibits rDNA transcription/elongation by decreased recruitment of UBF on rDNA promoter and coding regions (Cong et al., 2012).

Nucleolin also mediates the cleavage of 5'-ETS sequence of pre-rRNA, which is the first step of rRNA processing, via its interaction with U3 snoRNP (Ginisty et al., 1998). Nucleolin is capable of binding to rRNA both through the RBDs and the GAR domain. However, the presence of RBDs impart specificity to Nucleolin to bind to the 5'-ETS of rRNA (Ghisolfi et al., 1992).

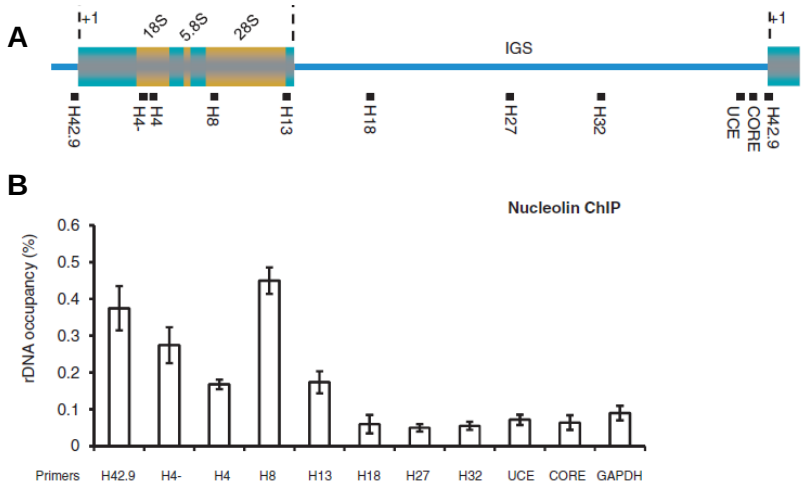

Figure 1.7. ChIP binding profile of Nucleolin along rDNA body and intergenic sequences.
A. Schematic of rDNA gene and intergenic regions showing primers used to assess Nucleolin binding. **B.** ChIP showing occupancy of Nucleolin in rDNA coding and intergenic sequemce. Reprinted with permission from (Cong et al., 2012).

Nucleolin binds to pre-rRNA and promotes secondary structure formation (Sipos and Olson, 1991). Thus, Nucleolin binding to NRE (Nucleolin recognition elements) stem-loops ensures proper folding and packaging of rRNA into pre-ribosomes (Allain et al., 2000). Pre-ribosome packaging seems to be sensitive to levels of Nucleolin as injection of excess Nucleolin

in stage VI *Xenopus* oocytes, causes erroneous packaging of 40S pre-ribosomes. Further, Nucleolin associated with many ribosomal proteins through its GAR domain (Bouvet et al., 1998). Thus it may also be necessary for import of ribosomal proteins into the nucleolus prior to their assembly with rRNA.

1.5.1.1.4. Non-ribosomal functions of Nucleolin

The plethora of functions played by Nucleolin is evident from its diverse and numerous set of proteins it interacts with (Fig 1.8). The multifunctional roles of Nucleolin is also due to its different sub-cellular localizations. Apart from the nucleolus, Nucleolin also localizes in the nucleoplasm, cytoplasm and cell surface (Borer et al., 1989; Hovanessian et al., 2000; Semenkovich et al., 1990). During mitosis, Nucleolin localizes to mitotic chromosome periphery and centrosomes, where it participates in choromosome congression (Ma et al., 2007).

(i) Functions of nucleoplasmic Nucleolin

In the nucleoplasm, Nucleolin regulates RNA Pol II mediated transcription, maintains genome stability and splicing (Das et al., 2013; Goldstein et al., 2013; González and Hurley, 2010; González et al., 2009; Shang et al., 2012; Uribe et al., 2011). Nucleolin is a histone chaperone with FACT (Facilitates Chromatin Transcription) like activity and associates with the SWI/SNF complex and ACF complex histone remodellers (Angelov et al., 2006; Gaume et al., 2011). Nucleolin facilitates nucleosome assembly on naked DNA by binding to H2A-H2B dimers and transferring them to pre-assembled H3-H4 tetrasomes on DNA (Godfrey et al., 1990). Nucleolin also increases turnover of H2A-H2B destabilizing histone octamers providing access to chromatin remodellers to DNA (Angelov et al., 2006). Nucleolin can also induce chromatin decondensation by by binding to Histone H1 and displacing it from chromatin (Erard et al., 1988). This histone chaperone activity of Nucleolin is likely to help in increased transcription (Kireeva et al., 2002). A second mechanism by which Nucleolin positively or negatively regulates transcription is by binding to GC rich DNA (G quadruplexes) in the promoters of vascular endothelial growth factor (VEGF) and c-Myc, respectively. Nucleolin also complexes with transcription factors like c-Jun to regulate cPLA2α gene expression. Nucleolin phosphorylated by PI3K and PKCζ, during oncogenic transformation, displaces the transcriptional repressor REST from the promoters and leads to the activation of CD59, Bcl211 and Mcl1 genes (Tediose et al., 2010).

Nucleolin also mediates DNA damage repair by complexing with several proteins – YB-1, PCNA, Rad51, γH2AX and Topoisomerase I (Bharti et al., 1996; De et al., 2006; Gaudreault et al., 2004; Kobayashi et al., 2012; Yang et al., 2009). Nucleolin also assists in DNA double strand break repair (DSB) by its nucleosome remodelling activity. Nucleolin was shown to be recruited to sites of DSB by ChIP assays. Upon recruitment to these sites, Nucleolin

evicts H2A-H2B from the damage site to facilitate binding of the repair machinery (Goldstein et al., 2013).

(ii) Functions of cytoplasmic Nucleolin

In the cytoplasm Nucleolin modulates translation, mRNA stability and apoptosis. A comprehensive RNA-IP of nucleolin with endogenous mRNA-protein complexes from HeLa cells, followed by microarray analysis, identified many target mRNAs bound by Nucleolin (Abdelmohsen et al., 2011). Many of these mRNAs were products of cancer-associated genes and genes involved in cell growth and proliferation pathways e.g. CCN1 (*CCN1*) and *AKT1*, translation, viral infection and cell metabolism (Abdelmohsen et al., 2011). Nucleolin binds to G-rich residues in the 3'-UTR, coding regions and 5'-UTR of these genes via its RNA binding domains and affects their translation without affecting mRNA. The most prominent target of Nucleolin is p53 mRNA whose translation is inhibited by Nucleolin upon DNA damage (Takagi et al., 2005). Nucleolin also represses translation of PGHS-1 by binding to the 5'-UTR (Bunimov et al., 2007). Conversely, Nucleolin binds to 3'-UTRs of MMP9 and other selenoprotein mRNAs, enhancing their translation (Fähling et al., 2005; Miniard et al., 2010).

Finally, Nucleolin also binds to the 3'-UTR and regulates the turnover and mRNA stability of β-globin, amyloid precursor protein (APP), gastrin, B-cell leukemia/lymphoma 2 (Bcl-2), Bcl-xL, interleukin 2 (IL-2) and Gadd45α (Ishimaru et al., 2010; Jiang et al., 2006; Lee et al., 2007; Sengupta et al., 2004; Wang et al., 2014; Zaidi and Malter, 1995; Zhang et al., 2015, 2008). Nucleolin inhibits apoptosis by binding to the AU-rich elements in the 3'-UTR of Bcl-2 and Bcl-xL anti-apoptotic factors (Ishimaru et al., 2010; Sengupta et al., 2004; Zhang et al., 2008).

Cell surface nucleolin is upregulated in cancers like colorectal carcinoma, hepatocellular carcinoma and angiogenic endothelial cells (Christian et al., 2003; Reyes-Reyes and Akiyama, 2008; Semenkovich et al., 1990; Wu et al., 2014). The cell surface localization of Nucleolin is unusual as it lacks a transmembrane domain or a GPI anchor (Hovanessian et al., 2010). Cytoplasmic nucleolin is encapsulated in vesicles and transported to the cell surface by an ER-Golgi independent but actin dependent pathway (Hovanessian et al., 2000). Cell surface translocation of Nucleolin is mediated by the actin motor protein non muscle myosin heavy chain (MyH9) (Huang et al., 2006). The heat shock protein Hsc70 enhances Nucleolin interaction with MyH9 and increases its cell surface localization (Ding et al., 2012). Nucleolin is glycosylated at the cell surface and inhibition of this glycosylation by tunicamycin reduces its cell surface localization (Losfeld et al., 2009). However, cell surface Nucleolin undergoes constant turnover with a half-life of only 45 min compared to 8 h of nuclear Nucleolin (Huang et al., 2006). Nucleolin transport to the cell surface is enhanced by VEGF and is also important for VEGF induced endothelial cell migration (Destouches et al., 2008). Cell surface Nucleolin

acts as a receptor for a plethora of ligands as to regulate cell signaling pathways as mentioned in Table 1.2 . Amongst these, its interaction with the Fas is of utmost importance as Nucleolin inhibits binding of Fas ligand (Fas L) to Fas, thereby inhibiting Fas-Fas L mediated apoptotic pathway in cancers (Wise et al., 2013). The surface expression of Nucleolin has been the target of cancer therapeutic drugs like HB-19, AS1411 that bind to cell surface Nucleolin and prevent its low affinity cell surface receptor activity (Destouches et al., 2008; Krust et al., 2011; Soundararajan et al., 2009).

Table. 1.2. Known ligands of cell surface Nucleolin
Reviewed in (Koutsioumpa and Papadimitriou, 2014)

Ligands	**Biological significance of the interaction**
Fas	Inhibition of Fas-mediated apoptosis in B-cell lymphomas (Wise et al., 2013)
Apo B and Apo E containing lipoprotein	Unknown (Semenkovich et al., 1990)
Ecto-protein kinase	NCL serves as a substrate (Jordan et al., 1994)
Laminin-1 (IKVAV site)	Differentiation of primary neurons and a variety of neural cell lines (Kleinman et al., 1991)
Complement regulator Factor J	Unknown (Larrucea et al., 1998)
L-selectin	Unknown (Harms et al., 2001)
Lipopolysaccharide (LPS)	Internalization of LPS / Participation in LPS-induced inflammation (Wang et al., 2011)
Poly-N-acetyl-lactosaminyl chains on CD43 caps	Recognition of early apoptotic cells by cell surface NCL on monocytes and macrophages (Hirano et al., 2005; Miki et al., 2013)
MK	Temperature-dependent active internalization process / Inhibition of HIV-1 infection (Said et al., 2005)
HGF	Regulatory interplay between stromal and epithelial cells within the prostate (Tate et al., 2006)
VEGF	VEGF165-induced endothelial cell migration (Destouches et al., 2008)
PTN	Temperature-dependent active internalization process / Inhibition of HIV-1 infection / PTN-induced endothelial cell migration (Koutsioumpa et al., 2013; Said et al., 2005)
Acharan sulfate	Anti-tumor activity in vitro and in vivo (Joo et al., 2005)
ADAMTS-2	Anti-angiogenic action in vitro and in vivo (Dubail et al., 2010)
Lactoferrin	Inhibition of the proliferation of cancerous mammary gland epithelial cells / Potent antiviral activity against HIV and CMV (Legrand et al., 2004)
ES	Transportation of ES in the nucleus / Anti-angiogenic and anti-tumor activities of ES in vivo / Anti-lymphangiogenic activities of ES (Shi et al., 2007; Zhuo et al., 2010)
scuPA	Transportation of scuPA in the nucleus / Induction of α-SMA expression in human fibroblasts (Stepanova et al., 2008)

Ligands	Biological significance of the interaction
Tumor-homing peptide F3	Internalization of F3 / Targeting cancer cells over-expressing NCL on their cell surface for diagnosis or targeted therapy (Christian et al., 2003; Drecoll et al., 2009; Hu et al., 2013)
RPTPβ/ζ	RPTPβ/ζ nuclear localization / Endothelial cell migration (Koutsioumpa et al., 2013)
Fas	Inhibition of Fas-mediated apoptosis in B-cell lymphomas (Wise et al., 2013)
Apo B and Apo E containing lipoprotein	Unknown (Semenkovich et al., 1990)
Ecto-protein kinase	NCL serves as a substrate (Jordan et al., 1994)
Laminin-1 (IKVAV site)	Differentiation of primary neurons and a variety of neural cell lines (Kleinman et al., 1991)
Complement regulator Factor J	Unknown (Larrucea et al., 1998)
L-selectin	Unknown (Harms et al., 2001)

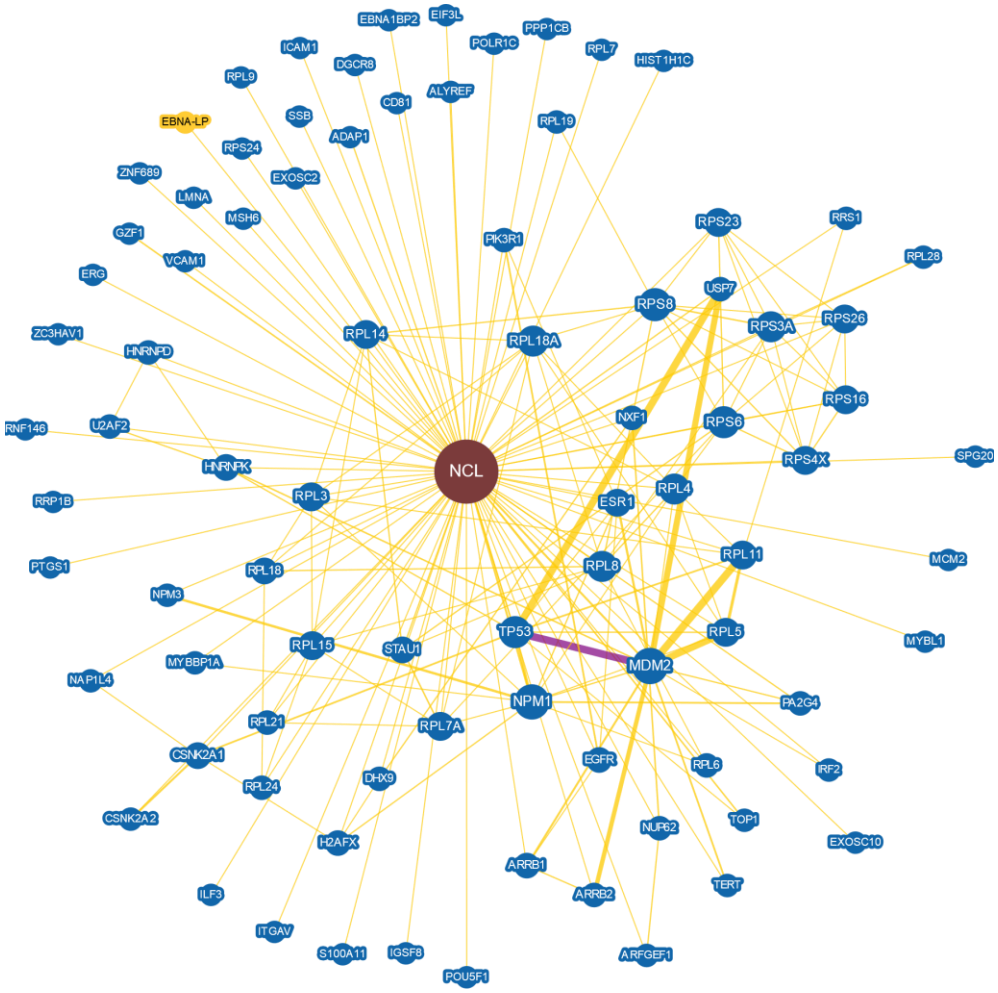

Figure 1.8. Numerous interactors of Nucleolin obtained by BioGrid analysis

1.5.1.2. Nucleophosmin

Nucleophosmin (NPM1), also known as B23, Numatrin and NO38, is an abundantly expressed nucleolar phosphoprotein (Feuerstein and Mond, 1987; Schmidt-Zachmann and Franke, 1988; Schmidt-Zachmann et al., 1987). It was initially described as a highly phosphorylated protein extracted from nucleoli of normal rat liver and rat hepatoma cells and named B23 because of its pattern of migration of 2D polyacrylamide gels (Kang et al., 1975). Nucleophosmin is encoded by *NPM1* gene located on Chr. 5q35. NPM1.1 (B23.1) is the largest transcript encoded by NPM1 gene resulting in a 294aa protein, the predominant isoform expressed in cells and localizing in the nucleolus (Wang et al., 1993). NPM1.3 (B23.2) protein resulting from an alternative splice variant of NPM1, lacks the last 35aa of B23.1, and is expressed at low levels in cells and localized in the cytoplasm (Wang et al., 1993). NPM1 is involved in ribosome biogenesis and its expression co-relates with proliferation potential of cells (Itahana et al., 2003).

1.5.1.2.1. Structure of Nucleophosmin

Nucleophosmin (NPM1) has a modular structure with an (i) N-terminal core domain (aa 1-120), (ii) a disordered central domain (aa 121-240), and (iii) a C-terminal domain (aa 241-294) (Hingorani et al., 2000). NPM1 can form homo-oligomers (upto pentamers) with its N-terminal oligomerization domain (OD) (Hingorani et al., 2000; Mitrea et al., 2014). Two donuts of these pentamers can then associate to form a decamer. The protein contains 3 acidic tracts A1 (aa 34-39) in the N-terminal domain; A2 (aa 120-133) and A3 (162-189) in the central domain. The acidic tract A1 mediates NPM1 interaction with R-motif ($RX_{n1}R$) containing proteins (Mitrea et al., 2016). The highly acidic central domain with A2 and A3 mediates interaction of NPM1 with histones H1, H3, H4, H2A, H2B, and its histone chaperoning activity (Gadad et al., 2011; Swaminathan et al., 2005). The basic C-terminal domain of NPM1 is essential for nucleic acid binding (hence termed NBD) (Wang et al., 1994). NPM1 contains a bipartite Nuclear localization signal (NLS) split between the central domain and the NBD (Dingwall et al., 1987). Immediately succeeding the NBD are two tryptophan residues (W287 and W289), which function as an atypical nucleolar localization signal (NoLS) that is missing in the isoform NPM1.3 (Nishimura et al., 2002). Besides, the central domain and part of the NBD is required for ribonuclease activity of NPM1 (Hingorani et al., 2000)

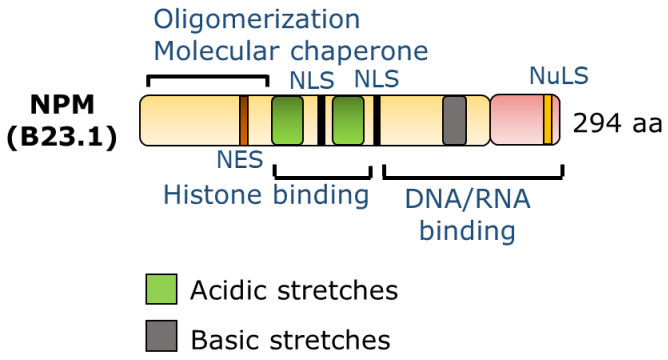

Figure 1.9. Domain structure of Nucleophosmin

1.5.1.2.2. Nucleophosmin post-translational modifications

NPM1 undergoes phosphorylation, ADP-ribosylation, SUMOylation and acetylation (Table 1.3). NPM1 is phosphorylated by several kinases – casein kinase II (CK2) (Szebeni et al., 2003), polo-like kinase 2 (PLK2) (Krause and Hoffmann, 2010), cdc2 (Peter et al., 1990) and cyclin E/CDK2 complex (Okuda et al., 2000). Phosphorylation of NPM1 impinges on its functions, nucleolar localization and dynamics (Negi and Olson, 2006). Further, very importantly, phosphorylation regulates oligomerization of NPM1 (Mitrea et al., 2014). Phosphorylation of NPM1 at Thr 95 and Ser 125, promotes equilibrium towards monomeric form of NPM1 which is likely to be nucleoplasmic, rather than the pentameric form which is required for phase-separation of NPM1 into the nucleolus (Mitrea et al., 2014, 2016).

Table 1.3. Selected post translational modifications of Nucleophosmin and their function

Post translational modification	Residue	Functional significance
Phosphorylation	CK2 – S125	Interphase. Required for retention in the nucleolus and ribosome biogenesis function (Negi and Olson, 2006)
	PLK1 – S4	M-phase, loss of phosphorylation shows aberrant centrosome numbers, incomplete cytokinesis (Zhang et al., 2004)
	PLK2 – S4	S-phase, controls centrosome duplication (Krause and Hoffmann, 2010)
	Aurora kinase B – S125	Cytokinesis failure (Shandilya et al., 2014)
	CDK2 – S125	Unknown
	IKKα – S125	Inhibition of centrosome duplication during

Post translational modification	Residue	Functional significance
		inflammatory signaling (Xia et al., 2013)
	CDK1 – T199, T219, T234, T237	Mitotic. Phosphorylation leads to loss of RNA binding (Okuwaki et al., 2002)
Acetylation	p300 – K212, K215, K229, K230, K257, K267	Nucleoplasmic localization. Transcriptional activation of genes (Shandilya et al., 2009; Swaminathan et al., 2005)
ADP-ribosylation	S207	Unknown
SUMOylation	TRIM28	Control of centrosome duplication (Neo et al., 2015)

1.5.1.2.3. Ribosomal functions of Nucleophosmin

NPM1, like Nucleolin, modulates multiple steps of ribosome biogenesis. NPM1 is a FACT like nucleolar histone chaperone binding to core histone H3 and transferring it to naked DNA (Okuwaki et al., 2001a) and its expression is co-related with enhanced rDNA transcription. Histone binding of NPM1 requires its decameric form (Namboodiri et al., 2004). siRNA mediated depletion of NPM1 reduces rDNA transcription (Murano et al., 2008). A similar effect of rDNA transcription downregulation is seen upon expression of a dominant negative B23 mutant lacking histone binding sites (Murano et al., 2008). ChIP-PCR analysis shows that NPM1 binds to the complete rDNA unit, however, it is most enriched at the transcription start site, similar to Nucleolin binding, and the 5.8S coding region (Murano et al., 2008). Knockdown of B23 or expression of B23 histone binding mutant, increases the density of histone occupancy on rDNA, thereby reducing transcription (Murano 2008). The RNA binding ability of NPM1 is necessary for its chromatin binding and rDNA transcription regulation (Hisaoka et al., 2010). Hence during mitosis when NPM1 is phosphorylated by cdc2 at T199, 219, 234 and 237 and its RNA binding ability is abolished, NPM1 binding to rDNA chromatin is also reduced (Hisaoka et al., 2010). Consequently, rRNA expression is also reduced at mitosis. Apart from this, NPM1 also regulates nucleolar localization of c-Myc and c-Myc induced rDNA transcription (Li and Hann, 2013).

NPM1 is required for processing of ITS2 of rRNA (Herrera et al., 1995; Savkur and Olson, 1998). It is also required for export of 40S and 60S pre-ribosomes from nucleus to the cytoplasm, as expression of shuttling deficient NPM1 mutants blocks this activity, and reduces export of pre-ribosomes, further reducing overall protein synthesis in cells (Maggi et al., 2008). NPM1 is also required for nucleolar localization of the RNA Pol I transcription termination factor TTF-I (Kuchenreuther and Weber, 2014).

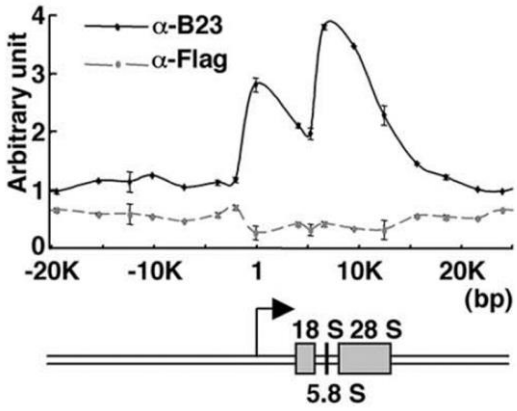

Figure 1.10. ChIP binding profile of Nucleophosmin along rDNA body and intergenic sequences. Reprinted with permission from (Murano et al., 2008)

1.5.1.2.4. Non-ribosomal functions of Nucleophosmin

Apart from ribosome biogenesis, NPM1 also functions in regulation of transcription, replication, DNA damage repair and centrosome duplication. Acetylation of NPM1 by p300 and its further interaction with acetylated core histones, disrupts nucleosomes and upregulates genes involved in oral cancer (Shandilya et al., 2009; Swaminathan et al., 2005). NPM1 is also acts as a context specific co-activator or co-repressor owing to its multiple interactions with cMyc, YY1, IRF1, p53, NFκB and many other transcriptional factors (Colombo et al., 2002; Dhar et al., 2004; Inouye and Seto, 1994; Kondo et al., 1997; Li and Hann, 2013).

Nucleophosmin promotes DNA Pol α mediated DNA replication by binding to pRb, and viral DNA replication, *in vitro* (Okuwaki et al., 2001b; Takemura et al., 1999). NPM1 also assists in DNA damage repair (Scott and Oeffinger, 2016). Upon IR damage, rDNA transcription is abrogated, and NPM1 translocates to the nucleoplasm, particularly to sites of IR damage (Koike et al., 2010). NPM1 expression is upregulated upon UV damage and shows enhanced RNA binding (Wu and Yung, 2002; Yang et al., 2002). Further, overexpression of NPM1 makes cells resistant to the UV mediated DNA damage. It is proposed that NPM1 function in DNA repair is linked to histone chaperone activity. NPM1 also modulates the Base Excision Repair (BER) proteins upon DNA damage (Poletto et al., 2014).

NPM1 also maintains structure of the nucleolus and depletion of NPM1 results in deformed nucleoli accompanied with re-arrangement of perinucleolar heterochromatin (Amin et al., 2008a, 2008b; Holmberg Olausson et al., 2014, 2015). NPM1 phosphorylation at Thr 199 and Ser 4, via a PPM1D phosphatase mediated cascade, is also important for nucleolar formation and control of nucleolar numbers (Kozakai et al., 2016). PPM1D is often upregulated in breast cancers where increase in nucleolar numbers is a prognostic marker (Helpap, 1989;

Lambros et al., 2010; Sood et al., 2013). NPM1 also contributes to genomic stability during mitosis, by binding to centrosomes during interphase, and only allowing centrosome duplication to happen only when it is phosphorylated by cdc2/Cyclin E, and released from unduplicated centrosomes (Okuda et al., 2000). Consequently loss of NPM1 leads to uncontrolled centrosome duplication and mitotic defects (Ugrinova et al., 2007).

1.5.1.2.5. Nucleophosmin and Cancer

NPM1 is frequently overexpressed and mutated in cancers (Table 1.4). NPM1 gene fusions independently with the retinoic acid receptor alpha gene (RARα), anaplastic lymphoma kinase (ALK) and myelodysplasia/myeloid leukaemia factor 1 (MLF1) lead to oncogenic fusion proteins, are common causes of lymphoid and myeloid leukaemias (Table 1.4).

NPM1 also functions as a tumor suppressor gene. In response to oncogenic stress, NPM1 sequesters the negative regulator of p53, MDM2 into the nucleolus and triggers p53 mediated apoptotic pathway (Colombo et al., 2002; Weber et al., 1999). Oncogenic cues also lead to overexpression of NPM1, thereby increasing ribosome biogenesis, p14ARF negatively regulates NPM1 and ribosome biogenesis and degrades MDM2, activating p53 pathway (Itahana et al., 2003; Sugimoto et al., 2003; Zhang et al., 1998).

Table. 1.4. Nucleophosmin is altered in cancer
(Reviewed in (Grisendi et al., 2006), reprinted with permission)

Alteration	Mutated products	Malignancies	References
Overexpression	Increased expression of the protein	Tumors of different histological origin (such as gastric, colon, ovarian, breast and prostate carcinomas)	(Nozawa et al., 1996; Shields et al., 1997; Skaar et al., 1998; Subong et al., 1999; Tanaka et al., 1992; Tsui et al., 2004)
Balanced translocations			
t(5;17)(q35;q12)	NPM-RARα	Acute promyelocytic leukaemia (APL)	(Redner et al., 1996)
t(2;5)(p23;q35)	NPM-ALK	Anaplastic large cell lymphoma (ALCL)	(Morris et al., 1994)
t(3;5)(q25;q35)	NPM-MLF1	Myelodysplastic syndrome (MDS) and Acute myeloid leukaemia (AML)	(Yoneda-Kato et al., 1996)
Mutation (exon 12)	NPMc+cytoplasmic mutant	AML with normal karyotype	(Falini et al., 2005)
Deletion (-5q35, -5)		MDS, AML and non-small-cell-lung carcinoma	(Mendes-da-Silva et al., 2000; Olney and Le Beau, 2002)

1.5.1.3. Fibrillarin

Fibrillarin is an S-adenosyl-L-methionine dependent RNA and protein methyltransferase present in the DFC of the nucleolus and Cajal bodies (Ochs et al., 1985; Snaar et al., 2000). Its main function is to carry out 2-O'-methylation of pre-rRNA and its processing (Kiss-László et al., 1996; Tollervey et al., 1993; Tycowski et al., 1996). Fibrillarin also acts as a protein methyltransferase from histone 2A (H2A) (Tessarz et al., 2014).

1.5.1.3.1. Structure of Fibrillarin

Fibrillarin is a 321 amino acid protein, composed of an N terminal GAR (glycine arginine rich) domain (aa 1-80), a central RNA binding domain (~90 aa) and a C-terminal α-helical domain (~30 aa) (Aris and Blobel, 1991). It is encoded by the *FBL* gene localized on Chr. 19q13.2, in humans. The RNA binding domain and the α-helical domain, together form the methyltransferase (Wang et al., 2000) while the GAR domain mediates interactions with the splicing factor 2-associated p32 (SF2A-p32) in Cajal bodies (Yanagida et al., 2004). The GAR domain likely contains the nucleolar localization signal of Fibrillarin as GAR domain mutants fail to localize into the nucleolus (Pih et al., 2000), however the α-helical domain is required to target Fibrillarin to the DFC (Snaar et al., 2000). The methyltransferase domain of Fibrillarin is very well conserved across evolution, beginning from archaebacteria *Methanococcus jannaschii* to yeast to higher eukaryotes *Xenopus* and humans. In fact Fibrillarin from *Xenopus* and *Arabidopsis* can substitute Nop1 (Fibrillarin homolog) function in yeast. Thus Fibrillarin function is conserved across evolution. However, archaebacteria do not possess the GAR domain seen in higher eukaryotes (Amiri, 1994; Wang et al., 2000).

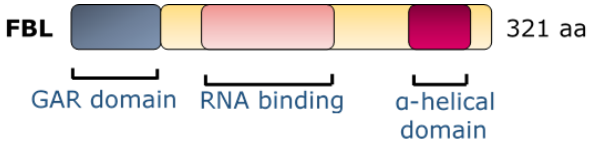

Figure 1.11. Domain structure of Fibrillarin

1.5.1.3.2. Function of Fibrillarin

Fibrillarin is part of the BOX C/D small nucleolar RNA (snoRNA) ribonucleoprotein (sno-RNP) complex guiding 2-O'-methylation of target RNAs (Kiss-László et al., 1996). The box C/D RNP comprises of Fibrillarin, box C/D sno-RNA and bridging proteins NOP56/58, 15.5k. Box C/D sno-RNAs are ~70nt long RNAs that contain the Box C (5'-RUGAUGA-3') and Box D (5'-CUGA-3') motifs (Kiss-László et al., 1998). These snoRNAs bind to rRNA through their antisense sequence and allow Fibrillarin to catalyze S-adenosyl-L-methionine

mediated methyltransfer to rRNA (Dunbar et al., 2000; Kiss-László et al., 1996; Tycowski et al., 1996). Further Fibrillarin complexes with U3, U8 and U13 snoRNAs and mediates cleavage of the 5'-ETS to generate 45S pre-rRNA from the 47S precursor (Craig et al., 1987).

Specific rRNA methylation and pseudouridylation patterns are necessary for translational fidelity, as aberrations in these methylation patterns lead to faulty ribosomes that promote nonsense suppression, amino acid misincorporation or internal ribosomal entry site (IRES) mediated translation of mRNAs of cancer-associated genes (Basu et al., 2011; Ruggero et al., 2003). Thus either upregulation or downregulation of Fibrillarin may lead to aberrant rRNA methylation. This is frequently seen in breast cancers where Fibrillarin is upregulated and p53 tumor suppressor negatively regulates Fibrillarin expression to maintain translational fidelity and prevent Fibrillarin mediated carcinogenesis (Marcel et al., 2013).

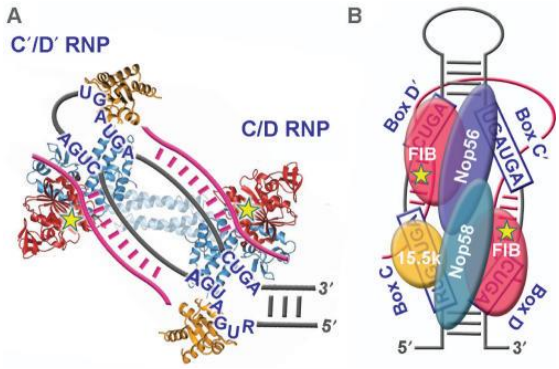

Figure 1.12. Fibrillarin in a Box C/D ribonucleoprotein complex.
A. Box C/D complex binding to ribosomal RNA via base pairing with snoRNAs. **B.** Fibrillarin methylates rRNA.

1.5.2. Nuclear envelope proteins

The nucleolus has potentially co-evolved with the nucleus in eukaryotes. In budding yeast, a single crescent shaped nucleolus is integrally associated with the nuclear envelope where the rDNA is anchored (Taddei and Gasser, 2012). Yeast cells undergo closed mitosis where nuclear envelope does not break down, unlike higher eukaryotes that undergo open mitosis (Boettcher and Barral, 2013). Similarly, the nucleolus also does not disintegrate during mitosis in yeast (Granot and Snyder, 1991). The nucleus is surrounded by a double layered membrane – outer nuclear membrane (INM) facing the cytoplasm, continuous with the endoplasmic reticulum and inner nuclear membrane (INM) facing the nucleoplasm. The linker of nucleoskeleton and cytoskeleton (LINC) complex (Sun and KASH proteins) are integral membrane proteins that span across the ONM and INM and connect the nucleus to the cytoskeleton (Starr and Fridolfsson, 2010). In higher eukaryotes, an elaborate meshwork of lamins – type V intermediate filament proteins underlie the INM providing mechanical strength to the nucleus (Aebi et al., 1986; Dechat et al., 2008). Yeast cells however, lack Lamin proteins (Taddei and Gasser, 2012). Several studies report the aberrations of the nucleolar structure, when nuclear envelope proteins – Sun1, Nesprin and lamins are downregulated in human cells (Buchwalter and Hetzer, 2017; Farley-Barnes et al., 2018; Martin et al., 2009; Matsumoto et al., 2016).

1.5.2.1. Lamins

Nuclear lamins are of two types – A type and B-type (Gerace and Blobel, 1980). A-type lamins include – Lamin A and Lamin C, which are alternatively spliced products of the *LMNA* gene located on Chr 1q22 in humans (Lin and Worman, 1993; Machiels et al., 1996). B-type lamins include Lamin B1 and Lamin B2, which are products of the *LMNB1* and *LMNB2* genes located on Chr 5q23.2 and Chr 19p13.3 (Höger et al., 1990). A third B-type lamin, Lamin B3, is found only in fish and amphibians and germ cells of mammals (Furukawa and Hotta, 1993; Goldberg et al., 1995). Most invertebrates express only B-type lamins (Erber et al., 1999; Riemer et al., 1993). Mammals express B-type lamins in all somatic cells, whereas A-type lamins are expressed in a developmentally regulated manner (Röber et al., 1989; Stewart and Burke, 1987). Lamins localize under the INM and are also part of the nucleoskeleton, providing structural integrity to the nucleus.

1.5.2.1.1. Structure of Lamins

All lamins are organized as N-terminal globular head domain, a central rod domain and a C-terminal tail domain. The rod domain of lamins are composed of four a-helical coil segments – 1A, 1B, 2A and 2B. The tail domain of lamins contain a nuclear localization signal (NLS), an immunoglobulin-like fold and a CAAX motif (Dittmer and Misteli, 2011).

Lamins form homo- or heterodimers via their central rod domain, which further organize into head to tail polymers (Heitlinger et al., 1991, 1992; Isobe et al., 2007). The IgG-like domain of lamins is mediate most protein-protein interactions of lamins (Krimm et al., 2002; Dhe-Paganon et al., 2002). Lamins are farnesylated and carboxymethylated at the cysteine residue of the CAAX motif (Beck et al., 1990; Chelsky et al., 1989; Holtz et al., 1989; Krohne et al., 1989). Lamin A undergoes a Zmpste24 enzyme mediated cleavage to generate mature Lamin A (Dominici et al., 2009; Sinensky et al., 1994). A mutant Lamin A commonly known as progerin, lacking 50 amino acids preceeding the CAAX motif (LAΔ50) fails to undergo Zmpste24 mediated cleavage and integrates into nuclear envelope, destabilizing it and leading to Hutchinson Gilford Progeria Syndrome (HGPS) (Eriksson et al., 2003). Moreover, over 100 other mutations have been mapped in all domains of Lamin A that cause cardiomyopathies, leukodystrophies, lipodystrophies, muscular and skeletal dystrophies collectively termed as "laminopathies" (Worman and Bonne, 2007). Most laminopathies are associated with severely disrupted nuclear morphology (Goldman et al., 2004; Roux and Burke, 2007).

Figure 1.12. Domain structure of Lamins

1.5.2.1.2. Functions of Lamins

Lamins are just as multifunctional as the previously described nucleolar proteins. The primary function of lamins is to maintain nuclear structure. Besides, lamins provide a nuclear scaffold for variety of nuclear functions like DNA transcription, replication, mRNA splicing, DNA damage repair, heterochromatin organization, telomere organization, histone dynamics, cellular senescence, apoptosis, cell cycle, chromosome organization, to name a few (Freund et al., 2012; Kumaran et al., 2002; Mahen et al., 2013; Melcer et al., 2012; Moir et al., 2000; Ranade et al., 2017; Sato et al., 2008; Spann et al., 2002; Wood et al., 2014). Lamins bind to regions of the genome termed as lamina associated domains (LADs) (Guelen et al., 2008). Binding of lamins at promoters of genes have been associated with both upregulation and downregulation of gene expression, in a context and cell-specific manner (Lund et al., 2013; Shevelyov et al., 2009). Binding of lamins to ribosomal DNA has not been determined yet.

Lamins form a scaffold for DNA replication foci and co-purify with DNA Polymerase subunits and the processivity factor PCNA (proliferating cell nuclear antigen) (Shumaker et al., 2008). Lamin A deficient MEFs show slower replication rates and while Lamin B1 depleted colon cancer cells show a prolonged S-phase (Camps et al., 2014; Moir et al., 2000). Downregulation of Lamin B2 is associated with aberrant cell cycle progression and generation of chromosomal aneuploidies (Kuga et al., 2014; Ranade et al., 2017). Finally, lamins are also important for function and organization of nuclear bodies like nuclear speckles that are depleted upon expression of N-terminal domain deletion mutant of Lamin A in HeLa cells (Kumaran et al., 2002). PML bodies are larger in area and their movement was faster in Lamin A depleted cells (Stixová et al., 2012). Lamins also affect number, morphology and function of the nucleolus (Matsumoto et al., 2016). Lamin B1 depletion in HeLa cells leads to nucleolar disruption and dispersal of nucleolar proteins into the nucleoplasm (Martin et al., 2009). Lamin A mutation and knockdown in HGPS fibroblasts is associated with increase in nucleolar size and ribosome biogenesis (Buchwalter and Hetzer, 2017).

1.6. Control of ribosome biogenesis by growth factor signaling

1.6.1. mTor signaling

The mTor pathway is a master regulator of cell growth and regulates ribosome biogenesis both by affecting rDNA transcription and translation of ribosomal proteins (Hardwick et al., 1999; Mayer and Grummt, 2006). Inhibition of mTor with Rapamycin reduces rDNA transcription and pre-rRNA processing (Hardwick et al., 1999; Mahajan, 1994; Powers and Walter, 1999). The major downstream mediator of mTor pathway is phosphorylated ribosomal protein S6 kinase (RSK or S6K) (Magnuson et al., 2012). The mTor protein regulates TIF-IA hyper-phosphorylation at Ser44 and hypo-phosphorylation at Ser199, a pattern that is reversed by treatment of cells with the mTor antagonist Rapamycin (Mayer et al., 2004). The phosphorylation of TIF-IA are potentially mediated by phospho-S6K via unknown intermediates, and regulate the occupancy of rDNA promoters and thereby rDNA transcription, by TIF-IA (Mayer et al., 2004). Rapamycin treatment disables complex formation between TIF-IA and RNA Pol I, and translocates TIF-IA from nucleus to the cytoplasm, thus downregulating rDNA transcription (Mayer et al., 2004). Further, mTor signaling increases S6K mediated phosphorylation of UBF in the C-terminal domain, increasing its binding with TFII-B/SL1 complex (Hannan et al., 2003). Finally, mTor pathway regulates the transcription of ribosomal protein coding genes via the transcription factors SFP1 and FHL1 (Marion et al., 2004; Martin et al., 2004). There is also significant cross-talk between other growth signaling pathways like ERK and Akt pathway with mTor to regulate ribosome biogenesis (James and Zomerdijk, 2004).

1.6.2. PI3K/Akt signaling

Treatment of cells with the mTor inhibitor - Rapamycin, only partially attenuates rDNA transcription. However treatment with the AZD8055, a combined inhibitor of mTor and Akt pathway, shows synergistic down-regulation of rRNA expression (Chan et al., 2011; Nguyen and Mitchell, 2013; Wu et al., 2016). This suggests that Akt controls rRNA expression, independent of the mTor pathway. (Bierhoff et al., 2008; Nguyen and Mitchell, 2013). p-Akt induces the nucleolar translocation of TIB-IA increasing its association with RNA Pol I in the pre-initiation complex, resulting in an increase in pre-rRNA expression (Nguyen and Mitchell, 2013). Further sustained Akt signaling is required for rRNA transcription elongation (Chan et al., 2011). Activated p-AKT induces a signaling cascade whereby it activates by phosphorylating CK2α at Thr 13, which further phosphorylates TIF-1A (Ser 170/172), necessary for promoter escape and transcription elongation (Bierhoff et al., 2008; Nguyen and Mitchell, 2013).

Akt induces SGK1 (serum/glucocorticoid regulated kinase) mediated phosphorylation and nucleolar localization of the histone demethylase JMJD2A/KDM4A, which converts "poised" rDNA to active form and is required for serum mediated activation of rDNA transcription (Salifou et al., 2016).

1.6.3. MAPK/ERK pathway

Upon replacement of serum to serum-starved NIH3T3 cells, rRNA expression levels increase by 10-fold (Zhao et al., 2003). Inhibition of the MAPK/ERK pathway by the specific MEK inhibitor PD98059 abolishes this increase (Zhao et al., 2003). Thus it was shown the ERK2/S6K complex binds to TIF-IA and phosphorylates it on Ser633 and Ser649, essential for rDNA transcription (Bierhoff et al., 2008).

1.6.4. c-Myc

The transcription factor c-Myc belongs to the bHLH family and regulates transcription of nearly 15% of the genome (Fernandez et al., 2003). Nucleophosmin regulates the nucleolar localization of c-Myc where it binds to ribosomal DNA and regulates Pol I transcription dependent transcription of 18S, 5.8S and 28S rRNA (Grandori et al., 2005; Li and Hann, 2013). c-Myc also upregulates expression of the RNA Pol III transcribed 5.8S rRNA and binds to consensus E box sequences in the promoter and terminator of rDNA (Grandori et al., 2005). Further, c-Myc interacts with the components of the TFIIB/SL1 complex and promotes recruitment of RNA Pol I at the promoter of rDNA. Notably, c-Myc also positively regulates the expression of its target gene – *UBTF* coding for UBF. The genes coding for rRNA processing and ribosome assembly factors – NOP56, BOP1, FBL, DKC1, NCL and NPM1 are targets of c-Myc and positively regulated by it (Watson et al., 2002). Further, c-Myc and N-Myc upregulate Pol II mediated transcription of many ribosomal proteins – RPS and RPL, thus affecting ribosome biogenesis at multiple levels (Boon et al., 2001; Schlosser et al., 2003).

1.6.5. Other growth factors

FGF-2 promotes rDNA transcription through the ERK pathway and also by directly interacting with UBF1 (Katz et al., 2007; Sheng et al., 2005; Zhao et al., 2003). FGF-2 translocates into the nucleolus and phosphorylates Nucleolin mediated by CK2 (Bonnet et al., 1996). FGF-2 binding is also seen on the rDNA gene and this binding enhances rRNA expression in a UBF dependent manner (Sheng et al., 2005). EGF also regulates rDNA transcription via the ERK pathway, by promoting rRNA elongation, by ERK-mediated phosphorylation of UBF (Stefanovsky et al., 2006).

Integrin mediated extracellular matrix adhesion enhances rDNA transcription (Wu et al., 2016). This is mediated by the activation of the PI3K/Akt signaling cascade by focal

adhesion kinase (FAK) upon integrin engagement (Wu et al., 2016). PTEN is a lipid phosphatase that represses PI3K/Akt and MAPK signaling (Gu et al., 1998; Tamura et al., 1999). It can repress rDNA transcription by repression of S6K phosphorylation, dissociation of the SL1 complex and reduced occupancy of SL1 on rDNA promoter (Zhang et al., 2005). The splice variant PTEN, PTENβ localizes to the nucleolus and dephosphorylates Nucleolin at Thr84, thereby downregulating rRNA expression (Liang et al., 2017).

Deprivation of amino acids from culture medium of HeLa cells affects rRNA transcriptional elongation in an S6K dependent manner (Kang et al., 2016).

1.7. Open questions

Notwithstanding the vast body of literature on the structure and function of the nucleolus, many open questions remain to be answered. The most pertinent questions are – since nucleoli behave like liquid droplets, (1) what prevents nucleoli to fuse into a single nucleolus, despite the absence of a surrounding membrane? Secondly, nucleolar structure is intimately linked with the ribosome biogenesis function. Cancer cells show dysregulated ribosome biogenesis - (2) how is nucleolar morphology and numbers affected in cancers. Literature survey shows compelling but circumstantial evidence of the role of nuclear envelope proteins in regulating nucleolar structure and function. Some of the key questions are (3) what is the mechanism by which lamins – the major nucleoskeletal proteins, modulate nucleolar structure and function? (4) Are both A-type and B-type lamins required to maintain nucleolar structure? (5) Is nuclear and nucleolar structure co-regulated by Lamins and nucleolar proteins? The nucleolus harbors ~4500 proteins. Investigations into the principles guiding phase separation of non-ribosomal proteins into the nucleolus and the physiological significance of the same, are unclear. Thus it remains to be answered (6) how do nucleoplasmic proteins relocalize into the nucleolus? We have attempted to answer these questions in this thesis under the following specific sub-aims –

1. To examine the role of nuclear lamins in maintaining nucleolar structure-function relationships.
2. To examine the role of nucleolar protein – Fibrillarin in modulating nucleolar and nuclear structure.
3. To examine the role of Nucleolin in guiding nucleolar sequestration of histone 2B.

Chapter 2:

Materials and Methods

2.1. Methods commonly used throughout the study

2.1.1. Cell lines and cell culture

All cells were maintained in respective medium supplemented with antibiotics penicillin (100 units/ml)-streptomycin (100 µg/ml) (Gibco, 15070-063) and 10% heat-inactivated fetal bovine serum (FBS) (Gibco, 6140). Cells were cultured at 37°C in the presence of 5% CO_2. Cells were sub-cultured when ~60-70% confluent and utilized in ~10-15 passages for all experiments. We ensured that cultures were free of *Mycoplasma* contamination by DAPI staining cells periodically.

Table 2.1. Cells and cell lines used in this study

Cell line	Origin	Source	Culture medium
CRL1790	Normal colon	ATCC	MEM
CRL1831	Normal colon	ATCC	DMEMF12 supplemented with 25 mM HEPES (final), 10 ng/ml cholera toxin, 0.005 mg/ml insulin, 0.005 mg/ml transferrin, 100 ng/ml hydrocortisone
DLD1	Colorectal adenocarcinoma	Dr. Thomas Ried Lab, NIH, USA	RPMI
SW480	Colorectal adenocarcinoma	Dr. Thomas Ried Lab, NIH, USA	DMEM
HCT116	Colorectal adenocarcinoma	Dr. Thomas Ried Lab, NIH, USA	DMEM
HT1080	Fibrosarcoma	Dr. Shantanu Chowdhury Lab, IGIB, Delhi	DMEM
A549	Lung adenocarcinoma	ATCC	DMEM
MCF7	Breast adenocarcinoma	Dr. Mayurika Lahiri Lab, IISER, Pune	DMEM

2.1.2. Karyotypic validation of cell lines

All cancer cell lines were periodically validated using DAPI Karyotyping to authenticate cell lines for the experiments. We relied on the validation from ATCC for the normal colon cells - CRL1790 and CRL1831 as we were unable to karyotype these cell types owing to their low mitotic index.

Table 2.2. Karyotypic validation of cell lines used in this study

Cell line	Modal chromosome number documented in literature	Modal chromosome number determined by DAPI Karyotyping
DLD1	44-46	44-46
SW480	52-58	57
HCT116	44-46	44
MCF7	82 Range 66-87	73
A549	66	66

Acknowledgements for Karyotyping:
A549: Maithilee Khot
SW480: Devika Ranade

2.1.3. siRNA and shRNA transfections

Transient siRNA transfections were performed using Lipofectamine RNAimax reagent (Invitrogen, 13778) or Lipofectamine 2000 reagent (Invitrogen, 116680) in reduced serum Opti-MEM (Gibco, 31985) for 6 h, after which cells were transferred to complete medium and incubated for 48h. On-target Plus non-targeting siRNA, respective scramble siRNAs and siLacZ siRNA, were used as negative controls.

For Nucleolin and Nucleophosmin knockdowns, cells were transfected with siNCL or siNPM1 using RNAimax reagent in reduced serum medium OptiMEM for 6h after which cells were transferred to complete medium. After 24h of first transfection, cells were pulsed again with siNCL or siNPM1 using the same protocol. Cells were assessed after 72h from first transfection. All knockdowns were performed at 100nM of final siRNA concentration.

The shRNA transfections were performed using Lipofectamine LTX and PLUS reagent. The shRNAs were procured from Sigma as a part of pLKO1 vectors which code for shRNA. DLD1 cells were transfected with 6-8 μg of the plasmids using medium with reduced serum (OptiMEM). The uptake of transfection mix was for 6 hours, followed by replacement with complete growth medium. At 48 hours post transfection, cells were subjected to selection by Puromycin (2 μg/mL for DLD1 cells). Colonies that were puromycin resistant, emerged at 7-8 days post selection. These colonies were picked using cloning discs (3.2 mm) and cultured in separate dishes. Colonies were screened for knockdown and positive colonies used for further assays. The siRNA and shRNA sequences used are tabulated in Table 2.3.

Table 2.3. siRNA and shRNA sequences used in this study

siRNAs	**Sequence**
On-target Plus non-targeting siRNAs	Dharmacon- D-001810-01-20, D-001810-02-20
siLacZ	5'-CGUACGCGGAAUACUUCGA-3'
siLMNA/C	5'-CAGUCUGCUGAGAGGAACA-3'
siLMNA/C Scramble	5'-GAUGAGGCGGUUAGAUGUA-3'
siLMNB2.1	5'-GAGCAGGAGAUGACGGAGA-3'
siLMNB2.2	5'-GCAAGUUUGUGCAGCUCAA-3'
siLMNB2.3	5'-GGAAGAGUGUGUUCGAGGA-3'
siLMNB2.1 Scramble	5'-GGAAGCGUAGACGGAAGAG-3'
siLMNB1	5'-AGACAAAGAGAGAGAGAUG-3'
siLMNB1 Scramble	5'-GAGGGAAACGTAAAGAAGA-3'
siFBL	5'- AGGAGAACATGAAGCCGCA-3'
siGNL3.1	5'-GCTTAAAACAAGAACAGAT-3'
siGNL3.2	5'-ATGTGGAACCTATGGAAAA-3'
siGNL3.1 Scramble	5'-ATAATCGAACGATAAGAAC-3'
siNCL	5'-TCCAAGGTAACTTTATTTCTT-3'
siNCL Scramble	5'-GCTAGCTTTATTCGTATATTA-3'
siNPM1	5'-AGATGATGATGATGATGAT-3'
siPLK1	5'-UGACCUACAUCGACGAGAA-3'
shRNA	**Sequence**
shLMNB2	5'-CCGGCGGCAGTTCTTTGTTAAAGATCTCGAGATCT TTAACAAAGAACTGCCGTTTTTG-3'

2.1.4. DNA transfections

For plasmid maxipreps, ~250 ml bacterial cultures were grown overnight at 37ºC at 180 rpm shaking. Extraction of DNA was performed using PureLink Maxiprep DNA Extraction Kit (Invitrogen), eluted in nuclease free water (NFW) and used for transfecting mammalian cells. For plasmids midipreps, ~50 ml bacterial cultures were grown as previously and plasmids were extracted using Exprep plasmid SV kit (GeneAll), eluted in nuclease free water (NFW) and used for transfecting mammalian cells. All plasmids used in this study were confirmed by sequencing.

Cells were transfected with plasmids using Lipofectamine LTX with Plus reagent (Invitrogen, 15338-100) in OptiMEM for 6h after which cells were transferred to complete medium, or using Trans-IT 2020 (Mirus) in complete medium.

Table 2.4. List of all constructs used in this study

Name	Source	Purpose
GFP-Nucleolin	Dr. Sui Huang	Expression/visualization of full length nucleolin
GFP-Nucleolin ΔN	Generated in lab (Gaurav Joshi)	Expression/visualization of nucleolin lacking N-terminal domain
GFP-Nucleolin ΔRBD	Generated in lab (Gaurav Joshi)	Expression/visualization of nucleolin lacking RNA binding domains
GFP-Nucleolin ΔGAR	Generated in lab (Gaurav Joshi)	Expression/visualization of nucleolin lacking GAR domain
H2B-ECFP	Dr. Jennifer Lippincot-Schwartz	Expression/visualization of histone 2B
NLS-CFP	Dr. Tom Misteli	Expression/visualization of Nuclear localization signal
Lamin B2-mCherry	Dr. T. Tomonaga	Expression/visualization of full length Lamin B2
Lamin B2-GFP	Dr. T. Tomonaga	Expression/visualization of full length Lamin B2
si*Lamin B2-GFP	Generated in lab (Devika Ranade)	Expression/visualization of siRNA resistant full length Lamin B2
Lamin B2 ΔHead-GFP	Generated in lab (Ayantika Sen Gupta)	Expression/visualization of Lamin B2 lacking head domain
si* Lamin B2 ΔHead-GFP	Generated in lab (Ayantika Sen Gupta)	Expression/visualization of siRNA resistant Lamin B2 lacking head domain
Lamin B2 ΔRod1-GFP	Generated in lab (Ayantika Sen Gupta)	Expression/visualization of Lamin B2 lacking aa28-210
si*Lamin B2 ΔRod1-GFP	Generated in lab (Ayantika Sen Gupta)	Expression/visualization of siRNA resistant Lamin B2 lacking aa28-210
siLamin B2 ΔRod2-GFP	Generated in lab (Ayantika Sen Gupta)	Expression/visualization of Lamin B2 lacking aa210-236
si*Lamin B2 ΔRod2-GFP	Generated in lab (Ayantika Sen Gupta)	Expression/visualization of siRNA resistant Lamin B2 lacking aa210-236
Lamin B2ΔSLS-GFP	Generated in lab (Ayantika Sen Gupta)	Expression/visualization of Lamin B2 lacking SLS peptide
si* Lamin B2ΔSLS-GFP	Generated in lab (Ayantika Sen Gupta)	Expression/visualization of siRNA resistant Lamin B2 lacking SLS peptide
GFP-NPM1	Dr. Sui Huang	Expression/visualization of Nucleophosmin
pUC9-rDNA-GFP	Dr. Brian McStay, NUI, Galway	Preparation of in-situ probe for visualization of rDNA intergenic sequence
HP1α-GFP	Addgene	Expression/visualization of heterochromatin binding protein α (HP1α)
pLKO shLamin B2 1-5	Sigma (TRCN0000072418-TRCN0000072422)	shRNA mediated knockdown of Lamin B2

2.1.5. Western blotting

SDS-PAGE and immunoblotting were performed as per standard protocols. Lysates were prepared in radioimmunoprecipitation assay (RIPA) buffer containing 1X protease inhibitory cocktail (PIC) (Roche), and the protein concentration was estimated using a bicinchoninic acid (BCA) kit (Pierce, 23225). Proteins were resolved by 10% SDS-PAGE and transferred to Immobilon-P membranes (GE). Blots were blocked in 5% non-fat dry milk. The blots were incubated with primary antibodies for 3 h at room temperature or overnight at 4°C, followed by incubation with secondary antibodies for 1 h at room temperature. Immunoblots were developed using the chemiluminescent substrate ECL Prime (GE, 89168-782) and imaged with ImageQuant LAS4000.

Antibodies used are listed in Table 2.5.

2.1.6. Co-immunoprecipitation

For co-immunoprecipitation (Co-IP) assays, ~10^7 cells (DLD1) were lysed in co-IP lysis buffer (50 mM Tris [pH 7.4], 150 mM NaCl, 0.5% NP-40, 1X PIC) vortexed and incubated on ice for 15 min, and centrifuged at 12,000 rpm and 4°C for 10 min. The lysate was precleared by incubating with Dynabeads protein A (Invitrogen, 10002D) for 1 h. Specific antibodies (~2 μg) or normal rabbit IgG was incubated with lysates overnight at 4°C. Protein A beads, pre-blocked with 0.5% BSA, were incubated with the immune-complex for 2 to 3 h. Beads were washed 6 times with co-IP lysis buffer (+ 0.5 mM phenylmethylsulfonyl fluoride [PMSF]) to minimize nonspecific binding. Bound protein was eluted from the beads by boiling in 2X Laemmli buffer for 15 min at 95°C.

Antibodies used are listed in Table 2.5.

2.1.7. Immunofluorescence assay (IFA)

Adherent cells were washed twice in 1X Phosphate Buffered Saline (PBS) (pH 7.4), permeabilized for 5 min with CSK buffer [0.1 M NaCl, 0.3 M sucrose, 3 mM $MgCl_2$, 10 mM piperazine-N,N'-bis(2-ethanesulfonic acid) (PIPES) (pH 7.4), 0.5% Triton X-100] on ice, fixed in 4% paraformaldehyde (PFA) (Sigma, P6148) for 10 min, and re-permeabilized in 0.5% Triton X-100 for 10 min. Cells were blocked in 1% bovine serum albumin (BSA) (Sigma, A2153) for 30 min and incubated with primary antibody (diluted in 0.5% BSA) for 1.5 h and with secondary antibodies (diluted in 1X PBS plus 0.1% Triton X-100 [PBST]) for 1 h. Cells were washed thrice in 1X PBS in between antibody incubations. Cells were counterstained with DAPI (4',6'-diamidino-2-phenylindole) and mounted in SlowFade gold antifade (Invitrogen, S36937).

The antibodies used are listed in Table 2.5.

Table 2.5. List of antibodies used in this study

Antibody	Purpose	Dilution
Anti-UBF (ab75781)	IFA	1:250
Anti-Nucleolin (ab13541)	IFA	1:300
Anti-Nucleolin (ab22758)	IFA Western Blotting IP	1:500 1:2,000 2 μg
Anti-Nucleolin (ab50279)	Immuno-RNA-FISH	1:500
Anti-Lamin A/C (Epitomics, 2966S)	IFA Western Blotting	1:600 1:5,000
Anti-Lamin A/C (ab40567)	IFA Western Blotting	1:50 1:200
Anti-Lamin A (ab26300)	IFA	1:500
Anti-Lamin B1 (ab16048)	IFA Western Blotting	1:500 1:1,000
Anti-Lamin B2 (ab8983)	IFA Western Blotting	1:400 1:400
Anti-Dnmt1 (ab19905)	Western Blotting IFA	1:1000 1:500
Anti-H3K27me3 (Millipore, 07-449)	IFA	1:500
Anti-GFP (ab290)	Western Blotting	1:1,000
Anti-Fibrillarin (ab5821)	IFA	1:500
Anti-Nucleophosmin (ab37659)	Western Blotting IP	1:1,000 2 μg
Anti-p84 (ab487)	IFA	1:500
Anti-Nucleophosmin (ab10530)	Western Blotting	1:1,000
Anti-H2B (Millipore, 07-371)	IFA Western Blotting	1:100 1:1,000
Anti-Actin (ab3280)	Western Blotting	1:400
Anti-GAPDH (Sigma, G9545)	Western Blotting	1:5,000
Anti-rabbit antibody–Alexa Fluor 488 (Molecular Probes)	IFA	1:1,000
Anti-rabbit antibody–Alexa Fluor 568 (Molecular Probes)	IFA	1:1,000
Anti-mouse antibody–Alexa Fluor 488 (Molecular Probes)	IFA	1:1000
Anti-mouse antibody–Alexa Fluor 568 (Molecular Probes)	IFA	1:1000
Anti-mouse antibody–Alexa Fluor 633 (Molecular Probes)	IFA	1:1000
Donkey anti-rabbit antibody–horseradish peroxidase (GE, NA9340V)	Western Blotting	1:10,000
Sheep anti-mouse antibody–horseradish peroxidase (GE, NA9310V)	Western blotting	1:10,000
Normal rabbit IgG	IP	2 μg
Phalloidin-Alexa 488	IFA	1:100

2.1.8. qRT-PCR analysis

RNA was prepared by lysing cells in TRIzol (Applied Biosciences) followed by phenol-chloroform extraction or by using PureLink RNA Mini Kit (12183018A). The cDNA was synthesized using the ImProm II reverse transcriptase system (Promega A3800). Quantitative real-time PCR (qRT-PCR) was performed using SYBR green (SAF Labs). *ACTIN* and *GAPDH* served as internal controls.

The primers used are listed in Table 2.6.

Table 2.6. qRT-PCR primers used in this study

Primer	Sequence
LMNA/C	Forward, 5'-CCGCAAGACCCTTGACTCA-3' Reverse, 5'-TGGTATTGCGCGCTTTCAG-3'
LMNB1	Forward, 5'-CGACCAGCTCCTCAACT-3' Reverse, 5'-CTTGATCTGGGCGCCATTA-3'
LMNB2	Forward, 5'-AGTTCACGCCCAAGTACATC-3'; Reverse, 5'-CTTCACAGTCCTCATGGCC-3'
FBL	Forward, 5'-GCATGAGGGTGTCTTCATTTG-3' Reverse, 5'-ATTCCCCAGGGACCAGGTT-3'
45S	Forward, 5'-GAACGGTGGTGTGTCGTT-3'; Reverse, 5'-GCGTCTCGTCTCGTCTCACT-3'
28S	Forward, 5'-AGAGGTAAACGGGTGGGGTC-3'; Reverse, 5'-GGGGTCGGGAGGAACGG-3'
18S	Forward, 5'-GATGGTAGTCGCCGTGCC-3'; Reverse, 5'-GCCTGCTGCCTTCCTTGG-3'
MALAT1	Forward, 5'-GACGGAGGTTGAGATGAAGC-3'; Reverse, 5'-ATTCGGGGCTCTGTAGTCCT-3'
ACTIN	Forward, 5'-GATTCCTATGTGGGCGAC-3' Reverse, 5'-GGTAGTCAGTCAGGTCCCG-3'
GAPDH	Forward, 5'-CGAGATCCCTCCAAAATCAAG-3' Reverse, 5'-GCAGAGATGATGACCCTTTTG-3'

2.1.9. Actinomycin D treatment

Cells were treated with 0.05 µg/ml actinomycin D (Act D) in complete medium for 4 h at 37°C with 5% CO_2 after which they were lysed to obtain RNA or protein. Equivalent volumes of diethyl sulfoxide (DMSO) were used as vehicle controls. Similarly, cells were treated with Act D and fixed for immunofluorescence, or live cells were imaged using confocal microscopy.

2.1.10. Microscopy

Cells were imaged on Zeiss LSM700, LSM710 and LSM780 confocal microscopes with 405-nm, 488 nm, 561 nm and 594 nm laser lines using a 63X Plan-Apochromat 1.4-numerical-aperture (NA) oil immersion objective at 2.0 to 2.5X digital zoom. Scanning was performed sequentially (*x-y*, 512 pixels by 512 pixels [1 pixel = 0.105 μm]), and z-stacks were collected at a step size of 0.34 μm and a pinhole size of 0.7μm (1 arbitrary unit [AU] for 405 nm laser line). The pixel depth was 8 bits, the line averaging was 2, and the scan speed was 10.

For super-resolution imaging of isolated nucleoli, a Zeiss LSM800 with an Airyscan detector was used.

For immuno-RNA-FISH experiments, fixed cells were imaged using a Leica TCS Sp8 microscope (*x-y*, 512pixels by 512 pixels (1 px ~0.1μm; *z*, 0.34 μm; frame averaging, 2; scan frequency, 400 Hz).

2.1.11. Live imaging

A Zeiss LSM710 or LSM780 confocal microscope equipped with a heated stage at 37°C was used for all photobleaching experiments and fluorescence image acquisitions. For live imaging, cells were grown on a 22 X 22 mm^2 coverslip glued onto a 35 mm petri dish coated with 100 μg/ml collagen (BD Biosciences; 354236); CO2-independent Leibovitz L-15 medium (Gibco; 21083-027) was used during microscopy.

2.1.12. Fluorescence recovery after photobleaching (FRAP) analysis

FRAP images were analyzed using the Zen 2011 FRAP analysis module, and relative fluorescence intensity (RFI) [also called as normalized fluorescence intensity (NFI)]was calculated as (Goldman et al., 2010).

$$\text{RFI or NFI} = \{[\text{ROI1}(t) - \text{ROI3}(t)]/[\text{ROI2}(t) - \text{ROI3}(t)]\} \times \{[\text{ROI2}(t = 0) - \text{ROI3}(t = 0)]/[\text{ROI1}(t = 0) \times \text{ROI3}(t = 0)]\},$$

where, ROI1 is the fluorescence intensity of the ROI that is bleached, ROI2 is the total nucleus fluorescence intensity, and ROI3 is the fluorescence intensity of a background region of equal size as ROI1, selected outside the nucleus. ROI1(t) denotes the postbleach fluorescence intensity at time t. ROI2(t) and ROI3(t) denote the same for the total nucleus and background, respectively. ROI1(t = 0) denotes the average prebleach fluorescence intensity. ROI2(t = 0) and ROI3(t = 0) denote the same for the whole nucleus and background, respectively.

The NFI was plotted as a function of time to generate double normalized FRAP curves.

Mobile fractions of H2B-ECFP were calculated as follows:

$$\%\text{Mobile fraction} = (Ffinal - Fbleach)/(Fprebleach - Fbleach) \times 100$$

Where, *Ffinal* is the NFI at maximum recovery, *Fbleach* is the NFI at the instant of bleaching and *Fpre-bleach* is the NFI before bleaching.

For assessing mobility of NCL-GFP in speckles, the double-normalized data were transformed on a scale of 0 to 1. Mobile fractions and $t1/2$ were calculated by fitting the normalized data (without transformation) with double-exponential fit using easyFRAP software (Rapsomaniki et al., 2012).

2.2. Specific methods for Chapter 3

2.2.1. Cloning and generation of Lamin B2 siRNA resistant and deletion mutants

Lamin B2 1257Δ1337, ΔHead and ΔSLS deletion mutants were generated from the Lamin B2-GFP plasmid by two consecutive PCRs. In the first PCR the N-terminal half of the deletion mutant and C-terminal half of the deletion mutant were generated by amplifying with CMV F-Δantisense primer and Δsense-EGFP-R primer sets. In the second PCR the products from the first PCR were used as mega-primers and ligated together using CMV F-EGFP R primer sets. Products from the second PCR were digested and cloned into the pEGFP-N1 vector to generate the Lamin B2 mutant with desired deletion.

The siRNA-resistant Lamin B2-GFP plasmids was generated by site-directed mutagenesis (SDM).

Table 2.7. Primers for generation of Lamin B2-GFP mutants

Primer	Sequence
SDM primer for generating si*LMNB2-GFP	Sense, 5'-ATGCTGGACGCCAAGGAACAAGAAATGACAGAAATGCGGGACGTGATGCA-3'; antisense, 5'-TGCATCACGTCCCGCATTTCTGTCATTTCTTGTTCCTTGGCGTCCAGCAT-3'
Primers for generating Lamin B2ΔHead mutant	Sense, 5'-CGAGCTCAAGCTTATATGGAGCTGCGCGAGC-3'; antisense, 5'-GCTCGCGCAGCTCCATATAAGCTTGAGCTCG-3'
Primers for generating Lamin B2ΔSLS mutant	Sense, 5'-GCAGCAGCGGCCTGGGCCGCAG-3'; antisense, 5'-CTGCGGCCCAGGCCGCTGCTGC-3'
CMV F	5'-CGCAAATGGGCGGTAGGCGTG-3'
EGFP R	5'-CGTCGCCGTCCAGCTCGACCAG-3'

2.2.2. Transfections

For experiments requiring both siRNA and plasmid DNA transfections, transfections were performed sequentially; siRNA transfection was performed as described in Section 2.1.3. DNA transfections were performed after 24 h as described in Section 2.1.4, and cells were processed 48 h after DNA transfection.

2.2.3. Nuclear matrix preparation

Nuclear matrix was prepared from DLD1 cells as previously described (Jagatheesan et al., 1999). DLD1 cells grown on coverslips were washed thrice in ice-cold cytoskeletal buffer

(10 mM PIPES [pH 6.8], 10 mM KCl, 300 mM sucrose, 3 mM $MgCl_2$, 1 mM EDTA, 0.05 mM PMSF, 1X PIC) and then incubated for 10 min in CSK buffer containing 0.5% Triton X-100 at 4°C. Cells were rinsed thrice in ice-cold RSB buffer (42.5 mM Tris-HCl [pH 8.3], 8.5 mM NaCl, 2.6 mM $MgCl_2$, 0.05 mM PMSF, 1X PIC) and incubated for 10 min in RSB buffer containing 1% (vol/vol) Tween 20 and 0.5% (vol/vol) sodium deoxycholate at 4°C. Cells were rinsed twice in ice-cold digestion buffer (10 mM PIPES [pH 8.3], 50 mM NaCl, 300 mM sucrose, 3 mM $MgCl_2$, 1 mM EGTA, 0.05 mM PMSF, 1X PIC) and then incubated for 30 min in digestion buffer containing 100 U/ml DNase I (Roche) at 30°C. Ammonium sulphate (1 M) was added to the cells to a final concentration of 0.25 M and incubated for 5 min to remove digested chromatin, followed by two washes in ice-cold digestion buffer. Cells were incubated in 2 M NaCl for 5 min at 4°C, washed twice in digestion buffer, fixed in 4% PFA, and immunostained.

2.2.4. Nucleolar isolation and immunostaining

Nucleolar isolation was performed as described previously (Liang et al., 2012). Briefly ~10^7 DLD1 cells were washed and scraped in ice-cold solution I (0.5 ml; 0.5 M sucrose with 3 mM magnesium chloride [$MgCl_2$] and 1X PIC). Cells were sonicated 5 times at 50% amplitude, 10 s on and 10 s off, on ice (Sonics Vibracell), layered over solution II (0.7 ml, 1.0 M sucrose, 3 mM $MgCl_2$), an centrifuged at 1,800 X *g* for 5 min at 4°C. The supernatant was removed carefully. The nucleolar pellet was re-suspended in 1X PBS, spotted on glass slides, air dried, and fixed with 4% PFA for 20 min. Nucleoli were blocked in 1% BSA for 60 min at room temperature and incubated with primary antibody and secondary antibodies for 30 min each, followed by three extensive washes with 1X PBST. The primary and secondary antibodies used were diluted in 1% BSA in 1X PBST. The preparation was mounted in DAPI-antifade. For Lamin B2 knockdown, nucleoli were isolated by pooling cells from 3 independent wells of a 6-well plate.

2.2.5. Imaging and scoring of nucleolar morphologies and numbers

Images were captured based on several random fields using DAPI staining and the extent of lamin knockdown in each nucleus. Nucleolar morphology and numbers were manually scored by visually inspecting nucleolin staining, across a number of nucleoli from several independent biological replicates (as indicated in each figure and figure legend).

2.2.6. Image processing and analysis

3D volume rendering and analysis of nuclei and nucleoli were performed using Image Pro Plus v7.1. MediaCybernetics, USA. Briefly, LSM files containing optical sections (z = 0.34 μm) of the immunostained nuclei were subjected to 3D surface rendering. 3D reconstructions

of each nucleus were performed on individually cropped nucleus. The acquired images were thresholded and surface rendered for each of the red, green, blue channels. 3x3x3 and 5x5x5 Lo-pass filters were used for thresholding nucleus and nucleolus, respectively. Volumes of nucleus and nucleoli were then calculated by Image pro plus software.

1.3. Specific methods for Chapter 4

1.3.1. RNA-FISH and 3D-immuno-RNA-FISH

(i) Fixation

RNA-FISH was performed as described previously (Chaumeil et al., 2008). All reagents for RNA-FISH were prepared in diethyl pyrocarbonate (DEPC)-treated water and supplemented with 2 mM vanadyl ribonucleoside complex (New England BioLabs). Briefly, cells were washed with 1X PBS, permeabilized with CSK buffer on ice for 5 min, fixed in 4% PFA for 10 min, and stored in 70% ethanol at -20°C until hybridization. For 3D-immuno-RNA-FISH, after fixation in 4% PFA, cells were permeabilized with 0.5% Triton X-100 in PBS, and immunostaining was performed as described earlier (88). Cells were post-fixed in 4% PFA for 10 min and washed twice with 2X SSC (1X SSC is 0.15 M NaCl plus 0.015 M sodium citrate), followed by hybridization.

(ii) FISH probe labelling

RNA-FISH probes for the ~12 Kbp intergenic sequence (IGS) upstream of the rDNA start site was prepared by nick translation of the pUC9-rDNA vector with Spectrum Red-conjugated dUTP, using DNase I (5 mU/µl)-DNA polymerase I (50 mU/µl) (Roche) for 3 h at 15°C. Nick-translated probe (6 µg) was precipitated overnight at -20°C with 20 µg human Cot1 DNA (Invitrogen) and 40 µg salmon sperm DNA (Invitrogen) using cold 100% ethanol and 1/10th volume of 3 M sodium acetate. The probe was re-suspended in deionized formamide at 37°C. Prior to hybridization, the probe was denatured at 80°C for 5 min, followed by addition of an equal volume of 2X hybridization mix containing 2 mM vanadyl ribonucleoside and incubation on ice for 30 min.

(iii) Hybridization and washes

Cells for RNA-FISH were dehydrated in an ethanol series (70%, 90%, and 100% ethanol) and air dried. Approximately 1 µg of probe (~4 to 6 µl) was spotted on an RNase-free slide, and cells on coverslips were inverted on the probe and sealed using nail varnish. Hybridization was carried out for 16 h at 37°C. Coverslips were washed thrice in 50% formamide‑2X SSC (pH 7.2), followed by three washes in 2X SSC (pH 7.2), for 5 min each at 42°C and mounted in DAPI-antifade.

2.3.2. 4D time lapse live imaging

To visualize nucleolin aggregates, cells were treated with Act D and immediately imaged for 3-4 h. z-stacks (0.34 µm slices) of cells were acquired every 1.3 min. Other parameters used are mentioned in Section 2.1.10.

2.3.3. Image processing and analysis

Volume measurements of nucleolin speckles from IFA, were performed using the ImageJ object counter 3D plugin. Colocalization analysis was performed using the JACOP plugin from ImageJ (89). 4D time-lapse images were analyzed using Imaris 8.0.0 software.

2.3.4. FRAP Experiments

For fluorescence recovery after photobleaching (FRAP) analysis, images were acquired using a 63X oil immersion objective, NA 1.4 at 2.5X digital zoom, at 2% laser power to avoid photobleaching.

(i) Nucleolin speckles

A 1-by 1-pixel square (1 pixel = 0.11 μm) region of interest (ROI) was used for bleaching nucleolin speckles. Ten images were acquired before photobleaching. Photobleaching was performed using 200 iterations of the 488-nm laser line at 100% power. Images were collected every 484 ms for a total duration of 25 s.

(ii) Nucleolar Nucleolin

A 10-by 10-pixel square (1 pixel = 0.11 μm) region of interest (ROI) was used for bleaching NCL-GFP. Ten images were acquired before photobleaching. The ROI was photobleached by 200 iterations of the 488-nm laser line at 100% power. Images were collected every 3.87 s for a total duration of 2.5 min.

(iii) HP1α-GFP

A 5-by 5-pixel square (1 pixel = 0.11 μm) region of interest (ROI) was used for bleaching HP1α foci. Ten images were acquired before photobleaching. The selected ROI was photobleached by 200 iterations of the 488-nm laser line at 100% power. Images were collected every 3.87 s for a total duration of 120 s. FRAP analysis was performed as described in Section 2.1.12.

2.3.5. Analysis of whole genome expression profiling upon Lamin B2 knockdown

Whole genome expression profiling upon Lamin B2 knockdown was performed using Microarray and published by *Ranade et. al* (Ranade et. al., 2016). This data was reanalysed by examining genes involved in ribosome biogenesis pathways. Annotated genes with fold change ≥ 1.2 (on a log scale), p value <0.05, were considered significant.

2.3.6. Gene Ontology (GO) analysis

Genes that were significantly deregulated upon Lamin B2 knockdown ≥ 1.2 fold (on a log scale), p value <0.05 were submitted to the online database DAVID (https://david.ncifcrf.gov/) to perform Gene annotation enrichment and functional annotation

clustering analyses. The output from the analysis consisted of GO categories from the Biological Process (BP), Molecular Function (MF) and Cellular Components (CC) sections. A graph was plotted for the $-\log_{10}$ (p-value) of enrichment for all GO categories obtained.

2.3.7. Overlap of nucleolar proteins with Lamin B2 knockdown deregulated genes

The geneset GO_nucleolus present in the Molecular Signatures Databse (MSigDB) (http://software.broadinstitute.org/gsea/msigdb) was downloaded and overlapped with genes deregulated upon Lamin B2 knockdown [≥ 1.2 fold (on a log scale), p value <0.05] using GeneVenn.

2.3.8. Overlap of ribosomal proteins with Lamin B2 knockdown deregulated genes

List of all human ribosomal proteins was downloaded from the Ribosomal Protein Gene Database (ribosome.med.miyazaki-u.ac.jp) and overlapped with genes deregulated upon Lamin B2 knockdown [≥1.4 fold (absolute scale), p value<0.05].

2.4. Specific methods for Chapter 5

2.4.1. MTT cell viability assay

Post 48h of siRNA transfection, cells were treated with 10% final volume of 5mg/ml MTT (3-(4, 5-dimethylthiazolyl-2)-2, 5-diphenyltetrazolium bromide) and incubated for 2-3 h at 37^0C, 5% CO_2. After incubation, the medium was discarded, cells were lysed and MTT crystals were dissolved in DMSO. The dissolved crystals were appropriately diluted in DMSO and colorimetric reading was obtained at 569 nm using a Varioskan Flash multiplate reader.

2.4.2. Gene expression profiling using qRT-PCR (TaqMan Array)

A custom TaqMAN gene expression microfluidic array card was obtained from Applied Biosystems to assess 43 nuclear architecture genes. Each well of the array consisted of a pair of unlabeled PCR primers and a TaqMan probe with an Applied Biosystems FAM label on the 5' end and minor groove binder (MGB) and nonfluorescent quencher (NFQ) on the 3' end. RNA was extracted from two independent biological replicates of Untreated, SINEG treated and siFBL treated cells using PureLink RNA Mini Kit (12183018A). RNA quality was checked by Bioanalyzer (Agilent) kit, and RIN was determined to be ≥1.8 for each sample. cDNA synthesis was performed using cDNA synthesis kit (Applied Biosystems) followed by a cDNA quantitation using *ACTIN* FAM coupled TaqMan gene expression assay (ABI). The microfluidic TaqMan Array card was loaded with equal amount of cDNA from each sample, TaqMan Master Mix (ABI) and run on a ViiA 7 real time PCR system (ABI). *GAPDH* gene expression was used as internal control.

2.4.3. Gene expression profiling using microarray

Control (untreated), siFBL treated and siGNL3 treated cells from three independent biological replicates were collected in RNA*later*™ (Invitrogen) and outsourced to Bionivid (Bangalore, India) for sample preparation, Microarray hybridization and data analysis. Hybridization was performed on the Illumina platform using Human HT12 V4 Expression BeadChip Kit. Standard probe level data pre-processing for all samples (Threshold: 1.0, logbase 2). Quantile normalization and median of all samples as baseline transformation, was applied. Analyses of gene expression levels were based on comparison of hybridizations between knockdown and control (untreated DLD1 cells) as reference. Gene expression levels (cut-off: absolute fold change ≥ 1.5, $p<0.05$) were used for further analyses.

2.4.4. Gene Ontology (GO) analysis

Gene ontology analysis was performed as described in Section 2.2.9 on genes that were significantly deregulated upon Fibrillarin and Nucleostemin knockdown ≥ 1.5 fold (on absolute scale), p value <0.05.

2.4.5. Gene Set Enrichment Analysis (GSEA) Analysis for motif enrichment and transcription factors in promoters of deregulated genes

The genes that were transcriptionally deregulated upon Fibrillarin and Nucleostemin knockdown were subjected to analysis to examine motifs enriched in their promoter sequences and transcription factors and miRNAs that bind to these motifs, if known. For this purpose, we used the Gene Set Enrichment Analysis (GSEA) - Molecular Signature Database (MSigDB) (Mootha et al., 2003; Subramanian et al., 2005). Gene lists from Fibrillarin and Nucleostemin Kd – up and downregulated sets were input into this database; and compared to gene sets with annotated motifs and miRNAs from the database. The top 20 gene set categories were obtained at a FDR (q) value of 0.05.

List of all human transcription factors was downloaded from Animal transcription factor database (Animal TFDB, http://bioinfo.life.hust.edu.cn/AnimalTFDB/) and overlapped with genes dysregulated upon FBL and GNL3 Kd using GeneVenn (http://genevenn.sourceforge.net) to determine transcription factors deregulated upon these knockdowns.

Transcription factors regulating deregulated nuclear architectural genes identified from TaqMAN array, were determined from ChIP Atlas database and overlapped with deregulated genes identified by microarray analysis.

2.4.6. Phalloidin staining

Cells washed twice with 1X PBS, fixed in 4% PFA for 7 min at room temperature (RT) and permeablized in 0.5% Triton X-100 10 min at RT. Cells were then incubated in Phalloidin-Alexa 488 (Invitrogen), 1:100 for 1 h, washed thrice in 1X PBS and counterstained with DAPI. For co-staining with Lamin B1, immunofluorescence was performed as described earlier in Section 2.1.7. and Phalloidin-Alexa 488 was added during secondary antibody incubation step.

2.4.7. Latrunculin A treatment

After 48 h of Fibrillarin knockdown, cells were treated with 50nM or 500nM Latrunculin A for 90 min at 37^0C, 5% CO_2, after which they were fixed for immunofluorescence. DMSO volume equivalent to 500nM drug, was added to cells as vehicle control.

2.4.8. 2D-Cell migration assay

DLD1 cells were transfected with control siRNA and siFBL for 24h in a 6 well plate. Thereafter cells were trypsinized and ~0.8 million cells were seeded in a single well of a 12 well plate in medium containing 10% FBS and allowed to attach for 8 h to achieve 100% confluence. Cells were washed and serum starved by replacing medium containing 0.1% FBS. After 12 h of serum starvation, a scratch was created in each well using a 10 µl micropipette tip, washed extensively with DPBS to eliminate floating cells and cells loosely adhered in the wound. Medium containing 0.1% FBS was replaced and the scratch was immediately imaged on the EVOS FL Auto Cell imaging system. Cells were subsequently imaged after 2 h, 6 h, 10 h and 24 h time points after scratch was made. Beacons were set on the microscope to allow acquisition of fixed regions in the wound at each time point. Images were analysed by Image J by manually marking and quantifying the area within the scratch at each time point.

2.5. Specific methods for Chapter 6

2.5.1. Cloning and generation of Nucleolin deletion mutants

Nucleolin deletion mutants were generated by restriction free (RF) cloning. RF cloning PCR was performed using sense and antisense deletion primers using GFP-NCL plasmid as a template with Accuprime Supermix (Invitrogen). The PCR product was treated with Dpn I enzyme at 16^0C overnight and used to transform competent *E. coli* DH5α cells. Positive clones were screened by sequencing. Primers used to generate the deletion mutants are listed in Table 2.8.

Table 2.8. Primers used to generate Nucleolin deletion mutants

Primer	Sequence
NCLΔN	Sense, 5'-GCAAGAATGCCAAGAAGCCTGTCAAAGAAGCACC-3' Antisense, 5'-GGTGCTTCTTTGACAGGCTTCTTGGCATTCTTGC-3'
NCLΔRBD1-4	Sense, 5'-GAACCGACTACGGCTAAGGGTGAAGGTGGC-3' Antisense, 5'-GCCACCTTCACCCTTAGCCGTAGTCGGTTC-3'
NCLΔGAR	Sense, 5'-CTGGGCCAAACCTAAGGACCACAAGCCACAAG-3'Antisense, 5'-CTTGTGGCTTGTGGTCCTTAGGTTTGGCCCAG-3'

2.5.2. Transfections

Transient plasmid transfections were performed using Lipofectamine LTX with Plus reagent (Invitrogen, 15338-100) and cells were imaged after 24 h of transfection. For FRAP analyses upon knockdowns, siRNA and DNA transfections were performed sequentially – siRNA transfection was performed as mentioned previously, while DNA transfections were performed after 24 h and cells were imaged by fluorescence microscopy, 24 h after DNA transfection.

2.5.3. FRAP and live imaging

The acquisition parameters were adjusted to avoid bleed-through of ECFP and GFP fluorescence. A 10 pixel X 10 pixel square (1 pixel = 0.11 μm) Region of Interest (ROI) was bleached in both nucleoplasmic and nucleolar H2B-ECFP. Photobleaching was performed using the 405 nm laser line at 100% power. Laser iterations of 120 and 150 were used to photobleach labeled H2B in the nucleus and nucleolus respectively. Images were collected every 3.87s for a total duration of 5 min.

Chapter 3:

Role of nuclear lamins in the maintenance of nucleolar structure in cancer cells

Results from this chapter are published as a part of the following paper –

Sen Gupta, A., and Sengupta, K. (2017). Lamin B2 modulates nucleolar morphology, dynamics, and function. Mol. Cell. Biol. *37*, e00274-17.

3.1 Introduction

The nucleolus evolved from a bipartite structure containing only Fibrillar strands and Granules in lower eukaryotes like yeast to a tripartite structure containing Fibrillar centres (FC), Dense Fibrillar component (DFC) and a Granular component (GC) in amniotes including humans (Thiry and Lafontaine, 2005). Ribosomal DNA (rDNA) transcription is initiated at the boundary of the FC and DFC in higher eukaryotes (Raska et al., 1995). Ribosomal RNA (rRNA) is processed in the DFC, which then complex with ribosomal proteins in the GC to form pre-ribosomes (Cheutin et al., 2002). Finally, the 40S and 60S pre-ribosomes are exported out of the nucleus into the cytoplasm (Ho et al., 2000; Sengupta et al., 2010).

Although the function of the DFC and GC are well characterized, the exact requirement for the FC is not very well understood. Previous studies suggest that the FC region of the nucleolus functions as a repository for non-engaged RNA Pol I and the transcription factor UBF (Goessens, 1984). During transcription, free RNA Pol I and UBF transition from the FC to the FC-DFC border where actively transcribing rDNA is located. The tripartite structure of the nucleolus co-evolved with nearly 10-fold increase in the lengths of the intergenic spacers between the arrays of ribosomal genes, from ~1 kbp in amphibians to ~13-14 kbp in mammals (Thiry and Lafontaine, 2005). The long intergenic spacers allowed looping out of inactive rDNA into the FC while the active rDNA localized to the FC-DFC border. Inhibition of nucleolar transcription, rRNA processing or its assembly into pre-ribosomes, perturbs the integrity of the nucleolar compartments (Nicolas et al., 2016; Shav-Tal et al., 2005; Wandrey et al., 2015). Inhibition of rRNA transcription by Actinomycin D (Act D), induces nucleolar cap formation, inversion of FC, DFC and GC, and dispersion of nucleolar proteins into the nucleoplasm (Shav-Tal et al., 2005). Physiological stresses such as DNA damage, serum starvation and hypoxia, which interfere with rDNA transcription, also disrupt nucleolar structure, underscoring the role of active rRNA transcription in maintaining nucleolar integrity (Boulon et al., 2010; Chan et al., 1985; Rubbi and Milner, 2003).

Nucleolar structure is a term that is interchangeably used to define nucleolar shape, morphology and ultrastructural features of the nucleolus that include fibrillar and dense fibrillar centres. Nucleolar structure and numbers vary greatly in different cell types and is highly influenced by rate of cell proliferation and activity of cells (Derenzini et al., 1998). Yeast nuclei have a crescent shaped nucleolus, while resting human lymphocytes possess ring shaped nucleoli (Raska et al., 1983; Yang et al., 1989). Nucleoli switch from irregular, lobulated to regular, spherical structures when HT1080 cells are treated with 8-chloro-cAMP - a protein kinase A (PKA) agonist (Krystosek, 1998). Coronavirus infection also alters nucleolar morphology with punctate distribution of Nucleolin and an enlarged FC (Dove et al., 2006).

Nucleolar structure is modulated by the rate of ribosome biogenesis in cells. Altered nucleolar numbers and structure correlate with cancers and ribosomopathies (Derenzini et al., 2009; Isaac et al., 2000). Thus, hyper-proliferative cancer cells and hypertrophic cardiomyocytes with elevated rate of protein synthesis and rRNA transcription, show increased numbers or enlarged nucleoli (Neuburger et al., 1998; Nguyen et al., 2015). Often these nucleoli are irregular in morphology and therefore serve as prognostic markers of carcinogenesis (Derenzini et al., 2009). Increased nucleolar area in cancer cells correlate with a higher RNA Polymerase I engagement on rDNA, increased expression of nucleolar proteins - Upstream Binding factor (UBF), Fibrillarin and DNA Topoisomerase I (Derenzini et al., 2009). Depletion of negative regulators of cell proliferation – p53 and pRb, also result in an increase in nucleolar area and increase in Fibrillarin expression in breast cancer cells (Marcel et al., 2013; Treré et al., 2004). However, nucleolar hypertrophy and changes in nucleolar morphology cannot be solely attributed to hyper-proliferation of cells. For instance, small cell anaplastic lung cancer cells, with greater proliferation rate, have smaller nucleoli, compared to slower proliferating large cell lung carcinoma cells (Zink et al., 2004). Moreover, human monocytes stimulated with IFNγ do not proliferate, albeit showing increase in rRNA synthesis, increase in nucleolar area and reticulate nucleolar morphology (Schedle et al., 1992). This suggests that nucleolar morphology is not just influenced by cell proliferation but also the metabolic state of the cell.

Nucleolar proteins - Nucleolin (C23), Nucleophosmin (B23) and Upstream Binding factor (UBF) are required for regulating nucleolar morphology (Grob et al., 2014; Okuwaki et al., 2001; Ugrinova et al., 2007). These proteins are directly involved in transcription or processing of rRNA (Ginisty et al., 1999; Learned et al., 1986; Murano et al., 2008). Nucleolar structure is also altered, when rRNA processing is compromised upon depletion of rRNA processing factors - NF90/NF110, or key ribosomal proteins uL18 (RPL5) and uL5 (RPL11) (Nicolas et al., 2016; Wandrey et al., 2015). However, several proteins affect nucleolar morphology, without any apparent effect on rRNA transcription. For example, knockdown of Arp6 (actin related protein-6) in HeLa cells, resulted in smaller FC and ring shaped GC, but did not affect rRNA expression (Kitamura et al., 2015).

The perinucleolar compartment is also an important factor in maintaining nucleolar integrity. *Drosophila* Su(var)3-9 mutants show multiple, lobulated nucleoli along with a loss in the heterochromatic mark H3K9me2, around the perinucleolar heterochromatin (Peng and Karpen, 2007). Epigenetic factors regulating nucleolar morphology include H4K16 methylation - altered in cells lacking Dnmt1 (Espada et al., 2007). Modulation of CARM1 in embryonic stem (ES) cells alter epigenetic marks (H3R17me2) on rDNA that affect nucleolar morphology (Franek et al., 2015). Truncation mutants of Telomere Recognition Factor (TRF2) results in acrocentric chromosomal fusions of NOR chromosomes that affect nucleolar stability (Stimpson et al., 2014).

Diploid human cells have 10 nucleolus organizer region (NOR) bearing chromosomes (Chromosomes 13, 14, 15, 21 and 22), that can potentially form 10 independent nucleoli. However, most normal cells have ~2-3 nucleoli (Andersen et al., 1998; Farley-Barnes et al., 2018; Wachtler et al., 1982). Previously, Nucleophosmin phosphorylation at Ser4 and Thr199 was shown to control nucleolar numbers (Kozakai et al., 2016). Recently, a high throughput genome wide screen has identified 139 proteins controlling ribosome biogenesis, which regulate nucleolar numbers in the human breast derived cell line - MCF10A (Farley-Barnes et al., 2018). Cancer cells have higher nucleolar numbers to increase rRNA production, to support their enormous requirement for ribosome production and protein synthesis during proliferation. It is unclear if increase in nucleolar numbers are due to an increase in the number of NOR chromosomes that often accompany cancer progression. Thus, the molecular mechanisms that regulate nucleolar morphology and numbers are poorly characterized.

In addition to aberrant nucleolar structures, cancer cells show large heterogeneities in their nuclear structure. This include nucleomegaly (nuclei enlarged >5 times the size of erythrocytes) seen in infiltrating ductal carcinoma, anisonucleosis (variations in nuclear size in a tissue) seen in differentiated pancreatic carcinoma, infolding of nuclear membrane seen in papillary carcinoma of thyroid, and multinucleate cells in colon carcinoma (Branca et al., 2016; Lin and Staerkel, 2003; Pandey et al., 2014; True and Jordan, 2008). A vast majority of these cancers show dysregulated Lamin expression, for example, downregulation of Lamin A/C is seen in lung, breast, ovarian, colon and prostate cancers; upregulation of Lamin A/C seen in colorectal and skin cancer; similarly B-type lamins are mainly upregulated in most cancer types – colorectal, ovarian, prostate, liver, pancreatic and show downregulation in breast and colon cancers (Irianto et al., 2016). Nuclear and nucleolar structural changes are perhaps co-regulated as Lamins, that are well established regulators of nuclear structure, also impinge on nucleolar structure and function (Buchwalter and Hetzer, 2017; Martin et al., 2009; Prokocimer et al., 2009).

In this chapter we have examined the factors that regulate nucleolar morphology in normal and cancer cells with a special emphasis on the lamin family of proteins. Here we assessed the role of Lamins - proteins that form the lamina and nucleoskeleton of mammalian cells, in the maintenance of nucleolar structure. We have also identified the molecular function of lamins by characterizing separation of function mutants of Lamin sub-pools at the nuclear periphery and nuclear interior and its impact on the maintenance of nuclear and nucleolar structure in cancer cells.

3.2 Results

3.2.1. Localization of endogenous nucleolar proteins in normal and cancer cells

We sought to examine the expression and localization of nucleolar proteins in normal and cancer cells. To this end, cells were immunostained for nucleolar markers - Upstream Binding Factor (UBF), Fibrillarin, Nucleolin and Nucleophosmin. UBF which is a transcription factor associated with RNA Polymerase I, showed a punctate staining, that marks the Fibrillar compartment (FC) of the nucleolus – the region of rRNA transcription (Fig. 3.1A). Fibrillarin also showed a punctate "grape-bunch" like structure inside the nucleolus, denoting the Dense Fibrillar Compartment (DFC) of the nucleolus. This is the region where newly transcribed 47S/45S rRNA is processed into mature 18S, 28S and 5.8S transcripts that are methylated and pseudo-uridylated. Nucleolin and Nucleophosmin showed similar ring-like localization demarcating the boundary of the nucleolus, in the outermost compartment - Granular Component (GC) – the region where rRNAs complex with ribosomal proteins to form 60S and 40S pre-ribosomes, that are then exported out of the nucleolus. We also detected that transfected histone 2B-ECFP (H2B-ECFP) localizes both in the nucleoplasm and in the nucleolus of a population of cells (Fig. 3.1B). The nucleolar localization of H2B-ECFP was ascertained by immunostaining these cells with Nucleolin that marks the nucleolar border around nucleolar H2B-ECFP (detailed in Chapter 6).

Figure 3.1

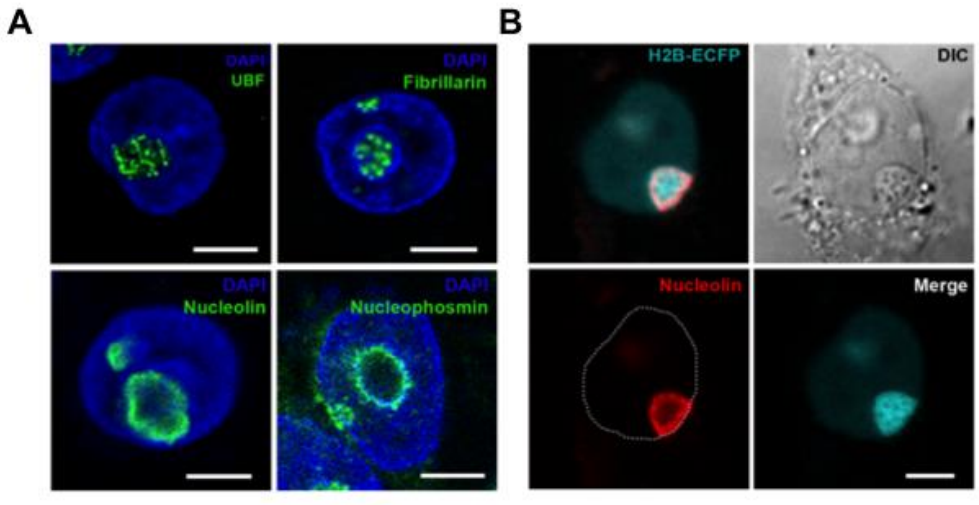

Figure 3.1. Localization of endogenous nucleolar proteins and transfected histone 2B-ECFP in the nucleolus.
A. Immunostaining for endogenous nucleolar proteins showing Upstream Binding Factor (UBF) localization in the FC, Fibrillarin (FBL) localization in the DFC and localization of Nucleolin (NCL) and Nucleophosmin (NPM1) in the granular component (GC) of the nucleolus. Scale bar ~ 5μm. **B.** Transfected histone 2B-ECFP (H2B-ECP) localizes in the nucleoplasm and in the nucleolus of cells. Nucleolar localization of H2B-ECFP is demarcated by Nucleolin staining. Scale bar ~ 5μm.

3.2.2. Nucleolar topology in normal and cancer cells

Nucleolar numbers and topology is an important parameter that is used to distinguish most cancer cells from their normal counterparts. Even within cancers like renal carcinomas, nucleolar topology is greatly altered in low grade vs high grade tumors (Helpap et al., 1990). We assessed nucleolar topology in cancer cell lines of varied origins and a normal colon cell type (Fig. 3.2A). CRL1831 (normal colon cells), DLD1 (colon adenocarcinoma), SW480 (colon adenocarcinoma), HCT116 (colon adenocarcinoma), HT1080 (fibrosarcoma) and A549 (lung carcinoma) cells were immunostained for Nucleolin to demarcate the nucleolus and nuclei were counterstained with DAPI. Nucleolin localizes at the Granular Component (GC) of each nucleolus and serves as a marker of nucleolar morphology and numbers across cell types. After performing confocal microscopy on cells immunostained with Nucleolin, 3D reconstructions were performed on the z-stacks.

We first assessed the number of nucleoli present in each cell line based on the number of Nucleolin signals in each nucleus (Fig. 3.2B). Nucleolar numbers predominantly ranged from 1-2 in normal colon epithelial cells CRL1831 to as high as 9 in breast cancer cell line MCF7 (Fig. 3.2B, Table 3.1). These analyses showed that the diploid colorectal cancer cells - DLD1 (2) and HCT116 (1) show fewer number of nucleoli in comparison to aneuploid cells - SW480 (3), MCF7 (5) and A549 (3-4), however the modal number of nucleoli seen in these cell lines did not directly correlate with the copy numbers of NOR chromosomes.

Table 3.1. Chromosomal ploidy, NOR chromosome copies and number of nucleoli in cells assessed in this study

Cell line	Ploidy (Modal number of chromosomes)	Copy numbers of NOR chromosomes (Spectral Karyotyping, T. Ried Lab)	Modal number of nucleoli
CRL1831	?	?	2
DLD1	44-46	SKYGRAM: All NOR chromosomes (2 copies)	2
SW480	57	SKYGRAM1: Chr 13 (3 copies) Chr 21 (3 copies) SKYGRAM2: Chr 13 (4 copies)	3
HCT116	44-46	SKYGRAM: All NOR chromosomes (2 copies)	1
MCF7	73	?	5
A549	66	SKYGRAM: Chr 14 (3 copies)	3-4

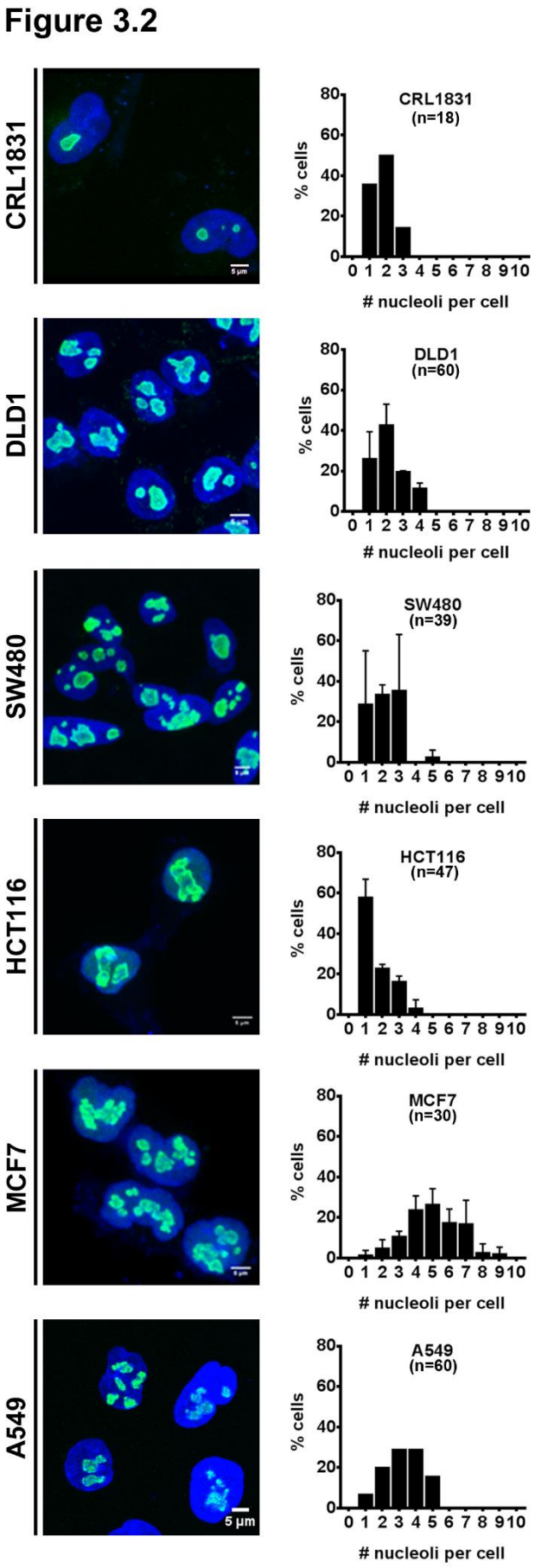

Figure 3.2. Number of nucleoli in normal and cancer cells

A. Maximum intensity projections of confocal z-stacks of CRL1831, DLD1, SW40, HCT116, MCF7 and A549 cells immunostained with Nucleolin (green) to mark the nucleolus and counterstained with DAPI (blue) to

Immunostaining cells with Nucleolin revealed striking differences in nucleolar morphology across cell lines, when we carefully assessed nucleolar morphology in these cell lines (Fig. 3.3A). Two primary categories of nucleolar morphologies were observed - (1) round and discrete, where nucleoli were regular and spherical in shape and multiple nucleoli were distinct from each other (2) aggregated - nucleoli were non-spherical and aggregated (Fig. 3.3A). Cells were visually inspected to quantify sub-populations showing discrete or aggregated nucleoli. If all nucleoli in a particular cell were discrete and spherical, these cells were classified as discrete. If even a single nucleolus within the nucleus showed aggregated morphology – nucleoli were classified as aggregated. Normal colon cells - CRL1831 showed the smallest sub-population of cells with aggregated nucleoli. In comparison colorectal cancer cell line DLD1 showed relatively higher nucleolar aggregates than CRL1831 cells. Nucleolar aggregates increased in the order CRL1831 < DLD1 < A549 < SW480 < HCT116=MCF7 < HT1080 (Fig. 3.3B, Table 3.2). We next quantified the volumes of nucleoli after 3D reconstruction using the software Image Pro Plus (Fig. 3.3C, Table 3.2). We found that the volumes of nucleoli were extremely heterogenous in cancer cells and increased in the order MCF7 < DLD1 < CRL1831 < SW480 < HT1080 < HCT116. Thus, nucleolar volumes did not scale with nucleolar aggregates (Table 3.2).

Figure 3.3

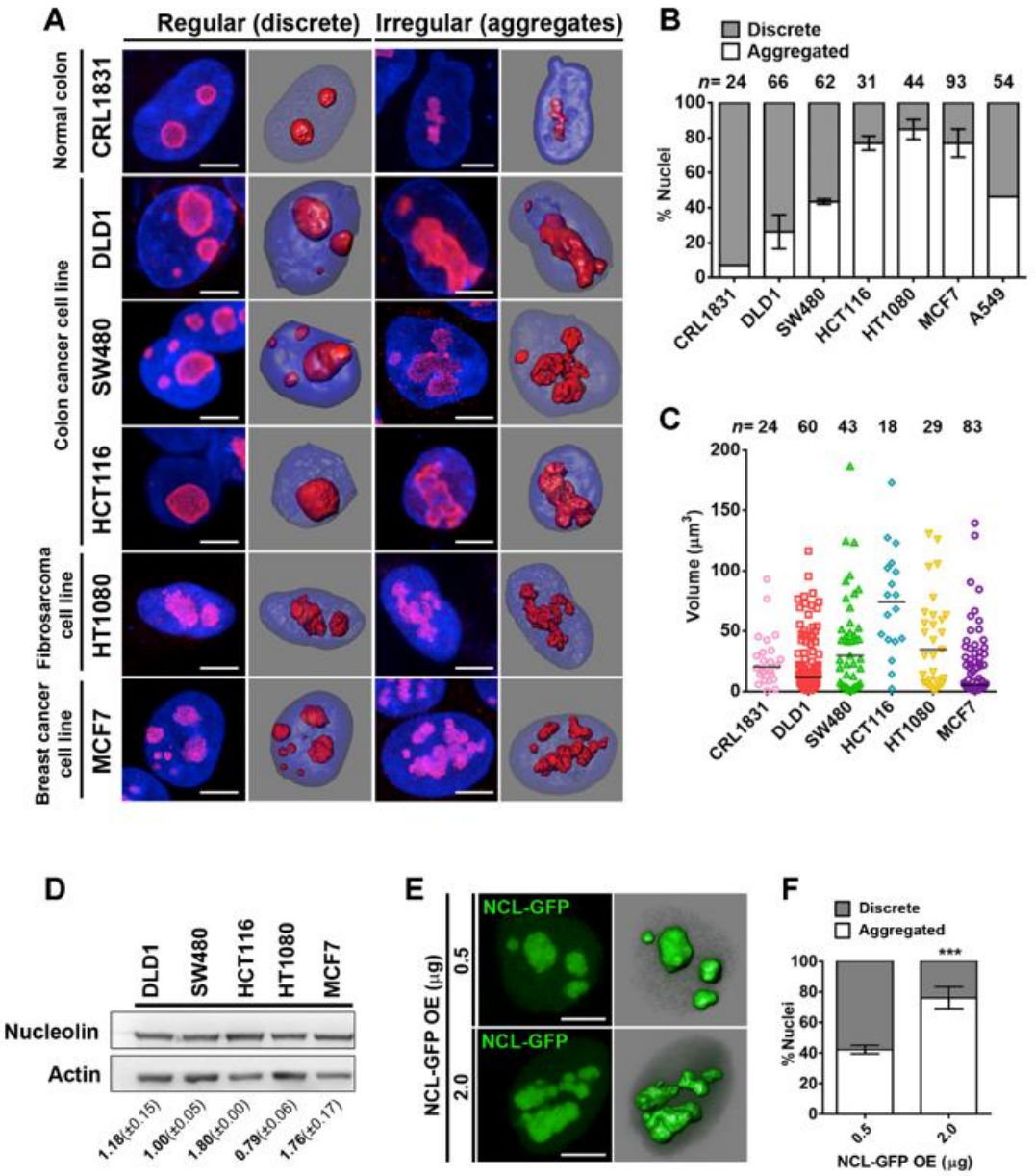

Figure 3.3. Cancer cell lines show regular and irregular nucleolar morphologies.
A. Maximum intensity projections of confocal z-stacks of CRL1831, DLD1, SW480, HCT116, MCF7 and HT1080 cells immunostained for Nucleolin and their 3D reconstructions showing classification of regular or irregular morphology of nucleoli, Scale bar ~5 µm. **B.** Percentage of nuclei showing regular and irregular nucleoli from **(A)**. Data for DLD1 cells from N=3 independent biological replicates and for other cell lines from two biological replicates, n: number of nuclei. Error bars: SD. **C.** Scatter plot showing the distribution of nucleolar volume distribution upon thresholding and 3D reconstruction using IPP software. n: number of nucleoli. **D.** Western blot showing expression levels of Nucleolin from whole cell lysates, loading control - Actin. Blot was quantified using ImageJ and mean (±SEM) expression level of Nucleolin for each cell line, normalized to Actin has been indicated below each lane. Data representative of N=2 biological replicates. **E.** Representative maximum intensity projection and 3D reconstructions from Z-stacks of live DLD1 cells transfected with 0.5 µg and 2.0 µg of NCL-GFP. Scale bar ~5 µm. **F.** Percentage of nuclei showing regular and irregular nucleoli in **(E)**. Fischer's exact test of proportions was used to compare percentages of nuclei with 0.5 µg and 2.0 µg of NCL-GFP. n=40, N=2. ***P<0.0001.

Table 3.2. Morphometry of nucleoli in normal and cancer cell lines

Cell line	Nucleolar morphology (%)		Nucleolar volume (μm^3)	
	Discrete	Aggregated	Median	IQR
CRL1831	93	7	21	23
DLD1	73	27	12	33
SW480	57	43	30	47
HCT116	23	77	74	60
HT1080	15	85	35	55
MCF7	23	77	5	24
A549	53	47	-	-

IQR: Inter-quartile range

Notably, nucleolar morphologies correlate with the extent of metastatic spread of colorectal cancer cell lines. DLD1 (Duke's Type C) and SW480 (Duke's Type B) were derived from relatively lower grade colorectal cancers (CRC), while HCT116 cells (Duke's Type D) was derived from a higher grade CRC and shows a greater extent of nucleolar aberrations (Baker et al., 2011). Furthermore, cell lines with nucleolar aggregates are relatively more aggressive than DLD1 cells as they form tumors in nude mice (Céspedes et al., 2007).

3.2.3. Nucleolin expression levels affect nucleolar morphology

We sought to examine nuclear factors that affect nucleolar morphology across cell lines. Since Nucleolin is a major nucleolar protein, localized at the Granular Compartment (GC) of the nucleolus and is required for the maintenance of nucleolar structure and function (Ma et al., 2007), we examined if disrupted nucleolar morphologies correlated with Nucleolin levels across cell lines. We assessed endogenous expression levels of Nucleolin across cell lines and found that colorectal cancer cells - DLD1, SW480 have comparable levels of endogenous Nucleolin (Fig. 3.3D, $p>0.05$). However, HCT116 showed significantly higher endogenous levels of Nucleolin compared to DLD1 (Fig. 3.3D, $p<0.05$). These studies revealed that colorectal cancer cells with relatively higher endogenous levels of Nucleolin correlate with irregular nucleolar morphologies. Notwithstanding similar levels of Nucleolin expression in HT1080 (compared to DLD1, $p>0.05$) and MCF7 (compared to DLD1, $p>0.05$) these cells show a higher incidence of aberrant nucleolar morphologies, suggesting Nucleolin independent mechanisms in the regulation of nucleolar morphology in fibrosarcoma and breast cancers. Taken together aberrations in nucleolar morphologies are largely consistent with Nucleolin levels and metastatic properties exhibited by these cancer cell lines.

Since aberrant nucleolar morphologies correlate with elevated Nucleolin levels, we sought to examine if ectopic overexpression of Nucleolin, affects nucleolar morphologies of DLD1 cells, which otherwise have relatively regular and spherical nucleoli (Fig. 3.3E). Visual

analyses of nucleolar morphologies revealed ~42% cells with irregular nucleoli in cells transfected with NCL-GFP (0.5 μg), while a significantly higher number of cells (~76%) showed irregular nucleolar morphologies when transfected with a higher amount of NCL-GFP (2.0 μg) (Fig. 3.3F). Irregular nucleolar morphologies in cells overexpressing NCL-GFP, were similar to the distorted nucleoli that we consistently found across the more aggressive cancer cell lines (Fig. 3.3A). Taken together, the extent of irregular nucleolar morphologies correlate with an increase in Nucleolin levels in colorectal cancers. This was corroborated by nucleolin overexpression. Nucleolin with a predominantly GC localization, therefore functions as a major regulator of nucleolar morphologies.

3.2.4. Lamin B2 but not Lamin A/C or B1 depletion disrupts nucleolar morphology

Nuclear envelope factors - Lamins and SUN1 are key regulators of nuclear structure and function across cell types (Chen et al., 2012; Prokocimer et al., 2009). Interestingly, Lamin A/C, Lamin B1, and SUN1 also regulate nucleolar structure and function (Buchwalter and Hetzer, 2017; Martin et al., 2009; Matsumoto et al., 2016). Here we sought to examine the effect of Lamin depletion on nucleolar morphology. We examined nucleolar morphology of DLD1 cells upon Lamin depletion. We selected DLD1 cells since – (i) they maintain near diploid chromosome numbers (45-46) across passages (ii) ~80% cells show 2 discrete nucleoli (iii) show comparable expression level of all Lamins - A/C, B1 and B2, which otherwise considerably vary in most other cell types (Kuga et al., 2014; Ranade et al., 2017; Swift et al., 2013).

To address the role of nuclear lamins in the maintenance of nucleolar morphology, we performed independent siRNA mediated knockdown of Lamins A/C, B1 and B2 in DLD1 cells (Fig. 3.4). While both Lamin A/C and B2 showed ~70-80% depletion, Lamin B1 showed ~50% depletion upon siRNA mediated knockdown (Fig. 3.4A-F). Furthermore, the knockdown of either of the lamins did not affect the levels of one another (Fig. 3.4D, E, F).

Figure 3.4

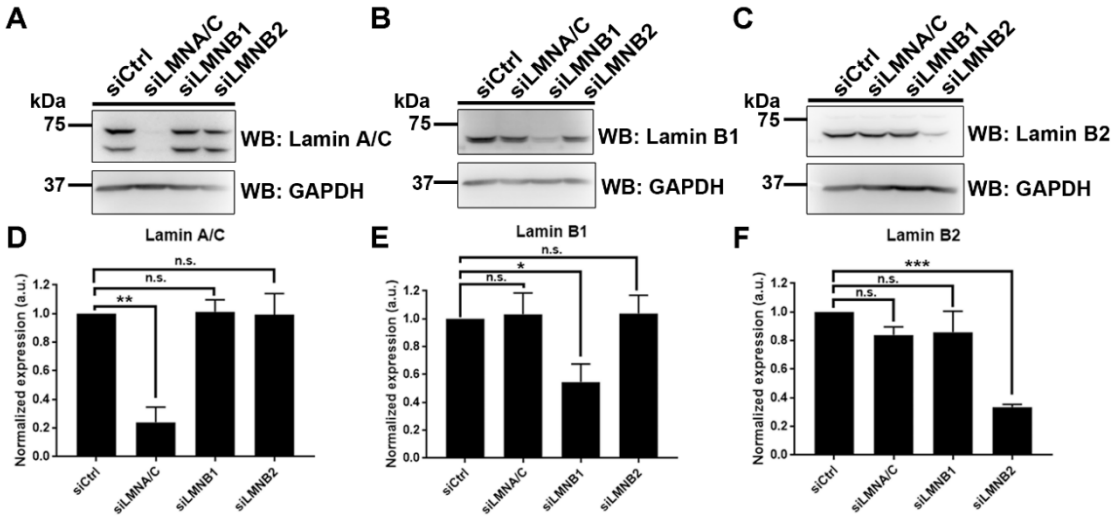

Figure 3.4. siRNA mediated knockdown of Lamins
A-C. DLD1 cells were independently depleted of Lamin A/C (siLMNA/C), Lamin B1 (siLMNB1) or Lamin B2 (siLMNB2) using siRNA mediated knockdown. Control cells (siCtrl) were treated with siRNA against *LacZ* gene (absent in human cells). **D-F.** Lamin A/C and B2 show 80% and 70% knockdown respectively. Lamin B1 shows 50% depletion. Depletion of one Lamin does not significantly affect the expression of other Lamins, as shown in quantification. Data from four independent blots (N=4). Error bar: SEM. Student's t-test, *p<0.05, **p<0.01, ***p<0.001, n.s. not significant.

We next examined nucleolar morphologies upon Lamin depletion by immunostaining cells with Nucleolin. Immunostaining of Nucleolin in DLD1 cells showed two contrasting nucleolar morphologies: (i) intact, i.e., discrete, spatially separate, and spherical nucleoli (Fig. 3.5A), and (ii) disrupted, i.e., aggregated and irregular nucleoli (Fig. 3.5A). We performed Lamin B2 depletion in these cells and examined nucleolar morphology (Fig. 3.5A). Lamin B2 depletion was ~70-80% as revealed by western blotting (Fig. 3.5B). We typically detected 2-3 discrete, spherical nucleoli in each nucleus in ~69% of the control cells, while ~31% of the cells showed disrupted nucleoli (Fig. 3.5C). However, Lamin B2 depletion, showed a significant increase in strikingly aberrant and disrupted nucleoli (Intact nucleoli: ~24% of cells, Disrupted nucleoli: ~76% of cells) (Fig. 3.5C). This was in sharp contrast to Lamin A/C depletion in these cells which did not show an effect on nucleolar morphology (Intact: ~80%, Disrupted: ~20%) (Fig. 3.6A, C). Also, Lamin B1 depletion, which was previously shown to disperse nucleoli in HeLa cells, did not show any effect on nucleolar morphology in these cells (Intact: ~64%, Disrupted: ~36%) compared to its corresponding control cells (Fig. 3.6D, E). The extent of Lamin A/C and Lamin B1 knockdown were assessed in these cells by western blotting (Fig. 3.6B, 3.4B).

Figure 3.5

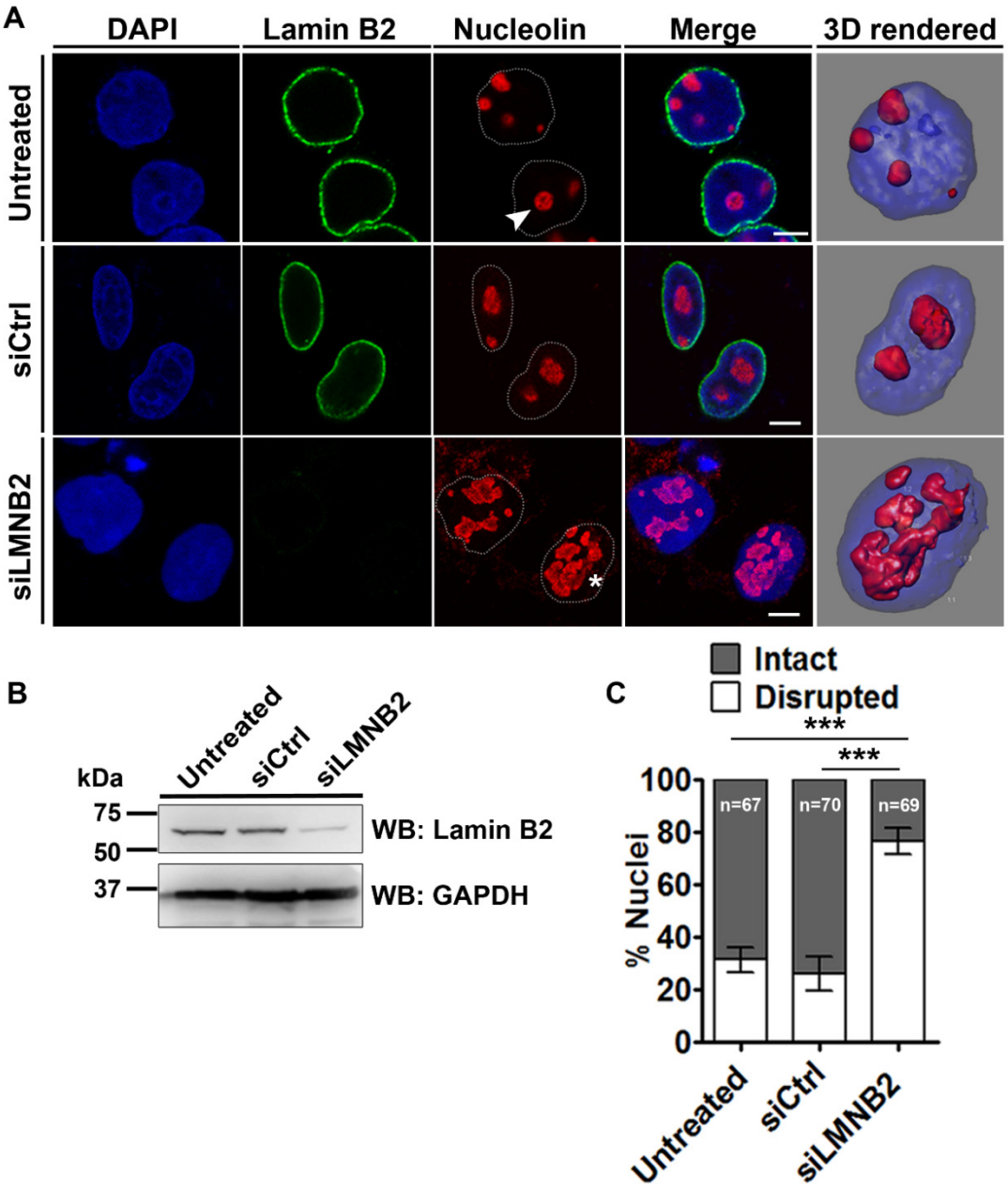

Figure 3.5. Lamin B2 depletion disrupts nucleolar morphology.
A. DLD1 cells were co-stained for Lamin B2 and Nucleolin. DAPI counterstains the nucleus. Untreated cells (Untreated), Lamin B2 knockdown cells (siLMNB2) or cells treated with non-targeting siRNA (siCtrl). Representative confocal images of control cells show discrete and intact nucleoli (arrowhead), siLMNB2 shows disrupted nucleolar morphology (white asterisk), also shown in 3D reconstructions. Scale bar ~ 5 µm. **B.** Western blot showing Lamin B2 depletion upon siRNA mediated knockdown. **C.** Quantification of nucleolar morphologies show a significant increase in disrupted nucleoli upon Lamin B2 knockdown (Fischer's exact test of proportions, ***p<0.001). Data from 3 independent biological replicates (N=3, n: number of nuclei). Error bar: SEM.

Figure 3.6

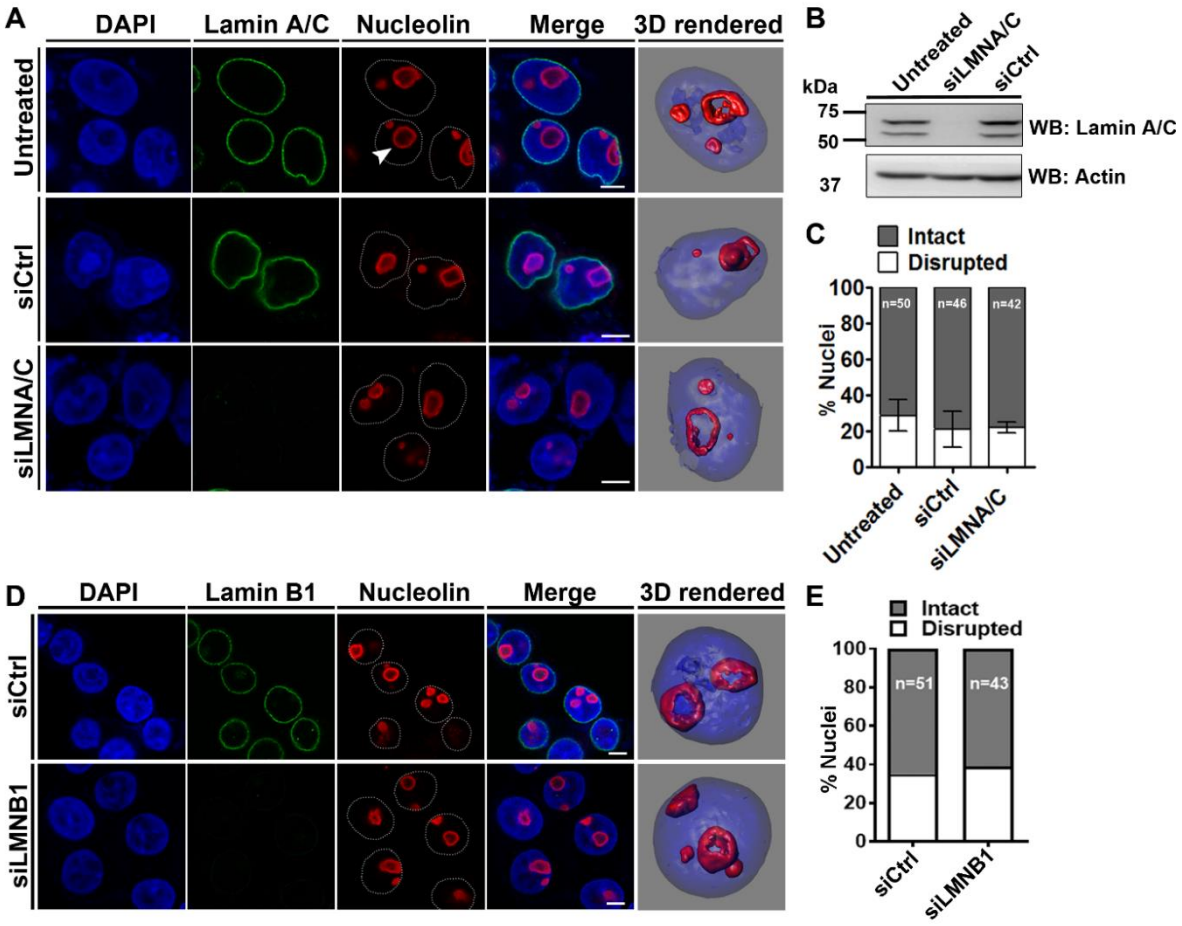

Figure 3.6. Lamin A/C and B1 depletion do not affect nucleolar morphology.
A. DLD1 cells were co-stained for Lamin A/C and Nucleolin. DAPI counterstains the nucleus. Untreated cells (Untreated), Lamin A/C knockdown cells (siLMNA/C) or cells treated with non-targeting siRNA (siCtrl). Representative confocal images of control and Lamin A/C depleted cells showing discrete nucleoli, also shown in 3D reconstructions. Scale bar ~ 5 µm. **B.** Western blot showing Lamin A/C depletion upon siRNA mediated knockdown. **C.** Quantification of nucleolar morphologies show no significant change (Fischer's exact test of proportions, $p>0.05$). Data from N=2 independent biological replicates, n: number of nuclei. Error bar: SD. **D.** Cells co-stained with Lamin B1 and Nucleolin. Representative confocal images of Lamin B1 depleted cells (siLMNB1) or cells treated with non-targeting siRNA (siCtrl) showing discrete nucleoli, also shown in 3D reconstructions. Scale bar ~ 5 µm. **E.** Quantification of nucleolar morphologies in control and siLMNB1 cells. Data from N=1 experiment, n: number of nuclei.

We also employed two independent siRNA oligonucleotides to knock down Lamin B2 and assessed the same by IFA and western blotting (Fig. 3.7A, B). Lamin B2 depletion using these siRNAs also showed comparable extents of disrupted nucleoli in DLD1 cells (siLMNB2.2, ~59%; siLMNB2.3, ~62%) (Fig. 3.7C). We further used an shRNA to stably knockdown Lamin B2, under selection (Fig. 3.7D). Two independent sub-clones of shLamin B2 cells (shB2-clone 3 and shB2-clone 5) showed ~50% depletion of Lamin B2 (Fig. 3.7E). The shLamin B2 treated cells showed that disrupted nucleoli were retained across passages upon long-term depletion of Lamin B2 (shB2-clone3: ~78%; shB2-clone5: 65%) (Fig. 3.7F).

To assess if the disrupted nucleolar morphology upon Lamin B2 depletion can be rescued, we overexpressed Lamin B2-GFP resistant to Lamin B2 siRNA (Fig. 3.8A). As seen previously, ~80% Lamin B2 depleted cells showed disrupted nucleoli, whereas upon overexpression of siRNA resistant Lamin B2-GFP, the percentage of cells showing disrupted nucleoli reduced to ~40% (Fig. 3.8B, C). This showed that nucleolar morphology can be rescued upon Lamin B2 overexpression. Taken together, these results reveal a specific role of Lamin B2 but not Lamin A/C or B1 in modulating nucleolar morphology in DLD1 cells.

Figure 3.7

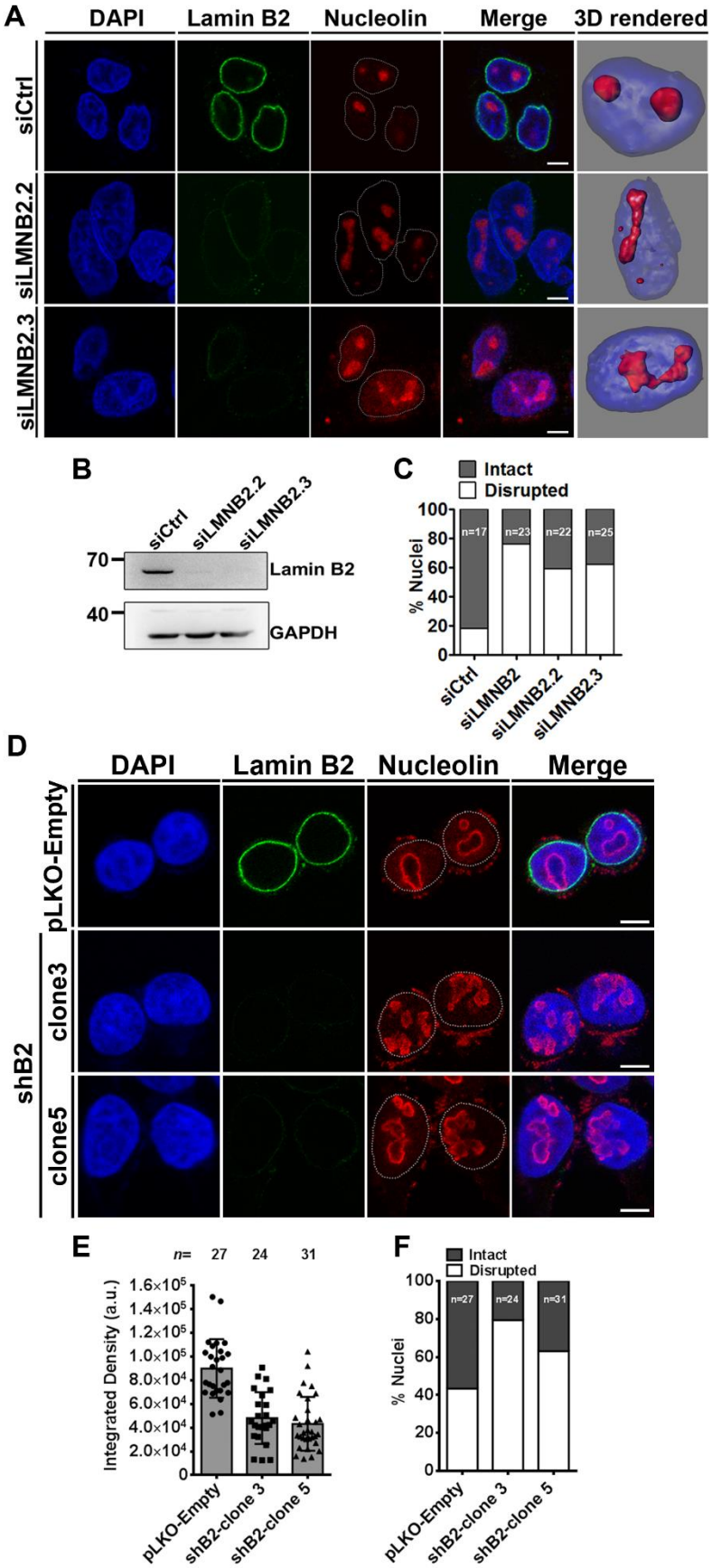

Figure 3.7. Lamin B2 depletion using alternate siRNAs and shRNA show nucleolar disruption
A. DLD1 cells were treated with two alternate siRNAs against Lamin B2 with distinct sequences (siLMNB2.2 and siLMNB2.3). Cells were immunostained with Lamin B2 and Nucleolin antibodies, and counterstained with DAPI. Knockdown with alternate Lamin B2 siRNAs also show disrupted nucleoli. Scale bar ~ 5µm. **B.** Western blot showing knockdown of Lamin B2 with siLMNB2.2 and siLMNB2.3 siRNAs. **C.** Quantification of nucleolar morphologies show an increase in disrupted

nucleoli upon Lamin B2 knockdown (N=1, n: number of nuclei). **D.** DLD1 cells were transfected with Lamin B2 shRNA and clones were selected by antibiotic selection for ~2 weeks. Cells were immunostained with Lamin B2 and Nucleolin, showing disrupted nucleoli in shLMNB2 positive clones (clone 3 and clone 5). Scale bar ~ 5µm. **E.** Quantification of relative Lamin B2 fluorescence intensity in control and shLamin B2 cells. n=number of nuclei, N=1. **F.** Quantification of nucleolar morphologies show an increase in disrupted nucleoli upon Lamin B2 knockdown using shRNA (N=1, n: number of nuclei).

Figure 3.8

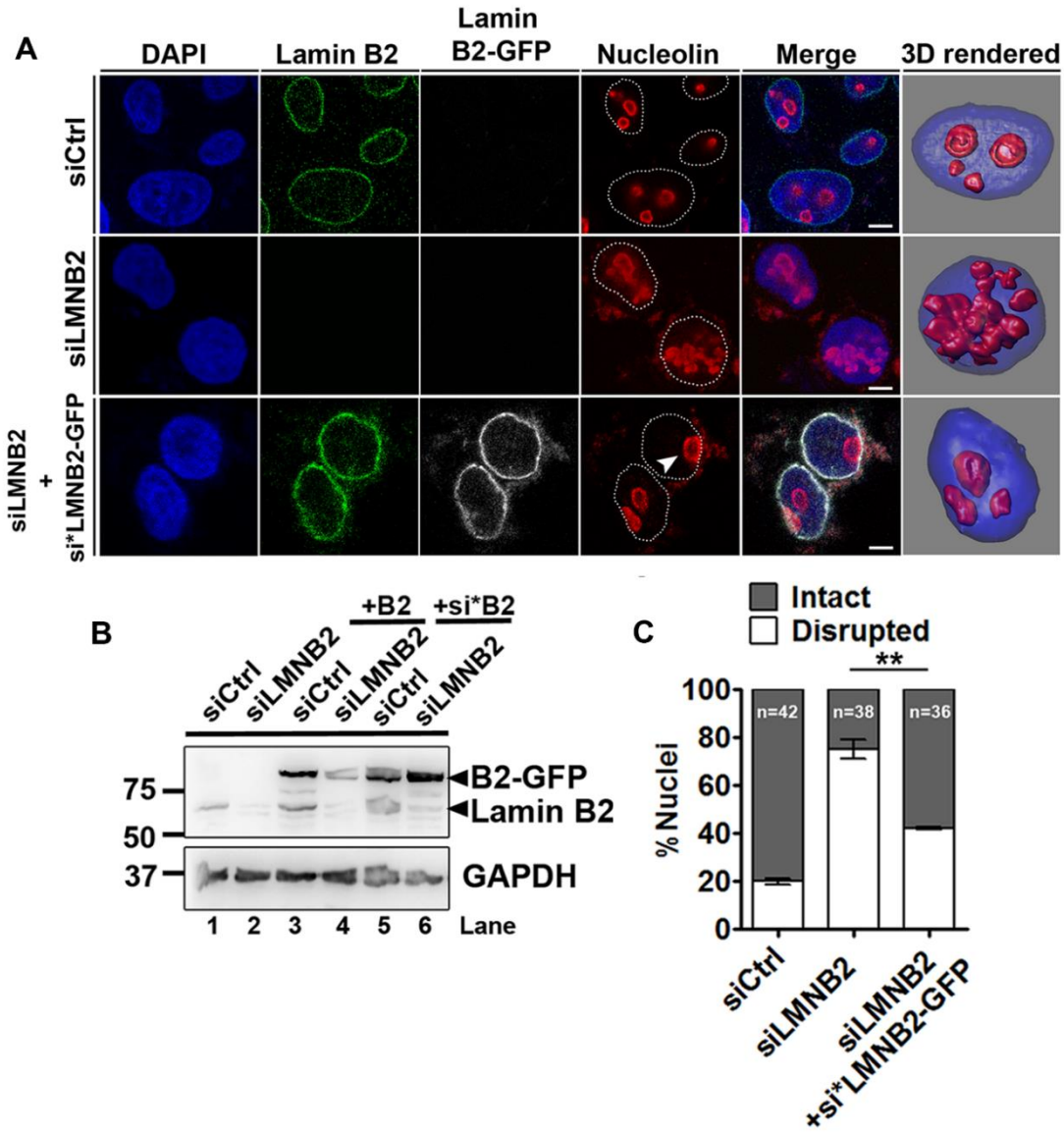

Figure 3.8. Nucleolar morphology is rescued upon overexpressing Lamin B2-GFP in Lamin B2 depleted cells.
A. Schematic showing time points of treating DLD1 cells with siRNA and siRNA resistant Lamin B2-GFP plasmid **B.** Intact nucleolar morphologies were restored in DLD1 cells transfected with siRNA resistant LMNB2-GFP (si*LMNB2-GFP, white arrow), Scale bar ~ 5 µm. **C.** Western blot showing overexpression of Lamin B2-GFP (B2-GFP) (Lane#3,4) and si resistant Lamin B2-GFP (si*B2) (Lane#5,6) in control and Lamin B2 depleted cells. **D.** Nucleolar morphology is restored upon overexpression of Lamin B2 (si*LMNB2-GFP) (Fischer's exact test of proportions, **p<0.01). N=2, n: number of nuclei. Error bar: SD.

3.2.5. Lamin B2 depletion affects nucleolar volume

Since nucleolar morphology was grossly affected upon Lamin B2 depletion, we assessed the number of nucleoli in these cells upon Lamin A/C and B2 depletion (Fig. 3.9A). We performed Nucleolin staining in these cells and examined the number of nucleoli in control, Lamin A/C and Lamin B2 depleted cells. Quantification of number of nucleoli showed that control DLD1 cells have a modal number of 2 nucleoli (Fig. 3.9A). This distribution was unaffected upon either Lamin B2 or Lamin A/C depletion, suggesting that Lamin depletion does not affect nucleolar numbers.

We next examined the effect of Lamin depletion on nucleolar volume, for which we performed 3D reconstructions of nucleoli from confocal images. This analyses reveals that a sub-population of cells have significantly larger nucleoli upon Lamin B2 depletion (Fig. 3.9B). We also assessed the volumes of nucleoli upon Lamin A/C depletion, which did not reveal a significant change in the volume of nucleoli in these cells (Fig. 3.9C). We further binned nucleolar volumes and found that cells showing nucleoli larger than >150 μm^3 were significantly enriched upon Lamin B2 depletion but did not show a change upon Lamin A/C depletion (Fig. 3.9D).

Figure 3.9

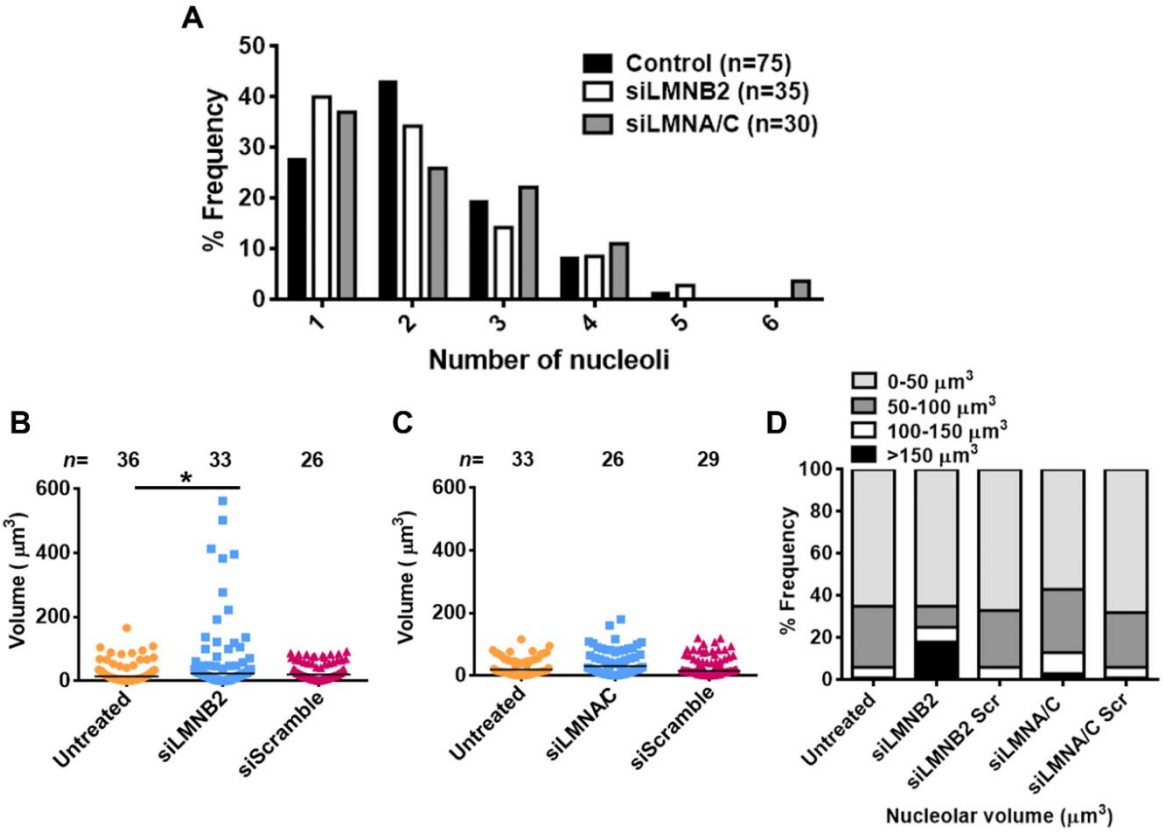

Figure 3.9. Nucleolar volumes increase upon Lamin B2 depletion.
A. Histogram showing number of nucleoli in control, Lamin B2 and Lamin A/C depleted cells. No significant change in nucleolar numbers were observed upon either knockdown. Fischer's exact test,

p>0.05. **B-C.** Volumes of nucleoli in control, Lamin B2 and Lamin A/C depleted cells. N=2, n=number of nuclei. Nucleolar volumes are significantly increased upon Lamin B2 knockdown but not upon Lamin A/C knockdown. Mann Whitney test. *p<0.05. **D.** Nucleolar volumes are binned into classes of 50 μm^3 show an in nucleoli larger than 150 μm^3 in size upon Lamin B2 depletion.

3.2.6. Sub-nuclear localization of Lamins

3.2.6.1. Lamins localize in the nuclear matrix as revealed by DNaseI digestion

It is well established that Lamin B2 localizes primarily at the inner nuclear membrane across cell types (Adam et al., 2013; Shimi et al., 2015). However, Lamin functions are not only restricted to the nuclear periphery as they also participate in regulation of numerous intranuclear functions such as DNA replication, transcription and genome organization (Prokocimer et al., 2009; Shimi et al., 2008). Thus we re-examined the localization of nuclear lamins as a means to address if lamins also localized near the nucleolus. Lamin staining in intact nuclei hardly show any intranuclear localization (Figs. 3.5, 3.6). We surmised that this could be due to inaccessibility of antibodies to intranuclear sub-pool of lamins. We therefore extracted soluble nuclear proteins using high salt buffers followed by Dnase I treatment to digest DNA, as described previously, to reveal intranuclear lamin organization (Hozák et al., 1995; Jagatheesan et al., 1999). The resulting nuclear matrix stained for the nuclear matrix protein p84, suggesting accessibility into the nuclear matrix (Fig. 3.10 A, B). This approach revealed a distinct intranuclear localization of Lamin B2 and Lamin A in the nucleus (Fig. 3.10 C-F). We also immunostained the nuclear matrix with Nucleolin to detect the nucleolus. Notably, Lamin B2 but not Lamin A localized proximal to the nucleolar border (indicated by arrows in line scan).

Figure 3.10

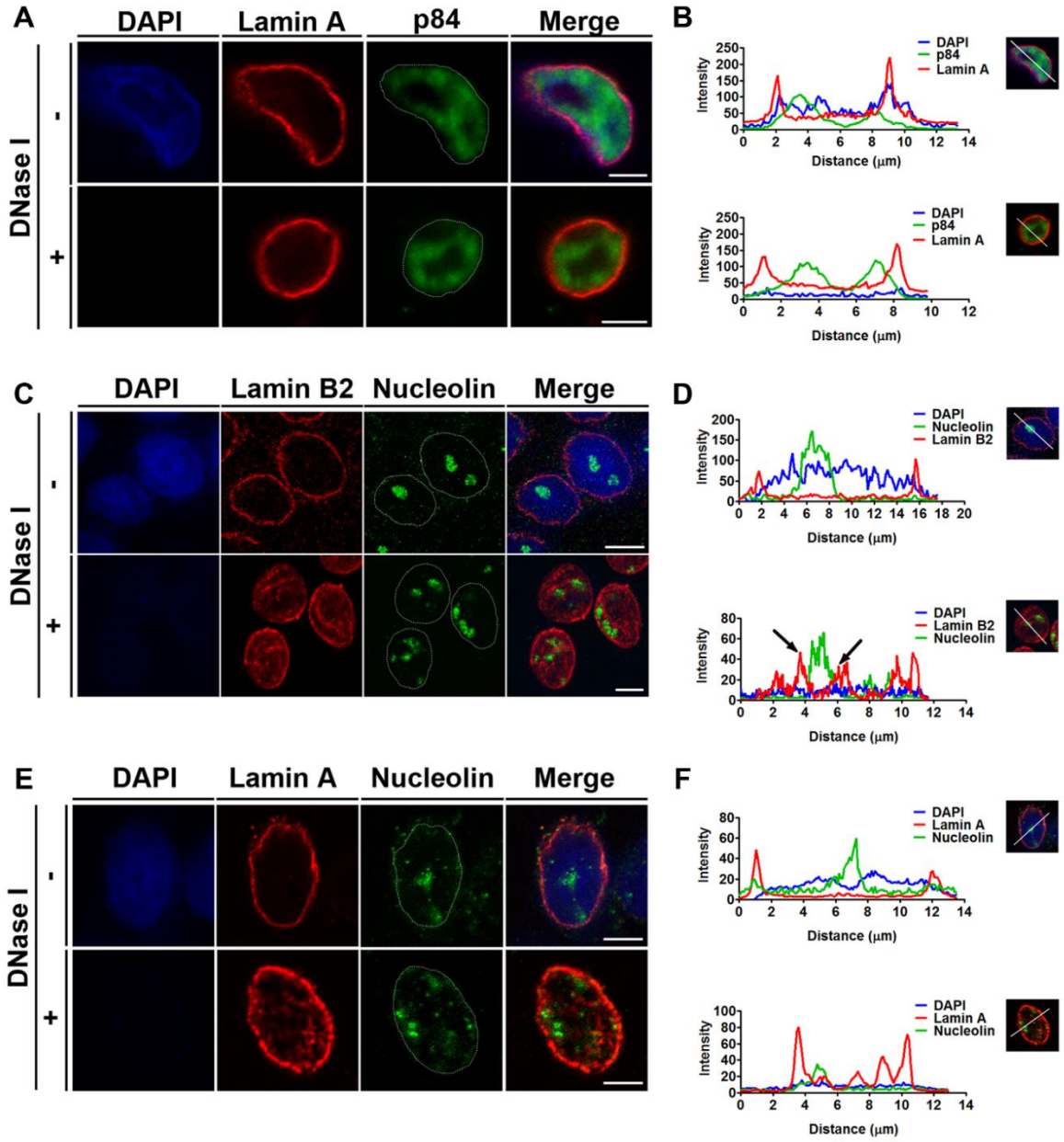

Figure 3.10. Lamin B2 and Lamin A/C also localize to the nuclear interior.
A. Nuclear matrix was prepared from DLD1 cells by sequential extractions with salt and detergents with (+) or without (-) DNAse I (100U/ml) treatment and immunostained for Lamin A/C and, the nuclear matrix protein p84. Notably, p84 staining within the nucleus is not altered in cells treated with DNase I from untreated cells. Loss of DAPI shows effective DNAse I treatment. Scale bar ~ 5 μm. **B.** Representative line scans through the nucleus showing the fluorescence intensity of p84, Lamin A/C and DAPI signals in (-) and (+) DNAse I treated preparations. **C.** Immunostaining for Lamin B2 performed on nuclear matrix preparations. Increase in internal staining of Lamin B2 upon DNAse I treatment. Nucleolar signals are detected by immunofluorescence for Nucleolin. Scale bar ~ 5 μm. **D.** Representative line scans across the nucleus show the distribution of Lamin B2, Nucleolin and DAPI in (-) and (+) DNAse I treated cells. **E.** Immunostaining for Lamin A/C and Nucleolin performed on nuclear matrix preparations. Internal pools of Lamin A/C was also detected upon DNAse I treatment. Scale bar ~ 5 μm. **F**. Representative line scans across the nucleus show the distribution of Lamin A/C, Nucleolin and DAPI in (-) and (+) DNAse I treated preparations. **G.** Live cells expressing NCL-GFP show the nucleolus and (J) Lamin A-mCherry or (K) Lamin B2-mCherry. Scale bar ~ 5 μm. **H.** Representative line scan across the nucleus showing the distribution of Lamin A, Lamin B2 and Nucleolin. **I.** Western blot showing overexpression of Lamin A and Lamin B2. Loading control: GAPDH. Scale bar ~5 μm. N=3 biological replicates.

3.2.6.2. Lamin B2 localizes at the nucleolar border

To determine if Lamin B2 indeed associates with the nucleolus we isolated intact nucleoli from a semi-confluent culture of DLD1 cells (Fig. 3.11A, B). We plated purified nucleoli on glass coverslips and performed immunofluorescence staining of Nucleolin and Lamin B2. Nucleolin staining on isolated nucleoli was indistinguishable from that seen around nucleoli within the nucleus. This showed that the structure of nucleoli was preserved even upon nucleolar isolation (Fig. 3.11B, C). Remarkably, isolated nucleoli showed a distinct localization and enrichment of Lamin B2 at the nucleolar border as foci in close proximity to Nucleolin (Fig. 3.11C, D inset, linescan). As a control to assess the specificity of Lamin B2 staining, we isolated nucleoli from Lamin B2 depleted cells, which did not show Lamin B2 staining, while Nucleolin staining was maintained at the nucleolar border (Fig. 3.11C, siLMNB2 panel). This further validated the specificity of Lamin B2 localization at the nucleolar border in isolated nucleoli.

We also performed super-resolution microscopy using Airyscan imaging to further resolve Lamin B2 and Lamin A/C localization within isolated nucleoli (Fig. 3.11D). This high-resolution imaging approach recapitulated Lamin B2 localization at the nucleolar border (Fig. 3.11D). In contrast, Lamin A/C showed a punctate distribution in the nucleolar interior, while Nucleolin localization was confined to the nucleolar border (Fig. 3.11D). The nucleolar localization of Lamin A/C is consistent with its detection in nucleolar extracts of HeLa cells, reported previously (Martin et al., 2009). Although confocal and super-resolution Airyscan imaging showed a close proximity of Lamin B2 with Nucleolin (Fig. 3.11C, line scans), we did not detect a colocalization between Lamin B2 and Nucleolin at all regions of isolated nucleoli.

Figure 3.11

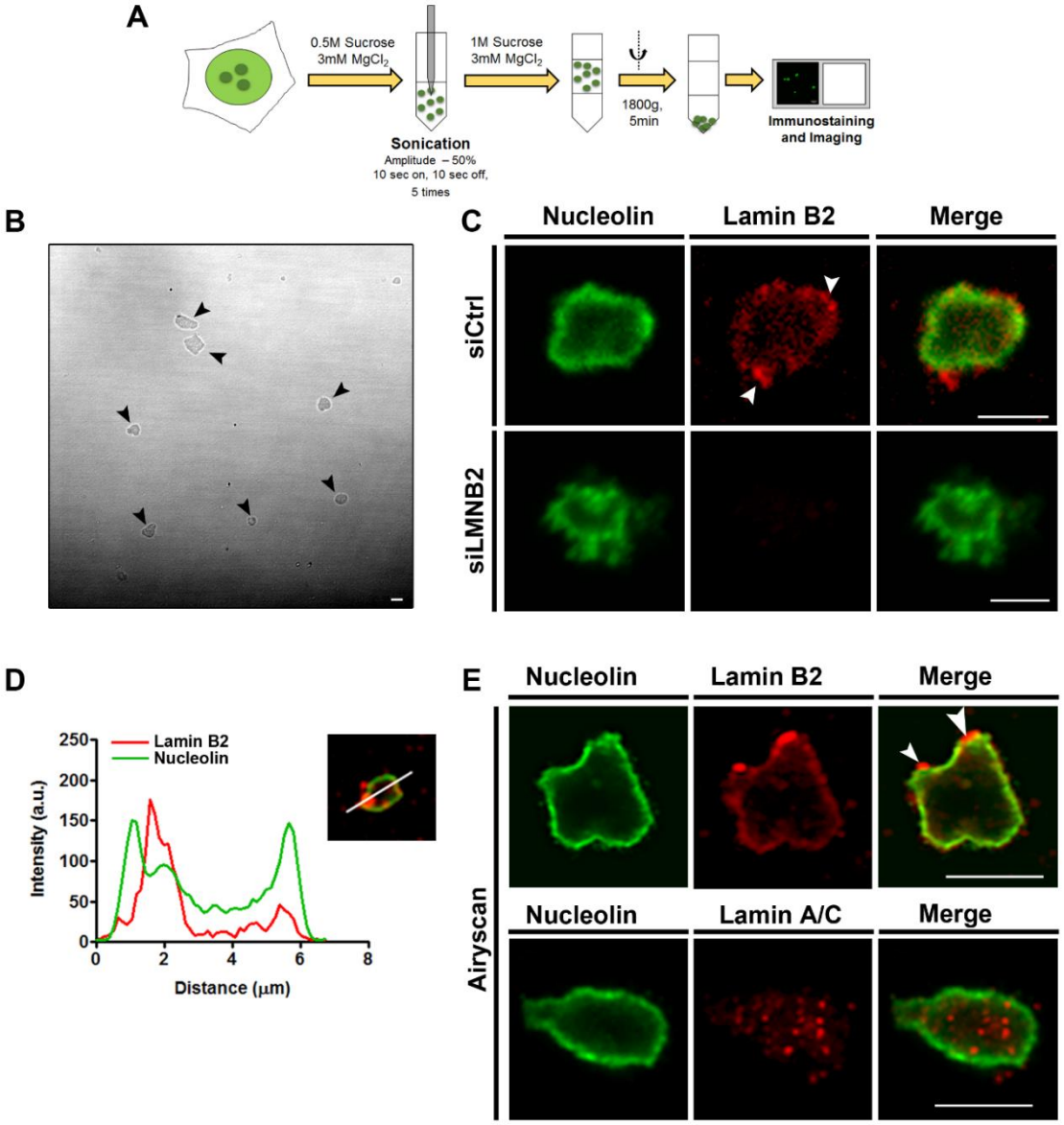

Figure 3.11. Lamin B2 is associated with the nucleolus.
A. Schematic representation of method followed for isolation and analysis of nucleoli. **B.** DIC images of isolated nucleoli (black arrowheads). Scale bar ~ 5μm. **C.** Isolated nucleoli were immunostained for Lamin B2 and Nucleolin. Border of nucleoli is demarcated by Nucleolin staining. Lamin B2 foci are enriched at the nucleolar border (siCtrl panel, white arrows). Absence of Lamin B2 staining at the nucleolar border in nucleoli isolated from Lamin B2 depleted cells (siLMNB2 panel), shows the specificity of Lamin B2 staining at the nucleolus. Scale bar ~5 μm. **D.** Line scan across an isolated nucleolus, shows Lamin B2 (red line) enrichment near the border of the nucleolus marked by Nucleolin (green line). **E.** High resolution Airyscan images of isolated nucleoli immunostained for Nucleolin, Lamin B2 and Lamin A/C. Lamin B2 foci are enriched at the nucleolar border, while Lamin A/C foci localize in the nucleolar interior. Scale bar ~5 μm.

3.2.6.3. Lamin B2 forms a complex with nucleolar GC proteins - Nucleolin and Nucleophosmin

Considering the proximity of Lamin B2 to the GC of the nucleolus, we asked if Lamin B2 associates with bonafide nucleolar GC proteins. We performed co-immunoprecipitation (co-IP) assays with Nucleolin and Nucleophosmin (NPM1) on whole-cell extracts of DLD1 cells (Fig. 3.12A). Under these conditions, we recapitulated the well-established interaction between Nucleolin and NPM1 (Fig. 3.12 A, panel i) (Li et al., 1996). Co-IP of Nucleolin specifically immunoprecipitated Lamin B2 but not Lamin A/C or Lamin B1 (Fig. 3.12A, panels ii-iv). Lamin B2 also co-immunoprecipitated with NPM1, underscoring the association of Lamin B2 with nucleolar proteins at the granular component (Fig. 3.12A, panel v). NPM1 however, also

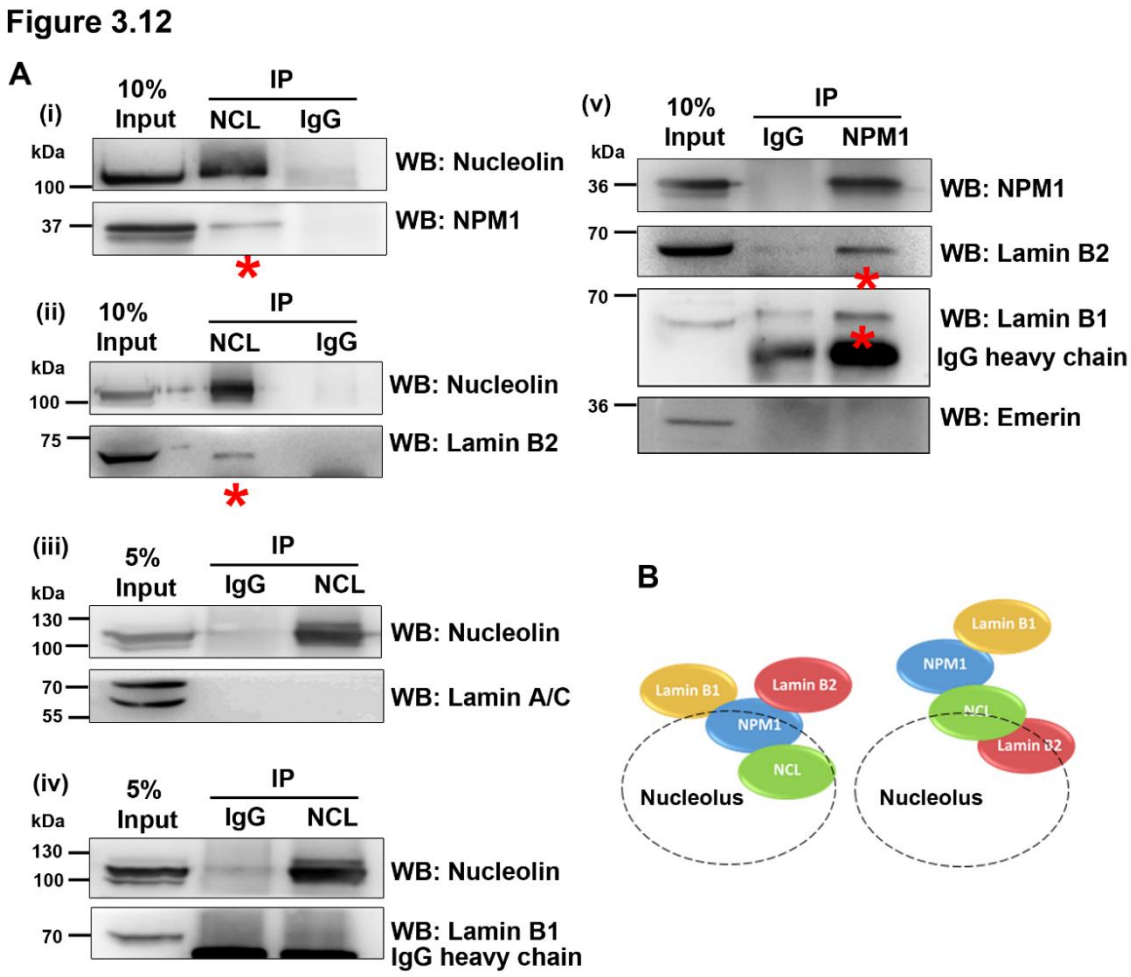

Figure 3.12. Lamin B2 forms a complex with Nucleolin and Nucleophosmin (NPM1).
A. (i) Co-immunoprecipitation of NPM1 with Nucleolin, serves as a positive control **(ii)** Lamin B2 co-immunoprecipitate with Nucleolin. Negative control: IgG **(iii-iv)** Lamin A/C and Lamin B1 do not co-immunoprecipitate with Nucleolin **(v)** Lamin B2 and Lamin B1 co-immunoprecipitate with NPM1, while Emerin does not. Co-IP experiments were performed in three independent biological replicates for Lamin B2 and two independent biological replicates for Lamin A/C, Lamin B1 and Emerin. **B.** Possible modes of interactions of Lamin B2 with nucleolar proteins.

showed a complex with Lamin B1, which was earlier shown in HeLa cells (Fig. 3.12A, panel v) (Martin et al., 2009). However, the inner nuclear membrane protein Emerin, did not associate with NPM1 (Fig. 3.12A, panel v). This suggests that B-type Lamins specifically interact with nucleolar GC proteins Nucleolin and NPM1, either directly or via Lamin B1 (Fig. 3.12B). In summary, these results strongly implicate Lamin B2 in the structural and potentially functional organization of the nucleolus.

3.2.6.4. Lamin B2 constitutes distinct complexes at the nuclear envelope and nucleolar border

Since super-resolution imaging and co-immunoprecipitation assays independently revealed Lamin B2 association with the nucleolus, we examined the interactions of Lamins with the nuclear periphery and the nucleolar periphery. A-type and B-type Lamins form differential interactions at the nuclear periphery. The primary interactors of Lamin A/C include B-type Lamins, Emerin, Barrier to autointegration factor (BAF), Lamina associated polypeptide 2α (LAP2A) and Linker of Nucleoskeleton and Cytoskeleton (LINC) Complex proteins - Sun1 and Sun2 (Simon and Wilson, 2013). Fewer interactors of B-type Lamins have been identified and these include Lamin B receptor (LBR), Heterochromatin binding protein 1 (HP1) and Lamina associated polypeptide 2β (LAP2B) (Simon and Wilson, 2013). We thus used STRING database to identify if Lamins associate with nuclear and nucleolar periphery. Our input proteins were

Lamin A, Lamin B1, Lamin B2, nuclear periphery proteins - Emerin, Sun1, Sun2, LBR and nucleolar proteins - Nucleolin, Nucleophosmin (NPM1), Fibrillarin and Upstream bonding factor (UBTF). STRING analysis revealed two distinct clusters of proteins constituting the nuclear periphery - EMD, LBR, LMNA, SUN1, SUN2 and a nucleolar cluster - NPM1, NCL, FBL and UBTF. Lamin B1 and Lamin B2 bridged the nuclear periphery and nucleolar clusters of proteins (Fig. 3.13). In summary we propose that Lamin B2 forms two distinct sub-interactomes – one at the nuclear periphery with nuclear envelope proteins and another with nucleolar GC proteins at the nucleolar border.

Figure 3.13

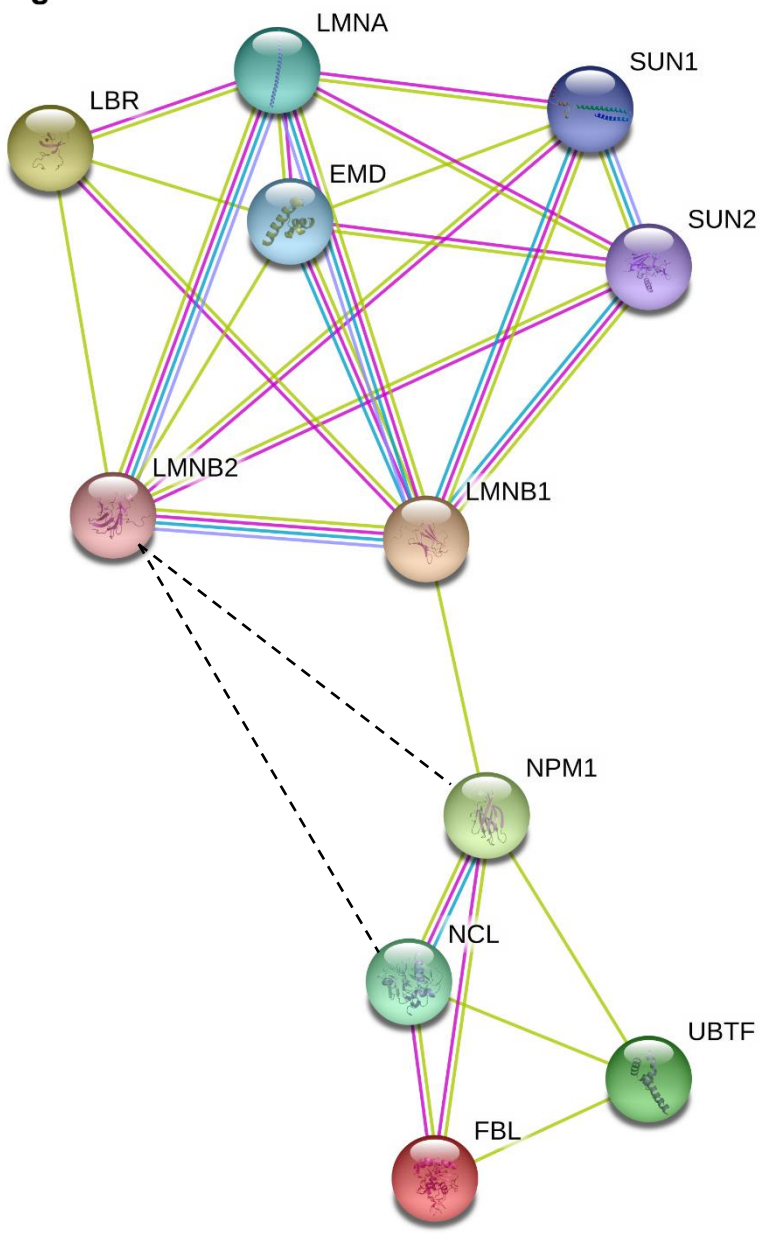

Figure 3.13. STRING output showing nuclear envelope and nucleolar interactors of Lamin B2
Lamin B2 and Lamin B1 are centrally located in the hub and show nuclear envelope and nucleolar interactomes. Dotted lines show the novel interaction of Lamin B2 with Nucleolin and Nucleophosmin identified in this study.

3.2.7. Lamin B2 shows separation of function at the nuclear periphery and nucleolar periphery

Lamins are known regulators of overall nuclear architecture. Since we found two different interactomes of Lamin B2 at the nuclear periphery and at the nucleolar border, we sought to examine differential functions of Lamin B2 at these two locations. We examined the amino acid sequence and structure of Lamin B2 protein. Lamin B2 has (i) N-terminal globular head domain (amino acids 1 to 28), (ii) central α-helical rod domain (aa 29 to 380), and (iii) C-terminal tail domain (aa 381 to 600) containing a globular immunoglobulin-fold (Fig. 3.14A) (Parry et al., 1986; Stuurman et al., 1998). At the nuclear envelope Lamin B2 forms a meshwork as follows - Lamin B2 molecules form a coiled-coil homodimer with their central rod domains, the dimers then organize into a half-staggered head-to-tail polymer and finally the head to tail polymers associate laterally to form a Lamin filament (Heitlinger et al., 1991, 1992; Turgay et al., 2017). Lamin B2 can also heterodimerize with Lamin B1 through its coiled-coiled rod domain (Heitlinger et al., 1991). The tail domain of Lamin B2 also has a highly acidic putative chromatin binding domain (aa 570-582) (Taniura et al., 1995). We also performed multiple sequence alignments between Lamin B1, B2 and A, and found two unique stretches of amino acids - SLSATGR (aa 404-410) and PLGSGPSVLGTG (aa 424-435) that are present in the tail domain of Lamin B2 but absent on either Lamin B1 or Lamin A/C.

To dissect potential separation of function of Lamin B2 in modulating nucleolar and nuclear morphologies, we made deletions in the N-terminal head domain, central rod domain and C-terminal tail domain of Lamin B2. We generated deletion constructs of Lamins such as (i) 1-28 aa (ΔHead) required for the head-tail organization of Lamin B2 dimers (ii) 210-236 aa (ΔRod1) (iii) 237-380 aa (ΔRod2), required for the coiled-coil dimerization of Lamin B2 (iv) Δ404-410 aa (ΔSLSATGR) - a unique stretch of amino acids in the C-terminal tail domain of Lamin B2 (Fig. 3.14A).

We first assessed the localization of Lamin B2 deletion mutants in DLD1 cells (Fig. 3.14B). Lamin B2-GFP localized to the nuclear envelope and colocalized with endogenous Lamin B2 staining. Similar to Lamin B2-GFP, the Lamin B2 head domain deletion mutant (ΔHead) localized at the nuclear periphery. In contrast, both the rod domain deletion mutant (ΔRod1 and ΔRod2) were mislocalized from the nuclear periphery. The ΔRod1 mutant formed foci inside the nucleoplasm while the ΔRod2 mutant formed large aggregates, while endogenous Lamin B2 staining is maintained at the nuclear periphery. The Lamin B2 tail mutant (ΔSLS) localized correctly at the nuclear periphery similar to endogenous Lamin B2. Since the ΔRod mutants were mislocalized, we performed subsequent assays with the ΔHead and ΔSLS mutants.

Figure 3.14

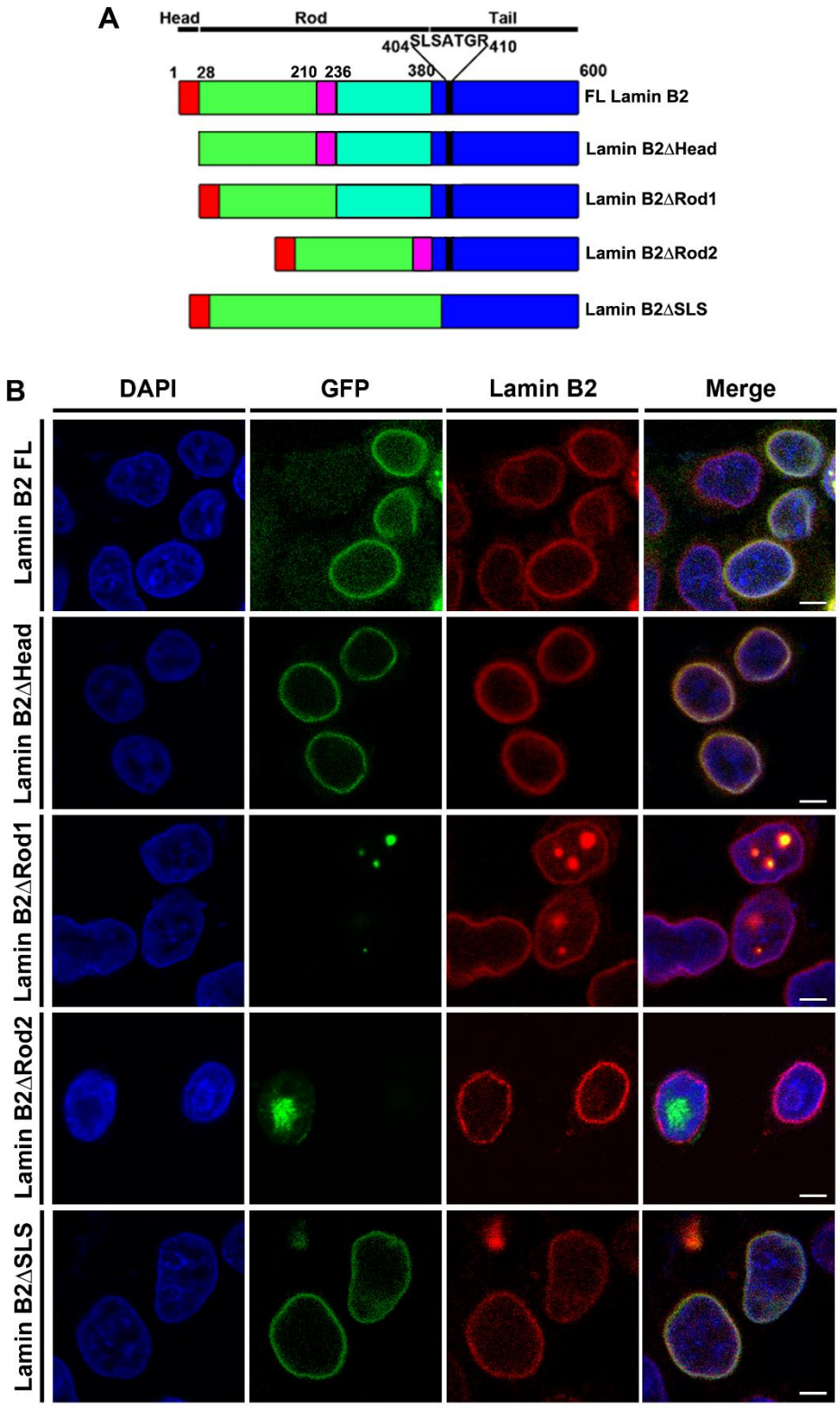

Figure 3.14. Expression of Lamin B2 mutants in DLD1 cells
A. Schematic representation of full-length Lamin B2 with the N-terminal head domain, central rod domain, and C-terminal tail domain. The Lamin B2ΔHead mutant lacks the head domain (aa 1 to 28) from the N terminus. ΔRod1 and ΔRod2 mutants lack aa and aa respectively. Lamin B2ΔSLS mutant lacks the sequence SLSATGR (aa 404 to 410) from the tail domain of Lamin B2. **B.** Immunofluorescence assay with endogenous Lamin B2 shows that full-length Lamin B2, Lamin B2ΔHead and Lamin B2ΔSLS mutants localize correctly at the nuclear envelope, while ΔRod1 and ΔRod2 mutants are mislocalized forming aggregates in the nucleoplasm. Scale ~5μm.

We next determined the effects of overexpressing siRNA-resistant (i) full-length Lamin B2 (ii) Lamin B2ΔHead, and (iii) Lamin B2ΔSLS on the nucleolar and nuclear morphologies in Lamin B2-depleted cells. Immunoblotting showed that the expression levels of full-length Lamin B2 and the deletion mutants were comparable in control and Lamin B2-depleted cells (Fig. 3.15A). We next expressed full-length Lamin B2 and its deletion mutants in DLD1 cells and examined nucleolar morphology by Nucleolin staining (Fig. 3.15B). We first examined the effect of overexpressing full-length siRNA-resistant Lamin B2 on nucleolar morphology in Lamin B2-depleted cells. Overexpression of full-length Lamin B2 in control cells reduced the number of disrupted nucleoli in control cells. Moreover, disrupted nucleoli induced upon Lamin B2 knockdown were also rescued to intact nucleoli upon overexpression of Lamin B2 in ~81% cells (Fig. 3.15B, C).

Transfection of the deletion constructs of Lamin B2 did not alter nucleolar morphology in control cells (Fig. 3.15B, D). Notably, the disrupted nucleolar morphology in Lamin B2-depleted cells was not restored to intact nucleoli upon overexpressing the Lamin B2 mutant lacking the head domain (Fig. 3.15B, C), while overexpression of the Lamin B2 mutant lacking the SLSATGR amino acid sequence at the tail domain restored intact nucleolar morphology in ~85% of the cells (comparable to the case for full-length Lamin B2) (Fig. 3.15B, C), suggesting that the SLSATGR sequence is dispensable for the maintenance of intact nucleoli. Taken together, the results show that the head domain of Lamin B2 is required for maintaining intact nucleolar morphologies. Lamin B2 knockout induces severe defects in the nuclear envelope (Coffinier et al., 2011).

Figure 3.15

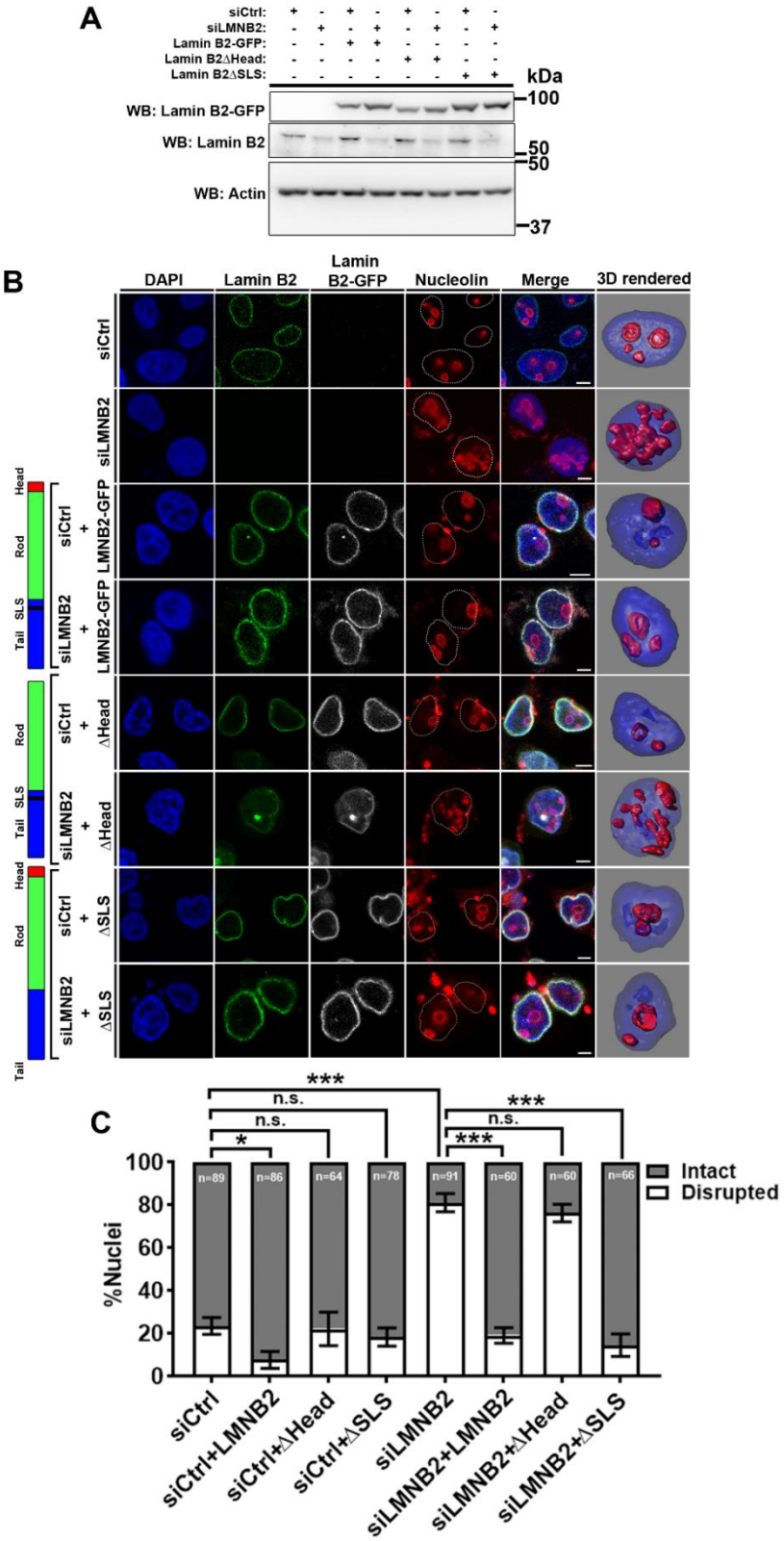

Figure 3.15. Lamin B2 head domain maintains nucleolar morphology

A. Western blot showing overexpression of siRNA-resistant full-length Lamin B2-GFP, Lamin B2ΔHead-GFP, and Lamin B2ΔSLS-GFP mutants in control and Lamin B2-depleted cells. The loading control was actin. **B.** Immunofluorescence staining of Nucleolin, showing the nucleolar morphology in control and Lamin B2-depleted cells overexpressing (i) full-length Lamin B2-GFP (+LMNB2), (ii) Lamin B2ΔHead (+ΔHead), and (iii) Lamin B2ΔSLS (+ΔSLS) constructs. Scale bars ~5 μm. **C.** Intact nucleolar morphology was restored upon overexpression of full-length Lamin B2 (siLMNB2+LMNB2) and Lamin B2ΔSLS (siLMNB2+ΔSLS) but not upon overexpression of Lamin B2ΔHead (siLMNB2+ΔHead). Fisher's exact test of proportions. *p<0.05, ***p<0.001, n.s., not significant. N=3 independent biological replicates, n: number of nuclei. Error bars: SEM.

We wanted to determine if Lamin B2 mutants exert mutually exclusive effects on the nucleolar and nuclear morphologies. To this end we examined the effect of Lamin B2 depletion on nuclear morphology. Confocal imaging of DLD1 cells immunostained for Lamin B1 consistently revealed a homogenous population of ellipsoidal nuclei, with a regular and uniform nuclear envelope (Fig. 3.16A, siCtrl). A small subpopulation (~1%) of control cells, however, showed nuclear blebs (Fig. 3.16B). Remarkably, Lamin B2 knockdown induced the formation of nuclear blebs in ~25% of DLD1 cells (Fig. 3.16A [siLMNB2, arrowhead], B). Overexpression of full-length Lamin B2 decreased nuclear blebs from ~25% to ~3% in Lamin B2-depleted cells (Fig. 3.16B, siLMNB2+LMNB2), while overexpression of Lamin B2ΔHead also reduced nuclear blebs to ~3% (Fig. 3.16B, siLMNB2ΔHead). In contrast, overexpression of Lamin B2ΔSLS mutant, did not reduce the extent of nuclear bleb formation in Lamin B2-depleted cells (Fig. 3.16B, siLMNB2ΔSLS), suggesting that the SLSATGR sequence is indeed required for maintaining normal and bleb-free nuclear morphology, while the head domain of Lamin B2 is dispensable for the same. We also found that overexpression of full-length Lamin B2, Lamin B2ΔHead, or Lamin B2ΔSLS did not induce nuclear blebs in control DLD1 cells (Fig. 3.16B). In summary, the analyses of Lamin B2 mutants was revealing at the mechanistic level, as this unraveled a distinct separation of function of Lamin B2 in independently modulating nucleolar and nuclear morphologies.

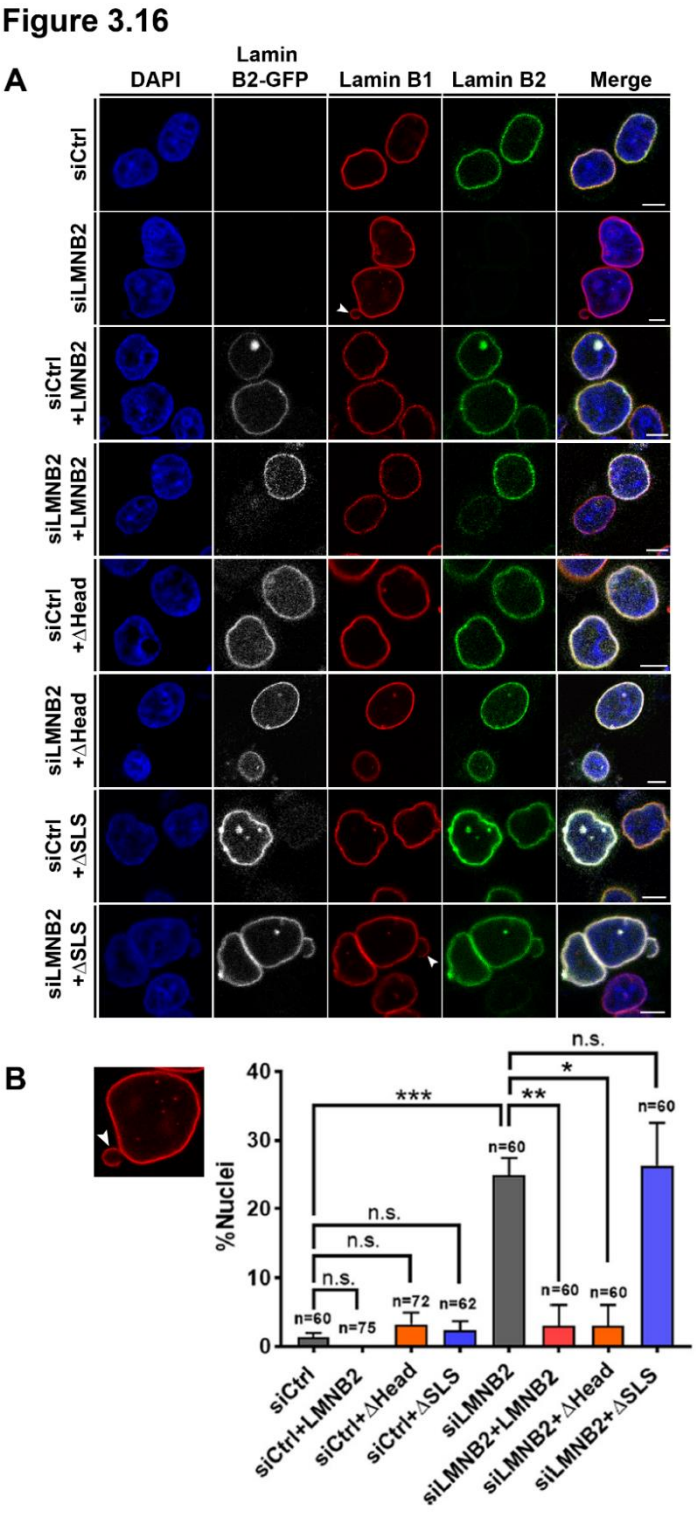

Figure 3.16. The SLSATGR sequence in the Lamin B2 tail domain maintains nuclear morphology

A. Immunofluorescence staining of Lamin B1, showing the nuclear morphology in control and Lamin B2-depleted cells overexpressing full-length Lamin B2-GFP (+LMNB2), (ii) Lamin B2ΔHead (+ΔHead), and (iii) Lamin B2ΔSLS (+ΔSLS) constructs. Control cells show ellipsoidal nuclei with uniform Lamin B1 staining at the nuclear periphery. Lamin B2-depleted cells show nuclear blebs that partially stain for Lamin B1 (arrowhead). Scale bars ~5 μm. **B.** The incidence of nuclear blebs in Lamin B2 depleted cells was reduced upon overexpression of full-length Lamin B2 (siLMNB2+LMNB2) and Lamin B2ΔHead (siLMNB2+ΔHead) but not upon overexpression of Lamin B2ΔSLS (siLMNB2+ΔSLS). Student's t test, *p<0.05, **p<0.01, ***p<0.001. N=3 independent biological replicates, n: number of nuclei. Error bars: SEM.

3.3. Discussion

Altered nucleolar morphology in cancer cells

Irregular nucleolar structures in carcinomas were first described by Pianese (Pianese, 1896). Thereafter, Ploton et. al. showed that nucleoli were were more intensely stained by silver stain in prostatic cancer compared to normal lymphocytes (Ploton et al., 1986). Enhanced silver staining of nucleoli denote an increase in argyrophilic proteins like UBF, RNA Pol I, Nucleolin and NPM1, in the nucleolus (Williams et al., 1982). Thus, cancer cells are usually associated with enhanced ribosome biogenesis activity to meet their increased requirement for protein sythesis (Belin et al., 2009; Derenzini et al., 1998). However, similar to previous observations of nucleoli in malignant tissue samples, our study reinstates that nucleolar morphology is highly variable in cancer cells and is potentially impacted by the fraction of proliferative cells present in the population (Fig. 3.3) (Derenzini and Ploton, 1991). Higher expression levels Nucleolin and Nucleophosmin usually co-relate with lower doubling time and faster proliferation of cells (Derenzini et al., 1998). In our study, we find corelation between increase in aggregated nucleolar morphologies with an increase in Nucleolin levels (Fig. 3.3). However, in this study, this co-relation only holds true for colorectal cancer cells, suggesting that Nucleolin could be an important factor in modulating nucleolar morphology in colorectal cancer cells. A larger repertoire of cell lines would have to be assessed to conclusively tell if higher Nucleolin levels indeed co-relate with nucleolar aberrations in other cell types.

Nucleolin and NPM1 are also important proteins that maintain nucleolar structure as prolonged loss of these proteins lead to nucleolar disruption (Amin et al., 2008; Ugrinova et al., 2007). Biophysical studies on *Xenopus* GV nucleoli show that nucleoli behave like liquid droplets that fuse when they contact each other and their volumes follow a power law distribution (Brangwynne et al., 2011). Further the physical properties of nucleolar proteins such as NPM1 and Fibrillarin, impart surface tension to the nucleolus, such that they assume a spherical shape (Feric et al., 2016). We do not know how post-translational modifications (PTMs) of Nucleolin and NPM1, affect their surface tension. It remains to be assessed if the PTMs of Nucleolin and NPM1 are dysregulated in cancer cells with subsequent changes in nucleolar morphology. It is suprising that volumes of nucleoli in cancer cells do not scale with their aggregated phenotype (Fig. 3.3). This possibly suggests that aggregated morphology of the nucleolus do not appear from fusions of adjacent nucleoli, rather once nucleoli are formed after mitosis, structural proteins are required to maintain their spherical shape, in absence of a surrounding membrane.

Intact nucleoskeleton is required to maintain nucleolar structure

The nucleoskeleton could thus serve as a platform to maintain the nucleolar structure, once nucleoli form. Lamins and nuclear actin are the major constituents of nucleoskeleton, required to co-ordinate many nuclear functions like DNA replication, transcription and mRNA export (Shumaker et al., 2003). *Xenopus* cells show enormous amounts of F-actin in the nucleus (Bohnsack et al., 2006). Nuclear actin is important to maintain discrete nucleoli in these cells as upon actin disruption by Cytochalasin D treatment, nucleoli merge with each other (Feric and Brangwynne, 2013). This suggests that nucleoskeletal tension is required to maintain discrete nucleoli. Human cells on the contrary show little nuclear F-actin due to the expression of Exportin 6 that exports actin-profilin complex outside the nucleus (Stüven et al., 2003). We surmise that in the absence of nuclear F-actin, Lamins play a predominat role in maintaining nucleolar structure. The localization of Lamin B2 around nucleoli is consistent with very early electron microscopic (EM) studies, which revealed pan-intermediate filaments connecting the nucleolus to the nucleoskeleton, at a time when specific antibodies towards Lamins were not available (Hozák et al., 1995). We surmise that Lamin B2 functions as a structural tether between the nucleolus and the nucleoskeleton, and the ensuing loss of nucleoskeletal tension upon Lamin B2 depletion, disrupts nucleolar structure.

Lamin B2 mutants exert mutually exclusive effects on nucleolar and nuclear morphologies

Lamins form structured polymers at the nuclear envelope as revealed by cryo-electron tomography and three-dimensional structured illumination microscopy (3D-SIM) (Shimi et al., 2015; Turgay et al., 2017). Lamins homo- or heterodimerize in vitro via their rod domains (Heitlinger et al., 1991). Lamin dimers form head-to-tail parallel polymers, which laterally associate to form stacks of lamin filaments (Heitlinger et al., 1992). We surmise that Lamin B2 organization at the nuclear periphery is strikingly different from that at the nucleolar border, owing to its stable association with Lamin A/C and B1 at the nuclear periphery (Fig. 3.11). The head domain of Lamin B2 is required for the head-to-tail polymerization of Lamin B2 dimers. Head domain deletion mutants of chicken Lamin B2 and mouse Lamin A do not form head-to-tail polymers in vitro (Heitlinger et al., 1992; Isobe et al., 2007). However, in mammalian cells, Lamin AΔHead did not localize at the nuclear periphery and showed nuclear aggregates, while Lamin B1ΔHead correctly localized to the nuclear periphery, with no effect on endogenous lamins (Izumi et al., 2000). This suggests differential localization and function of the head domains of A-type and B-type lamins at the nuclear envelope. Interestingly, our studies suggest that the head domain of Lamin B2 is required for maintaining nucleolar morphology but not nuclear morphology (Fig. 3.15 and 3.16).

It is possible that Lamin B2 forms head-to-tail polymers at the nucleolar periphery in order to maintain the spherical morphology and discrete organization of the nucleolus. A

possibility remains that the Lamin B2ΔHead mutant heterodimerizes with endogenous Lamin A/C or Lamin B1 via its rod domain at the nuclear envelope, thereby rescuing the extent of nuclear blebs (Georgatos et al., 1988).

Nuclear rupture and nuclear blebs during cancer cell migration are enhanced upon Lamin B2 depletion (Denais et al., 2016). Consistent with previous reports, nuclear blebs were enriched in regions of the nuclear membrane with reduced Lamin B1 levels (Fig. 3.16, arrowhead) (Denais et al., 2016; Funkhouser et al., 2013). The tail domains of lamins with the CAAX motif and IgG fold are required for their integration into the nuclear membrane and interaction with emerin and histones (Krohne et al., 1989; Sakaki et al., 2001; Taniura et al., 1995). It is interesting that the relatively uncharacterized and unique amino acid stretch SLSATGR in the C-terminal region of Lamin B2 modulates the formation of nuclear blebs (Fig. 3.16). This shows that the SLSATGR sequence is required for the proper organization of the nuclear lamina, as its absence increases the propensity for nuclear blebs.

In summary, we show that in addition to providing mechanical and structural integrity to the nucleus (Coffinier et al., 2011), Lamin B2, and its head domain in particular, is required for maintaining the intact and discrete morphology of the nucleolus. Lamin B2 potentially exerts its nucleolar function by localizing at the nucleolar border and by associating with nucleolar factors such as Nucleolin and Nucleophosmin.

Figure 3.17

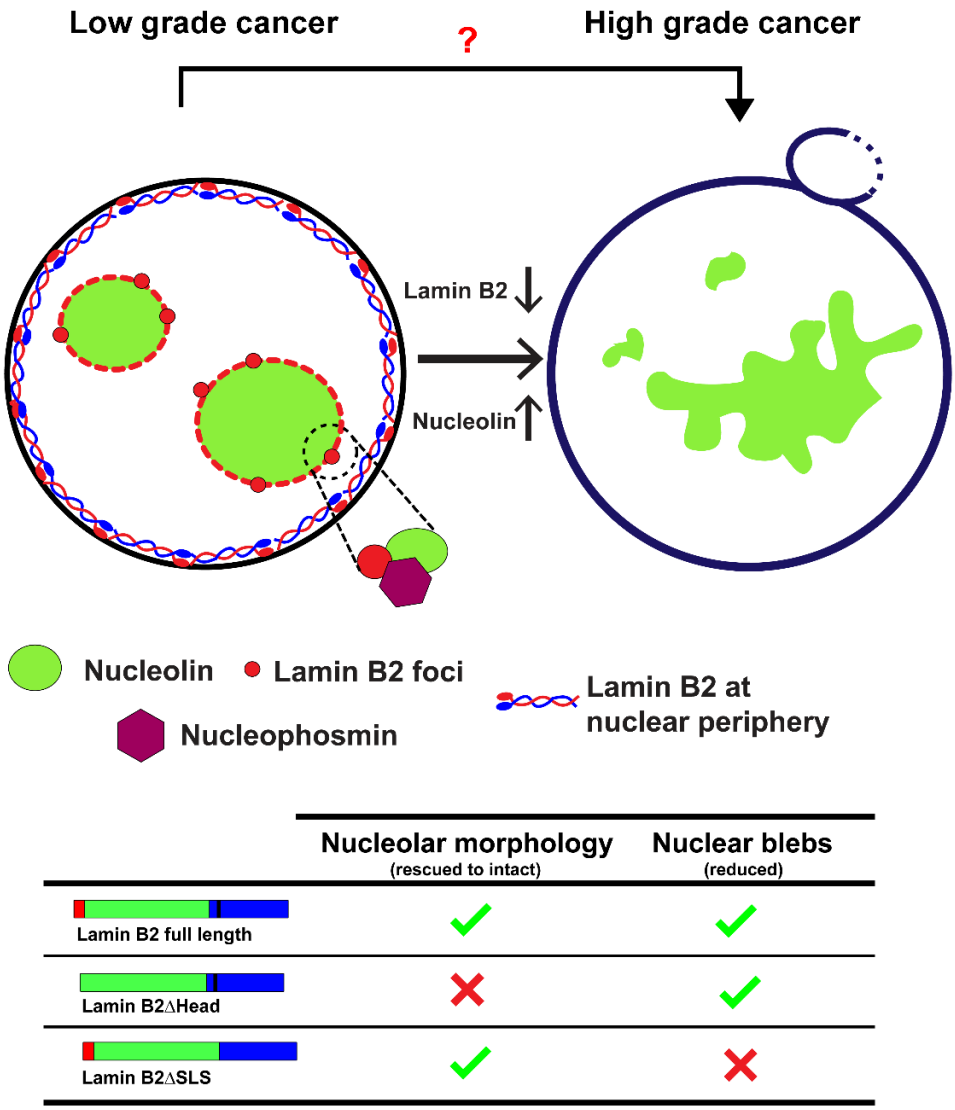

Figure 3.17. Model depicting role of Lamin B2 in modulating nucleolar structure
Higher grade of cancers co-relate with increased nucleolar aggregates and Nucleolin expression levels. Lamin B2 is localized predominantly at the nuclear periphery. However, Lamin B2 also localizes at the nucleolar border and potentially interacts with Nucleolin and NPM1. Lamin B2 depletion shows disrupted nucleolar morphology. The Lamin B2 head domain is required for the maintenance of intact nucleolar morphology, while the Lamin B2 SLSATGR amino acid sequence is required for maintaining bleb-free nuclei.

Chapter 4:

Impact of Lamin B2 on nucleolar function and dynamics

Results from this chapter are published as a part of the following paper –

Sen Gupta, A., and Sengupta, K. (2017). Lamin B2 modulates nucleolar morphology, dynamics, and function. Mol. Cell. Biol. *37*, e00274-17.

4.1. Introduction

The nucleolus is a multifunctional nuclear sub-organelle whose main function is the production of ribosomal RNA (rRNA), its processing and packaging into pre-ribosomes. The nucleolus assembles on the p-arms of NOR bearing chromosomes that harbor several repeats of ribosomal DNA. A recent study showed that humans and mice show high variability in rDNA copy numbers from (Human: 14-410; Mouse: 31-289 copies of 45S) (Gibbons et al., 2015), while only ~ 50% of these genes are actively transcribed (Birch and Zomerdijk, 2008; Miller and Beatty, 1969; Moss and Stefanovsky, 2002). Loss in the copy numbers and deregulation of methylation patterns of rDNA, are seen in pathological conditions like cancer and neurodegenerative disorders – dementia with Lewy bodies (DLB) and Alzheimer's disease (Hallgren et al., 2014; Pietrzak et al., 2011; Xu et al., 2017). It is surprising that cancer cells with higher requirement for ribosome biogenesis, would show a loss of copy numbers of ribosomal DNA, however this loss has been seen to be associated with an increase in growth inducing mTor signaling (Xu et al., 2017).

Each ribosomal transcription unit in humans is ~43 kbp long, with ~13 kbp coding sequences and ~30 kbp of intergenic sequence comprising of regulatory elements (Fig. 3.1). Upstream of the rRNA start site is the rDNA promoter and ~100 bp upstream of this lie the upstream control elements (UCE) required for rRNA gene transcription. The pre-initiation complex TIF1B/SL1 recruits RNA Polymerase I to the rDNA promoter. Further upstream are located spacer promoters and spacer terminators (T_{SP}). The rDNA gene is flanked on the 5' end by a single termination site (T_0) and on the 3' end by multiple termination sites (T_1-T_{10}), which are bound by TTF-I to terminate rDNA transcription. The rRNA gene is further divided into coding sequences for 18S, 5.8S and 28S rRNA, interspersed by internal transcribed sequences (ITS1 and ITS2), respectively. Transcription of rDNA generates relatively short lived 47S precursor RNA, which is immediately cleaved at sites in the 5' and 3' ETS to generate the 45S rRNA. 45S rRNA is further processed in multiple steps to produce the 18S, 5.8S and 28S rRNAs (Henras et al., 2015).

Transcription of rDNA and processing must be critically regulated in cells to meet their metabolic demands. For example during lack of nutrient availability rDNA transcription is shut off, while early developing *Xenopus* embryos show progressive increase in rRNA expression (Bird et al., 1981; Kang et al., 2016). Cells do not necessarily need a change in rDNA copy numbers to modulate rRNA expression as this is can be achieved by varying the rate of transcription per gene or by varying the proportion of active and inactive rRNA genes.

Figure 4.1

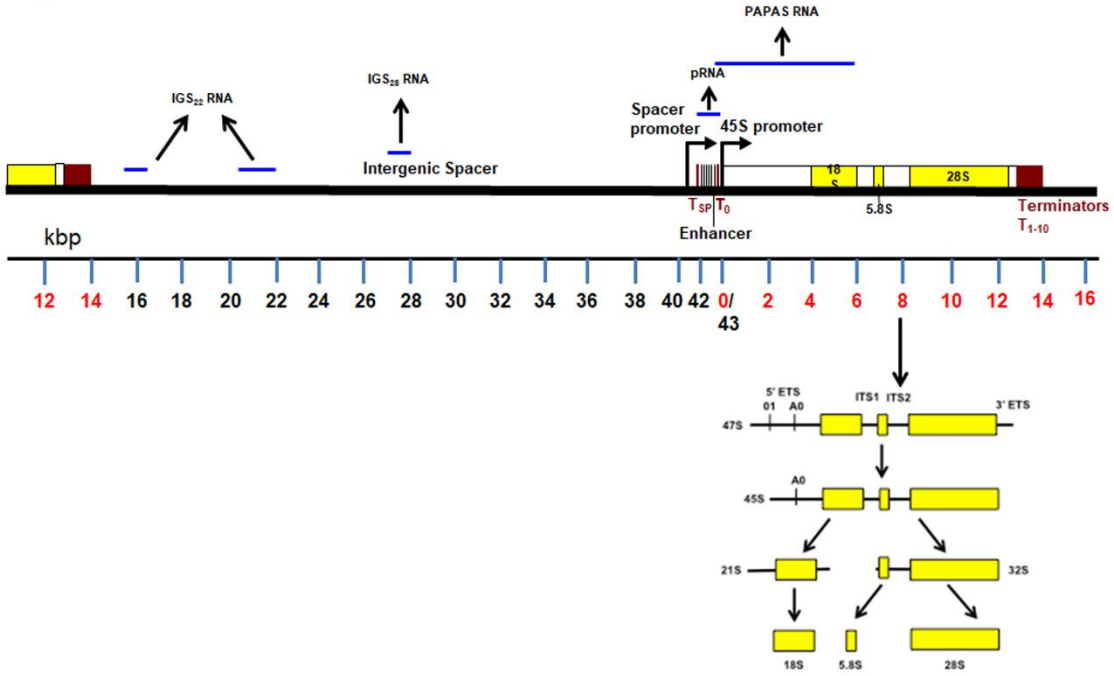

Figure 4.1. Organization of ribosomal DNA genic and intergenic regions.
Ribosomal genes organized as repeats on p-arms of NOR chromosomes. Coding regions are interspersed by intergenic regions. T_{SP} – Spacer terminator, T_0 – Termination site, T_{1-10} – termination sites, ETS – External transcribed sequence. rDNA is transcribed in a 47S pre-rRNA that is immediately cleaved into 45S pre-rRNA by cleavage at site 01 in the 5'-ETS and the 3'-ETS. Subsequent processing events yield the 18S, 5.8S and 28S rRNA. Non-coding RNAs are transcribed from intergenic regions.

Epigenetic regulators of ribosomal DNA transcription

Ribosomal DNA repeats exist in two distinct chromatin states - transcriptionally active euchromatic "open" state and repressed heterochromatic state, as revealed by psolaren cross-linking experiments (Conconi et al., 1989; Stancheva et al., 1997). Each chromatin state of rDNA have specific epigenetic marks associated with itself. Transcriptionally active euchromatic rDNA is associated with DNA hypomethylation, histone H4 acetylation, histone H3 dimethylation (H3K4me2). Repressed heterochromatic rDNA repeats are associated with DNA hypermethylation, histone H4 hypoacetylation, H3K9me3, H3K27me3 and H4K20me3. The transcription termination factor (TTF-I) binds to the T0 site upstream of rDNA promoter and can induce either active or repressive states of rDNA depending on its interactions with transcriptional activators or repressors. Recruitment of the DNA dependent ATPase CSB (Cocayne Syndrome protein B) and the histone methyltransferase G9a by TTF-I promotes rDNA transcription and elongation. On the other hand, TTF-I recruits Tip5 (TTF-I Interacting

protein 5), the large subunit of the NoRC (Nucleolar remodeling complex) at T_0, which induces heretochromatic marks on rDNA by further recruiting histone modifiers (HDAC1) and DNA methyltransferases (Dnmt1 and Dnmt3) (Santoro and Grummt, 2005; Santoro et al., 2002; Zhou et al., 2002). Although depletion of Dnmt1 affects rDNA promoter CpG methylation and nucleolar organization, this is not sufficient to increase rate of rDNA transcription (Espada et al., 2007).

Nucleolar retention of protein complexes by intergenic non-coding RNAs

Although the intergenic regions of ribosomal DNA were initially considered transcriptionally inactive, studies have now shown expression of multiple non-coding RNAs from these intergenic sites. Mouse cells express pRNAs (promoter associated RNA) that are 150-250nt long, transcribed by RNA Pol I from the spacer promoters located ~2kbp upstream of the rDNA promoter (Santoro et al., 2010). The pRNAs associate with Tip5 and promote NoRC mediated rDNA silencing. Interaction of Tip5 with pRNA is required for its nucleolar localization (Schmitz et al., 2010). PAPAS (promoter and pre-rRNA antisense) are long non-coding (lnc) RNAs transcribed in the antisense direction of rRNA by RNA Polymerase II during quiescence, serum starvation and heat-shock. PAPAS recruits Suv4-20h2 and CHD4 complex to rDNA and promotes H4K20me3, thus negatively regulating rDNA transcription (Bierhoff et al., 2010, 2014; Zhao et al., 2016a). Further, IGS_{22} and IGS_{28} RNAs are transcribed from ~22kbp and 28kbp upstream of rRNA start site during heat shock and acidosis response, respectively. These ncRNAs sequester Hsp70 and von-Hippel Lindau (VHL) tumor suppressor protein into the nucleolus, thereby reducing rRNA transcription during such stresses, and also acts as a means for post-translational regulation for these proteins (Audas et al., 2012; Mekhail et al., 2006).

Role of RNAs in the maintenance of nucleolar structure

Nucleolar structure is integrally connected to its function, hence inhibition of RNA Pol I mediated rRNA synthesis by Actinomycin D, greatly affects nucleolar structure (Shav-Tal et al., 2005). Further, inhibition of RNA polymerase II by α-amanitin also shows nucleolar disruption, due to decreased abundance of intronic Alu-element containing RNAs (Alu RNA) (Caudron-Herger et al., 2015). Although the exact role of Alu RNAs in maintaining nucleolar structure is unknown, these RNAs were shown to upregulate pre-rRNA synthesis in cells (Caudron-Herger et al., 2015). Further, inhibition of pre-rRNA synthesis in the nucleolus and accumulation of unprocessed rRNA is seen in interphase pre-nucleolar bodies (iPNBs) that appear upon hypotonic stress (Musinova et al., 2016; Zhao et al., 2016a). The synthesis of pre-rRNA in the nucleolus and processing of RNAs in iPNBs resumes upon returning cells to

isotonic medium, thus allowing transfer of Nucleophosmin from iPNBs to the nucleolus (Musinova et al., 2016). This shows that rRNA not only regulates nucleolar function but are also required for the stability of nucleolar structure.

With this background and having seen that Lamin B2 depletion causes such large-scale nucleolar disruptions, we asked the following questions in this chapter – (i) Does Lamin B2 depletion affect nucleolar function of rRNA synthesis? (ii) Does Lamin B2 depletion affect modulators of rRNA transcription? (iii) Does Lamin B2 regulate non coding RNA expression from the rDNA locus? and (iv) Do non-coding RNAs play a role in regulating dynamics of nucleolar proteins?

4.2. Results

4.2.1. Impact of Lamin B2 depletion on nucleolar function

Since we observed strikingly disrupted nucleolar morphologies in cells upon depletion of Lamin B2, we determined the effect of Lamin B2 knockdown on nucleolar function.

4.2.1.1. Lamin B2 depletion increases ribosomal and intergenic RNA expression

The primary function of the nucleolus is transcription of ribosomal RNA (rRNA) which is transcribed as a 47S/45S precursor and further processed into 28S, 5.8S, and 18S rRNAs (Fig. 4.1, 4.2A) (Boisvert et al., 2007). We examined the expression levels of 45S pre-RNA upon Lamin B2 depletion using quantitative real-time PCR (qRT-PCR) (Fig. 4.2B). Remarkably, cells showed a significant increase in the levels of the RNA Pol I-transcribed 45S pre-rRNA (fold change, ~2.7) upon Lamin B2 depletion (Fig. 4.2B). As a control, we also examined the expression levels of the RNA Pol II transcribed, non-nucleolar long ncRNA MALAT1, upon Lamin B2 knockdown (Fig. 4.2B). Expression levels of MALAT1 remained unaffected in Lamin B2 depleted cells.

To ascertain the specificity of 45S pre-rRNA upregulation, we inhibited the RNA Pol I activity by its inhibitor Actinomycin D (Act D, 0.05µg/ml). As expected, 45S pre-rRNA expression significantly declined (~84% decrease, fold change – 0.16) upon Act D treatment (Fig. 4.2B, siCtrl+Act D). 45S pre-rRNA was also significantly reduced in Lamin B2 depleted cells upon Act D treatment (fold change ~0.38). This showed that 45S upregulation upon Lamin B2 depletion was specific and is repressed by the inhibition of RNA Pol I activity. Expression levels of 28S and 18S processed rRNA transcripts were not significantly altered upon Lamin B2 depletion suggesting that Lamin B2 depletion may not affect processing of 45S pre-rRNA (Fig. 4.2B). Since Act D treatment affects production of newly transcribed pre-rRNA and not rRNA processing, 28S and 18S levels remained unaltered upon Act D treatment. Taken together, these findings reveal a unique role for Lamin B2 and underscores its specificity in upregulating 45S pre-rRNA levels.

Figure 4.2

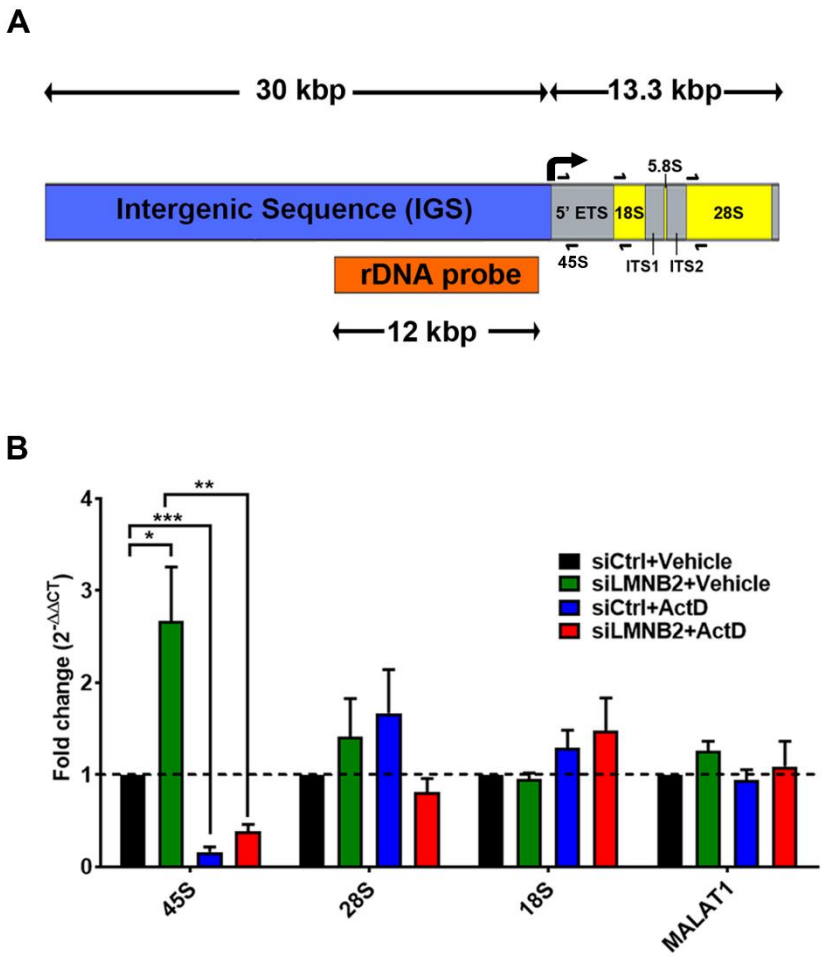

Figure 4.2. rRNA expression increases upon Lamin B2 knockdown
A. Schematic representation of the rDNA encoding the ~13.3-kbp 45S rRNA and ~30-kbp intergenic sequence. The primer pairs used for qRT-PCR (half arrows) and the ~12-kbp probe for RNA-FISH are indicated. **B.** qRT-PCR shows a significant increase in 45S transcript levels upon Lamin B2 depletion. Act D treatment significantly reduces expression levels of the 45S rRNA transcript in both control and Lamin B2-depleted cells. Lamin B2 depletion does not show a significant change in the levels of 28S and 18S transcripts (number of independent biological replicates [N] = 3). MALAT1 expression levels are not altered upon Lamin B2 depletion and serve as a negative control (N = 3; *p < 0.05; **p < 0.01; ***p < 0.001 [by Student's t test]).

In addition to ribosomal RNA, several non-coding RNA transcripts are expressed from rDNA intergenic regions in response to serum starvation, heat shock, or acidosis (Audas et al., 2012; Santoro and Grummt, 2005; Zhao et al., 2016b). These include ncRNAs such as pRNAs, PAPAS RNA and IGS_{28}RNA. Interestingly, these ncRNAs regulate 45S pre-rRNA expression, or sequester chaperones like heat shock proteins (HSPs) and Von Hippel-Lindau tumor suppressor protein (VHL) into the nucleolus (Audas et al., 2012; Zhao et al., 2016b). Having detected an increase in 45S pre-rRNA levels, we determined if Lamin B2 depletion affects the expression of ncRNAs from rDNA intergenic regions. However, since the intergenic RNAs are not very well characterized, we examined expression and nuclear localization of non-coding RNAs from the intergenic region by RNA fluorescent *in-situ* hybridization (RNA FISH) (Fig. 4.3A) using a probe spanning a 12 kbp region upstream of the 45S rRNA start site.

RNA-FISH signals were as follows in the nucleus (i) a single IGS RNA focus (~65% of cells) (ii) 2 IGS RNA foci (~33% of cells) and (iii) >2 IGS RNA foci (~2% of the cells) (Fig. 4.3B, gray bars). RNase treatment of cells did not show IGS RNA signals, suggesting the specificity of RNA FISH. Lamin B2 depletion showed a marked decrease in cells with a single focus (~31% of the cells) and a concomitant increase in cells with 2 foci (~46% of the cells) and >2 foci (~23% of the cells) (Fig. 4.3B, white bars). This suggests that Lamin B2 depletion upregulates IGS RNA transcripts. Remarkably, Lamin B2 overexpression rescued levels of IGS RNA signals to a single focus (~71%), comparable to control cells (Fig. 4.3B, black bars). In summary, Lamin B2 upregulates levels of 45S pre-rRNA and nucleolus specific intergenic transcripts.

Figure 4.3

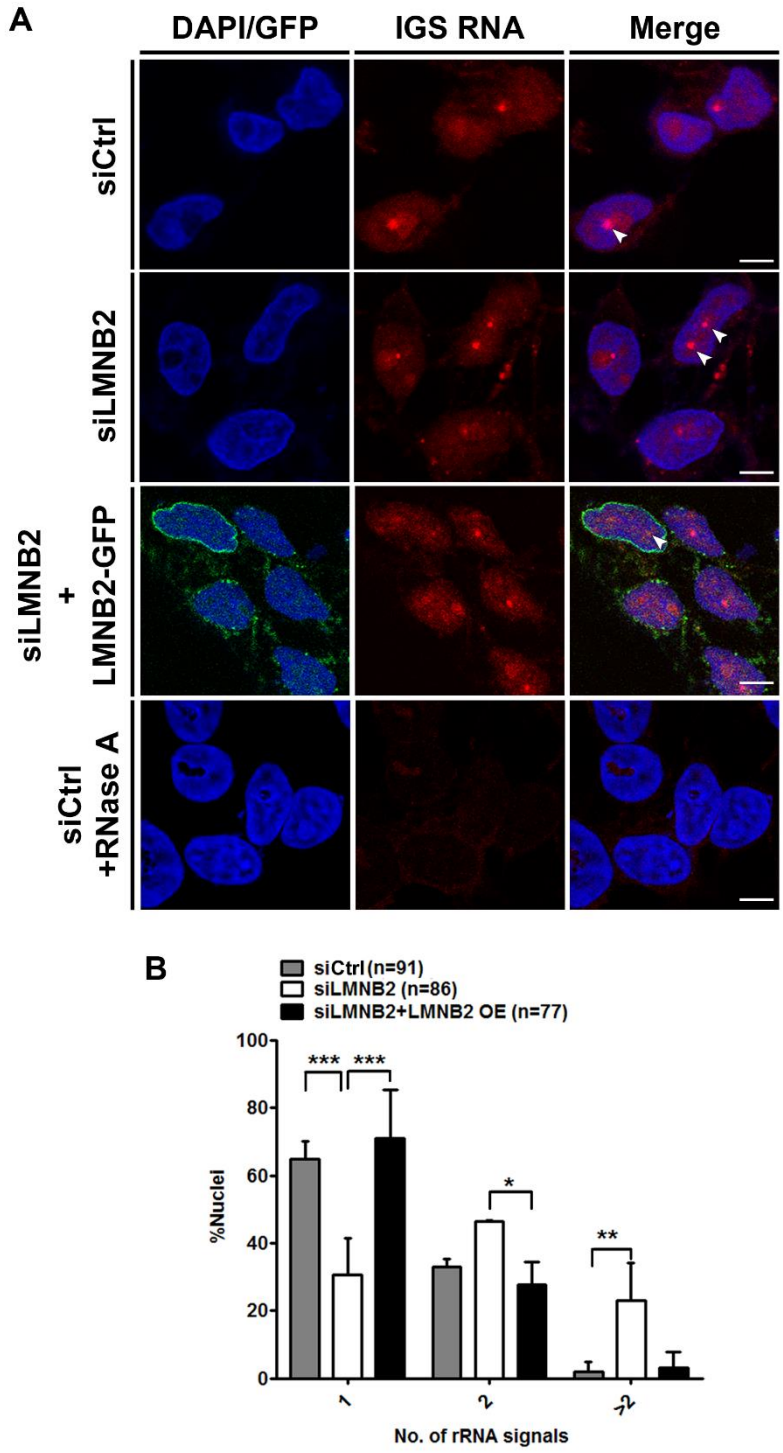

Figure 4.3. IGS RNA transcripts upregulated upon Lamin B2 knockdown
A. RNA-FISH labels intergenic sequence (IGS) RNA in the nucleolus. Lamin B2-depleted cells show amplification of IGS RNA (siLMNB2 panel, arrowhead). Overexpression of siRNA-resistant Lamin B2-GFP in Lamin B2-depleted cells (siLMNB2+LMNB2-GFP) restores the number of IGS RNA-FISH signals. The absence of RNA signals in cells upon RNase A treatment shows specificity of IGS RNA-FISH foci. Scale bar ~ 5µm. **B.** Quantification of RNA-FISH foci shows a significant increase (>2 foci) upon Lamin B2 depletion, while overexpression of Lamin B2 restores IGS transcripts to a single focus. Error bars, SD. (*P < 0.05; **P < 0.01; ***, P < 0.001 [by Fisher's exact test of proportions]) (N = 3, n, number of nuclei).

4.2.1.2. Lamin B2 depletion affects rDNA methyltransferase Dnmt1 – a regulator of nucleolar structure

To investigate the mechanisms by which Lamin B2 regulates rDNA transcription, we examined regulators of rDNA transcription (Fig. 4.4A). Methylation of rDNA promoters and enhancers by DNA methyltransferases is a key mechanism by which rDNA is regulated (Ghoshal et al., 2004). We examined the levels of DNA methyltransferase I (Dnmt1) in Lamin B2 depleted cells. Immunofluorescence assay of Dnmt1 revealed a punctate localization of Dnmt1 in the nucleoplasm of control cells (Fig. 4.4A). Quantification of the fluorescence intensity of Dnmt1 foci showed a significant reduction upon Lamin B2 depletion (Fig. 4.4B). Furthermore, Dnmt1 protein levels estimated by western blotting from whole cell lysates, also showed a significant reduction by ~40% (Fig. 4.4C). We surmise that the increase in rRNA expression upon Lamin B2 depletion is potentially mediated by loss of rDNA methylation by Dnmt1.

The inactive heterochromatin mark - H3K27me3 is localized as foci associated with heterochromatin towards the nuclear and nucleolar periphery (Fig. 4.4D) (Németh et al., 2010). Interestingly, H3K27me3 showed an overall increase in the entire nucleus upon Lamin B2 depletion and was not just limited to nucleolar chromatin (Fig. 4.4E, F). Taken together, this suggests that de-repression of rDNA transcription is independent of the levels of H3K27 trimethylation.

Suv39H1 mutant *Drosophila* S2 cells show destabilization of the HP1/heterochromatin marks that perturb nucleolar morphologies (Peng and Karpen, 2007). We sought to examine if Lamin B2 depletion affects the dynamics of perinucleolar heterochromatin that impinges on nucleolar morphology and rDNA transcription. HP1α-GFP – a marker of nuclear heterochromatin was enriched as foci within the nucleoplasm. Further, we detected HP1α foci surrounding the nucleolus (Fig. 4.4G, arrows). Photobleaching of HP1α-GFP foci in Lamin B2 depleted cells showed an increase in HP1α-GFP recovery within ~120 seconds of photobleaching (Fig. 4.4H, I). In summary, these results suggest that Lamin B2 modulates heterochromatin associated factors that potentially regulate levels and dynamics of nucleolar transcripts.

Figure 4.4

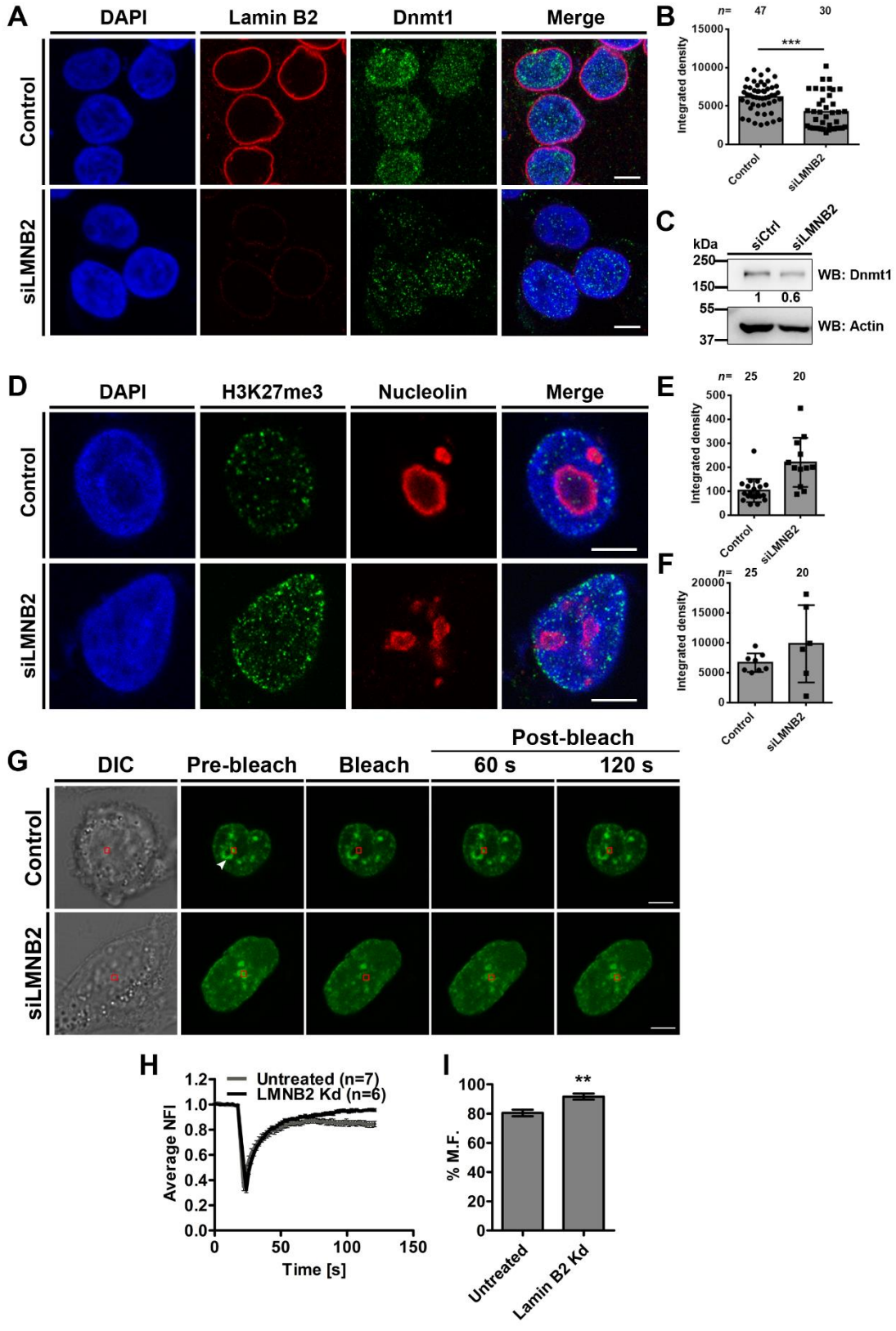

Figure 4.4. Lamin B2 depletion affects Dnmt1 and histone marks

A. Immunostaining for DNA methyltransferase (Dnmt1) in control and Lamin B2 knockdown cells. Scale ~ 5 μm. **B.** Quantification of total Dnmt1 intensity in control and Lamin B2 knockdown cells. N=2, n= number of nuclei. Student's t-test, ***p<0.001. **C.** Western blot showing Dnmt1 expression levels in control and Lamin B2 knockdown cells. Numbers below blot show relative quantification of

Dnmt1 levels calculated by Image J. N=1, data from a single experiment **D.** Immunostaining for H3K27me3 in control and Lamin B2 knockdown cells. Scale ~ 5 μm. **E.** Quantification of H3K27me3 intensity surrounding the nucleolus. **F.** Quantification of H3K27me3 in total nucleus. N=1, data from a single experiment, n=number of nuclei. **G.** FRAP of HP1α in control and Lamin B2 depleted cells. Red box: Photobleaching ROI. **H.** FRAP curve showing recovery of HP1α in control and Lamin B2 depleted cells. N=1, data from a single experiment, n=number of nuclei **I.** Percent mobile fraction (M.F.) of HP1α as calculated from (I). Student's t-test, **p<0.01.

4.2.1.3. Lamin B2 depletion affects gene families associated with ribosome biogenesis

Since we observed a deregulation of ribosomal DNA transcription upon Lamin B2 depletion, we were also interested to assess the global impact of Lamin B2 depletion on expression of genes involved in rDNA transcription, processing and assembly, from transcriptomic analyses of Lamin B2 knockdown cells.

(i) Pathways affected upon Lamin B2 depletion

We first performed **G**ene **O**ntology (GO) analyses of genes deregulated (both upregulated and downregulated) upon Lamin B2 depletion using the DAVID Functional Annotation Tool (Dennis et al., 2003). GO categories of genes dysregulated upon Lamin B2 depletion primarily include – (1) alternative splicing (2) positive regulation of cytoskeleton organization (3) chromosomal rearrangements (4) regulation of organelle organization (Fig. 4.5A, $p<0.05$). Furthermore, GO classification also revealed the following categories – (1) negative regulation of RNA metabolic process ($p<0.05$); and (2) translation, ribosomal structure and biogenesis ($p=0.05$) (Fig. 4.5A). The genes categorized under negative regulation of RNA metabolic process include *EHMT* which is an H3K9-methyltransferase with similar activity as SUV39H1; and *JARID2* (Jumonji- and AT-rich interaction domain (ARID)-domain-containing protein) which modulates methyltransferase activity of PRC2 complex and is a transcriptional repressor (Li et al., 2010; Tachibana et al., 2005). Although *JARID2* function with respect to ribosomal DNA transcription is not reported, it localizes in the nucleolus during spermatogenesis in *Drosophila* in a PRC2 dependent manner (Goto et al., 2016). In addition, a closely related Jumonji domain 2 family protein JMJD2A is a lysine demethylase and required for serum induced activation of rDNA transcription (Salifou et al., 2016). Thus *EHMT* and *JARID2* are likely downstream targets of Lamin B2 that modulate rDNA transcription. Additional genes categorized under translation, ribosomal structure and biogenesis include *NMD3* Ribosome export adaptor required for exit of 60S ribosome subunit through the nuclear pore into the cytoplasm (Ho et al., 2000), and *EXOSC2* which catalyzes 3'-to-5' processing of ribosomal RNA (Mitchell et al., 1996).

Figure 4.5

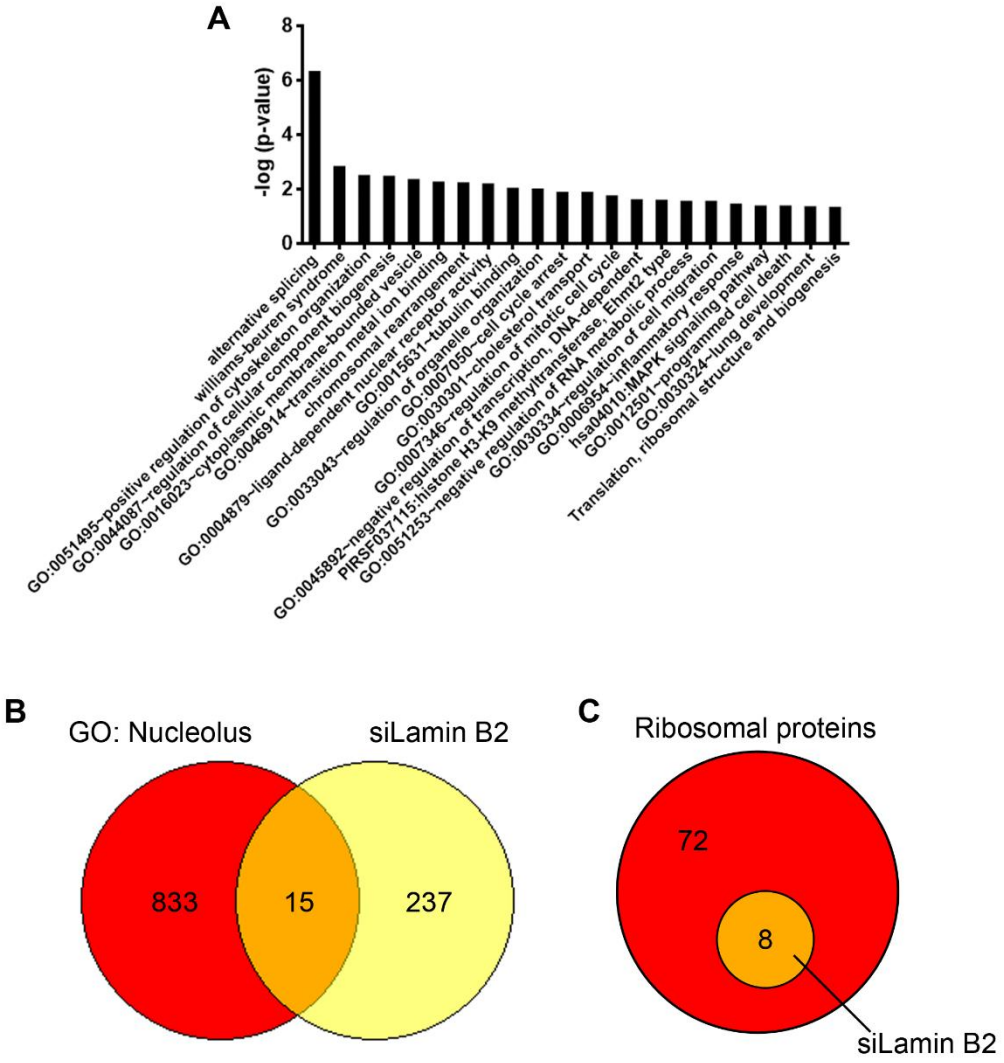

Figure 4.5. Microarray analysis of Lamin B2 depleted cells.
A. GO categories of genes dysregulated upon Lamin B2 knockdown in DLD1 cells. Y-axis represents $-\log_{10}$(p-value) of functional categories. $p<0.05$. **B.** Overlap of genes dysregulated (up- and downregulated combined) with genes annotated in GO_Nucleus from MsigDB. **C.** Overlap of ribosomal protein coding genes dysregulated upon Lamin B2 knockdown, with all 80 ribosomal protein coding genes.

(ii) Nucleolar genes are deregulated upon Lamin B2 depletion

We next examined differential regulation of 848 genes annotated under the specific geneset: GO_Nucleolus in the MSigDB (Fig. 4.5B). These genes encode for proteins that localize to the nucleolus and are involved in maintenance of nucleolar structure, multiple steps of ribosome biogenesis (e.g. *NCL*, *NPM1*, *BOP1*, *FBL*, *UBTF*, *TAF1A*, *TAF1B*, *RPL5*, *RPL7*, TTF1) and non-ribosomal nucleolar functions like DNA damage response (e.g. *TOP1*, *TCOF1*, *BLM*, *WRN*), cell cycle (*CCND2*, *CDC14B*, *MYC*) and apoptosis (e.g. *TP53*), to name a few. This analysis revealed that 15 out of 848 genes in the nucleolus were dysregulated upon Lamin B2 depletion (Fig. 4.5B, Table 4.1). Interestingly, all 15 genes in this category, were upregulated (≥1.2 fold on log scale) upon Lamin B2 depletion, which includes *MYC*, a known positive regulator of rDNA transcription (Table 4.1) (Li and Hann, 2013).

(iii) Ribosomal proteins affected upon Lamin B2 depletion

A comprehensive siRNA based screen by Nicolas et. al. revealed that depletion of ~20-24 out of 80 human ribosomal proteins affected nucleolar structure, pre-rRNA processing and p53 expression levels (Nicolas et al., 2016). We overlapped the Lamin B2 knockdown transcriptome with each of the 80 human ribosomal genes, to assess for altered gene expression levels (Fig. 4.5C). We found that 8 out of 80 ribosomal protein coding genes were deregulated upon Lamin B2 depletion, 7 out of these 8 genes – *RPL12*, *RPS18*, *RPS15*, *RPS16*, *RPL28*, *RPS5* and *RPL27A* were upregulated upon Lamin B2 depletion, whereas *RPS11* was downregulated (Fig. 4.4C, Table 4.2). Amongst these genes, dysregulation of *RPL27A* disrupts nucleolar structure (Nicolas et al., 2016).

Table 4.1. GO_Nucleolus genes dysregulated upon Lamin B2 knockdown

Gene Name	Description	Function
CDC14B	Cell Division Cycle 14B	Nucleolar dual-specificity phosphatase involved in DNA damage response, dephosphorylation and regulation of p53
CHD3	Chromodomain Helicase DNA Binding Protein 3	Component of the histone deacetylase NuRD complex. Among its related pathways are Chromatin organization and RNA Polymerase I Promoter Escape
CTSB	Cathepsin B	This gene encodes a member of the C1 family of peptidases, involved in the proteolytic processing of amyloid precursor protein (APP)
EXOSC2	Exosome Component 2	Catalyzes 3'-to-5' processing of ribosomal RNA
KLHL7	Kelch Like Family Member 7	Promotes TUT1 ubiquitination associated with nucleolar integrity
MYC	Proto-Oncogene C-Myc	Activates RNA polymerase (pol) I-mediated transcription of ribosomal RNA (rRNA) genes

Gene Name	Description	Function
NFIB	Nuclear Factor I B	Transcription factor essential in embryonic development and works together with its gene complex to initiate tissue differentiation in the fetus. Nucleolar function unknown.
NMD3	NMD3 Ribosome Export Adaptor	involved in the passage of the 60S subunit through the nuclear pore complex and into the cytoplasm
RPL12	60S Ribosomal Protein L12	component of the 60S subunit
RPP21	Ribonuclease P/MRP Subunit P21	Subunit of nuclear ribonuclease P. Among its related pathways are rRNA processing in the nucleus and cytosol. Localizes in the nucleolus when expressed at high levels.
RREB1	Ras Responsive Element Binding Protein 1	zinc finger transcription factor that binds to RAS-responsive elements (RREs) of gene promoters. Nucleolar function unknown.
SRPK2	SRSF Protein Kinase 2	involved in the phosphorylation of SR splicing factors and the regulation of splicing. Nucleolar function unknown
SURF6	Surfeit 6	May function as a nucleolar-matrix protein with nucleic acid-binding properties. Implicated in regulation of 18S rRNA and ribosome biogenesis
TERF1	Telomeric Repeat Binding Factor 1 (TRF1)	telomere specific protein which is a component of the telomere nucleoprotein complex. Nucleoplasmic concentration is regulated by sequestration into the nucleolus
ZNF655	Zinc Finger Protein 655	Encodes a zinc finger protein. May be involved in transcriptional regulation, nucleolar function unknown.

Table 4.2. Ribosomal proteins dysregulated upon Lamin B2 knockdown[#]

Small subunit		Large subunit		
RPSA	*RPS15A*	*RPL3*	*RPL18*	*RPL35*
RPS2	***RPS16***	*RPL4*	*RPL18A*	*RPL35A*
RPS3	*RPS17*	*RPL5*	*RPL19*	*RPL36*
RPS3A	***RPS18***	*RPL6*	*RPL21*	*RPL36A*
RPS4X	*RPS19*	*RPL7*	*RPL22*	*RPL37*
RPS4Y	*RPS20*	*RPL7A*	*RPL23*	*RPL37A*
RPS5	*RPS21*	*RPL8*	*RPL23A*	*RPL38*
RPS6	*RPS23*	*RPL9*	*RPL24*	*RPL39*
RPS7	*RPS24*	*RPL10*	*RPL26*	*RPL40*
RPS8	*RPS25*	*RPL10A*	*RPL27*	*RPL41*
RPS9	*RPS26*	*RPL11*	***RPL27A***	*RPLP0*
RPS10	*RPS27*	***RPL12***	***RPL28***	*RPLP1*
RPS11	*RPS27A*	*RPL13*	*RPL29*	*RPLP2*
RPS12	*RPS28*	*RPL13A*	*RPL30*	
RPS13	*RPS29*	*RPL14*	*RPL31*	
RPS14	*RPS30*	*RPL15*	*RPL32*	
RPS15		*RPL17*	*RPL34*	

[#]Genes significantly upregulated and downregulated (Fold change > 1.5 fold absolute scale, $p<0.05$) upon Lamin B2 knockdown are indicated in red and green, respectively.

4.2.2. Impact of Lamin B2 on nucleolar dynamics

4.2.2.1. Lamin B2 depletion enhances Nucleolin aggregation in the nucleoplasm

Active transcription by RNA polymerase I (Pol I) is essential for the maintenance of nucleolar structure and function (Shav-Tal et al., 2005). This was corroborated by actinomycin D (Act D)-mediated inhibition of RNA Pol I, which induces reorganization of Fibrillarin and UBF into nucleolar caps and dispersal of Nucleolin and NPM1 into the nucleoplasm (Shav-Tal et al., 2005). Act D treatment is a useful experimental paradigm to address the effects of potential regulators on the morphology and function of the nucleolus. We determined the effect of Lamin B2 depletion on the subnuclear localization of Nucleolin and nucleolar morphology upon Act D treatment. Immunostaining of Nucleolin in Act D-treated cells consistently showed cells with (i) smaller and hollow nucleoli (Fig. 4.6A, asterisk), (ii) nucleolar cap formation, and (iii) Nucleolin dispersion into the nucleoplasm (Fig. 4.6A, siCtrl+Act D, arrowhead). Furthermore, Nucleolin was enriched at the nuclear periphery, consistent with Nucleolin shuttling out of the nucleolus in Act D-treated cells (51). Act D treatment induced Nucleolin aggregates in the nucleoplasm (Fig. 4.6A, siCtrl+Act D, arrowhead). Of note, Lamin B2-depleted cells treated with Act D showed a significant increase in cells with Nucleolin aggregates (siCtrl, ~54%; siLMNB2, ~80%) (Fig. 4.6B) and an increase in their volume (~1.3-fold) (Fig. 4.6C). Notably, Fibrillarin co-localized with Nucleolin aggregates, suggesting the association of nucleolar RNA binding proteins within Nucleolin aggregates upon destabilization of the nucleolus (Fig. 4.7A). Fibrillarin also showed a relatively higher intensity in these aggregates upon Lamin B2 depletion (Fig. 4.7B).

Figure 4.6

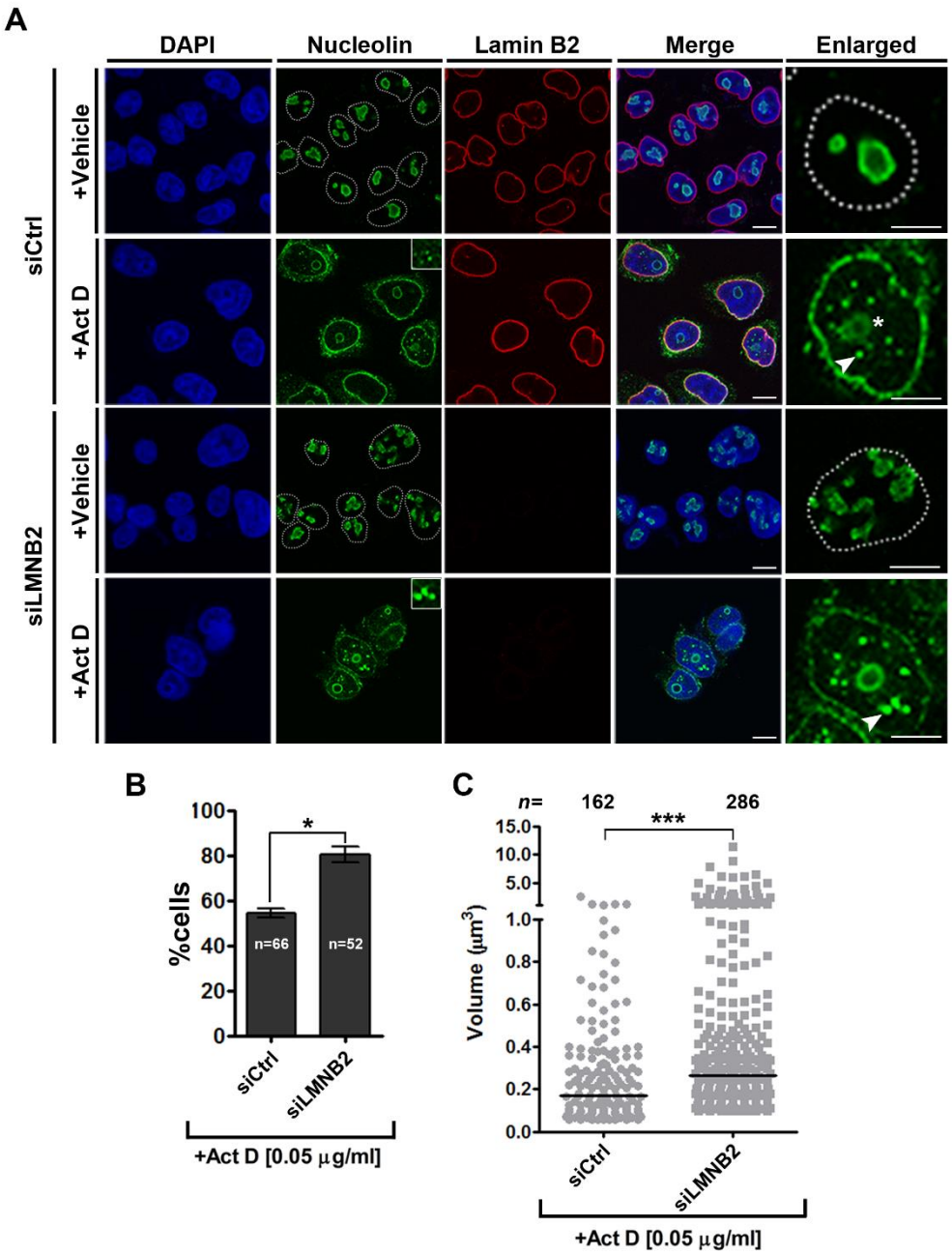

Figure 4.6. Lamin B2 depletion increases the volume of Nucleolin aggregates.
A. Control or Lamin B2-depleted cells were treated with DMSO (vehicle control) or actinomycin D (+Act D) and immunostained for Nucleolin. Vehicle-treated control (siCtrl) and Lamin B2-depleted (siLMNB2) cells show Nucleolin restricted to the nucleolus. Vehicle-treated Lamin B2-depleted cells show an irregular nucleolar morphology (siLMNB2+Vehicle panel). Act D-treated control (siCtrl+Act D) or Lamin B2-depleted (siLMNB2+Act D) cells show Nucleolin aggregates in the nucleoplasm (insets, enlarged panels [arrowhead]). Act D treatment shows spherical nucleoli (asterisk, enlarged panel). Scale bars ~5 µm. **B.** Lamin B2 depletion shows a significant increase in cells with Nucleolin aggregates upon Act D treatment (*$p < 0.05$ by Student's t test) (number of independent biological replicates [N] = 3; n, number of nuclei). Error bars indicate SEM. **C.** Scatter plots showing an increase in the volumes of Nucleolin aggregates upon Lamin B2 depletion followed by Act D treatment (***$p < 0.001$ by Mann-Whitney test). Bar, median (N = 3; n, number of aggregates; siCtrl, 32 nuclei; siLMNB2, 35 nuclei).

Figure 4.7

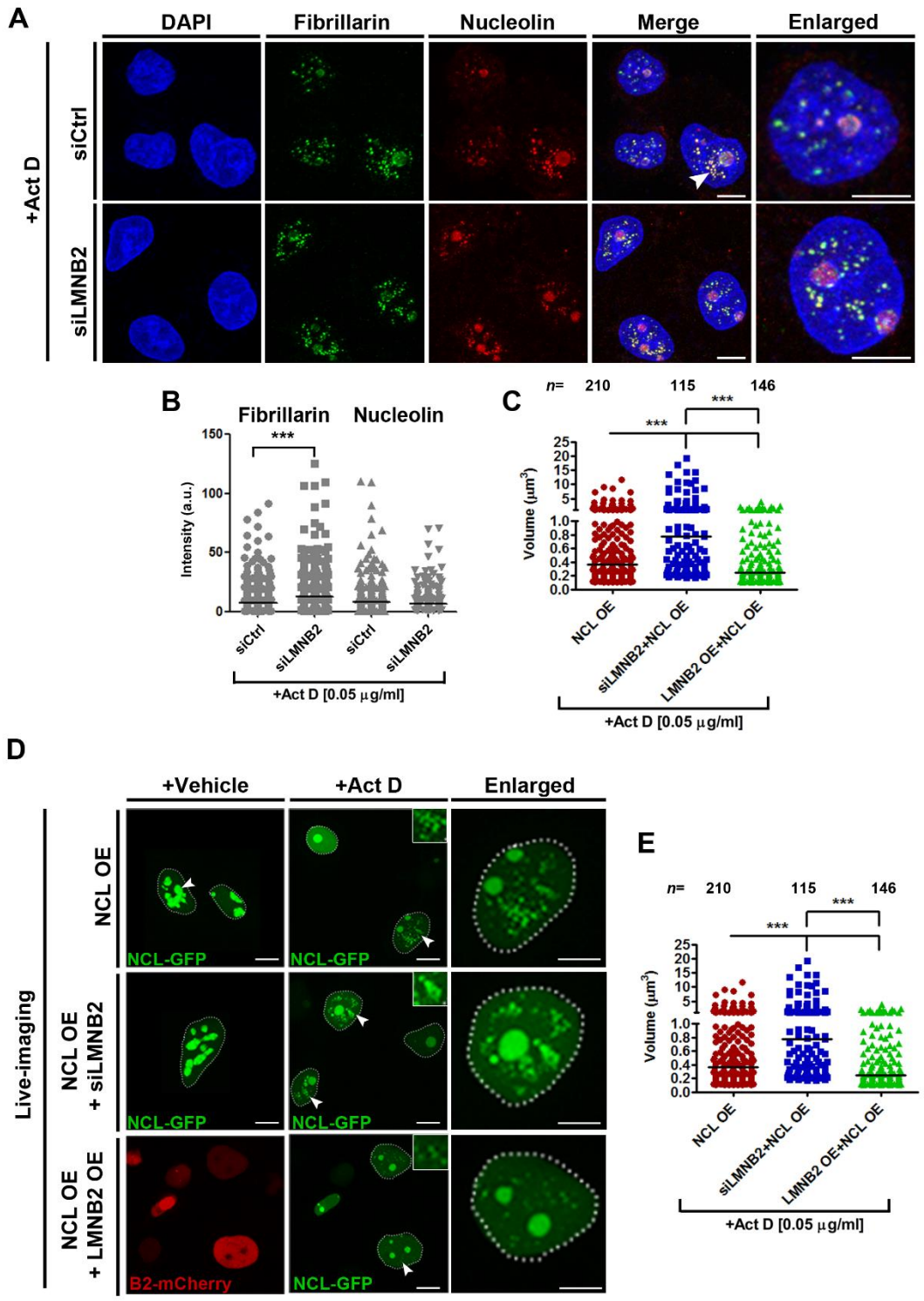

Figure 4.7. Nucleolin aggregates are rescued by Lamin B2 overexpression
A. Fibrillarin colocalizes with nucleolin aggregates upon Act D treatment (arrowhead). Scale bars ~5 µm. **B.** Lamin B2-depleted cells show a significant increase in Fibrillarin intensity within nucleolin aggregates (***p < 0.001 by Mann-Whitney test) (N=2; siCtrl, 28 nuclei; siLMNB2, 30 nuclei). **C.** Live imaging of DLD1 cells overexpressing nucleolin (NCL-GFP OE) following Act D or vehicle treatment. NCL-GFP-transfected cells phenocopy disrupted nucleolar morphology comparably to Lamin B2 depletion (NCL-GFP OE, arrowhead). Act D-treated cells show aggregates of nucleolin in the nucleoplasm (arrowhead). Lamin B2-depleted cells overexpressing nucleolin show relatively larger aggregates in the nucleoplasm (NCL OE+siLMNB2, inset). Cells co-expressing Lamin B2-mCherry and NCL-GFP show smaller aggregates, suggesting a rescue of the phenotype of Lamin B2 depletion (NCL OE+LMNB2 OE, inset). Insets, nucleolin aggregates. Scale bars ~5 µm. **D.** Scatter plots showing volumes of nucleolin aggregates. Lamin B2 depletion significantly increases the volumes of nucleolin aggregates (siLMNB2_NCL OE), while coexpression of Lamin B2 and nucleolin (LMNB2 OE+NCL OE) rescues the volume of nucleolin aggregates to basal levels. Bars, median (***p<0.001 by Mann-Whitney test) (N=3, n=number of aggregates; NCL OE, 30 nuclei; siLMNB2+NCL OE, 30 nuclei; LMNB2 OE+NCL OE, 25 nuclei).

We determined whether Lamin B2 modulates the status of Nucleolin aggregates in cells overexpressing Nucleolin. Interestingly, Nucleolin overexpression phenocopied the disrupted nucleolar morphologies that we consistently detect upon Lamin B2 depletion (Fig. 4.7C, NCL OE+vehicle, arrowhead). Additionally, Nucleolin overexpression showed Nucleolin aggregates in the nucleoplasm upon Act D treatment (Fig. 4.7C, D, NCL OE+Act D) (volume = 0.36 μm^3 (median)). Lamin B2 knockdown showed a significant increase in the volume of Nucleolin aggregates (M=0.77 μm^3) of ~2.13-fold, while Lamin B2 overexpression rescued the volume of Nucleolin aggregates to near-basal levels (M=0.25 μm^3) (Fig. 4.7C, D). In summary, Lamin B2 modulates Nucleolin aggregation in the nucleoplasm.

4.2.2.2. Nucleolin aggregates persist in the nucleoplasm upon Lamin B2 depletion

We determined the effect of Lamin B2 depletion on the dynamics of Nucleolin aggregates by live-cell imaging. This revealed a progressive increase in Nucleolin aggregates originating from the nucleolus, from ~40 min after Act D addition (Fig. 4.8A siCtrl, B). In control cells, nucleoplasmic aggregates of Nucleolin showed a steady decline and were hardly detectable after ~2 h, suggesting a dispersal of Nucleolin into the nucleoplasm (Fig. 4.8A, B [blue dots]). Remarkably, Nucleolin aggregates in Lamin B2-depleted cells persisted in the nucleoplasm even after ~3 h of Act D treatment (Fig. 4.8A, B [red dots]). This suggests that Lamin B2 depletion promotes the long-term retention of Nucleolin aggregates in the nucleoplasm. We performed fluorescence recovery after photobleaching (FRAP) to examine whether Lamin B2 regulates Nucleolin dynamics within the aggregates (Fig. 4.8C, D). Nucleolin showed ~95% recovery, suggesting a free exchange of Nucleolin into the aggregates (Fig. 4.8D, E). This is consistent with the free diffusion of Nucleolin in the nucleoplasm of HeLa cells treated with Act D (52). Although the relative mobile fractions of Nucleolin within the aggregates were comparable (Fig. 4.9E), Nucleolin recovery was significantly faster upon Lamin B2 depletion (half-life [$t_{1/2}$] = 1.2 s) than that of control cells ($t_{1/2}$ = 1.7 s) (Fig. 4.8F). Taken together, these results suggest an increased recruitment of Nucleolin into the aggregates upon Lamin B2 depletion.

Figure 4.8

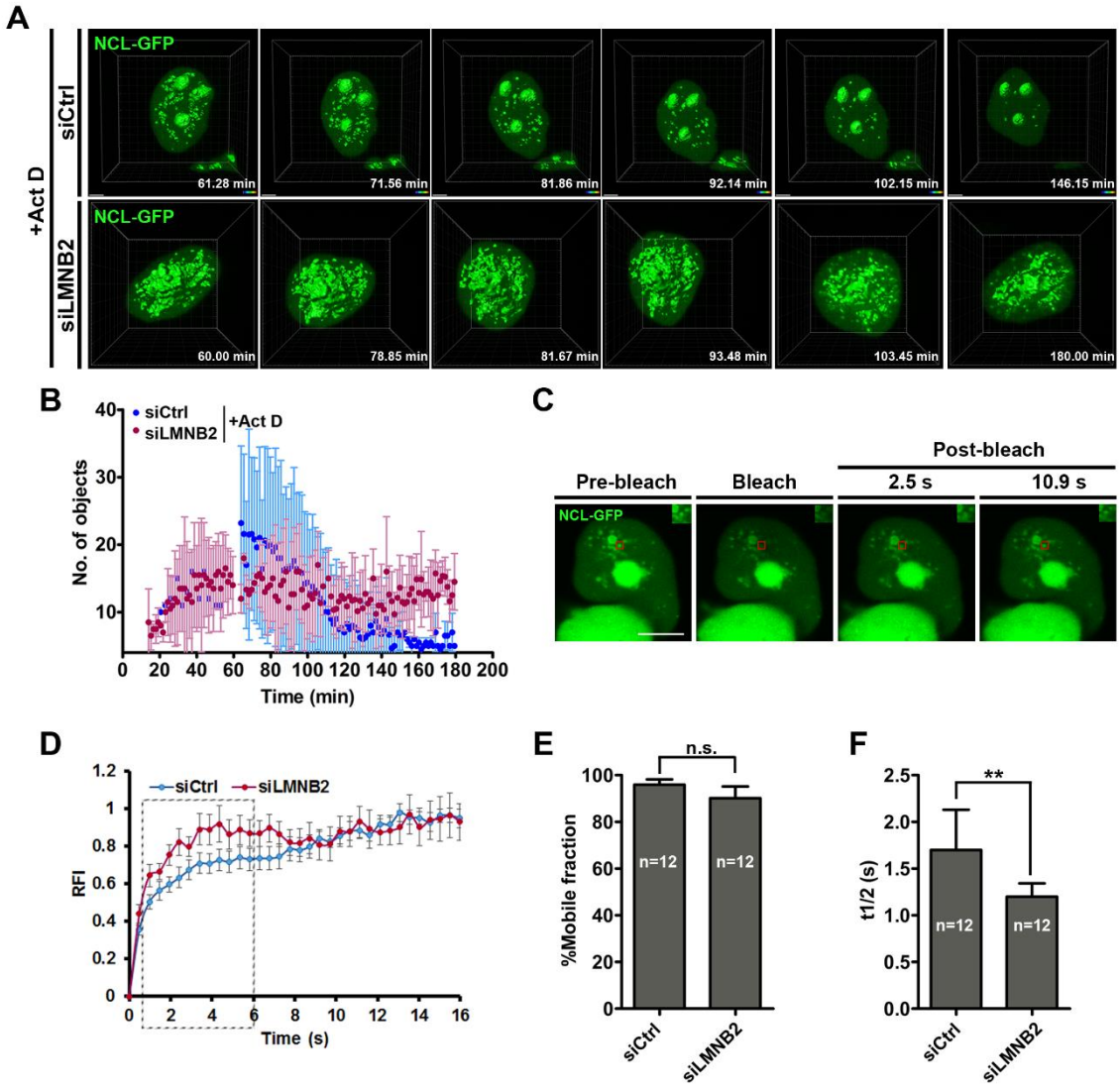

Figure 4.8. Persistence of Nucleolin aggregates upon Lamin B2 depletion.
A. Control and Lamin B2-depleted cells were transfected with NCL-GFP and treated with Act D. 4D time-lapse confocal imaging shows Nucleolin aggregates that peak at ~1 h after Act D addition and gradually disperse into the nucleoplasm (siCtrl panel). In Lamin B2-depleted cells, Nucleolin aggregates persist for ~3 h (siLMNB2 panel). Scale bars ~2 μm. **B.** Quantification of Nucleolin aggregates from reconstructions of 4D time-lapse movies, plotted as a function of time (number of independent biological replicates [N] =3; n=6 nuclei each), shows the persistence of Nucleolin aggregates upon Lamin B2 depletion. **C.** Nucleolin aggregates (NCL-GFP) were photobleached to assess Nucleolin dynamics. Representative images of Nucleolin speckles from control cells are shown. Red boxes bleach ROI. Insets, photobleached ROI. Scale bar ~5 μm. (D) FRAP curve shows recovery of Nucleolin in aggregates from Lamin B2-depleted and control cells. Dashed box, initial phase of recovery is faster upon Lamin B2 depletion. **E.** The mobile fraction of Nucleolin calculated from panel C is not altered upon Lamin B2 depletion. Error bars, SEM (*p < 0.05 by Student's t test) (N = 3; n, number of nuclei). **F.** Nucleolin recovery is significantly faster upon Lamin B2 depletion (**p < 0.01 by Student's t test) (N = 3; n, number of nuclei).

4.2.2.3. IGS RNA colocalize with Nucleolin aggregates

We asked if Nucleolin aggregates formed upon Act D treatment contained RNA, like iPNBs that were generated upon hypotonic treatment of cells (Musinova et al., 2016). Hence we co-stained Act D treated cells with Nucleolin and propidium iodide, after DNase I treatment, to detect RNA (Fig. 4.9A). Propidium iodide staining showed RNA in Nucleolin aggregates (Fig. 4.9A, inset). We examined the nuclear localization of IGS RNA upon Pol I inhibition (Fig. 4.9B). In contrast to the distinct foci of IGS RNA signals in untreated cells (Fig. 4.3B), IGS RNA localization was relatively diffuse upon Act D treatment. Furthermore, IGS RNA colocalized with Nucleolin aggregates upon Act D treatment as observed by confocal and super-resolution STED imaging (Fig. 4.9B, C). IGS RNA and Nucleolin colocalization was enhanced in Lamin B2-depleted cells (Fig. 4.9B, D). In summary, Lamin B2 depletion promotes the stability of Nucleolin-IGS RNA aggregates in the nucleoplasm. We conclude that Lamin B2 functions as a key modulator of Nucleolin dynamics, and function.

Figure 4.9

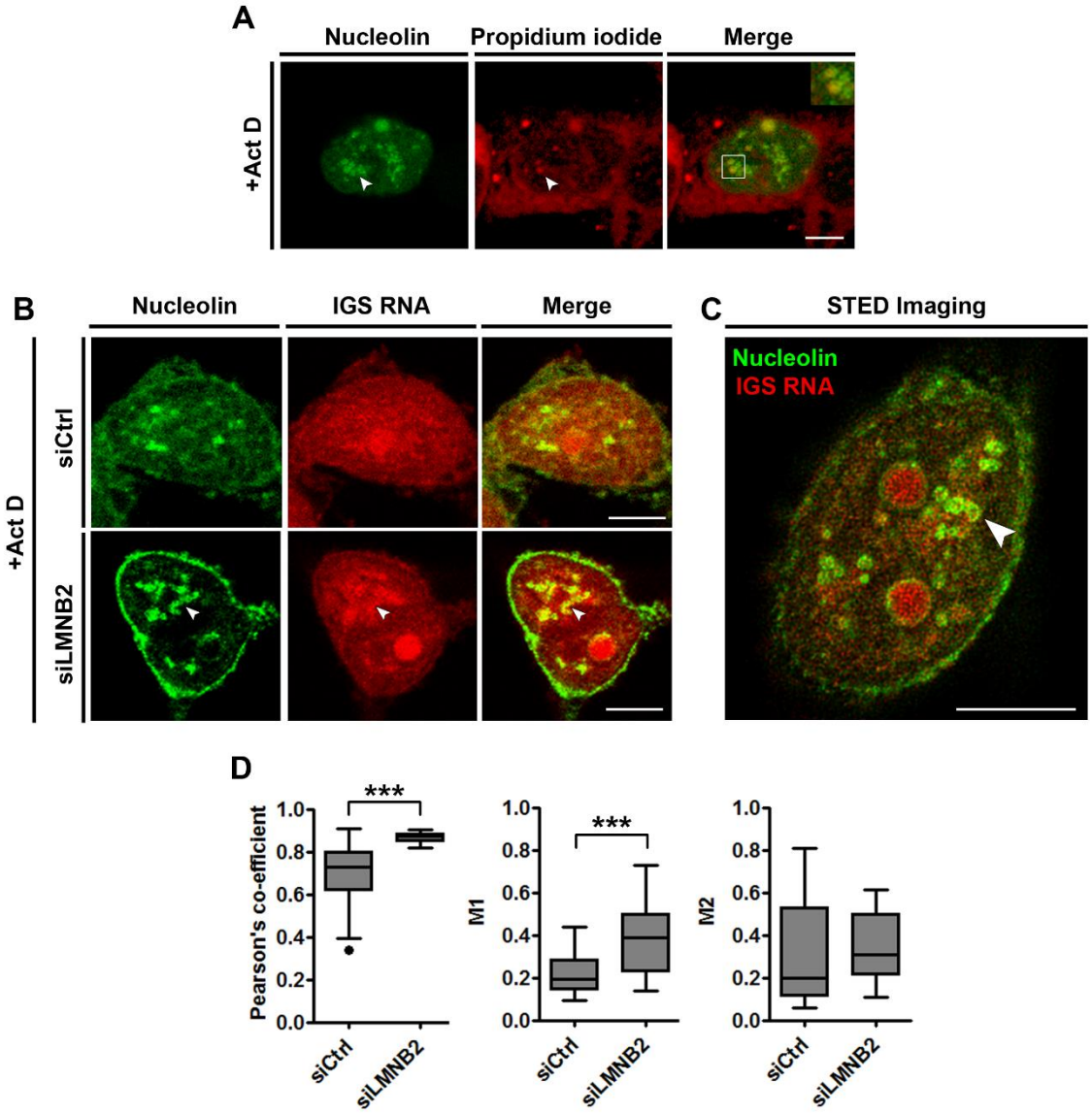

Figure 4.9. IGS RNA colocalizes with Nucleolin aggregates.
A. Cells treated with Act D were fixed and DNase I treated to digest DNA. Cells were immunostained with anti-Nucleolin antibody and counterstained with propidium iodide to detect RNA. RNA localizes in Nucleolin aggregates (white arrowheads, enlarged inset in Merge panel). Scale bar ~5μm. **B.** Immuno-RNA-FISH shows colocalization of Nucleolin speckles with IGS transcripts in control or Lamin B2-depleted cells treated with Act D (arrowhead). Scale bar, ~5μm. **C.** Super-resolution STED (stimulated emission depletion) image of Nucleolin aggregates containing IGS RNA. Scale bar ~5μm **D.** Increased colocalization of IGS transcripts with Nucleolin in the nucleoplasm upon Lamin B2 knockdown (Pearson colocalization index median values: control, 0.7; siLMNB2, 0.88). Manders coefficient (M1), overlap of IGS RNA with Nucleolin (median values; control, 0.19; siLMNB2, 0.38). Manders coefficient (M2), overlap of Nucleolin with IGS RNA (median values: control, 0.2; siLMNB2, 0.31 [not significant]). Whiskers, Tukey (***p<0.001 by Mann-Whitney test) (N = 3; siCtrl, 28 nuclei; siLMNB2, 32 nuclei).

4.3. Discussion

Here we have assessed the role of Lamin B2 in regulating rRNA expression – which is the primary function of the nucleolus (Russell and Zomerdijk, 2005). The expression of rRNA is stringently regulated in cells and deregulated expression is a characteristic of both solid tumors like prostate cancers, cervical cancer and blood cancers like myelodysplasia (Raval et al., 2012; Uemura et al., 2012; Zhou et al., 2016). These assays reveal that 45S rRNA expression levels were elevated upon Lamin B2 depletion (Fig. 4.2B). Further, Lamin B2 depletion also enhances expression levels of IGS RNA (Fig. 4.3A, B). Therefore, the regulatory role of Lamin B2 also extends to the upstream regions of pre-rRNA and is not limited to the pre-rRNA promoter.

We find that Dnmt1, the methyltransferase guiding rDNA promoter methylation was downregulated upon Lamin B2 depletion (Fig. 4.4A-C). Promoter methylation is a common mechanism by which RNA Pol II-transcribed genes, are repressed (Razin and Cedar, 1991). However, there are contradictory reports on rDNA transcriptional repression by DNA methylation. While promoter hypomethylation co-relates with increased rRNA expression in hepatocellular carcinoma, rRNA expression remained independent of promoter methylation status in DNMT1 and DNMT3b knockout cell lines (Espada et al., 2007; Ghoshal et al., 2004; Raval et al., 2012; Richter AM and Dammann RH, 2015). However, Dnmt1 knockout cells show severely disrupted nucleoli (Espada et al., 2007). Hence modulating Dnmt1 expression levels could be a mechanism by which rDNA transcription and/or nucleolar structure is altered in Lamin B2 depleted cells. Further, microarray analysis upon Lamin B2 depletion identified deregulation of other chromatin modifiers – the H3K9 methyltransferase EHMT1 and the PRC2 co-regulator JARID2, which may further contribute to chromatin remodeling and activation of the rDNA locus.

Our assays show that Lamin B2 depletion increases HP1α mobility in foci around the nucleolus (Fig. 4.4G-I). This raises the possibility that Lamin B2 depletion leads to chromatin decondensation at rDNA clusters, thus upregulating transcription from rDNA genes and intergenic regions. Repressed rDNA genes associate with heterochromatin binding factors such as HP1 and MacroH2A (Cong et al., 2014; Zhou et al., 2002). The loss of MacroH2A.1 disrupts nucleoli and upregulates 45S rRNA, effects that are similar to those of Lamin B2 depletion (Cong et al., 2014; Douet et al., 2017; Fu et al., 2015). It is interesting to note that Lamin B2 can potentially engage in macromolecular complexes with both HP1α via Lamin B receptor (LBR) and MacroH2A.1 via Lamin B1 (Fu et al., 2015; Ye et al., 1997). We have shown previously that Lamin B2 associates with Nucleolin (Fig. 3.12). It is conceivable that Lamin B2 may modulate the recruitment of Nucleolin or MacroH2A.1, which are enriched on the rDNA promoter regions as revealed by chromatin immunoprecipitation (ChIP) (Cong et al., 2012).

Further, expression levels of c-Myc (*MYC*) is upregulated (~1.51 fold) upon Lamin B2 knockdown. The transcription factor - c-Myc binds to rDNA promoter and enhances rDNA transcription by recruiting TF-IIB/SL1, necessary for rDNA transcription initiation (Grandori et al., 2005). Effectively, the concerted association of Lamin B2 with activators of rDNA transcription such as c-Myc and Nucleolin; or repressors such as Dnmt1, EHMT1, JARID2 and MacroH2A, is likely to impinge on rDNA transcription.

We have also uncovered enhanced expression of rRNAs from the rDNA intergenic regions (Fig. 4.3). Cellular stresses such as acidosis are associated with the expression of noncoding RNAs from intergenic rDNA sites that sequester stress-responsive proteins such as HSP70 and VHL in the nucleolus (Audas et al., 2012). An increase in the expression levels of IGS RNA in Lamin B2-depleted cells could suggest of cellular stress (Fig. 4.3). Analogous to the formation of interphase pre-nucleolar bodies (iPNBs) associated with unprocessed rRNA in cells under hypotonic stress (Musinova et al., 2016), here, we find that the inhibition of RNA Pol I by Act D treatment induces the aggregation of Nucleolin speckles in the nucleoplasm (Fig. 4.7). Nucleolin speckles are further enhanced upon Lamin B2 depletion (Fig. 4.8). The enhanced co-localization of Nucleolin with IGS RNA upon Act D treatment in Lamin B2-depleted cells suggests the stabilization of the Nucleolin-IGS RNA complex (Fig. 4.10). This is consistent with the faster recovery of Nucleolin into the aggregates (Fig. 4.9D-F), and prolonged retention of Nucleolin speckles in the nucleoplasm (Fig. 4.9A, B), upon Lamin B2 depletion, potentially due to the affinity of Nucleolin to IGS RNA (Fig. 4.10). Nucleolin mobility and sequestration into the nucleolus is modulated by ncRNAs such as Alu RNA and intergenic RNAs expressed upon acidosis (Caudron-Herger et al., 2015). We envisage three potential mechanisms by which loss of Lamin B2 enhances Nucleolin stability, i.e., (i) promoting self-oligomerization of Nucleolin, (ii) stable association of Nucleolin with other nucleolar proteins such as Fibrillarin (Fig. 4.8A), or (iii) Nucleolin-RNA complex formation (Fig. 4.10A), collectively resulting in the prolonged stability of Nucleolin aggregates (Caudron-Herger et al., 2015; Chen et al., 2012). We surmise that the RNA binding domains of Nucleolin regulate Nucleolin-RNA dynamics in a Lamin B2-dependent manner (Ghisolfi-Nieto et al., 1996).

In summary, these studies uncover Lamin B2 as a modulator of not only nucleolar function of rDNA transcription but also the dynamics of nucleolar proteins essential for ribosome biogenesis.

Figure 4.10

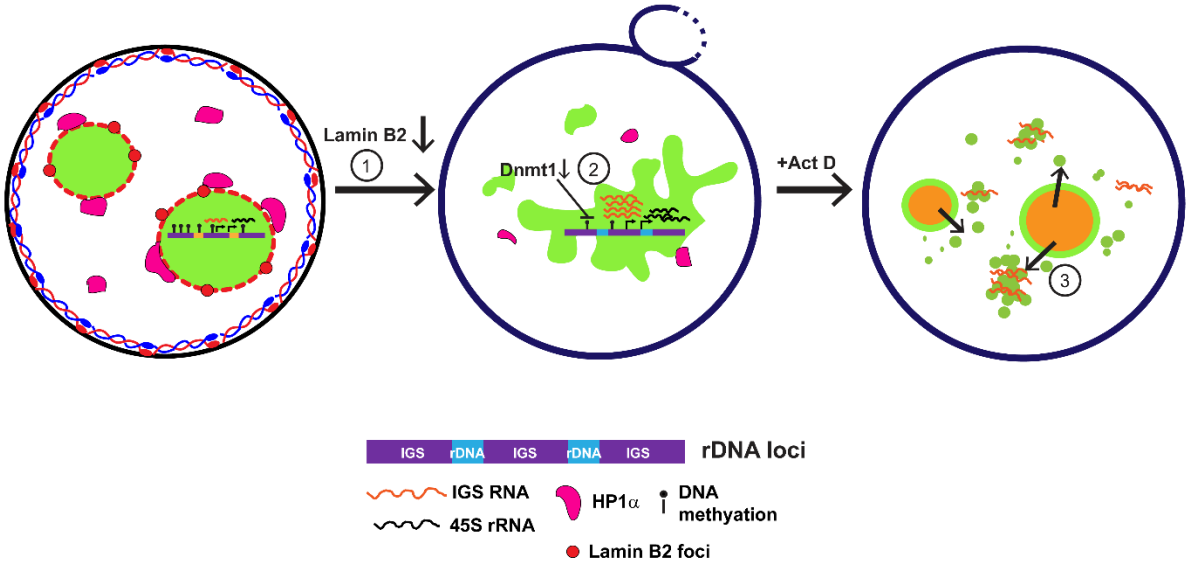

Figure 4.10. Model depicting a role for Lamin B2 in modulating nucleolar function and dynamics. Lamin B2 depletion shows disrupted nucleolar morphology, increased expression of 45S rRNA and intergenic sequence RNA (IGS RNA). Lamin B2 depleted cells show downregulation of Dnmt1 expression and increased HP1α mobility. Lamin B2-depleted cells treated with actinomycin D (Act D) have increased Nucleolin-IGS RNA aggregates that persist in the nucleoplasm.

Chapter 5:

Role of Fibrillarin in modulating nuclear, nucleolar and cellular architecture

5.1. Introduction

Although the nucleolus is a phase-separated nuclear sub-organelle, it is connected to the nucleus via the nucleoskeleton (Hozák et al., 1995). The impact of nucleolar proteins over nucleolar structure, ribosome biogenesis, and protein translation has been well studied (Farley-Barnes et al., 2018). Similarly, two key nucleolar proteins – Fibrillarin (FBL) and Nucleophosmin (NPM1) modulate nuclear shapes (Amin et al., 2007, 2008a). Both NPM1 and FBL depleted cells show abnormal nuclear shapes. The defects in nuclear shapes upon NPM1 knockdown is attributed to altered cytoskeletal microtubule polymerization (Amin et al., 2008a), however, the mechanisms by which Fibrillarin depletion affects nuclear shapes is not known.

Fibrillarin is a protein present in the DFC of the nucleolus and involved in pre-rRNA processing (Cerdido and Medina, 1995). It is a part of the Box C/D ribonucleoprotein complex and catalyzes 2-O'-ribose methylation of rRNA (Dunbar et al., 2000). Post-transcriptional modifications of rRNA i.e. methylation and pseudouridylation are important to produce functional ribosomes (Baxter-Roshek et al., 2007; Sloan et al., 2017). Aberrantly methylated rRNAs are preponderant in breast cancers and ribosomopathies, and lead to altered translational fidelity, promoting internal ribosome entry site (IRES) mediated translation instead of 5' mRNA cap mediated translation, misincorporation of amino acids and non-sense suppression (Basu et al., 2011; Baxter-Roshek et al., 2007; Ruggero et al., 2003). Fibrillarin gene expression is modulated by the tumor suppressor p53, which binds to the intronic p53-responsive elements (p53-RE) of the *FBL* gene and represses it (Marcel et al., 2013). Thus in p53 mutated breast cancer cells, upregulation of Fibrillarin correlates with increased translation of cancer related genes – *IGF1R*, *MYC*, *FGF1*, *FGF2* and *VEGFA (Marcel et al., 2013)*.

Besides rRNA methylation, Fibrillarin also methylates conserved glutamine residues on histone H2A across yeast, human and plants (Loza-Muller et al., 2015; Tessarz et al., 2014). Glutamine methylated H2A is only localized in the nucleolus and associated with active rDNA (Tessarz et al., 2014).

Fibrillarin is highly expressed in mouse embryonic stem cells and its methyltransferase activity is required to maintain their pluoripotency (Watanabe-Susaki et al., 2014). Fibrillarin is also necessary for neuronal differentiation in dorsal midbrain and retina of Zebrafish embryos (Bouffard et al., 2018).

The role of Fibrillarin in regulating nuclear integrity is unclear. Here we have assessed the global impact of Fibrillarin depletion in colorectal cancer cells. We also asked – how does Fibrillarin affect nuclear structure and what is the impact of Fibrillarin on cell architecture?

5.2. Results

5.2.1. Depletion of Fibrillarin in DLD1 cells

To characterize the functions of Fibrillarin in diploid colon cancer cells, we performed siRNA mediated knockdown Fibrillarin in DLD1 cells (Fig. 5.1A). >80% depletion of Fibrillarin depletion was achieved with 100 nM siRNA (Fig. 5.1A). Fibrillarin depletion followed by cell viability assay using MTT showed ~69% viable cells (Fig. 5.1B). Immunofluorescence assays revealed ~70% depletion of Fibrillarin at the single cell level (Fig. 5.1C, D).

Figure 5.1

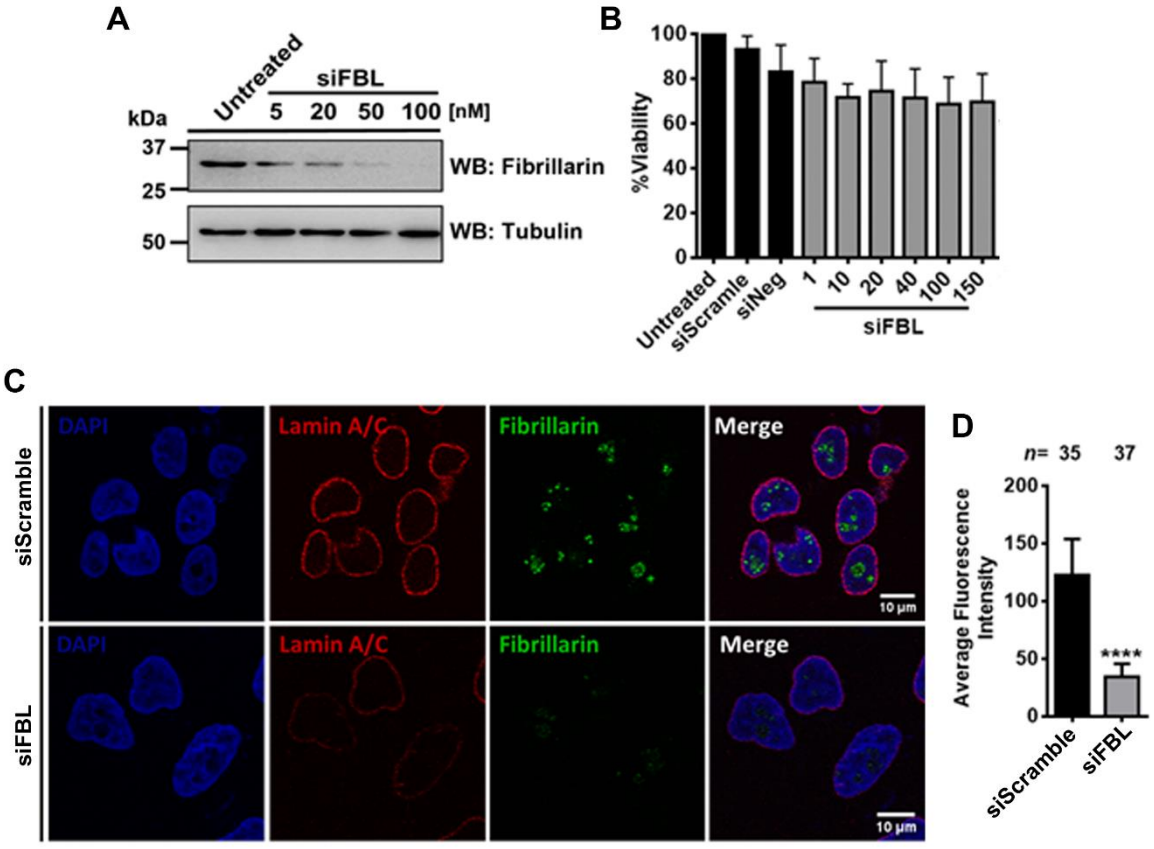

Figure 5.1. siRNA mediated knockdown of Fibrillarin.
A. Western blot showing Fibrillarin levels from whole cell extracts of DLD1 cells treated with increasing concentration of Fibrillarin siRNA (5, 20, 50, 100 nM). Loading control: Tubulin. **B.** MTT assay showing cell viability upon Fibrillarin knockdown. Error bar – S.E. N=3 biological replicates. **C.** Immunostaining showing Fibrillarin staining in control and Fibrillarin knockdown. Lamin A marks the nuclear boundary. Scale ~ 10µm. **D.** Average fluorescence intensity of Fibrillarin from control and siFBL treated cells showing significant reduction of Fibrillarin. Error bar – S.D. N=2 biological replicates. Student's t-test, ****p<0.0001.

5.2.2. Effect of Fibrillarin depletion on the transcriptome

To understand the role of Fibrillarin, we performed transcriptomic analyses upon Fibrillarin knockdown in DLD1 cells. We further compared the transcriptomic changes induced by Fibrillarin knockdown with the knockdown of another independent nucleolar protein - Nucleostemin (GNL3), to examine if the transcriptional changes were specific to Fibrillarin knockdown. Nucleostemin is a marker of stem cells and upregulated in cancers including gastric carcinomas (Asadi et al., 2014; Kafienah et al., 2006). Nucleostemin localizes to the granular component of the nucleolus and regulates cell cycle and differentiation (Huang et al., 2015; Romanova et al., 2009a).

Microarray analyses showed that 1118 genes were significantly dysregulated (both up and downregulated) upon Fibrillarin knockdown, whereas 106 genes were significantly dysregulated upon Nucleostemin knockdown (Fig. 5.2). Amongst the genes dysregulated upon Fibrillarin knockdown, 494 genes were upregulated while 624 genes were downregulated (Fig. 5.2A). Whereas, upon Nucleostemin knockdown, 72 genes were upregulated while 34 genes were downregulated (Fig. 5.2B). Few genes were common between the two datasets (Fig. 5.2C), which include *PTGS2* (Prostaglandin-endoperoxide synthase), which is implicated in colorectal cancer, consistent with the *SCARNA2*, the U2 snRNA, consistent with the overlapping roles of Fibillarin and Nucleostemin in rRNA processing and carcinogenesis (Asadi et al., 2014; Dunbar et al., 2000; Marcel et al., 2013; Romanova et al., 2009a, 2009b).

Figure 5.2

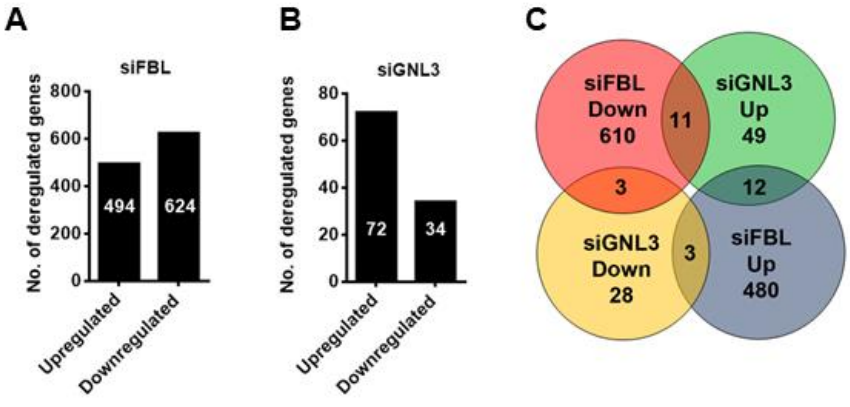

Figure 5.2. Microarray analysis of Fibrillarin and Nucleostemin depleted cells.
A. Total number of genes up- or down-regulated upon Fibrillarin (FBL) knockdown. **B.** Total number of genes up- or down-regulated upon Nucleostemin (GNL3) knockdown. **C.** Common and uniquely deregulated genes upon Fibrillarin and Nucleostemin knockdown in DLD1 cells.

5.2.3. Functional categories of genes dysregulated upon Fibrillarin knockdown

We next sought to examine biological functions that are affected upon Fibrillarin knockdown and if these functions are related to the changes observed in nuclear morphologies of DLD1 cells. To this end, we performed GO analysis on genes dysregulated upon Fibrillarin knockdown (Fig. 5.3). Genes that were upregulated upon Fibrillarin knockdown clustered under the following categories – (i) innate immune response in mucosa, (ii) methylation, (iii) TNF signaling pathway, (iv) cell chemotaxis, and so on (Fig. 5.3A). Genes that were downregulated upon Fibrillarin knockdown clustered under the following categories – (i) Transferase (methyltransferase), (ii) Transcription factor activity, (iii) Golgi cisterna membrane, (iv) regulation of cell shape, (v) nervous system development, (vi) methylation and so on (Fig. 5.3B). In contrast, genes upregulated upon Nucleostemin knockdown grouped under the categories – (i) EGF like-1, (ii) TNF signaling, (iii) negative regulation of cell division, (iv) astrocyte development (Fig. 5.4A), and downregulated genes grouped under – (i) glucose metabolic process, (ii) Toll-like receptor signaling pathway, (iii) Osteoclast differentiation, (iv) Ras signaling pathway and so on (Fig. 5.4B). Thus except the effect on TNF signaling pathway, Fibrillarin and Nucleostemin knockdown affected distinct classes of genes.

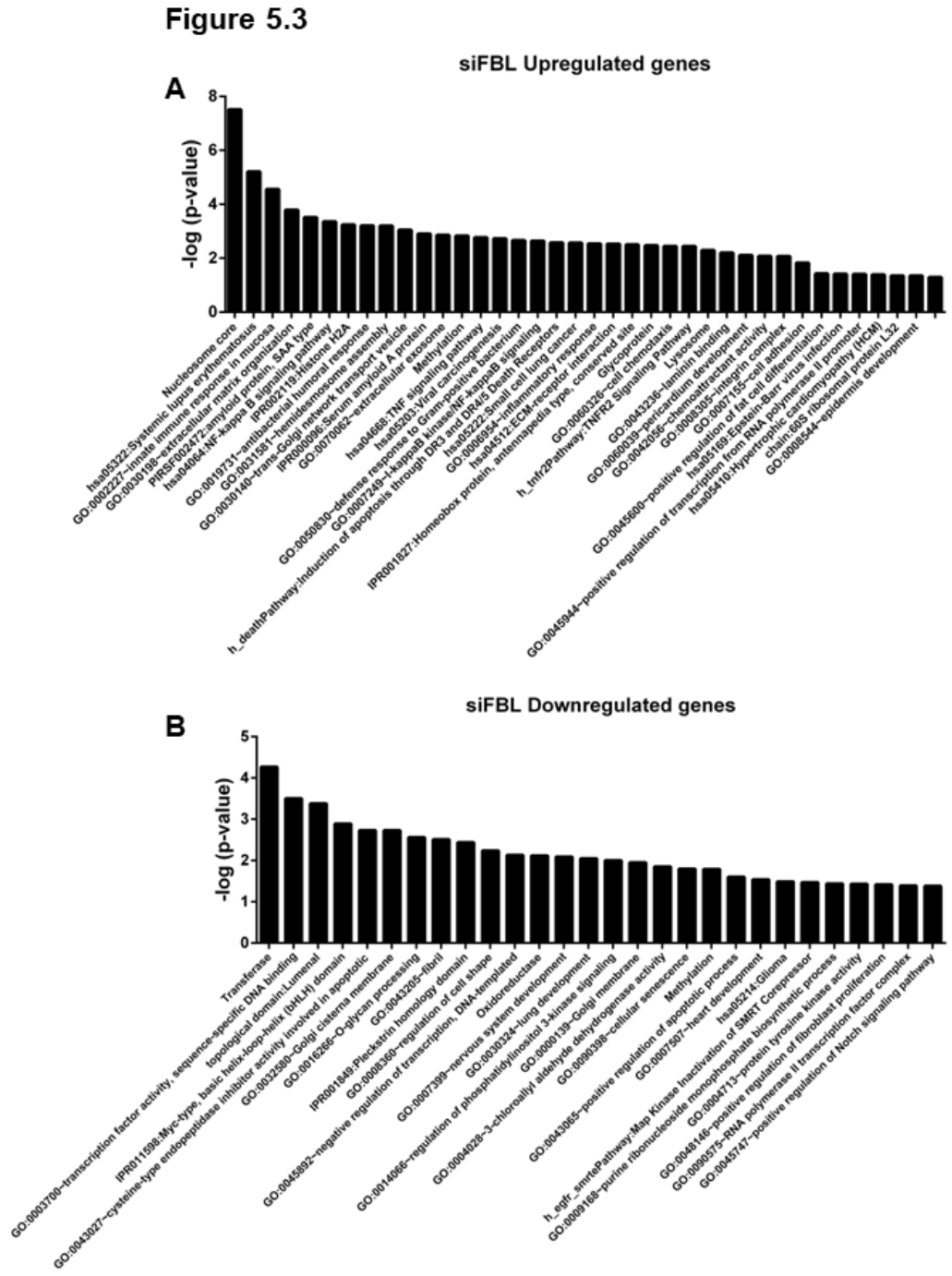

Figure 5.3. Gene ontology analysis of genes dysregulated upon Fibrillarin knockdown.
Significantly enriched GO categories (Biological processes, Cellular component, Molecular functional all inclusive) of genes **A.** upregulated and **B.** downregulated upon Fibrillarin knockdown ($p<0.05$). Enrichment plotted as −log (p value) of shortlisted GO categories.

Figure 5.4

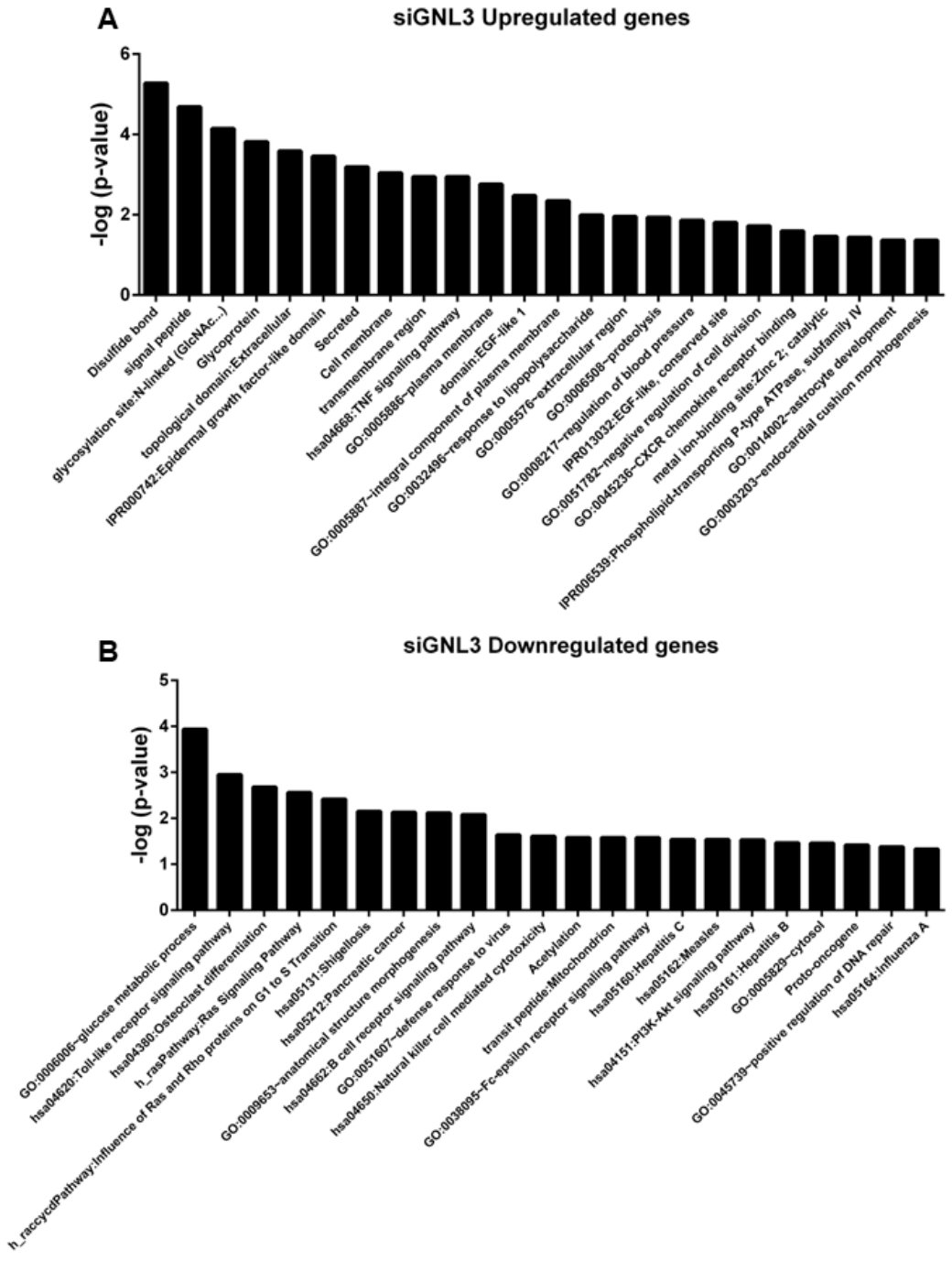

Figure 5.4. Gene ontology analysis of genes dysregulated upon Nucleostemin knockdown. Significantly enriched GO categories (Biological processes, Cellular component, Molecular functional all inclusive) of genes **A.** upregulated and **B.** downregulated upon Nucleostemin knockdown ($p<0.05$). Enrichment plotted as −log (p value) of shortlisted GO categories.

5.2.4. Transcription factors (TFs) affected upon Fibrillarin knockdown

We examined the regulation of genes encoding transcription factors to address transcriptional changes mediated upon Fibrillarin knockdown. To this end we overlapped the list of deregulated genes upon Fibrillarin knockdown with known human transcription factor genes (curated on the Animal Transcription Factor Database) (Zhang et al., 2012). We found that 74 genes that were deregulated upon Fibrillarin knockdown coded for transcription factors, 24 out of these 74 transcription factor genes were upregulated while 50 genes were downregulated (Fig. 5.5, Table 5.1). Upregulated transcription factors belonged to zinc finger nuclease (ZNF), homeobox and ETS families. Downregulated transcription factors belonged to MYB, bHLH and homeobox families.

5.2.5. Enriched TF binding motifs in promoters of dysregulated genes

We examined if genes dysregulated upon Fibrillarin knockdown were enriched for consensus motifs for transcription factors in their promoters. We performed gene set enrichment (GSEA) analysis and compared enriched gene sets with annotated gene sets for consensus motifs for binding of transcription factors and micro RNAs. The top 20 TFs and their consensus sequence (if known) are listed in Table 5.2 and Table 5.3. Genes upregulated upon Fibrillarin knockdown showed sequences enriched for binding of NFAT, E12, SP1, AP1, ETS2 (Table 5.2). Genes downregulated upon Fibrillarin knockdown showed sequences enriched for binding of MAZ, SP1, E12, LEF1 (Table 5.3). It is interesting to note that genes downregulated upon Fibrillarin knockdown showed enrichment for the TF NMYC, which itself is also downregulated by Fibrillarin depletion. Additionally, there were many common TF binding motifs between genes dysregulated upon Fibrillarin knockdown (Table 5.2 and Table 5.3). Thus transcriptional deregulation seen upon Fibrillarin depletion is likely to be mediated by these transcription factors.

Figure 5.5

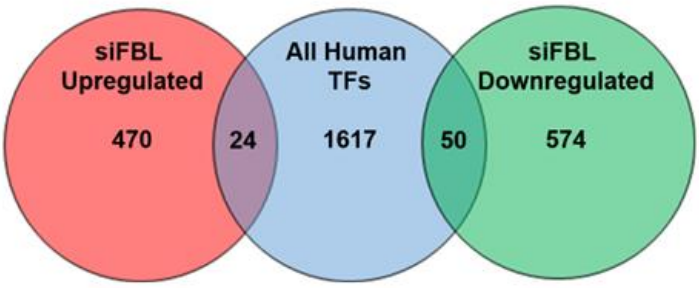

Figure 5.5. Analysis of human transcription factors affected upon Fibrillarin.
Genes dysregulated upon Fibrillarin knockdown were overlapped with all human transcription factors annotated in Animal Transcription Factor Database. 24 and 50 transcription factors were upregulated and downregulated upon Fibrillarin knockdown, respectively.

Table 5.1. Genes encoding transcription factors dysregulated upon Fibrillarin knockdown

Upregulated			Downregulated				
• *ZNF425*	• *ZKSCAN2*	• *HOXA2*	• *SPDEF*	• *ELK1*	• *CIC*	• *MKX*	• *ZNF573*
• *ZFP2*	• *CREBL2*	• *IRF1*	• *MYB*	• *ZBTB42*	• *NFIC*	• *CEBPA*	• *GLI2*
• *ELF3*	• *TFAP2E*	• *ZNF250*	• *PITX1*	• *ZNF165*	• *RARA*	• *SIM2*	• *TRERF1*
• *HOXB4*	• *NRIH2*	• *TADA2B*	• *MLXIPL*	• *ARID3A*	• *SLC2A4RG*	• *SRF*	• *HES6*
• *ATF3*	• *NFKB2*		• *TCF3*	• *SP5*	• *FOXD2*	• *KLF9*	• *E2F1*
• *ZNF669*	• *ZNF574*		• *LBX2*	• *NCOR2*	• *IRF7*	• *ZSCAN5A*	• *MAFB*
• *HOXA4*	• *OVOL2*		• *MYCN*	• *IMGA1*	• *E2F2*	• *DMBX1*	• *ZNF589*
• *RELB*	• *SMAD3*		• *ASCL2*	• *ZNF219*	• *ID3*	• *FOXD1*	• *MESP1*
• *CCRN4L*	• *TERF2*		• *DMRT1*	• *ATOH8*	• *ZNF488*	• *ZNF485*	• *ZNF484*
• *HOXA3*	• *NRID2*		• *HEYL*	• *STAT2*	• *ZNF841*	• *TBX2*	• *ZNF672*

Table 5.2. Motifs/microRNA enriched in promoters of upregulated genes upon Fibrillarin knockdown

Transcription factor/miRNA	Motif	p-value
NFAT	TGGAAA	6.25E-14
E12	CAGGTG	7.66E-12
MIR19A, MIR19B	TTTGCAC	1.14E-11
Unknown	KRCTCNNNNMANAGC	1.68E-11
SP1	GGGCGGR	9.71E-11
Unknown	TTTNNANAGCYR	2.47E-10
Unknown	AACTTT	2.33E-08
AP1	TGANTCA	3.60E-08
MIR15A, MIR16, MIR15B, MIR195, MIR424	TGCTGCT	6.23E-07
ETS2	RYTTCCTG	6.63E-07
LEF1	CTTTGT	1.37E-06
Unknown	TGGNNNNNNKCCAR	1.68E-06
NFKB	GGGNNTTTCC	3.51E-06
STAT5A	TTC(T/C)N(G/A)GAA	5.43E-06
TEF1	WGGAATGY	9.21E-06
ERR1	TGACCTY	9.42E-06
MIR506	GTGCCTT	1.07E-05

Table 5.3. Motifs/microRNA enriched in promoters of downregulated genes upon Fibrillarin knockdown

Transcription factor/miRNA	Motif	p-value
MAZ	GGGAGGRR	7.05E-19
SP1	GGGCGGR	2.82E-17
E12	CAGGTG	2.89E-10
LEF1	CTTTGT	4.13E-09
Unknown	AACTTT	4.47E-08
FOXO4	TTGTTT	4.58E-08
AP4	CAGCTG	6.13E-08
MEIS1	TGACAGNY	7.70E-08
NFY	GATTGGY	1.85E-07
MIR30A5P, MIR30C, MIR30D, MIR30B, MIR30E5P	TGTTTAC	5.50E-07
FREAC2	RTAAACA	7.07E-07
PAX4	GGGTGGRR	8.92E-07
MIR27A	ACTGTGA	1.20E-06
MYOD	GCANCTGNY	2.34E-06
MYC	CACGTG	2.58E-06
ERR1	TGACCTY	3.20E-06

5.2.6. Effects of Fibrillarin knockdown at the single cell level

5.2.6.1. Nucleolar morphology

Since Fibrillarin is integral factor of the nucleolar Dense Fibrillar Component (DFC) and essential for methylation and processing of ribosomal RNA (Tollervey et al., 1993), we first assessed the effect of its depletion on nucleolar morphology. Fibrillarin knockdown was performed in DLD1 cells, followed by immunofluorescence assays with Nucleolin to visualize nucleoli (Fig. 5.6A). Interestingly, quantifications revealed that nucleolar disruptions were not significantly different between control (~28%) and Fibrillarin depleted cells (~20%) (Fig. 5.6B). This result corroborates previous findings where Fibrillarin knockdown does not affect nucleolar structure of HeLa cells.

5.2.6.2. Nuclear morphology

Although Fibrillarin knockdown does not affect nucleolar morphology, it results in severely distorted nuclei in HeLa cells (Amin et al., 2007). However, cells with chromosomal instabilities such as hypertriploid (3n+) HeLa cells, typically show heterogenous and aberrant nuclear morphologies (Ohshima, 2008). To examine the effect on nuclear morphology in diploid cells, we performed Fibrillarin knockdown in DLD1 cells and immunostained with Lamin A/C (Fig. 5.6C). Nuclei in control DLD1 cells were ellipsoidal and nuclear envelope was free of invaginations. Fibrillarin knockdown followed by immunofluorescence assays and imaging revealed a significant increase in cells with nuclear deformities such as nuclear envelope invaginations, misshapen and lobulated nuclei (Control: ~14%, siFBL: ~48%) (Fig. 5.6D). Thus, Fibrillarin knockdown significantly increased nuclear aberrations across cancer cell types.

Figure 5.6

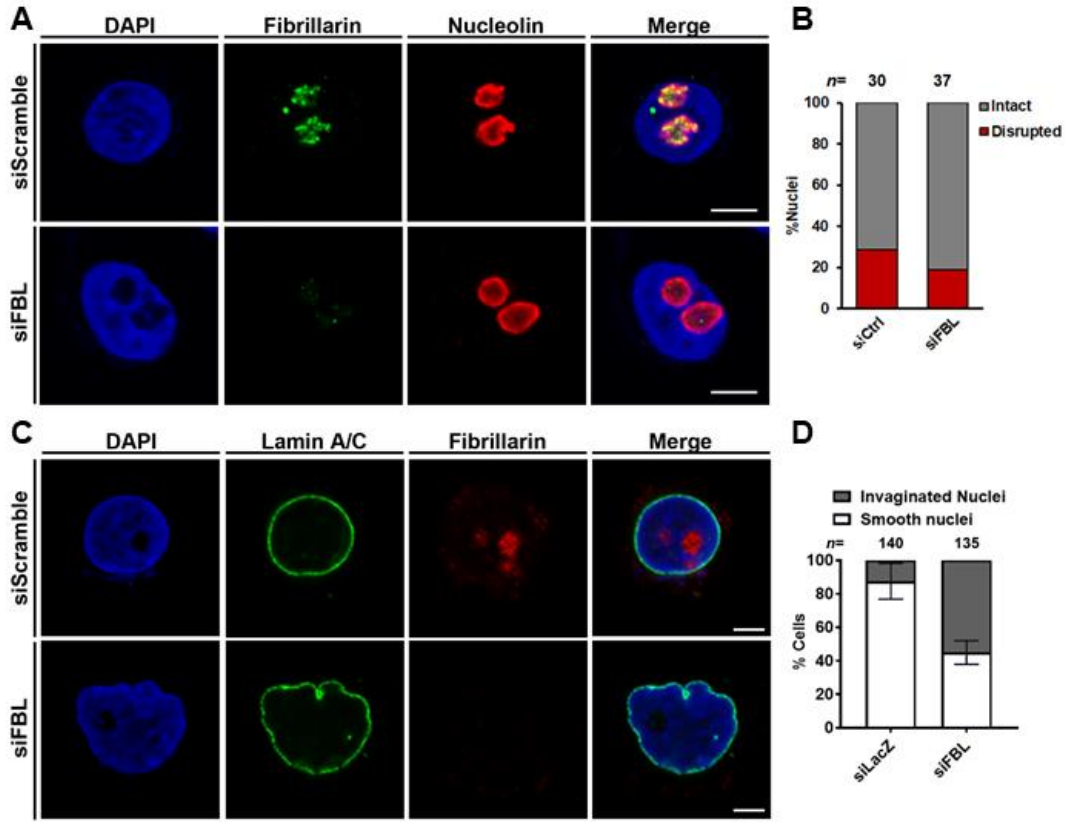

Figure 5.6. Nucleolar and nuclear morphology upon Fibrillarin knockdown.
A. Control and Fibrillarin depleted cells were immunostained with anti-Nucleolin antibody to demarcate the nucleolus. Scale bar ~ 5 μm. **B.** Nucleolar morphology is unaffected upon Fibrillarin knockdown. n=number of nuclei assessed from N=1, a single experiment. **C.** Control and Fibrillarin depleted cells were immunostained for Lamin A/C. Nuclei show invaginations upon Fibrillarin knockdown. Scale bar ~ 5 μm. **D.** Quantification showing increased percentage of cells with nuclear invaginations upon Fibrillarin knockdown. Error bar – S.D. n=number of nuclei assessed from N=2 biological replicates.

5.2.6.3. Cell morphology

Genes dysregulated upon Fibrillarin knockdown clustered under cell chemotaxis and regulation of cell shape categories (Fig. 5.3). Nuclear morphology and cell morphology are integrally connected, since the nuclear lamina is connected to cellular actin via the LINC proteins (Starr and Fridolfsson, 2010). Extracellular forces are transmitted into the nucleus by mechanotransduction (Haase et al., 2016). We surmised that changes in nuclear morphology upon Fibrillarin knockdown is likely to be coupled to changes in cell architecture.

To assess morphology of DLD1 cells, we immunostained control and Fibrillarin depleted cells with Phalloidin (Fig. 5.7). Phalloidin binds to F-actin structures in the cytoplasm (Vandekerckhove et al., 1985). Immunostaining of control DLD1 cells showed cobble-stone morphology with actin enrichment at the cell periphery (Fig. 5.7A). Fibrillarin depleted cells showed spreading, with a significant increase in the cell surface area (siCtrl: ~258 cm^2, siFBL: ~359 cm^2) (Fig. 5.7A, B). F-actin intensity in Fibrillarin depleted cells was significantly higher as compared to control cells (siCtrl: 5634 a.u., siFBL: 8235 a.u.) (Fig. 5.7C). In addition, cells showed altered actin organization upon Fibrillarin depletion, with ~50% of cells showing large aggregates of actin inside the cell juxtaposed to the nucleus (Fig. 5.7D, E). In control cells, these actin aggregates were observed in ~15% of cells (Fig. 5.7E). The nucleus showed invaginations potentially owing to the proximity of actin aggregates external to the nucleus (Fig. 5.7D). Fibrillarin depleted cells also showed an increased number of filopodia per cell (siCtrl: 5, siFBL: 20), a characteristic of enhanced cell motility (Fig. 5.7F, G).

Figure 5.7

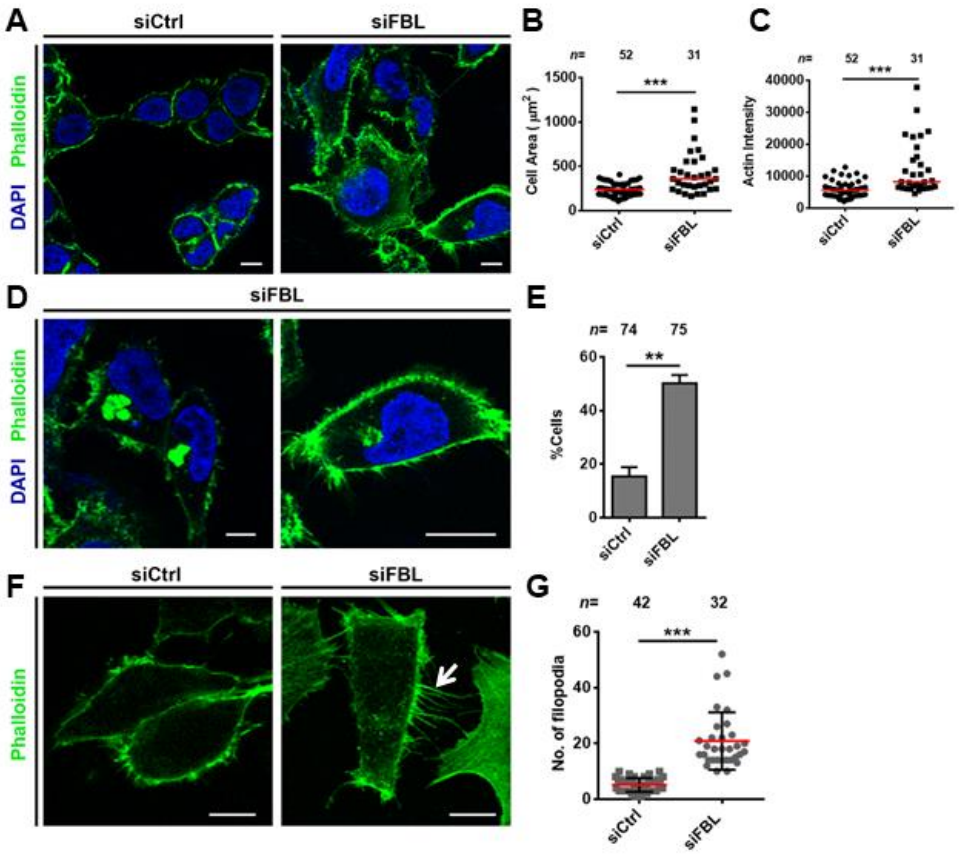

Figure 5.7. Cell morphology is affected upon Fibrillarin knockdown.
A. Control and Fibrillarin depleted cells were immunostained with Phalloidin to demarcate actin and the cell boundary. Scale bar ~ 5 µm. **B.** Cell area is significantly increased in Fibrillarin depleted cells. Red bar – median. n=number of nuclei assessed from N=2 biological replicates. Mann-Whitney test, ***p<0.001. **C.** Total actin intensity is significantly increased in Fibrillarin depleted cells. Red bar – median. n=number of nuclei assessed from N=2 biological replicates. Mann-Whitney test, ***p<0.001. **D.** Fibrillarin depleted cells show actin accumulation adjacent to indented nucleus. Scale bar ~ 5 µm. **E.** Cells with accumulated actin foci are significantly increased upon Fibrillarin knockdown. Error bars – S.D. n=number of nuclei assessed from N=2 biological replicates. Mann-Whitney test, **p<0.01. **F.** Fibrillarin depleted cells show increase in filopodia (white arrow). Scale bar ~ 5 µm. **G.** Quantification showing significantly increased number of filopodia in each cell, upon Fibrillarin knockdown. Red bar – mean. n=number of nuclei assessed from N=2 biological replicates. Mann-Whitney test, ***p<0.001.

Gene expression profiling revealed upregulation of multiple integrins (α2, α6, β5, β8) and extracellular matrix proteins – collagen16α1, laminins (β3, γ1) that affect cell adhesion and cytoskeletal reorganization and cell morphology (Fig. 5.3). Modulators of F-actin organization were also dysregulated upon Fibrillarin depletion. These included coronin1A (*CORO1A*) that modulates Arp2/3 activity; plexin-B2 (*PLXNB2*) that regulates the Rac and Cdc42 GTPases; and Arf6-GAP *(ARAP3)* that activates Rho kinase (Fig. 5.3) (Gandhi and Goode, 2013; Krugmann et al., 2004; Roney et al., 2011).

To assess actin stability in Fibrillarin depleted cells, we treated these cells with Latrunculin A (Fig. 5.8A). Latrunculin A (Lat A) acts by binding to monomeric G-actin and preventing actin polymerization. We detected a decrease in actin intensity and cell area (Median cell area – DMSO: ~404 μm^2, 50nM: ~379 μm^2, 500nM: ~214 μm^2) (Fig. 5.8B, C). At each concentration of Lat A, Fibrillarin depleted cells showed higher actin intensity than control cells (Fig. 5.8B). Further, cell area was significantly higher in Fibrillarin depleted cells compared to control cells (Median cell area, siCtrl+Lat A: 379, siFBL+Lat A: 836) treated with Lat A (50 nM) (Fig. 5.8C). This suggests that Fibrillarin depleted cells are resistant to actin depolymerisation by Lat A treatment.

Figure 5.8

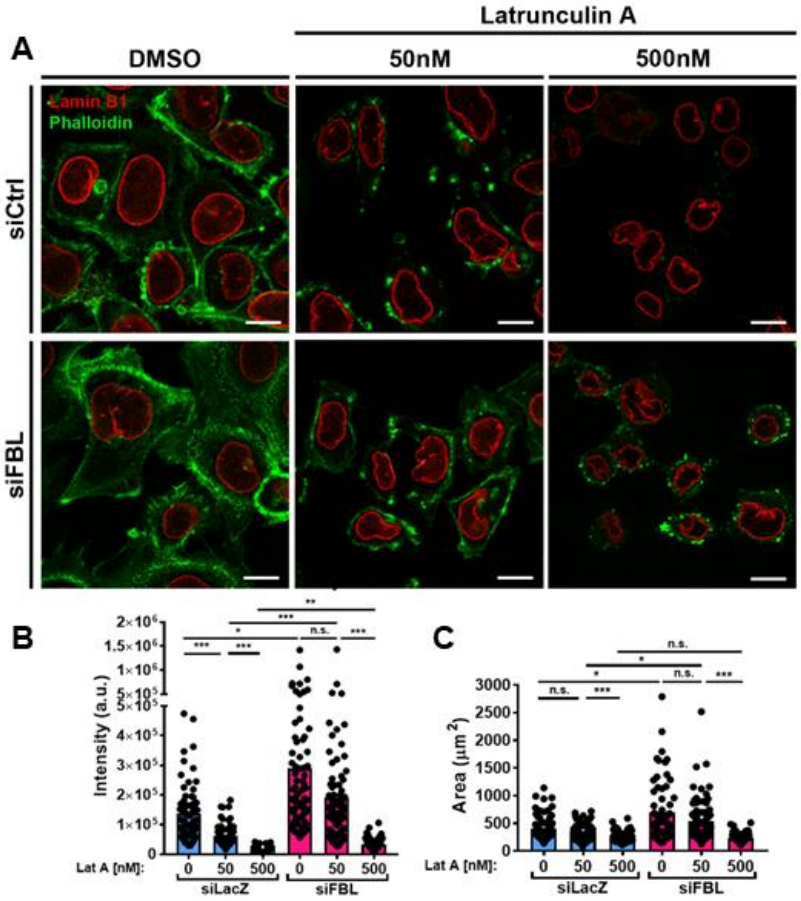

Figure 5.8. Fibrillarin depleted cells are resistant to actin depolymerization.
A. Control and Fibrillarin depleted cells were treated with Latrunculin A (50 nM and 500 nM) or vehicle control DMSO, and immunostained with Phalloidin. Scale bar ~ 5 μm. **B.** Actin intensity progressively decreases in cells upon treatment with increasing concentrations of Lat A. Fibrillarin depleted cells show significantly higher actin intensity at each assessed concentration of Lat A. n=number of cells assessed from N=2 biological replicates. Mann-Whitney test, *p<0.05, **p<0.01, ***p<0.001. **C.** Cell area progressively decreases upon increasing concentrations of Lat A treatment. Fibrillarin depleted cells show significantly higher actin intensity upto 50nM of Lat A concentration, compared with control siRNA treated cells. n=number of cells assessed from N=2 biological replicates. Mann-Whitney test, *p<0.05, **p<0.01, ***p<0.001.

5.2.7. Fibrillarin depletion affects nuclear architectural genes

Since Fibrillarin depletion showed a significant increase in nuclear aberrations with invaginated nuclear envelope (Fig. 5.6C), we examined the expression levels of nuclear architecture genes upon Fibrillarin knockdown using a customized Taqman based array (Fig. 5.9A). This custom array was composed of labeled probes for 43 genes including nuclear architectural genes, nucleolar proteins, transcription factors and chromatin remodellers. Fibrillarin transcripts were downregulated by ~96% upon siFBL treatment. Fibrillarin depletion induced significant downregulation in the transcript levels of other genes coding for nucleolar proteins – *GNL3*, *NCL*, *NPM1* and *EMG1*. Further, Fibrillarin knockdown also showed downregulation of (i) nuclear envelope genes – *BANF1*, *TMEM48*, *EMD*, *TMPO* and *LMNA*; (ii) nucleoporin encloding genes – *NUP93*, *SEC13*; (iii) transcription factors – *E2F1*, *SREBF1*, *POU5F1* and (iv) DNA methytransferase – *DNMT1*. Upregulated genes included histone binding protein – *CBX5*, transcription factor – *FOS* and cell-cell junction protein – *CDH1* (Fig. 5.9A). In summary, nuclear architecture genes were affected upon Fibrillarin knockdown, which could lead to weakening of the nuclear lamina, thus leading to nuclear distortions and invaginations.

We also examined if transcription factors specifically regulating nuclear envelope genes were deregulated upon Fibrillarin knockdown. We examined ChIP-Atlas database to identify transcription factors that regulate expression levels of nuclear envelope genes ($p<0.05$). We next overlapped these transcription factors to genes that were deregulated upon Fibrillarin knockdown, from the microarray data (Fig. 5.9B). We found two key transcription factors – *NMYC* and *ATF3* that regulate nuclear envelope genes (Fig. 5.9B). While *ATF3* was upregulated, *NMYC* was downregulated upon Fibrillarin depletion.

Figure 5.9

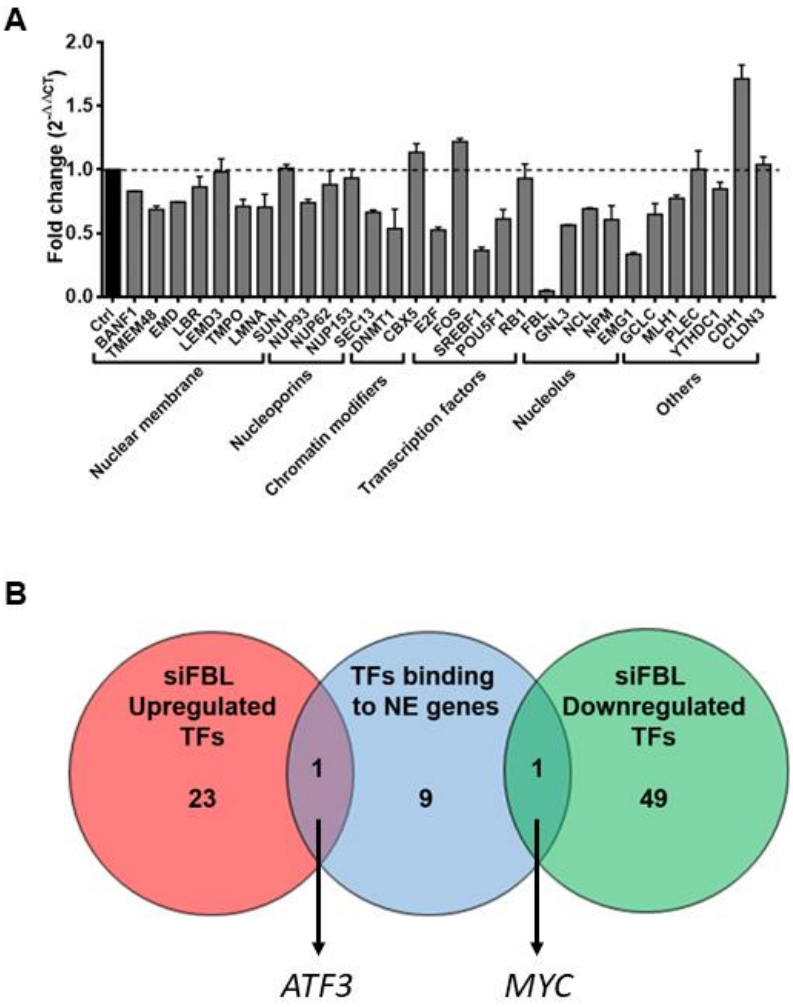

Figure 5.9. Nuclear architecture genes are dysregulated upon Fibrillarin knockdown. A. Expression profiling of genes coding for nuclear architectural (N.A.) proteins, upon Fibrillarin knockdown. Data shown is a compilation of three independent biological replicates, normalized to expression levels of *GAPDH*. Error bars – S.E.M. **B.** Overlap of transcription factors (T.F.s) affected upon Fibrillarin knockdown, with T.F.s regulating nuclear architectural genes affected in (A). *ATF3* and *MYC* are dysregulated TFs that regulate N.A. genes affected upon Fibrillarin knockdown.

5.2.8. Fibrillarin depletion affects Lamin expression levels

One of the most notable nuclear genes downregulated upon Fibrillarin knockdown was *LMNA* (~0.75 fold) (Fig. 5.9A). Lamins maintain nuclear structure and function across most cell types. In particular, mutations in LMNA gene (E145K, R471C, R527C, G608S) prevent processing of pre-lamin A into mature Lamin A, known to cause Hutchinson Gilford Progeria Syndrome (HGPS), characterized by severely misshapen nuclei (Vidak and Foisner, 2016). To understand if misshapen and invaginated nuclei seen upon Fibrillarin knockdown is due to altered Lamin levels, we examined expression and localization of lamins upon Fibrillarin knockdown. We immunostained cells for Lamin A/C, B2 and B1 (Fig. 5.10A-C). Lamin A/C and B2 were significantly downregulated in single cells, upon Fibrillarin knockdown while Lamin B1 levels remained unchanged (Fig. 5.10D-F). Furthermore, qRT-PCR analyses showed a significant decrease in *LMNA* (~0.72 fold) and *LMNB2* (~0.76 fold) transcript levels upon Fibrillarin knockdown, while LMNB1 (~0.81 fold) gene expression was unaffected (Fig. 5.10G). Further, western blotting revealed a significant depletion of Lamins upon Fibrillarin knockdown, which corroborated with the imaging results, showing ~50% downregulation in both Lamin A/C and Lamin B2 (Fig. 5.10H).

In summary, aberrations in nuclear structure upon Fibrillarin knockdown, is potentially mediated by downregulation of Lamin A/C and B2.

Figure 5.10

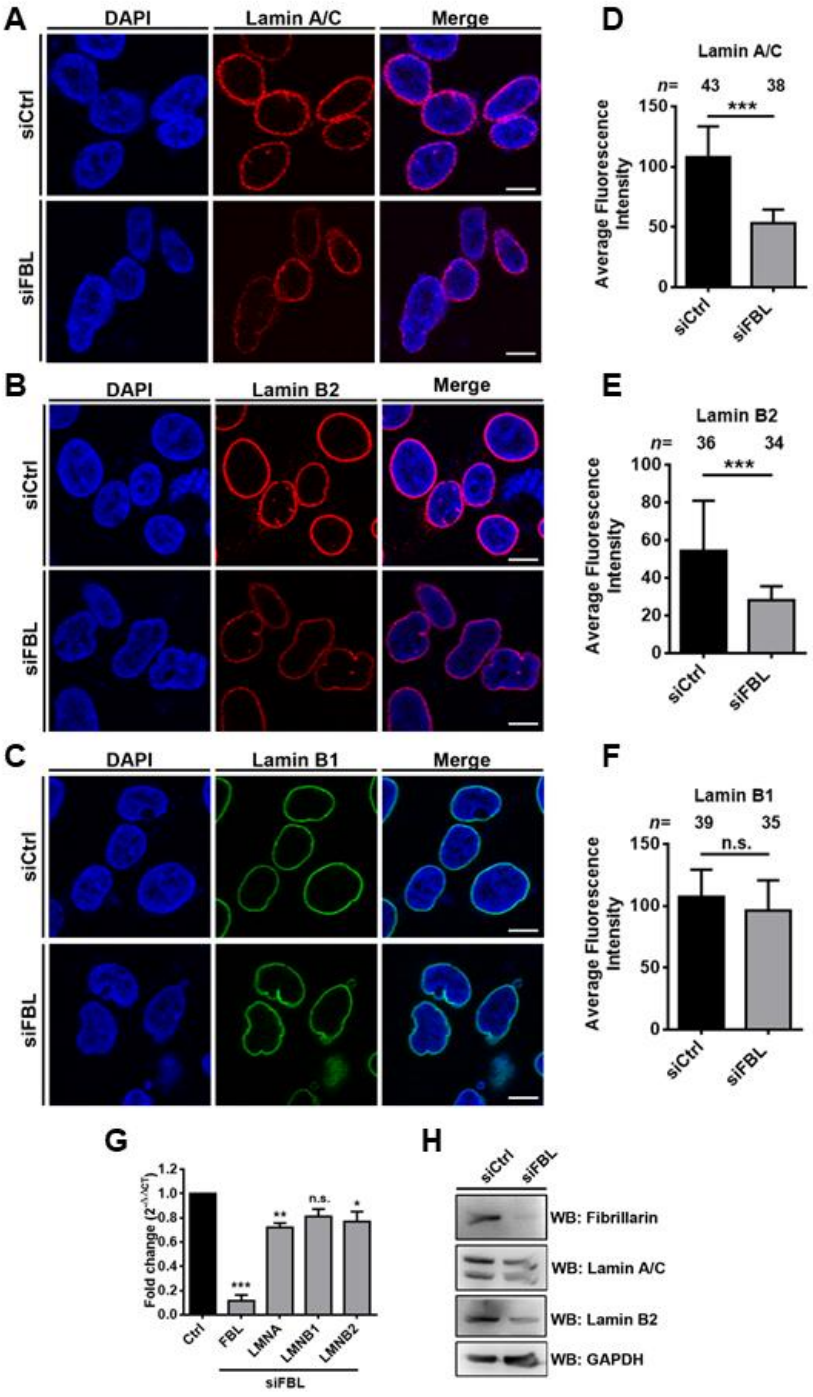

Figure 5.10. Lamin A/C and B2 are downregulated upon Fibrillarin knockdown.
A-C. Cells were immunostained with antibodies against Lamin A/C, B2 and B1 upon Fibrillarin knockdown, showing nuclear deformities. Scale bar ~ 5 μm. **D-F.** Quantification of average fluorescence intensity of Lamins A/C, B2 and B1 in Fibrillarin depleted cells. Error bars – S.D. n=number of nuclei assessed from N=3 biological replicates. **G.** qRT-PCR showing transcript levels of Lamins A, B1 and B2 upon Fibrillarin knockdown. **H.** Western blot showing protein expression levels of Lamin A/C and B2, upon Fibrillarin knockdown.

5.2.9. Fibrillarin depleted cells show enhanced cell migration

Given the striking changes in cell and nuclear morphology and actin organization in Fibrillarin depleted cells, we next determined cell migration in these cells. We surmised that cell migration could be affected in Fibrillarin depleted cell primarily because of the following reasons – (i) Fibrillarin depleted cells showed upregulation of genes associated with chemotaxis, (ii) these cells showed distinct changes in actin organization, (iii) these cells showed distorted nuclei and downregulation of Lamins A/C and B2. Migration of cells through tight interstitial spaces in the extracellular matrix, require large-scale deformation of the cell and the nucleus (Tong et al., 2012). Cells show highly contorted nuclei during migration through tissues. This is usually accompanied by a weakening of nuclear lamina with downregulation of lamins and LINC complex proteins (Rowat et al., 2013). The role of Lamin A has been widely studied in this aspect and higher expression levels of Lamin A, has been shown to impede cell migration (Swift et al., 2013). Fibrillarin depleted cells presented an interesting case of downregulation of nuclear lamina components (especially Lamin A/C) (Fig. 5.10) and a change in cell architecture (Fig. 5.7).

We thus assessed migration of Fibrillarin depleted DLD1 cells using 2D wound healing assay on tissue culture plastic. DLD1 cells show ~40% wound healing in 24h (Fig. 5.11A, B). However, Fibrillarin depleted cells showed increased wound healing 6h onwards at each assessed time point compared to control siRNA treated cells, finally showing ~75% wound healing at the end of 24h (Fig. 5.11A, B). We performed these assays under serum-starved conditions to negate the effects of cell proliferation. In summary, Fibrillarin depletion shows enhanced migratory potential in DLD1 cells.

Taken together, these assays showed that depletion of the essential nucleolar protein Fibrillarin leads to changes in cell and nuclear architecture. Fibrillarin shows a transcriptional and translational feedback with nuclear lamins. The changes in nuclear architecture, is potentially an outcome of weakened nuclear envelope and aberrant actin accumulation. The changes in cell architecture, is potentially mediated by dysregulation of genes affecting cell shape and cytoskeletal organization. Finally, Fibrillarin depletion in colorectal cancer cells also leads to enhanced cell migration.

Figure 5.11

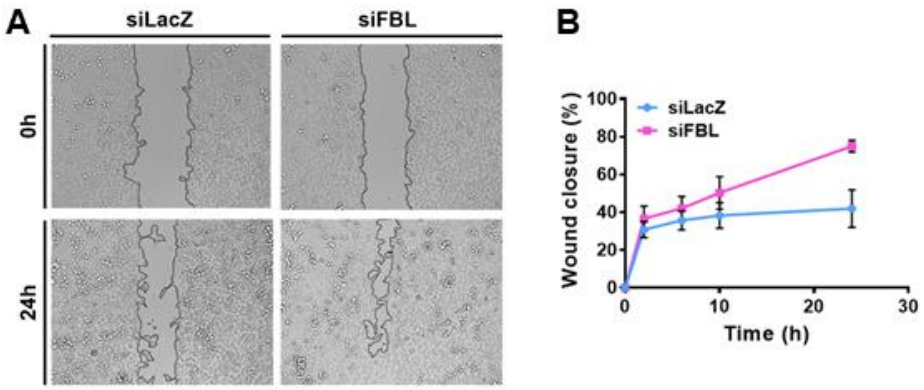

Figure 5.11. Enhanced migration of DLD1 cells upon Fibrillarin knockdown.
A. Representative images from wound healing assay in control and Fibrillarin depleted cells at 0 h and after 24 h of wound. **B.** Quantification of the percent closure of wound at 0 h, 6 h, 8 h, 10 h and 24 h after wound, showing enhanced cell migration in Fibrillarin depleted cells. n=6 fields per time point, N=1 biological replicate. Error bars – S.E.M.

5.3. Discussion

Effect of Fibrillarin knockdown on transcriptome

Our experiments show that Fibrillarin knockdown shows transcriptional deregulation (Fig. 5.2). So far, the role of Fibrillarin in affecting transcript levels through direct binding to DNA, has not been demonstrated. Therefore it is difficult to attribute the observed effects directly to the loss of Fibrillarin. From bioinformatics analyses, we identified several transcription factors that regulate genes affected upon Fibrillarin knockdown that include – NFAT, E12, SP1, AP1, MAZ, LEF1, NFKB, MYOD, MYC and PAX4 (Table 5.1). This could be due to aberrant IRES mediated translation or faulty ribosomes, that preferentially translate certain mRNA pools (Marcel et al., 2013; Shi et al., 2017). Interestingly SP1, AP1, MYC, LEF1, all contain IRES(s), which are otherwise rare in housekeeping genes (Hung et al., 2014; Jimenez et al., 2005; Komar et al., 2012; Shi et al., 2005; Vesely et al., 2009). Further studies using Fibrillarin mutated for methyltransferase activity (T172A mutant), may help delineate translational effects of Fibrillarin from direct transcriptional roles.

Nevertheless, genes that were dysregulated upon Fibrillarin knockdown include transcription factors and genes essential for developmental pathways such as *HOX* genes, *PITX1* and SMAD3, reiterating the important role of Fibrillarin in development (Fig. 5.3, Fig. 5.5, Table 5.1) (Bouffard et al., 2018; Liu et al., 2004; Mallo and Alonso, 2013; Marcil et al., 2003; Newton et al., 2003). This is in contrast with Nucleostemin knockdown, which specifically targeted genes involved in astrocyte and osteoclast differentiation, consistent with its role as a promoter of stemness in these cell types (Fig. 5.4) (Kafienah et al., 2006; Yaghoobi et al., 2005).

Lamin dependent regulation of nuclear structure by Fibrillarin

Fibrillarin knockdown severely affects nuclear structure (Fig. 5.6). To understand the mechanism by which Fibrillarin modulates nuclear morphology, we assessed the expression of several nuclear architectural genes (Fig. 5.9). We found that Lamins A/C and B2 were downregulated upon Fibrillarin knockdown, both at the transcript and the protein level (Fig. 5.9). Since, lamins are the major factors that maintain nuclear architecture, we surmise that the downregulation of Lamins A/C and B2 contributes to the occurrence of invaginated nuclei upon Fibrillarin depletion. Nucleolar structure was unaffected in Fibrillarin depleted cells, although Lamin B2 is downregulated by ~50%, suggesting that a critical threshold of Lamin B2 downregulation (~80-90%) is required to disrupt nucleoli (Fig. 5.6).

Lamin expression is mainly regulated at the transcript level, however regulatory transcription factors for Lamins, remain poorly characterized (Freund et al., 2012; Hamid et al., 1996; Mattia et al., 1992). Interestingly, Fibrillarin knockdown shows differential effects on the expression of Lamins – while A/C and B2 are downregulated, Lamin B1 remains unaffected

(Fig. 5.6). Epitope binding analysis from ChIP-Atlas suggests c-Myc as a transcription factor that binds to both Lamin A and B2 promoters, but not Lamin B1. Myc is downregulated upon Fibrillarin knockdown, and a potential candidate via which Fibrillarin mediates differential regulation of Lamins, although this remains to be experimentally validated. Further, stoichiometries of A-type and B-type lamins determine the arrangement of Lamin filaments at the nuclear envelope and consequently contribute to mechanical properties of the nucleus. B-type lamin knockout cells show an increase in the size of the Lamin A meshwork (Shimi et al., 2015). Large lamin meshwork sizes upon depletion of B-type lamins also co-relate with nuclear blebs (Funkhouser et al., 2013). A higher A:B1 lamin ratio is found in tissues with higher stiffness like bone and muscle, while a lower A:B1 ratio is found in soft tissues like brain and neuroendocrine tissues (Swift et al., 2013). Lamin B2 expression is generally constant across tissue types. Greater A:B ratio also indicates an increase in nuclear stiffness and rigidity, as depletion of Lamin A in A549 cells without affecting B-type lamins, leads to softer, compliant nuclei (Pajerowski et al., 2007). Taken together, the downregulation of Lamin A and B2, upon Fibrillarin depletion potentially affects nuclear structure.

Altered cytoskeletal structure in Fibrillarin depleted cells

Our studies show for the first time, an impact of Fibrillarin on cell shape and cytoskeletal organization. Fibrillarin depleted cells are larger in size, show numerous filopodia and aberrant actin accumulation in the cytoplasm (Fig. 5.7). These cells are also more resistant to Actin depolymerization by Latrunculin treatment (Fig. 5.8). We envisage two potential mechanisms by which Actin cytoskeleton could be modulated in Fibrillarin knockdown cells – (i) dysregulation of Actin remodeling proteins (ii) Lamin A/C mediated effects on actin polymerization.

Rho, Rac and cdc42 are the primary GTPases that regulate actin organization in the cytoplasm (Fig. 5.3). Rac responds to growth factor signaling and promotes actin branching and lamellipodia formation in an Arp2/3 dependent manner, while inhibiting Rho (Jaffe and Hall, 2005). Rho promotes actin stress fibre and focal adhesion formation, while cdc42 induces filopodia formation (Gupton and Gertler, 2007; Wheeler and Ridley, 2004). Microarray analysis, showed that multiple regulators of these GTPases, were downregulated upon Fibrillarin knockdown including – *PLXNB2* (negative regulator of Rac) and ARAP3 (activator of Rho). Further, *CORO1A*, which promotes actin turnover, was downregulated upon Fibrillarin knockdown. Thus, downregulation of these genes is potentially a mechanism by which actin cytoskeletal reorganizations are seen upon Fibrillarin knockdown. ChIP-seq experiments show that the transcription factor SREBF1 (SREBP-1) has binding sites on the promoters of *PLXNB2* and *CORO1A* (Seo et al., 2009). Thus the transcriptional downregulation of *PLXNB2* and

CORO1A could be mediated by SREBF-1, which itself is downregulated upon Fibrillarin depletion.

Lamin A/C connects to cytoplasmic actin via the LINC complex (Rowland et al., 2003). Cytoplasmic actin is highly mobile in LMNA$^{-/-}$ cells (Ho et al., 2013). Further, actin stress fibre re-assembly after Cytochalasin treatment and wash-off, is slower in LMNA$^{-/-}$ cells, suggesting altered actin polymerization (Ho et al., 2013). Lamin A also promotes actin polymerization in activated T-cells, which is necessary for immunological synapse formation (González-Granado et al., 2014). Thus, the altered actin arrangement and accumulation of actin in Fibrillarin depleted cells could result from downregulation of Lamin A/C.

Nuclear morphology and cell cytoskeleton are co-regulated

Experiments involving cells cultured on micro-patterned substrates show that nuclear shape is highly dependent on cell adhesion geometry (Versaevel et al., 2012). The crucial role of perinuclear actin, in maintaining nuclear shape is demonstrated, when it is disrupted by actin depolymerizing drugs Latrunculin A, or by knocking down LINC complex proteins that de-links that nucleus from the actin cytoskeleton (Fig. 5.8) (Khatau et al., 2009). The perinuclear actin cap is essentially composed of contractile acto-myosin cables that lie above the interphase nucleus connected to the nuclear envelope via the LINC proteins. Lamin A mutant and null cells show a lack of perinuclear actin cap, show nuclear ruffles when cells are stretched, showing that Lamin A/C and perinuclear actin prevent nuclear deformation (Kim et al., 2017). Thus, the unusual actin organization upon Fibrillarin knockdown, coupled with Lamin A/C downregulation potentially affects nuclear morphology in these cells.

Lamin A$^{-/-}$ and Lamin A mutant cells show lower cell stiffness, analogous to metastatic cancer cells that show higher mechanical compliance compared to non-metastatic cells (Lee et al., 2007a; Swaminathan et al., 2011). Reduced Lamin A levels and softer nuclei, allow the passage of cells through constrictions of the extra cellular matrix (Rowat et al., 2013). We have uncovered an increase in 2D cell migration upon Fibrillarin knockdown (Fig. 5.11). This could be attributed to the increase in expression of chemotactic genes and genes involved in extracellular matrix organization, upon Fibrillarin knockdown. It would be useful to assess the role of Lamin A/C in regulating cell migration in Fibrillarin depleted cells. Fibrillarin overexpression has been previously shown to increase tumorigenesis by increasing translation of oncogenes – *MYC*, *FGF1*, *FGF2* and *VEGFA* (Marcel et al., 2013). In this study, we find that decrease in Fibrillarin levels can also induce phenotypic changes in cells, typically observed during cancer cell metastasis.

In summary, we have uncovered a unique feedback between a nucleolar protein – Fibrillarin and nuclear Lamins, in regulating nuclear and cell architecture.

Figure 5.12

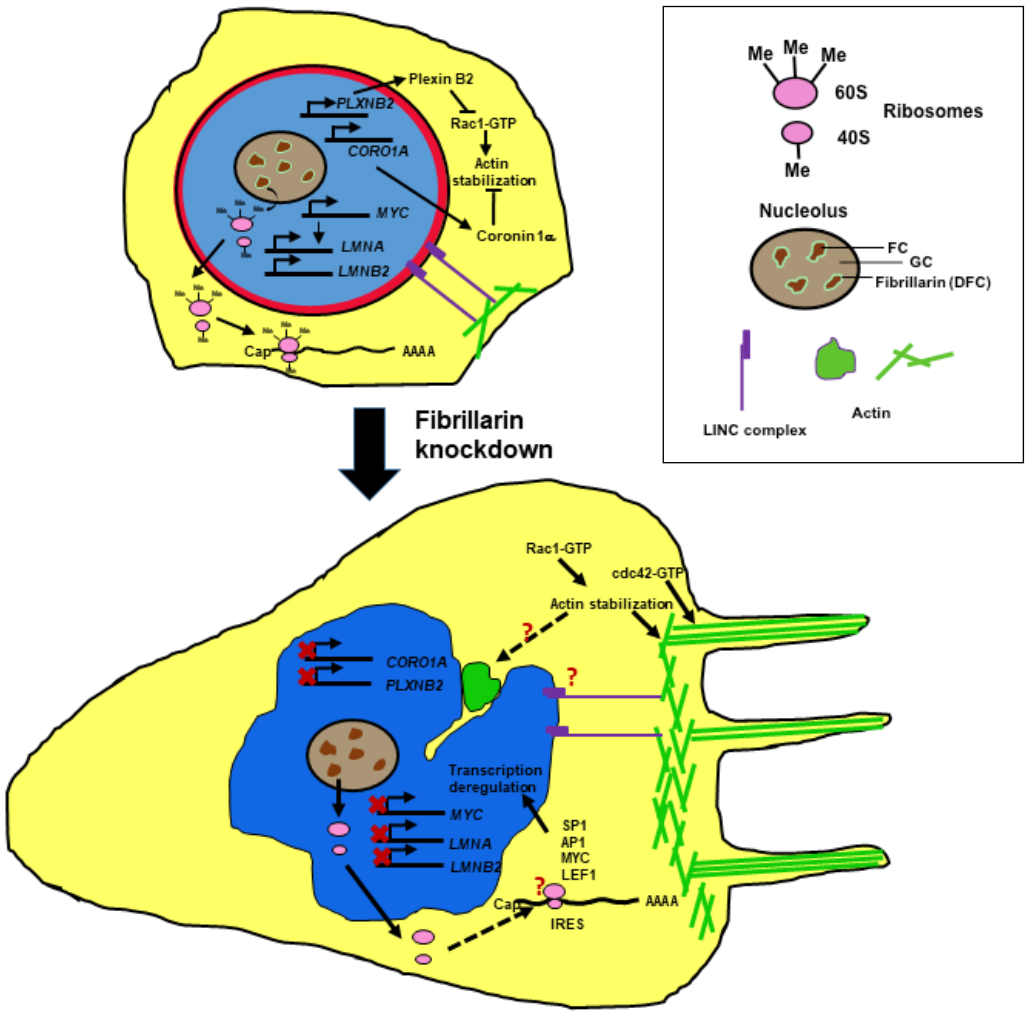

Figure 5.12. Model depicting a role for Fibrillarin in modulating nuclear and cell architecture
Fibrillarin depleted cells show invaginated nucleiand downregulation of Lamin gene expression. Cells show larger surface area, Actin aggregates and increased filopodia upon Fibrillarin knockdown. Fibrillarin knockdown affects methylation of rRNA. Aberrantly methylated ribosomes potentially show IRES mediated translation of transcription factors that further deregulate gene expression. Downregulation of *CORO1A* and *PLXNB2* potentially affects Actin organization upon Fibrillarin knockdown.

Chapter 6:
Role of Nucleolin in modulating nucleolar localization of histone 2B

Data acknowledgements –
Figure 6.1A, B – Sumit Pawar
Figure 6.4A, B – Sumit Pawar
Figure 6.6D – Gaurav Joshi

Results from this chapter are published as a part of the following paper –

Sen Gupta, A., Joshi, G., Pawar, S. and Sengupta, K. (2018). Nucleolin modulates compartmentalization and dynamics of histone 2B-ECFP in the nucleolus. Nucleus. 1-18.

6.1. Introduction

The nucleolus is a multifunctional nuclear sub-organelle. Proteomic studies of isolated nucleoli have identified over 4500 proteins that stably or dynamically localize to the nucleolus and this number is still expanding (Ahmad et al., 2009). Further, SILAC (stable isotope labelling with amino acids) based quantitative proteomic analysis has shown how the nucleolar proteome is altered during viral infections, stress induced senescence, serum stimulation and DNA damage (Boisvert and Lamond, 2010; Emmott et al., 2010a, 2010b; Kar et al., 2011; Lam et al., 2010; Liang et al., 2012). The massive repertoire of nucleolar proteins unrelated to ribosome biogenesis, underscore the role of the nucleolus in various cellular processes like regulation of cell cycle, apoptosis, signaling and cellular stress sensing (Bański et al., 2010; Bywater et al., 2012; Gaulden and Perry, 1958). The import and sequestration of protein and RNA into nucleolus modulates their nucleoplasmic concentration and function. The nucleolus functions as a stress-sensing compartment that sequesters oncoproteins such as BRCA1 and regulators of p53, that are released into the nucleoplasm upon DNA damage (Boyd et al., 2011; Guerra-Rebollo et al., 2012), while, HSP70 and VHL proteins are immobilized in the nucleolus during thermal stress and acidosis respectively, that negatively affect rDNA transcription (Audas et al., 2012). Thus sequestration of proteins or their exit from the nucleolus, is an important mode of post-translational regulation of proteins and impinges onto cell homeostasis.

Protein targeting to different organelles require specific signal peptide like KDEL for the endoplasmic reticulum (ER), SKL for lysosomes and basic lysine-arginine rich Nuclear localization signal (NLS) sequences for nuclear localization (Gould et al., 1989; Lange et al., 2007; Munro and Pelham, 1987). The presence of targeting signals on proteins are recognized by specialized machinery like the signal recognition particle (SRP) that target proteins to the ER and the importin complex that allows entry of proteins into the nucleus (Janda et al., 2010; Lange et al., 2007). Once localized, these proteins are usually stably associated with the organelle. Unlike other organelles like the ER and the nucleus, intranuclear bodies like the nucleolus are not membrane bound. Furthermore, nucleolar proteins are in dynamic equilibrium with the nucleoplasm. Mechanisms by which proteins are targeted to the nucleolus are still not very well understood. Several studies show the role of a nucleolar localization signal (NoLS) in targeting proteins to the nucleolus (Table 6.1) (Emmott and Hiscox, 2009; Scott et al., 2011). However, NoLS motifs are not very distinct from NLS motifs in terms of their sequence composition and can also show overlap (Valdez et al., 1994). Systematic characterization of 46 NoLS motifs has shown that in general NoLS sequences are short basic motifs rich in lysine and arginine amino acids (~48% basic residues) and usually localized at the termini of proteins (Scott et al., 2010).

Table 6.1. Nucleolar localization sequences of selected proteins
(Reviewed Emmott and Hiscox, 2009)

Protein	NoLS sequence	References
IBV N protein	WRRQARFK	(Reed et al., 2008)
ApLLP	MAKSIRSKHRRQMRMMKRE	(Kim et al., 2003)
HIV-1 TAT	RKKRRQRRRAHQ	(Siomi et al., 1990)
GGNNVα	RRRANNRRR	(Guo et al., 2003)
Angiogenin	IMRRRGL	(Lixin et al., 2001)
HSV type 1 γ(1)34.5	MARRRRHRGPRRPRPP	(Cheng et al., 2002)
HIV-1 REV	RRNRRRRWRERQRQI	(Cochrane et al., 1990)
FGF2	RSRKYTSWYVALKR	(Sheng et al., 2004)
MDM2	KKLKKRNK	(Lohrum et al., 2000)
NIK	RKKRKKK	(Birbach et al., 2004)
Nuclear VCP-like protein	KRKGKLKNKGSKRKK	(Nagahama et al., 2004)
p120	SKRLSSRARKRAAKRRLG	(Valdez et al., 1994)
HIC p40	GRCRRLANFGPRKRRRRRR	(Thébault et al., 2000)
MDV MEQ protein	RRRKRNRDARRRRRKQ	(Liu et al., 1997)
HVS ORF57	KRPR-RRPSRPFRKP (a bipartite NoLS; 25 residues separate the two halves in wild type, but it retains its functionality when they are joined)	(Boyne and Whitehouse, 2006)
LIMK2	KKRTLRKNDRKKR	(Goyal et al., 2006)
PRRSV N protein	PGKKNKKKNPEKPHFP LATEDDVRHHFTPSER	(Rowland et al., 1999, 2003)

ApLLP, *Aplysia* LAPS18-like protein; FGF2, fibroblast growth factor 2; GGNNVα, betanodavirus greasy grouper (*Epinephelus tauvina*) nervous necrosis virus protein α; HIC p40, human I-mfa domain-containing protein, p40; HIV-1 Rev, human immunodeficiency virus-1 regulator of virion protein; HIV-1 TAT, human immunodeficiency virus-1 transactivator of transcription protein; HVS, herpesvirus saimiri; HSV type 1 γ(1) 34.5, herpes simplex virus type 1 γ(1) 34.5 protein; IBV N, infectious bronchitis virus nucleocapsid; LIMK2, LIM kinases 2; MDM2, murine double minute 2 protein; MDV, Marek disease virus; MEQ, MDV Eco Q; NIK, nuclear factor-κB inducing kinase; NoLS, nucleolar localization signal; ORF57, open reading frame 57; PRRSV N, porcine reproductive and respiratory syndrome virus nucleocapsid; VCP, nuclear valosin-containing protein

Although VHL protein contains an NoLS, it localizes to the nucleolus only under acidic conditions of cell medium (Mekhail et al., 2005). This suggests that mere presence of an NoLS is not sufficient for nucleolar localization of proteins. It was later demonstrated that the nucleolar localization and retention of VHL was facilitated by its association nucleolar non-coding RNA, whose expression is induced upon acidosis (Audas et al., 2012). Further PP1 protein localizes to the nucleolus, even though it does not contain an NoLS, by interacting with the NoLS containing protein Nom1 (Gunawardena et al., 2008). Thus, localization and retention

of proteins in the nucleolus can be mediated by their binding to nucleolar "hub" proteins, nucleolar RNA or DNA (Emmott and Hiscox, 2009). Nucleolar "hub" proteins include Nucleolin and Nucleophosmin (NPM1) (Emmott and Hiscox, 2009). Surprisingly, Nucleophosmin, itself does not contain a characteristic NoLS (Scott et al., 2010). NPM1 binds to NoLS of PNRC (proline-rich nuclear receptor coregulatory protein), HIV tat protein, Nucleolin, p120 and shuttles them to the nucleolus (Li, 1997; Li et al., 1996; Valdez et al., 1994; Wang et al., 2011b). The influenza virus NS1 protein localizes to the nucleolus via its interaction with Nucleolin through the NoLS of NS1 (Melén et al., 2012). Nucleolin and NPM1, both contain predicted disordered regions in their N and C termini, respectively. These disordered regions mediate interaction of Nucleolin and NPM1 with multiple binding partners and also with RNA (Fujiwara et al., 2011; Mitrea et al., 2016).

Mass spectrometric analyses of nucleolar extracts identified the presence of isoforms of each histone family – H1, H2, H3, H4 and histone-modifying enzymes in the nucleolus (Leung et al., 2006). Core histones are very stably associated with nucleoplasmic chromatin by incorporation into octamers. Furthermore, histones are largely bound to nuclear chromatin, considering their low recovery in photobleaching experiments (Kimura and Cook, 2001). Histone 2B has been detected in the nucleoli of Bovine liver cells and chicken erythrocytes using antibodies raised against its first 58 amino acids (di Padua Mathieu et al., 1981). Localization of H2B in the nucleolus is attributed to stretches of basic amino acid residues (KKRKRSRK), similar to the NoLS motifs: (R/K)(R/K)X(RK) or (R/K)X(R/K)(R/K) (Musinova et al., 2011). The NoLS signals in histone 2B overlap with its NLS, hence making it difficult to verify the specific role of NoLS in targeting histone 2B to the nucleolus. Also, the function of nucleolar histone 2B is not understood.

In vitro studies implicate Nucleolin as a histone chaperone with FACT-like activity, which regulates Swi-SNF function and ACF chromatin remodelers (Angelov et al., 2006). Nucleolin has a High Mobility Group (HMG)-like N-terminal domain with four acidic stretches of glutamate and aspartate residues, interspersed with basic lysine residues (Erard et al., 1988). The acidic stretches interact with histone H1 while the basic residues interact with DNA (Erard et al., 1988). Nucleolin also has four central RNA binding domains (RBD1-4) and a C-terminal GAR (Glycine Arginine Rich) domain. The RNA binding domain specifically binds to a 5' external transcribed sequence (ETS) site on nascent ribosomal RNA. The GAR domain of Nucleolin binds specifically to DNA and non-specifically to RNA, while the RBDs confer specificity to RNA binding (Ghisolfi et al., 1992; Serin et al., 1996, 1997). ChIP-Seq analysis reveals the recruitment of Nucleolin to sites of DNA damage, resulting in the eviction of histones - H2A and H2B thereby allowing access to the DNA double strand break repair machinery (Goldstein et al., 2013).

Here we investigated the role of Nucleolin in modulating nucleolar localization and dynamics of histone 2B. Furthermore, since our previous studies suggested the role of Lamins and nucleolar proteins – Fibrillarin and Nucleostemin in regulating nucleolar and nuclear structure-function, we also examined if these proteins modulate histone 2B dynamics in the nucleus and nucleolus respectively.

6.2. Results

6.2.1. Histone 2B (H2B) compartmentalizes in the nucleolus

The nucleolus is the largest nuclear sub-organelle and is essential for ribosomal RNA (rRNA) and protein synthesis (Mélèse and Xue, 1995). However, the mechanisms that regulate the sequestration of proteins within the nucleolus remain unclear. For instance, overexpressed H2B is sequestered in the nucleolus (Musinova et al., 2011). Here we sought to investigate the mechanisms that modulate the sequestration and dynamics of H2B in the nucleolus. We transfected H2B-ECFP into DLD1 cells and found that although H2B localizes in the nucleoplasm of all cells, a significant sub-population of cells (~40%) show H2B-ECFP in the nucleolus (Fig.6.1A, B). While, the Nuclear Localization Signal (NLS) sequence tagged with CFP localizes in the nucleolus of nearly all transfected cells (~98%) (Fig. 6.1A, B). We surmise that the relatively small NLS-CFP freely diffuses into the nucleolus, while the nucleolar localization of H2B-ECFP in a sub-population of ~40% cells, is potentially guided by additional interactions with nucleolar factors. H2B-ECFP localizes in the nucleolus of diverse cancer cell lines such as HCT116 (colorectal cancer cell line), MCF7 (breast cancer cell line) as well as DLD1 cells (Fig. 6.1C). In addition to visualizing nucleolar localization of overexpressed H2B-ECFP, we found that endogenous H2B localizes in the nucleolus as revealed by immunofluorescence assays (Fig. 6.1D).

Lamin A regulates nuclear histone dynamics, while Lamin B1 and Lamin B2 modulate nucleolar organization and function (Martin et al., 2009; Melcer et al., 2012; Sen Gupta and Sengupta, 2017). We thus asked if nuclear Lamins or nucleolar factors - Fibrillarin (FBL) and Nucleostemin (GNL3), modulate the compartmentalization of H2B-ECFP in the nucleolus (Fig. 6.1E). We independently knocked down nuclear Lamins, Fibrillarin (FBL) and Nucleostemin (GNL3) in DLD1 cells. Interestingly, knockdown of Lamin A/C (LMNA/C), Lamin B1 (LMNB1), Lamin B2 (LMNB2) or nucleolar factors - Fibrillarin (FBL) and Nucleostemin (GNL3) did not significantly affect the extent of H2B-ECFP localization within the nucleolus (Fig. 6.1E). Taken together, these results suggest that the nucleolar localization of H2B is unaffected by the depletion of Lamins or nucleolar factors such as FBL and GNL3.

Figure 6.1

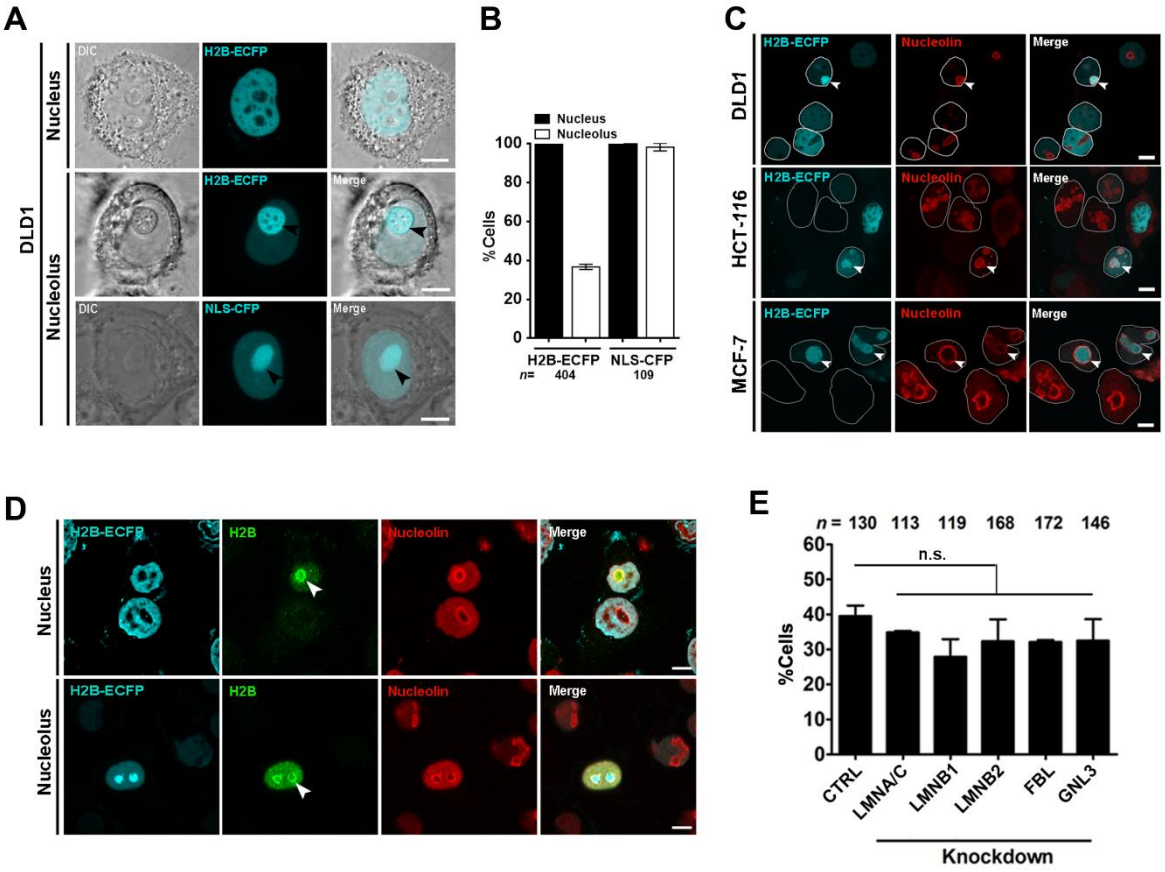

Figure 6.1. Histone 2B localizes in the nucleolus.
A. H2B-ECFP is distinctly localized in the nucleoplasm and the nucleolus. (Top panel, Nucleus): nucleoplasmic localization of H2B-ECFP. (Lower panel, Nucleolus): localization of H2B-ECFP in the nucleolus (black arrowhead). NLS-CFP localizes to the nucleoplasm and the nucleolus (black arrowhead). Scale bar ~ 5µm. **B.** All transfected cells show H2B-ECFP in the nucleoplasm, while ~40% of these cells harbor H2B-ECFP in the nucleolus. All cells show NLS-CFP in the nucleoplasm, while ~98% cells show NLS-CFP in the nucleolus, n=number of nuclei, data compiled from N=2 independent biological replicates. **C.** Immunostaining of Nucleolin reveals nucleolar localization of H2B-ECFP in DLD1, HCT-116 and MCF-7 cells (white arrows). White outline demarcates single nucleus, Scale bar ~ 5µm. **D.** Cells transfected with H2B-ECFP were immunostained with anti-histone 2B antibody and anti-nucleolin antibody to demarcate the nucleolus (white arrows). Anti-histone 2B antibody detected both transfected and endogenous H2B in the nucleolus. Scale bar ~ 5µm. **E.** Independent knockdowns of Lamin A/C, B1, B2, FBL and GNL3 do not affect nucleolar localization of labeled H2B-ECFP, n=number of nuclei, data compiled from N=3 independent biological replicates, error bars: SEM. Student's t-test, p>0.05 (n.s: not significant).

6.2.2. Lamin B1 enhances mobility of H2B in the nucleolus

Since, nuclear Lamins maintain the structural and functional integrity of the nucleus (Shimi et al., 2008; Taimen et al., 2009), we asked if Lamins regulate H2B dynamics. We performed siRNA mediated knockdown followed by immunoblotting, which showed ~70% depletion of Lamins in DLD1 cells (Fig. 6.2A-C). We next performed FRAP of H2B-ECFP in the nucleolus and the nucleus upon Lamin depletion (Fig. 6.2D, E). Interestingly, Lamin A/C knockdown did not affect H2B-ECFP dynamics in the nucleolus (M.F. ~38.77%) (Fig. 6.2F, I, Table 6.2), while Lamin B1 knockdown showed a significant increase in the mobile fraction of H2B-ECFP (M.F ~61.63%) (Fig. 6.2G, I, Table 6.2). Lamin B2 knockdown also showed a marginal increase in H2B mobility (~48.98%) (Fig. 6.2H, I, Table 6.2). In sharp contrast, Lamin knockdowns did not significantly alter H2B mobility in the nucleus (Fig. 6.2J-M, Table 6.2).

Table 6.2. Mobile fractions of H2B-ECFP

	H2B-ECFP Mobile fraction (%) ± S.E.M.	
	Nucleus	**Nucleolus**
Control	18.79 ± 2.19 (n=17)	44.3 ± 3.44 (n=16)
Lamin A Kd	21.14 ± 1.13 (n=15, p=0.62)	38.77 ± 9.27 (n=8, p=0.59)
Lamin B1 Kd	18.01 ± 0.47 (n=11, p=0.77)	61.63 ± 5.05 (n=11, *p=0.015)
Lamin B2 Kd	22.25 ± 0.87 (n=15, p=0.39)	48.98 ± 7.9 (n=7, p=0.599)
Fibrillarin Kd	17.11 ± 2.22 (n=13, p=0.59)	68.81 ± 8.09 (n=7, *p=0.02)
Nucleostemin Kd	12.75 ± 0.46 (n=13, *p=0.03)	69.44 ± 3.16 (n=11, **p=0.0058)
Nucleolin GFP OE	-	71.76 ± 3.43 (n=17, **p=0.0048)

Figure 6.2

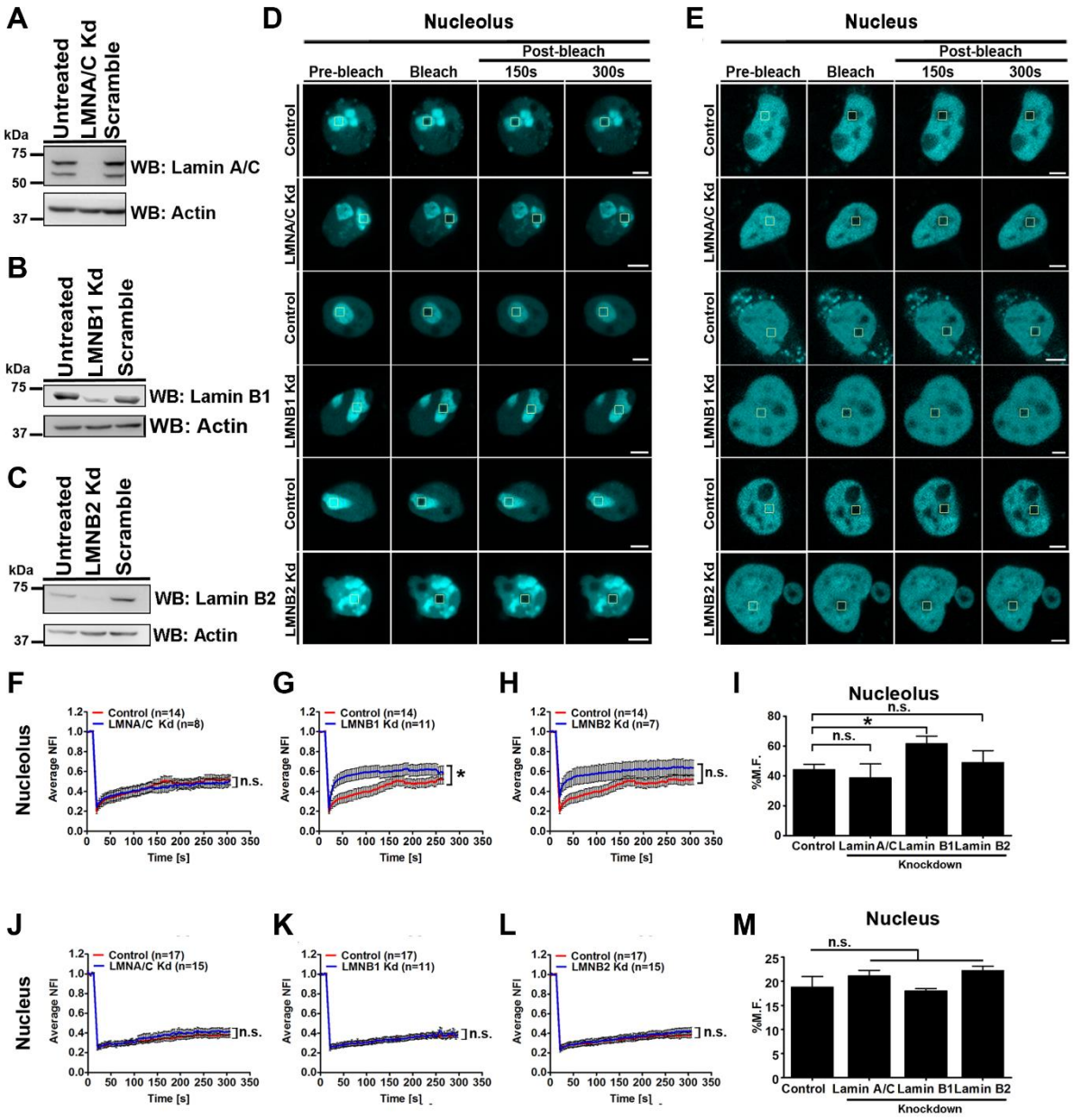

Figure 6.2. Lamin B1 depletion enhances H2B–ECFP mobility in the nucleolus.
A-C. Western blots of whole cell lysates prepared from (A) LMNA/C (B) LMNB1 and (C) LMNB2 knockdown. Controls: Untreated, scramble siRNA. Loading control: Actin. **D-E.** FRAP of H2B-ECFP in the nucleolus and nucleus. Representative nucleus of control, LMNA Kd, LMNB1 Kd and LMNB2 Kd cells, respectively. Yellow box represents bleached ROI. Scale bar ~ 5 µm. **F-H.** Normalized fluorescence recovery curves comparing recovery of H2B-ECFP in the nucleolus of control, (F) LMNA Kd (G) LMNB1 Kd and (H) LMNB2 Kd cells. **I.** Relative mobile fractions of H2B-ECFP in the nucleolus as calculated from (F-H), showing increased mobility of H2B-ECFP in the nucleolus upon Lamin B1 Kd. **J-L.** Normalized fluorescence recovery curves of H2B-ECFP in the nucleus of control, (J) LMNA Kd (K) LMNB1 Kd (L) LMNB2 Kd cells. **M.** Relative mobile fractions of H2B-ECFP in the nucleus as calculated from (J-L). Lamin Kd does not affect H2B-ECFP mobility in the nucleus, n=number of nuclei, data compiled from N=3 independent biological replicates, error bars: SEM in recovery curves and bar graph. Student's t-test, *p<0.05.

6.2.3. Fibrillarin (FBL) and Nucleostemin (GNL3) modulate H2B dynamics within the nucleolus

We sought to examine if bonafide nucleolar proteins of the DFC and GC regions of the nucleolus - Fibrillarin (FBL) and Nucleostemin (GNL3), respectively, modulate H2B dynamics within the nucleolus (Fig. 6.3) (Cerdido and Medina, 1995; Romanova et al., 2009a). We performed siRNA mediated knockdown of FBL and GNL3 in DLD1 cells, followed by western blotting, which showed ~80% depletion (Fig. 6.3A, B). We next examined H2B dynamics in the nucleolus and nucleus respectively upon FBL and GNL3 depletion (Fig. 6.3C, D). FBL and GNL3 knockdown significantly increased the mobility of H2B-ECFP in the nucleolus (FBL Kd: M.F ~68.81%), (GNL3 Kd: M.F ~69.44%) (Fig. 6.3E-G, Table 6.2). Interestingly photobleaching the nuclear sub-pool of H2B-ECFP, showed a marginal decrease in its nuclear dynamics (FBL Kd: M.F ~17.11%) (Fig. 3H, J, Table 6.2), while Nucleostemin (GNL3) depletion showed a significant decrease in the mobile fraction of H2B-ECFP (GNL3 Kd: M.F ~12.75%) in the nucleus (Fig. 3I, J, Table 6.2). Taken together, these results reveal that Fibrillarin and Nucleostemin depletions modulate the dynamics of H2B in the nucleolus, further underscoring the role of FBL and GNL3 in maintaining the microenvironment and stability of the nucleolus.

Figure 6.3

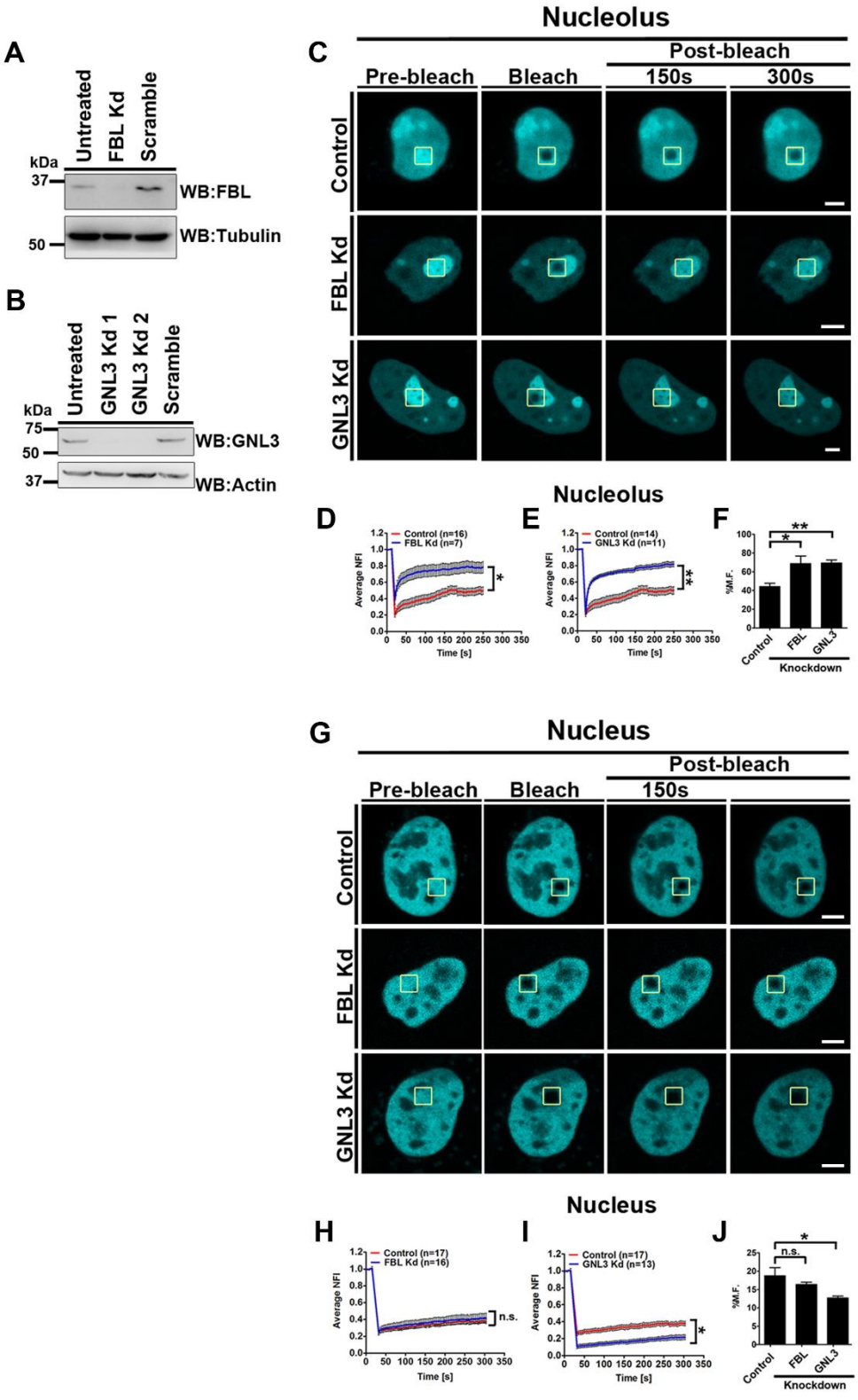

Figure 6.3. Depletion of Fibrillarin (FBL) and Nucleostemin (GNL3) enhances H2B–ECFP mobility in the nucleolus.
A-B. Western blots of whole cell lysates prepared from DLD1 cells upon knockdown of (A) Fibrillarin (FBL) (B) Nucleostemin (GNL3), Controls: untreated and respective scramble siRNA treated cells. Loading controls: Tubulin, Actin. **C-D.** FRAP of H2B-ECFP in the nucleolus and nucleus of control, FBL and GNL3 Kd cells, respectively. Yellow box represents bleached ROI. Scale bar ~ 5 µm.

E-F. Normalized fluorescence recovery curves comparing recovery of H2B-ECFP in the nucleolus of control (E) FBL Kd and (F) GNL3 Kd cells. **G.** Relative mobile fractions of H2B-ECFP in the nucleolus as calculated from (E-F). **H-I.** Normalized fluorescence recovery curves comparing recovery of H2B-ECFP in the nucleus of control, (H) FBL Kd (I) GNL3 Kd cells. **J.** Relative mobile fractions of H2B-ECFP in the nucleus as calculated from (H-I), n=number of nuclei, data from N=3 independent biological replicates, error bars: SEM in recovery curves and bar graph. Student's t-test, *p<0.05, **p<0.01.

6.2.4. Nucleolin modulates compartmentalization of H2B in the nucleolus

Nucleolin is a bonafide GC component protein that maintains nucleolar integrity and stability (Ma et al., 2007). We asked if Nucleolin modulates the sequestration of H2B in the nucleolus. We knocked down Nucleolin, followed by H2B-ECFP transfection into DLD1 cells (Fig. 6.4A, B). Interestingly, Nucleolin depletion revealed a striking reduction in the number of cells with H2B-ECFP in the nucleolus (<10%), as compared to control cells (~36%) (Fig. 6.4C). H2B-ECFP expression was marginally higher in Nucleolin depleted cells (Fig. 6.4B (ii)). This contrasts with Lamin, FBL and GNL3 depletion, which did not alter the extent of H2B compartmentalization in the nucleolus (Fig. 6.1E). The independent depletion of another nucleolar GC protein namely Nucleophosmin (NPM1), also showed a marginal reduction of H2B-ECFP in the nucleolus (~30%) as compared to control cells (~38%) (Fig. 6.4C). Decrease in nucleolar H2B-ECFP upon NPM1 knockdown, is consistent with the association between NPM1 and core, linker histones (H1, H3, H4, H2A, H2B) (Gadad et al., 2011; Swaminathan et al., 2005). In contrast, the GC protein Nucleostemin (GNL3), does not affect nucleolar localization of H2B-ECFP (Fig. 6.1E). Of note, the localization of NLS-CFP in the nucleolus was unaltered upon Nucleolin knockdown (~95%) as compared to control cells (~96%) (Fig. 6.4C). In summary, Nucleolin is a key factor, which modulates the localization of H2B-ECFP in the nucleolus.

Since Nucleolin knockdown reduced H2B-ECFP compartmentalization in the nucleolus, we performed the converse experiment of overexpressing Nucleolin. Interestingly, Nucleolin co-expression showed a consistent and enhanced retention of nucleolar H2B-ECFP in ~67% cells (24h), which declined to ~42% (48h), and ~24% (72h) post transfection (Fig. 6.4D, black bars), while nucleolar H2B-ECFP declined rapidly over time from ~35% (24h), ~10% (48h) and ~5% (72h) in control cells (Fig. 4D, white bars). Essentially, H2B-ECFP retention was significantly higher upon Nucleolin co-expression at each time point. Independently, NPM1 co-expression showed a moderate increase in nucleolar retention of H2B-ECFP (~57%, after 24h), which was lower than upon Nucleolin co-expression (~67%) (Fig. 6.4D). Taken together, Nucleolin regulates H2B-ECFP retention in the nucleolus.

We asked if the compartmentalization of H2B-ECFP in the nucleolus, correlates with endogenous levels of Nucleolin across cell lines (Fig. 6.4E-G). Immunoblotting of whole cell extracts across cell lines showed an increase in Nucleolin levels as follows: CRL1790 < DLD1

< HCT116 <MCF7 (Fig. 6.4F). Furthermore, increased nucleolar sequestration of H2B-ECFP positively correlates with an increase in the endogenous levels of Nucleolin in these cell lines (Fig. 6.4E, G). We further corroborated this by overexpressing Nucleolin in DLD1 cells, which dramatically increased nucleolar compartmentalization of H2B in ~67% cells, as compared to control cells (~40%) (Fig. 6.4G). In summary, an increase in the endogenous or overexpressed levels of Nucleolin, positively correlates with the extent of H2B-ECFP in the nucleolus and Nucleolin therefore functions as a positive regulator of H2B-ECFP sequestration into the nucleolus.

Figure 6.4

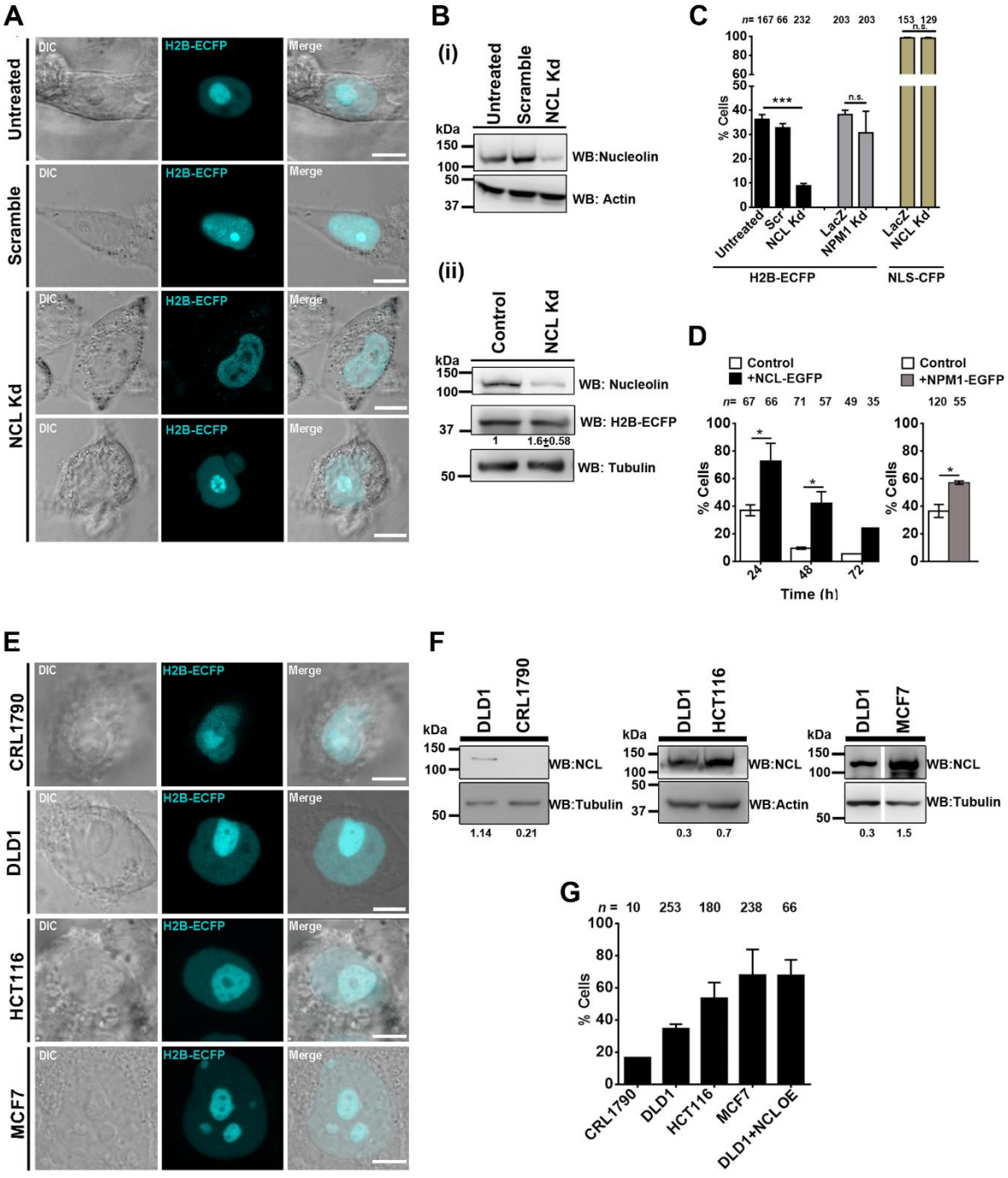

Figure 6.4. Nucleolin levels modulate compartmentation of H2B-ECFP in the nucleolus.
A. Representative images from live imaging of H2B-ECFP upon Nucleolin knockdown (NCL Kd) in DLD1 cells. Controls: untreated and scrambled siRNA treated cells. Scale bar ~ 5µm. **B.** (i) Western blots performed on whole cell lysates to detect Nucleolin levels in untreated, scramble and NCL siRNA treated DLD1 cells. Loading control: Actin. (ii) H2B-ECFP expression remains is marginally increased upon Nucleolin knockdown. Loading control: Tubulin. **C.** Percent cells showing nucleolar H2B-ECFP compartments upon NCL Knockdown (Kd). n=number of nuclei, data from N=3 independent biological replicates, error bars: SEM. Percent cells showing nucleolar H2B-ECFP upon NPM1 knockdown (Kd), n=number of nuclei, data from N=2 independent biological replicates, error bars: SD. Percent cells showing nucleolar NLS-CFP upon

NCL Kd. Percent cells showing nucleolar H2B-ECFP upon NPM1 knockdown (Kd), n=number of nuclei, data from N=2 independent biological replicates, error bars: SD. Student's t-test, ***p<0.001. **D.** Nucleolar H2B-ECFP upon NCL-GFP overexpression. DLD1 cells transfected with H2B-ECFP only (control, white bars) and co-transfected with H2B-ECFP and NCL-GFP (+NCL-GFP, black bars) imaged at intervals of 24, 48, and 72 h post transfection. Percent cells showing nucleolar H2B-ECFP upon 24h of NPM1-GFP overexpression. n=number of nuclei, data from two independent biological replicates, N=2, error bars: SD. **E.** Representative images from live imaging H2B-ECFP transfected CRL-1790, DLD1, HCT-116 and MCF-7 cells showing nucleolar localization of H2B-ECFP. Scale bar ~ 5 μm **F.** Western blots showing endogenous levels of NCL in CRL-1790, DLD1, HCT116, and MCF7 cells. Loading controls: Tubulin, Actin. Intensity of Nucleolin normalized to loading control. **G.** Extent of H2B-ECFP in the nucleolus in CRL-1790, DLD1, HCT116, MCF7 cells and in DLD1 cells co-transfected with NCL-GFP, n=number of nuclei, data from two independent biological replicates, N=2.

6.2.5. Nucleolin modulates H2B dynamics in the nucleolus

Nucleolin is a histone chaperone and evicts histones from DNA (Gaume et al., 2011; Goldstein et al., 2013). We monitored fluorescence recovery of labelled H2B in order to address the impact of Nucleolin on the mobility of H2B (Fig. 6.5A, B). Interestingly, H2B-ECFP showed a higher mobile fraction in HCT116 (M.F. ~59%) and MCF7 cells (M.F. ~68%) respectively, as compared to DLD1 cells (M.F. ~40%) (Fig. 6.5C). Furthermore, DLD1 cells overexpressing Nucleolin showed a significantly higher mobility of H2B-ECFP in the nucleolus (DLD1+NCL OE: M.F. ~72%) as compared to control cells (M.F. ~40%) (Fig. 6.5C). Taken together, the mobility of H2B-ECFP in the nucleolus positively correlates with an increase in the levels of Nucleolin.

Figure 6.5

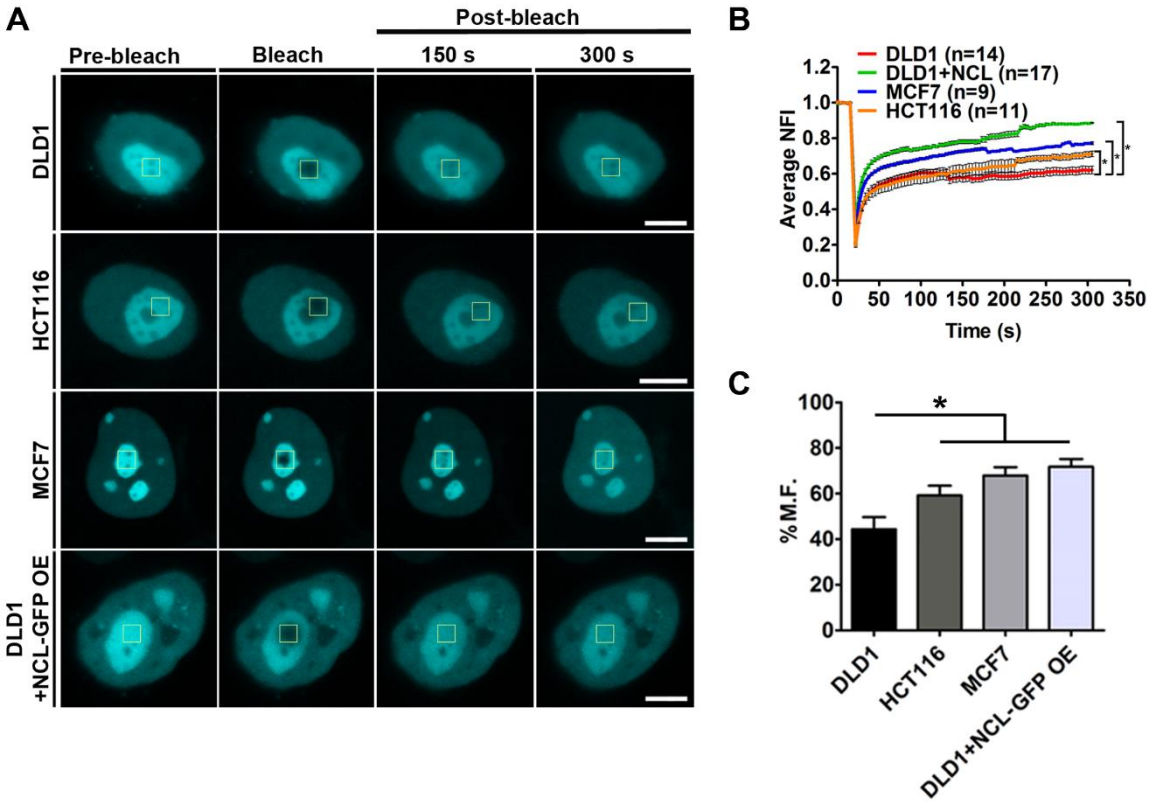

Figure 6.5. Nucleolin levels positively correlate with H2B mobility.
A. FRAP of H2B-ECFP in the nucleolus of DLD1, HCT116, MCF7 and DLD1 cells co-transfected with NCL-GFP (DLD1+ NCL-GFP OE), Scale bar ~ 5 µm. **B.** Normalized fluorescence recovery curves of H2B-ECFP in the nucleolus. **C.** Relative mobile fractions of H2B-ECFP as calculated from (B), n=number of nuclei, data from N=3 independent biological replicates, error bars: SEM in recovery curves and bar graph. Student's t-test, *p<0.05.

6.2.6. Nucleolin interacts with H2B-ECFP

Since Nucleolin modulates the retention and dynamics of H2B-ECFP in the nucleolus (Fig. 6.4, 6.5), we sought to examine if Nucleolin associates with H2B-ECFP. Remarkably, we found that H2B-ECFP co-immunoprecipitates with endogenous Nucleolin and independently with co-expressed NCL-GFP (Fig. 6.6A). Furthermore, H2B-ECFP and NCL-GFP, co-localize in the nucleolus reiterating the association between Nucleolin and H2B-ECFP (Fig. 6.6B).

We sought to investigate into the mechanisms of Nucleolin mediated sequestration of H2B-ECFP in the nucleolus. Towards this end, we examined the effect of co-expressing deletion mutants of Nucleolin into DLD1 cells, and scored for H2B-ECFP compartments in the nucleolus. We co-expressed H2B-ECFP with (i) full length NCL FL (ii) NCLΔN (N-terminal deleted) (iii) NCLΔRBD (RBD1-4 deleted) and (iv) NCLΔGAR (GAR domain deleted). We observed a comparable localization of NCLΔN in the nucleolus as that of full-length NCL,

while NCLΔRBD and NCLΔGAR partially mislocalized in the nucleoplasm, consistent with previous studies (Fig. 6.6B) (Creancier et al., 1993; Heine et al., 1993; Schmidt-Zachmann and Nigg, 1993). Co-expression of full length NCL showed a significant increase in nucleolar H2B-ECFP (~74%), as compared to cells transfected with H2B-ECFP alone (~32%) (Fig. 6.6C). Interestingly, co-expression of NCLΔN and NCLΔRBD did not enhance H2B-ECFP localization in the nucleolus, since both conditions showed ~31% cells with nucleolar H2B-ECFP (Fig. 6.6C). In contrast, co-expression of NCLΔGAR showed a comparable extent of nucleolar H2B-ECFP as that of full length NCL (~77%) (Fig. 6.6C). Taken together, the N-terminal and RNA binding domains of Nucleolin are essential for the enhanced localization of H2B-ECFP in the nucleolus.

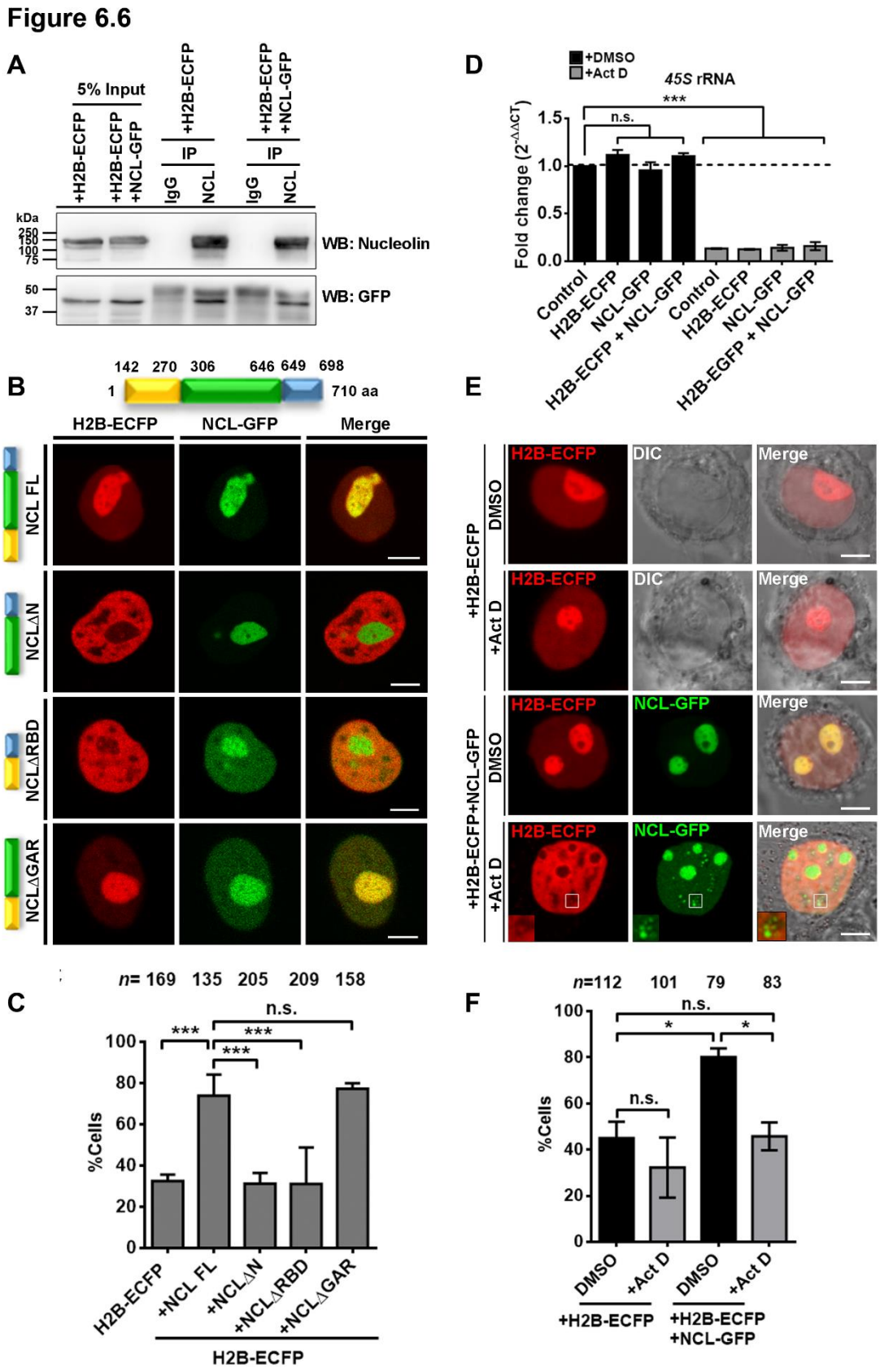

Figure 6.6. Nucleolin associates with H2B-ECFP in the nucleolus.
A. Co-immunoprecipitation (Co-IP) of endogenous Nucleolin and NCL-GFP with anti-Nucleolin antibody reveals its interaction with H2B-ECFP. Normal IgG used as a control for Co-IP. Anti-GFP

antibody was used in western blot to detect H2B-ECFP. Data from N=2 independent biological replicates. **B.** Representative images of DLD1 cells co-transfected with H2B-ECFP and Full length NCL (NCL FL), N-terminal deletion (NCLΔN), RNA binding domain deletion (NCLΔRBD) or GAR domain deletion (NCLΔGAR). H2B-ECFP and FL NCL show co-localization in the nucleolus. NCLΔRBD and NCLΔGAR show nucleoplasmic localization in addition to nucleolar localization. Scale bar ~ 5μm. **C.** Percent cells showing nucleolar H2B-ECP upon co-expression of NCL FL, NCLΔN, NCLΔRBD and NCLΔGAR, n=number of nuclei, data from N=3 independent biological replicates, error bars: SEM. ANOVA, ***p<0.001. **D.** qRT-PCR for 45S pre-rRNA in vehicle (DMSO) and Actinomycin D (Act D, 0.05μg/ml) treated cells, N=2. 45S pre-rRNA level is downregulated in all cells upon Act D treatment. All statistics performed with respect to Control (+DMSO) cells, ANOVA, ***p<0.001. **E.** Representative images of cells expressing H2B-ECFP alone, or co-expressing NCL-GFP, upon DMSO or Act D treatment. Inset - Nucleolin speckles upon Act D treatment, do not show H2B-ECFP. Scale bar ~ 5μm. **F.** Quantification of percent cells showing nucleolar H2B-ECFP upon Act D treatment (from E), n=number of nuclei, N=2 independent biological replicates. ANOVA, *p<0.05.

6.2.7. Nucleolin mediated nucleolar localization of H2B-ECFP is pre-rRNA dependent

Since NCLΔRBD did not enhance nucleolar H2B-ECFP localization, we determined if rRNA was necessary for NCL mediated localization of H2B-ECFP in the nucleolus. We treated DLD1 cells with Actinomycin D (0.05 μg/ml) for 4 hours, which showed a significant decrease in 45S rRNA levels (Fig. 6.6D).

We asked if nucleolar localization of H2B-ECFP was affected upon inhibition of rDNA transcription by Act D treatment (Fig. 6.6E). H2B-ECFP localized in the nucleolus in ~45% control cells (Fig. 6.6E, F). This sub-population of cells marginally reduced upon Act D treatment (~32%) (Fig. 6.6E, F). Co-expressing NCL-GFP enhanced nucleolar localization of H2B-ECFP in ~80% control cells (Fig. 6.6E, F). However, upon Act D treatment, the NCL-GFP mediated increase in nucleolar H2B-ECFP (~77%) showed a significant reduction to ~46% (Fig. 6.6E, F). This suggests a requirement of 45S rRNA in the the sequestration of H2B-ECFP in the nucleolus.

It is noteworthy that upon Act D treatment, Nucleolin speckles in the nucleoplasm did not colocalize with H2B-ECFP (Fig. 6.6E, inset). However, Nucleolin shows a distinctive co-localization with H2B-ECFP in the nucleolus, in the presence of 45S pre-rRNA in the nucleolus. Taken together, Nucleolin and 45S rRNA are required for the compartmentalization of H2B-ECFP in the nucleolus.

6.3. Discussion

Overexpressed H2B localizes in the nucleolus

The nucleolus is a complex milieu of ribosomal DNA, RNA, proteins and non-ribosomal proteins (Sirri et al., 2008). Sequestration into the nucleolus is an important mode of post translational regulation of proteins such as ARF and cdc14 that control cell cycle and apoptosis (Weber et al., 1999). Histones and histone variants are commonly enriched in the nucleolus. The histone H1 variant H1.0, localizes in the nucleolus and is strongly associated with non-transcribed regions of ribosomal DNA and interacts with nucleolar proteins involved in RNA processing (Kalashnikova et al., 2013; Szerlong et al., 2015). Another histone variant - macroH2A also localizes at the nucleolus and is directly involved in rDNA repression (Cong et al., 2014). Histone 2A methylated by Fibrillarin at Q104 in humans and Q105 in yeast, is exclusively localized in the nucleolus (Tessarz et al., 2014). However, H2B transiently localizes in the nucleolus upon transfection and disperses into the nucleoplasm over time, either integrating or exchanging with nuclear chromatin (Musinova et al., 2011). In vitro, a higher concentration of histones octamers to DNA (>0.76 mass ratio), aggregates chromatin and inhibits transcription (Steger and Workman, 1999). Furthermore, excess histone expression in budding yeast shows cytotoxicity and is deleterious to these cells (Gunjan and Verreault, 2003; Singh et al., 2010). We surmise, that the nucleolar sequestration of excess H2B, is a preferred paradigm for preventing the potentially deleterious effects of histone overexpression in the nucleus and toxicity across most cell types.

Lamins as modulators of nuclear histone dynamics

Histones are hyperdynamic in ES cells which have a relatively open chromatin conformation (Meshorer et al., 2006). Histone dynamics is dampened during differentiation and lineage commitment, as chromatin undergoes compaction. Lamin A/C levels are relatively lower in ES cells but increase during differentiation (Constantinescu et al., 2006). Consequently, Lamin A/C overexpression in ES cells, restricts histone H1 mobility (Melcer et al., 2012). Furthermore, Lamin B1 expression is lower in senescent cells with compact chromatin and Senescence Associated Heterochromatic Foci (SAHF) (Freund et al., 2012). Lamin depletion in differentiated DLD1 cells, did not show an appreciable effect on H2B dynamics in the nucleoplasm (Fig. 6.2). This is consistent with reduced chromatin dynamics in differentiated cells upon masking of the histone binding domain of Lamin A/C (Dixon et al., 2017). We envisage the following scenarios of the role of Lamins in the modulation of histone dynamics - (1) Consistent with previous data, reduced expression levels of Lamin A/C or B-type lamins does not appreciably affect histone mobility in differentiated cells (Fig. 6.2) (Constantinescu et al., 2006; Melcer et al., 2012) (2) It is likely that the combined depletion of Lamin A/C and B-type Lamins is required to alter histone mobility, in differentiated cell types

(3) Lamin interactors such as Emerin, Lamin B receptor (LBR) and barrier to autointegration factor (BAF) with histone binding domains, maintain histone dynamics in the absence of Lamins (Hirano et al., 2012; Montes de Oca et al., 2005). On the other hand, Nucleostemin is highly expressed and therefore a marker of cancer stem cells (Tin et al., 2014). Furthermore cancer stem cells show increased DNA accessibility as assessed by formaldehyde-assisted isolation of regulatory elements-sequencing (FAIRE-seq), suggesting open chromatin conformation (Gomez et al., 2016; Hardy et al., 2016). We surmise that, the decrease in H2B-ECFP mobility in the nucleoplasm upon Nucleostemin loss suggests reduced accessibility to chromatin in cancer stem cells. Interestingly, independent knockdowns of Lamin B1, Fibrillarin and Nucleostemin enhance H2B-ECFP mobility in the nucleolus (Fig. 6.3). We surmise that Fibrillarin and Nucleostemin are bonafide nucleolar factors that control the nucleolar microenvironment, as their depletion enhances H2B-ECFP dynamics to a significantly greater extent than nuclear lamin B1 (Fig. 6.2, 6.3). Furthermore, the loss of Fibrillarin, Nucleostemin or Lamin B1, potentially alter the relative stoichiometries of bound and unbound sub-fractions of H2B with nucleolar chromatin and consequently enhance histone dynamics in the nucleolus (Martin et al., 2009; Romanova et al., 2009a; Tollervey et al., 1993).

Nucleolin modulates H2B localization into the nucleolus

Nucleolin exhibits a dominant role in sequestering H2B into the nucleolus (Fig. 6.4). Nucleolin is a high mobility group protein and is a major constituent of the granular component of the nucleolus (Mongelard and Bouvet, 2007). Nucleolin is involved in rRNA transcription and processing (Cong et al., 2012; Ginisty et al., 1998). Nucleolin is closely related to another nucleolar phosphoprotein - Nucleophosmin. Phase separation of Nucleophosmin and Fibrillarin to a relatively more viscous nucleolar phase is critical to the maintenance of nucleolar integrity (Feric et al., 2016; Mitrea et al., 2016). In addition, ribosomal proteins - L3 and S3A and non-ribosomal proteins - Lamin B2 and HIV-rev, localize into the nucleolus by virtue of their interaction with Nucleolin and Nucleophosmin (Bouvet et al., 1998; Fankhauser et al., 1991; Sen Gupta and Sengupta, 2017). H2B is localized into the nucleolus through its nucleolar localization signal (NoLS) and electrostatic interaction with nucleolar components (Musinova et al., 2011). Here, we discovered the requirement of Nucleolin for the sequestration and retention of H2B-ECFP in the nucleolus. Nucleolin plays a more dominant role in the localization of H2B-ECFP in the nucleolus, since the loss of Nucleolin strikingly decreases nucleolar H2B-ECFP, while the co-expression of Nucleolin retains H2B in the nucleolus over a considerably longer duration (Fig. 6.4). More importantly, the N-terminal domain, previously shown to interact with histones H1 and H2A-H2B dimers; and the RNA binding domain of Nucleolin, are indispensable for the nucleolar retention of H2B-ECFP (Angelov et al., 2006; Erard et al., 1988) (Fig. 6.6). Taken together, the interaction between H2B-ECFP and Nucleolin

in the nucleolus serves as a mechanism for the nucleolar localization and retention of overexpressed H2B.

Nucleolin modulates nucleolar H2B dynamics

Nucleolin levels modulate H2B-ECFP retention and dynamics in the nucleolus across cell types (Fig. 6.4, 6.5). Furthermore, the N-terminal domain and RBD of Nucleolin regulate H2B-ECFP compartmentation in the nucleolus (Fig. 6.6). Nucleolin functions as a histone chaperone facilitating exchange of H2A-H2B dimers from chromatin (Angelov et al., 2006; Gaume et al., 2011). However, nucleoplasmic and nucleolar H2B exist in distinct microenvironments. The nucleoplasmic pool of H2B largely associates with DNA, whereas nucleolar sub-pools of H2B reside in the microenvironment of nucleolar DNA, ribosomal RNA, non-coding RNAs such as snoRNAs, ribosomal and non-ribosomal proteins, which may collectively impinge on H2B dynamics in the nucleolus.

We surmise that the N-terminal domain of Nucleolin rich in acidic amino acid stretches binds to nucleoplasmic H2B-ECFP and transports it to the nucleolus (Fig. 6.7) (Angelov et al., 2006; Erard et al., 1988). Thus with increased Nucleolin expression, there is enhanced H2B-ECFP import into the nucleolus, which correlates with an increase in the recovery of H2B-ECFP (Fig. 5). We surmise that the enhanced retention of H2B-ECFP in the nucleolus upon NCL overexpression is also rRNA dependent. However, Act D treatment redistributes a sub-population of Nucleolin to the nucleoplasm, likely to contribute to lowered retention of H2B in the nucleolus. The RNA binding domains of Nucleolin specifically mediate its interaction with the 5'-ETS of pre-rRNA while GAR domain of Nucleolin non-specifically bind to any RNA (Ghisolfi-Nieto et al., 1996; Serin et al., 1997). In summary, the nucleolar retention of H2B-ECFP is dependent upon Nucleolin-45S rRNA complex.

Thus the sub-domains of Nucleolin differentially affect nucleolar H2B-ECFP compartmentation. While the N-terminal domain is potentially required for translocating H2B-ECFP to the nucleolus, the RNA binding domain is also necessary for the retention of H2B-ECFP in the nucleolus.

While it was previously proposed that overexpressed H2B localizes in the nucleolus, via charge based interactions between the positively charged H2B and the negatively charged nucleic acids within the nucleolar milieu, our studies for the first time unravel a novel Nucleolin guided mechanism that modulates the sequestration, retention and dynamics of H2B in the nucleolus (Musinova et al., 2011). This implicates Nucleolin, 45S rRNA and potentially other bonafide nucleolar factors such as Nucleophosmin in directing the fate of overexpressed and therefore excess nuclear proteins, into the nucleolus. Considering that the nucleolus is maintained as discrete phase separated entities in the nucleus, the mechanisms involved in targeting nuclear factors into or out of the nucleolus are largely unclear (Emmott and Hiscox,

2009). Histone gene expression is tightly regulated and coupled to DNA replication during S-phase (Gunjan and Verreault, 2003; Robbins and Borun, 1967). Imbalances in histone expression and its accumulation can induce G1 cell cycle arrest, genomic instability and affect transcription (Meeks-Wagner and Hartwell, 1986; Mei et al., 2017; Morillo-Huesca et al., 2010). It is therefore conceivable that Nucleolin/Nucleophosmin are specifically involved in dual roles of chaperoning out excess nuclear proteins such as histones into the nucleolus.

Furthermore, this study also unravels the key involvement of ribosomal RNA as an essential mediator that facilitates the retention of nucleolar H2B. A combination of nucleolar factors and their interaction with rRNA is potentially involved in the generation of the phase separated nucleolus – a unique non-membranous milieu within the nucleoplasm, for the rapid but regulated entry and exit of factors that potentially facilitate rRNA biogenesis. In summary, this study unravels a unique and novel mechanism whereby proteins are guided and retained into phase separated systems such as the nucleolus. This suggests potential implications towards the targeted therapeutic intervention of the dysregulated “cancer nucleoli”.

Figure 6.7

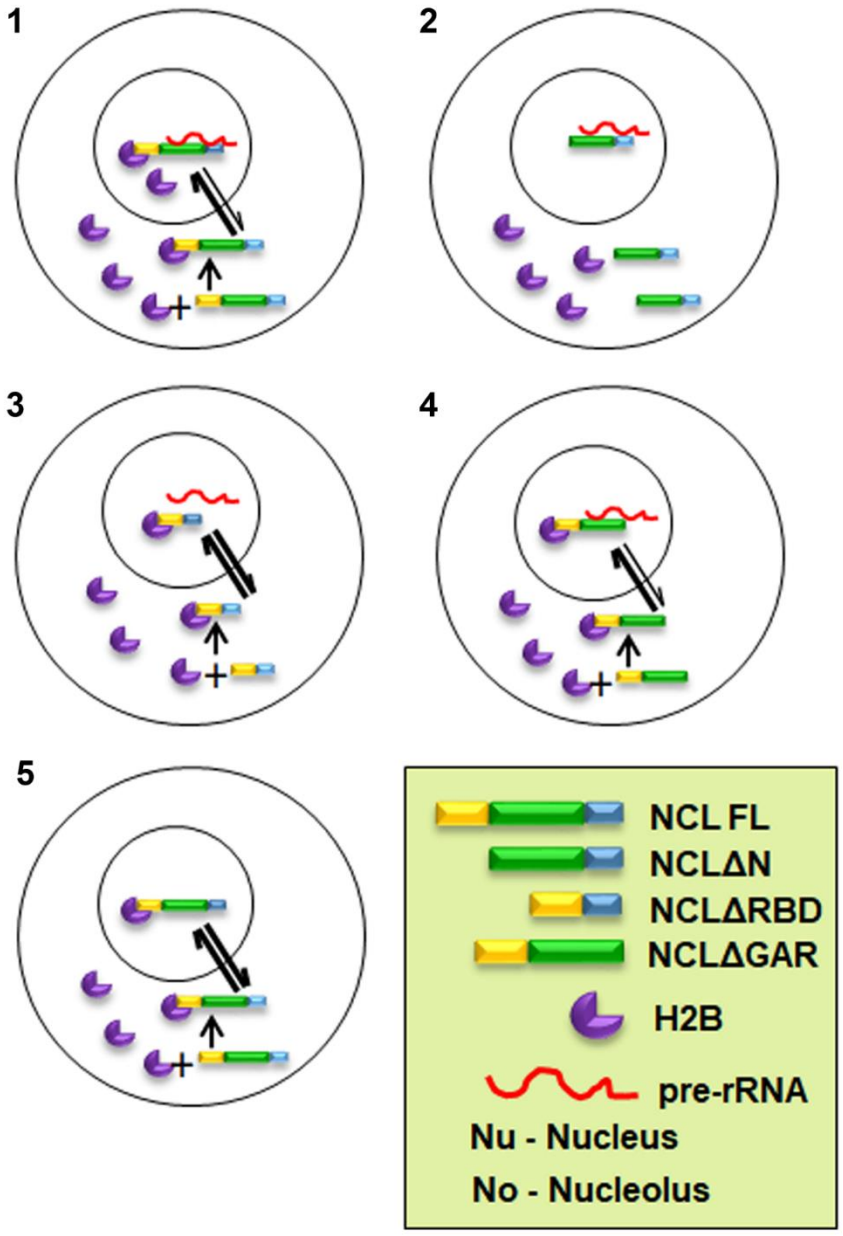

Figure 6.7. Speculative model of Nucleolin regulating nucleolar compartmentation and dynamics of H2B. 1. Nucleolin interacts with H2B-ECFP via its N-terminal domain and shuttles it into the nucleolus. In the nucleolus, Nucleolin binds to pre-rRNA via its RNA binding domain and H2B-ECFP via its N-terminal domain, thus retaining H2B-ECFP in the nucleolus. It is likely that the relative rate of import of H2B-ECFP into the nucleolus is greater in the presence of Nucleolin. 2. In absence of the N-terminal domain, Nucleolin does not bind to H2B-ECFP, thereby reducing nucleolar pools of H2B-ECFP. 3. Nucleolin RBD deletion mutant binds to H2B-ECFP through its N-terminal domain and sequesters H2B-ECFP into the nucleolus. However in the absence of RBD, H2B-ECFP is not retained in the nucleolus, as the RBD is required for binding to pre-rRNA. 4. GAR domain deletion mutant binds to H2B-ECFP and pre-rRNA and shows enhanced recruitment of H2B-ECFP into the nucleolus, similar to full length Nucleolin. 5. Nucleolin imports H2B-ECFP in the nucleolus but is unable to retain it in the nucleolus in the absence of pre-rRNA transcription by Act D.

Chapter 7:

Discussion and future perspectives

In this thesis, we have contributed to the existing literature on nucleolar morphology, dynamics and function. We show for the first time, a novel role of Lamin B2 in modulating nucleolar structure-function. We have uncovered the function of distinct domains of Lamin B2 that are required to maintain nuclear and nucleolar structure. Further we have uncovered interesting effects of Fibrillarin knockdown. This reveals a previously unknown interplay between nucleolar proteins and Lamins in maintaining nuclear and cellular structure function. Finally we have addressed the question of how proteins are compartmentalized into the nucleolus, along with a predominant role of Nucleolin in the shuttling of proteins into the nucleolus.

7.1. Nucleolar morphology and rRNA expression across cancer cells

Pathologists have historically used nucleolar morphology and numbers to distinguish cancer tissue from normal (Derenzini et al., 2009). We assessed several cancer cell lines for nucleolar numbers and morphology; and found that these parameters vary between normal and cancer cells, and also across different grades of cancers (Fig. 3.2). We found that diploid colon cancer cell lines – DLD1 and HCT116 showed comparable number of nucleoli with that of normal colon cells (CRL1831) (Table 3.2). However, the aneuploid cancer cell lines – SW480, MCF7 and A549 showed more number of nucleoli (Table 3.2). Thus, our data suggests that number of nucleoli cannot be a single parameter to distinguish cancer from normal cells. On the contrary, close examination of nucleolar morphologies revealed reproducible signatures of discrete and aggregated nucleoli for each cell line assessed (Fig. 3.3). We found that cancer cell lines showed higher percentages of aggregated nucleolar morphology compared to normal cells. Further, the propensity of aggregated nucleolar morphology increased with the stage of progression of colon cancer with – DLD1 and SW480 cells (Duke's type C and B, respectively) showed fewer cells with aggregated nucleoli than the more aggressive HCT116 cells (Duke's type D) (Fig. 3.3). Further metastatic HT1080 and A549 cells showed highly aggregated nucleolar morphology. While HT1080 cells form aggressive angiogenic tumors, subcutaneously injected A549 cells show lung metastases in nude mice (Jakubowska et al., 2013; Misra et al., 2012). Increase in nucleolar number and size has been previously shown to accompany breast cancer aggressiveness when ribosome biogenesis is increased upon knockdown of ADP ribosylation factor like 2 (Arl-2) (Belin et al., 2009). Thus our study corroborates nucleolar morphology as an important parameter to distinguish between normal and cancer cells and generally, more aggressive cancer cells from less aggressive ones.

Aberrant nucleolar phenotypes typically correlate with increased ribosome biogenesis activity of cells. Thus the question arises – do cells showing aggregated nucleolar morphology synthesize more ribosomal RNA? A recent study assessed 45S pre-rRNA levels across a panel of colorectal cancer cell lines that include DLD1, HCT116 and SW480 cells (Tsoi et al., 2017).

This data showed that pre-rRNA expression in DLD1 and HCT116 cells were not significantly different, even though DLD1 and HCT116 cells show distinctly different nucleolar morphologies, in our study (Fig. 7.1) (Tsoi et al., 2017). This suggests that nucleolar morphology may be modulated, independent of 45S pre-rRNA expression levels. We surmised that structural proteins of the nucleus and nucleolus impinge on nucleolar morphology. We have observed that higher endogenous levels of the nucleolar architectural protein – Nucleolin, and its ectopic overexpression in cells, co-relates with aggregated nucleolar morphology.

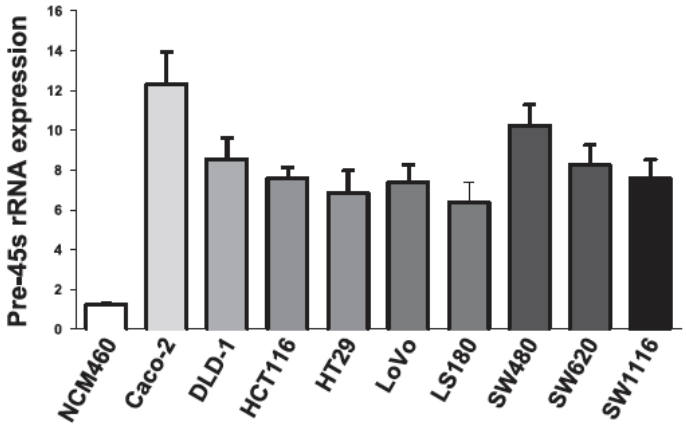

Figure 7.1. 45S pre-rRNA levels across normal and colorectal cancer cell lines.
Reprinted from (Tsoi et al., 2017)

7.2. Differential roles of Lamins in regulating nucleolar morphology

Although Lamins are the major structural factors in higher eukaryotes, it is largely unclear if they modulate nucleolar structure. We compared the effects of Lamins B2, A/C and B1 depletion on nucleolar structure in DLD1 cells. Our studies show the exclusive role of Lamin B2 in maintaining discrete and spherical nucleolar morphology in DLD1 cells, while Lamin A/C and Lamin B1 hardly show any effects. This is in contrast with previous studies that show a role for Lamin B1 in maintaining normal nucleolar morphology and function in HeLa cells, and downregulation of Lamin A in primary human fibroblasts showing nucleolar expansion (Buchwalter and Hetzer, 2017; Martin et al., 2009). This is suggestive of cell type specific predominance in the functions of A-type and B-type Lamins. Such differential regulation of nuclear functions by A-type and B-type lamins is also seen with respect to regulation of ploidy in colorectal cancer cells, where loss of Lamin B2 but not Lamin A/C, leads to aneuploidy (Kuga et al., 2014). Further, while loss or mutations of Lamin A/C particularly affect functioning of connective tissues like skeletal, muscle or fat cells, owing to their roles in nuclear and cell mechanics; Lamin B1 and B2 functions predominate in softer tissues such as the brain and gut (De Castro et al., 2012; Coffinier et al., 2011; Lee et al., 2007a; Ranade et al., 2017).

The differences in Lamin functions with respect to the nucleolus may be attributed to their differential interactors and localizations in the nucleolus (Fig. 3.11). We found that Lamin B2 and A/C localize in distinct compartments of the nucleolus. While Lamin A/C is localized in the interior of the nucleolus (potentially FC and DFC regions), Lamin B2 localizes at the boundary of the GC of the nucleolus. Further, we found that Lamin B2 interacts with the GC proteins Nucleolin and Nucleophosmin (B23), while Lamin A/C does not. The distinct localizations of Lamin B2 and Lamin A/C could arise from their differential interactors, in the GC and DFC, respectively.

Moreover, we found a predominant role of the head domain of Lamin B2, but not the tail domain, in maintaining nucleolar structure (Fig. 3.15). Sequence alignments of the head domains of Lamin A/C and Lamin B2 show significant stretches of amino acids that are present on Lamin B2 but not on Lamin A/C (Fig. 7.2). It is possible that Lamin B2 localizes to the nucleolus by interacting with Nucleolin and NPM1, via its head domain.

```
CLUSTAL 2.1 multiple sequence alignment


LMNA            --METPSQRRATRSG------------AQASSTPLSPTRITRLQEKE
LMNB2           MSPPSPGRRREQRRPRAAATMATPLPGRAGGPATPLSPTRLSRLQEKE
                    :*.:**  *               * ..:*******::******
```

Figure 7.2. Sequence alignments of the head domains of Lamin A/C and Lamin B2

7.3. Crosstalk of Lamin B2 with regulators of rDNA transcription

The unique localization of Lamin B2 adjacent to the nucleolar GC, invokes Lamin B2 as an important factor to relay signals from the nucleoplasm to the phase-separated nucleolus and vice-versa. We imagine that this role is similar to the role of Lamin A/C at the nuclear periphery, where it transduces extracellular cytoplasmic signals to the nucleus (Osmanagic-Myers et al., 2015). Localization of Lamin B2 also potentially functions as an interface between the intranucleolar rDNA and the perinucleolar heterochromatin. Perinucleolar heterochromatin is composed of repressed rDNA repeats, rDNA flanking distal junction (DJ) sequences, centromeric and pericentromeric satellite repeats from NOR and non-NOR bearing chromosomes, and low gene density regions (Floutsakou et al., 2013; van Koningsbruggen et al., 2010; Németh et al., 2010). These heterochromatic domains either return to the periphery of the nucleolus or contact the nuclear periphery, in daughter cells, post-mitosis, suggesting the importance of Lamins in maintaining heterochromatin organization (van Koningsbruggen et al., 2010). Bioinformatics analysis and literature survey suggest that Lamin B2 potentially forms a

network with factors required for stably maintaining heterochromatin and repress gene expression (Fig. 7.3). These include macroH2A, DNA methyltransfereases – DNMT1, DNMT3a, DNMT3b, histone deacetylase HDAC1, SIRT7, RBBP4 and CHD4. Further, through microarray analysis, we have identified histone modifiers such as JARID2 and EHMT1 required for gene repression and heterochromatin maintenance, which are deregulated upon Lamin B2 knockdown. Analysis of the rDNA promoter and UCE in HGPS (Lamin A mutated) cells has shown significant reduction in DNA methylation (Buchwalter and Hetzer, 2017). Our assays show that Dnmt1 levels are significantly reduced upon Lamin B2 depletion (Fig. 4.4). Bisulphite-sequencing assays are likely to identify if rDNA methylation is altered upon Lamin B2 knockdown in colorectal cancer cells, which may modulate rRNA levels. Further chromatin immunoprecipitation (ChIP) studies are also required to assess direct binding of Lamin B2 on the rDNA and thereby its regulation.

Thus, a loss of Lamin B2 could potentially alter heterochromatin organization in cells, which manifest in increased mobility of the heterochromatin binding protein – HP1α (Fig. 4.4). Although we uncovered changes in the global heterochromatin binder - HP1α dynamics upon Lamin B2 depletion, we surmise that this effect would be more pronounced for HP1β and HP1γ proteins, which are predominant perinucleolar heterochromatin binding proteins, which need to be addressed in further studies (Bártová et al., 2010).

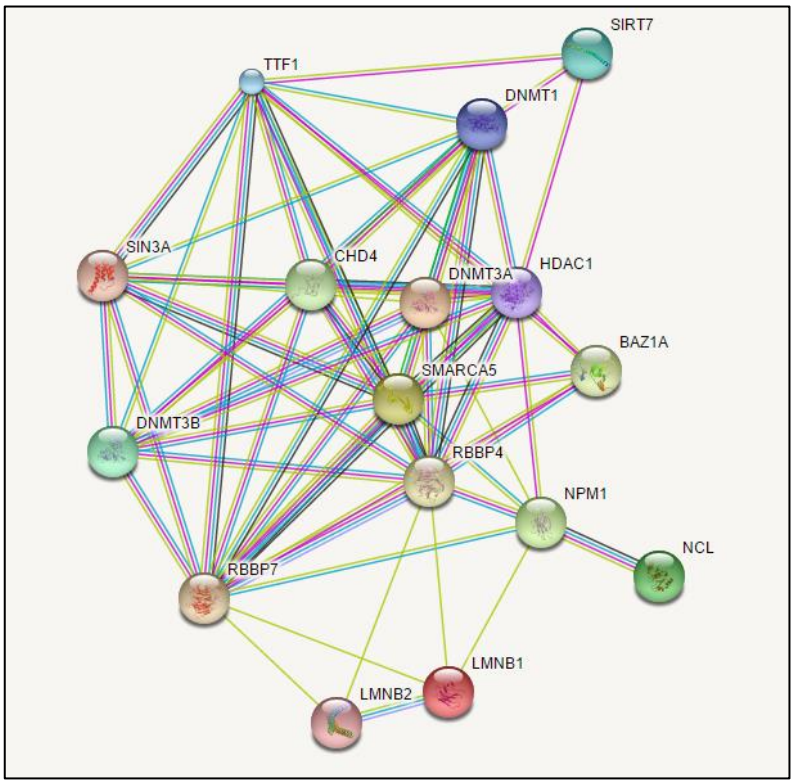

Figure 7.3. Protein protein interaction map generated by STRING depicting B-type lamins with regulators of rDNA transcription.

The two major pathways regulating ribosome biogenesis are the mTor and the Akt signaling pathway (Chan et al., 2011; Hannan et al., 2003; James and Zomerdijk, 2004). Enhanced mTor signaling with increased S6K phosphorylation has been observed in Lamin A$^{-/-}$ mouse skeletal and cardiac cells (Ramos et al., 2012). Treatment of HGPS cells with the mTor inhibitor Rapamycin partially rescues the abnormal nuclear shapes in these cells. This suggests dysregulation of the mTor pathway in cells lacking Lamin A. Although crosstalk of Lamin B2 with the mTor and Akt pathway has not been investigated so far, it will be important to test the downstream effectors of these signaling pathways in Lamin B2 proficient and deficient backgrounds, to examine if growth signaling pathways impinge on Lamin B2 mediated rDNA repression.

7.4. Lamin B2 – possible implications in nucleolar phase separation

Nucleolar reformation after mitosis and its assembly on NOR-bearing chromosomes, has been an active area of research, recently (Brangwynne et al., 2011; Grob et al., 2014). Liquid-liquid phase separation (LLPS) of nucleolar proteins from the nucleoplasm, to active sites of rDNA transcription, is a driving force in keeping the nucleolus together, in the absence of a bounding membrane (Falahati et al., 2016). Besides ribosomal RNA, non-coding Alu RNAs have been identified as nucleators of nucleolar proteins (Caudron-Herger et al., 2015). Further, non-coding RNAs from rDNA intergenic locus also sequester proteins into the nucleolus, under stress conditions (Audas et al., 2012). We found that presence Lamin B2, not only represses transcription from the rDNA promoter, but also impinges on transcription from rDNA intergenic regions (Fig. 4.2, 4.3). It is unclear if (1) IGS transcripts comprise of long non-coding RNAs? or, (2) whether there are indeed multiple RNAs that originate from these regions in absence of Lamin B2? or, (3) which RNA Polymerase transcribes these RNAs? Nevertheless, we speculate that these IGS RNA transcripts potentially mediate LLPS of Nucleolin and subsequently lead to the aggregated morphology of the nucleolus.

It is likely that inhibition of rDNA transcription by RNA Pol I inhibitors, represents the reverse process of phase-separation, whereby nucleolar proteins now disperse into the nucleoplasm, in absence of their nucleator – RNA (Fig. 4.6). However, upon Lamin B2 the nucleolar protein – Nucleolin, failed to disperse into the nucleoplasm after prolonged Actinomycin D treatment. We found that the same IGS transcripts that were upregulated upon Lamin B2 knockdown, were enriched in nucleoplasmic speckles of Nucleolin. This suggests the possibility that IGS transcripts can act as “molecular glue” to aggregate nucleolar proteins and thereby the nucleolus. Thus, Lamin B2 at the periphery of the nucleolus, potentially works as a guardian for controlled dynamics of nucleolar proteins like Nucleolin and NPM1, in an RNA-dependent manner.

7.5. Crosstalk between lamins and nucleolar protein – Fibrillarin to maintain nuclear and cell architecture

Our study shows that just as Lamins regulate nucleolar structure, likewise nucleolar proteins crosstalk with the nuclear lamina to maintain nuclear and cell architecture. In this respect, we have studied the role of Fibrillarin, a methyltransferase, required for efficient processing of rRNA, yielding functional ribosomes (Tollervey et al., 1993). Deregulation of translational fidelity of ribosomes is a major setback in cellular quality control, and causal to production of defective proteins that are widespread in cancers (Belin et al., 2009). Whole genome microarray analysis upon Fibrillarin depletion, show significant transcriptional deregulation in colon cancer cells (Fig. 5.2). Fibrillarin is an RNA binding protein and its binding to DNA has not been reported. Hence we speculate that Fibrillarin knockdown generates a cascade of events whereby a specific set of transcription factors (SP1, AP1, MYC, LEF1) are aberrantly translated by IRES mediated translation instead of 5' CAP mediated mRNA translation (Hung et al., 2014; Jimenez et al., 2005; Shi et al., 2005; Vesely et al., 2009). These transcription factors may deregulate transcription of their target genes, which further include transcription factors (e.g. ATF3, N-MYC, SMAD3, SP5, MYB, HOXB4), nuclear architectural genes (e.g. LMNA, LMNB2, EMD, NUP93) and cytoskeleton organizing genes (e.g. ITGA2, ITGA6, ITGB5, ITGB8, COL16A, LAMB3, LAMG1, PLXNB2, CORO1A) (Table 5.1).

Fibrillarin depletion was previously associated with changes in nuclear morphology (Amin et al., 2007). We show here that several nuclear envelope proteins are dysregulated upon Fibrillarin knockdown – the most noted amongst these being Lamin A/C and Lamin B2, while surprisingly Lamin B1 expression remains constant (Fig. 5.10). However, contrary to the nuclear blebs observed upon single knockdown of Lamin B2 (Fig. 3.16), we observed invaginations of the nuclear envelope upon Fibrillarin knockdown, where both Lamin A/C and Lamin B2 were downregulated (Fig. 5.6). In addition, we show for the first time, that Fibrillarin knockdown leads to significant changes in the cytoskeleton organization, with actin forming aggregates adjacent to the nuclear periphery (Fig. 5.7). Such aggresomes or inclusion bodies of F-actin have been previously reported in Alzheimer's disease (AD), chronic alcoholism and myopathies (Hirano, 1994; Laas and Hagel, 1994; Maloney et al., 2005; Podlubnaia and Nowak, 2006), although we are unsure if the molecular compositions of actin inclusion bodies in AD are similar to the aggregates that we observe upon Fibrillarin knockdown. Consistent with the possible neuroprotective role of Fibrillarin by preventing actin inclusion bodies, we find a high expression of Fibrillarin in the cerebellar and hippocampal tissues of the brain. Actin aggresomes are also induced in cells upon treatment with the actin-stabilizing drug – Jasplakinolide (Lázaro-Diéguez et al., 2008). This, and our experiments with Lat A treatments, suggest that actin in Fibrillarin depleted cells is more stable. This is also consistent with low

Fibrillarin expression in heart and skeletal muscle cells that show highly stable contractile actin structures, compared to non-muscle cells that show labile actin structures (Tilney, 1975).

We surmise that a concerted effect of the weakening of nuclear lamina and aggregation of actin outside the nucleus leads to nuclear morphology changes. Nuclear morphology changes are closely associated with transcriptional deregulation. In future, it will be interesting to assess if effects on nuclear morphology and transcriptome, seen upon Fibrillarin knockdown, are recapitulated by simply treating cells with Jasplakinolide and stabilizing actin.

We also found that Fibrillarin depleted cells show enhanced migration. Yet again, this can be contributed by the downregulation of Lamin A/C, altered cytoskeletal organization (increase in filopodia) and an increase in chemokine signaling pathways, uncovered upon Fibrillarin knockdown. Although previously, Fibrillarin overexpression has been corelated with carcinogenesis in breast cells, our study suggests that critical levels of Fibrillarin are necessary to maintain normal cell functions (Marcel et al., 2013). We suggest that both hypermethylation of rRNA due to overexpression of Fibrillarin, or hypomethylation due to Fibrillarin loss, could potentially generate abnormal ribosomes leading to a lack of control on translation, leading to altered nuclear and cell architecture.

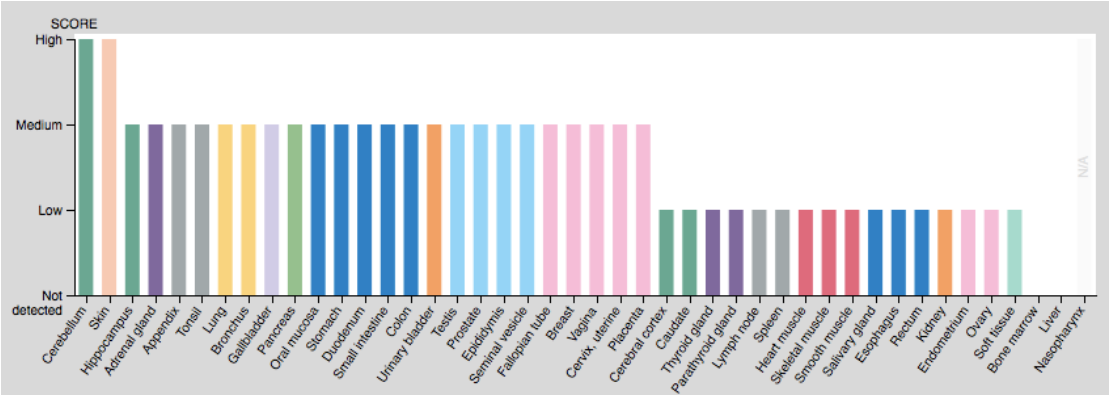

Figure 7.4. Relative expression levels of Fibrillarin protein across tissues from Human Protein Atlas

7.6. Nucleolar targeting of proteins by Nucleolin

A long-standing debate in the field has been the mechanisms that target proteins into the nucleolus. While several groups have reported the presence of a lysine-rich nucleolar localization signal (NoLS) as necessary and sufficient for the localization of proteins inside the nucleolus (Antoine et al., 1997; Dang and Lee, 1989; Musinova et al., 2011; Schmidt-Zachmann and Nigg, 1993; Scott et al., 2010), many bonafide nucleolar proteins like Nucleophosmin (NPM1) do not possess such “characteristic” motifs predicted by Nucleolar Localization

Sequence Detector, (NoD, http://www.compbio.dundee.ac.uk/www-nod/) (Scott et al., 2011). Instead, NPM1 is a nuclear-nucleolar shuttling protein and one of the several mechanisms by which it is retained in the nucleolus is via its interactions with G-quadruplexes on rDNA chromatin (Chiarella et al., 2013). Further, NPM1 localization to the nucleolus could also be via its interaction with Nucleolin as it relocalizes to the nucleoplasm in Nucleolin knockout cells (Li et al., 1996; Storck et al., 2009).

Our studies with H2B-ECFP nucleolar localization have been revealing and suggest that nucleolar localization of histone 2B is dependent on Nucleolin. Histone 2B was previously shown to localize into the nucleolus via its highly positively charged nucleolar localization/retention signal KKGGKKRKRSRK (aa24-35) (Musinova et al., 2011). However, these studies were performed in Nucleolin proficient HeLa cells. The study also showed the dependence of histone 2B on RNA for nucleolar localization. Our study extends these results and shows that the nucleolar localization of histone 2B is largely dependent on its interaction with Nucleolin, as the nucleolar localization of histone 2B sharply declines upon knockdown of Nucleolin (Fig. 6.4). We also show the specific role of nucleolar 45S pre-rRNA in nucleolar retention of histone 2B in a Nucleolin dependent manner. We surmise that Nucleolin mediated sequestration of proteins may be a post-translational mechanism to regulate their nucleoplasmic concentration and function. Further studies will reveal if Nucleolin dependent localization is a general mechanism by which other proteins localize to the nucleolus.

We also find that Lamin B2 localizes to the nucleolus and interacts with Nucleolin and NPM1 (Fig. 3.12). It is unclear if this localization of Lamin B2 at nucleolar periphery is "dependent" on Nucleolin or NPM1. However, NPM1 was shown to interact with R-motif containing proteins ($RX_{n1}R$, where X is any amino acid, $n1 \leq 2$), via its N-terminal oligomerization domain and disordered region (aa 1-130) (Mitrea et al., 2016). This interaction helps localize R-motif containing proteins to the nucleolus and further assist the phase separation of NPM1 from the nucleoplasmic phase into a more structured nucleolar phase (Mitrea et al., 2016). We found several such R-motifs on Lamin B2. Thus, it needs to be experimentally verified if these R-motifs are necessary for nucleolar localization of Lamin B2 and if they help in nucleolar phase separation of Nucleolin and NPM1.

1
MSPPSPGRRREQRRPRAAATMATPLPGRAGGPATPLSPTRLSRLQEKEELRELNDRLAHY
61
IDRVRALELENDRLLLKISEKEEVTTREVSGIKALYESELADARRVLDETARERARLQIE
121
IGKLRAELDEVNKSAKKREGELTVAQGRVKDLESLFHRSEVELAAALSDKRGLESDVAEL
181
RAQLAKAEDGHAVAKKQLEKETLMRVDLENRCQSLQEELDFRKSVFEEEVRETRRRHERR
241
LVEVDSSRQQEYDFKMAQALEELRSQHDEQVRLYKLELEQTYQAKLDSAKLSSDQNDKAA
301
SAAREELKEARMRLESLSYQLSGLQKQASAAEDRIRELEEAMAGERDKFRKMLDAKEQEM
361
TEMRDVMQQQLAEYQELLDVKLALDMEINAYRKLLEGEEERLKLSPSPSSRVTVSRATSS
421
SSGSLSATGRLGRSKRKRLEVEEPLGSGPSVLGTGTGGSGGFHLAQQASASGSVSIEEID
481
LEGKFVQLKNNSDKDQSLGNWRIKRQVLEGEEIAYKFTPKYILRAGQMVTVWAAGAGVAH
541
SPPSTLVWKGQSSWGTGESFRTVLVNADGEEVAMRTVKKSSVMRENENGEEEEEEAEFGE
601
EDLFHQQGDPRTTSRGCYVM

Figure 7.5. Amino acid sequence of Lamin B2 protein (Uniprot ID: Q03252) indicating possible R-motifs highlighted in yellow

7.7. Implications of Lamin and nucleolar protein convergence in neurodegenerative diseases

Lamins mutations have long been associated with the accelerated ageing disease – HGPS. Very recently, lowered expression of B-type Lamins has been shown to mediate loss of heterochromatinization and neuronal cell death in a *Drosophila* model of Alzheimer's disease (Frost et al., 2016). This is consistent with the important role of B-type Lamins in maintaining nuclear shape in neuronal cells and associated developmental disorder (Coffinier et al., 2011). Further, rDNA copy numbers show an increase in brain samples from the neurodegenerative diseases - dementia with Lewy bodies (DLB) and Alzheimer's disease denoting genomic instability at the rDNA locus during disease progression (Hallgren et al., 2014; Pietrzak et al., 2011). Further an enhanced expression of 18S and 28S rRNAs has been observed in AD (Rasmussen et al., 2015). This is contrary to reports that show aberrant hypermethylation and silencing of rDNA in AD and reduction in rRNA synthesis, nucleolar size during ageing (García Moreno et al., 1997; Pietrzak et al., 2011). In our study, we find that rRNA expression is deregulated upon Lamin B2 knockdown with a subsequent decrease Dnmt1 expression levels (Fig. 4.4). Further Lamin B2 downregulation is associated with genomic instability (Ranade et al., 2017). Thus, it will be interesting to investigate if Lamin B2 regulates rDNA stability and expression during pathogenesis of DLB and AD. Further, reduction in Nucleolin binding to

rDNA promoters is reduced in polyglutaminopathies like Huntington's disease due to sequestration of Nucleolin by mutant CAG repeat transcripts, resulting in reduced rDNA transcription and nucleolar stress (Tsoi and Chan, 2013). Finally cdc2 phosphorylated Nucleolin localize to cytoplasmic neurofibrillary tangles (NFTs), which contain aggregates of hyperphosphorylated Tau protein, characteristic of AD pathogenesis (Brion, 1998; Dranovsky et al., 2001). Our study demonstrates that Lamin B2 plays an important role in modulating Nucleolin aggregation. It would be of interest in future to assess if Lamin B2 also regulates aggregation of Nucleolin and other proteins like Tau in NFTs to drive neurodegeneration.

References

Abdelmohsen, K., Tominaga, K., Lee, E.K., Srikantan, S., Kang, M.J., Kim, M.M., Selimyan, R., Martindale, J.L., Yang, X., Carrier, F., et al. (2011). Enhanced translation by Nucleolin via G-rich elements in coding and non-coding regions of target mRNAs. Nucleic Acids Res. *39*, 8513–8530.

Adam, S.A., Butin-Israeli, V., Cleland, M.M., Shimi, T., and Goldman, R.D. (2013). Disruption of lamin B1 and Lamin B2 processing and localization by farnesyltransferase inhibitors. Nucleus *4*, 142–150.

Aebi, U., Cohn, J., Buhle, L., and Gerace, L. (1986). The nuclear lamina is a meshwork of intermediate-type filaments. Nature *323*, 560–564.

Ahmad, Y., Boisvert, F.-M., Gregor, P., Cobley, A., and Lamond, A.I. (2009). NOPdb: Nucleolar Proteome Database--2008 update. Nucleic Acids Res. *37*, D181-4.

Al-Baker, E.A., Boyle, J., Harry, R., and Kill, I.R. (2004). A p53-independent pathway regulates nucleolar segregation and antigen translocation in response to DNA damage induced by UV irradiation. Exp. Cell Res. *292*, 179–186.

Albert, B., Perez-Fernandez, J., Léger-Silvestre, I., and Gadal, O. (2012). Regulation of ribosomal RNA production by RNA polymerase I: does elongation come first? Genet Res Int *2012*, 276948.

Allain, F.H., Bouvet, P., Dieckmann, T., and Feigon, J. (2000). Molecular basis of sequence-specific recognition of pre-ribosomal RNA by nucleolin. EMBO J. *19*, 6870–6881.

Amin, M.A., Matsunaga, S., Ma, N., Takata, H., Yokoyama, M., Uchiyama, S., and Fukui, K. (2007). Fibrillarin, a nucleolar protein, is required for normal nuclear morphology and cellular growth in HeLa cells. Biochem. Biophys. Res. Commun. *360*, 320–326.

Amin, M.A., Matsunaga, S., Uchiyama, S., and Fukui, K. (2008a). Depletion of nucleophosmin leads to distortion of nucleolar and nuclear structures in HeLa cells. Biochem J *415*, 345–351.

Amin, M.A., Matsunaga, S., Uchiyama, S., and Fukui, K. (2008b). Nucleophosmin is required for chromosome congression, proper mitotic spindle formation, and kinetochore-microtubule attachment in HeLa cells. FEBS Lett *582*, 3839–3844.

Amiri, K.A. (1994). Fibrillarin-like proteins occur in the domain Archaea. J Bacteriol *176*, 2124–2127.

Anastassova-Kristeva, M. (1977). The nucleolar cycle in man. J. Cell Sci. *25*, 103–110.

Andersen, J.S., Lyon, C.E., Fox, A.H., Leung, A.K.L., Lam, Y.W., Steen, H., Mann, M., and Lamond, A.I. (2002). Directed proteomic analysis of the human nucleolus. Curr. Biol. *12*, 1–11.

Andersen, J.S., Lam, Y.W., Leung, A.K.L., Ong, S.-E., Lyon, C.E., Lamond, A.I., and Mann, M. (2005). Nucleolar proteome dynamics. Nature *433*, 77–83.

Andersen, L., Kayser, L., Keiding, N., and Thomsen, J. (1998). A morphometric analysis of nucleoli in cultured carcinoma cells of the human thyroid. Anal. Cell. Pathol. *16*, 131–140.

Anderson, S.J., Sikes, M.L., Zhang, Y., French, S.L., Salgia, S., Beyer, A.L., Nomura, M., and Schneider, D.A. (2011). The transcription elongation factor Spt5 influences transcription by RNA polymerase I positively and negatively. J. Biol. Chem. *286*, 18816–18824.

Angelov, D., Bondarenko, V.A., Almagro, S., Menoni, H., Mongélard, F., Hans, F., Mietton, F., Studitsky, V.M., Hamiche, A., Dimitrov, S., et al. (2006). Nucleolin is a histone chaperone with FACT-like activity and assists remodeling of nucleosomes. EMBO J. *25*, 1669–1679.

Antoine, M., Reimers, K., Dickson, C., and Kiefer, P. (1997). Fibroblast growth factor 3, a protein with dual subcellular localization, is targeted to the nucleus and nucleolus by the concerted action of two nuclear localization signals and a nucleolar retention signal. J. Biol. Chem. *272*, 29475–29481.

Aris, J.P., and Blobel, G. (1991). cDNA cloning and sequencing of human fibrillarin, a conserved nucleolar protein recognized by autoimmune antisera. Proc Natl Acad Sci USA *88*, 931–935.

Asadi, M.H., Derakhshani, A., and Mowla, S.J. (2014). Concomitant upregulation of nucleostemin and downregulation of Sox2 and Klf4 in gastric adenocarcinoma. Tumour Biol *35*, 7177–7185.

Audas, T.E., Jacob, M.D., and Lee, S. (2012). Immobilization of proteins in the nucleolus by ribosomal intergenic spacer noncoding RNA. Mol. Cell *45*, 147–157.

Baker, A.M., Cox, T.R., Bird, D., Lang, G., Murray, G.I., Sun, X.-F., Southall, S.M., Wilson, J.R., and Erler, J.T. (2011). The role of lysyl oxidase in SRC-dependent proliferation and metastasis of colorectal cancer. J. Natl. Cancer. Inst. *103*, 407–424.

Bański, P., Mahboubi, H., Kodiha, M., Shrivastava, S., Kanagaratham, C., and Stochaj, U. (2010). Nucleolar targeting of the chaperone hsc70 is regulated by stress, cell signaling, and a composite targeting signal which is controlled by autoinhibition. J. Biol. Chem. *285*, 21858–21867.

Bártová, E., Horáková, A.H., Uhlírová, R., Raska, I., Galiová, G., Orlova, D., and Kozubek, S. (2010). Structure and epigenetics of nucleoli in comparison with non-nucleolar compartments. J. Histochem. Cytochem. *58*, 391–403.

Bartsch, I., Schoneberg, C., and Grummt, I. (1988). Purification and characterization of TTFI, a factor that mediates termination of mouse ribosomal DNA transcription. Mol. Cell Biol. *8*, 3891–3897.

Basu, A., Das, P., Chaudhuri, S., Bevilacqua, E., Andrews, J., Barik, S., Hatzoglou, M., Komar, A.A., and Mazumder, B. (2011). Requirement of rRNA methylation for 80S ribosome assembly on a cohort of cellular internal ribosome entry sites. Mol. Cell Biol. *31*, 4482–4499.

Baxter-Roshek, J.L., Petrov, A.N., and Dinman, J.D. (2007). Optimization of ribosome structure and function by rRNA base modification. PLoS One *2*, e174.

Bazett-Jones, D.P., Leblanc, B., Herfort, M., and Moss, T. (1994). Short-range DNA looping by the Xenopus HMG-box transcription factor, xUBF. Science (80-.). *264*, 1134–1137.

Beck, L.A., Hosick, T.J., and Sinensky, M. (1990). Isoprenylation is required for the processing of the lamin A precursor. J. Cell Biol. *110*, 1489–1499.

Belenguer, P., Baldin, V., Mathieu, C., Prats, H., Bensaid, M., Bouche, G., and Amalric, F. (1989). Protein kinase NII and the regulation of rDNA transcription in mammalian cells. Nucleic Acids Res. *17*, 6625–6636.

Belenguer, P., Caizergues-Ferrer, M., Labbé, J.C., Dorée, M., and Amalric, F. (1990). Mitosis-specific phosphorylation of nucleolin by p34cdc2 protein kinase. Mol. Cell Biol. *10*, 3607–3618.

Belin, S., Beghin, A., Solano-Gonzàlez, E., Bezin, L., Brunet-Manquat, S., Textoris, J., Prats, A.-C., Mertani, H.C., Dumontet, C., and Diaz, J.J. (2009). Dysregulation of ribosome biogenesis and translational capacity is associated with tumor progression of human breast cancer cells. PLoS One *4*, e7147.

Bharti, A.K., Olson, M.O., Kufe, D.W., and Rubin, E.H. (1996). Identification of a nucleolin binding site in human topoisomerase I. J. Biol. Chem. *271*, 1993–1997.

Bhatt, P., d'Avout, C., Kane, N.S., Borowiec, J.A., and Saxena, A. (2012). Specific domains of nucleolin interact with Hdm2 and antagonize Hdm2-mediated p53 ubiquitination. FEBS J *279*, 370–383.

Bierhoff, H., Dundr, M., Michels, A.A., and Grummt, I. (2008). Phosphorylation by casein kinase 2 facilitates rRNA gene transcription by promoting dissociation of TIF-IA from elongating RNA polymerase I. Mol. Cell Biol. *28*, 4988–4998.

Bierhoff, H., Schmitz, K., Maass, F., Ye, J., and Grummt, I. (2010). Noncoding transcripts in sense and antisense orientation regulate the epigenetic state of ribosomal RNA genes. Cold Spring Harb. Symp. Quant. Biol. *75*, 357–364.

Bierhoff, H., Dammert, M.A., Brocks, D., Dambacher, S., Schotta, G., and Grummt, I. (2014). Quiescence-induced LncRNAs trigger H4K20 trimethylation and transcriptional silencing. Mol. Cell *54*, 675–682.

Biggiogera, M., Bürki, K., Kaufmann, S.H., Shaper, J.H., Gas, N., Amalric, F., and Fakan, S. (1990). Nucleolar distribution of proteins B23 and nucleolin in mouse preimplantation embryos as visualized by immunoelectron microscopy. Development *110*, 1263–1270.

Birbach, A., Bailey, S.T., Ghosh, S., and Schmid, J.A. (2004). Cytosolic, nuclear and nucleolar localization signals determine subcellular distribution and activity of the NF-kappaB inducing kinase NIK. J. Cell Sci. *117*, 3615–3624.

Birch, J.L., and Zomerdijk, J.C.B.M. (2008). Structure and function of ribosomal RNA gene chromatin. Biochem. Soc. Trans. *36*, 619–624.

Bird, A., Taggart, M., and Macleod, D. (1981). Loss of rDNA methylation accompanies the onset of ribosomal gene activity in early development of X. laevis. Cell *26*, 381–390.

Boettcher, B., and Barral, Y. (2013). The cell biology of open and closed mitosis. Nucleus *4*, 160–165.

Bohnsack, M.T., Stüven, T., Kuhn, C., Cordes, V.C., and Görlich, D. (2006). A selective block of nuclear actin export stabilizes the giant nuclei of Xenopus oocytes. Nat. Cell Biol. *8*, 257–263.

Boisvert, F.M., and Lamond, A.I. (2010). p53-Dependent subcellular proteome localization following DNA damage. Proteomics *10*, 4087–4097.

Boisvert, F.M., van Koningsbruggen, S., Navascués, J., and Lamond, A.I. (2007). The multifunctional nucleolus. Nat. Rev. Mol. Cell Biol. *8*, 574–585.

Bonnet, H., Filhol, O., Truchet, I., Brethenou, P., Cochet, C., Amalric, F., and Bouche, G. (1996). Fibroblast growth factor-2 binds to the regulatory beta subunit of CK2 and directly stimulates CK2 activity toward nucleolin. J. Biol. Chem. *271*, 24781–24787.

Boon, K., Caron, H.N., van Asperen, R., Valentijn, L., Hermus, M.C., van Sluis, P., Roobeek, I., Weis, I., Voûte, P.A., Schwab, M., et al. (2001). N-myc enhances the expression of a large set of genes functioning in ribosome biogenesis and protein synthesis. EMBO J. *20*, 1383–1393.

Borer, R.A., Lehner, C.F., Eppenberger, H.M., and Nigg, E.A. (1989). Major nucleolar proteins shuttle between nucleus and cytoplasm. Cell *56*, 379–390.

Bouche, G., Caizergues-Ferrer, M., Bugler, B., and Amalric, F. (1984). Interrelations between the maturation of a 100 kDa nucleolar protein and pre rRNA synthesis in CHO cells. Nucleic Acids Res. *12*, 3025–3035.

Bouffard, S., Dambroise, E., Brombin, A., Lempereur, S., Hatin, I., Simion, M., Corre, R., Bourrat, F., Joly, J.S., and Jamen, F. (2018). Fibrillarin is essential for S-phase progression and neuronal differentiation in zebrafish dorsal midbrain and retina. Dev. Biol. *437*, 1–16.

Boulon, S., Westman, B.J., Hutten, S., Boisvert, F.M., and Lamond, A.I. (2010). The nucleolus under stress. Mol. Cell *40*, 216–227.

Bouvet, P., Diaz, J.J., Kindbeiter, K., Madjar, J.J., and Amalric, F. (1998). Nucleolin interacts with several ribosomal proteins through its RGG domain. J. Biol. Chem. *273*, 19025–19029.

Boyd, M.T., Vlatkovic, N., and Rubbi, C.P. (2011). The nucleolus directly regulates p53 export and degradation. J. Cell Biol. *194*, 689–703.

Boyne, J.R., and Whitehouse, A. (2006). Nucleolar trafficking is essential for nuclear export of intronless herpesvirus mRNA. Proc. Natl. Acad. Sci. USA *103*, 15190–15195.

Branca, G., Barresi, V., Ieni, A., Irato, E., and Caruso, R.A. (2016). Pleomorphic carcinoma of the colon: morphological and immunohistochemical findings. Case Rep. Gastroenterol. *10*, 233–240.

Brangwynne, C.P., Mitchison, T.J., and Hyman, A.A. (2011). Active liquid-like behavior of nucleoli determines their size and shape in Xenopus laevis oocytes. Proc. Natl. Acad. Sci. USA *108*, 4334–4339.

Brion, J.P. (1998). Neurofibrillary tangles and Alzheimer's disease. Eur Neurol *40*, 130–140.

Brown, D.D., and Gurdon, J.B. (1964). Absence of ribosomal RNA synthesis in the anucleolate mutant of Xenopus laevis. Proc. Natl. Acad. Sci. USA *51*, 139-146.

Buchwalter, A., and Hetzer, M.W. (2017). Nucleolar expansion and elevated protein translation in premature aging. Nat Commun *8*, 328.

Bugler, B., Caizergues-Ferrer, M., Bouche, G., Bourbon, H., and Amalric, F. (1982). Detection and localization of a class of proteins immunologically related to a 100-kDa nucleolar protein. Eur J Biochem *128*, 475–480.

Bunimov, N., Smith, J.E., Gosselin, D., and Laneuville, O. (2007). Translational regulation of PGHS-1 mRNA: 5' untranslated region and first two exons conferring negative regulation. Biochim Biophys Acta *1769*, 92–105.

Bywater, M.J., Poortinga, G., Sanij, E., Hein, N., Peck, A., Cullinane, C., Wall, M., Cluse, L., Drygin, D., Anderes, K., et al. (2012). Inhibition of RNA polymerase I as a therapeutic strategy to promote cancer-specific activation of p53. Cancer Cell *22*, 51–65.

Caburet, S., Conti, C., Schurra, C., Lebofsky, R., Edelstein, S.J., and Bensimon, A. (2005). Human ribosomal RNA gene arrays display a broad range of palindromic structures. Genome Res. *15*, 1079–1085.

Caizergues-Ferrer, M., Belenguer, P., Lapeyre, B., Amalric, F., Wallace, M.O., and Olson, M.O. (1987). Phosphorylation of nucleolin by a nucleolar type NII protein kinase. Biochemistry *26*, 7876–7883.

Camps, J., Wangsa, D., Falke, M., Brown, M., Case, C.M., Erdos, M.R., and Ried, T. (2014). Loss of lamin B1 results in prolongation of S phase and decondensation of chromosome territories. FASEB J. *28*, 3423–3434.

Carpentier, M., Morelle, W., Coddeville, B., Pons, A., Masson, M., Mazurier, J., and Legrand, D. (2005). Nucleolin undergoes partial N- and O-glycosylations in the extranuclear cell compartment. Biochemistry *44*, 5804–5815.

Carron, C., Balor, S., Delavoie, F., Plisson-Chastang, C., Faubladier, M., Gleizes, P.E., and O'Donohue, M.F. (2012). Post-mitotic dynamics of pre-nucleolar bodies is driven by pre-rRNA processing. J. Cell Sci. *125*, 4532–4542.

Caudron-Herger, M., Pankert, T., Seiler, J., Németh, A., Voit, R., Grummt, I., and Rippe, K. (2015). Alu element-containing RNAs maintain nucleolar structure and function. EMBO J. *34*, 2758–2774.

Cerdido, A., and Medina, F.J. (1995). Subnucleolar location of fibrillarin and variation in its levels during the cell cycle and during differentiation of plant cells. Chromosoma *103*, 625–634.

Céspedes, M.V., Espina, C., García-Cabezas, M.A., Trias, M., Boluda, A., Gómez del Pulgar, M.T., Sancho, F.J., Nistal, M., Lacal, J.C., and Mangues, R. (2007). Orthotopic microinjection of human colon cancer cells in nude mice induces tumor foci in all clinically relevant metastatic sites. Am. J. Pathol. *170*, 1077–1085.

Chan, J.C., Hannan, K.M., Riddell, K., Ng, P.Y., Peck, A., Lee, R.S., Hung, S., Astle, M.V., Bywater, M., Wall, M., et al. (2011). AKT promotes rRNA synthesis and cooperates with c-MYC to stimulate ribosome biogenesis in cancer. Sci Signal *4*, ra56.

Chan, P.K., Aldrich, M., and Busch, H. (1985). Alterations in immunolocalization of the phosphoprotein B23 in HeLa cells during serum starvation. Exp. Cell Res. *161*, 101–110.

Chaumeil, J., Augui, S., Chow, J.C., and Heard, E. (2008). Combined immunofluorescence, RNA fluorescent in situ hybridization, and DNA fluorescent in situ hybridization to study chromatin changes, transcriptional activity, nuclear organization, and X-chromosome inactivation. Methods Mol. Biol. *463*, 297–308.

Chelsky, D., Sobotka, C., and O'Neill, C.L. (1989). Lamin B methylation and assembly into the nuclear envelope. J. Biol. Chem. *264*, 7637–7643.

Chen, D., and Huang, S. (2001). Nucleolar components involved in ribosome biogenesis cycle between the nucleolus and nucleoplasm in interphase cells. J. Cell Biol. *153*, 169–176.

Chen, J., Guo, K., and Kastan, M.B. (2012). Interactions of nucleolin and ribosomal protein L26 (RPL26) in translational control of human p53 mRNA. J. Biol. Chem. *287*, 16467–16476.

Cheng, G., Brett, M.E., and He, B. (2002). Signals that dictate nuclear, nucleolar, and cytoplasmic shuttling of the gamma(1)34.5 protein of herpes simplex virus type 1. J. Virol. *76*, 9434–9445.

Cheutin, T., O'Donohue, M.-F., Beorchia, A., Vandelaer, M., Kaplan, H., Deféver, B., Ploton, D., and Thiry, M. (2002). Three-dimensional organization of active rRNA genes within the nucleolus. J. Cell Sci. *115*, 3297–3307.

Chiarella, S., De Cola, A., Scaglione, G.L., Carletti, E., Graziano, V., Barcaroli, D., Lo Sterzo, C., Di Matteo, A., Di Ilio, C., Falini, B., et al. (2013). Nucleophosmin mutations alter its nucleolar localization by impairing G-quadruplex binding at ribosomal DNA. Nucleic Acids Res. *41*, 3228–3239.

Christian, S., Pilch, J., Akerman, M.E., Porkka, K., Laakkonen, P., and Ruoslahti, E. (2003). Nucleolin expressed at the cell surface is a marker of endothelial cells in angiogenic blood vessels. J. Cell Biol. *163*, 871–878.

Cimato, T.R., Tang, J., Xu, Y., Guarnaccia, C., Herschman, H.R., Pongor, S., and Aletta, J.M. (2002). Nerve growth factor-mediated increases in protein methylation occur predominantly at type I arginine methylation sites and involve protein arginine methyltransferase 1. J Neurosci Res *67*, 435–442.

Clos, J., Buttgereit, D., and Grummt, I. (1986). A purified transcription factor (TIF-IB) binds to essential sequences of the mouse rDNA promoter. Proc Natl Acad Sci USA *83*, 604–608.

Cochrane, A.W., Perkins, A., and Rosen, C.A. (1990). Identification of sequences important in the nucleolar localization of human immunodeficiency virus Rev: relevance of nucleolar localization to function. J. Virol. *64*, 881–885.

Coffinier, C., Jung, H.-J., Nobumori, C., Chang, S., Tu, Y., Barnes, R.H., Yoshinaga, Y., de Jong, P.J., Vergnes, L., Reue, K., et al. (2011). Deficiencies in lamin B1 and Lamin B2 cause neurodevelopmental defects and distinct nuclear shape abnormalities in neurons. Mol. Biol. Cell *22*, 4683–4693.

Colombo, E., Marine, J.C., Danovi, D., Falini, B., and Pelicci, P.G. (2002). Nucleophosmin regulates the stability and transcriptional activity of p53. Nat. Cell Biol. *4*, 529–533.

Comai, L., Tanese, N., and Tjian, R. (1992). The TATA-binding protein and associated factors are integral components of the RNA polymerase I transcription factor, SL1. Cell *68*, 965–976.

Conconi, A., Widmer, R.M., Koller, T., and Sogo, J.M. (1989). Two different chromatin structures coexist in ribosomal RNA genes throughout the cell cycle. Cell *57*, 753–761.

Cong, R., Das, S., Ugrinova, I., Kumar, S., Mongelard, F., Wong, J., and Bouvet, P. (2012). Interaction of nucleolin with ribosomal RNA genes and its role in RNA polymerase I transcription. Nucleic Acids Res. *40*, 9441–9454.

Cong, R., Das, S., Douet, J., Wong, J., Buschbeck, M., Mongelard, F., and Bouvet, P. (2014). macroH2A1 histone variant represses rDNA transcription. Nucleic Acids Res. *42*, 181–192.

Constantinescu, D., Gray, H.L., Sammak, P.J., Schatten, G.P., and Csoka, A.B. (2006). Lamin A/C expression is a marker of mouse and human embryonic stem cell differentiation. Stem Cells *24*, 177–185.

Craig, N., Kass, S., and Sollner-Webb, B. (1987). Nucleotide sequence determining the first cleavage site in the processing of mouse precursor rRNA. Proc Natl Acad Sci USA *84*, 629–633.

Creancier, L., Prats, H., Zanibellato, C., Amalric, F., and Bugler, B. (1993). Determination of the functional domains involved in nucleolar targeting of nucleolin. Mol. Biol. Cell *4*, 1239–1250.

Dang, C.V., and Lee, W.M. (1989). Nuclear and nucleolar targeting sequences of c-erb-A, c-myb, N-myc, p53, HSP70, and HIV tat proteins. J. Biol. Chem. *264*, 18019–18023.

Daniely, Y., Dimitrova, D.D., and Borowiec, J.A. (2002). Stress-dependent nucleolin mobilization mediated by p53-nucleolin complex formation. Mol. Cell. Biol. *22*, 6014–6022.

Das, S., Cong, R., Shandilya, J., Senapati, P., Moindrot, B., Monier, K., Delage, H., Mongelard, F., Kumar, S., Kundu, T.K., et al. (2013). Characterization of nucleolin K88 acetylation defines a new pool of nucleolin colocalizing with pre-mRNA splicing factors. FEBS Lett *587*, 417–424.

De, A., Donahue, S.L., Tabah, A., Castro, N.E., Mraz, N., Cruise, J.L., and Campbell, C. (2006). A novel interaction [corrected] of nucleolin with Rad51. Biochem Biophys Res Commun *344*, 206–213.

De Castro, S.C.P., Malhas, A., Leung, K.-Y., Gustavsson, P., Vaux, D.J., Copp, A.J., and Greene, N.D.E. (2012). Lamin b1 polymorphism influences morphology of the nuclear envelope, cell cycle progression, and risk of neural tube defects in mice. PLoS Genet. *8*, e1003059.

Dechat, T., Pfleghaar, K., Sengupta, K., Shimi, T., Shumaker, D.K., Solimando, L., and Goldman, R.D. (2008). Nuclear lamins: major factors in the structural organization and function of the nucleus and chromatin. Genes Dev. *22*, 832–853.

Denais, C.M., Gilbert, R.M., Isermann, P., McGregor, A.L., te Lindert, M., Weigelin, B., Davidson, P.M., Friedl, P., Wolf, K., and Lammerding, J. (2016). Nuclear envelope rupture and repair during cancer cell migration.

Science (80-.). *352*, 353–358.

Denissov, S., van Driel, M., Voit, R., Hekkelman, M., Hulsen, T., Hernandez, N., Grummt, I., Wehrens, R., and Stunnenberg, H. (2007). Identification of novel functional TBP-binding sites and general factor repertoires. EMBO J. *26*, 944–954.

Denissov, S., Lessard, F., Mayer, C., Stefanovsky, V., van Driel, M., Grummt, I., Moss, T., and Stunnenberg, H.G. (2011). A model for the topology of active ribosomal RNA genes. EMBO Rep *12*, 231–237.

Dennis, G., Sherman, B.T., Hosack, D.A., Yang, J., Gao, W., Lane, H.C., and Lempicki, R.A. (2003). DAVID: Database for Annotation, Visualization, and Integrated Discovery. Genome Biol.

Derenzini, M., and Ploton, D. (1991). Interphase nucleolar organizer regions in cancer cells. Int Rev Exp Pathol.

Derenzini, M., Trerè, D., Pession, A., Montanaro, L., Sirri, V., and Ochs, R.L. (1998). Nucleolar function and size in cancer cells. Am. J. Pathol. *152*, 1291–1297.

Derenzini, M., Ceccarelli, C., Santini, D., Taffurelli, M., and Treré, D. (2004). The prognostic value of the AgNOR parameter in human breast cancer depends on the pRb and p53 status. J. Clin. Pathol. *57*, 755–761.

Derenzini, M., Montanaro, L., and Treré, D. (2009). What the nucleolus says to a tumour pathologist. Histopathology *54*, 753–762.

Destouches, D., El Khoury, D., Hamma-Kourbali, Y., Krust, B., Albanese, P., Katsoris, P., Guichard, G., Briand, J.P., Courty, J., and Hovanessian, A.G. (2008). Suppression of tumor growth and angiogenesis by a specific antagonist of the cell-surface expressed nucleolin. PLoS One *3*, e2518.

Dhar, S.K., Lynn, B.C., Daosukho, C., and St Clair, D.K. (2004). Identification of nucleophosmin as an NF-kappaB co-activator for the induction of the human SOD2 gene. J. Biol. Chem. *279*, 28209–28219.

Dhe-Paganon, S., Werner, E.D., Chi, Y.I., and Shoelson, S.E. (2002). Structure of the globular tail of nuclear lamin. J. Biol. Chem. *277*, 17381–17384.

Ding, Y., Song, N., Liu, C., He, T., Zhuo, W., He, X., Chen, Y., Song, X., Fu, Y., and Luo, Y. (2012). Heat shock cognate 70 regulates the translocation and angiogenic function of nucleolin. Arterioscler Thromb Vasc Biol *32*, e126-34.

Dingwall, C., Dilworth, S.M., Black, S.J., Kearsey, S.E., Cox, L.S., and Laskey, R.A. (1987). Nucleoplasmin cDNA sequence reveals polyglutamic acid tracts and a cluster of sequences homologous to putative nuclear localization signals. EMBO J. *6*, 69–74.

Dittmer, T.A., and Misteli, T. (2011). The lamin protein family. Genome Biol. *12*, 222.

Dixon, C.R., Platani, M., Makarov, A.A., and Schirmer, E.C. (2017). Microinjection of Antibodies Targeting the Lamin A/C Histone-Binding Site Blocks Mitotic Entry and Reveals Separate Chromatin Interactions with HP1, CenpB and PML. Cells *6*.

Dominici, S., Fiori, V., Magnani, M., Schena, E., Capanni, C., Camozzi, D., D'Apice, M.R., Le Dour, C., Auclair, M., Caron, M., et al. (2009). Different prelamin A forms accumulate in human fibroblasts: a study in experimental models and progeria. Eur. J. Histochem. *53*, 43-52.

Douet, J., Corujo, D., Malinverni, R., Renauld, J., Sansoni, V., Posavec Marjanović, M., Cantariño, N., Valero, V., Mongelard, F., Bouvet, P., et al. (2017). MacroH2A histone variants maintain nuclear organization and heterochromatin architecture. J. Cell Sci. *130*, 1570–1582.

Dove, B.K., You, J.-H., Reed, M.L., Emmett, S.R., Brooks, G., and Hiscox, J.A. (2006). Changes in nucleolar morphology and proteins during infection with the coronavirus infectious bronchitis virus. Cell Microbiol. *8*, 1147–1157.

Dranovsky, A., Vincent, I., Gregori, L., Schwarzman, A., Colflesh, D., Enghild, J., Strittmatter, W., Davies, P., and Goldgaber, D. (2001). Cdc2 phosphorylation of nucleolin demarcates mitotic stages and Alzheimer's disease pathology. Neurobiol Aging *22*, 517–528.

Drecoll, E., Gaertner, F.C., Miederer, M., Blechert, B., Vallon, M., Müller, J.M., Alke, A., Seidl, C.,

Bruchertseifer, F., Morgenstern, A., et al. (2009). Treatment of peritoneal carcinomatosis by targeted delivery of the radio-labeled tumor homing peptide bi-DTPA-[F3]2 into the nucleus of tumor cells. PLoS One *4*, e5715.

Dubail, J., Kesteloot, F., Deroanne, C., Motte, P., Lambert, V., Rakic, J.M., Lapière, C., Nusgens, B., and Colige, A. (2010). ADAMTS-2 functions as anti-angiogenic and anti-tumoral molecule independently of its catalytic activity. Cell Mol. Life Sci. *67*, 4213–4232.

Dunbar, D.A., Wormsley, S., Lowe, T.M., and Baserga, S.J. (2000). Fibrillarin-associated box C/D small nucleolar RNAs in Trypanosoma brucei. Sequence conservation and implications for 2'-O-ribose methylation of rRNA. J. Biol. Chem. *275*, 14767–14776.

Eberhard, D., Tora, L., Egly, J.M., and Grummt, I. (1993). A TBP-containing multiprotein complex (TIF-IB) mediates transcription specificity of murine RNA polymerase I. Nucleic Acids Res. *21*, 4180–4186.

Egyhazi, E., Pigon, A., Chang, J.H., Ghaffari, S.H., Dreesen, T.D., Wellman, S.E., Case, S.T., and Olson, M.O. (1988). Effects of anti-C23 (nucleolin) antibody on transcription of ribosomal DNA in Chironomus salivary gland cells. Exp Cell Res *178*, 264–272.

El Hage, A., Koper, M., Kufel, J., and Tollervey, D. (2008). Efficient termination of transcription by RNA polymerase I requires the 5' exonuclease Rat1 in yeast. Genes Dev *22*, 1069–1081.

Emmott, E., and Hiscox, J.A. (2009). Nucleolar targeting: the hub of the matter. EMBO Rep. *10*, 231–238.

Emmott, E., Wise, H., Loucaides, E.M., Matthews, D.A., Digard, P., and Hiscox, J.A. (2010b). Quantitative proteomics using SILAC coupled to LC-MS/MS reveals changes in the nucleolar proteome in influenza A virus-infected cells. J Proteome Res *9*, 5335–5345.

Emmott, E., Rodgers, M.A., Macdonald, A., McCrory, S., Ajuh, P., and Hiscox, J.A. (2010a). Quantitative proteomics using stable isotope labeling with amino acids in cell culture reveals changes in the cytoplasmic, nuclear, and nucleolar proteomes in Vero cells infected with the coronavirus infectious bronchitis virus. Mol Cell Proteomics *9*, 1920–1936.

Erard, M.S., Belenguer, P., Caizergues-Ferrer, M., Pantaloni, A., and Amalric, F. (1988). A major nucleolar protein, nucleolin, induces chromatin decondensation by binding to histone H1. Eur J Biochem *175*, 525–530.

Erber, A., Riemer, D., Hofemeister, H., Bovenschulte, M., Stick, R., Panopoulou, G., Lehrach, H., and Weber, K. (1999). Characterization of the Hydra lamin and its gene: A molecular phylogeny of metazoan lamins. J. Mol. Evol. *49*, 260–271.

Eriksson, M., Brown, W.T., Gordon, L.B., Glynn, M.W., Singer, J., Scott, L., Erdos, M.R., Robbins, C.M., Moses, T.Y., Berglund, P., et al. (2003). Recurrent de novo point mutations in lamin A cause Hutchinson-Gilford progeria syndrome. Nature *423*, 293–298.

Espada, J., Ballestar, E., Santoro, R., Fraga, M.F., Villar-Garea, A., Németh, A., Lopez-Serra, L., Ropero, S., Aranda, A., Orozco, H., et al. (2007). Epigenetic disruption of ribosomal RNA genes and nucleolar architecture in DNA methyltransferase 1 (Dnmt1) deficient cells. Nucleic Acids Res. *35*, 2191–2198.

Fähling, M., Steege, A., Perlewitz, A., Nafz, B., Mrowka, R., Persson, P.B., and Thiele, B.J. (2005). Role of nucleolin in posttranscriptional control of MMP-9 expression. Biochim Biophys Acta *1731*, 32–40.

Falahati, H., Pelham-Webb, B., Blythe, S., and Wieschaus, E. (2016). Nucleation by rRNA Dictates the Precision of Nucleolus Assembly. Curr. Biol. *26*, 277–285.

Falini, B., Mecucci, C., Tiacci, E., Alcalay, M., Rosati, R., Pasqualucci, L., La Starza, R., Diverio, D., Colombo, E., Santucci, A., et al. (2005). Cytoplasmic nucleophosmin in acute myelogenous leukemia with a normal karyotype. N. Engl. J. Med. *352*, 254–266.

Fankhauser, C., Izaurralde, E., Adachi, Y., Wingfield, P., and Laemmli, U.K. (1991). Specific complex of human immunodeficiency virus type 1 rev and nucleolar B23 proteins: dissociation by the Rev response element. Mol. Cell. Biol. *11*, 2567–2575.

Farley-Barnes, K.I., McCann, K.L., Ogawa, L.M., Merkel, J., Surovtseva, Y.V., and Baserga, S.J. (2018).

Diverse regulators of human ribosome biogenesis discovered by changes in nucleolar number. Cell Rep. *22*, 1923–1934.

Feric, M., and Brangwynne, C.P. (2013). A nuclear F-actin scaffold stabilizes ribonucleoprotein droplets against gravity in large cells. Nat. Cell Biol. *15*, 1253–1259.

Feric, M., Vaidya, N., Harmon, T.S., Mitrea, D.M., Zhu, L., Richardson, T.M., Kriwacki, R.W., Pappu, R.V., and Brangwynne, C.P. (2016). Coexisting liquid phases underlie nucleolar subcompartments. Cell *165*, 1686–1697.

Fernandez, P.C., Frank, S.R., Wang, L., Schroeder, M., Liu, S., Greene, J., Cocito, A., and Amati, B. (2003). Genomic targets of the human c-Myc protein. Genes Dev *17*, 1115–1129.

Feuerstein, N., and Mond, J.J. (1987). Identification of a prominent nuclear protein associated with proliferation of normal and malignant B cells. J Immunol *139*, 1818–1822.

Floutsakou, I., Agrawal, S., Nguyen, T.T., Seoighe, C., Ganley, A.R.D., and McStay, B. (2013). The shared genomic architecture of human nucleolar organizer regions. Genome Res. *23*, 2003–2012.

Franek, M., Legartová, S., Suchánková, J., Milite, C., Castellano, S., Sbardella, G., Kozubek, S., and Bártová, E. (2015). CARM1 modulators affect epigenome of stem cells and change morphology of nucleoli. Physiol. Res.

French, S.L., Sikes, M.L., Hontz, R.D., Osheim, Y.N., Lambert, T.E., El Hage, A., Smith, M.M., Tollervey, D., Smith, J.S., and Beyer, A.L. (2011). Distinguishing the roles of Topoisomerases I and II in relief of transcription-induced torsional stress in yeast rRNA genes. Mol. Cell Biol. *31*, 482–494.

Freund, A., Laberge, R.-M., Demaria, M., and Campisi, J. (2012). Lamin B1 loss is a senescence-associated biomarker. Mol. Biol. Cell *23*, 2066–2075.

Frost, B., Bardai, F.H., and Feany, M.B. (2016). Lamin dysfunction mediates neurodegeneration in tauopathies. Curr. Biol. *26*, 129–136.

Fu, Y., Lv, P., Yan, G., Fan, H., Cheng, L., Zhang, F., Dang, Y., Wu, H., and Wen, B. (2015). MacroH2A1 associates with nuclear lamina and maintains chromatin architecture in mouse liver cells. Sci. Rep. *5*, 17186.

Fujiwara, Y., Fujiwara, K., Goda, N., Iwaya, N., Tenno, T., Shirakawa, M., and Hiroaki, H. (2011). Structure and function of the N-terminal nucleolin binding domain of nuclear valosin-containing protein-like 2 (NVL2) harboring a nucleolar localization signal. J. Biol. Chem. *286*, 21732–21741.

Funkhouser, C.M., Sknepnek, R., Shimi, T., Goldman, A.E., Goldman, R.D., and Olvera de la Cruz, M. (2013). Mechanical model of blebbing in nuclear lamin meshworks. Proc. Natl. Acad. Sci. USA *110*, 3248–3253.

Furukawa, K., and Hotta, Y. (1993). cDNA cloning of a germ cell specific lamin B3 from mouse spermatocytes and analysis of its function by ectopic expression in somatic cells. EMBO J.

Gadad, S.S., Senapati, P., Syed, S.H., Rajan, R.E., Shandilya, J., Swaminathan, V., Chatterjee, S., Colombo, E., Dimitrov, S., Pelicci, P.G., et al. (2011). The multifunctional protein nucleophosmin (NPM1) is a human linker histone H1 chaperone. Biochemistry *50*, 2780–2789.

Gandhi, M., and Goode, B.L. (2013). Coronin: The Double-Edged Sword of Actin Dynamics. Subcell Biochem. *48*, 72-87.

García Moreno, L.M., Cimadevilla, J.M., González Pardo, H., Zahonero, M.C., and Arias, J.L. (1997). NOR activity in hippocampal areas during the postnatal development and ageing. Mech. Ageing Dev. *97*, 173–181.

Gaudreault, I., Guay, D., and Lebel, M. (2004). YB-1 promotes strand separation in vitro of duplex DNA containing either mispaired bases or cisplatin modifications, exhibits endonucleolytic activities and binds several DNA repair proteins. Nucleic Acids Res. *32*, 316–327.

Gaulden, M.E., and Perry, R.P. (1958). Influence of the nucleolus on mitosis as revealed by ultraviolet microbeam irradiation. Proc. Natl. Acad. Sci. USA *44*, 553–559.

Gaume, X., Monier, K., Argoul, F., Mongelard, F., and Bouvet, P. (2011). In vivo Study of the Histone Chaperone Activity of Nucleolin by FRAP. Biochem Res Int *2011*, 187624.

Gautier, T., Robert-Nicoud, M., Guilly, M.N., and Hernandez-Verdun, D. (1992). Relocation of nucleolar

proteins around chromosomes at mitosis. A study by confocal laser scanning microscopy. J. Cell Sci. *102 (Pt 4)*, 729–737.

Gavet, O., and Pines, J. (2010). Progressive activation of CyclinB1-Cdk1 coordinates entry to mitosis. Dev. Cell *18*, 533–543.

Gébrane-Younès, J., Fomproix, N., and Hernandez-Verdun, D. (1997). When rDNA transcription is arrested during mitosis, UBF is still associated with non-condensed rDNA. J. Cell Sci. *110 (Pt 19)*, 2429–2440.

Georgatos, S.D., Stournaras, C., and Blobel, G. (1988). Heterotypic and homotypic associations between the nuclear lamins: site-specificity and control by phosphorylation. Proc. Natl. Acad. Sci. USA *85*, 4325–4329.

Gerace, L., and Blobel, G. (1980). The nuclear envelope lamina is reversibly depolymerized during mitosis. Cell *19*, 277–287.

Ghisolfi, L., Kharrat, A., Joseph, G., Amalric, F., and Erard, M. (1992). Concerted activities of the RNA recognition and the glycine-rich C-terminal domains of nucleolin are required for efficient complex formation with pre-ribosomal RNA. Eur J Biochem *209*, 541–548.

Ghisolfi-Nieto, L., Joseph, G., Puvion-Dutilleul, F., Amalric, F., and Bouvet, P. (1996). Nucleolin is a sequence-specific RNA-binding protein: characterization of targets on pre-ribosomal RNA. J Mol Biol *260*, 34–53.

Ghoshal, K., Majumder, S., Datta, J., Motiwala, T., Bai, S., Sharma, S.M., Frankel, W., and Jacob, S.T. (2004). Role of human ribosomal RNA (rRNA) promoter methylation and of methyl-CpG-binding protein MBD2 in the suppression of rRNA gene expression. J. Biol. Chem. *279*, 6783–6793.

Gibbons, J.G., Branco, A.T., Godinho, S.A., Yu, S., and Lemos, B. (2015). Concerted copy number variation balances ribosomal DNA dosage in human and mouse genomes. Proc. Natl. Acad. Sci. USA *112*, 2485–2490.

Ginisty, H., Amalric, F., and Bouvet, P. (1998). Nucleolin functions in the first step of ribosomal RNA processing. EMBO J. *17*, 1476–1486.

Ginisty, H., Sicard, H., Roger, B., and Bouvet, P. (1999). Structure and functions of nucleolin. J. Cell Sci. *112 (Pt 6)*, 761–772.

Godfrey, J.E., Baxevanis, A.D., and Moudrianakis, E.N. (1990). Spectropolarimetric analysis of the core histone octamer and its subunits. Biochemistry *29*, 965–972.

Goessens, G. (1984). Nucleolar structure. Int Rev Cytol *87*, 107–158.

Goldberg, M., Jenkins, H., Allen, T., Whitfield, W.G., and Hutchison, C.J. (1995). Xenopus lamin B3 has a direct role in the assembly of a replication competent nucleus: evidence from cell-free egg extracts. J. Cell Sci. *108 (11)*, 3451–3461.

Goldman, R.D., Shumaker, D.K., Erdos, M.R., Eriksson, M., Goldman, A.E., Gordon, L.B., Gruenbaum, Y., Khuon, S., Mendez, M., Varga, R., et al. (2004). Accumulation of mutant lamin A causes progressive changes in nuclear architecture in Hutchinson-Gilford progeria syndrome. Proc. Natl. Acad. Sci. USA *101*, 8963–8968.

Goldman, R.D., Swedlow, J.R., and Spector, D.L. (2010). Live Cell Imaging (Cold Spring Harbor Laboratory Press: Cold Spring Harbor Laboratory Press).

Goldstein, M., Derheimer, F.A., Tait-Mulder, J., and Kastan, M.B. (2013). Nucleolin mediates nucleosome disruption critical for DNA double-strand break repair. Proc Natl Acad Sci USA *110*, 16874–16879.

Gomez, N.C., Hepperla, A.J., Dumitru, R., Simon, J.M., Fang, F., and Davis, I.J. (2016). Widespread Chromatin Accessibility at Repetitive Elements Links Stem Cells with Human Cancer. Cell Rep. *17*, 1607–1620.

González, V., and Hurley, L.H. (2010). The C-terminus of nucleolin promotes the formation of the c-MYC G-quadruplex and inhibits c-MYC promoter activity. Biochemistry *49*, 9706–9714.

González, V., Guo, K., Hurley, L., and Sun, D. (2009). Identification and characterization of nucleolin as a c-myc G-quadruplex-binding protein. J. Biol. Chem. *284*, 23622–23635.

González-Granado, J.M., Silvestre-Roig, C., Rocha-Perugini, V., Trigueros-Motos, L., Cibrián, D., Morlino, G., Blanco-Berrocal, M., Osorio, F.G., Freije, J.M.P., López-Otín, C., et al. (2014). Nuclear envelope lamin-A

couples actin dynamics with immunological synapse architecture and T cell activation. Sci. Signal. *7*, ra37.

Goodpasture, C., and Bloom, S.E. (1975). Visualization of nucleolar organizer regions in mammalian chromosomes using silver staining. Chromosoma.

Gorski, J.J., Pathak, S., Panov, K., Kasciukovic, T., Panova, T., Russell, J., and Zomerdijk, J.C. (2007). A novel TBP-associated factor of SL1 functions in RNA polymerase I transcription. EMBO J. *26*, 1560–1568.

Goto, M., Toda, N., Shimaji, K., Suong, D.N., Vo, N., Kimura, H., Yoshida, H., Inoue, Y.H., and Yamaguchi, M. (2016). Polycomb-dependent nucleolus localization of Jumonji/Jarid2 during Drosophila spermatogenesis. Spermatogenesis *6*, e1232023.

Gould, S.J., Keller, G.A., Hosken, N., Wilkinson, J., and Subramani, S. (1989). A conserved tripeptide sorts proteins to peroxisomes. J. Cell Biol. *108*, 1657–1664.

Goyal, P., Pandey, D., and Siess, W. (2006). Phosphorylation-dependent regulation of unique nuclear and nucleolar localization signals of LIM kinase 2 in endothelial cells. J. Biol. Chem. *281*, 25223–25230.

Grandori, C., Gomez-Roman, N., Felton-Edkins, Z.A., Ngouenet, C., Galloway, D.A., Eisenman, R.N., and White, R.J. (2005). c-Myc binds to human ribosomal DNA and stimulates transcription of rRNA genes by RNA polymerase I. Nat. Cell Biol. *7*, 311–318.

Granot, D., and Snyder, M. (1991). Segregation of the nucleolus during mitosis in budding and fission yeast. Cell Motil. Cytoskeleton *20*, 47–54.

Grisendi, S., Mecucci, C., Falini, B., and Pandolfi, P.P. (2006). Nucleophosmin and cancer. Nat. Rev. Cancer *6*, 493–505.

Grob, A., Colleran, C., and McStay, B. (2014). Construction of synthetic nucleoli in human cells reveals how a major functional nuclear domain is formed and propagated through cell division. Genes Dev. *28*, 220–230.

Grummt, I., Roth, E., and Paule, M.R. (1982). Ribosomal RNA transcription in vitro is species specific. Nature *296*, 173–174.

Grummt, I., Maier, U., Ohrlein, A., Hassouna, N., and Bachellerie, J.P. (1985). Transcription of mouse rDNA terminates downstream of the 3' end of 28S RNA and involves interaction of factors with repeated sequences in the 3' spacer. Cell *43*, 801–810.

Gu, J., Tamura, M., and Yamada, K.M. (1998). Tumor suppressor PTEN inhibits integrin- and growth factor-mediated mitogen-activated protein (MAP) kinase signaling pathways. J. Cell Biol. *143*, 1375–1383.

Guelen, L., Pagie, L., Brasset, E., Meuleman, W., Faza, M.B., Talhout, W., Eussen, B.H., de Klein, A., Wessels, L., de Laat, W., et al. (2008). Domain organization of human chromosomes revealed by mapping of nuclear lamina interactions. Nature *453*, 948–951.

Guerra-Rebollo, M., Mateo, F., Franke, K., Huen, M.S.Y., Lopitz-Otsoa, F., Rodríguez, M.S., Plans, V., and Thomson, T.M. (2012). Nucleolar exit of RNF8 and BRCA1 in response to DNA damage. Exp. Cell Res. *318*, 2365–2376.

Gunawardena, S.R., Ruis, B.L., Meyer, J.A., Kapoor, M., and Conklin, K.F. (2008). NOM1 targets protein phosphatase I to the nucleolus. J. Biol. Chem. *283*, 398–404.

Gunjan, A., and Verreault, A. (2003). A Rad53 kinase-dependent surveillance mechanism that regulates histone protein levels in S. cerevisiae. Cell *115*, 537–549.

Guo, Y.X., Dallmann, K., and Kwang, J. (2003). Identification of nucleolus localization signal of betanodavirus GGNNV protein alpha. Virology *306*, 225–235.

Gupton, S.L., and Gertler, F.B. (2007). Filopodia: the fingers that do the walking. Sci STKE *2007*, re5.

Haase, K., Macadangdang, J.K.L., Edrington, C.H., Cuerrier, C.M., Hadjiantoniou, S., Harden, J.L., Skerjanc, I.S., and Pelling, A.E. (2016). Extracellular forces cause the nucleus to deform in a highly controlled anisotropic manner. Sci. Rep. *6*, 21300.

Hallgren, J., Pietrzak, M., Rempala, G., Nelson, P.T., and Hetman, M. (2014). Neurodegeneration-associated

instability of ribosomal DNA. Biochim. Biophys. Acta *1842*, 860–868.

Haltiner, M.M., Smale, S.T., and Tjian, R. (1986). Two distinct promoter elements in the human rRNA gene identified by linker scanning mutagenesis. Mol. Cell. Biol. *6*, 227–235.

Hamid, Q.A., Fatima, S., Thanumalayan, S., and Parnaik, V.K. (1996). Activation of the lamin A gene during rat liver development. FEBS Lett. *392*, 137–142.

Hanada, K., Song, C.Z., Yamamoto, K., Yano, K., Maeda, Y., Yamaguchi, K., and Muramatsu, M. (1996). RNA polymerase I associated factor 53 binds to the nucleolar transcription factor UBF and functions in specific rDNA transcription. EMBO J.

Hannan, K.M., Brandenburger, Y., Jenkins, A., Sharkey, K., Cavanaugh, A., Rothblum, L., Moss, T., Poortinga, G., McArthur, G.A., Pearson, R.B., et al. (2003). mTOR-dependent regulation of ribosomal gene transcription requires S6K1 and is mediated by phosphorylation of the carboxy-terminal activation domain of the nucleolar transcription factor UBF. Mol. Cell Biol. *23*, 8862–8877.

Hardwick, J.S., Kuruvilla, F.G., Tong, J.K., Shamji, A.F., and Schreiber, S.L. (1999). Rapamycin-modulated transcription defines the subset of nutrient-sensitive signaling pathways directly controlled by the Tor proteins. Proc Natl Acad Sci USA *96*, 14866–14870.

Hardy, K., Wu, F., Tu, W., Zafar, A., Boulding, T., McCuaig, R., Sutton, C.R., Theodoratos, A., and Rao, S. (2016). Identification of chromatin accessibility domains in human breast cancer stem cells. Nucleus *7*, 50–67.

Harms, G., Kraft, R., Grelle, G., Volz, B., Dernedde, J., and Tauber, R. (2001). Identification of nucleolin as a new L-selectin ligand. Biochem. J. *360*, 531–538.

Heine, M.A., Rankin, M.L., and DiMario, P.J. (1993). The Gly/Arg-rich (GAR) domain of Xenopus nucleolin facilitates in vitro nucleic acid binding and in vivo nucleolar localization. Mol. Biol. Cell *4*, 1189–1204.

Heitlinger, E., Peter, M., Häner, M., Lustig, A., Aebi, U., and Nigg, E.A. (1991). Expression of chicken Lamin B2 in Escherichia coli: characterization of its structure, assembly, and molecular interactions. J. Cell Biol. *113*, 485–495.

Heitlinger, E., Peter, M., Lustig, A., Villiger, W., Nigg, E.A., and Aebi, U. (1992). The role of the head and tail domain in lamin structure and assembly: analysis of bacterially expressed chicken lamin A and truncated B2 lamins. J. Struct. Biol. *108*, 74–89.

Heix, J., and Grummt, I. (1995). Species specificity of transcription by RNA polymerase I. Curr Opin Genet Dev *5*, 652–656.

Heix, J., Zomerdijk, J.C., Ravanpay, A., Tjian, R., and Grummt, I. (1997). Cloning of murine RNA polymerase I-specific TAF factors: conserved interactions between the subunits of the species-specific transcription initiation factor TIF-IB/SL1. Proc Natl Acad Sci USA *94*, 1733–1738.

Heix, J., Vente, A., Voit, R., Budde, A., Michaelidis, T.M., and Grummt, I. (1998). Mitotic silencing of human rRNA synthesis: inactivation of the promoter selectivity factor SL1 by cdc2/cyclin B-mediated phosphorylation. EMBO J. *17*, 7373–7381.

Helpap, B. (1989). Nucleolar grading of breast cancer. Comparative studies on frequency and localization of nucleoli and histology, stage, hormonal receptor status and lectin histochemistry. Virchows Arch A Pathol Anat Histopathol *415*, 501–508.

Helpap, B., Knüpffer, J., and Essmann, S. (1990). Nucleolar grading of renal cancer. Correlation of frequency and localization of nucleoli to histologic and cytologic grading and stage of renal cell carcinomas. Mod. Pathol. *3*, 671–678.

Henderson, A.S., Warburton, D., and Atwood, K.C. (1972). Location of ribosomal DNA in the human chromosome complement. Proc. Natl. Acad. Sci. USA *69*, 3394–3398.

Henras, A.K., Plisson-Chastang, C., O'Donohue, M.F., Chakraborty, A., and Gleizes, P.E. (2015). An overview of pre-ribosomal RNA processing in eukaryotes. Wiley Interdiscip Rev RNA *6*, 225–242.

Hernandez-Verdun, D., Roussel, P., Thiry, M., Sirri, V., and Lafontaine, D.L.J. (2010). The nucleolus: structure/function relationship in RNA metabolism. Wiley Interdiscip Rev RNA *1*, 415–431.

Herrera, J.E., Savkur, R., and Olson, M.O. (1995). The ribonuclease activity of nucleolar protein B23. Nucleic Acids Res. *23*, 3974–3979.

Hingorani, K., Szebeni, A., and Olson, M.O. (2000). Mapping the functional domains of nucleolar protein B23. J. Biol. Chem. *275*, 24451–24457.

Hirano, A. (1994). Hirano bodies and related neuronal inclusions. Neuropathology and Applied Neurobiology.

Hirano, K., Miki, Y., Hirai, Y., Sato, R., Itoh, T., Hayashi, A., Yamanaka, M., Eda, S., and Beppu, M. (2005). A multifunctional shuttling protein nucleolin is a macrophage receptor for apoptotic cells. J. Biol. Chem. *280*, 39284–39293.

Hirano, Y., Hizume, K., Kimura, H., Takeyasu, K., Haraguchi, T., and Hiraoka, Y. (2012). Lamin B receptor recognizes specific modifications of histone H4 in heterochromatin formation. J. Biol. Chem. *287*, 42654–42663.

Hirschler-Laszkiewicz, I., Cavanaugh, A.H., Mirza, A., Lun, M., Hu, Q., Smink, T., and Rothblum, L.I. (2003). Rrn3 becomes inactivated in the process of ribosomal DNA transcription. J. Biol. Chem. *278*, 18953–18959.

Hisaoka, M., Ueshima, S., Murano, K., Nagata, K., and Okuwaki, M. (2010). Regulation of nucleolar chromatin by B23/nucleophosmin jointly depends upon its RNA binding activity and transcription factor UBF. Mol. Cell Biol. *30*, 4952–4964.

Ho, C.Y., Jaalouk, D.E., Vartiainen, M.K., and Lammerding, J. (2013). Lamin A/C and emerin regulate MKL1-SRF activity by modulating actin dynamics. Nature *497*, 507–511.

Ho, J.H., Kallstrom, G., and Johnson, A.W. (2000). Nmd3p is a Crm1p-dependent adapter protein for nuclear export of the large ribosomal subunit. J. Cell Biol. *151*, 1057–1066.

Höger, T.H., Zatloukal, K., Waizenegger, I., and Krohne, G. (1990). Characterization of a second highly conserved B-type lamin present in cells previously thought to contain only a single B-type lamin. Chromosoma *100*, 67–69.

Holmberg Olausson, K., Nistér, M., and Lindström, M.S. (2014). Loss of nucleolar histone chaperone NPM1 triggers rearrangement of heterochromatin and synergizes with a deficiency in DNA methyltransferase DNMT3A to drive ribosomal DNA transcription. J. Biol. Chem. *289*, 34601–34619.

Holmberg Olausson, K., Elsir, T., Moazemi Goudarzi, K., Nistér, M., and Lindström, M.S. (2015). NPM1 histone chaperone is upregulated in glioblastoma to promote cell survival and maintain nucleolar shape. Sci Rep *5*, 16495.

Holtz, D., Tanaka, R.A., Hartwig, J., and McKeon, F. (1989). The CaaX motif of lamin A functions in conjunction with the nuclear localization signal to target assembly to the nuclear envelope. Cell *59*, 969–977.

Hovanessian, A.G., Puvion-Dutilleul, F., Nisole, S., Svab, J., Perret, E., Deng, J.S., and Krust, B. (2000). The cell-surface-expressed nucleolin is associated with the actin cytoskeleton. Exp Cell Res *261*, 312–328.

Hovanessian, A.G., Soundaramourty, C., El Khoury, D., Nondier, I., Svab, J., and Krust, B. (2010). Surface expressed nucleolin is constantly induced in tumor cells to mediate calcium-dependent ligand internalization. PLoS One *5*, e15787.

Hozák, P., Sasseville, A.M., Raymond, Y., and Cook, P.R. (1995). Lamin proteins form an internal nucleoskeleton as well as a peripheral lamina in human cells. J. Cell Sci. *108 (Pt 2)*, 635–644.

Hu, Q., Gu, G., Liu, Z., Jiang, M., Kang, T., Miao, D., Tu, Y., Pang, Z., Song, Q., Yao, L., et al. (2013). F3 peptide-functionalized PEG-PLA nanoparticles co-administrated with tLyp-1 peptide for anti-glioma drug delivery. Biomaterials *34*, 1135–1145.

Huang, G., Meng, L., and Tsai, R.Y. (2015). p53 Configures the G2/M Arrest Response of Nucleostemin-Deficient Cells. Cell Death Discov *1*.

Huang, Y., Shi, H., Zhou, H., Song, X., Yuan, S., and Luo, Y. (2006). The angiogenic function of nucleolin is

mediated by vascular endothelial growth factor and nonmuscle myosin. Blood *107*, 3564–3571.

Hung, C.-Y., Yang, W.B., Wang, S.A., Hsu, T.I., Chang, W.C., and Hung, J.J. (2014). Nucleolin enhances internal ribosomal entry site (IRES)-mediated translation of Sp1 in tumorigenesis. Biochim. Biophys. Acta *1843*, 2843–2854.

Inouye, C.J., and Seto, E. (1994). Relief of YY1-induced transcriptional repression by protein-protein interaction with the nucleolar phosphoprotein B23. J. Biol. Chem. *269*, 6506–6510.

Irianto, J., Pfeifer, C.R., Ivanovska, I.L., Swift, J., and Discher, D.E. (2016). Nuclear lamins in cancer. Cell Mol. Bioeng. *9*, 258–267.

Isaac, C., Marsh, K.L., Paznekas, W.A., Dixon, J., Dixon, M.J., Jabs, E.W., and Meier, U.T. (2000). Characterization of the nucleolar gene product, treacle, in Treacher Collins syndrome. Mol. Biol. Cell *11*, 3061–3071.

Ishimaru, D., Zuraw, L., Ramalingam, S., Sengupta, T.K., Bandyopadhyay, S., Reuben, A., Fernandes, D.J., and Spicer, E.K. (2010). Mechanism of regulation of bcl-2 mRNA by nucleolin and A+U-rich element-binding factor 1 (AUF1). J. Biol. Chem. *285*, 27182–27191.

Isobe, K., Gohara, R., Ueda, T., Takasaki, Y., and Ando, S. (2007). The last twenty residues in the head domain of mouse lamin A contain important structural elements for formation of head-to-tail polymers in vitro. Biosci. Biotechnol. Biochem. *71*, 1252–1259.

Itahana, K., Bhat, K.P., Jin, A., Itahana, Y., Hawke, D., Kobayashi, R., and Zhang, Y. (2003). Tumor suppressor ARF degrades B23, a nucleolar protein involved in ribosome biogenesis and cell proliferation. Mol. Cell *12*, 1151–1164.

Izumi, M., Vaughan, O.A., Hutchison, C.J., and Gilbert, D.M. (2000). Head and/or CaaX domain deletions of lamin proteins disrupt preformed lamin A and C but not lamin B structure in mammalian cells. Mol. Biol. Cell *11*, 4323–4337.

Jaffe, A.B., and Hall, A. (2005). Rho GTPases: biochemistry and biology. Annu. Rev. Cell Dev. Biol. *21*, 247–269.

Jagatheesan, G., Thanumalayan, S., Muralikrishna, B., Rangaraj, N., Karande, A.A., and Parnaik, V.K. (1999). Colocalization of intranuclear lamin foci with RNA splicing factors. J. Cell Sci. *112 (Pt 24)*, 4651–4661.

Jakubowska, M., Sniegocka, M., Podgórska, E., Michalczyk-Wetula, D., Urbanska, K., Susz, A., Fiedor, L., Pyka, J., and Plonka, P.M. (2013). Pulmonary metastases of the A549-derived lung adenocarcinoma tumors growing in nude mice. A multiple case study. Acta Biochim. Pol. *60*, 323–330.

James, M.J., and Zomerdijk, J.C. (2004). Phosphatidylinositol 3-kinase and mTOR signaling pathways regulate RNA polymerase I transcription in response to IGF-1 and nutrients. J. Biol. Chem. *279*, 8911–8918.

James, A., Wang, Y., Raje, H., Rosby, R., and DiMario, P. (2014). Nucleolar stress with and without p53. Nucleus *5*, 402–426.

Janda, C.Y., Li, J., Oubridge, C., Hernández, H., Robinson, C.V., and Nagai, K. (2010). Recognition of a signal peptide by the signal recognition particle. Nature *465*, 507–510.

Jansa, P., and Grummt, I. (1999). Mechanism of transcription termination: PTRF interacts with the largest subunit of RNA polymerase I and dissociates paused transcription complexes from yeast and mouse. Mol Gen Genet *262*, 508–514.

Jantzen, H.M., Admon, A., Bell, S.P., and Tjian, R. (1990). Nucleolar transcription factor hUBF contains a DNA-binding motif with homology to HMG proteins. Nature *344*, 830–836.

Jiang, Y., Xu, X.S., and Russell, J.E. (2006). A nucleolin-binding 3' untranslated region element stabilizes beta-globin mRNA in vivo. Mol. Cell Biol. *26*, 2419–2429.

Jimenez, J., Jang, G.M., Semler, B.L., and Waterman, M.L. (2005). An internal ribosome entry site mediates translation of lymphoid enhancer factor-1. RNA *11*, 1385–1399.

Joo, E.J., ten Dam, G.B., van Kuppevelt, T.H., Toida, T., Linhardt, R.J., and Kim, Y.S. (2005). Nucleolin:

acharan sulfate-binding protein on the surface of cancer cells. Glycobiology *15*, 1–9.

Jordan, P., Heid, H., Kinzel, V., and Kübler, D. (1994). Major cell surface-located protein substrates of an ecto-protein kinase are homologs of known nuclear proteins. Biochemistry *33*, 14696–14706.

Kafienah, W., Mistry, S., Williams, C., and Hollander, A.P. (2006). Nucleostemin is a marker of proliferating stromal stem cells in adult human bone marrow. Stem Cells *24*, 1113–1120.

Kalashnikova, A.A., Winkler, D.D., McBryant, S.J., Henderson, R.K., Herman, J.A., DeLuca, J.G., Luger, K., Prenni, J.E., and Hansen, J.C. (2013). Linker histone H1.0 interacts with an extensive network of proteins found in the nucleolus. Nucleic Acids Res. *41*, 4026–4035.

Kang, J., Kusnadi, E.P., Ogden, A.J., Hicks, R.J., Bammert, L., Kutay, U., Hung, S., Sanij, E., Hannan, R.D., Hannan, K.M., et al. (2016). Amino acid-dependent signaling via S6K1 and MYC is essential for regulation of rDNA transcription. Oncotarget *7*, 48887–48904.

Kang, Y.J., Olson, M.O., Jones, C., and Busch, H. (1975). Nucleolar phosphoproteins of normal rat liver and Novikoff hepatoma ascites cells. Cancer Res. *35*, 1470–1475.

Kar, B., Liu, B., Zhou, Z., and Lam, Y.W. (2011). Quantitative nucleolar proteomics reveals nuclear re-organization during stress- induced senescence in mouse fibroblast. BMC Cell Biol *12*, 33.

Katz, M., Amit, I., and Yarden, Y. (2007). Regulation of MAPKs by growth factors and receptor tyrosine kinases. Biochim Biophys Acta *1773*, 1161–1176.

Kawauchi, J., Mischo, H., Braglia, P., Rondon, A., and Proudfoot, N.J. (2008). Budding yeast RNA polymerases I and II employ parallel mechanisms of transcriptional termination. Genes Dev *22*, 1082–1092.

Khatau, S.B., Hale, C.M., Stewart-Hutchinson, P.J., Patel, M.S., Stewart, C.L., Searson, P.C., Hodzic, D., and Wirtz, D. (2009). A perinuclear actin cap regulates nuclear shape. Proc. Natl. Acad. Sci. USA *106*, 19017–19022.

Kim, H., Chang, D.J., Lee, J.A., Lee, Y.S., and Kaang, B.K. (2003). Identification of nuclear/nucleolar localization signal in Aplysia learning associated protein of slug with a molecular mass of 18 kDa homologous protein. Neurosci. Lett. *343*, 134–138.

Kim, J.-K., Louhghalam, A., Lee, G., Schafer, B.W., Wirtz, D., and Kim, D.H. (2017). Nuclear lamin A/C harnesses the perinuclear apical actin cables to protect nuclear morphology. Nat Commun *8*, 2123.

Kimura, H., and Cook, P.R. (2001). Kinetics of core histones in living human cells: little exchange of H3 and H4 and some rapid exchange of H2B. J. Cell Biol. *153*, 1341–1353.

Kireeva, M.L., Walter, W., Tchernajenko, V., Bondarenko, V., Kashlev, M., and Studitsky, V.M. (2002). Nucleosome remodeling induced by RNA polymerase II: loss of the H2A/H2B dimer during transcription. Mol. Cell *9*, 541–552.

Kiss-László, Z., Henry, Y., Bachellerie, J.P., Caizergues-Ferrer, M., and Kiss, T. (1996). Site-specific ribose methylation of preribosomal RNA: a novel function for small nucleolar RNAs. Cell *85*, 1077–1088.

Kiss-László, Z., Henry, Y., and Kiss, T. (1998). Sequence and structural elements of methylation guide snoRNAs essential for site-specific ribose methylation of pre-rRNA. EMBO J. *17*, 797–807.

Kitamura, H., Matsumori, H., Kalendova, A., Hozak, P., Goldberg, I.G., Nakao, M., Saitoh, N., and Harata, M. (2015). The actin family protein ARP6 contributes to the structure and the function of the nucleolus. Biochem. Biophys. Res. Commun. *464*, 554–560.

Kleinman, H.K., Weeks, B.S., Cannon, F.B., Sweeney, T.M., Sephel, G.C., Clement, B., Zain, M., Olson, M.O., Jucker, M., and Burrous, B.A. (1991). Identification of a 110-kDa nonintegrin cell surface laminin-binding protein which recognizes an A chain neurite-promoting peptide. Arch. Biochem. Biophys. *290*, 320–325.

Kobayashi, J., Fujimoto, H., Sato, J., Hayashi, I., Burma, S., Matsuura, S., Chen, D.J., and Komatsu, K. (2012). Nucleolin participates in DNA double-strand break-induced damage response through MDC1-dependent pathway. PLoS One *7*, e49245.

Koike, A., Nishikawa, H., Wu, W., Okada, Y., Venkitaraman, A.R., and Ohta, T. (2010). Recruitment of

phosphorylated NPM1 to sites of DNA damage through RNF8-dependent ubiquitin conjugates. Cancer Res. *70*, 6746–6756.

Komar, A.A., Mazumder, B., and Merrick, W.C. (2012). A new framework for understanding IRES-mediated translation. Gene *502*, 75–86.

Kondo, T., Minamino, N., Nagamura-Inoue, T., Matsumoto, M., Taniguchi, T., and Tanaka, N. (1997). Identification and characterization of nucleophosmin/B23/numatrin which binds the anti-oncogenic transcription factor IRF-1 and manifests oncogenic activity. Oncogene *15*, 1275–1281.

van Koningsbruggen, S., Gierlinski, M., Schofield, P., Martin, D., Barton, G.J., Ariyurek, Y., den Dunnen, J.T., and Lamond, A.I. (2010). High-resolution whole-genome sequencing reveals that specific chromatin domains from most human chromosomes associate with nucleoli. Mol. Biol. Cell *21*, 3735–3748.

Kopp, K., Gasiorowski, J.Z., Chen, D., Gilmore, R., Norton, J.T., Wang, C., Leary, D.J., Chan, E.K., Dean, D.A., and Huang, S. (2007). Pol I transcription and pre-rRNA processing are coordinated in a transcription-dependent manner in mammalian cells. Mol. Biol. Cell *18*, 394–403.

Koutsioumpa, M., and Papadimitriou, E. (2014). Cell surface nucleolin as a target for anti-cancer therapies. Recent Pat. Anticancer. Drug Discov. *9*, 137–152.

Koutsioumpa, M., Polytarchou, C., Courty, J., Zhang, Y., Kieffer, N., Mikelis, C., Skandalis, S.S., Hellman, U., Iliopoulos, D., and Papadimitriou, E. (2013). Interplay between αvβ3 integrin and nucleolin regulates human endothelial and glioma cell migration. J. Biol. Chem. *288*, 343–354.

Kozakai, Y., Kamada, R., Furuta, J., Kiyota, Y., Chuman, Y., and Sakaguchi, K. (2016). PPM1D controls nucleolar formation by up-regulating phosphorylation of nucleophosmin. Sci Rep *6*, 33272.

Krause, A., and Hoffmann, I. (2010). Polo-like kinase 2-dependent phosphorylation of NPM/B23 on serine 4 triggers centriole duplication. PLoS One *5*, e9849.

Krimm, I., Ostlund, C., Gilquin, B., Couprie, J., Hossenlopp, P., Mornon, J.P., Bonne, G., Courvalin, J.-C., Worman, H.J., and Zinn-Justin, S. (2002). The Ig-like structure of the C-terminal domain of lamin A/C, mutated in muscular dystrophies, cardiomyopathy, and partial lipodystrophy. Structure *10*, 811–823.

Krohne, G., Waizenegger, I., and Höger, T.H. (1989). The conserved carboxy-terminal cysteine of nuclear lamins is essential for lamin association with the nuclear envelope. J. Cell Biol. *109*, 2003–2011.

Krugmann, S., Williams, R., Stephens, L., and Hawkins, P.T. (2004). ARAP3 is a PI3K- and rap-regulated GAP for RhoA. Curr. Biol. *14*, 1380–1384.

Krust, B., El Khoury, D., Nondier, I., Soundaramourty, C., and Hovanessian, A.G. (2011). Targeting surface nucleolin with multivalent HB-19 and related Nucant pseudopeptides results in distinct inhibitory mechanisms depending on the malignant tumor cell type. BMC Cancer *11*, 333.

Krystosek, A. (1998). Repositioning of human interphase chromosomes by nucleolar dynamics in the reverse transformation of HT1080 fibrosarcoma cells. Exp. Cell Res. *241*, 202–209.

Kuchenreuther, M.J., and Weber, J.D. (2014). The ARF tumor-suppressor controls Drosha translation to prevent Ras-driven transformation. Oncogene *33*, 300–307.

Kuga, T., Nie, H., Kazami, T., Satoh, M., Matsushita, K., Nomura, F., Maeshima, K., Nakayama, Y., and Tomonaga, T. (2014). Lamin B2 prevents chromosome instability by ensuring proper mitotic chromosome segregation. Oncogenesis *3*, e94.

Kuhn, A., and Grummt, I. (1992). Dual role of the nucleolar transcription factor UBF: trans-activator and antirepressor. Proc Natl Acad Sci USA *89*, 7340–7344.

Kumaran, R.I., Muralikrishna, B., and Parnaik, V.K. (2002). Lamin A/C speckles mediate spatial organization of splicing factor compartments and RNA polymerase II transcription. J. Cell Biol. *159*, 783–793.

Kurki, S., Peltonen, K., Latonen, L., Kiviharju, T.M., Ojala, P.M., Meek, D., and Laiho, M. (2004). Nucleolar protein NPM interacts with HDM2 and protects tumor suppressor protein p53 from HDM2-mediated degradation.

Cancer Cell *5*, 465–475.

Laas, R., and Hagel, C. (1994). Hirano bodies and chronic alcoholism. Neuropathology and Applied Neurobiology.

Lam, Y.W., Evans, V.C., Heesom, K.J., Lamond, A.I., and Matthews, D.A. (2010). Proteomics analysis of the nucleolus in adenovirus-infected cells. Mol Cell Proteomics *9*, 117–130.

Lambros, M.B., Natrajan, R., Geyer, F.C., Lopez-Garcia, M.A., Dedes, K.J., Savage, K., Lacroix-Triki, M., Jones, R.L., Lord, C.J., Linardopoulos, S., et al. (2010). PPM1D gene amplification and overexpression in breast cancer: a qRT-PCR and chromogenic in situ hybridization study. Mod Pathol *23*, 1334–1345.

Lange, A., Mills, R.E., Lange, C.J., Stewart, M., Devine, S.E., and Corbett, A.H. (2007). Classical nuclear localization signals: definition, function, and interaction with importin alpha. J. Biol. Chem. *282*, 5101–5105.

Lapeyre, B., Bourbon, H., and Amalric, F. (1987). Nucleolin, the major nucleolar protein of growing eukaryotic cells: an unusual protein structure revealed by the nucleotide sequence. Proc Natl Acad Sci USA *84*, 1472–1476.

Larrucea, S., González-Rubio, C., Cambronero, R., Ballou, B., Bonay, P., López-Granados, E., Bouvet, P., Fontán, G., Fresno, M., and López-Trascasa, M. (1998). Cellular adhesion mediated by factor J, a complement inhibitor. Evidence for nucleolin involvement. J. Biol. Chem. *273*, 31718–31725.

Lázaro-Diéguez, F., Aguado, C., Mato, E., Sánchez-Ruíz, Y., Esteban, I., Alberch, J., Knecht, E., and Egea, G. (2008). Dynamics of an F-actin aggresome generated by the actin-stabilizing toxin jasplakinolide. J. Cell Sci. *121*, 1415–1425.

Learned, R.M., Learned, T.K., Haltiner, M.M., and Tjian, R.T. (1986). Human rRNA transcription is modulated by the coordinate binding of two factors to an upstream control element. Cell *45*, 847–857.

Lee, J.S.H., Hale, C.M., Panorchan, P., Khatau, S.B., George, J.P., Tseng, Y., Stewart, C.L., Hodzic, D., and Wirtz, D. (2007a). Nuclear lamin A/C deficiency induces defects in cell mechanics, polarization, and migration. Biophys. J. *93*, 2542–2552.

Lee, P.T., Liao, P.C., Chang, W.C., and Tseng, J.T. (2007b). Epidermal growth factor increases the interaction between nucleolin and heterogeneous nuclear ribonucleoprotein K/poly(C) binding protein 1 complex to regulate the gastrin mRNA turnover. Mol. Biol. Cell *18*, 5004–5013.

Legrand, D., Vigié, K., Said, E.A., Elass, E., Masson, M., Slomianny, M.-C., Carpentier, M., Briand, J.-P., Mazurier, J., and Hovanessian, A.G. (2004). Surface nucleolin participates in both the binding and endocytosis of lactoferrin in target cells. Eur. J. Biochem. *271*, 303–317.

Leitinger, N., and Wesierska-Gadek, J. (1993). ADP-ribosylation of nucleolar proteins in HeLa tumor cells. J Cell Biochem *52*, 153–158.

Leporé, N., and Lafontaine, D.L. (2011). A functional interface at the rDNA connects rRNA synthesis, pre-rRNA processing and nucleolar surveillance in budding yeast. PLoS One *6*, e24962.

Leung, A.K.L., Trinkle-Mulcahy, L., Lam, Y.W., Andersen, J.S., Mann, M., and Lamond, A.I. (2006). Nopdb: nucleolar proteome database. Nucleic Acids Res. *34*, D218-20.

Li, Y.P. (1997). Protein B23 is an important human factor for the nucleolar localization of the human immunodeficiency virus protein Tat. J. Virol. *71*, 4098–4102.

Li, Z., and Hann, S.R. (2013). Nucleophosmin is essential for c-Myc nucleolar localization and c-Myc-mediated rDNA transcription. Oncogene *32*, 1988–1994.

Li, G., Margueron, R., Ku, M., Chambon, P., Bernstein, B.E., and Reinberg, D. (2010). Jarid2 and PRC2, partners in regulating gene expression. Genes Dev *24*, 368–380.

Li, Y.P., Busch, R.K., Valdez, B.C., and Busch, H. (1996). C23 interacts with B23, a putative nucleolar-localization-signal-binding protein. Eur. J. Biochem. *237*, 153–158.

Liang, H., Chen, X., Yin, Q., Ruan, D., Zhao, X., Zhang, C., McNutt, M.A., and Yin, Y. (2017). PTENβ is an alternatively translated isoform of PTEN that regulates rDNA transcription. Nat. Commun. *8*, 14771.

Liang, Y.M., Wang, X., Ramalingam, R., So, K.Y., Lam, Y.W., and Li, Z.F. (2012). Novel nucleolar isolation

method reveals rapid response of human nucleolar proteomes to serum stimulation. J. Proteomics *77*, 521–530.

Lin, F., and Staerkel, G. (2003). Cytologic criteria for well differentiated adenocarcinoma of the pancreas in fine-needle aspiration biopsy specimens. Cancer *99*, 44–50.

Lin, F., and Worman, H.J. (1993). Structural organization of the human gene encoding nuclear lamin A and nuclear lamin C. J. Biol. Chem. *268*, 16321–16326.

Lischwe, M.A., Roberts, K.D., Yeoman, L.C., and Busch, H. (1982). Nucleolar specific acidic phosphoprotein C23 is highly methylated. J. Biol. Chem. *257*, 14600–14602.

Liu, J.L., Lee, L.F., Ye, Y., Qian, Z., and Kung, H.J. (1997). Nucleolar and nuclear localization properties of a herpesvirus bZIP oncoprotein, MEQ. J. Virol. *71*, 3188–3196.

Liu, Y., Festing, M., Thompson, J.C., Hester, M., Rankin, S., El-Hodiri, H.M., Zorn, A.M., and Weinstein, M. (2004). Smad2 and Smad3 coordinately regulate craniofacial and endodermal development. Dev. Biol. *270*, 411–426.

Lixin, R., Efthymiadis, A., Henderson, B., and Jans, D.A. (2001). Novel properties of the nucleolar targeting signal of human angiogenin. Biochem. Biophys. Res. Commun. *284*, 185–193.

Lohrum, M.A., Ashcroft, M., Kubbutat, M.H., and Vousden, K.H. (2000). Identification of a cryptic nucleolar-localization signal in MDM2. Nat. Cell Biol. *2*, 179–181.

Losfeld, M.E., Khoury, D.E., Mariot, P., Carpentier, M., Krust, B., Briand, J.P., Mazurier, J., Hovanessian, A.G., and Legrand, D. (2009). The cell surface expressed nucleolin is a glycoprotein that triggers calcium entry into mammalian cells. Exp Cell Res *315*, 357–369.

Loza-Muller, L., Rodríguez-Corona, U., Sobol, M., Rodríguez-Zapata, L.C., Hozak, P., and Castano, E. (2015). Fibrillarin methylates H2A in RNA polymerase I trans-active promoters in Brassica oleracea. Front. Plant Sci. *6*, 976.

Lund, E., Oldenburg, A.R., Delbarre, E., Freberg, C.T., Duband-Goulet, I., Eskeland, R., Buendia, B., and Collas, P. (2013). Lamin A/C-promoter interactions specify chromatin state-dependent transcription outcomes. Genome Res. *23*, 1580–1589.

Ma, N., Matsunaga, S., Takata, H., Ono-Maniwa, R., Uchiyama, S., and Fukui, K. (2007). Nucleolin functions in nucleolus formation and chromosome congression. J. Cell Sci. *120*, 2091–2105.

Machiels, B.M., Zorenc, A.H., Endert, J.M., Kuijpers, H.J., van Eys, G.J., Ramaekers, F.C., and Broers, J.L. (1996). An alternative splicing product of the lamin A/C gene lacks exon 10. J. Biol. Chem. *271*, 9249–9253.

Maden, B.E., Dent, C.L., Farrell, T.E., Garde, J., McCallum, F.S., and Wakeman, J.A. (1987). Clones of human ribosomal DNA containing the complete 18 S-rRNA and 28 S-rRNA genes. Characterization, a detailed map of the human ribosomal transcription unit and diversity among clones. Biochem. J. *246*, 519–527.

Maggi, L.B., Kuchenruether, M., Dadey, D.Y., Schwope, R.M., Grisendi, S., Townsend, R.R., Pandolfi, P.P., and Weber, J.D. (2008). Nucleophosmin serves as a rate-limiting nuclear export chaperone for the Mammalian ribosome. Mol. Cell Biol. *28*, 7050–7065.

Magnuson, B., Ekim, B., and Fingar, D.C. (2012). Regulation and function of ribosomal protein S6 kinase (S6K) within mTOR signalling networks. Biochem J *441*, 1–21.

Mahajan, P.B. (1994). Modulation of transcription of rRNA genes by rapamycin. Int J Immunopharmacol *16*, 711–721.

Mahen, R., Hattori, H., Lee, M., Sharma, P., Jeyasekharan, A.D., and Venkitaraman, A.R. (2013). A-type lamins maintain the positional stability of DNA damage repair foci in mammalian nuclei. PLoS One *8*, e61893.

Mais, C., Wright, J.E., Prieto, J.-L., Raggett, S.L., and McStay, B. (2005). UBF-binding site arrays form pseudo-NORs and sequester the RNA polymerase I transcription machinery. Genes Dev. *19*, 50–64.

Mallo, M., and Alonso, C.R. (2013). The regulation of Hox gene expression during animal development. Development *140*, 3951–3963.

Maloney, M.T., Minamide, L.S., and Kinley, A.W., Boyle, J.A., Bamburg, J.R. (2005). Beta-secretase-cleaved amyloid precursor protein accumulates at actin inclusions induced in neurons by stress or amyloid beta: a feedforward mechanism for Alzheimer's disease. J. Neurosci. *25*, 11313-21.

Mamrack, M.D., Olson, M.O., and Busch, H. (1979). Amino acid sequence and sites of phosphorylation in a highly acidic region of nucleolar nonhistone protein C23. Biochemistry *18*, 3381–3386.

Marcel, V., Ghayad, S.E., Belin, S., Therizols, G., Morel, A.P., Solano-Gonzàlez, E., Vendrell, J.A., Hacot, S., Mertani, H.C., Albaret, M.A., et al. (2013). p53 acts as a safeguard of translational control by regulating fibrillarin and rRNA methylation in cancer. Cancer Cell *24*, 318–330.

Marcil, A., Dumontier, E., Chamberland, M., Camper, S.A., and Drouin, J. (2003). Pitx1 and Pitx2 are required for development of hindlimb buds. Development *130*, 45–55.

Marilley, M., and Pasero, P. (1996). Common DNA structural features exhibited by eukaryotic ribosomal gene promoters. Nucleic Acids Res. *24*, 2204–2211.

Marion, R.M., Regev, A., Segal, E., Barash, Y., Koller, D., Friedman, N., and O'Shea, E.K. (2004). Sfp1 is a stress- and nutrient-sensitive regulator of ribosomal protein gene expression. Proc Natl Acad Sci USA *101*, 14315–14322.

Martin, C., Chen, S., Maya-Mendoza, A., Lovric, J., Sims, P.F.G., and Jackson, D.A. (2009). Lamin B1 maintains the functional plasticity of nucleoli. J. Cell Sci. *122*, 1551–1562.

Martin, D.E., Soulard, A., and Hall, M.N. (2004). TOR regulates ribosomal protein gene expression via PKA and the Forkhead transcription factor FHL1. Cell *119*, 969–979.

Mason, S.W., Sander, E.E., and Grummt, I. (1997). Identification of a transcript release activity acting on ternary transcription complexes containing murine RNA polymerase I. EMBO J. *16*, 163–172.

Matsumoto, A., Sakamoto, C., Matsumori, H., Katahira, J., Yasuda, Y., Yoshidome, K., Tsujimoto, M., Goldberg, I.G., Matsuura, N., Nakao, M., et al. (2016). Loss of the integral nuclear envelope protein SUN1 induces alteration of nucleoli. Nucleus *7*, 68–83.

Mattia, E., Hoff, W.D., den Blaauwen, J., Meijne, A.M., Stuurman, N., and van Renswoude, J. (1992). Induction of nuclear lamins A/C during in vitro-induced differentiation of F9 and P19 embryonal carcinoma cells. Exp. Cell Res. *203*, 449–455.

Mayer, C., and Grummt, I. (2006). Ribosome biogenesis and cell growth: mTOR coordinates transcription by all three classes of nuclear RNA polymerases. Oncogene *25*, 6384–6391.

Mayer, C., Zhao, J., Yuan, X., and Grummt, I. (2004). mTOR-dependent activation of the transcription factor TIF-IA links rRNA synthesis to nutrient availability. Genes Dev *18*, 423–434.

McClintock, B. (1934). The relation of a particular chromosomal element to the development of the nucleoli in Zea mays. Z. Zellforsch. *21*, 294–326.

Meeks-Wagner, D., and Hartwell, L.H. (1986). Normal stoichiometry of histone dimer sets is necessary for high fidelity of mitotic chromosome transmission. Cell *44*, 43–52.

Mei, Q., Huang, J., Chen, W., Tang, J., Xu, C., Yu, Q., Cheng, Y., Ma, L., Yu, X., and Li, S. (2017). Regulation of DNA replication-coupled histone gene expression. Oncotarget *8*, 95005–95022.

Mekhail, K., Khacho, M., Carrigan, A., Hache, R.R.J., Gunaratnam, L., and Lee, S. (2005). Regulation of ubiquitin ligase dynamics by the nucleolus. J. Cell Biol. *170*, 733–744.

Mekhail, K., Rivero-Lopez, L., Khacho, M., and Lee, S. (2006). Restriction of rRNA synthesis by VHL maintains energy equilibrium under hypoxia. Cell Cycle *5*, 2401–2413.

Melcer, S., Hezroni, H., Rand, E., Nissim-Rafinia, M., Skoultchi, A., Stewart, C.L., Bustin, M., and Meshorer, E. (2012). Histone modifications and lamin A regulate chromatin protein dynamics in early embryonic stem cell differentiation. Nat Commun *3*, 910.

Melén, K., Tynell, J., Fagerlund, R., Roussel, P., Hernandez-Verdun, D., and Julkunen, I. (2012). Influenza A

H3N2 subtype virus NS1 protein targets into the nucleus and binds primarily via its C-terminal NLS2/NoLS to nucleolin and fibrillarin. Virol J. *9*, 167.

Mélèse, T., and Xue, Z. (1995). The nucleolus: an organelle formed by the act of building a ribosome. Curr. Opin. Cell Biol. *7*, 319–324.

Mendes-da-Silva, P., Moreira, A., Duro-da-Costa, J., Matias, D., and Monteiro, C. (2000). Frequent loss of heterozygosity on chromosome 5 in non-small cell lung carcinoma. MP, Mol Pathol *53*, 184–187.

Meshorer, E., Yellajoshula, D., George, E., Scambler, P.J., Brown, D.T., and Misteli, T. (2006). Hyperdynamic plasticity of chromatin proteins in pluripotent embryonic stem cells. Dev. Cell *10*, 105–116.

Miki, Y., Oguri, E., Hirano, K., and Beppu, M. (2013). Macrophage recognition of cells with elevated calcium is mediated by carbohydrate chains of CD43. Cell Struct Funct *38*, 43–54.

Miller, O.L., and Beatty, B.R. (1969). Visualization of nucleolar genes. Science *164*, 955–957.

Miller, G., Panov, K.I., Friedrich, J.K., Trinkle-Mulcahy, L., Lamond, A.I., and Zomerdijk, J.C. (2001). hRRN3 is essential in the SL1-mediated recruitment of RNA Polymerase I to rRNA gene promoters. EMBO J. *20*, 1373–1382.

Miller, O.J., Miller, D.A., Dev, V.G., Tantravahi, R., and Croce, C.M. (1976). Expression of human and suppression of mouse nucleolus organizer activity in mouse-human somatic cell hybrids. Proc Natl Acad Sci USA *73*, 4531–4535.

Miniard, A.C., Middleton, L.M., Budiman, M.E., Gerber, C.A., and Driscoll, D.M. (2010). Nucleolin binds to a subset of selenoprotein mRNAs and regulates their expression. Nucleic Acids Res. *38*, 4807–4820.

Misra, R.M., Bajaj, M.S., and Kale, V.P. (2012). Vasculogenic mimicry of HT1080 tumour cells in vivo: critical role of HIF-1α-neuropilin-1 axis. PLoS One *7*, e50153.

Mitchell, P., Petfalski, E., and Tollervey, D. (1996). The 3' end of yeast 5.8S rRNA is generated by an exonuclease processing mechanism. Genes Dev *10*, 502–513.

Mitrea, D.M., Grace, C.R., Buljan, M., Yun, M.K., Pytel, N.J., Satumba, J., Nourse, A., Park, C.G., Madan Babu, M., White, S.W., et al. (2014). Structural polymorphism in the N-terminal oligomerization domain of NPM1. Proc Natl Acad Sci USA *111*, 4466–4471.

Mitrea, D.M., Cika, J.A., Guy, C.S., Ban, D., Banerjee, P.R., Stanley, C.B., Nourse, A., Deniz, A.A., and Kriwacki, R.W. (2016). Nucleophosmin integrates within the nucleolus via multi-modal interactions with proteins displaying R-rich linear motifs and rRNA. Elife *5*.

Moir, R.D., Spann, T.P., Herrmann, H., and Goldman, R.D. (2000). Disruption of nuclear lamin organization blocks the elongation phase of DNA replication. J. Cell Biol. *149*, 1179–1192.

Mongelard, F., and Bouvet, P. (2007). Nucleolin: a multiFACeTed protein. Trends Cell Biol. *17*, 80–86.

Montes de Oca, R., Lee, K.K., and Wilson, K.L. (2005). Binding of barrier to autointegration factor (BAF) to histone H3 and selected linker histones including H1.1. J. Biol. Chem. *280*, 42252–42262.

Morillo-Huesca, M., Maya, D., Muñoz-Centeno, M.C., Singh, R.K., Oreal, V., Reddy, G.U., Liang, D., Géli, V., Gunjan, A., and Chávez, S. (2010). FACT prevents the accumulation of free histones evicted from transcribed chromatin and a subsequent cell cycle delay in G1. PLoS Genet. *6*, e1000964.

Morris, S.W., Kirstein, M.N., Valentine, M.B., Dittmer, K.G., Shapiro, D.N., Saltman, D.L., and Look, A.T. (1994). Fusion of a kinase gene, ALK, to a nucleolar protein gene, NPM, in non-Hodgkin's lymphoma. Science *263*, 1281–1284.

Moss, T., and Stefanovsky, V.Y. (2002). At the center of eukaryotic life. Cell *109*, 545–548.

Munro, S., and Pelham, H.R. (1987). A C-terminal signal prevents secretion of luminal ER proteins. Cell *48*, 899–907.

Murano, K., Okuwaki, M., Hisaoka, M., and Nagata, K. (2008). Transcription regulation of the rRNA gene by a multifunctional nucleolar protein, B23/nucleophosmin, through its histone chaperone activity. Mol. Cell Biol. *28*,

3114–3126.

Musinova, Y.R., Lisitsyna, O.M., Golyshev, S.A., Tuzhikov, A.I., Polyakov, V.Y., and Sheval, E.V. (2011). Nucleolar localization/retention signal is responsible for transient accumulation of histone H2B in the nucleolus through electrostatic interactions. Biochim. Biophys. Acta *1813*, 27–38.

Musinova, Y.R., Lisitsyna, O.M., Sorokin, D.V., Arifulin, E.A., Smirnova, T.A., Zinovkin, R.A., Potashnikova, D.M., Vassetzky, Y.S., and Sheval, E.V. (2016). RNA-dependent disassembly of nuclear bodies. J. Cell Sci. *129*, 4509–4520.

Nagahama, M., Hara, Y., Seki, A., Yamazoe, T., Kawate, Y., Shinohara, T., Hatsuzawa, K., Tani, K., and Tagaya, M. (2004). NVL2 is a nucleolar AAA-ATPase that interacts with ribosomal protein L5 through its nucleolar localization sequence. Mol. Biol. Cell *15*, 5712–5723.

Namboodiri, V.M., Akey, I.V., Schmidt-Zachmann, M.S., Head, J.F., and Akey, C.W. (2004). The structure and function of Xenopus NO38-core, a histone chaperone in the nucleolus. Structure *12*, 2149–2160.

Negi, S.S., and Olson, M.O.J. (2006). Effects of interphase and mitotic phosphorylation on the mobility and location of nucleolar protein B23. J. Cell Sci. *119*, 3676–3685.

Németh, A., Guibert, S., Tiwari, V.K., Ohlsson, R., and Längst, G. (2008). Epigenetic regulation of TTF-I-mediated promoter-terminator interactions of rRNA genes. EMBO J. *27*, 1255–1265.

Németh, A., Conesa, A., Santoyo-Lopez, J., Medina, I., Montaner, D., Péterfia, B., Solovei, I., Cremer, T., Dopazo, J., and Längst, G. (2010). Initial genomics of the human nucleolus. PLoS Genet. *6*, e1000889.

Neo, S.H., Itahana, Y., Alagu, J., Kitagawa, M., Guo, A.K., Lee, S.H., Tang, K., and Itahana, K. (2015). TRIM28 Is an E3 Ligase for ARF-Mediated NPM1/B23 SUMOylation That Represses Centrosome Amplification. Mol. Cell Biol. *35*, 2851–2863.

Neuburger, M., Herget, G.W., Plaumann, L., Falk, A., Schwalb, H., and Adler, C.P. (1998). Change in size, number and morphology of the nucleoli in human hearts as a result of hyperfunction. Pathol Res Pract *194*, 385–389.

Newton, K., Petfalski, E., Tollervey, D., and Cáceres, J.F. (2003). Fibrillarin is essential for early development and required for accumulation of an intron-encoded small nucleolar RNA in the mouse. Mol. Cell. Biol. *23*, 8519–8527.

Nguyen, L.X., and Mitchell, B.S. (2013). Akt activation enhances ribosomal RNA synthesis through casein kinase II and TIF-IA. Proc Natl Acad Sci USA.

Nguyen, L.X.T., Raval, A., Garcia, J.S., and Mitchell, B.S. (2015). Regulation of ribosomal gene expression in cancer. J. Cell Physiol. *230*, 1181–1188.

Nicolas, E., Parisot, P., Pinto-Monteiro, C., de Walque, R., De Vleeschouwer, C., and Lafontaine, D.L.J. (2016). Involvement of human ribosomal proteins in nucleolar structure and p53-dependent nucleolar stress. Nat Commun *7*, 11390.

Nishimura, Y., Ohkubo, T., Furuichi, Y., and Umekawa, H. (2002). Tryptophans 286 and 288 in the C-terminal region of protein B23.1 are important for its nucleolar localization. Biosci Biotechnol Biochem *66*, 2239–2242.

Nozawa, Y., Van Belzen, N., Van der Made, A.C., Dinjens, W.N., and Bosman, F.T. (1996). Expression of nucleophosmin/B23 in normal and neoplastic colorectal mucosa. J Pathol *178*, 48–52.

Ochs, R.L., Lischwe, M.A., Spohn, W.H., and Busch, H. (1985). Fibrillarin: a new protein of the nucleolus identified by autoimmune sera. Biol Cell *54*, 123–133.

Ohshima, S. (2008). Abnormal mitosis in hypertetraploid cells causes aberrant nuclear morphology in association with H2O2-induced premature senescence. Cytometry A *73*, 808–815.

Okuda, M., Horn, H.F., Tarapore, P., Tokuyama, Y., Smulian, A.G., Chan, P.K., Knudsen, E.S., Hofmann, I.A., Snyder, J.D., Bove, K.E., et al. (2000). Nucleophosmin/B23 is a target of CDK2/cyclin E in centrosome duplication. Cell *103*, 127–140.

Okuwaki, M., Matsumoto, K., Tsujimoto, M., and Nagata, K. (2001a). Function of nucleophosmin/B23, a nucleolar acidic protein, as a histone chaperone. FEBS Lett *506*, 272–276.

Okuwaki, M., Iwamatsu, A., Tsujimoto, M., and Nagata, K. (2001b). Identification of nucleophosmin/B23, an acidic nucleolar protein, as a stimulatory factor for in vitro replication of adenovirus DNA complexed with viral basic core proteins. J Mol Biol *311*, 41–55.

Okuwaki, M., Tsujimoto, M., and Nagata, K. (2002). The RNA binding activity of a ribosome biogenesis factor, nucleophosmin/B23, is modulated by phosphorylation with a cell cycle-dependent kinase and by association with its subtype. Mol. Biol. Cell *13*, 2016–2030.

Olney, H.J., and Le Beau, M.M. (2002). The Myelodysplastic Syndromes: Pathobiology And Clinical Management (New York: Marcel Dekker).

Olson, M.O., Ezrailson, E.G., Guetzow, K., and Busch, H. (1975). Localization and phosphorylation of nuclear, nucleolar and extranucleolar non-histone proteins of Novikoff hepatoma ascites cells. J Mol Biol *97*, 611–619.

Orrick, L.R., Olson, M.O., and Busch, H. (1973). Comparison of nucleolar proteins of normal rat liver and Novikoff hepatoma ascites cells by two-dimensional polyacrylamide gel electrophoresis. Proc Natl Acad Sci USA *70*, 1316–1320.

Osmanagic-Myers, S., Dechat, T., and Foisner, R. (2015). Lamins at the crossroads of mechanosignaling. Genes Dev. *29*, 225–237.

di Padua Mathieu, D., Mura, C.V., Frado, L.L., Woodcock, C.L., and Stollar, B.D. (1981). Differing accessibility in chromatin of the antigenic sites of regions 1-58 and 63-125 of histone H2B. J. Cell Biol. *91*, 135–141.

Pajerowski, J.D., Dahl, K.N., Zhong, F.L., Sammak, P.J., and Discher, D.E. (2007). Physical plasticity of the nucleus in stem cell differentiation. Proc. Natl. Acad. Sci. USA *104*, 15619–15624.

Pandey, P., Dixit, A., Chandra, S., and Kaur, S. (2014). A comparative and evaluative study of two cytological grading systems in breast carcinoma with histological grading: an important prognostic factor. Anal. Cell. Pathol. (Amst). *2014*, 767215.

Panov, K.I., Friedrich, J.K., and Zomerdijk, J.C. (2001). A step subsequent to preinitiation complex assembly at the ribosomal RNA gene promoter is rate limiting for human RNA polymerase I-dependent transcription. Mol. Cell Biol. *21*, 2641–2649.

Panov, K.I., Friedrich, J.K., Russell, J., and Zomerdijk, J.C. (2006). UBF activates RNA polymerase I transcription by stimulating promoter escape. EMBO J. *25*, 3310–3322.

Parry, D.A., Conway, J.F., and Steinert, P.M. (1986). Structural studies on lamin. Similarities and differences between lamin and intermediate-filament proteins. Biochem. J. *238*, 305–308.

Peng, J.C., and Karpen, G.H. (2007). H3K9 methylation and RNA interference regulate nucleolar organization and repeated DNA stability. Nat. Cell Biol. *9*, 25–35.

Percipalle, P., Fomproix, N., Cavellán, E., Voit, R., Reimer, G., Krüger, T., Thyberg, J., Scheer, U., Grummt, I., and Farrants, A.K. (2006). The chromatin remodelling complex WSTF-SNF2h interacts with nuclear myosin 1 and has a role in RNA polymerase I transcription. EMBO Rep *7*, 525–530.

Peter, M., Nakagawa, J., Dorée, M., Labbé, J.C., and Nigg, E.A. (1990). Identification of major nucleolar proteins as candidate mitotic substrates of cdc2 kinase. Cell *60*, 791–801.

Pianese, G. (1896). Beitrag zur Histologie und Aetiologie der Carcinoma. Histologische und experimentelle Untersuchungen. Beitr. Pathol. Anat. *142*, 1–193.

Pietrzak, M., Rempala, G., Nelson, P.T., Zheng, J.J., and Hetman, M. (2011). Epigenetic silencing of nucleolar rRNA genes in Alzheimer's disease. PLoS One *6*, e22585.

Pih, K.T., Yi, M.J., Liang, Y.S., Shin, B.J., Cho, M.J., Hwang, I., and Son, D. (2000). Molecular cloning and targeting of a fibrillarin homolog from Arabidopsis. Plant Physiol *123*, 51–58.

Ploton, D., Menager, M., Jeannesson, P., Himber, G., Pigeon, F., and Adnet, J.J. (1986). Improvement in the staining and in the visualization of the argyrophilic proteins of the nucleolar organizer region at the optical level. The Histochemical Journal *18(1)*, 5-14.

Podlubnaia, Z.A., and Nowak, E. (2006). The C-terminal fragment of thymopoietin forms F-actin bundles: electron microscopic data]. Biofizika *51*, 804–809.

Poletto, M., Lirussi, L., Wilson, D.M., and Tell, G. (2014). Nucleophosmin modulates stability, activity, and nucleolar accumulation of base excision repair proteins. Mol. Biol. Cell *25*, 1641–1652.

Powers, T., and Walter, P. (1999). Regulation of ribosome biogenesis by the rapamycin-sensitive TOR-signaling pathway in Saccharomyces cerevisiae. Mol. Biol. Cell *10*, 987–1000.

Prestayko, A.W., Klomp, G.R., Schmoll, D.J., and Busch, H. (1974). Comparison of proteins of ribosomal subunits and nucleolar preribosomal particles from Novikoff hepatoma ascites cells by two-dimensional polyacrylamide gel electrophoresis. Biochemistry *13*, 1945–1951.

Prokocimer, M., Davidovich, M., Nissim-Rafinia, M., Wiesel-Motiuk, N., Bar, D.Z., Barkan, R., Meshorer, E., and Gruenbaum, Y. (2009). Nuclear lamins: key regulators of nuclear structure and activities. J. Cell Mol. Med. *13*, 1059–1085.

Raman, B. (2001). Nomega-arginine dimethylation modulates the interaction between a Gly/Arg-rich peptide from human nucleolin and nucleic acids. Nucleic Acids Res. *29*, 3377–3384.

Ramos, F.J., Chen, S.C., Garelick, M.G., Dai, D.-F., Liao, C.-Y., Schreiber, K.H., MacKay, V.L., An, E.H., Strong, R., Ladiges, W.C., et al. (2012). Rapamycin reverses elevated mTORC1 signaling in lamin A/C-deficient mice, rescues cardiac and skeletal muscle function, and extends survival. Sci Transl Med *4*, 144ra103.

Ranade, D., Koul, S., Thompson, J., Prasad, K.B., and Sengupta, K. (2017). Chromosomal aneuploidies induced upon Lamin B2 depletion are mislocalized in the interphase nucleus. Chromosoma *126*, 223–244.

Rao, S.V., Mamrack, M.D., and Olson, M.O. (1982). Localization of phosphorylated highly acidic regions in the NH2-terminal half of nucleolar protein C23. J. Biol. Chem. *257*, 15035–15041.

Rapsomaniki, M.A., Kotsantis, P., Symeonidou, I.-E., Giakoumakis, N.-N., Taraviras, S., and Lygerou, Z. (2012). easyFRAP: an interactive, easy-to-use tool for qualitative and quantitative analysis of FRAP data. Bioinformatics *28*, 1800–1801.

Raska, I., Rychter, Z., and Smetana, K. (1983). Fibrillar centres and condensed nucleolar chromatin in resting and stimulated human lymphocytes. Z. Mikrosk. Anat. Forsch. *97*, 15–32.

Raska, I., Dundr, M., Koberna, K., Melcák, I., Risueño, M.C., and Török, I. (1995). Does the synthesis of ribosomal RNA take place within nucleolar fibrillar centers or dense fibrillar components? A critical appraisal. J. Struct. Biol. *114*, 1–22.

Rasmussen, L., de Labio, R.W., Viani, G.A., Chen, E., Villares, J., Bertolucci, P.H., Minett, T.S., Turecki, G., Cecyre, D., Drigo, S.A., et al. (2015). Differential expression of ribosomal genes in brain and blood of alzheimer's disease patients. Curr Alzheimer Res *12*, 984–989.

Raval, A., Sridhar, K.J., Patel, S., Turnbull, B.B., Greenberg, P.L., and Mitchell, B.S. (2012). Reduced rRNA expression and increased rDNA promoter methylation in CD34+ cells of patients with myelodysplastic syndromes. Blood *120*, 4812–4818.

Razin, A., and Cedar, H. (1991). DNA methylation and gene expression. Microbiol Rev *55*, 451–458.

Redner, R.L., Rush, E.A., Faas, S., Rudert, W.A., and Corey, S.J. (1996). The t(5;17) variant of acute promyelocytic leukemia expresses a nucleophosmin-retinoic acid receptor fusion. Blood *87*, 882–886.

Reed, B.D., Charos, A.E., Szekely, A.M., Weissman, S.M., and Snyder, M. (2008). Genome-wide occupancy of SREBP1 and its partners NFY and SP1 reveals novel functional roles and combinatorial regulation of distinct classes of genes. PLoS Genet. *4*, e1000133.

Reeder, R.H., Guevara, P., and Roan, J.G. (1999). Saccharomyces cerevisiae RNA polymerase I terminates

transcription at the Reb1 terminator in vivo. Mol. Cell Biol. *19*, 7369–7376.

Reyes-Reyes, E.M., and Akiyama, S.K. (2008). Cell-surface nucleolin is a signal transducing P-selectin binding protein for human colon carcinoma cells. Exp Cell Res *314*, 2212–2223.

Richter AM, T.S., and Dammann RH, L.B. (2015). Aberrant DNA methylation of ribosomal RNA genes in human cancer. Mol. Biol. (NY) *04*.

Rickards, B., Flint, S.J., Cole, M.D., and LeRoy, G. (2007). Nucleolin is required for RNA polymerase I transcription in vivo. Mol. Cell Biol. *27*, 937–948.

Riemer, D., Dodemont, H., and Weber, K. (1993). A nuclear lamin of the nematode Caenorhabditis elegans with unusual structural features; cDNA cloning and gene organization. Eur. J. Cell Biol. *62*, 214–223.

Robbins, E., and Borun, T.W. (1967). The cytoplasmic synthesis of histones in hela cells and its temporal relationship to DNA replication. Proc. Natl. Acad. Sci. USA *57*, 409–416.

Röber, R.A., Weber, K., and Osborn, M. (1989). Differential timing of nuclear lamin A/C expression in the various organs of the mouse embryo and the young animal: a developmental study. Development *105*, 365–378.

Romanova, L., Grand, A., Zhang, L., Rayner, S., Katoku-Kikyo, N., Kellner, S., and Kikyo, N. (2009a). Critical role of nucleostemin in pre-rRNA processing. J. Biol. Chem. *284*, 4968–4977.

Romanova, L., Kellner, S., Katoku-Kikyo, N., and Kikyo, N. (2009b). Novel role of nucleostemin in the maintenance of nucleolar architecture and integrity of small nucleolar ribonucleoproteins and the telomerase complex. J. Biol. Chem. *284*, 26685–26694.

Roney, K.E., O'Connor, B.P., Wen, H., Holl, E.K., Guthrie, E.H., Davis, B.K., Jones, S.W., Jha, S., Sharek, L., Garcia-Mata, R., et al. (2011). Plexin-B2 negatively regulates macrophage motility, Rac, and Cdc42 activation. PLoS One *6*, e24795.

Roux, K.J., and Burke, B. (2007). Nuclear envelope defects in muscular dystrophy. Biochim. Biophys. Acta *1772*, 118–127.

Rowat, A.C., Jaalouk, D.E., Zwerger, M., Ung, W.L., Eydelnant, I.A., Olins, D.E., Olins, A.L., Herrmann, H., Weitz, D.A., and Lammerding, J. (2013). Nuclear envelope composition determines the ability of neutrophil-type cells to passage through micron-scale constrictions. J. Biol. Chem. *288*, 8610–8618.

Rowland, R.R., Kervin, R., Kuckleburg, C., Sperlich, A., and Benfield, D.A. (1999). The localization of porcine reproductive and respiratory syndrome virus nucleocapsid protein to the nucleolus of infected cells and identification of a potential nucleolar localization signal sequence. Virus Res. *64*, 1–12.

Rowland, R.R.R., Schneider, P., Fang, Y., Wootton, S., Yoo, D., and Benfield, D.A. (2003). Peptide domains involved in the localization of the porcine reproductive and respiratory syndrome virus nucleocapsid protein to the nucleolus. Virology *316*, 135–145.

Rubbi, C.P., and Milner, J. (2003). Disruption of the nucleolus mediates stabilization of p53 in response to DNA damage and other stresses. EMBO J. *22*, 6068–6077.

Ruggero, D., Grisendi, S., Piazza, F., Rego, E., Mari, F., Rao, P.H., Cordon-Cardo, C., and Pandolfi, P.P. (2003). Dyskeratosis congenita and cancer in mice deficient in ribosomal RNA modification. Science *299*, 259–262.

Russell, J., and Zomerdijk, J.C.B.M. (2005). RNA-polymerase-I-directed rDNA transcription, life and works. Trends Biochem. Sci. *30*, 87–96.

Said, E.A., Courty, J., Svab, J., Delbé, J., Krust, B., and Hovanessian, A.G. (2005). Pleiotrophin inhibits HIV infection by binding the cell surface-expressed nucleolin. FEBS J. *272*, 4646–4659.

Sakaki, M., Koike, H., Takahashi, N., Sasagawa, N., Tomioka, S., Arahata, K., and Ishiura, S. (2001). Interaction between emerin and nuclear lamins. J. Biochem. *129*, 321–327.

Salifou, K., Ray, S., Verrier, L., Aguirrebengoa, M., Trouche, D., Panov, K.I., and Vandromme, M. (2016). The histone demethylase JMJD2A/KDM4A links ribosomal RNA transcription to nutrients and growth factors availability. Nat. Commun. *7*, 10174.

Santoro, R., and Grummt, I. (2005). Epigenetic mechanism of rRNA gene silencing: temporal order of NoRC-mediated histone modification, chromatin remodeling, and DNA methylation. Mol. Cell. Biol. *25*, 2539–2546.

Santoro, R., Li, J., and Grummt, I. (2002). The nucleolar remodeling complex NoRC mediates heterochromatin formation and silencing of ribosomal gene transcription. Nat. Genet. *32*, 393–396.

Santoro, R., Schmitz, K.M., Sandoval, J., and Grummt, I. (2010). Intergenic transcripts originating from a subclass of ribosomal DNA repeats silence ribosomal RNA genes in trans. EMBO Rep. *11*, 52–58.

Sato, A., Hiramoto, A., Satake, A., Miyazaki, E., Naito, T., Wataya, Y., and Kim, H.S. (2008). Association of nuclear membrane protein lamin B1 with necrosis and apoptosis in cell death induced by 5-fluoro-2'-deoxyuridine. Nucleosides Nucleotides Nucleic Acids *27*, 433–438.

Savino, T.M., Gébrane-Younès, J., De Mey, J., Sibarita, J.B., and Hernandez-Verdun, D. (2001). Nucleolar assembly of the rRNA processing machinery in living cells. J. Cell Biol. *153*, 1097–1110.

Savkur, R.S., and Olson, M.O. (1998). Preferential cleavage in pre-ribosomal RNA byprotein B23 endoribonuclease. Nucleic Acids Res. *26*, 4508–4515.

Schedle, A., Willheim, M., Zeitelberger, A., Gessl, A., Frauendorfer, K., Schöfer, C., Wachtler, F., Schwarzacher, H.G., and Boltz-Nitulescu, G. (1992). Nucleolar morphology and rDNA in situ hybridisation in monocytes. Cell Tissue Res. *269*, 473–480.

Scherl, A., Couté, Y., Déon, C., Callé, A., Kindbeiter, K., Sanchez, J.-C., Greco, A., Hochstrasser, D., and Diaz, J.J. (2002). Functional proteomic analysis of human nucleolus. Mol. Biol. Cell *13*, 4100–4109.

Schlosser, I., Hölzel, M., Mürnseer, M., Burtscher, H., Weidle, U.H., and Eick, D. (2003). A role for c-Myc in the regulation of ribosomal RNA processing. Nucleic Acids Res. *31*, 6148–6156.

Schmidt-Zachmann, M.S., and Franke, W.W. (1988). DNA cloning and amino acid sequence determination of a major constituent protein of mammalian nucleoli. Correspondence of the nucleoplasmin-related protein NO38 to mammalian protein B23. Chromosoma *96*, 417–426.

Schmidt-Zachmann, M.S., and Nigg, E.A. (1993). Protein localization to the nucleolus: a search for targeting domains in nucleolin. J. Cell Sci. *105 (Pt 3)*, 799–806.

Schmidt-Zachmann, M.S., Hügle-Dörr, B., and Franke, W.W. (1987). A constitutive nucleolar protein identified as a member of the nucleoplasmin family. EMBO J. *6*, 1881–1890.

Schmitz, K.-M., Mayer, C., Postepska, A., and Grummt, I. (2010). Interaction of noncoding RNA with the rDNA promoter mediates recruitment of DNMT3b and silencing of rRNA genes. Genes Dev. *24*, 2264–2269.

Schneider, D.A., French, S.L., Osheim, Y.N., Bailey, A.O., Vu, L., Dodd, J., Yates, J.R., Beyer, A.L., and Nomura, M. (2006). RNA polymerase II elongation factors Spt4p and Spt5p play roles in transcription elongation by RNA polymerase I and rRNA processing. Proc Natl Acad Sci USA *103*, 12707–12712.

Schneider, D.A., Michel, A., Sikes, M.L., Vu, L., Dodd, J.A., Salgia, S., Osheim, Y.N., Beyer, A.L., and Nomura, M. (2007). Transcription elongation by RNA polymerase I is linked to efficient rRNA processing and ribosome assembly. Mol. Cell *26*, 217–229.

Schwab, M.S., and Dreyer, C. (1997). Protein phosphorylation sites regulate the function of the bipartite NLS of nucleolin. Eur J Cell Biol *73*, 287–297.

Scott, D.D., and Oeffinger, M. (2016). Nucleolin and nucleophosmin: nucleolar proteins with multiple functions in DNA repair. Biochem Cell Biol *94*, 419–432.

Scott, M.S., Boisvert, F.M., McDowall, M.D., Lamond, A.I., and Barton, G.J. (2010). Characterization and prediction of protein nucleolar localization sequences. Nucleic Acids Res. *38*, 7388–7399.

Scott, M.S., Troshin, P.V., and Barton, G.J. (2011). NoD: a Nucleolar localization sequence detector for eukaryotic and viral proteins. BMC Bioinformatics *12*, 317.

Semenkovich, C.F., Ostlund, R.E., Olson, M.O., and Yang, J.W. (1990). A protein partially expressed on the surface of HepG2 cells that binds lipoproteins specifically is nucleolin. Biochemistry *29*, 9708–9713.

Sen Gupta, A., and Sengupta, K. (2017). Lamin B2 modulates nucleolar morphology, dynamics, and function. Mol. Cell. Biol. *37*.

Sengupta, J., Bussiere, C., Pallesen, J., West, M., Johnson, A.W., and Frank, J. (2010). Characterization of the nuclear export adaptor protein Nmd3 in association with the 60S ribosomal subunit. J. Cell Biol. *189*, 1079–1086.

Sengupta, T.K., Bandyopadhyay, S., Fernandes, D.J., and Spicer, E.K. (2004). Identification of nucleolin as an AU-rich element binding protein involved in bcl-2 mRNA stabilization. J. Biol. Chem. *279*, 10855–10863.

Seo, Y.-K., Chong, H.K., Infante, A.M., Im, S.-S., Xie, X., and Osborne, T.F. (2009). Genome-wide analysis of SREBP-1 binding in mouse liver chromatin reveals a preference for promoter proximal binding to a new motif. Proc. Natl. Acad. Sci. USA *106*, 13765–13769.

Serin, G., Joseph, G., Faucher, C., Ghisolfi, L., Bouche, G., Amalric, F., and Bouvet, P. (1996). Localization of nucleolin binding sites on human and mouse pre-ribosomal RNA. Biochimie *78*, 530–538.

Serin, G., Joseph, G., Ghisolfi, L., Bauzan, M., Erard, M., Amalric, F., and Bouvet, P. (1997). Two RNA-binding domains determine the RNA-binding specificity of nucleolin. J. Biol. Chem. *272*, 13109–13116.

Shandilya, J., Swaminathan, V., Gadad, S.S., Choudhari, R., Kodaganur, G.S., and Kundu, T.K. (2009). Acetylated NPM1 localizes in the nucleoplasm and regulates transcriptional activation of genes implicated in oral cancer manifestation. Mol. Cell Biol. *29*, 5115–5127.

Shandilya, J., Senapati, P., Dhanasekaran, K., Bangalore, S.S., Kumar, M., Kishore, A.H., Bhat, A., Kodaganur, G.S., and Kundu, T.K. (2014). Phosphorylation of multifunctional nucleolar protein nucleophosmin (NPM1) by aurora kinase B is critical for mitotic progression. FEBS Lett *588*, 2198–2205.

Shang, Y., Kakinuma, S., Nishimura, M., Kobayashi, Y., Nagata, K., and Shimada, Y. (2012). Interleukin-9 receptor gene is transcriptionally regulated by nucleolin in T-cell lymphoma cells. Mol Carcinog *51*, 619–627.

Shav-Tal, Y., Blechman, J., Darzacq, X., Montagna, C., Dye, B.T., Patton, J.G., Singer, R.H., and Zipori, D. (2005). Dynamic sorting of nuclear components into distinct nucleolar caps during transcriptional inhibition. Mol. Biol. Cell *16*, 2395–2413.

Sheng, Z., Lewis, J.A., and Chirico, W.J. (2004). Nuclear and nucleolar localization of 18-kDa fibroblast growth factor-2 is controlled by C-terminal signals. J. Biol. Chem. *279*, 40153–40160.

Sheng, Z., Liang, Y., Lin, C.Y., Comai, L., and Chirico, W.J. (2005). Direct regulation of rRNA transcription by fibroblast growth factor 2. Mol. Cell Biol. *25*, 9419–9426.

Shevelyov, Y.Y., Lavrov, S.A., Mikhaylova, L.M., Nurminsky, I.D., Kulathinal, R.J., Egorova, K.S., Rozovsky, Y.M., and Nurminsky, D.I. (2009). The B-type lamin is required for somatic repression of testis-specific gene clusters. Proc. Natl. Acad. Sci. USA *106*, 3282–3287.

Shi, H., Huang, Y., Zhou, H., Song, X., Yuan, S., Fu, Y., and Luo, Y. (2007). Nucleolin is a receptor that mediates antiangiogenic and antitumor activity of endostatin. Blood *110*, 2899–2906.

Shi, Y., Sharma, A., Wu, H., Lichtenstein, A., and Gera, J. (2005). Cyclin D1 and c-myc internal ribosome entry site (IRES)-dependent translation is regulated by AKT activity and enhanced by rapamycin through a p38 MAPK- and ERK-dependent pathway. J. Biol. Chem. *280*, 10964–10973.

Shi, Z., Fujii, K., Kovary, K.M., Genuth, N.R., Röst, H.L., Teruel, M.N., and Barna, M. (2017). Heterogeneous Ribosomes Preferentially Translate Distinct Subpools of mRNAs Genome-wide. Mol. Cell *67*, 71–83.e7.

Shields, L.B., Gerçel-Taylor, C., Yashar, C.M., Wan, T.C., Katsanis, W.A., Spinnato, J.A., and Taylor, D.D. (1997). Induction of immune responses to ovarian tumor antigens by multiparity. J Soc Gynecol Investig *4*, 298–304.

Shimi, T., Pfleghaar, K., Kojima, S., Pack, C.-G., Solovei, I., Goldman, A.E., Adam, S.A., Shumaker, D.K., Kinjo, M., Cremer, T., et al. (2008). The A- and B-type nuclear lamin networks: microdomains involved in chromatin organization and transcription. Genes Dev. *22*, 3409–3421.

Shimi, T., Kittisopikul, M., Tran, J., Goldman, A.E., Adam, S.A., Zheng, Y., Jaqaman, K., and Goldman, R.D.

(2015). Structural organization of nuclear lamins A, C, B1, and B2 revealed by superresolution microscopy. Mol. Biol. Cell *26*, 4075–4086.

Shumaker, D.K., Kuczmarski, E.R., and Goldman, R.D. (2003). The nucleoskeleton: lamins and actin are major players in essential nuclear functions. Curr. Opin. Cell Biol. *15*, 358–366.

Shumaker, D.K., Solimando, L., Sengupta, K., Shimi, T., Adam, S.A., Grunwald, A., Strelkov, S.V., Aebi, U., Cardoso, M.C., and Goldman, R.D. (2008). The highly conserved nuclear lamin Ig-fold binds to PCNA: its role in DNA replication. J. Cell Biol. *181*, 269–280.

Simon, D.N., and Wilson, K.L. (2013). Partners and post-translational modifications of nuclear lamins. Chromosoma *122*, 13–31.

Sinensky, M., Fantle, K., Trujillo, M., McLain, T., Kupfer, A., and Dalton, M. (1994). The processing pathway of prelamin A. J. Cell Sci. *107 (Pt 1)*, 61–67.

Singh, R.K., Liang, D., Gajjalaiahvari, U.R., Kabbaj, M.-H.M., Paik, J., and Gunjan, A. (2010). Excess histone levels mediate cytotoxicity via multiple mechanisms. Cell Cycle *9*, 4236–4244.

Siomi, H., Shida, H., Maki, M., and Hatanaka, M. (1990). Effects of a highly basic region of human immunodeficiency virus Tat protein on nucleolar localization. J. Virol. *64*, 1803–1807.

Sipos, K., and Olson, M.O. (1991). Nucleolin promotes secondary structure in ribosomal RNA. Biochem Biophys Res Commun *177*, 673–678.

Sirri, V., Roussel, P., and Hernandez-Verdun, D. (2000). The AgNOR proteins: qualitative and quantitative changes during the cell cycle. Micron *31*, 121–126.

Sirri, V., Urcuqui-Inchima, S., Roussel, P., and Hernandez-Verdun, D. (2008). Nucleolus: the fascinating nuclear body. Histochem. Cell Biol. *129*, 13–31.

Skaar, T.C., Prasad, S.C., Sharareh, S., Lippman, M.E., Brünner, N., and Clarke, R. (1998). Two-dimensional gel electrophoresis analyses identify nucleophosmin as an estrogen regulated protein associated with acquired estrogen-independence in human breast cancer cells. J Steroid Biochem Mol Biol *67*, 391–402.

Sloan, K.E., Warda, A.S., Sharma, S., Entian, K.D., Lafontaine, D.L.J., and Bohnsack, M.T. (2017). Tuning the ribosome: The influence of rRNA modification on eukaryotic ribosome biogenesis and function. RNA Biol *14*, 1138–1152.

Snaar, S., Wiesmeijer, K., Jochemsen, A.G., Tanke, H.J., and Dirks, R.W. (2000). Mutational analysis of fibrillarin and its mobility in living human cells. J. Cell Biol. *151*, 653–662.

Sood, N., Nigam, J.S., Yadav, P., Rewri, S., Sharma, A., Omhare, A., and Malhotra, J. (2013). Comparative Study of Cytomorphological Robinson's Grading for Breast Carcinoma with Modified Bloom-Richardson Histopathological Grading. Patholog Res Int *2013*, 146542.

Soundararajan, S., Wang, L., Sridharan, V., Chen, W., Courtenay-Luck, N., Jones, D., Spicer, E.K., and Fernandes, D.J. (2009). Plasma membrane nucleolin is a receptor for the anticancer aptamer AS1411 in MV4-11 leukemia cells. Mol Pharmacol *76*, 984–991.

Spann, T.P., Goldman, A.E., Wang, C., Huang, S., and Goldman, R.D. (2002). Alteration of nuclear lamin organization inhibits RNA polymerase II-dependent transcription. J. Cell Biol. *156*, 603–608.

Srivastava, M., Fleming, P.J., Pollard, H.B., and Burns, A.L. (1989). Cloning and sequencing of the human nucleolin cDNA. FEBS Lett *250*, 99–105.

Srivastava, M., McBride, O.W., Fleming, P.J., Pollard, H.B., and Burns, A.L. (1990). Genomic organization and chromosomal localization of the human nucleolin gene. J. Biol. Chem. *265*, 14922–14931.

Srivastava, R., Srivastava, R., and Ahn, S.H. (2016). The epigenetic pathways to ribosomal DNA silencing. Microbiol. Mol. Biol. Rev. *80*, 545–563.

Stancheva, I., Lucchini, R., Koller, T., and Sogo, J.M. (1997). Chromatin structure and methylation of rat rRNA genes studied by formaldehyde fixation and psoralen cross-linking. Nucleic Acids Res. *25*, 1727–1735.

Starr, D.A., and Fridolfsson, H.N. (2010). Interactions between nuclei and the cytoskeleton are mediated by SUN-KASH nuclear-envelope bridges. Annu. Rev. Cell Dev. Biol. *26*, 421–444.

Stefanovsky, V., Langlois, F., Gagnon-Kugler, T., Rothblum, L.I., and Moss, T. (2006). Growth factor signaling regulates elongation of RNA polymerase I transcription in mammals via UBF phosphorylation and r-chromatin remodeling. Mol. Cell *21*, 629–639.

Stefanovsky, V.Y., Pelletier, G., Bazett-Jones, D.P., Crane-Robinson, C., and Moss, T. (2001). DNA looping in the RNA polymerase I enhancesome is the result of non-cooperative in-phase bending by two UBF molecules. Nucleic Acids Res. *29*, 3241–3247.

Steger, D.J., and Workman, J.L. (1999). Transcriptional analysis of purified histone acetyltransferase complexes. Methods *19*, 410–416.

Stepanova, V., Lebedeva, T., Kuo, A., Yarovoi, S., Tkachuk, S., Zaitsev, S., Bdeir, K., Dumler, I., Marks, M.S., Parfyonova, Y., et al. (2008). Nuclear translocation of urokinase-type plasminogen activator. Blood *112*, 100–110.

Stewart, C., and Burke, B. (1987). Teratocarcinoma stem cells and early mouse embryos contain only a single major lamin polypeptide closely resembling lamin B. Cell *51*, 383–392.

Stimpson, K.M., Sullivan, L.L., Kuo, M.E., and Sullivan, B.A. (2014). Nucleolar organization, ribosomal DNA array stability, and acrocentric chromosome integrity are linked to telomere function. PLoS One *9*, e92432.

Stixová, L., Matula, P., Kozubek, S., Gombitová, A., Cmarko, D., Raška, I., and Bártová, E. (2012). Trajectories and nuclear arrangement of PML bodies are influenced by A-type lamin deficiency. Biol Cell *104*, 418–432.

Storck, S., Thiry, M., and Bouvet, P. (2009). Conditional knockout of nucleolin in DT40 cells reveals the functional redundancy of its RNA-binding domains. Biol Cell *101*, 153–167.

Stuurman, N., Heins, S., and Aebi, U. (1998). Nuclear lamins: their structure, assembly, and interactions. J. Struct. Biol. *122*, 42–66.

Stüven, T., Hartmann, E., and Görlich, D. (2003). Exportin 6: a novel nuclear export receptor that is specific for profilin.actin complexes. EMBO J. *22*, 5928–5940.

Subong, E.N., Shue, M.J., Epstein, J.I., Briggman, J.V., Chan, P.K., and Partin, A.W. (1999). Monoclonal antibody to prostate cancer nuclear matrix protein (PRO:4-216) recognizes nucleophosmin/B23. Prostate *39*, 298–304.

Sugimoto, M., Kuo, M.L., Roussel, M.F., and Sherr, C.J. (2003). Nucleolar Arf tumor suppressor inhibits ribosomal RNA processing. Mol. Cell *11*, 415–424.

Swaminathan, V., Kishore, A.H., Febitha, K.K., and Kundu, T.K. (2005). Human histone chaperone nucleophosmin enhances acetylation-dependent chromatin transcription. Mol. Cell Biol. *25*, 7534–7545.

Swaminathan, V., Mythreye, K., O'Brien, E.T., Berchuck, A., Blobe, G.C., and Superfine, R. (2011). Mechanical stiffness grades metastatic potential in patient tumor cells and in cancer cell lines. Cancer Res. *71*, 5075–5080.

Swift, J., Ivanovska, I.L., Buxboim, A., Harada, T., Dingal, P.C.D.P., Pinter, J., Pajerowski, J.D., Spinler, K.R., Shin, J.-W., Tewari, M., et al. (2013). Nuclear lamin-A scales with tissue stiffness and enhances matrix-directed differentiation. Science *341*, 1240104.

Szebeni, A., Hingorani, K., Negi, S., and Olson, M.O. (2003). Role of protein kinase CK2 phosphorylation in the molecular chaperone activity of nucleolar protein b23. J. Biol. Chem. *278*, 9107–9115.

Szerlong, H.J., Herman, J.A., Krause, C.M., DeLuca, J.G., Skoultchi, A., Winger, Q.A., Prenni, J.E., and Hansen, J.C. (2015). Proteomic characterization of the nucleolar linker histone H1 interaction network. J. Mol. Biol. *427*, 2056–2071.

Tachibana, M., Ueda, J., Fukuda, M., Takeda, N., Ohta, T., Iwanari, H., Sakihama, T., Kodama, T., Hamakubo, T., and Shinkai, Y. (2005). Histone methyltransferases G9a and GLP form heteromeric complexes and are both crucial for methylation of euchromatin at H3-K9. Genes Dev *19*, 815–826.

Taddei, A., and Gasser, S.M. (2012). Structure and function in the budding yeast nucleus. Genetics *192*, 107–129.

Taimen, P., Pfleghaar, K., Shimi, T., Möller, D., Ben-Harush, K., Erdos, M.R., Adam, S.A., Herrmann, H., Medalia, O., Collins, F.S., et al. (2009). A progeria mutation reveals functions for lamin A in nuclear assembly, architecture, and chromosome organization. Proc. Natl. Acad. Sci. USA *106*, 20788–20793.

Takagi, M., Absalon, M.J., McLure, K.G., and Kastan, M.B. (2005). Regulation of p53 translation and induction after DNA damage by ribosomal protein L26 and nucleolin. Cell *123*, 49–63.

Takemura, M., Sato, K., Nishio, M., Akiyama, T., Umekawa, H., and Yoshida, S. (1999). Nucleolar Protein B23.1 Binds to Retinoblastoma Protein and Synergistically Stimulates DNA Polymerase α Activity. The Journal of Biochemistry.

Tamura, M., Gu, J., Danen, E.H., Takino, T., Miyamoto, S., and Yamada, K.M. (1999). PTEN interactions with focal adhesion kinase and suppression of the extracellular matrix-dependent phosphatidylinositol 3-kinase/Akt cell survival pathway. J. Biol. Chem. *274*, 20693–20703.

Tanaka, M., Sasaki, H., Kino, I., Sugimura, T., and Terada, M. (1992). Genes preferentially expressed in embryo stomach are predominantly expressed in gastric cancer. Cancer Res. *52*, 3372–3377.

Taniura, H., Glass, C., and Gerace, L. (1995). A chromatin binding site in the tail domain of nuclear lamins that interacts with core histones. J. Cell Biol. *131*, 33–44.

Tate, A., Isotani, S., Bradley, M.J., Sikes, R.A., Davis, R., Chung, L.W.K., and Edlund, M. (2006). Met-Independent Hepatocyte Growth Factor-mediated regulation of cell adhesion in human prostate cancer cells. BMC Cancer *6*, 197.

Tediose, T., Kolev, M., Sivasankar, B., Brennan, P., Morgan, B.P., and Donev, R. (2010). Interplay between REST and nucleolin transcription factors: a key mechanism in the overexpression of genes upon increased phosphorylation. Nucleic Acids Res. *38*, 2799–2812.

Teng, Y., Girvan, A.C., Casson, L.K., Pierce, W.M., Qian, M., Thomas, S.D., and Bates, P.J. (2007). AS1411 alters the localization of a complex containing protein arginine methyltransferase 5 and nucleolin. Cancer Res. *67*, 10491–10500.

Tessarz, P., Santos-Rosa, H., Robson, S.C., Sylvestersen, K.B., Nelson, C.J., Nielsen, M.L., and Kouzarides, T. (2014). Glutamine methylation in histone H2A is an RNA-polymerase-I-dedicated modification. Nature *505*, 564–568.

Thébault, S., Basbous, J., Gay, B., Devaux, C., and Mesnard, J.M. (2000). Sequence requirement for the nucleolar localization of human I-mfa domain-containing protein (HIC p40). Eur. J. Cell Biol. *79*, 834–838.

Thiry, M., and Lafontaine, D.L.J. (2005). Birth of a nucleolus: the evolution of nucleolar compartments. Trends Cell Biol. *15*, 194–199.

Tilney, L.G. (1975). The role of actin in nonmuscle cell motility. Soc Gen Physiol Ser *30*, 339–388.

Tin, A.S., Park, A.H., Sundar, S.N., and Firestone, G.L. (2014). Essential role of the cancer stem/progenitor cell marker nucleostemin for indole-3-carbinol anti-proliferative responsiveness in human breast cancer cells. BMC Biol. *12*, 72.

Tollervey, D., Lehtonen, H., Jansen, R., Kern, H., and Hurt, E.C. (1993). Temperature-sensitive mutations demonstrate roles for yeast fibrillarin in pre-rRNA processing, pre-rRNA methylation, and ribosome assembly. Cell *72*, 443–457.

Tong, Z., Balzer, E.M., Dallas, M.R., Hung, W.C., Stebe, K.J., and Konstantopoulos, K. (2012). Chemotaxis of cell populations through confined spaces at single-cell resolution. PLoS One *7*, e29211.

Treré, D., Ceccarelli, C., Montanaro, L., Tosti, E., and Derenzini, M. (2004). Nucleolar size and activity are related to pRb and p53 status in human breast cancer. J. Histochem. Cytochem. *52*, 1601–1607.

True, L.D., and Jordan, C.D. (2008). The cancer nuclear microenvironment: interface between light microscopic cytology and molecular phenotype. J. Cell Biochem. *104*, 1994–2003.

Tsoi, H., and Chan, H.Y.E. (2013). Expression of expanded CAG transcripts triggers nucleolar stress in Huntington's disease. Cerebellum *12*, 310–312.

Tsoi, H., Lam, K.C., Dong, Y., Zhang, X., Lee, C.K., Zhang, J., Ng, S.C., Ng, S.S.M., Zheng, S., Chen, Y., et al. (2017). Pre-45s rRNA promotes colon cancer and is associated with poor survival of CRC patients. Oncogene *36*, 6109–6118.

Tsui, K.H., Cheng, A.J., Chang, P.E., Pan, T.L., and Yung, B.Y. (2004). Association of nucleophosmin/B23 mRNA expression with clinical outcome in patients with bladder carcinoma. Urology *64*, 839–844.

Turgay, Y., Eibauer, M., Goldman, A.E., Shimi, T., Khayat, M., Ben-Harush, K., Dubrovsky-Gaupp, A., Sapra, K.T., Goldman, R.D., and Medalia, O. (2017). The molecular architecture of lamins in somatic cells. Nature *543*, 261–264.

Tycowski, K.T., Smith, C.M., Shu, M.D., and Steitz, J.A. (1996). A small nucleolar RNA requirement for site-specific ribose methylation of rRNA in Xenopus. Proc Natl Acad Sci USA *93*, 14480–14485.

Uemura, M., Zheng, Q., Koh, C.M., Nelson, W.G., Yegnasubramanian, S., and De Marzo, A.M. (2012). Overexpression of ribosomal RNA in prostate cancer is common but not linked to rDNA promoter hypomethylation. Oncogene *31*, 1254–1263.

Ugrinova, I., Monier, K., Ivaldi, C., Thiry, M., Storck, S., Mongelard, F., and Bouvet, P. (2007). Inactivation of nucleolin leads to nucleolar disruption, cell cycle arrest and defects in centrosome duplication. BMC Mol Biol *8*, 66.

Uribe, D.J., Guo, K., Shin, Y.J., and Sun, D. (2011). Heterogeneous nuclear ribonucleoprotein K and nucleolin as transcriptional activators of the vascular endothelial growth factor promoter through interaction with secondary DNA structures. Biochemistry *50*, 3796–3806.

Valdez, B.C., Perlaky, L., Henning, D., Saijo, Y., Chan, P.K., and Busch, H. (1994). Identification of the nuclear and nucleolar localization signals of the protein p120. Interaction with translocation protein B23. J. Biol. Chem. *269*, 23776–23783.

Valentin, G. (1836). Repertorium für Anatomie und Physiologie (Berlin).

Vandekerckhove, J., Deboben, A., Nassal, M., and Wieland, T. (1985). The phalloidin binding site of F-actin. EMBO J. *4*, 2815–2818.

Versaevel, M., Grevesse, T., and Gabriele, S. (2012). Spatial coordination between cell and nuclear shape within micropatterned endothelial cells. Nat Commun *3*, 671.

Vesely, P.W., Staber, P.B., Hoefler, G., and Kenner, L. (2009). Translational regulation mechanisms of AP-1 proteins. Mutat. Res. *682*, 7–12.

Vidak, S., and Foisner, R. (2016). Molecular insights into the premature aging disease progeria. Histochem. Cell Biol. *145*, 401–417.

Voit, R., Seiler, J., and Grummt, I. (2015). Cooperative Action of Cdk1/cyclin B and SIRT1 Is Required for Mitotic Repression of rRNA Synthesis. PLoS Genet. *11*, e1005246.

Wachtler, F., Schwarzacher, H.G., and Ellinger, A. (1982). The influence of the cell cycle on structure and number of nucleoli in cultured human lymphocytes. Cell Tissue Res. *225*, 155–163.

Wagner, R. (1834). Einige bemerkungen und fragen über das keimbläschen (vesicular germinativa). Müller's Archiv Anat Physiol Wissenschaft Med.

Wandrey, F., Montellese, C., Koos, K., Badertscher, L., Bammert, L., Cook, A.G., Zemp, I., Horvath, P., and Kutay, U. (2015). The NF45/NF90 Heterodimer Contributes to the Biogenesis of 60S Ribosomal Subunits and Influences Nucleolar Morphology. Mol. Cell. Biol. *35*, 3491–3503.

Wang, D., Umekawa, H., and Olson, M.O. (1993). Expression and subcellular locations of two forms of nucleolar protein B23 in rat tissues and cells. Cell Mol Biol Res *39*, 33–42.

Wang, D., Baumann, A., Szebeni, A., and Olson, M.O. (1994). The nucleic acid binding activity of nucleolar

protein B23.1 resides in its carboxyl-terminal end. J. Biol. Chem. *269*, 30994–30998.

Wang, H., Boisvert, D., Kim, K.K., Kim, R., and Kim, S.H. (2000). Crystal structure of a fibrillarin homologue from Methanococcus jannaschii, a hyperthermophile, at 1.6 A resolution. EMBO J. *19*, 317–323.

Wang, W.H., Childress, M.O., and Geahlen, R.L. (2014). Syk interacts with and phosphorylates nucleolin to stabilize Bcl-x(L) mRNA and promote cell survival. Mol. Cell Biol. *34*, 3788–3799.

Wang, Y., Mao, M., and Xu, J. (2011a). Cell-surface nucleolin is involved in lipopolysaccharide internalization and signalling in alveolar macrophages. Cell Biol. Int. *35*, 677–685.

Wang, Y., Chen, B., Li, Y., Zhou, D., and Chen, S. (2011b). PNRC accumulates in the nucleolus by interaction with B23/nucleophosmin via its nucleolar localization sequence. Biochim. Biophys. Acta *1813*, 109–119.

Watanabe-Susaki, K., Takada, H., Enomoto, K., Miwata, K., Ishimine, H., Intoh, A., Ohtaka, M., Nakanishi, M., Sugino, H., Asashima, M., et al. (2014). Biosynthesis of ribosomal RNA in nucleoli regulates pluripotency and differentiation ability of pluripotent stem cells. Stem Cells *32*, 3099–3111.

Watson, J.D., Oster, S.K., Shago, M., Khosravi, F., and Penn, L.Z. (2002). Identifying genes regulated in a Myc-dependent manner. J. Biol. Chem. *277*, 36921–36930.

Weber, J.D., Taylor, L.J., Roussel, M.F., Sherr, C.J., and Bar-Sagi, D. (1999). Nucleolar Arf sequesters Mdm2 and activates p53. Nat. Cell Biol. *1*, 20–26.

West, S., Gromak, N., and Proudfoot, N.J. (2004). Human 5' --> 3' exonuclease Xrn2 promotes transcription termination at co-transcriptional cleavage sites. Nature *432*, 522–525.

Wheeler, A.P., and Ridley, A.J. (2004). Why three Rho proteins? RhoA, RhoB, RhoC, and cell motility. Exp. Cell Res. *301*, 43–49.

Williams, M.A., Kleinschmidt, J.A., Krohne, G., and Franke, W.W. (1982). Argyrophilic nuclear and nucleolar proteins of Xenopus laevis oocytes identified by gel electrophoresis. Exp. Cell Res. *137*, 341–351.

Wise, J.F., Berkova, Z., Mathur, R., Zhu, H., Braun, F.K., Tao, R.H., Sabichi, A.L., Ao, X., Maeng, H., and Samaniego, F. (2013). Nucleolin inhibits Fas ligand binding and suppresses Fas-mediated apoptosis in vivo via a surface nucleolin-Fas complex. Blood.

Wood, A.M., Rendtlew Danielsen, J.M., Lucas, C.A., Rice, E.L., Scalzo, D., Shimi, T., Goldman, R.D., Smith, E.D., Le Beau, M.M., and Kosak, S.T. (2014). TRF2 and lamin A/C interact to facilitate the functional organization of chromosome ends. Nat Commun *5*, 5467.

Worman, H.J., and Bonne, G. (2007). "Laminopathies": a wide spectrum of human diseases. Exp. Cell Res. *313*, 2121–2133.

Wu, M.H., and Yung, B.Y.M. (2002). UV stimulation of nucleophosmin/B23 expression is an immediate-early gene response induced by damaged DNA. J. Biol. Chem. *277*, 48234–48240.

Wu, C., You, J., Fu, J., Wang, X., and Zhang, Y. (2016). Phosphatidylinositol 3-Kinase/Akt Mediates Integrin Signaling To Control RNA Polymerase I Transcriptional Activity. Mol. Cell Biol. *36*, 1555–1568.

Wu, D.M., Zhang, P., Liu, R.Y., Sang, Y.X., Zhou, C., Xu, G.C., Yang, J.L., Tong, A.P., and Wang, C.T. (2014). Phosphorylation and changes in the distribution of nucleolin promote tumor metastasis via the PI3K/Akt pathway in colorectal carcinoma. FEBS Lett *588*, 1921–1929.

Xia, X., Liu, S., Xiao, Z., Zhu, F., Song, N.Y., Zhou, M., Liu, B., Shen, J., Nagashima, K., Veenstra, T.D., et al. (2013). An IKKα-nucleophosmin axis utilizes inflammatory signaling to promote genome integrity. Cell Rep *5*, 1243–1255.

Xiao, S., Caglar, E., Maldonado, P., Das, D., Nadeem, Z., Chi, A., Trinité, B., Li, X., and Saxena, A. (2014). Induced expression of nucleolin phosphorylation-deficient mutant confers dominant-negative effect on cell proliferation. PLoS One *9*, e109858.

Xu, B., Li, H., Perry, J.M., Singh, V.P., Unruh, J., Yu, Z., Zakari, M., McDowell, W., Li, L., and Gerton, J.L. (2017). Ribosomal DNA copy number loss and sequence variation in cancer. PLoS Genet. *13*, e1006771.

Yaghoobi, M.M., Mowla, S.J., and Tiraihi, T. (2005). Nucleostemin, a coordinator of self-renewal, is expressed in rat marrow stromal cells and turns off after induction of neural differentiation. Neurosci. Lett. *390*, 81–86.

Yanagida, M., Hayano, T., Yamauchi, Y., Shinkawa, T., Natsume, T., Isobe, T., and Takahashi, N. (2004). Human fibrillarin forms a sub-complex with splicing factor 2-associated p32, protein arginine methyltransferases, and tubulins alpha 3 and beta 1 that is independent of its association with preribosomal ribonucleoprotein complexes. J. Biol. Chem. *279*, 1607–1614.

Yang, C., Maiguel, D.A., and Carrier, F. (2002). Identification of nucleolin and nucleophosmin as genotoxic stress-responsive RNA-binding proteins. Nucleic Acids Res. *30*, 2251–2260.

Yang, C., Kim, M.S., Chakravarty, D., Indig, F.E., and Carrier, F. (2009). Nucleolin binds to the proliferating cell nuclear antigen and inhibits nucleotide excision repair. Mol Cell Pharmacol *1*, 130–137.

Yang, C.H., Lambie, E.J., Hardin, J., Craft, J., and Snyder, M. (1989). Higher order structure is present in the yeast nucleus: autoantibody probes demonstrate that the nucleolus lies opposite the spindle pole body. Chromosoma *98*, 123–128.

Ye, J., Zhao, J., Hoffmann-Rohrer, U., and Grummt, I. (2008). Nuclear myosin I acts in concert with polymeric actin to drive RNA polymerase I transcription. Genes Dev *22*, 322–330.

Ye, Q., Callebaut, I., Pezhman, A., Courvalin, J.C., and Worman, H.J. (1997). Domain-specific interactions of human HP1-type chromodomain proteins and inner nuclear membrane protein LBR. J. Biol. Chem. *272*, 14983–14989.

Yoneda-Kato, N., Look, A.T., Kirstein, M.N., Valentine, M.B., Raimondi, S.C., Cohen, K.J., Carroll, A.J., and Morris, S.W. (1996). The t(3;5)(q25.1;q34) of myelodysplastic syndrome and acute myeloid leukemia produces a novel fusion gene, NPM-MLF1. Oncogene *12*, 265–275.

Zaidi, S.H., and Malter, J.S. (1995). Nucleolin and heterogeneous nuclear ribonucleoprotein C proteins specifically interact with the 3'-untranslated region of amyloid protein precursor mRNA. J. Biol. Chem. *270*, 17292–17298.

Zhang, C., Comai, L., and Johnson, D.L. (2005). PTEN represses RNA Polymerase I transcription by disrupting the SL1 complex. Mol. Cell Biol. *25*, 6899–6911.

Zhang, D., Liang, Y., Xie, Q., Gao, G., Wei, J., Huang, H., Li, J., Gao, J., and Huang, C. (2015). A novel post-translational modification of nucleolin, SUMOylation at Lys-294, mediates arsenite-induced cell death by regulating gadd45α mRNA stability. J. Biol. Chem. *290*, 4784–4800.

Zhang, H., Shi, X., Paddon, H., Hampong, M., Dai, W., and Pelech, S. (2004). B23/nucleophosmin serine 4 phosphorylation mediates mitotic functions of polo-like kinase 1. J. Biol. Chem. *279*, 35726–35734.

Zhang, H.-M., Chen, H., Liu, W., Liu, H., Gong, J., Wang, H., and Guo, A.Y. (2012). AnimalTFDB: a comprehensive animal transcription factor database. Nucleic Acids Res. *40*, D144-9.

Zhang, J., Tsaprailis, G., and Bowden, G.T. (2008). Nucleolin stabilizes Bcl-X L messenger RNA in response to UVA irradiation. Cancer Res. *68*, 1046–1054.

Zhang, Y., Xiong, Y., and Yarbrough, W.G. (1998). ARF promotes MDM2 degradation and stabilizes p53: ARF-INK4a locus deletion impairs both the Rb and p53 tumor suppression pathways. Cell *92*, 725–734.

Zhao, J., Yuan, X., Frödin, M., and Grummt, I. (2003). ERK-dependent phosphorylation of the transcription initiation factor TIF-IA is required for RNA polymerase I transcription and cell growth. Mol. Cell *11*, 405–413.

Zhao, Z., Dammert, M.A., Grummt, I., and Bierhoff, H. (2016a). lncRNA-Induced Nucleosome Repositioning Reinforces Transcriptional Repression of rRNA Genes upon Hypotonic Stress. Cell Rep. *14*, 1876–1882.

Zhao, Z., Dammert, M.A., Hoppe, S., Bierhoff, H., and Grummt, I. (2016b). Heat shock represses rRNA synthesis by inactivation of TIF-IA and lncRNA-dependent changes in nucleosome positioning. Nucleic Acids Res. *44*, 8144–8152.

Zhou, H., Wang, Y., Lv, Q., Zhang, J., Wang, Q., Gao, F., Hou, H., Zhang, H., Zhang, W., and Li, L. (2016). Overexpression of Ribosomal RNA in the Development of Human Cervical Cancer Is Associated with rDNA

Promoter Hypomethylation. PLoS One *11*, e0163340.

Zhou, Y., Santoro, R., and Grummt, I. (2002). The chromatin remodeling complex NoRC targets HDAC1 to the ribosomal gene promoter and represses RNA polymerase I transcription. EMBO J. *21*, 4632–4640.

Zhuo, W., Luo, C., Wang, X., Song, X., Fu, Y., and Luo, Y. (2010). Endostatin inhibits tumour lymphangiogenesis and lymphatic metastasis via cell surface nucleolin on lymphangiogenic endothelial cells. J. Pathol. *222*, 249–260.

Zink, D., Fischer, A.H., and Nickerson, J.A. (2004). Nuclear structure in cancer cells. Nat. Rev. Cancer *4*, 677–687.

Publications

AMERICAN SOCIETY FOR MICROBIOLOGY | Molecular and Cellular Biology®

RESEARCH ARTICLE

Lamin B2 Modulates Nucleolar Morphology, Dynamics, and Function

Ayantika Sen Gupta, Kundan Sengupta

Biology, Indian Institute of Science Education and Research, Pune, India

ABSTRACT The nucleolus is required for ribosome biogenesis. Human cells have 2 or 3 nucleoli associated with nucleolar organizer region (NOR)-bearing chromosomes. An increase in number and altered nucleolar morphology define cancer cells. However, the mechanisms that modulate nucleolar morphology and function are unclear. Here we show that in addition to localizing at the nuclear envelope, lamin B2 localizes proximal to nucleolin at the granular component (GC) of the nucleolus and associates with the nucleolar proteins nucleolin and nucleophosmin. Lamin B2 knockdown severely disrupted the nucleolar morphology, which was rescued to intact and discrete nucleoli upon lamin B2 overexpression. Furthermore, two mutually exclusive lamin B2 deletion mutants, ΔHead and ΔSLS, rescued nuclear and nucleolar morphology defects, respectively, induced upon lamin B2 depletion, suggesting independent roles for lamin B2 at the nucleolus and nuclear envelope. Lamin B2 depletion increased nucleolin aggregation in the nucleoplasm, implicating lamin B2 in stabilizing nucleolin within the nucleolus. Lamin B2 knockdown upregulated nucleolus-specific 45S rRNA and upstream intergenic sequence (IGS) transcripts. The IGS transcripts colocalized with aggregates of nucleolin speckles, which were sustained in the nucleoplasm upon lamin B2 depletion. Taken together, these studies uncover a novel role for lamin B2 in modulating the morphology, dynamics, and function of the nucleolus.

KEYWORDS lamin, nucleolin, nucleolus, nucleophosmin, nucleus, rDNA, rRNA

Received 24 May 2017 **Returned for modification** 5 July 2017 **Accepted** 29 September 2017

Accepted manuscript posted online 9 October 2017

Citation Sen Gupta A, Sengupta K. 2017. Lamin B2 modulates nucleolar morphology, dynamics, and function. Mol Cell Biol 37:e00274-17. https://doi.org/10.1128/MCB.00274-17.

Address correspondence to Kundan Sengupta, kunsen@iiserpune.ac.in.

The nucleolus is the largest nuclear subcompartment and is the site of ribosomal DNA (rDNA) transcription, processing, and ribosome biogenesis (1). The nucleolus undergoes cycles of disassembly and reassembly during mitosis (2). At the end of mitosis, small prenucleolar bodies (PNBs) assemble on human chromosomes 13, 14, 15, 21, and 22 bearing the nucleolar organizer regions (NOR), which then coalesce to form the nucleolus (3). Altered nucleolar numbers and structure correlate with cancers and ribosomopathies (4, 5).

Electron microscopy (EM) revealed that the nucleolus in amniotes has a tripartite organization consisting of the innermost fibrillar compartment (FC), the intermediate dense fibrillar compartment (DFC), and the outermost granular component (GC) (6). Inhibition of nucleolar transcription, rRNA processing, or assembly into preribosomes perturbs the integrity of the nucleolar compartments. Inhibition of rRNA transcription by actinomycin D (Act D) induces nucleolar cap formation, inversion of the FC, DFC, and GC, and dispersion of nucleolar proteins into the nucleoplasm, underscoring the role of active transcription of rDNA in maintaining nucleolar integrity (7). Thus, nucleolar morphologies are affected by altered metabolic rates and physiological stresses, such as nutrient deprivation, DNA damage, and hypoxia, that inhibit rDNA transcription (8–11). On the other hand, hyperproliferative cancer cells and hypertrophic cardiomyocytes with elevated protein synthesis and rDNA transcription show increased numbers of or enlarged nucleoli (12, 13). Often these nucleoli are irregular in morphology and therefore serve as prognostic markers of carcinogenesis (14). The nucleolar structure is also altered when rRNA processing is compromised upon depletion of the rRNA-

processing factors NF90/NF110 or the key ribosomal proteins uL18 (RPL5) and uL5 (RPL11) (15, 16).

Mass spectrometric analysis of isolated nucleoli identified ~4,500 nucleolar proteins that modulate ribosome biogenesis, cell cycle control, and DNA damage repair (17). However, the majority of nucleolar proteins remain uncharacterized in terms of their potential to modulate nucleolar structure and function. Upstream binding factor (UBF), nucleolin, and nucleophosmin are well-characterized nucleolar proteins that are essential for nucleolar formation and morphology (18–21). Fibrillarin and nucleophosmin, which are associated with ribosome biogenesis, phase-separate from the soluble nucleoplasm into nucleoli in an rRNA-dependent manner (22, 23).

The nucleolus nevertheless remains dynamic in its tripartite organization and is connected to the nuclear matrix by intermediate filament (IF) proteins (24, 25). Lamins are type V intermediate filament proteins at the inner nuclear membrane that maintain nuclear architecture (26). B-type lamins (B1 and B2) are expressed in most vertebrate cells, while lamin A/C is expressed predominantly in differentiated cells (27, 28). Although lamins localize primarily to the nuclear periphery, intranuclear pools of lamins modulate chromatin dynamics, splicing, and DNA damage repair (29–32). Lamin A/C and lamin B1 are implicated in maintaining nucleolar structure and function (33–36). However, the role of lamin B2 in nucleolar structure-function modulation remains unclear.

Here we have uncovered a novel role for lamin B2 in modulating nucleolar morphology and function. We show that lamin B2 localizes at the granular component and associates with nucleolar factors such as nucleolin and nucleophosmin (NPM1) in diploid DLD-1 cells. Furthermore, lamin B2 depletion strikingly disrupts nucleolar morphology and upregulates levels of nucleolar transcripts such as the 45S rRNA and intergenic sequence (IGS) transcripts. The upregulated IGS transcripts show an increased colocalization with nucleolin aggregates in the nucleoplasm. Taken together, these studies unravel a novel role for lamin B2 in modulating nucleolar morphology, dynamics, and function.

RESULTS

Lamin B2 depletion disrupts nucleolar morphology. Lamins and SUN1, which are proteins of the nuclear envelope, regulate nuclear structure and function across cell types (37, 38). Interestingly, lamin A/C, lamin B1, and SUN1 also regulate nucleolar structure and function (33, 35). Here we sought to examine the relatively unappreciated role of lamin B2 in the modulation of nucleolar structure and function in diploid colorectal cancer (DLD-1) cells. We selected DLD-1 cells for our experiments owing to their stable and near diploid karyotype of 44 to 46 chromosomes across passages (data not shown). Furthermore, the levels of all three nuclear lamins, i.e., lamins A/C, B1, and B2, are comparable in DLD-1 cells but vary considerably in most other cell types (39–41).

We performed small interfering RNA (siRNA)-mediated gene silencing of lamins B2 and A/C, followed by immunoblotting assays, which showed ~70% knockdown of lamin B2 and lamin A/C, independently, in DLD-1 cells (Fig. 1A and B). Since the depletion of the closely related lamin B1 disperses nucleoli in HeLa cells, we ascertained that lamin B2 depletion does not alter the levels of lamin B1 in DLD-1 cells (Fig. 1C) (35). We next examined nucleolar morphologies upon lamin depletion by immunostaining cells with nucleolin, a bona fide nucleolar protein (Fig. 1D and F). Nucleolin localizes at the granular component (GC) of each nucleolus and serves as a marker of nucleolar morphology and numbers across cell types (19, 42). Immunostaining of nucleolin in DLD-1 cells showed two contrasting nucleolar morphologies: (i) intact, i.e., discrete, spatially separate, and spherical nucleoli (Fig. 1D, arrowhead), and (ii) disrupted, i.e., aggregated and irregular nucleoli (Fig. 1D, asterisk). We typically detected 2 or 3 discrete, spherical nucleoli in each nucleus in ~69% of the cells, while ~31% of the cells showed disrupted nucleoli (Fig. 1E). Interestingly, lamin B2 depletion revealed a significant increase in strikingly aberrant and disrupted nucleoli in ~76% of the cells

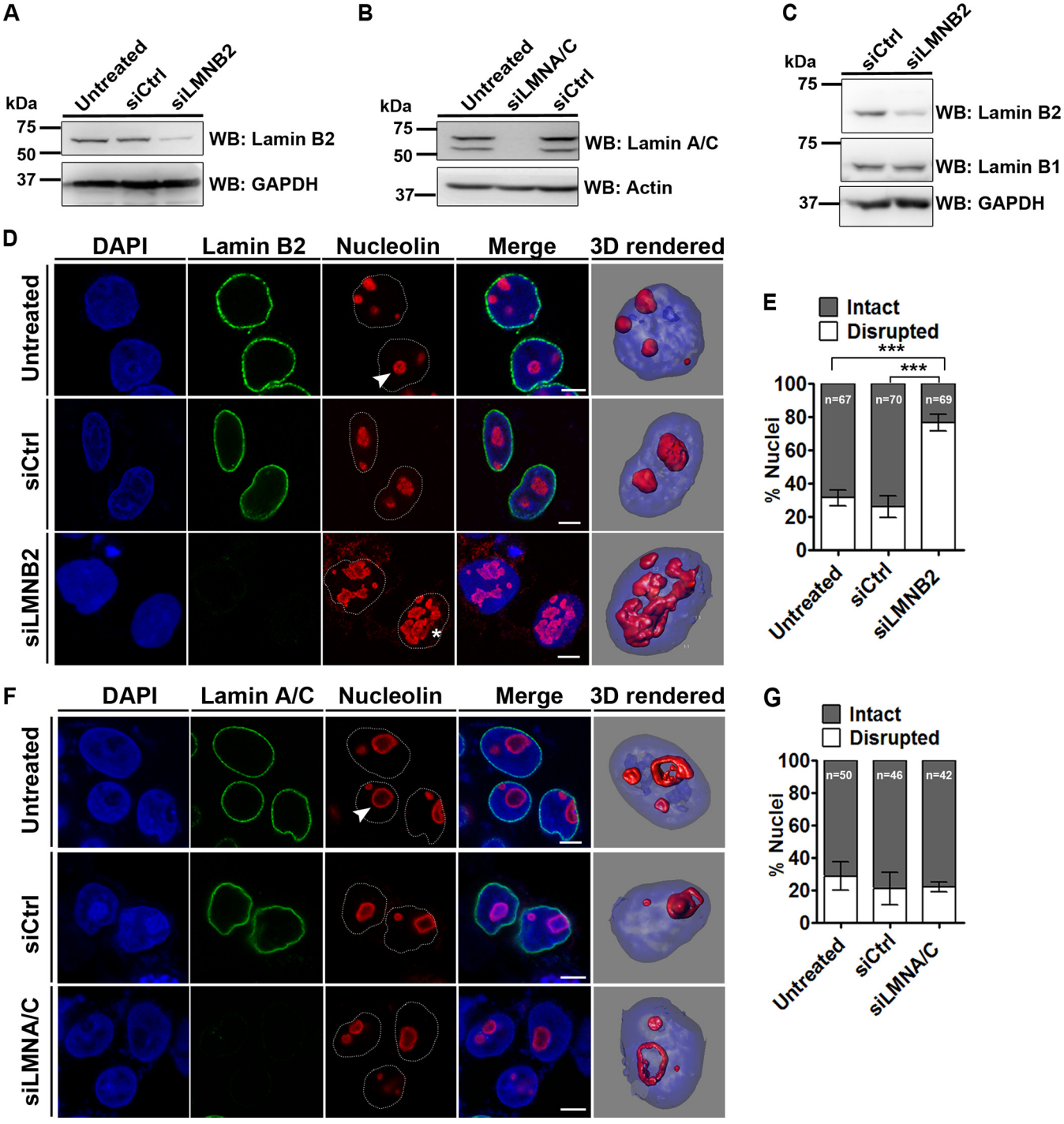

FIG 1 Lamin B2 depletion disrupts nucleolar morphology. (A and B) Western blots (WB) showing siRNA-mediated depletion of lamin B2 (A) and lamin A/C (B). (C) Lamin B1 levels are unaltered upon lamin B2 knockdown. Loading controls were GAPDH (glyceraldehyde-3-phosphate dehydrogenase) and actin. (D) Coimmunostaining of lamin B2 and nucleolin in DLD-1 cells. DAPI counterstains the nucleus. Untreated cells, lamin B2 knockdown cells (siLMNB2), or cells treated with nontargeting siRNA (siCtrl) were used. Representative confocal images of control cells show discrete and intact nucleoli (arrowhead), and siLMNB2 shows disrupted nucleolar morphology (asterisk) (also shown in 3D reconstructions). Scale bars, ~5 μm. (E) Quantification of nucleolar morphologies shows a significant increase in disrupted nucleoli upon lamin B2 knockdown (***, $P < 0.001$ by Fisher's exact test of proportions) (number of independent biological replicates [N] = 3; n, number of nuclei). Error bars indicate standard errors of means (SEM). (F) Coimmunostaining of lamin A/C and nucleolin. No change in nucleolar morphology was observed upon siLMNA/C (arrowhead) or siCtrl treatment (also shown in 3D reconstructions). Scale bars, ~5 μm. (G) Quantification of nucleolar morphologies upon lamin A/C knockdown ($P > 0.05$ by Fisher's exact test of proportions) ($N = 2$; n, number of nuclei). Error bars indicate standard deviations (SD).

(Fig. 1D [asterisk] and E). In marked contrast, lamin A/C knockdown did not affect nucleolar morphologies (intact, ~80% of the cells; disrupted, ~20% of the cells) (Fig. 1F and G). We also employed two independent siRNA oligonucleotides to knock down lamin B2, which showed comparable extents of disrupted nucleoli in DLD-1 cells (siLMNB2.2, ~59%; siLMNB2.3, ~62%) (data not shown). Furthermore, nucleolar volumes showed a significant increase (~1.5-fold) upon lamin B2 but not lamin A/C depletion, consistent with the large-scale nucleolar disruptions that we detected in lamin B2-depleted cells (data not shown). Lamin B2 knockdown, however, did not alter nucleolin levels (data not shown). Taken together, these results underscore a novel role for lamin B2 in the maintenance of discrete and intact nucleolar morphologies.

Distinct domains of lamin B2 modulate nucleolar and nuclear morphologies. To dissect potential separation of the function of lamin B2 in modulating nucleolar and nuclear morphologies, we targeted two amino acid sequences in the N- and C-terminal domains of lamin B2. Lamin B2 is organized as (i) an N-terminal globular head domain (amino acids [aa] 1 to 28), (ii) a central rod domain (aa 29 to 380), and (iii) a C-terminal tail domain (aa 381 to 600) (Fig. 2A) (43, 44). We created two independent deletion mutants of lamin B2: (i) lamin B2ΔHead (with the first 28 amino acids of lamin B2 deleted), required for the head-tail organization of lamin B2 dimers (45), and (ii) lamin B2ΔSLS, with a 7-amino-acid deletion of the SLSATGR sequence from the C-terminal tail domain (Fig. 2A). This amino acid stretch is unique to lamin B2 and absent in lamin A/C and lamin B1.

We determined the effects of overexpressing siRNA-resistant (i) full-length lamin B2, (ii) lamin B2ΔHead, and (iii) lamin B2ΔSLS on the nucleolar and nuclear morphologies in lamin B2-depleted cells. Immunoblotting showed that the expression levels of full-length lamin B2 and the deletion mutants were comparable in control and lamin B2-depleted cells (Fig. 2B). We next expressed full-length lamin B2 and its deletion mutants in DLD-1 cells and examined the nucleolar morphology by nucleolin staining (Fig. 2C).

We first examined the effect of overexpressing full-length siRNA-resistant lamin B2 on nucleolar morphology in lamin B2-depleted cells. Overexpression of full-length lamin B2 reduced the number of disrupted nucleoli in control cells. Disrupted nucleoli induced upon lamin B2 knockdown were also rescued to intact nucleoli upon overexpression of lamin B2 in ~81% of the cells (Fig. 2C and D). Taken together, these data suggest that an intact nucleolar morphology was rescued upon the restoration of lamin B2 levels.

Transfection of the deletion constructs of lamin B2 did not alter the nucleolar morphology in control cells (Fig. 2C and D). Notably, the disrupted nucleolar morphology in lamin B2-depleted cells was not restored to intact nucleoli upon overexpressing the lamin B2 mutant lacking the head domain (Fig. 2C and D), while overexpression of the lamin B2 mutant lacking the SLSATGR amino acid sequence at the tail domain restored intact nucleolar morphology in ~85% of the cells (comparable to the case for full-length lamin B2) (Fig. 2C and D), suggesting that the SLSATGR sequence is dispensable for the maintenance of intact nucleoli. Taken together, the results show that the head domain of lamin B2 is required for maintaining intact nucleolar morphologies.

Lamin B2 knockout induces severe defects in the nuclear envelope (37). We were curious to determine if lamin B2 mutants exert mutually exclusive effects on the nucleolar and nuclear morphologies. We examined the effect of lamin B2 depletion on nuclear morphology. Confocal imaging of DLD-1 cells immunostained for lamin B1 consistently revealed a homogenous population of ellipsoidal nuclei, with a regular and uniform nuclear envelope (Fig. 3A, siCtrl). A small subpopulation (~1%) of control cells, however, showed nuclear blebs (Fig. 3B). Remarkably, lamin B2 knockdown induced the formation of nuclear blebs in ~25% of DLD-1 cells (Fig. 3A [siLMNB2, arrowhead] and B). Overexpression of full-length lamin B2 decreased nuclear blebs from ~25% to ~3% in lamin B2-depleted cells (Fig. 3B, siLMNB2+LMNB2), while overexpression of lamin

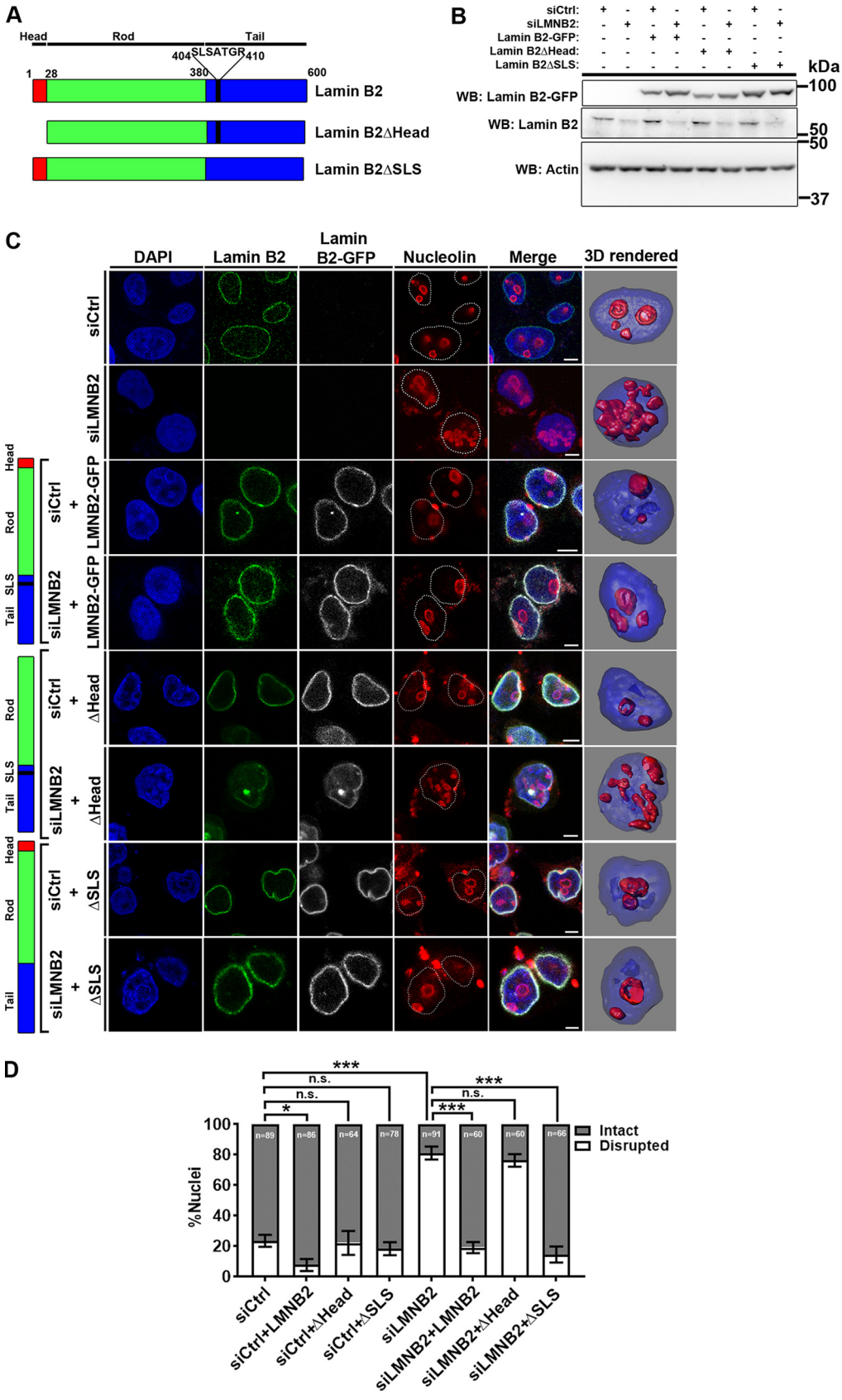

FIG 2 The lamin B2 head domain maintains nucleolar morphology. (A) Schematic representation of full-length lamin B2 with the N-terminal head domain, central rod domain, and C-terminal tail domain. The lamin B2ΔHead mutant lacks the

(Continued on next page)

B2ΔHead also reduced nuclear blebs to ~3% (Fig. 3B, siLMNB2+ΔHead). Overexpression of the lamin B2ΔSLS mutant, in contrast, did not reduce the extent of nuclear bleb formation in lamin B2-depleted cells (Fig. 3B, siLMNB2+ΔSLS), suggesting that the SLSATGR sequence is indeed required for maintaining the normal and bleb-free nuclear morphology, while the head domain of lamin B2 is dispensable for the same. We also found that overexpression of full-length lamin B2, lamin B2ΔHead, or lamin B2ΔSLS did not induce nuclear blebs in control DLD-1 cells (Fig. 3B). In summary, the analyses of lamin B2 mutants was revealing at the mechanistic level, as this unraveled a distinct separation of function of lamin B2 in independently modulating nucleolar and nuclear morphologies.

Lamin B2 localizes at the nucleolar border and associates with nucleolin and nucleophosmin. It is well established that lamin B2 localizes primarily at the inner nuclear membrane across cell types (46, 47). Lamin B2 staining in intact nuclei shows hardly any intranuclear localization (Fig. 1D). We therefore permeabilized the nucleus by salt extractions and DNase I treatment in order to facilitate antibody accessibility into the nuclear matrix (48, 49). This approach revealed a distinct intranuclear localization of lamin B2 and lamin A/C inside the nucleus. Notably, lamin B2 but not lamin A/C localized proximal to the nucleolar border (data not shown).

To determine if lamin B2 indeed associates with the nucleolus, we performed immunofluorescence staining of lamin B2 on isolated nucleoli from a semiconfluent culture of DLD-1 cells (Fig. 4A). Remarkably, isolated nucleoli showed a distinct localization and enrichment of lamin B2 at the nucleolar border as foci in close proximity to nucleolin (Fig. 4A [siCtrl, arrowheads] and B [line scan]). Nucleoli isolated from lamin B2-depleted cells did not show lamin B2 staining, while nucleolin staining was maintained at the nucleolar border (Fig. 4A, siLMNB2). This further validated the specificity of lamin B2 localization at the nucleolar border in isolated nucleoli.

We also performed superresolution microscopy using Airyscan imaging to further resolve lamin B2 and lamin A/C localization within isolated nucleoli (Fig. 4C). This high-resolution imaging approach recapitulated lamin B2 localization at the nucleolar border (Fig. 4C). In contrast, lamin A/C showed a punctate distribution in the nucleolar interior, while nucleolin localization was confined to the nucleolar border (Fig. 4C). The nucleolar localization of lamin A/C is consistent with its detection in nucleolar extracts of HeLa cells by mass spectrometry (35). Although confocal and superresolution Airyscan imaging showed a close proximity of lamin B2 with nucleolin (Fig. 4B, line scans), we did not detect a colocalization between lamin B2 and nucleolin at all regions of isolated nucleoli.

Considering the proximity of lamin B2 to nucleolin, we asked if lamin B2 associates with bona fide nucleolar proteins. We performed coimmunoprecipitation (co-IP) assays with nucleolin and nucleophosmin (NPM1) on whole-cell extracts of DLD-1 cells (Fig. 4D). Coimmunoprecipitation of nucleolin specifically immunoprecipitated lamin B2 but not lamin A/C or lamin B1 (Fig. 4D, panels i to iii). Under similar conditions, we recapitulated the well-established interaction between nucleolin and NPM1 (50) (Fig. 4D, panel iv). Lamin B2 also coimmunoprecipitated with NPM1, underscoring the association of lamin B2 with nucleolar proteins at the granular component (Fig. 4D, panel v). In summary, these results strongly implicate lamin B2 in the structural and potentially functional organization of the nucleolus.

FIG 2 Legend (Continued)
head domain (aa 1 to 28) from the N terminus. The lamin B2ΔSLS mutant lacks the sequence SLSATGR (aa 404 to 410) from the tail domain of lamin B2. (B) Western blot showing overexpression of siRNA-resistant full-length lamin B2-GFP, lamin B2ΔHead-GFP, and lamin B2ΔSLS-GFP mutants in control and lamin B2-depleted cells. The loading control was actin. (C) Immunofluorescence staining of nucleolin, showing the nucleolar morphology in control and lamin B2-depleted cells overexpressing (i) full-length lamin B2-GFP (+LMNB2), (ii) lamin B2ΔHead (+ΔHead), and (iii) lamin B2ΔSLS (+ΔSLS) constructs. Scale bars, ~5 μm. (D) Intact nucleolar morphology was restored upon overexpression of full-length lamin B2 (siLMNB2+LMNB2) and lamin B2ΔSLS (siLMNB2+ΔSLS) but not upon overexpression of lamin B2ΔHead (siLMNB2+ΔHead). (*, $P < 0.05$; ***, $P < 0.001$; n.s., not significant [by Fisher's exact test of proportions]) (number of independent biological replicates [N] = 3; n, number of nuclei). Error bars indicate SEM.

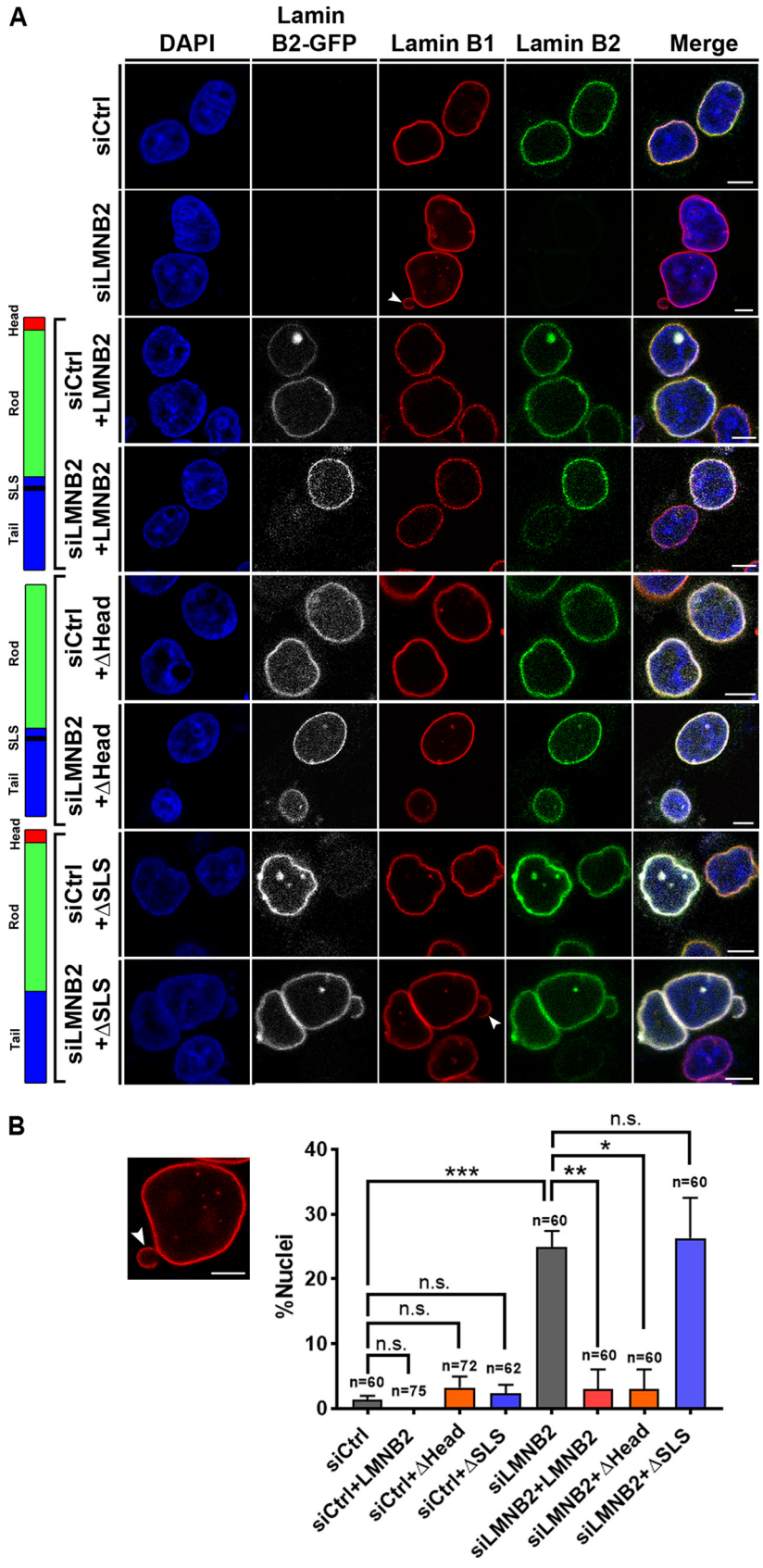

FIG 3 The SLSATGR sequence in the lamin B2 tail domain maintains nuclear morphology. (A) Immunofluorescence staining of lamin B1, showing the nuclear morphology in control and lamin

(Continued on next page)

Lamin B2 depletion enhances nucleolin aggregation in the nucleoplasm. Active transcription by RNA polymerase I (Pol I) is essential for the maintenance of nucleolar structure and function. This was corroborated by actinomycin D (Act D)-mediated inhibition of RNA Pol I, which induces reorganization of fibrillarin and UBF into nucleolar caps and dispersal of nucleolin and NPM1 into the nucleoplasm (7). Act D treatment is a useful experimental paradigm to address the effects of potential regulators on the morphology and function of the nucleolus. We determined the effect of lamin B2 depletion on the subnuclear localization of nucleolin and nucleolar morphology upon Act D treatment. Immunostaining of nucleolin in Act D-treated cells consistently showed cells with (i) smaller and hollow nucleoli (Fig. 5A, asterisk), (ii) nucleolar cap formation, and (iii) nucleolin dispersion into the nucleoplasm (Fig. 5A, siCtrl+Act D, arrowhead). Furthermore, nucleolin was enriched at the nuclear periphery, consistent with nucleolin shuttling out of the nucleolus in Act D-treated cells (51). Act D treatment induced nucleolin aggregates in the nucleoplasm (Fig. 5A, siCtrl+Act D, arrowhead). Of note, lamin B2-depleted cells treated with Act D showed a significant increase in cells with nucleolin aggregates (siCtrl, ~54%; siLMNB2, ~80%) (Fig. 5B) and also an increase in their volume (~1.3-fold) (Fig. 5C). Notably, fibrillarin costained with nucleolin aggregates, suggesting the association of nucleolar RNA binding proteins within these aggregates and destabilization of the nucleolus (Fig. 5D). Fibrillarin also showed a relatively higher intensity in these aggregates upon lamin B2 depletion (Fig. 5E).

We determined whether lamin B2 modulates the status of nucleolin aggregates in cells overexpressing nucleolin. Interestingly, nucleolin overexpression phenocopied the disrupted nucleolar morphologies that we consistently detect upon lamin B2 depletion (Fig. 5F, NCL OE + vehicle, arrowhead). Additionally, nucleolin overexpression showed nucleolin aggregates in the nucleoplasm upon Act D treatment (Fig. 5F and G, NCL OE + Act D) (volume [M] = 0.36 μm^3). Lamin B2 knockdown showed a significant increase in the volume of nucleolin aggregates (M = 0.77 μm^3) of ~2.13-fold, while lamin B2 overexpression rescued the volume of nucleolin aggregates to near-basal levels (M = 0.25 μm^3) (Fig. 5F and G). Taking the data together, we conclude that lamin B2 modulates nucleolin aggregation in the nucleoplasm.

Nucleolin aggregates persist in the nucleoplasm upon lamin B2 depletion. We determined the effect of lamin B2 depletion on the dynamics of nucleolin aggregates by live-cell imaging. This revealed a progressive increase in nucleolin aggregates originating from the nucleolus, from ~40 min after Act D addition (Fig. 6A [siCtrl] and B; see Movie S1 in the supplemental material). In control cells, nucleoplasmic aggregates of nucleolin showed a steady decline and were hardly detectable after ~2 h, suggesting a dispersal of nucleolin into the nucleoplasm (Fig. 6A and B [blue circles]). Remarkably, nucleolin aggregates in lamin B2-depleted cells persisted in the nucleoplasm even after ~3 h of Act D treatment (Fig. 6A and B [red circles]; see Movies S2 and S3 in the supplemental material). This suggests that lamin B2 depletion promotes the long-term retention of nucleolin aggregates in the nucleoplasm. We performed fluorescence recovery after photobleaching (FRAP) to examine whether lamin B2 regulates nucleolin dynamics within the aggregates (Fig. 6C and D). Nucleolin showed ~95% recovery, suggesting a free exchange of nucleolin into the aggregates (Fig. 6D and E). This is consistent with the free diffusion of nucleolin in the nucleoplasm of HeLa cells treated with Act D (52). Although the relative mobile fractions of nucleolin within the aggregates were comparable (Fig. 6E), nucleolin recovery was significantly faster upon

FIG 3 Legend (Continued)
B2-depleted cells overexpressing full-length lamin B2-GFP (+LMNB2), (ii) lamin B2ΔHead (+ΔHead), and (iii) lamin B2ΔSLS (+ΔSLS) constructs. Control cells show ellipsoidal nuclei with uniform lamin B1 staining at the nuclear periphery. Lamin B2-depleted cells show nuclear blebs that partially stain for lamin B1 (arrowhead). Scale bars, ~5 μm. (B) The incidence of nuclear blebs in lamin B2 depleted cells was reduced upon overexpression of full-length lamin B2 (siLMNB2+LMNB2) and lamin B2ΔHead (siLMNB2+ΔHead) but not upon overexpression of lamin B2ΔSLS (siLMNB2+ΔSLS). (*, $P < 0.05$; **, $P < 0.01$; ***, $P < 0.001$ [by Student's t test]) (number of independent biological replicates [N] = 3; n, number of nuclei). Error bars indicate SEM.

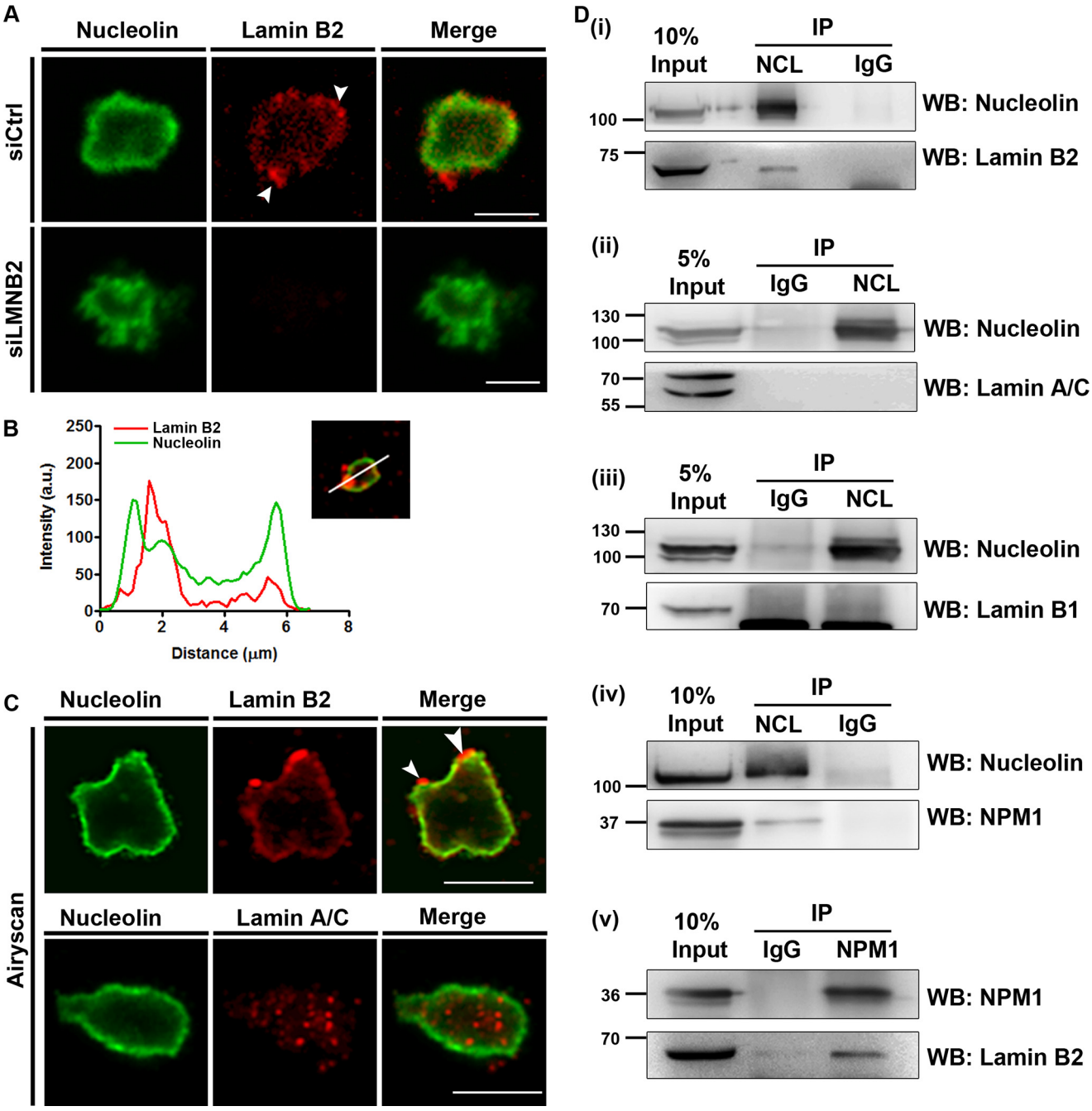

FIG 4 Lamin B2 associates with the nucleolus. (A) Isolated nucleoli were immunostained for lamin B2 and nucleolin. Nucleolin localizes largely at the nucleolar edge. Lamin B2 foci were enriched at the nucleolar periphery (siCtrl panel, arrowheads). The absence of lamin B2 staining in nucleoli isolated from lamin B2-depleted cells (siLMNB2 panel) shows the specificity of lamin B2 staining at the nucleolus. Scale bars, ~5 μm. (B) A representative line scan across an isolated nucleolus shows lamin B2 (red line) enrichment near the edge of the nucleolus marked by nucleolin (green line). (C) Superresolution Airyscan images of isolated nucleoli immunostained for nucleolin, lamin B2, and lamin A/C. Lamin B2 is enriched at the nucleolar border (arrowheads), while lamin A/C foci localize in the nucleolar interior. Scale bars, ~5 μm. (D) (i) Coimmunoprecipitation of lamin B2 with nucleolin (NCL). Negative control, IgG. (ii and iii) Lamin A/C (ii) and lamin B1 (iii) do not coimmunoprecipitate with nucleolin. (iv) Nucleolin pulls down NPM1, which serves as a positive control. (v) Lamin B2 coimmunoprecipitates with NPM1. Co-IP experiments were performed in three independent biological replicates for lamin B2 and two independent biological replicates for lamin A/C and lamin B1.

lamin B2 depletion (half-life [$t_{1/2}$], ~1.2 s) than that for control cells ($t_{1/2}$, ~1.7 s) (Fig. 6F). Taken together, these results suggest an increased recruitment of nucleolin into the aggregates upon lamin B2 depletion.

Lamin B2 depletion increases rRNA expression. Lamin B2 depletion significantly disrupts the nucleolar morphology and affects the dynamics of nucleolin aggregates

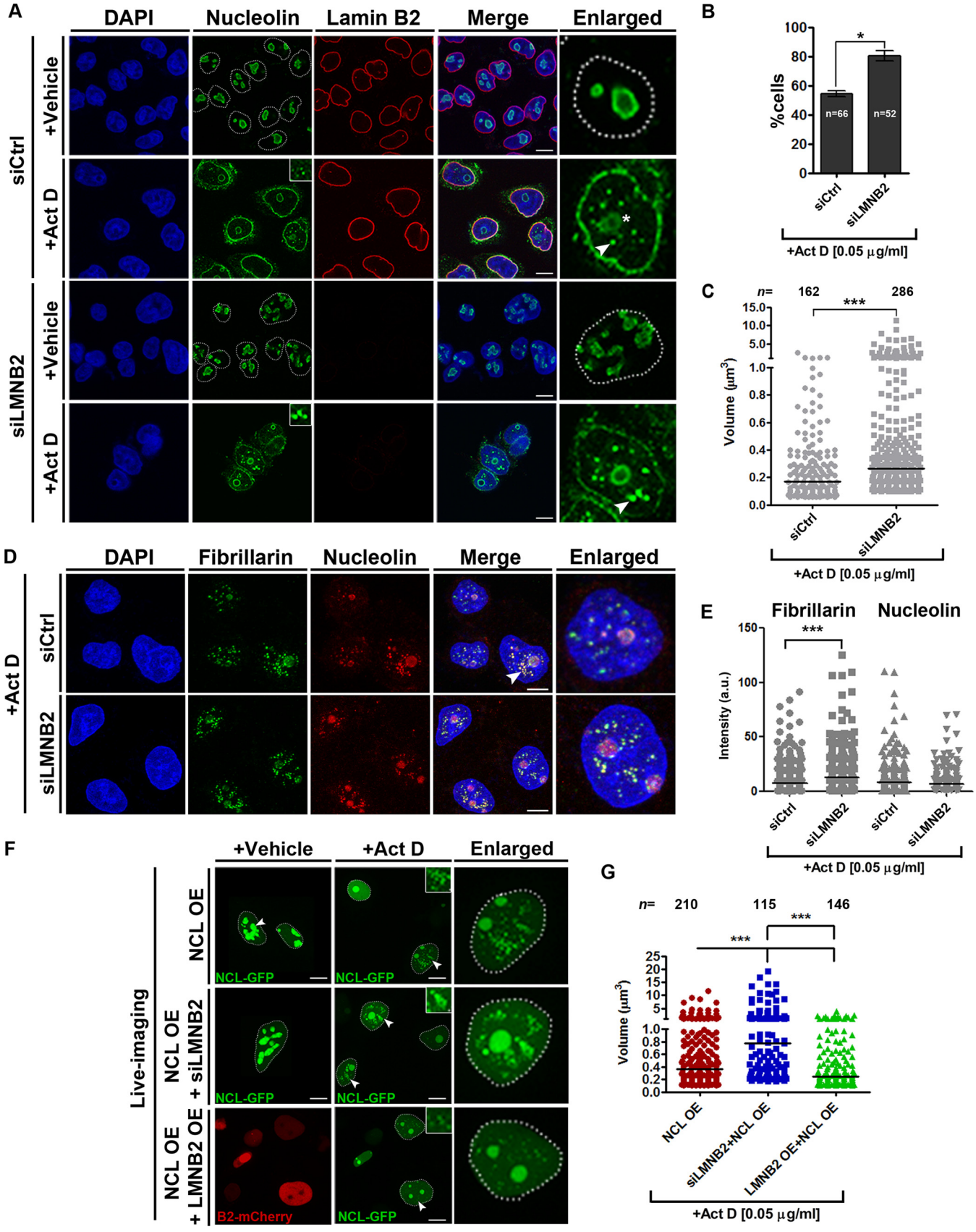

FIG 5 Lamin B2 depletion increases the volume of nucleolin aggregates. (A) Control or lamin B2-depleted cells were treated with DMSO (vehicle control) or actinomycin D (+Act D) and immunostained for nucleolin. Vehicle-treated control (siCtrl) and lamin B2-depleted (siLMNB2) cells show nucleolin restricted to

(Continued on next page)

(Fig. 1D and E and 6D to F). We determined whether lamin B2 also modulates nucleolar function by monitoring the levels of nucleolus-specific transcripts. We examined the expression levels of key nucleolar transcripts (by quantitative real-time PCR [qRT-PCR]) from two independent regions of the rDNA repeat cluster, i.e., (i) 45S rRNA, an ~13-kbp rRNA coding region which is further processed into 28S, 5.8S, and 18S rRNAs, and (ii) the intergenic sequence (IGS), an ~12-kbp region upstream of the 45S rRNA start site, by RNA fluorescent *in situ* hybridization (RNA-FISH) (Fig. 7A). The rDNA IGS encodes noncoding RNAs (ncRNAs) such as promoter-associated RNAs (pRNAs) and promoter and pre-rRNA antisense (PAPAS) in response to serum starvation, heat shock, or acidosis (53–55). Interestingly, these ncRNAs regulate 45S rRNA expression, or sequester chaperones (heat shock proteins [HSPs] and Von Hippel-Lindau tumor suppressor protein [VHL]) into the nucleolus (54, 55).

Remarkably, lamin B2 depletion showed a significant increase in the levels of the RNA Pol I-transcribed 45S rRNA (fold change, ~2.7), while the long noncoding MALAT1 RNA (transcribed by RNA Pol II) was unaffected (Fig. 7B). Taken together, these findings reveal a unique role for lamin B2 and underscores its specificity in upregulating 45S rRNA levels. The expression levels of 45S rRNA showed a significant decline (~84% decrease) upon Act D treatment (Fig. 7B, siCtrl+Act D). Although Act D treatment downregulated 45S rRNA levels in control cells by ~84%, the decrease in 45S rRNA levels was only ~61% in lamin B2-depleted cells. This reiterates that the reduction in lamin B2 levels counters the effect of Act D in downmodulating the levels of 45S rRNA (Fig. 7B). Levels of 28S and 18S processed rRNA transcripts were not significantly altered upon lamin B2 depletion or Act D treatment, suggesting that lamin B2 depletion may not affect processing of 45S pre-rRNA (Fig. 7B).

Having detected a specific increase in 45S rRNA levels, we examined the expression levels and nuclear localization of IGS RNA by RNA-FISH upon lamin B2 depletion (Fig. 7C). RNA-FISH revealed three subpopulations of cells showing IGS foci: (i) a single focus (~65% of the cells), (ii) 2 foci (~33% of the cells), and (iii) >2 foci (~2% of the cells) (Fig. 7D, gray bars). Lamin B2 depletion showed a marked decrease in cells with a single focus (~31% of the cells) and a concomitant increase in cells with 2 foci (~46% of the cells) and >2 foci (23% of the cells) (Fig. 7D, white bars). Taking the results together, in addition to the 45S rRNA, lamin B2 also upregulates expression levels of nucleolus-specific intergenic transcripts. Remarkably, lamin B2 overexpression rescued levels of IGS RNA signals to a single focus (~71%), comparable to the case for control cells (Fig. 7D, black bars).

We next examined the nuclear localization of IGS RNA upon Pol I inhibition (Fig. 7E). In contrast to the distinct foci of IGS RNA signals in untreated cells (Fig. 7C), IGS RNA localization was relatively diffuse upon Act D treatment. Furthermore, IGS RNA colocalized with nucleolin aggregates upon Act D treatment (Fig. 7E). IGS RNA and nucleolin colocalization was enhanced in lamin B2-depleted cells (Fig. 7E and F). In summary, lamin B2 depletion promotes the stability of nucleolin-IGS RNA aggregates in the

FIG 5 Legend (Continued)
the nucleolus. Vehicle-treated lamin B2-depleted cells show an irregular nucleolar morphology (siLMNB2, +Vehicle panel). Act D-treated control (siCtrl+Act D) or lamin B2-depleted (siLMNB2+Act D) cells show nucleolin aggregates in the nucleoplasm (insets, enlarged panels [arrowhead]). Act D treatment shows spherical nucleoli (asterisk, enlarged panel). Scale bars, ~5 μm. (B) Lamin B2 depletion shows a significant increase in cells with nucleolin aggregates upon Act D treatment (*, $P < 0.05$ by Student's *t* test) (number of independent biological replicates [*N*] = 3; *n*, number of nuclei). Error bars indicate SEM. (C) Scatter plots showing an increase in the volumes of nucleolin aggregates upon lamin B2 depletion followed by Act D treatment (***, $P < 0.001$ by Mann-Whitney test). Bar, median ($N = 3$; *n*, number of aggregates; siCtrl, 32 nuclei; siLMNB2, 35 nuclei). (D) Fibrillarin colocalizes with nucleolin aggregates upon Act D treatment (arrowhead). Scale bars, ~5 μm. (E) Lamin B2-depleted cells show a significant increase in fibrillarin intensity within nucleolin aggregates (***, $P < 0.001$ by Mann-Whitney test) ($N = 2$; siCtrl, 28 nuclei; siLMNB2, 30 nuclei). (F) Live imaging of DLD-1 cells overexpressing nucleolin (NCL-GFP OE) following Act D or vehicle treatment. NCL-GFP-transfected cells phenocopy disrupted nucleolar morphology comparably to lamin B2 depletion (NCL-GFP OE, arrowhead). Act D-treated cells show aggregates of nucleolin in the nucleoplasm (arrowhead). Lamin B2-depleted cells overexpressing nucleolin show relatively larger aggregates in the nucleoplasm (NCL OE+ siLMNB2, inset). Cells coexpressing lamin B2-mCherry and NCL-GFP show smaller aggregates, suggesting a rescue of the phenotype of lamin B2 depletion (NCL OE+ LMNB2 OE, inset). Insets, nucleolin aggregates. Scale bars, ~5 μm. (G) Scatter plots showing volumes of nucleolin aggregates. Lamin B2 depletion significantly increases the volumes of nucleolin aggregates (siLMNB2+NCL OE), while coexpression of lamin B2 and nucleolin (LMNB2 OE + NCL OE) rescues the volume of nucleolin aggregates to basal levels. Bars, median (***, $P < 0.001$ by Mann-Whitney test) ($N = 3$, *n*, number of aggregates; NCL OE, 30 nuclei; siLMNB2+NCL OE, 30 nuclei; LMNB2 OE+NCL OE, 25 nuclei).

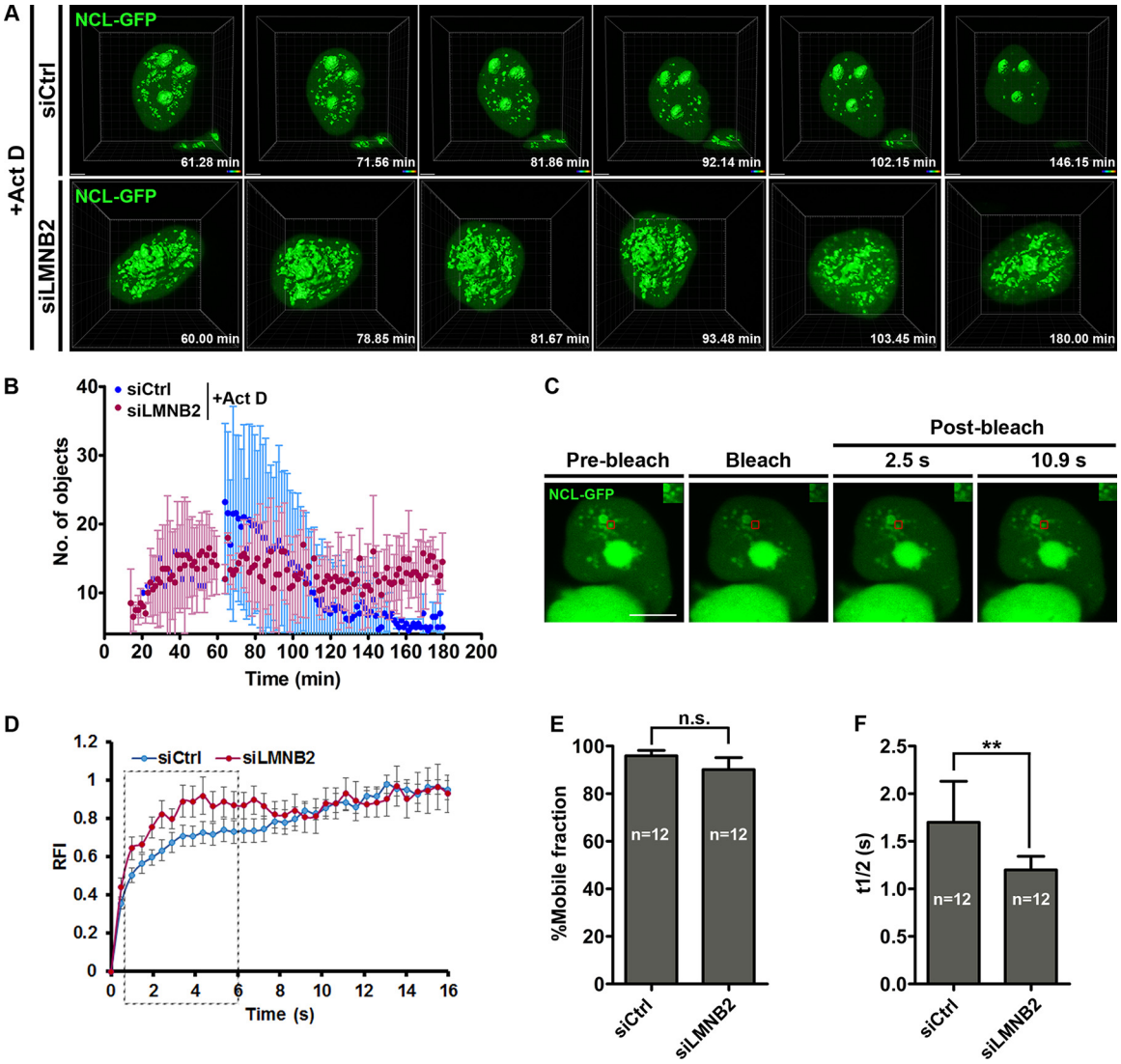

FIG 6 Persistence of nucleolin aggregates upon lamin B2 depletion. (A) Control and lamin B2-depleted cells were transfected with NCL-GFP and treated with Act D. 4D time-lapse confocal imaging shows nucleolin aggregates that peak at ~1 h after Act D addition and gradually disperse into the nucleoplasm (siCtrl,). In lamin B2-depleted cells, nucleolin aggregates persist for ~3 h (siLMNB2 panel). Scale bars, ~2 μm. (B) Quantification of nucleolin aggregates from reconstructions of 4D time-lapse movies, plotted as a function of time (number of independent biological replicates [*N*] = 3; *n* = 6 nuclei each), shows the persistence of nucleolin aggregates upon lamin B2 depletion. (C) Nucleolin aggregates (NCL-GFP) were photobleached to assess nucleolin dynamics. Representative images of nucleolin speckles from control cells are shown. Red boxes, bleach ROI. Insets, photobleached ROI. Scale bar, ~5 μm. (D) FRAP curve shows recovery of nucleolin in aggregates from lamin B2-depleted and control cells. Dashed box, initial phase of recovery is faster upon lamin B2 depletion. (E) The mobile fraction of nucleolin calculated from panel C is not altered upon lamin B2 depletion. Error bars, SEM ($P > 0.05$ by Student's *t* test) (*N* = 3; *n*, number of nuclei). (F) Nucleolin recovery is significantly faster upon lamin B2 depletion (**, $P < 0.01$ by Student's *t* test) (*N* = 3; *n*, number of nuclei).

nucleoplasm. We conclude that lamin B2 functions as a key modulator of nucleolar morphology, dynamics, and function.

DISCUSSION

It is well established that lamins are required for the maintenance of nuclear architecture and function (56). Here we show that in addition to providing mechanical and structural integrity to the nucleus (37), lamin B2, and its head domain in particular, is required for maintaining the intact and discrete morphology of the nucleolus. Lamin B2 potentially exerts its nucleolar function by localizing at the nucleolar border and by associating with nucleolar factors such as nucleolin and nucleophosmin. Furthermore, lamin B2 modulates the extent of nucleolin aggregation and dynamics in the nucleus.

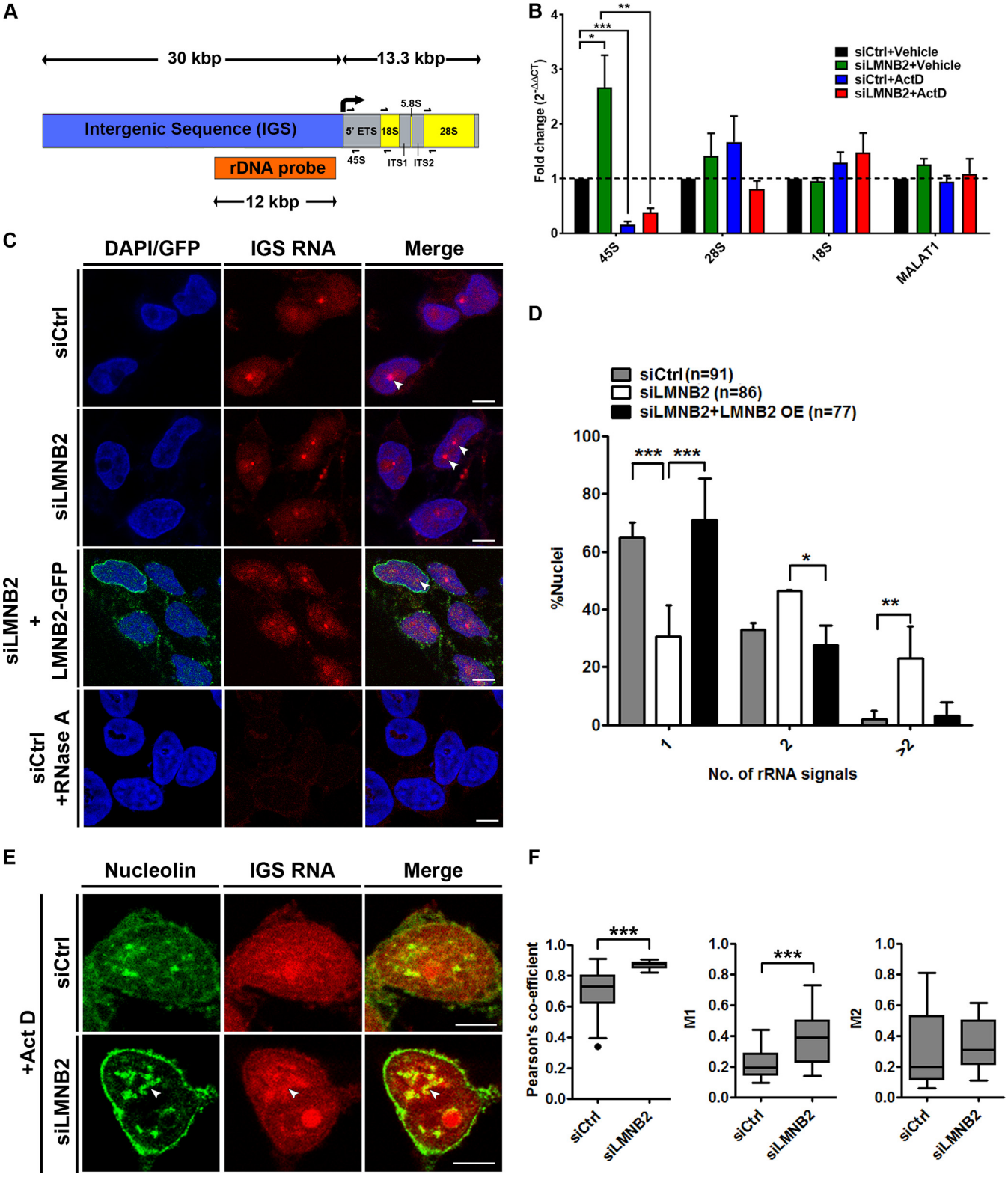

FIG 7 Lamin B2 depletion upregulates expression levels of nucleolar transcripts. (A) Schematic representation of the rDNA encoding the ~13.3-kbp 45S rRNA and ~30-kbp intergenic sequence. The primer pairs used for qRT-PCR (half arrows) and the ~12-kbp probe for RNA-FISH are indicated. (B) qRT-PCR shows a significant increase in 45S transcript levels upon lamin B2 depletion. Act D treatment significantly reduces expression levels of the 45S rRNA transcript in both control and lamin B2-depleted cells. Lamin B2 depletion does not show a significant change in the levels of 28S and 18S transcripts (number of independent biological replicates [*N*] = 3). MALAT1 expression levels are not altered upon lamin B2 depletion and serve as a negative control (*N* = 3; *, $P < 0.05$; **, $P < 0.01$; ***, $P < 0.001$ [by Student's *t* test]). (C) RNA-FISH labels intergenic sequence (IGS) RNA in the nucleolus. Lamin B2-depleted cells show amplification of IGS RNA (siLMNB2 panel, arrowhead). Overexpression of siRNA-resistant lamin B2-GFP in lamin B2-depleted cells (siLMNB2+LMNB2-GFP) restores the number

(Continued on next page)

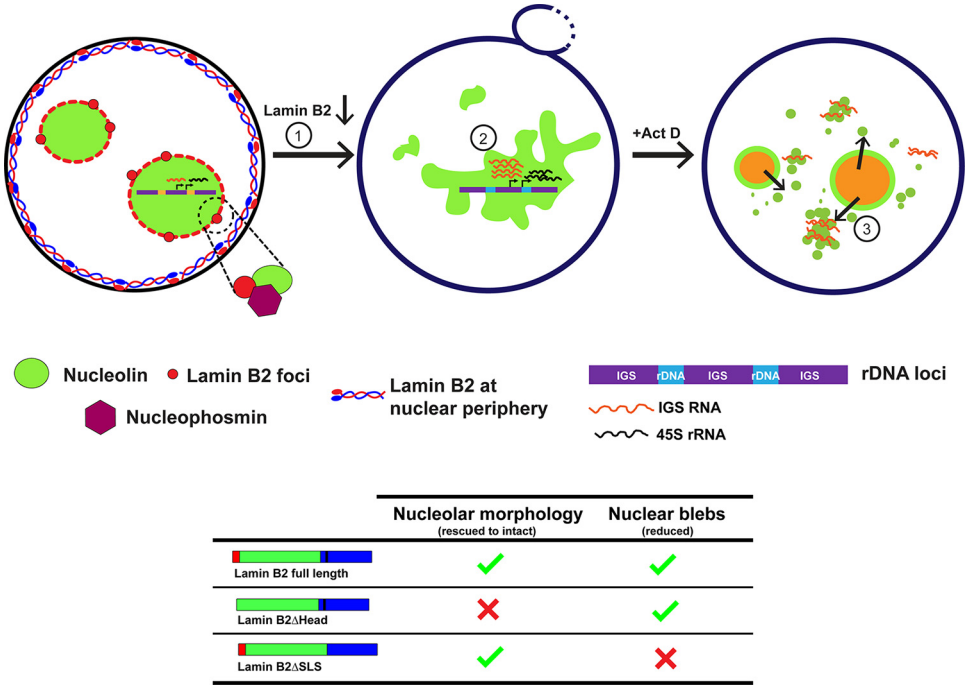

FIG 8 Model depicting a role for lamin B2 in modulating nucleolar structure and function. Lamin B2 is localized predominantly at the nuclear periphery. However, lamin B2 also localizes at the nucleolar border and potentially interacts with nucleolin and NPM1. Lamin B2 depletion shows disrupted nucleolar morphology (1) and increased expression of 45S rRNA and intergenic sequence RNA (IGS RNA) (2). Lamin B2-depleted cells treated with actinomycin D (Act D) have increased nucleolin-IGS RNA aggregates that persist in the nucleoplasm (3). The lamin B2 head domain is required for the maintenance of intact nucleolar morphology, while the lamin B2 SLSATGR amino acid sequence is required for maintaining bleb-free nuclei.

Lamin B2 depletion strikingly increases the expression levels of key nucleolus-specific transcripts such as the 45S rRNA and the upstream IGS RNA (Fig. 8). Taken together, the results of this study unravel a novel role for nuclear lamin B2 in the maintenance of nucleolar structure and function.

Although the nucleus does not have membrane-bound subcompartments, the nucleolus achieves a remarkable level of compartmentalization by phase separation through nucleolar proteins such as nucleophosmin and fibrillarin, which also maintain the relatively spherical morphology of the nucleolus (22, 23, 57). Nucleolin and NPM1 have alternate stretches of basic and acidic amino acid residues at the N terminus, which are likely to function in the phase separation of the nucleolus. We surmise that given the uniquely peripheral localization of lamin B2 at the nucleolar border (Fig. 4), lamin B2 may associate with the negatively charged regions of nucleolin and NPM1 and further assist them in phase separating the nucleolus. It is evident that the loss of lamin B2 disorganizes the nucleolus and enhances the formation of nucleolin aggregates in the nucleoplasm, further implicating lamin B2 in modulating nucleolar phase separation (Fig. 1D and 5A). The contribution of the cytoskeleton in conjunction with nuclear lamins and LINC complex proteins in phase separating nuclear suborganelles is an active area of investigation. The nuclear membrane proteins SUN1, lamin A/C, and lamin B1 regulate nucleolar structure and function in human mammary epithelial

FIG 7 Legend (Continued)
of IGS RNA-FISH signals. The absence of RNA signals in cells upon RNase A treatment shows specificity of IGS RNA-FISH foci. Scale bars, ~5 μm. (D) Quantification of RNA-FISH foci shows a significant increase (>2 foci) upon lamin B2 depletion, while overexpression of lamin B2 restores IGS transcripts to a single focus. Error bars, SD. (*, $P < 0.05$; **, $P < 0.01$; ***, $P < 0.001$ [by Fisher's exact test of proportions]) ($N = 3$, n, number of nuclei). (E) Immuno-RNA-FISH shows colocalization of nucleolin speckles with IGS transcripts in control or lamin B2-depleted cells treated with Act D (arrowhead). (F) Increased colocalization of IGS transcripts with nucleolin in the nucleoplasm upon lamin B2 knockdown (Pearson colocalization index median values: control, 0.7; siLMNB2, 0.88). Manders coefficient (M1), overlap of IGS RNA with nucleolin (median values; control, 0.19; siLMNB2, 0.38). Manders coefficient (M2), overlap of nucleolin with IGS RNA (median values: control, 0.2; siLMNB2, 0.31 [not significant]). Whiskers, Tukey (***, $P < 0.001$ by Mann-Whitney test) ($N = 3$; siCtrl, 28 nuclei; siLMNB2, 32 nuclei).

MCF10A cells and in HeLa cells (33, 35). Further, the disruption of F-actin filaments by latrunculin treatment results in nucleolar aggregates in *Xenopus* germinal vesicle nuclei. This suggests that nucleoskeletal tension between the nucleolus and nuclear matrix potentially contributes to the discreteness of individual nucleoli (58). Of note, lamin A/C knockdown led to nucleolar expansion in MCF10A cells and fibroblasts (33, 34), while lamin B1 depletion in HeLa cells resulted in nucleolar dispersal (35). This suggests that lamin function in the regulation of nucleolar structure and function is cell type specific.

Lamin B2 mutants exert mutually exclusive effects on nucleolar and nuclear morphologies. Lamins form structured polymers at the nuclear membrane as revealed by cryo-electron tomography and three-dimensional structured illumination microscopy (3D-SIM) (46, 59). Lamins homo- or heterodimerize *in vitro* via their rod domains (45). Lamin dimers form head-to-tail parallel polymers, which laterally associate to form stacks of lamin filaments (60). We surmise that the lamin B2 organization at the nuclear periphery is strikingly different from that at the nucleolar border, owing to its stable association with lamin A/C and B1 at the nuclear periphery (Fig. 4). The head domain of lamin B2 is required for the head-to-tail polymerization of lamin B2 dimers. Head domain deletion mutants of chicken lamin B2 and mouse lamin A do not form head-to-tail polymers *in vitro* (60, 61). However, in mammalian cells, lamin AΔHead did not localize at the nuclear periphery and showed nuclear aggregates, while lamin B1ΔHead correctly localized to the nuclear periphery, with no effect on endogenous lamins (62). This suggests the differential localization and function of the head domains of A-type and B-type lamins at the nuclear envelope. Interestingly, our studies suggest that the head domain of lamin B2 is required for maintaining nucleolar morphology but not nuclear morphology (Fig. 2 and 3).

It is possible that lamin B2 forms head-to-tail polymers at the nucleolar periphery in order to maintain the spherical morphology and discrete organization of the nucleolus. A possibility remains that the lamin B2ΔHead mutant heterodimerizes with endogenous lamin A/C or lamin B1 via its rod domain at the nuclear envelope, thereby rescuing the extent of nuclear blebs (63).

Nuclear rupture and nuclear blebs during cancer cell migration are enhanced upon lamin B2 depletion (64). Consistent with previous reports, nuclear blebs were enriched in regions of the nuclear membrane with reduced lamin B1 levels (Fig. 3B, arrowhead) (64). The tail domains of lamins with the CAAX motif and IgG fold are required for their integration into the nuclear membrane and interaction with emerin and histones (65–67). It is interesting that the relatively uncharacterized and unique amino acid stretch SLSATGR in the C-terminal region of lamin B2 modulates the formation of nuclear blebs (Fig. 3). This suggests that the SLSATGR sequence is required for the proper organization of the nuclear lamina, as its absence increases the propensity for nuclear blebs.

Lamin B2 associates with the nucleolus and interacts with nucleolar factors. The nucleolar localization sequence (NoLS) guides the localization of several ribosomal and nonribosomal proteins, such as human telomerase reverse transcriptase (hTERT) and fibroblast growth factor 3 (FGF-3), in the nucleolus (68–70). In addition to the NoLS, c-Myc protein for instance is recruited to the nucleolus via its interaction with NPM1 (71). Furthermore, NPM1 phase-separates and integrates into the nucleolus by interacting with RXn1R motif-containing proteins (22). Interestingly, we found several RXn1R motifs in lamin B2 that may facilitate its nucleolar localization. We propose that lamin B2 localized at the GC compartment functions as a barrier (Fig. 4A) and limits nucleolin mobility in and out of the nucleolus, since lamin B2 depletion was associated with increased rates of nucleolin recovery into nucleolin aggregates in the nucleoplasm (Fig. 6F). Nucleolin stability within the nucleolus is important, as its nucleoplasmic localization is associated with the degradation of p53 mRNA (72, 73).

Lamin B2 modulates nucleolin aggregation. The formation of interphase prenucleolar bodies (iPNBs) associated with unprocessed rRNA is induced in cells under hypotonic stress (74). Here, we show that the inhibition of RNA Pol I by Act D treatment induces the aggregation of nucleolin speckles in the nucleoplasm, which is further

enhanced upon lamin B2 depletion (Fig. 5A and F). We envisage three potential mechanisms by which loss of lamin B2 enhances nucleolin stability, i.e., (i) promoting self-oligomerization of nucleolin, (ii) stable association of nucleolin with other nucleolar proteins such as fibrillarin (Fig. 5D), or (iii) nucleolin-RNA complex formation (Fig. 7E), collectively resulting in the prolonged stability of nucleolin aggregates (72, 75).

Cellular stresses such as acidosis are associated with the expression of noncoding RNAs from intergenic rDNA sites that sequester stress-responsive proteins such as HSP70 and VHL in the nucleolus (55). An increase in the expression levels of IGS RNA in lamin B2-depleted cells is suggestive of cellular stress (Fig. 7C and D). The enhanced colocalization of nucleolin with IGS RNA upon Act D treatment in lamin B2-depleted cells suggests the stabilization of the nucleolin-IGS RNA complex (Fig. 7E and F). This is consistent with the faster recovery of nucleolin into the aggregates (Fig. 6F), potentially due to its affinity to IGS RNA. Nucleolin mobility and sequestration into the nucleolus are also modulated by ncRNAs such as Alu RNA and intergenic RNAs expressed upon acidosis (75). We surmise that the RNA binding domains of nucleolin regulate nucleolin-RNA dynamics in a lamin B2-dependent manner (76).

Lamin B2 regulates rRNA expression. rRNA expression is stringently regulated in cells (77, 78). Our assays reveal that 45S rRNA expression levels are elevated upon lamin B2 depletion (Fig. 7B). However, lamin B2 depletion also enhances expression levels of IGS RNA (Fig. 7C and D). Therefore, the regulatory role of lamin B2 also extends to the upstream regions of pre-rRNA and is not limited to the pre-rRNA promoter. A tempting possibility is the decondensation of rDNA clusters in the absence of lamin B2, which otherwise associate with heterochromatin binding factors such as HP1 and MacroH2A (79, 80). Consistent with these findings, the loss of MacroH2A.1 disrupts nucleoli and upregulates 45S rRNA, effects that are similar to those of lamin B2 depletion (80–82). It is conceivable that lamin B2 may modulate the recruitment of nucleolin or MacroH2A.1, which are enriched on the rDNA promoter regions as revealed by chromatin immunoprecipitation (ChIP) (83). Effectively, the concerted association of lamin B2 with activators of rDNA transcription such as nucleolin or repressors such as MacroH2A is likely to regulate rDNA transcription.

Our studies reveal a novel and unique role for lamin B2, and its head domain in particular, in maintaining nucleolar structure. Lamin B2 depletion therefore modulates nucleolar morphology, alters nucleoplasmic dynamics of nucleolin, and elevates nucleolar transcripts (Fig. 8). Taken together, our studies implicate lamin B2 as a unique orchestrator of the structural and functional organization of the nucleolus.

MATERIALS AND METHODS

Cell lines, cell culture, and transfections. DLD-1 colorectal adenocarcinoma cells (a gift from Thomas Ried, NCI/NIH, USA), were grown in RPMI medium (Gibco, 11875) supplemented with penicillin (100 units/ml)-streptomycin (100 μg/ml) (Gibco, 15070-063) and 10% heat-inactivated fetal bovine serum (FBS) (Gibco, 6140). Cells were cultured at 37°C in the presence of 5% CO_2. We repeatedly validated DLD-1 cells across passages by karyotyping and consistently found near-diploid chromosome numbers (44–46) (data not shown). We ensured that all cultures were free of *Mycoplasma*.

Transient siRNA transfections were performed using Lipofectamine RNAimax reagent (Invitrogen, 13778) in reduced serum Opti-MEM (Gibco, 31985) for 6 h, after which cells were transferred to complete medium and incubated for 48 h. Cells were transfected with plasmids using Lipofectamine LTX with Plus reagent (Invitrogen, 15338-100) or Trans-IT 2020 (Mirus). Green fluorescent protein (GFP)-nucleolin, lamin B2-mCherry, and lamin B2-GFP constructs were kind gifts from Sui Huang and T. Tomonaga (41, 52). Lamin B2 ΔHead and ΔSLS deletion mutants were generated from the lamin B2-GFP construct by two consecutive PCRs and cloned into the pEGFP-N1 vector. The siRNA-resistant lamin B2-GFP plasmids was generated by site-directed mutagenesis (SDM). For experiments requiring both siRNA and plasmid DNA, transfections were performed sequentially; siRNA transfection was performed as mentioned above, DNA transfections were performed after 24 h, and cells were processed after 48 h. The siRNAs used are listed in Table 1.

Act D treatment. Cells were treated with 0.05 μg/ml actinomycin D (Act D) in complete medium for 4 h at 37°C with 5% CO_2 after which they were lysed to obtain RNA or protein. Equivalent volumes of dimethyl sulfoxide (DMSO) were used as vehicle controls. Similarly, cells were treated with Act D and fixed for immunofluorescence, or live cells were imaged using confocal microscopy.

Immunofluorescence assay (IFA). Adherent DLD-1 cells were washed twice in 1× phosphate-buffered saline (PBS) (pH 7.4), permeabilized for 5 min with CSK buffer [0.1 M NaCl, 0.3 M sucrose, 3 mM $MgCl_2$, 10 mM piperazine-*N*,*N*′-bis(2-ethanesulfonic acid) (PIPES) (pH 7.4), 0.5% Triton X-100] on ice, fixed

TABLE 1 siRNAs and primers used in this study

siRNA or primer(s)	Sequence(s)
siRNAs	
siLMNB2	5′-GAGCAGGAGAUGACGGAGA-3′
siLMNA/C	5′-CAGUCUGCUGAGAGGAACA-3′
siCtrl1 (LMNB2 scramble)	5′-GGAAGCGUAGACGGAAGAG-3′
siCtrl2 (LacZ)	5′-CGUACGCGGAAUACUUCGA-3′
siCtrl3 (LMNA/C scramble)	5′-GGAGGUCGAGCCAAUAUCA-3′
siLMNB2.2	5′-CCAAGAAGAGGGAGGGCGA-3′
siLMNB2.3	5′-GGAAGAGUGUGUUCGAGGA-3′
Primers	
SDM primer for generating si*LMNB2-GFP	Sense, 5′-ATGCTGGACGCCAAGGAACAAGAAATGACAGAAATGCGGGACGTGATGCA-3′; antisense, 5′-TGCATCACGTCCCGCATTTCTGTCATTTCTTGTTCCTTGGCGTCCAGCAT-3′
Primers for generating lamin B2ΔHead mutant	Sense, 5′-CGAGCTCAAGCTTATATGGAGCTGCGCGAGC-3′; antisense, 5′-GCTCGCGCAGCTCCATATAAGCTTGAGCTCG-3′
Primers for generating lamin B2ΔSLS mutant	Sense, 5′-GCAGCAGCGGCCTGGGCCGCAG-3′; antisense, 5′-CTGCGGCCCAGGCCGCTGCTGC-3′
CMV F	Forward, 5′-CGCAAATGGGCGGTAGGCGTG-3′
EGFP R	Forward, 5′-CGTCGCCGTCCAGCTCGACCAG-3′
LMNB2	Forward, 5′-AGTTCACGCCCAAGTACATC-3′; reverse, 5′-CTTCACAGTCCTCATGGCC-3′
45S	Forward, 5′-GAACGGTGGTGTGTCGTT-3′; reverse, 5′-GCGTCTCGTCTCGTCTCACT-3′
28S	Forward, 5′-AGAGGTAAACGGGTGGGGTC-3′; reverse, 5′-GGGGTCGGGAGGAACGG-3′
18S	Forward, 5′-GATGGTAGTCGCCGTGCC-3′; reverse, 5′-GCCTGCTGCCTTCCTTGG-3′
MALAT1	Forward, 5′-GACGGAGGTTGAGATGAAGC-3′; reverse, 5′-ATTCGGGGCTCTGTAGTCCT-3′

in 4% paraformaldehyde (PFA) (Sigma, P6148) for 10 min, and repermeabilized in 0.5% Triton X-100 for 10 min. Cells were blocked in 1% bovine serum albumin (BSA) (Sigma, A2153) for 30 min and incubated with primary antibody (diluted in 0.5% BSA) for 1.5 h and with secondary antibodies (diluted in 1× PBS plus 0.1% Triton X-100 [PBST]) for 1 h. Cells were washed thrice in 1× PBS in between antibody incubations. Cells were counterstained with DAPI (4′,6′-diamidino-2-phenylindole) and mounted in SlowFade gold antifade (Invitrogen, S36937). The antibodies used are listed in Table 2.

Western blotting and co-IP. SDS-PAGE and immunoblotting were performed as per standard protocols. Lysates were prepared in radioimmunoprecipitation assay (RIPA) buffer containing 1× protease inhibitory cocktail (PIC) (Roche), and the protein concentration was estimated using a bicinchoninic

TABLE 2 Antibodies used in this study

Antibody	Purpose	Dilution or amt
Antinucleolin (ab13541)	IFA	1:300
Antinucleolin (ab22758)	IFA	1:500
	Western blotting	1:2,000
	IP	2 μg
Antinucleolin (ab50279)	Immuno-RNA-FISH	1:500
Anti-lamin A/C (Epitomics, 2966S)	IFA	1:600
	Western blotting	1:5,000
Anti-lamin A/C (ab40567)	IFA	1:50
	Western blotting	1:200
Anti-lamin B2 (ab8983)	IFA	1:400
	Western blotting	1:400
Antifibrillarin (ab5821)	IFA	1:500
Antinucleophosmin (ab37659)	Western blotting	1:1,000
	IP	2 μg
Anti-p84 (ab487)	IFA	1:500
Antinucleophosmin (ab10530)	Western blotting	1:500
Antiactin	Western blotting	1:400
Anti-GAPDH	Western blotting	1:5,000
Anti-rabbit antibody–Alexa Fluor 488	IFA	1:1,000
Anti-rabbit antibody–Alexa Fluor 568	IFA	1:1,000
Anti-mouse antibody–Alexa Fluor 488	IFA	1:1,000
Anti-mouse antibody–Alexa Fluor 568	IFA	1:1,000
Anti-mouse antibody–Alexa Fluor 633	IFA	1:1,000
Donkey anti-rabbit antibody–horseradish peroxidase (GE, NA9340V)	Western blotting	1:10,000
Sheep anti-mouse antibody–horseradish peroxidase (GE, NA9310V)	Western blotting	1:10,000
Normal rabbit IgG	IP	2 μg

acid (BCA) kit (Pierce, 23225). Proteins were resolved by 10% SDS-PAGE and transferred to Immobilon-P membranes (GE). Blots were blocked in 5% nonfat dry milk. The blots were incubated with primary antibodies for 3 h at room temperature or overnight at 4°C, followed by incubation with secondary antibodies for 1 h at room temperature. Immunoblots were developed using the chemiluminescent substrate ECL Prime (GE, 89168-782) and imaged with ImageQuant LAS4000. The antibodies used are listed in Table 2.

For coimmunoprecipitation (Co-IP) assays, ~10^7 cells (DLD-1) were lysed in co-IP lysis buffer (50 mM Tris [pH 7.4], 150 mM NaCl, 0.5% NP-40, 1× PIC) vortexed and incubated on ice for 15 min, and centrifuged at 12,000 rpm and 4°C for 10 min. The lysate was precleared by incubating with Dynabeads protein A (Invitrogen, 10002D) for 1 h. Two micrograms of specific antibody or normal rabbit IgG was incubated with lysates overnight at 4°C. Protein A beads, preblocked with 0.5% BSA, were incubated with the immunocomplex for 2 to 3 h. Beads were washed 6 times with co-IP lysis buffer (plus 0.5 mM phenylmethylsulfonyl fluoride [PMSF]) to minimize nonspecific binding. Bound protein was eluted from the beads by boiling in 2× Laemmli buffer for 15 min at 95°C.

Nucleolar isolation and immunostaining. Nucleolar isolation was performed as described previously (84). Briefly ~10^7 cells (DLD-1) were washed and scraped in ice-cold solution I (0.5 ml; 0.5 M sucrose with 3 mM magnesium chloride [$MgCl_2$] and 1× PIC). Cells were sonicated 5 times at 50% amplitude, 10 s on and 10 s off, on ice (Sonics Vibracell), layered over solution II (0.7 ml, 1.0 M sucrose, 3 mM $MgCl_2$), an centrifuged at 1,800 × *g* for 5 min at 4°C. The supernatant was removed carefully. The nucleolar pellet was resuspended in 1× PBS, spotted on glass slides, air dried, and fixed with 4% PFA for 20 min. Nucleoli were blocked in 1% BSA for 60 min at room temperature and incubated with primary antibody and secondary antibodies for 30 min each, followed by three extensive washes with 1× PBST. The primary and secondary antibodies used were diluted in 1% BSA in 1× PBST. The preparation was mounted in DAPI-antifade. For lamin B2 knockdown, nucleoli were isolated by pooling cells from 3 independent wells of a 6-well plate.

Nuclear matrix preparation. Nuclear matrix was prepared from DLD-1 cells as previously described (85). DLD-1 cells grown on coverslips were washed thrice in ice-cold cytoskeletal buffer (10 mM PIPES [pH 6.8], 10 mM KCl, 300 mM sucrose, 3 mM $MgCl_2$, 1 mM EDTA, 0.05 mM PMSF, 1× PIC) and then incubated for 10 min in CSK buffer containing 0.5% Triton X-100 at 4°C. Cells were rinsed thrice in ice-cold RSB buffer (42.5 mM Tris-HCl [pH 8.3], 8.5 mM NaCl, 2.6 mM $MgCl_2$, 0.05 mM PMSF, 1× PIC) and incubated for 10 min in RSB buffer containing 1% (vol/vol) Tween 20 and 0.5% (vol/vol) sodium deoxycholate at 4°C. Cells were rinsed twice in ice-cold digestion buffer (10 mM PIPES [pH 8.3], 50 mM NaCl, 300 mM sucrose, 3 mM $MgCl_2$, 1 mM EGTA, 0.05 mM PMSF, 1× PIC) and then incubated for 30 min in digestion buffer containing 100 U/ml DNase I (Roche) at 30°C. Ammonium sulfate (1 M) was added to the cells to a final concentration of 0.25 M and incubated for 5 min to remove digested chromatin, followed by two washes in ice-cold digestion buffer. Cells were incubated in 2 M NaCl for 5 min at 4°C, washed twice in digestion buffer, fixed in 4% PFA, and immunostained.

Microscopy. Cells were imaged on Zeiss LSM710 and LSM780 confocal microscopes with 405-nm, 488-nm, and 561-nm laser lines using a 63× Plan-Apochromat 1.4-numerical-aperture (NA) oil immersion objective at 2.0 to 2.5× digital zoom. Scanning was performed sequentially (*x-y*, 512 pixels by 512 pixels [1 pixel ~ 0.105 μm]), and z-stacks were collected at a step size of 0.34 μm and a pinhole size of ~0.7 μm (1 arbitrary unit [AU]). The pixel depth was 8 bits, the line averaging was 2, and the scan speed was 10. For superresolution imaging of isolated nucleoli, a Zeiss LSM800 with an Airyscan detector was used. For immuno-RNA-FISH experiments, fixed cells were imaged using a Leica TCS Sp8 microscope (*x-y*, 512 pixels by 512 pixels; *z*, 0.34 μm; frame averaging, 2; scan frequency, 400 Hz).

Imaging and scoring of nucleolar morphologies. Images were captured based on several random fields using DAPI staining and the extent of lamin knockdown in each nucleus. Nucleolar morphology was scored by inspecting nucleolin staining. Nucleoli were visually inspected across a number of independent nuclei. Intact nucleoli were spherical and discrete, whereas disrupted nucleoli were irregular aggregates.

Live imaging of cells and FRAP analysis. A Zeiss LSM710 or LSM780 confocal microscope equipped with a heated stage at 37°C was used for all photobleaching experiments and fluorescence image acquisitions. For live imaging, cells were grown on a 22- by 22-mm^2 coverslip glued onto a 35-mm petri dish coated with 100 μg/ml collagen (BD Biosciences; 354236); CO_2-independent Leibovitz L-15 medium (Gibco; 21083-027) was used during microscopy. To visualize nucleolin aggregates, cells were treated with Act D and imaged. z-stacks (~0.34 μm) of cells were acquired every 1.3 min.

For fluorescence recovery after photobleaching (FRAP) analysis, images were acquired using a 63× oil immersion objective, NA 1.4 at 2.5× digital zoom, at 2% laser power to avoid photobleaching. A 1- by 1-pixel square (1 pixel = 0.11 μm) region of interest (ROI) was used for bleaching nucleolin speckles. Ten images were acquired before photobleaching. Photobleaching was performed using 200 iterations of the 488-nm laser line at 100% power. Images were collected every 484 ms for a total duration of 25 s. Images were analyzed using the Zen 2011 FRAP analysis module, and relative fluorescence intensity (RFI) was calculated as (86) $RFI = \{[ROI1(t) - ROI3(t)]/[ROI2(t) - ROI3(t)]\} \times \{[ROI2(t = 0) - ROI3(t = 0)]/[ROI1(t = 0) - ROI3(t = 0)]\}$, where ROI1 is the fluorescence intensity of the 1- by 1-pixel ROI that is bleached, ROI2 is the total nucleus fluorescence intensity, and ROI3 is the fluorescence intensity of a 1- by 1-pixel background region selected outside the nucleus. ROI1(*t*) denotes the postbleach fluorescence intensity at time *t*. ROI2(*t*) and ROI3(*t*) denote the same for the total nucleus and background, respectively. ROI1($t = 0$) denotes the average prebleach fluorescence intensity. ROI2($t = 0$) and ROI3($t = 0$) denote the same for the whole nucleus and background, respectively. The double-normalized data were transformed on a scale of 0 to 1. Mobile fractions and $t_{1/2}$ were calculated by fitting the normalized data (without transformation) with double-exponential fit using easyFRAP software (87).

qRT-PCR analysis. RNA was prepared by lysing cells in TRIzol (Applied Biosciences) and phenol-chloroform extraction. cDNA was synthesized using the ImProm II reverse transcriptase system (Promega A3800). Quantitative real-time PCR (qRT-PCR) was performed using SYBR green (SAF Labs). The primers used are listed in Table 1. Actin served as an internal control.

RNA-FISH and 3D-immuno-RNA-FISH. (i) Fixation. RNA-FISH was performed as described previously (88). All reagents for RNA-FISH were prepared in diethyl pyrocarbonate (DEPC)-treated water and supplemented with 2 mM vanadyl ribonucleoside complex (New England BioLabs). Briefly, cells were washed with 1× PBS, permeabilized with CSK buffer on ice for 5 min, fixed in 4% PFA for 10 min, and stored in 70% ethanol at −20°C until hybridization. For 3D-immuno-RNA-FISH, after fixation in 4% PFA, cells were permeabilized with 0.5% Triton X-100 in PBS, and immunostaining was performed as described earlier (88). Cells were postfixed in 4% PFA for 10 min and washed twice with 2× SSC (1× SSC is 0.15 M NaCl plus 0.015 M sodium citrate), followed by hybridization.

(ii) FISH probe labeling. RNA-FISH probes for the ~12-kbp intergenic sequence (IGS) upstream of the rDNA start site was prepared by nick translation of the pUC9-rDNA vector (a gift from Brian McStay) with Spectrum Red-conjugated dUTP, using DNase I (5 mU/μl)-DNA polymerase I (50 mU/μl) (Roche) for 3 h at 15°C. Six micrograms of nick-translated probe was precipitated overnight at −20°C with 20 μg human Cot1 DNA (Invitrogen) and 40 μg salmon sperm DNA (Invitrogen) using cold 100% ethanol and 1/10 volume of 3 M sodium acetate. The probe was resuspended in deionized formamide at 37°C. Prior to hybridization, the probe was denatured at 80°C for 5 min, followed by addition of an equal volume of 2× hybridization mix containing 2 mM vanadyl ribonucleoside and incubation on ice for 30 min.

(iii) Hybridization and washes. Cells for RNA-FISH were dehydrated in an ethanol series (70%, 90%, and 100% ethanol) and air dried. Approximately 1 μg of probe (~4 to 6 μl) was spotted on an RNase-free slide, and cells on coverslips were inverted on the probe and sealed using nail varnish. Hybridization was carried out for 16 h at 37°C. Coverslips were washed thrice in 50% formamide–2× SSC (pH 7.2), followed by three washes in 2× SSC (pH 7.2), for 5 min each at 42°C and mounted in DAPI-antifade.

Image processing and analysis. 3D volume rendering and analysis of nuclei and nucleoli were performed using Image Pro Plus v7.1. Volume measurements of nucleolin speckles were performed using the ImageJ object counter 3D plugin. Colocalization analysis was performed using the JACOP plugin from ImageJ (89). 4D time-lapse images were analyzed using Imaris 8.0.0.

Statistical analysis and graphs. Statistical analyses were performed for each experiment as described in the figure legends, and graphs were plotted using GraphPad Prism 5 software; a P value of <0.05 was considered significant. We imaged and analyzed a minimum of 20 to 30 cells for each biological replicate in fixed preparations, while a minimum of 2 or 3 nuclei were tracked and analyzed during prolonged live imaging of nucleolin speckles. In the figures and legends, N is the number of independent biological replicates and n is as defined for each figure.

SUPPLEMENTAL MATERIAL

Supplemental material for this article may be found at https://doi.org/10.1128/MCB.00274-17.

SUPPLEMENTAL FILE 1, MP4 file, 8.6 MB.

SUPPLEMENTAL FILE 2, MP4 file, 1.5 MB.

SUPPLEMENTAL FILE 3, MP4 file, 2.0 MB.

ACKNOWLEDGMENTS

We gratefully acknowledge IISER, Pune, for facilities. We acknowledge the microscopy facility of IISER, Pune. We thank Carl Zeiss India for the usage of the superresolution Airyscan microscope. We thank Sanjeev Galande for sharing reagents. We thank Chromosome Biology Lab members and Richa Rikhy for critical inputs during experiments and writing of the manuscript.

A.S.G. thanks CSIR, New Delhi, for a senior research fellowship. K.S. thanks IISER, Pune, for intramural funding and the Wellcome Trust-Department of Biotechnology India Alliance Intermediate Fellowship for extramural funding (award no. 500164/Z/09/Z).

A.S.G. and K.S. designed the experiments. A.S.G. performed the experiments, analyzed the data, and prepared the figures. A.S.G. and K.S. wrote the manuscript.

We declare that we have no competing interests.

REFERENCES

1. Leary DJ, Huang S. 2001. Regulation of ribosome biogenesis within the nucleolus. FEBS Lett 509:145–150. https://doi.org/10.1016/S0014-5793(01)03143-X.
2. Hernandez-Verdun D. 2011. Assembly and disassembly of the nucleolus during the cell cycle. Nucleus 2:189–194. https://doi.org/10.4161/nucl.2.3.16246.
3. Dundr M, Misteli T, Olson MO. 2000. The dynamics of postmitotic reassembly of the nucleolus. J Cell Biol 150:433–446. https://doi.org/10.1083/jcb.150.3.433.
4. Derenzini M, Montanaro L, Treré D. 2009. What the nucleolus says to a tumour pathologist. Histopathology 54:753–762. https://doi.org/10.1111/j.1365-2559.2008.03168.x.

5. Isaac C, Marsh KL, Paznekas WA, Dixon J, Dixon MJ, Jabs EW, Meier UT. 2000. Characterization of the nucleolar gene product, treacle, in Treacher Collins syndrome. Mol Biol Cell 11:3061–3071. https://doi.org/10.1091/mbc.11.9.3061.
6. Cheutin T, O'Donohue M-F, Beorchia A, Vandelaer M, Kaplan H, Deféver B, Ploton D, Thiry M. 2002. Three-dimensional organization of active rRNA genes within the nucleolus. J Cell Sci 115:3297–3307.
7. Shav-Tal Y, Blechman J, Darzacq X, Montagna C, Dye BT, Patton JG, Singer RH, Zipori D. 2005. Dynamic sorting of nuclear components into distinct nucleolar caps during transcriptional inhibition. Mol Biol Cell 16:2395–2413. https://doi.org/10.1091/mbc.E04-11-0992.
8. Tsang CK, Bertram PG, Ai W, Drenan R, Zheng XFS. 2003. Chromatin-mediated regulation of nucleolar structure and RNA Pol I localization by TOR. EMBO J 22:6045–6056. https://doi.org/10.1093/emboj/cdg578.
9. Mayer C, Zhao J, Yuan X, Grummt I. 2004. mTOR-dependent activation of the transcription factor TIF-IA links rRNA synthesis to nutrient availability. Genes Dev 18:423–434. https://doi.org/10.1101/gad.285504.
10. van Sluis M, McStay B. 2015. A localized nucleolar DNA damage response facilitates recruitment of the homology-directed repair machinery independent of cell cycle stage. Genes Dev 29:1151–1163. https://doi.org/10.1101/gad.260703.115.
11. Mekhail K, Rivero-Lopez L, Khacho M, Lee S. 2006. Restriction of rRNA synthesis by VHL maintains energy equilibrium under hypoxia. Cell Cycle 5:2401–2413. https://doi.org/10.4161/cc.5.20.3387.
12. Nguyen LXT, Raval A, Garcia JS, Mitchell BS. 2015. Regulation of ribosomal gene expression in cancer. J Cell Physiol 230:1181–1188. https://doi.org/10.1002/jcp.24854.
13. Neuburger M, Herget GW, Plaumann L, Falk A, Schwalb H, Adler CP. 1998. Change in size, number and morphology of the nucleoli in human hearts as a result of hyperfunction. Pathol Res Pract 194:385–389. https://doi.org/10.1016/S0344-0338(98)80028-9.
14. Ribeiro CV, Vasconcelos AC, Andrade Filho JDS. 2015. Apoptosis and expression of argyrophilic nucleolus organizer regions in epithelial neoplasms of the larynx. Braz J Otorhinolaryngol 81:158–166. https://doi.org/10.1016/j.bjorl.2014.12.003.
15. Wandrey F, Montellese C, Koos K, Badertscher L, Bammert L, Cook AG, Zemp I, Horvath P, Kutay U. 2015. The NF45/NF90 heterodimer contributes to the biogenesis of 60S ribosomal subunits and influences nucleolar morphology. Mol Cell Biol 35:3491–3503. https://doi.org/10.1128/MCB.00306-15.
16. Nicolas E, Parisot P, Pinto-Monteiro C, de Walque R, De Vleeschouwer C, Lafontaine DLJ. 2016. Involvement of human ribosomal proteins in nucleolar structure and p53-dependent nucleolar stress. Nat Commun 7:11390. https://doi.org/10.1038/ncomms11390.
17. Ahmad Y, Boisvert F-M, Gregor P, Cobley A, Lamond AI. 2009. NOPdb: Nucleolar Proteome Database—2008 update. Nucleic Acids Res 37:D181–D184. https://doi.org/10.1093/nar/gkn804.
18. Grob A, Colleran C, McStay B. 2014. Construction of synthetic nucleoli in human cells reveals how a major functional nuclear domain is formed and propagated through cell division. Genes Dev 28:220–230. https://doi.org/10.1101/gad.234591.113.
19. Ma N, Matsunaga S, Takata H, Ono-Maniwa R, Uchiyama S, Fukui K. 2007. Nucleolin functions in nucleolus formation and chromosome congression. J Cell Sci 120:2091–2105. https://doi.org/10.1242/jcs.008771.
20. Amin MA, Matsunaga S, Uchiyama S, Fukui K. 2008. Depletion of nucleophosmin leads to distortion of nucleolar and nuclear structures in HeLa cells. Biochem J 415:345–351. https://doi.org/10.1042/BJ20081411.
21. Kozakai Y, Kamada R, Furuta J, Kiyota Y, Chuman Y, Sakaguchi K. 2016. PPM1D controls nucleolar formation by up-regulating phosphorylation of nucleophosmin. Sci Rep 6:33272. https://doi.org/10.1038/srep33272.
22. Mitrea DM, Cika JA, Guy CS, Ban D, Banerjee PR, Stanley CB, Nourse A, Deniz AA, Kriwacki RW. 2016. Nucleophosmin integrates within the nucleolus via multi-modal interactions with proteins displaying R-rich linear motifs and rRNA. eLife 5:e13571. https://doi.org/10.7554/eLife.13571.
23. Feric M, Vaidya N, Harmon TS, Mitrea DM, Zhu L, Richardson TM, Kriwacki RW, Pappu RV, Brangwynne CP. 2016. Coexisting liquid phases underlie nucleolar subcompartments. Cell 165:1686–1697. https://doi.org/10.1016/j.cell.2016.04.047.
24. Andersen JS, Lam YW, Leung AKL, Ong S-E, Lyon CE, Lamond AI, Mann M. 2005. Nucleolar proteome dynamics. Nature 433:77–83. https://doi.org/10.1038/nature03207.
25. Nickerson JA, Krockmalnic G, Wan KM, Penman S. 1997. The nuclear matrix revealed by eluting chromatin from a cross-linked nucleus. Proc Natl Acad Sci U S A 94:4446–4450. https://doi.org/10.1073/pnas.94.9.4446.
26. Prokocimer M, Davidovich M, Nissim-Rafinia M, Wiesel-Motiuk N, Bar DZ, Barkan R, Meshorer E, Gruenbaum Y. 2009. Nuclear lamins: key regulators of nuclear structure and activities. J Cell Mol Med 13:1059–1085. https://doi.org/10.1111/j.1582-4934.2008.00676.x.
27. Eckersley-Maslin MA, Bergmann JH, Lazar Z, Spector DL. 2013. Lamin A/C is expressed in pluripotent mouse embryonic stem cells. Nucleus 4:53–60. https://doi.org/10.4161/nucl.23384.
28. Constantinescu D, Gray HL, Sammak PJ, Schatten GP, Csoka AB. 2006. Lamin A/C expression is a marker of mouse and human embryonic stem cell differentiation. Stem Cells 24:177–185. https://doi.org/10.1634/stemcells.2004-0159.
29. Moir RD, Montag-Lowy M, Goldman RD. 1994. Dynamic properties of nuclear lamins: lamin B is associated with sites of DNA replication. J Cell Biol 125:1201–1212. https://doi.org/10.1083/jcb.125.6.1201.
30. Camps J, Wangsa D, Falke M, Brown M, Case CM, Erdos MR, Ried T. 2014. Loss of lamin B1 results in prolongation of S phase and decondensation of chromosome territories. FASEB J 28:3423–3434. https://doi.org/10.1096/fj.14-250456.
31. Bronshtein I, Kepten E, Kanter I, Berezin S, Lindner M, Redwood AB, Mai S, Gonzalo S, Foisner R, Shav-Tal Y, Garini Y. 2015. Loss of lamin A function increases chromatin dynamics in the nuclear interior. Nat Commun 6:8044. https://doi.org/10.1038/ncomms9044.
32. Mahen R, Hattori H, Lee M, Sharma P, Jeyasekharan AD, Venkitaraman AR. 2013. A-type lamins maintain the positional stability of DNA damage repair foci in mammalian nuclei. PLoS One 8:e61893. https://doi.org/10.1371/journal.pone.0061893.
33. Matsumoto A, Sakamoto C, Matsumori H, Katahira J, Yasuda Y, Yoshidome K, Tsujimoto M, Goldberg IG, Matsuura N, Nakao M, Saitoh N, Hieda M. 2016. Loss of the integral nuclear envelope protein SUN1 induces alteration of nucleoli. Nucleus 7:68–83. https://doi.org/10.1080/19491034.2016.1149664.
34. Buchwalter A, Hetzer MW. 2017. Nucleolar expansion and elevated protein translation in premature aging. Nat Commun 8:328. https://doi.org/10.1038/s41467-017-00322-z.
35. Martin C, Chen S, Maya-Mendoza A, Lovric J, Sims PFG, Jackson DA. 2009. Lamin B1 maintains the functional plasticity of nucleoli. J Cell Sci 122:1551–1562. https://doi.org/10.1242/jcs.046284.
36. Louvet E, Yoshida A, Kumeta M, Takeyasu K. 2014. Probing the stiffness of isolated nucleoli by atomic force microscopy. Histochem Cell Biol 141:365–381. https://doi.org/10.1007/s00418-013-1167-9.
37. Coffinier C, Jung H-J, Nobumori C, Chang S, Tu Y, Barnes RH, Yoshinaga Y, de Jong PJ, Vergnes L, Reue K, Fong LG, Young SG. 2011. Deficiencies in lamin B1 and lamin B2 cause neurodevelopmental defects and distinct nuclear shape abnormalities in neurons. Mol Biol Cell 22:4683–4693. https://doi.org/10.1091/mbc.E11-06-0504.
38. Chen C-Y, Chi Y-H, Mutalif RA, Starost MF, Myers TG, Anderson SA, Stewart CL, Jeang K-T. 2012. Accumulation of the inner nuclear envelope protein Sun1 is pathogenic in progeric and dystrophic laminopathies. Cell 149:565–577. https://doi.org/10.1016/j.cell.2012.01.059.
39. Ranade D, Koul S, Thompson J, Prasad KB, Sengupta K. 2017. Chromosomal aneuploidies induced upon lamin B2 depletion are mislocalized in the interphase nucleus. Chromosoma 126:223–244. https://doi.org/10.1007/s00412-016-0580-y.
40. Swift J, Ivanovska IL, Buxboim A, Harada T, Dingal PCDP, Pinter J, Pajerowski JD, Spinler KR, Shin J-W, Tewari M, Rehfeldt F, Speicher DW, Discher DE. 2013. Nuclear lamin-A scales with tissue stiffness and enhances matrix-directed differentiation. Science 341:1240104. https://doi.org/10.1126/science.1240104.
41. Kuga T, Nie H, Kazami T, Satoh M, Matsushita K, Nomura F, Maeshima K, Nakayama Y, Tomonaga T. 2014. Lamin B2 prevents chromosome instability by ensuring proper mitotic chromosome segregation. Oncogenesis 3:e94. https://doi.org/10.1038/oncsis.2014.6.
42. Ginisty H, Sicard H, Roger B, Bouvet P. 1999. Structure and functions of nucleolin. J Cell Sci 112:761–772.
43. Parry DA, Conway JF, Steinert PM. 1986. Structural studies on lamin. Similarities and differences between lamin and intermediate-filament proteins. Biochem J 238:305–308.
44. Stuurman N, Heins S, Aebi U. 1998. Nuclear lamins: their structure, assembly, and interactions. J Struct Biol 122:42–66. https://doi.org/10.1006/jsbi.1998.3987.
45. Heitlinger E, Peter M, Häner M, Lustig A, Aebi U, Nigg EA. 1991. Expression of chicken lamin B2 in Escherichia coli: characterization of its

structure, assembly, and molecular interactions. J Cell Biol 113:485–495. https://doi.org/10.1083/jcb.113.3.485.
46. Shimi T, Kittisopikul M, Tran J, Goldman AE, Adam SA, Zheng Y, Jaqaman K, Goldman RD. 2015. Structural organization of nuclear lamins A, C, B1, and B2 revealed by superresolution microscopy. Mol Biol Cell 26: 4075–4086. https://doi.org/10.1091/mbc.E15-07-0461.
47. Adam SA, Butin-Israeli V, Cleland MM, Shimi T, Goldman RD. 2013. Disruption of lamin B1 and lamin B2 processing and localization by farnesyltransferase inhibitors. Nucleus 4:142–150. https://doi.org/10.4161/nucl.24089.
48. Kumaran RI, Muralikrishna B, Parnaik VK. 2002. Lamin A/C speckles mediate spatial organization of splicing factor compartments and RNA polymerase II transcription. J Cell Biol 159:783–793. https://doi.org/10.1083/jcb.200204149.
49. Hozák P, Sasseville AM, Raymond Y, Cook PR. 1995. Lamin proteins form an internal nucleoskeleton as well as a peripheral lamina in human cells. J Cell Sci 108:635–644.
50. Li YP, Busch RK, Valdez BC, Busch H. 1996. C23 interacts with B23, a putative nucleolar-localization-signal-binding protein. Eur J Biochem 237:153–158. https://doi.org/10.1111/j.1432-1033.1996.0153n.x.
51. Borer RA, Lehner CF, Eppenberger HM, Nigg EA. 1989. Major nucleolar proteins shuttle between nucleus and cytoplasm. Cell 56:379–390. https://doi.org/10.1016/0092-8674(89)90241-9.
52. Chen D, Huang S. 2001. Nucleolar components involved in ribosome biogenesis cycle between the nucleolus and nucleoplasm in interphase cells. J Cell Biol 153:169–176. https://doi.org/10.1083/jcb.153.1.169.
53. Santoro R, Schmitz K-M, Sandoval J, Grummt I. 2010. Intergenic transcripts originating from a subclass of ribosomal DNA repeats silence ribosomal RNA genes in trans. EMBO Rep 11:52–58. https://doi.org/10.1038/embor.2009.254.
54. Zhao Z, Dammert MA, Hoppe S, Bierhoff H, Grummt I. 2016. Heat shock represses rRNA synthesis by inactivation of TIF-IA and lncRNA-dependent changes in nucleosome positioning. Nucleic Acids Res 44: 8144–8152. https://doi.org/10.1093/nar/gkw496.
55. Audas TE, Jacob MD, Lee S. 2012. Immobilization of proteins in the nucleolus by ribosomal intergenic spacer noncoding RNA. Mol Cell 45:147–157. https://doi.org/10.1016/j.molcel.2011.12.012.
56. Dechat T, Pfleghaar K, Sengupta K, Shimi T, Shumaker DK, Solimando L, Goldman RD. 2008. Nuclear lamins: major factors in the structural organization and function of the nucleus and chromatin. Genes Dev 22: 832–853. https://doi.org/10.1101/gad.1652708.
57. Brangwynne CP, Mitchison TJ, Hyman AA. 2011. Active liquid-like behavior of nucleoli determines their size and shape in Xenopus laevis oocytes. Proc Natl Acad Sci U S A 108:4334–4339. https://doi.org/10.1073/pnas.1017150108.
58. Feric M, Brangwynne CP. 2013. A nuclear F-actin scaffold stabilizes ribonucleoprotein droplets against gravity in large cells. Nat Cell Biol 15:1253–1259. https://doi.org/10.1038/ncb2830.
59. Turgay Y, Eibauer M, Goldman AE, Shimi T, Khayat M, Ben-Harush K, Dubrovsky-Gaupp A, Sapra KT, Goldman RD, Medalia O. 2017. The molecular architecture of lamins in somatic cells. Nature 543:261–264. https://doi.org/10.1038/nature21382.
60. Heitlinger E, Peter M, Lustig A, Villiger W, Nigg EA, Aebi U. 1992. The role of the head and tail domain in lamin structure and assembly: analysis of bacterially expressed chicken lamin A and truncated B2 lamins. J Struct Biol 108:74–89. https://doi.org/10.1016/1047-8477(92)90009-Y.
61. Isobe K, Gohara R, Ueda T, Takasaki Y, Ando S. 2007. The last twenty residues in the head domain of mouse lamin A contain important structural elements for formation of head-to-tail polymers in vitro. Biosci Biotechnol Biochem 71:1252–1259. https://doi.org/10.1271/bbb.60674.
62. Izumi M, Vaughan OA, Hutchison CJ, Gilbert DM. 2000. Head and/or CaaX domain deletions of lamin proteins disrupt preformed lamin A and C but not lamin B structure in mammalian cells. Mol Biol Cell 11: 4323–4337. https://doi.org/10.1091/mbc.11.12.4323.
63. Georgatos SD, Stournaras C, Blobel G. 1988. Heterotypic and homotypic associations between the nuclear lamins: site-specificity and control by phosphorylation. Proc Natl Acad Sci U S A 85:4325–4329. https://doi.org/10.1073/pnas.85.12.4325.
64. Denais CM, Gilbert RM, Isermann P, McGregor AL, te Lindert M, Weigelin B, Davidson PM, Friedl P, Wolf K, Lammerding J. 2016. Nuclear envelope rupture and repair during cancer cell migration. Science 352:353–358. https://doi.org/10.1126/science.aad7297.
65. Krohne G, Waizenegger I, Höger TH. 1989. The conserved carboxy-terminal cysteine of nuclear lamins is essential for lamin association with the nuclear envelope. J Cell Biol 109:2003–2011. https://doi.org/10.1083/jcb.109.5.2003.
66. Sakaki M, Koike H, Takahashi N, Sasagawa N, Tomioka S, Arahata K, Ishiura S. 2001. Interaction between emerin and nuclear lamins. J Biochem 129: 321–327. https://doi.org/10.1093/oxfordjournals.jbchem.a002860.
67. Taniura H, Glass C, Gerace L. 1995. A chromatin binding site in the tail domain of nuclear lamins that interacts with core histones. J Cell Biol 131:33–44. https://doi.org/10.1083/jcb.131.1.33.
68. Scott MS, Boisvert F-M, McDowall MD, Lamond AI, Barton GJ. 2010. Characterization and prediction of protein nucleolar localization sequences. Nucleic Acids Res 38:7388–7399. https://doi.org/10.1093/nar/gkq653.
69. Yang Y, Chen Y, Zhang C, Huang H, Weissman SM. 2002. Nucleolar localization of hTERT protein is associated with telomerase function. Exp Cell Res 277:201–209. https://doi.org/10.1006/excr.2002.5541.
70. Antoine M, Reimers K, Dickson C, Kiefer P. 1997. Fibroblast growth factor 3, a protein with dual subcellular localization, is targeted to the nucleus and nucleolus by the concerted action of two nuclear localization signals and a nucleolar retention signal. J Biol Chem 272:29475–29481. https://doi.org/10.1074/jbc.272.47.29475.
71. Li Z, Hann SR. 2013. Nucleophosmin is essential for c-Myc nucleolar localization and c-Myc-mediated rDNA transcription. Oncogene 32: 1988–1994. https://doi.org/10.1038/onc.2012.227.
72. Chen J, Guo K, Kastan MB. 2012. Interactions of nucleolin and ribosomal protein L26 (RPL26) in translational control of human p53 mRNA. J Biol Chem 287:16467–16476. https://doi.org/10.1074/jbc.M112.349274.
73. Takagi M, Absalon MJ, McLure KG, Kastan MB. 2005. Regulation of p53 translation and induction after DNA damage by ribosomal protein L26 and nucleolin. Cell 123:49–63. https://doi.org/10.1016/j.cell.2005.07.034.
74. Musinova YR, Lisitsyna OM, Sorokin DV, Arifulin EA, Smirnova TA, Zinovkin RA, Potashnikova DM, Vassetzky YS, Sheval EV. 2016. RNA-dependent disassembly of nuclear bodies. J Cell Sci 129:4509–4520.
75. Caudron-Herger M, Pankert T, Seiler J, Németh A, Voit R, Grummt I, Rippe K. 2015. Alu element-containing RNAs maintain nucleolar structure and function. EMBO J 34:2758–2774. https://doi.org/10.15252/embj.201591458.
76. Ghisolfi-Nieto L, Joseph G, Puvion-Dutilleul F, Amalric F, Bouvet P. 1996. Nucleolin is a sequence-specific RNA-binding protein: characterization of targets on pre-ribosomal RNA. J Mol Biol 260:34–53. https://doi.org/10.1006/jmbi.1996.0380.
77. Grummt I. 2003. Life on a planet of its own: regulation of RNA polymerase I transcription in the nucleolus. Genes Dev 17:1691–1702. https://doi.org/10.1101/gad.1098503R.
78. Russell J, Zomerdijk JCBM. 2005. RNA-polymerase-I-directed rDNA transcription, life and works. Trends Biochem Sci 30:87–96. https://doi.org/10.1016/j.tibs.2004.12.008.
79. Santoro R, Li J, Grummt I. 2002. The nucleolar remodeling complex NoRC mediates heterochromatin formation and silencing of ribosomal gene transcription. Nat Genet 32:393–396. https://doi.org/10.1038/ng1010.
80. Cong R, Das S, Douet J, Wong J, Buschbeck M, Mongelard F, Bouvet P. 2014. macroH2A1 histone variant represses rDNA transcription. Nucleic Acids Res 42:181–192. https://doi.org/10.1093/nar/gkt863.
81. Douet J, Corujo D, Malinverni R, Renauld J, Sansoni V, Marjanović MP, Cantari'o N, Valero V, Mongelard F, Bouvet P, Imhof A, Thiry M, Buschbeck M. 2017. MacroH2A histone variants maintain nuclear organization and heterochromatin architecture. J Cell Sci 130:1570–1582. https://doi.org/10.1242/jcs.199216.
82. Fu Y, Lv P, Yan G, Fan H, Cheng L, Zhang F, Dang Y, Wu H, Wen B. 2015. MacroH2A1 associates with nuclear lamina and maintains chromatin architecture in mouse liver cells. Sci Rep 5:17186. https://doi.org/10.1038/srep17186.
83. Cong R, Das S, Ugrinova I, Kumar S, Mongelard F, Wong J, Bouvet P. 2012. Interaction of nucleolin with ribosomal RNA genes and its role in RNA polymerase I transcription. Nucleic Acids Res 40:9441–9454. https://doi.org/10.1093/nar/gks720.
84. Liang YM, Wang X, Ramalingam R, So KY, Lam YW, Li ZF. 2012. Novel nucleolar isolation method reveals rapid response of human nucleolar proteomes to serum stimulation. J Proteomics 77:521–530. https://doi.org/10.1016/j.jprot.2012.09.031.
85. Jagatheesan G, Thanumalayan S, Muralikrishna B, Rangaraj N, Karande AA, Parnaik VK. 1999. Colocalization of intranuclear lamin foci with RNA splicing factors. J Cell Sci 112:4651–4661.
86. Bancaud A, Huet S, Rabut G, Ellenberg J. *In* Goldman RD, Swedlow JR, Spector DL (ed). 2010. Live cell imaging: a laboratory manual, 2nd ed. Cold Spring Harbor Laboratory Press, Cold Spring Harbor, NY.

87. Rapsomaniki MA, Kotsantis P, Symeonidou I-E, Giakoumakis N-N, Taraviras S, Lygerou Z. 2012. easyFRAP: an interactive, easy-to-use tool for qualitative and quantitative analysis of FRAP data. Bioinformatics 28:1800–1801. https://doi.org/10.1093/bioinformatics/bts241.
88. Chaumeil J, Augui S, Chow JC, Heard E. 2008. Combined immunofluorescence, RNA fluorescent in situ hybridization, and DNA fluorescent in situ hybridization to study chromatin changes, transcriptional activity, nuclear organization, and X-chromosome inactivation. Methods Mol Biol 463:297–308. https://doi.org/10.1007/978-1-59745-406-3_18.
89. Bolte S, Cordelières FP. 2006. A guided tour into subcellular colocalization analysis in light microscopy. J Microsc 224:213–232. https://doi.org/10.1111/j.1365-2818.2006.01706.x.

Nucleus

ISSN: 1949-1034 (Print) 1949-1042 (Online) Journal homepage: http://www.tandfonline.com/loi/kncl20

Nucleolin modulates compartmentalization and dynamics of histone 2B-ECFP in the nucleolus

Ayantika Sen Gupta, Gaurav Joshi, Sumit Pawar & Kundan Sengupta

To cite this article: Ayantika Sen Gupta, Gaurav Joshi, Sumit Pawar & Kundan Sengupta (2018): Nucleolin modulates compartmentalization and dynamics of histone 2B-ECFP in the nucleolus, Nucleus, DOI: 10.1080/19491034.2018.1471936

To link to this article: https://doi.org/10.1080/19491034.2018.1471936

NUCLEUS
https://doi.org/10.1080/19491034.2018.1471936

Taylor & Francis
Taylor & Francis Group

RESEARCH ARTICLE

OPEN ACCESS Check for updates

Nucleolin modulates compartmentalization and dynamics of histone 2B-ECFP in the nucleolus

Ayantika Sen Gupta, Gaurav Joshi, Sumit Pawar, and Kundan Sengupta

Biology, Indian Institute of Science Education and Research (IISER), Pune, India

ABSTRACT

Eukaryotic cells have 2 to 3 discrete nucleoli required for ribosome synthesis. Nucleoli are phase separated nuclear sub-organelles. Here we examined the role of nuclear Lamins and nucleolar factors in modulating the compartmentalization and dynamics of histone 2B (H2B-ECFP) in the nucleolus. Live imaging and Fluorescence Recovery After Photobleaching (FRAP) of labelled H2B, showed that the depletion of Lamin B1, Fibrillarin (FBL) or Nucleostemin (GNL3), enhances H2B-ECFP mobility in the nucleolus. Furthermore, Nucleolin knockdown significantly decreases H2B-ECFP compartmentalization in the nucleolus, while H2B-ECFP residence and mobility in the nucleolus was prolonged upon Nucleolin overexpression. Co-expression of N-terminal and RNA binding domain (RBD) deletion mutants of Nucleolin or inhibiting 45S rRNA synthesis reduces the sequestration of H2B-ECFP in the nucleolus. Taken together, these studies reveal a crucial role of Nucleolin-rRNA complex in modulating the compartmentalization, stability and dynamics of H2B within the nucleolus.

KEYWORDS

Nucleolus; H2B; nucleolin; lamin; nucleus; rRNA

Introduction

The nucleus houses chromatin and several non-membranous nuclear bodies involved in transcription [1], splicing [2] and nuclear transport [3]. The absence of membranes within the nucleus facilitates dynamic but regulated exchange of molecules between nuclear bodies and chromatin [4]. The import and sequestration of protein and RNA into nuclear bodies modulates their nucleoplasmic concentration and function. The nucleolus is the largest nuclear sub-organelle essential for ribosome biogenesis [5]. The nucleolus also functions as a stress-sensing compartment that sequesters oncoproteins such as BRCA1 and regulators of p53, that are released into the nucleoplasm upon DNA damage [6,7], while, HSP70 and VHL proteins are immobilized in the nucleolus during thermal stress and acidosis respectively [8]. Key mechanisms of protein sequestration into the nucleolus are (i) interaction of proteins with resident nucleolar factors such as Nucleolin and Nucleophosmin [9–11] (ii) nucleolar localization signal (NoLS) enriched in lysine and arginine rich repeats [12] and (iii) interaction of proteins with non-coding RNA transcribed from intergenic sequence of the rDNA [8]. Mass spectrometric analyses of nucleolar extracts identified ~4500 proteins, which include isoforms of each histone family – H1, H2, H3, H4 and histone-modifying enzymes [13].

Electron microscopy reveals a remarkable tripartite structure of the nucleolus with a central Fibrillar Center (FC), surrounded by the Dense Fibrillar Component (DFC) and the Granular Component (GC). Such an organization facilitates ribosome biogenesis [5,14]. The nucleolus partitions into sub-compartments as a result of the separation of immiscible phases of Fibrillarin and Nucleophosmin [15]. Nucleolar structure is maintained by ongoing rDNA transcription, as its inhibition by Actinomycin D induces nucleolar segregation [16]. Nucleolar structure is also regulated by Nucleolin – one of the most abundant proteins of the GC [17]. Nucleolin has diverse roles in rDNA transcription, ribosome biogenesis [18], DNA damage repair [19] and regulation of apoptosis [20]. *In vitro* studies implicate Nucleolin

CONTACT Kundan Sengupta kunsen@iiserpune.ac.in Biology, Indian Institute of Science Education and Research (IISER), Dr. Homi Bhabha Road, Pashan, Pune 411 008, India

Supplemental data for this article can be accessed here.

as a histone chaperone with FACT-like activity, which regulates SWI-SNF function and ACF chromatin remodelers [21]. Nucleolin has a High Mobility Group (HMG)-like N-terminal domain with four acidic stretches of glutamate and aspartate residues, interspersed with basic lysine residues [22]. The acidic stretches interact with histone H1 while the basic residues interact with DNA [22]. Nucleolin also has four central RNA binding domains (RBD1-4) and a C-terminal GAR (Glycine Arginine Rich) domain. The RNA binding domain specifically binds to a 5′ external transcribed sequence (ETS) site on nascent ribosomal RNA. The GAR domain of Nucleolin binds specifically to DNA and non-specifically to RNA, while the RBDs confer specificity to RNA binding [23–25]. ChIP-Seq analysis reveals the recruitment of Nucleolin to sites of DNA damage, resulting in the eviction of histones – H2A and H2B thereby allowing access to the DNA double strand break repair machinery [19]. H2B has been detected in the nucleoli of Bovine liver cells and chicken erythrocytes using antibodies raised against its first 58 amino acids [26]. Localization of H2B in the nucleolus is attributed to stretches of basic amino acid residues (KKRKRSRK), similar to the NoLS motifs: (R/K)(R/K)X(RK) or (R/K)X(R/K)(R/K) [27].

Here we show the RNA-dependent function of Nucleolin in modulating the localization, dynamics and retention of Histone 2B (H2B-ECFP) in the nucleolus.

Results

Histone 2B (H2B) compartmentalizes in the nucleolus

The nucleolus is the largest nuclear sub-organelle and is essential for ribosomal RNA (rRNA) and protein synthesis [28]. However, the mechanisms that regulate the sequestration of proteins within the nucleolus remain unclear. For instance, overexpressed H2B is sequestered in the nucleolus [27]. Here we sought to investigate the mechanisms that modulate the sequestration and dynamics of H2B-ECFP in the nucleolus. We transfected H2B-ECFP into DLD1 colorectal cancer cells and found that although H2B-ECFP localizes in the nucleoplasm of all cells, a significant sub-population of cells (~40%) show H2B-ECFP in the nucleolus (Figure 1(a,b)). While, the Nuclear Localization Signal (NLS) sequence tagged with CFP localizes in the nucleolus of nearly all transfected cells (~98%) (Figure 1(a,b)). We surmise that the relatively small NLS-CFP freely diffuses into the nucleolus, while the nucleolar localization of H2B-ECFP in a sub-population of ~40% cells, is potentially guided by additional interactions with nucleolar factors. H2B-ECFP localizes in the nucleolus of diverse cancer cell lines such as HCT116 (colorectal cancer cell line), MCF7 (breast cancer cell line) as well as DLD1 cells (Figure 1(c)). In addition to visualizing nucleolar localization of overexpressed H2B-ECFP, we found that endogenous H2B also localizes in the nucleolus as revealed by immunofluorescence assays (Figure 1(d)).

Lamin A regulates nuclear histone dynamics, while Lamin B1 and Lamin B2 modulate nucleolar organization and function [29–31]. We asked if nuclear Lamins or nucleolar factors i.e fibrillarin (FBL) and nucleostemin (GNL3), modulate the compartmentalization of H2B-ECFP in the nucleolus (Figure 1(e)). We independently knocked down nuclear Lamins, Fibrillarin (FBL) and Nucleostemin (GNL3) in DLD1 cells. Interestingly, knockdown of Lamin A/C (LMNA/C), Lamin B1 (LMNB1), Lamin B2 (LMNB2) or nucleolar factors – Fibrillarin (FBL) and Nucleostemin (GNL3) did not significantly affect the extent of H2B-ECFP localization within the nucleolus (Figure 1(e)). Taken together, these results suggest that the nucleolar localization of H2B-ECFP is unaffected by the depletion of Lamins or nucleolar factors such as FBL and GNL3.

Lamin B1 enhances mobility of H2B-ECFP in the nucleolus

We sought to investigate the dynamics of fluorescently labelled H2B in the nucleolus and nucleus by Fluorescence Recovery After Photobleaching (FRAP) (Fig. S1A, B). Interestingly, photobleaching H2B in the nucleolus showed a significantly higher mobile fraction (M.F. ~40%) as compared to the nuclear sub-pool (M.F ~18%) (Fig. S1C). While NLS-CFP showed complete and immediate recovery further underscoring its ability to freely diffuse into the nucleus as well as the nucleolus (Fig. S1D, E).

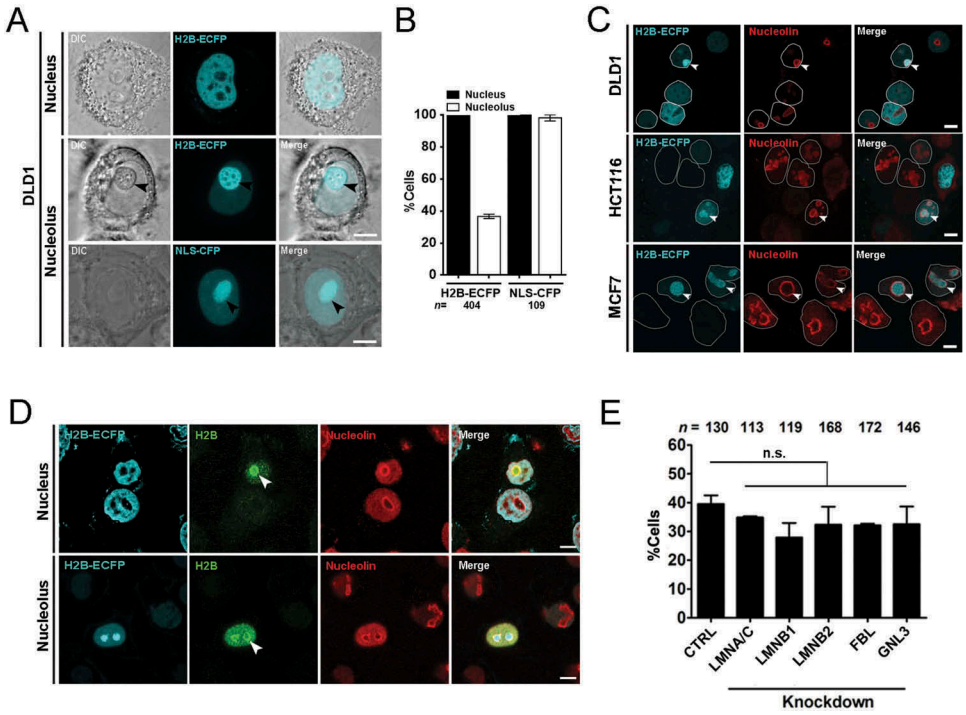

Figure 1. Histone 2B-ECFP localizes in the nucleolus. (a) H2B-ECFP is distinctly localized in the nucleoplasm and the nucleolus. Top panel: nucleoplasmic localization of H2B-ECFP, Middle panel: localization of H2B-ECFP in the nucleolus (black arrowhead). Bottom panel: NLS-CFP localizes to the nucleoplasm and the nucleolus (black arrowhead). Scale bar ~5 µm. (b) All transfected cells show H2B-ECFP in the nucleoplasm, while ~40% of these cells harbor H2B-ECFP in the nucleolus. All cells show NLS-CFP in the nucleoplasm, while ~98% cells show NLS-CFP in the nucleolus, n = number of nuclei, data compiled from N = 2 independent biological replicates. (c) Immunostaining of Nucleolin marks nucleoli with H2B-ECFP in DLD1, HCT116 and MCF7 cells (white arrows). White outline demarcates single nucleus, scale bar ~5 µm. (d) Cells transfected with H2B-ECFP were immunostained with anti-histone 2B antibody and anti-nucleolin antibody to demarcate the nucleolus (white arrows), anti-histone 2B antibody detects both transfected and endogenous H2B in the nucleolus. (e) Independent knockdowns of Lamin A/C, B1, B2, FBL and GNL3 do not affect the extent of nucleolar localization of labeled H2B-ECFP, n = number of nuclei, data compiled from N = 3 independent biological replicates, error bars: SEM. Student's t-test, $p > 0.05$ (n.s: not significant).

Since, nuclear Lamins maintain the structural and functional integrity of the nucleus [32,33], we asked if Lamins regulate H2B-ECFP dynamics. We performed siRNA mediated knockdown followed by immunoblotting, which showed ~70% depletion of Lamins in DLD1 cells (Figure 2(a–c)). We next performed FRAP of H2B-ECFP in the nucleolus and the nucleus respectively upon Lamin depletion (Figure 2(d,e)). Interestingly, Lamin A/C knockdown did not affect H2B-ECFP dynamics in the nucleolus (M.F. ~38.77%) (Figure 2(f,i), Table 1), while Lamin B1 knockdown showed a significant increase in the mobile fraction of H2B-ECFP (M.F ~61.63%) (Figure 2(g, i), Table 1). Lamin B2 knockdown also showed a marginal increase in H2B-ECFP mobility (~48.98%) (Figure 2(h,i), Table 1). In sharp contrast, Lamin knockdowns did not significantly alter H2B-ECFP mobility in the nucleus (Figure 2 (j–m), Table 1). Of note, neither endogenous nor overexpressed levels of H2B were altered upon Lamin knockdowns (Fig. S1F). Taken together, Lamin B1 knockdown enhances H2B-ECFP mobility in the nucleolus.

Fibrillarin (FBL) and Nucleostemin (GNL3) modulate H2B-ECFP dynamics within the nucleolus

We sought to examine if bonafide nucleolar proteins of the DFC and GC regions of the nucleolus – Fibrillarin (FBL) and Nucleostemin (GNL3),

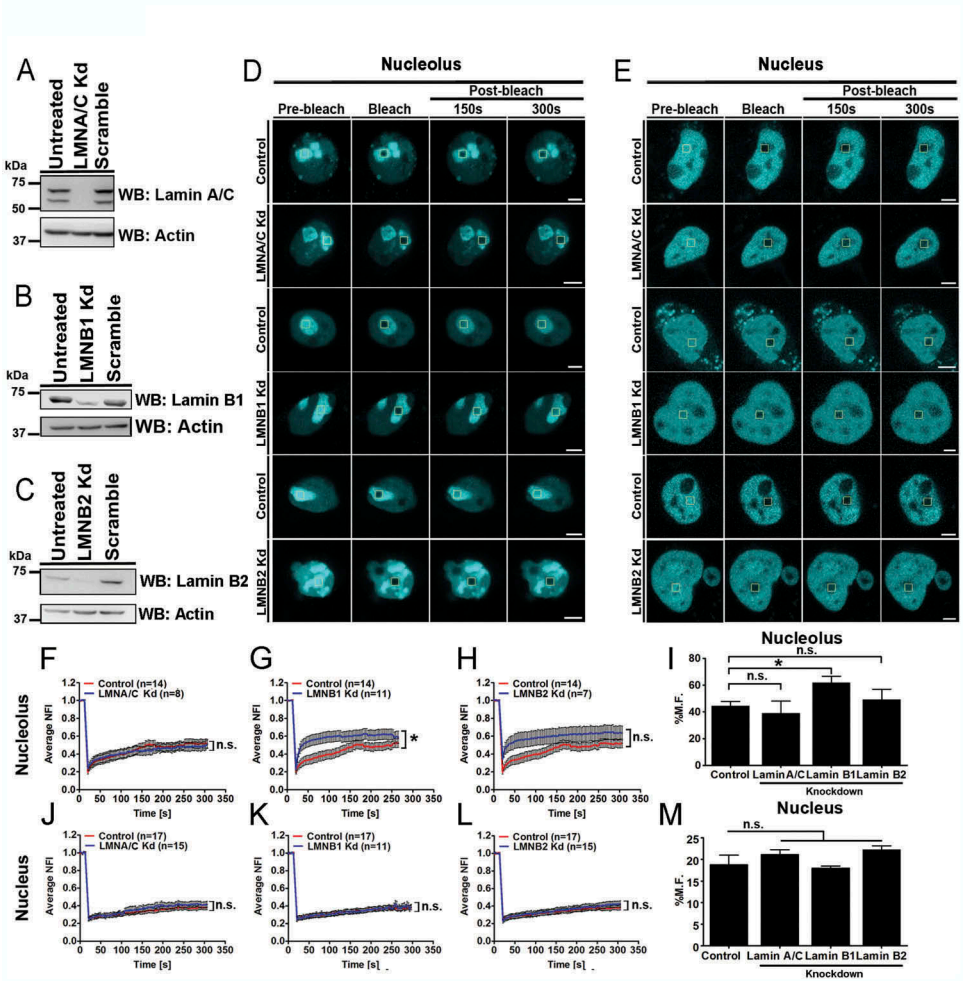

Figure 2. Lamin B1 depletion enhances H2B–ECFP mobility in the nucleolus. (a–c) Western blots of whole cell lysates prepared from (a) LMNA/C (b) LMNB1 and (c) LMNB2 knockdown. Controls: Untreated, scramble siRNA. Loading control: Actin. (d–e) Representative images showing FRAP of H2B-ECFP in (d) nucleolus and (e) nucleus of control, LMNA/C Kd, LMNB1 Kd and LMNB2 Kd cells. Yellow box represents bleached ROI. Scale bar ~5 µm. (f–h) Normalized fluorescence recovery curves comparing recovery of H2B-ECFP in the nucleolus of control, (f) LMNA/C Kd (g) LMNB1 Kd and (h) LMNB2 Kd cells. (i) Relative mobile fractions of H2B-ECFP in the nucleolus as calculated from (f–h), showing increased mobility of H2B-ECFP in the nucleolus upon Lamin B1 Kd. (j–l) Normalized fluorescence recovery curves of H2B-ECFP in the nucleus of control, (j) LMNA/C Kd (k) LMNB1 Kd (l) LMNB2 Kd cells. (m) Relative mobile fractions of H2B-ECFP in the nucleus as calculated from (j–l). Lamin knockdown does not affect H2B-ECFP mobility in the nucleus, n = number of nuclei, data compiled from N = 3 independent biological replicates, error bars: SEM in recovery curves and bar graph. Student's t-test, *p < 0.05.

respectively, modulate H2B-ECFP dynamics in the nucleolus (Figure 3) [34,35]. We performed siRNA mediated knockdown of FBL and GNL3 in DLD1 cells, followed by western blotting, which showed ~80% depletion (Figure 3(a,b)). We next examined H2B-ECFP dynamics in the nucleolus and nucleus respectively upon FBL and GNL3 depletion (Figure 3(c,d)). FBL and GNL3 knockdown significantly increased the mobility of H2B-ECFP in the nucleolus (FBL Kd: M.F ~68.81%), (GNL3 Kd: M.F ~69.44%) (Figure 3(e–g), Table 1). Interestingly photobleaching the nuclear sub-pool of H2B-ECFP, showed a marginal decrease in its nuclear dynamics (FBL Kd: M.F ~17.11%) (Figure 3(h,j), Table 1), while Nucleostemin (GNL3) depletion showed a significant decrease in the mobile fraction of H2B-ECFP (GNL3 Kd: M.F ~12.75%) in the nucleus (Figure 3(i,j), Table 1). Taken together, these results reveal that Fibrillarin and Nucleostemin depletions modulate the dynamics

Table 1. Mobile fractions of H2B-ECFP calculated from fluorescence recovery after photobleaching (FRAP) in the nucleus and nucleolus of DLD1 cells in Control, knockdowns of Lamin A, B1, B2, Fibrillarin, Nucleostemin, Nucleolin; and Nucleolin overexpression. Error represents SEM, p-value <0.05 considered significant as calculated from unpaired Students t-test (two-tailed).

	H2B-ECFP Mobile fraction (%) ± S.E.M.	
	Nucleus	Nucleolus
Control	18.79 ± 2.19 (n = 17)	44.3 ± 3.44 (n = 16)
Lamin A Kd	21.14 ± 1.13 (n = 15, p = 0.62)	38.77 ± 9.27 (n = 8, p = 0.59)
Lamin B1 Kd	18.01 ± 0.47 (n = 11, p = 0.77)	61.63 ± 5.05 (n = 11, *p = 0.015)
Lamin B2 Kd	22.25 ± 0.87 (n = 15, p = 0.39)	48.98 ± 7.9 (n = 7, p = 0.599)
Fibrillarin Kd	17.11 ± 2.22 (n = 13, p = 0.59)	68.81 ± 8.09 (n = 7, *p = 0.02)
Nucleostemin Kd	12.75 ± 0.46 (n = 13, *p = 0.03)	69.44 ± 3.16 (n = 11, **p = 0.0058)
Nucleolin GFP OE	–	71.76 ± 3.43 (n = 17, **p = 0.0048)

*p < 0.05, **p < 0.01.

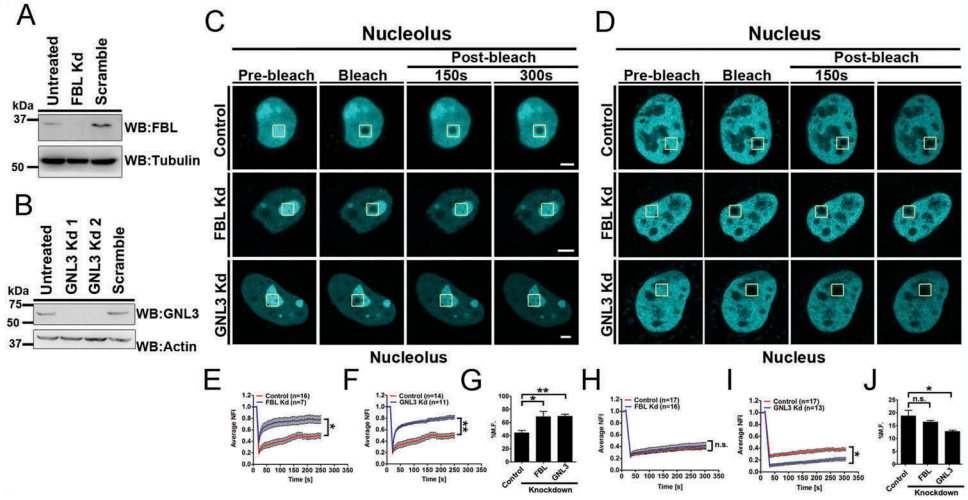

Figure 3. Depletion of Fibrillarin (FBL) and Nucleostemin (GNL3) enhances H2B–ECFP mobility in the nucleolus. (a, b) Western blots of whole cell lysates prepared from DLD1 cells upon knockdown of (a) Fibrillarin (FBL) (b) Nucleostemin (GNL3), Controls: untreated and respective scramble siRNA treated cells. Loading controls: Tubulin, Actin. (c, d) FRAP of H2B-ECFP in the (c) nucleolus and (d) nucleus of control, FBL and GNL3 Kd cells, respectively. Yellow box represents bleached ROI. Scale bar ~5 µm. (e, f) Normalized fluorescence recovery curves comparing recovery of H2B-ECFP in the nucleolus of control (e) FBL Kd and (f) GNL3 Kd cells. (g) Relative mobile fractions of H2B-ECFP in the nucleolus as calculated from (e, f). (h, i) Normalized fluorescence recovery curves comparing recovery of H2B-ECFP in the nucleus of control, (h) FBL Kd (i) GNL3 Kd cells. (j) Relative mobile fractions of H2B-ECFP in the nucleus as calculated from (h, i), n = number of nuclei, data from N = 3 independent biological replicates, error bars: SEM in recovery curves and bar graph. Student's t-test, *p < 0.05, **p < 0.01.

of H2B-ECFP in the nucleolus, further underscoring the role of FBL and GNL3 in maintaining the microenvironment and stability of the nucleolus.

Nucleolin modulates compartmentalization of H2B-ECFP in the nucleolus

Nucleolin is a bonafide GC component protein that maintains nucleolar integrity and stability [36]. We asked if Nucleolin modulates the sequestration of H2B-ECFP in the nucleolus. We knocked down Nucleolin, followed by H2B-ECFP transfection into DLD1 cells (Figure 4(a,b)(i)). Interestingly, Nucleolin depletion revealed a striking reduction in the number of cells with H2B-ECFP in the nucleolus (<10%), as compared to control cells (~36%) (Figure 4(c)). H2B-ECFP expression was marginally higher in Nucleolin depleted cells (Figure 4(b)(ii)). This contrasts with

Lamin, FBL and GNL3 depletion, which did not alter the extent of H2B-ECFP compartmentalization in the nucleolus (Figure 1(e)). The independent depletion of another nucleolar GC protein namely Nucleophosmin (NPM1), also showed a marginal reduction of H2B-ECFP in the nucleolus (~30%) as compared to control cells (~38%) (Figure 4(c), Fig. S2B). Decrease in nucleolar H2B-ECFP upon NPM1 knockdown, is consistent with the association between NPM1 and core, linker histones (H1, H2A,

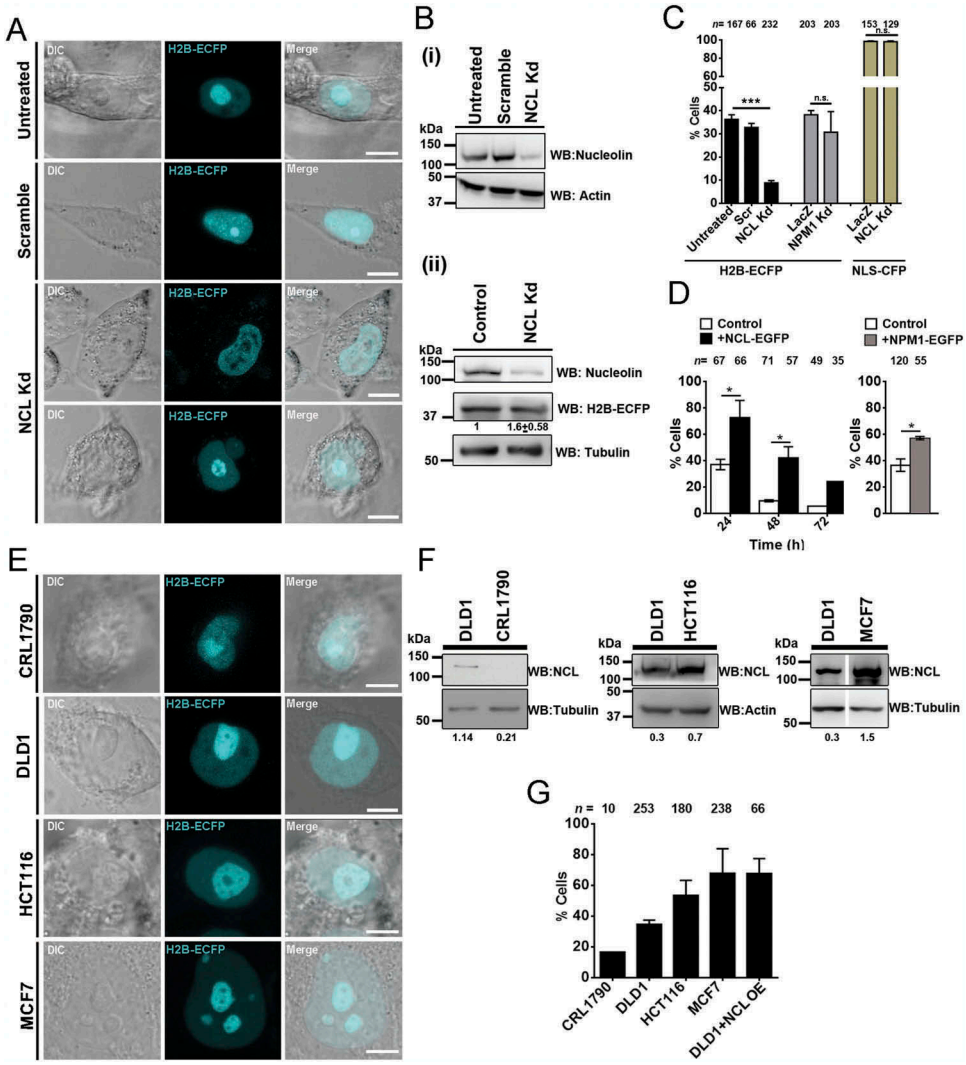

Figure 4. Nucleolin levels modulate compartmentation of H2B-ECFP in the nucleolus. (a) Representative images from live imaging of H2B-ECFP upon Nucleolin knockdown (NCL Kd) in DLD1 cells. Controls: untreated and scrambled siRNA treated cells. Scale bar ~5 µm. (b) (i) Western blots performed on whole cell lysates to detect Nucleolin levels in untreated, scramble and NCL siRNA treated DLD1 cells. Loading control: Actin. (ii) H2B-ECFP expression is marginally increased upon Nucleolin knockdown. Loading control: Tubulin. (c) Percent cells showing nucleolar H2B-ECFP compartments upon NCL Knockdown (Kd), n = number of nuclei, data from N = 3 independent biological replicates, error bars: SEM. Percent cells showing nucleolar H2B-ECFP upon NPM1 knockdown, n = number of nuclei, data from N = 2 independent biological replicates, error bars: SD. Percent cells showing nucleolar NLS-CFP upon NCL Kd, n = number of nuclei, data from N = 2 independent biological replicates, error bars: SD. Student's t-test, ***$p < 0.001$. (d) Nucleolar H2B-ECFP upon NCL-GFP overexpression. DLD1 cells transfected with H2B-ECFP only (control, white bars) and co-transfected with H2B-ECFP and NCL-GFP (+NCL-GFP, black bars) imaged at intervals of 24, 48, and 72 h post transfection. Percent cells showing nucleolar H2B-ECFP upon 24 h of NPM1-GFP overexpression, n = number of nuclei, data from two independent biological replicates, N = 2, error bars: SD. (e) Representative images from live imaging H2B-ECFP transfected CRL1790, DLD1, HCT116 and MCF7 cells showing nucleolar localization of H2B-ECFP. Scale bar ~5 µm. (f) Western blots showing endogenous levels of NCL in CRL1790, DLD1, HCT116, and MCF7 cells. Loading controls: Tubulin, Actin. Intensity of Nucleolin normalized to loading control. (g) Extent of H2B-ECFP in the nucleolus in CRL1790, DLD1, HCT116, MCF7 cells and in DLD1 cells co-transfected with NCL-GFP, n = number of nuclei, data from two independent biological replicates, N = 2.

H2B, H3 and H4) [37,38]. In contrast, the GC protein Nucleostemin (GNL3), does not affect nucleolar localization of H2B-ECFP (Figure 1(e)). Of note, the localization of NLS-CFP in the nucleolus was unaltered upon Nucleolin knockdown (~95%) as compared to control cells (~96%) (Figure 4(c), Fig. S2A). In summary, Nucleolin is a key factor which modulates the localization of H2B-ECFP in the nucleolus.

Since Nucleolin knockdown reduced H2B-ECFP compartmentalization in the nucleolus, we performed the converse experiment of overexpressing Nucleolin. Interestingly, Nucleolin co-expression showed a consistent and enhanced retention of nucleolar H2B-ECFP in ~67% cells (24 h), which declined to ~42% (48 h), and ~24% (72 h) post transfection (Figure 4(d), black bars), while nucleolar H2B-ECFP declined rapidly over time from ~35% (24 h), ~10% (48 h) and ~5% (72 h) in control cells (Figure 4(d), white bars). Essentially, H2B-ECFP retention was significantly higher upon Nucleolin co-expression at each time point. Independently, NPM1 co-expression showed a moderate increase in nucleolar retention of H2B-ECFP (~57%, after 24 h), which was lower than upon Nucleolin co-expression (~67%) (Figure 4(d)). Taken together, Nucleolin regulates H2B-ECFP retention in the nucleolus.

We asked if the compartmentalization of H2B-ECFP in the nucleolus, correlates with endogenous levels of Nucleolin across cell lines (Figure 4(e–g)). Immunoblotting of whole cell extracts across cell lines showed an increase in Nucleolin levels as follows: CRL1790 < DLD1 < HCT116 < MCF7 (Figure 4(f)). Furthermore, increased nucleolar sequestration of H2B-ECFP positively correlates with an increase in the endogenous levels of Nucleolin in these cell lines (Figure 4(e,g)). We further corroborated this by overexpressing Nucleolin in DLD1 cells, which dramatically increased nucleolar compartmentalization of H2B-ECFP in ~67% cells, as compared to control cells (~40%) (Figure 4(g)). In summary, an increase in the endogenous or overexpressed levels of Nucleolin, positively correlates with the extent of H2B-ECFP in the nucleolus and Nucleolin therefore functions as a positive regulator of H2B-ECFP sequestration into the nucleolus.

Nucleolin modulates H2B-ECFP dynamics in the nucleolus

Nucleolin is a histone chaperone and evicts histones from DNA [19,39]. We monitored fluorescence recovery of labelled H2B in order to address the impact of Nucleolin on the mobility of H2B-ECFP (Figure 5(a,b)). Interestingly, H2B-ECFP showed a higher mobile fraction in HCT116 (M.F. ~59%) and MCF7 cells (M.F. ~68%) respectively, as compared to DLD1 cells (M.F. ~40%) (Figure 5(c)). Furthermore, DLD1 cells overexpressing Nucleolin showed a significantly higher mobility of H2B-ECFP in the nucleolus (DLD1 + NCL OE: M.F. ~72%) as compared to control cells (M.F. ~40%) (Figure 5(c)). Taken together, the mobility of H2B-ECFP in the nucleolus positively correlates with an increase in the levels of Nucleolin.

Nucleolin interacts with H2B-ECFP

Since Nucleolin modulates the retention and dynamics of H2B-ECFP in the nucleolus (Figures 4 and 5), we sought to examine if Nucleolin associates with H2B-ECFP. Remarkably, we found that H2B-ECFP co-immunoprecipitates with endogenous Nucleolin and independently with co-expressed NCL-GFP (Figure 6(a)). Furthermore, H2B-ECFP and NCL-GFP, co-localize in the nucleolus reiterating the association between Nucleolin and H2B-ECFP (Figure 6(b)).

We sought to investigate into the mechanisms of Nucleolin mediated sequestration of H2B-ECFP in the nucleolus. Towards this end, we examined the effect of co-expressing deletion mutants of Nucleolin into DLD1 cells and scored for H2B-ECFP compartments in the nucleolus. We co-expressed H2B-ECFP with (i) full length NCL FL (ii) NCLΔN (N-terminal deleted) (iii) NCLΔRBD (RBD1-4 deleted) and (iv) NCLΔGAR (GAR domain deleted). We observed a comparable localization of NCLΔN in the nucleolus as that of full length NCL, while NCLΔRBD and NCLΔGAR partially mislocalized in the nucleoplasm, consistent with previous studies (Figure 6(b)) [40–42]. Co-

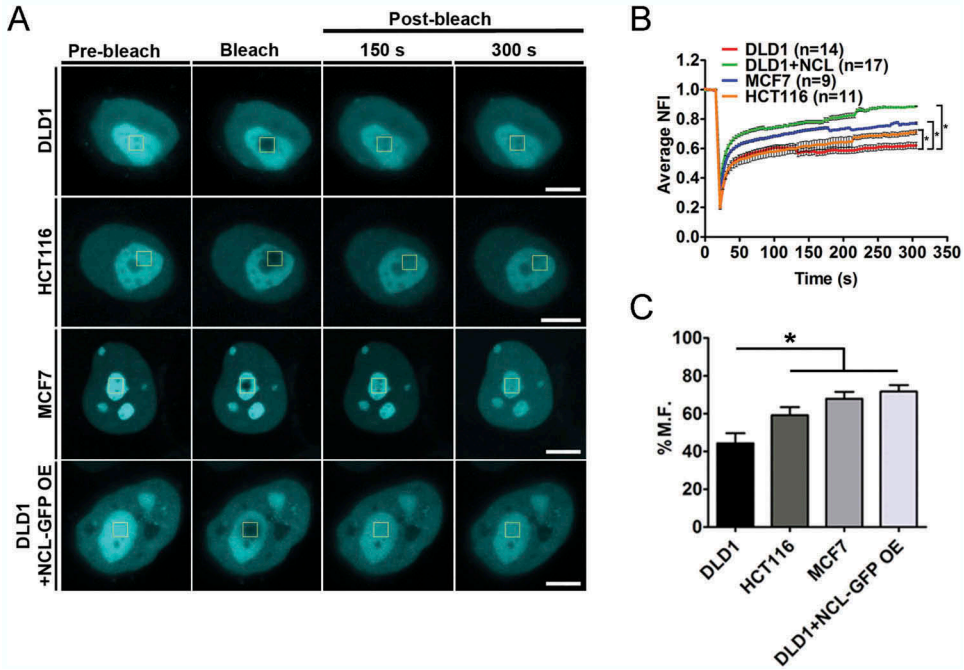

Figure 5. Nucleolin levels positively correlate with H2B-ECFP mobility. (a) FRAP of H2B-ECFP in the nucleolus of DLD1, HCT116, MCF7 and DLD1 cells co-transfected with NCL-GFP (DLD1+ NCL-GFP OE), Scale bar ~5 µm. (b) Normalized fluorescence recovery curves of H2B-ECFP in the nucleolus. (c) Relative mobile fractions of H2B-ECFP as calculated from (b), n = number of nuclei, data from N = 3 independent biological replicates, error bars: SEM in recovery curves and bar graph. Student's t-test, *p < 0.05.

expression of full length NCL showed a significant increase in nucleolar H2B-ECFP (~74%), as compared to cells transfected with H2B-ECFP alone (~32%) (Figure 6(c)). Interestingly, co-expression of NCLΔN and NCLΔRBD did not enhance H2B-ECFP localization in the nucleolus, since both conditions showed ~31% cells with nucleolar H2B-ECFP (Figure 6(c)). In contrast, co-expression of NCLΔGAR showed a comparable extent of nucleolar H2B-ECFP as that of full length NCL (~77%) (Figure 6(c)). Taken together, the N-terminal and RNA binding domains of Nucleolin are essential for the enhanced localization of H2B-ECFP in the nucleolus.

Nucleolin mediated nucleolar localization of H2B-ECFP is pre-rRNA dependent

Since NCLΔRBD did not enhance nucleolar H2B-ECFP localization, we determined if rRNA was necessary for NCL mediated localization of H2B-ECFP in the nucleolus. We treated DLD1 cells with Actinomycin D (0.05 µg/ml) for 4 hours, which showed a significant decrease in 45S rRNA levels (Figure 6(d)).

We asked if nucleolar localization of H2B-ECFP was affected upon inhibition of rDNA transcription by Act D treatment (Figure 6(e)). H2B-ECFP localized in the nucleolus in ~45% control cells (Figure 6(e,f)). This sub-population of cells marginally reduced upon Act D treatment (~32%) (Figure 6(e,f)). Co-expressing NCL-GFP enhanced nucleolar localization of H2B-ECFP in ~80% control cells (Figure 6(e,f)). However, upon Act D treatment, the NCL-GFP mediated increase in nucleolar H2B-ECFP (~77%) showed a significant reduction to ~46% (Figure 6(e,f)). This suggests a requirement of 45S rRNA in the sequestration of H2B-ECFP in the nucleolus.

It is noteworthy that upon Act D treatment, Nucleolin speckles in the nucleoplasm do not colocalize with H2B-ECFP (Figure 6(e), inset). However, Nucleolin shows a distinctive co-localization with H2B-ECFP in the nucleolus, in the presence of 45S pre-rRNA in the nucleolus.

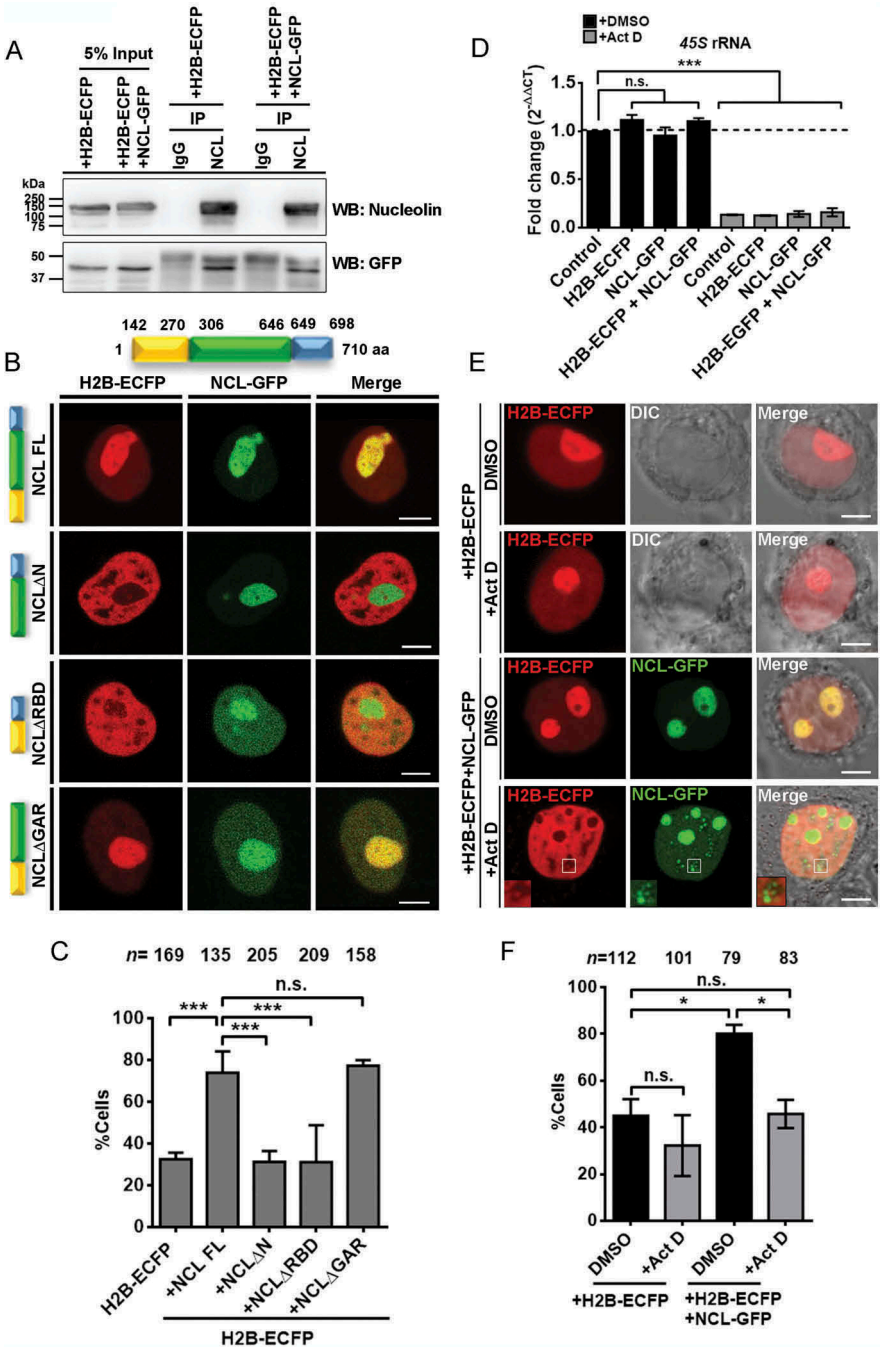

Figure 6. Nucleolin associates with H2B-ECFP in the nucleolus. (a) Co-immunoprecipitation (Co-IP) of endogenous Nucleolin and NCL-GFP with anti-Nucleolin antibody reveals its interaction with H2B-ECFP. Normal IgG used as a control for Co-IP. Anti-GFP antibody was used in western blot to detect H2B-ECFP. Data from N = 2 independent biological replicates. (b) Schematic showing three major domains of Nucleolin. The numbers denote the amino acid positions of the respective domains of Nucleolin. Representative images of DLD1 cells co-transfected with H2B-ECFP and Full length NCL (NCL FL), N-terminal deletion (NCLΔN), RNA binding domain deletion (NCLΔRBD) or GAR domain deletion (NCLΔGAR). H2B-ECFP and FL NCL show co-localization in the nucleolus. NCLΔRBD and NCLΔGAR show nucleoplasmic localization in addition to nucleolar localization. Scale bar, 5 µm. (c) Percent cells showing nucleolar H2B-ECP upon co-expression of NCL FL, NCLΔN, NCLΔRBD and NCLΔGAR, n = number of nuclei, data from N = 3 independent biological replicates, error bars: SEM. ANOVA, ***p < 0.001. (d) qRT-PCR for 45S pre-rRNA in vehicle (DMSO) and Actinomycin D (Act D, 0.05 µg/ml) treated cells, N = 2. 45S pre-rRNA level is downregulated in all cells upon Act D treatment. All statistics performed with respect to Control (+DMSO) cells, ANOVA, ***p < 0.001. (e) Representative images of cells expressing H2B-ECFP alone, or co-expressing NCL-GFP, upon DMSO or Act D treatment. Inset – Nucleolin speckles upon Act D treatment, do not show H2B-ECFP, Scale bar ~5 µm. (f) Quantification of percent cells showing nucleolar H2B-ECFP upon Act D treatment (from e), n = number of nuclei, N = 2 independent biological replicates. ANOVA, *p < 0.05.

Taken together, Nucleolin and 45S rRNA are required for the compartmentalization of H2B-ECFP in the nucleolus.

Discussion

Overexpressed H2B localizes in the nucleolus

The nucleolus is a complex milieu of ribosomal DNA, RNA, proteins and non-ribosomal proteins [5]. Sequestration into the nucleolus is an important mode of post translational regulation of proteins such as ARF and Cdc14 that control cell cycle and apoptosis [43]. Histones and histone variants are commonly enriched in the nucleolus. The histone H1 variant H1.0, localizes in the nucleolus and is strongly associated with non-transcribed regions of ribosomal DNA and interacts with nucleolar proteins involved in rRNA processing [44,45]. Another histone variant – macroH2A also localizes at the nucleolus and is directly involved in rDNA repression [46]. Histone 2A methylated by Fibrillarin at Q104 in humans and Q105 in yeast, is exclusively localized in the nucleolus [47]. However, H2B transiently localizes in the nucleolus upon transfection and disperses into the nucleoplasm over time, either integrating or exchanging with nuclear chromatin [27]. In vitro, a higher concentration of histone octamers to DNA (>0.76 mass ratio), aggregates chromatin and inhibits transcription [48]. Furthermore, excess histone expression in budding yeast shows cytotoxicity and is deleterious to these cells [49,50]. We surmise, that the nucleolar sequestration of excess H2B, is a preferred paradigm for preventing the potentially deleterious effects of histone overexpression in the nucleus and toxicity across most cell types.

Lamins as modulators of nuclear histone dynamics

Histones are hyperdynamic in ES cells which have a relatively open chromatin conformation [51]. Histone dynamics is dampened during differentiation and lineage commitment, as chromatin undergoes compaction. Lamin A/C levels are relatively lower in ES cells but increase during differentiation [52]. Consequently, Lamin A overexpression in ES cells, restricts histone H1 mobility [29]. Furthermore, Lamin B1 expression is lower in senescent cells with compact chromatin and Senescence Associated Heterochromatic Foci (SAHF) [53]. Lamin depletion in differentiated DLD1 cells, did not show an appreciable effect on H2B-ECFP dynamics in the nucleoplasm (Figure 2). This is consistent with relatively unaltered chromatin dynamics in differentiated cells upon masking of the histone binding domain of Lamin A/C [54]. We envisage the following scenarios of the role of Lamins in the modulation of histone dynamics – (1) Consistent with previous data, reduced expression levels of Lamin A/C or B-type lamins do not appreciably affect histone mobility in differentiated cells (Figure 2) [29,52] (2) It is likely that the combined depletion of Lamin A/C and B-type Lamins, alter histone mobility, in differentiated cell types (3) Lamin interactors such as Emerin, Lamin B receptor (LBR) and barrier to autointegration factor (BAF) with histone binding domains, maintain histone dynamics in the absence of Lamins [55,56].

On the other hand, Nucleostemin is highly expressed and is a marker of cancer stem cells [57]. Furthermore cancer stem cells show increased DNA accessibility as assessed by formaldehyde-assisted isolation of regulatory elements-sequencing (FAIRE-seq), suggesting open chromatin conformation [58,59]. We surmise that the decrease in H2B-ECFP mobility in the nucleoplasm upon Nucleostemin loss suggests reduced accessibility to chromatin in cancer stem cells. Interestingly, independent knockdowns of Lamin B1, Fibrillarin and Nucleostemin enhance H2B-ECFP mobility in the nucleolus (Figure 3). We surmise that Fibrillarin and Nucleostemin are bonafide nucleolar factors, that control the nucleolar microenvironment, as their depletion enhances H2B-ECFP dynamics to a significantly greater extent than nuclear lamin B1 (Figures 2 and 3). Furthermore, the loss of Fibrillarin, Nucleostemin or Lamin B1, potentially alter the relative stoichiometries of bound and unbound sub-fractions of H2B-ECFP with

nucleolar chromatin and consequently enhance histone dynamics in the nucleolus [30,35,60].

Nucleolin modulates H2B-ECFP localization into the nucleolus

Nucleolin exhibits a dominant role in sequestering H2B-ECFP into the nucleolus (Figure 4). Nucleolin is a high mobility group protein and is a major constituent of the granular component of the nucleolus [61]. Nucleolin is involved in rRNA transcription and processing [18,62]. Nucleolin is closely related to another nucleolar phosphoprotein – Nucleophosmin. Phase separation of Nucleophosmin and Fibrillarin to a relatively more viscous nucleolar phase is critical to the maintenance of nucleolar integrity [15,63]. In addition, ribosomal proteins – L3 and S3A and non-ribosomal proteins – Lamin B2 and HIV-rev, localize into the nucleolus by virtue of their interaction with Nucleolin and Nucleophosmin [9,31,64]. H2B is localized into the nucleolus through its nucleolar localization signal (NoLS) and electrostatic interaction with nucleolar components [27]. Here, we discovered the requirement of Nucleolin for the sequestration and retention of H2B-ECFP in the nucleolus. Nucleolin plays a more dominant role in the localization of H2B-ECFP in the nucleolus, since the loss of Nucleolin strikingly decreases nucleolar H2B-ECFP, while the co-expression of Nucleolin, retains H2B-ECFP in the nucleolus over a considerably longer duration (Figure 4). More importantly, the N-terminal domain, previously shown to interact with histones H1 and H2A-H2B dimers and the RNA binding domain of Nucleolin, are indispensable for the nucleolar retention of H2B-ECFP [21,22] (Figure 6). Taken together, the interaction between H2B-ECFP and Nucleolin in the nucleolus serves as a mechanism for the nucleolar localization and retention of overexpressed H2B.

Nucleolin modulates nucleolar H2B-ECFP dynamics

Nucleolin levels modulate H2B-ECFP retention and dynamics in the nucleolus across cell types (Figures 4 and 5). Furthermore, the N-terminal domain and RBD of Nucleolin regulate H2B-ECFP compartmentation in the nucleolus (Figure 6). Nucleolin functions as a histone chaperone facilitating exchange of H2A-H2B dimers from chromatin [21,39]. However, nucleoplasmic and nucleolar H2B exist in distinct microenvironments. The nucleoplasmic pool of H2B largely associates with DNA, whereas nucleolar subpools of H2B reside in the microenvironment of nucleolar DNA, ribosomal RNA, non-coding RNAs such as snoRNAs, ribosomal and non-ribosomal proteins, which may collectively impinge on H2B dynamics in the nucleolus.

We surmise that the N-terminal domain of Nucleolin rich in acidic amino acid stretches binds to nucleoplasmic H2B-ECFP and transports it to the nucleolus (Figure 7) [21,22]. Thus, with increased Nucleolin expression, there is enhanced H2B-ECFP import into the nucleolus, which correlates with an increase in the recovery of H2B-ECFP (Figure 5). We surmise that the enhanced retention of H2B-ECFP in the nucleolus upon NCL overexpression is also rRNA dependent. However, Act D treatment redistributes a subpopulation of Nucleolin to the nucleoplasm, potentially resulting in the lowered retention of H2B in the nucleolus. The RNA binding domains of Nucleolin specifically interacts with the 5′-ETS of pre-rRNA while GAR domain of Nucleolin non-specifically binds to any RNA [25,65]. In summary, the nucleolar retention of H2B-ECFP is dependent upon Nucleolin-45S rRNA complex. Therefore, the sub-domains of Nucleolin differentially affect nucleolar H2B-ECFP compartmentation. While the N-terminal domain is potentially required for translocating H2B-ECFP to the nucleolus, the RNA binding domain is also necessary for the retention of H2B-ECFP in the nucleolus.

Implications

While it was previously proposed that overexpressed H2B localizes in the nucleolus, via charge based interactions between the positively charged H2B and the negatively charged nucleic acids within the nucleolar milieu, our studies for the first time unravel a novel Nucleolin guided mechanism that modulates the sequestration, retention and dynamics of H2B in the nucleolus

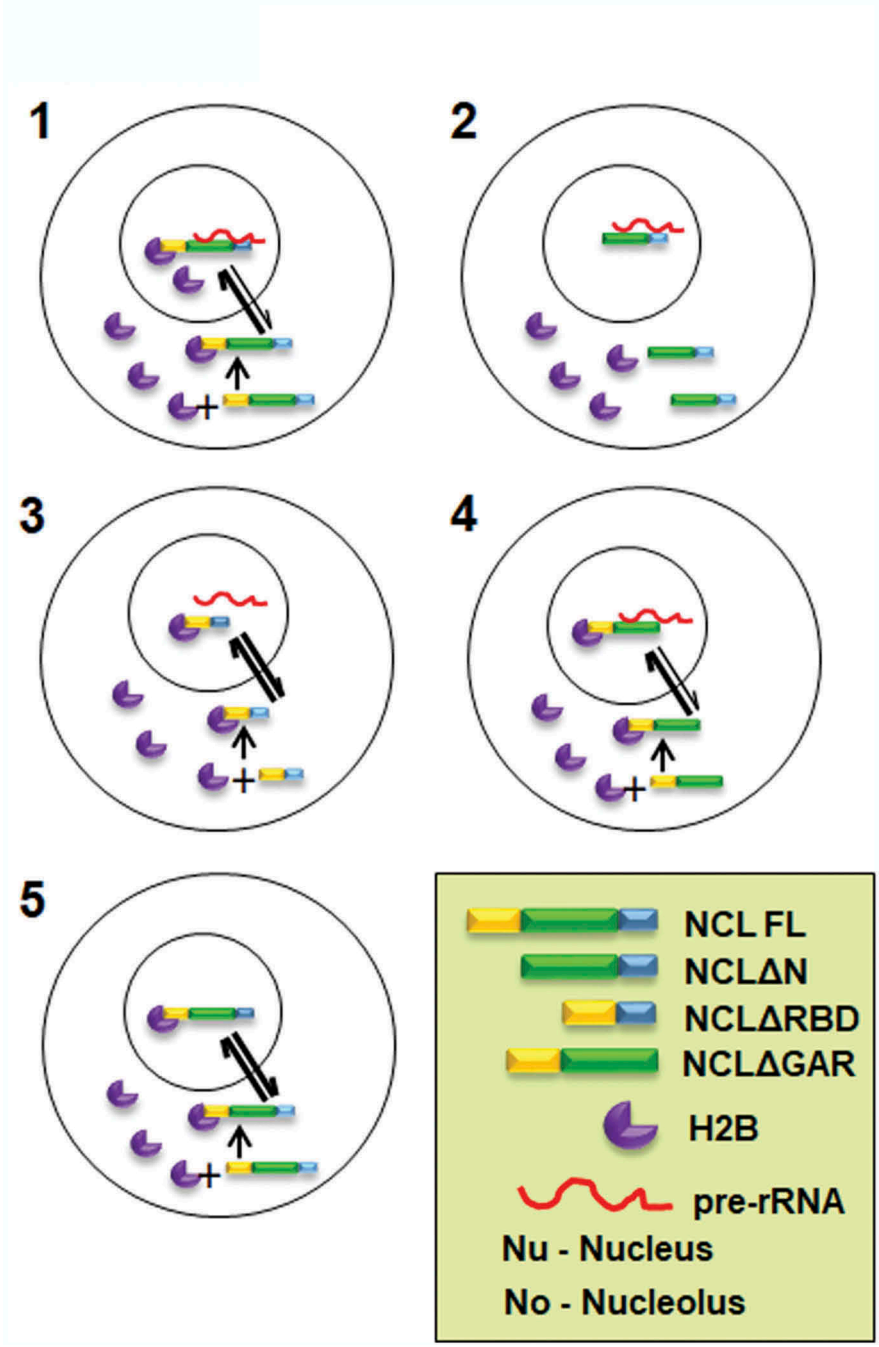

Figure 7. Speculative model of Nucleolin regulating nucleolar compartmentation and dynamics of H2B-ECFP. 1. Nucleolin interacts with H2B-ECFP via its N-terminal domain and shuttles it into the nucleolus. In the nucleolus, Nucleolin binds to pre-rRNA via its RNA binding domain and H2B-ECFP via its N-terminal domain, thus retaining H2B-ECFP in the nucleolus. It is likely that the relative rate of import of H2B-ECFP into the nucleolus is greater in the presence of Nucleolin. 2. In absence of the N-terminal domain, Nucleolin does not bind to H2B-ECFP, thereby reducing nucleolar pools of H2B-ECFP. 3. Nucleolin RBD deletion mutant binds to H2B-ECFP through its N-terminal domain and sequesters H2B-ECFP into the nucleolus. However, in the absence of RBD, H2B-ECFP is not retained in the nucleolus, as the RBD is required for binding to pre-rRNA. 4. GAR domain deletion mutant binds to H2B-ECFP and pre-rRNA and shows enhanced recruitment of H2B-ECFP into the nucleolus, similar to full length Nucleolin. 5. Nucleolin imports H2B-ECFP in the nucleolus but is unable to retain it in the nucleolus in the absence of pre-rRNA transcription inhibited by Act D.

[27]. This implicates Nucleolin, 45S rRNA and potentially other bonafide nucleolar factors namely Nucleophosmin in directing the fate of overexpressed and therefore excess nuclear proteins such as histones, into the nucleolus. Considering that the nucleolus is maintained as discrete phase separated entities in the nucleus, the mechanisms involved in targeting nuclear factors into or out of the nucleolus are largely unclear [12]. Histone gene expression is tightly regulated and coupled to DNA replication during S-phase [50,66]. Imbalances in histone expression and its accumulation can induce G1 cell cycle arrest, genomic instability and affect transcription [67–69]. It is therefore conceivable that Nucleolin/Nucleophosmin are specifically involved in dual roles of chaperoning out excess nuclear proteins such as histones into the nucleolus. Furthermore, this study also unravels the key involvement of ribosomal RNA as an essential mediator that facilitates the retention of nucleolar H2B. A combination of nucleolar factors and their interaction with rRNA is potentially involved in the generation of the phase separated nucleolus – a unique non-membranous milieu within the nucleoplasm, for the rapid but regulated entry and exit of factors that potentially facilitate rRNA biogenesis. In summary, this study unravels a unique and novel mechanism whereby proteins are guided and retained into phase separated systems such as the nucleolus. This suggests potential implications towards the targeted therapeutic intervention of dysregulated 'cancer nucleoli'.

Materials and methods

Plasmids

H2B-ECFP [70], GFP-nucleolin [71], GFP-NPM1 and NLS-CFP plasmids were kind gifts from Jennifer Lippincott-Schwartz, Sui Huang and Tom Misteli, respectively. NCLΔN, NCLΔRBD and NCLΔGAR plasmids were generated from GFP-nucleolin by restriction free (RF) cloning. Primers used for RF cloning are as follows: NCLΔN: Sense, 5′-GCAAGAATGCCAAGAAGCCTGTCAAAGAAGCACC-3′, Antisense, 5′-GGTGCTTCTTTGACAGGCTTCTTGGCATTCTTGC-3′; NCLΔRBD: Sense, 5′-GAACCGACTACGGCTAAGGGTGAAGGTGGC-3′, Antisense, 5′-GCCACCTTCACCCTTAGCCGTAGTCGGTTC-3′; NCLΔGAR: Sense, 5′-CTGGGCCAAACCTAAGGACCACAAGCCACAAG-3′, Antisense, 5′-CTTGTGGCTTGTGGTCCTTAGGTTTGGCCCAG-3′.

Cell lines, cell culture and transfections

DLD1 colorectal adenocarcinoma cells (Gift from Thomas Ried, NCI/NIH) were grown in RPMI medium (Gibco, 11875), HCT116 colorectal carcinoma and MCF7 breast adenocarcinoma (ATCC) cells were grown in DMEM (Gibco, 11995), CRL1790 normal colon cells were grown in MEM (Gibco, 11095). All media were supplemented with Penicillin (100 units/ml)/Streptomycin (100 µg/ml) (Gibco, 15070-063) and 10% heat inactivated FBS (Gibco, 6140). Cells were cultured at 37°C in the presence of 5% CO_2. We authenticated cell lines by karyotyping metaphases derived from each of these cell lines. We routinely tested cells in culture and found them free of mycoplasma contamination. Transient transfections were performed using Lipofectamine RNAimax reagent and siRNA (100 nM) (Invitrogen, 13778) in reduced serum medium OptiMEM (Gibco, 31985) for 6 h, after which cells were transferred to complete medium and incubated for a total duration of 48 h at 37°C. The siRNA oligonucleotide sequences were – FBL: 5′-AGGAGAACAUGAAGCCGCA-3′, FBL Scramble: 5′-GAAGAACGAUCAGGACAAU-3′; GNL3: 5′-GCUUAAAACAAGAACAGAU-3′, 5′-AUGUGGAACCUAUGGAAAA-3′; GNL3 Scramble: 5′-AUAAUCGAACGAUAAGAAC-3′; LMNA/C: 5′-CAGUCUGCUGAGAGGAACA-3′;LMNA/C Scramble: 5′-GGAGGUCGAGCCAAUAUCA-3′; LMNB1: 5′-AGACAAAGAGAGAGAGAUG-3′; LMNB1 Scramble: 5′-GAGGGAAACGUAAAGAAGA-3′; LMNB2: 5′-GAGCAGGAGAUGACGGAGA-3′; LMNB2 Scramble: 5′-GGAAGCGUAGACGGAAGAG-3′. NCL: 5′-UCCAAGGUAACUUUAUUUCUU-3′; NCL Scramble: 5′-GCUAGCUUUAUUCGUAUAUUA-3′, NPM1: 5′-AGATGATGATGATGATGAT-3′. Transient plasmid transfections were performed using Lipofectamine LTX with Plus reagent (Invitrogen, 15338-100) and cells were imaged after 24 h of transfection at 37°C. For FRAP analyses upon knockdowns, siRNA

and DNA transfections were performed sequentially – siRNA transfection was performed as mentioned previously, while DNA transfections were performed after 24 h and cells were imaged by fluorescence microscopy, after 48h of siRNA transfection at 37°C.

Western blot, antibodies and co-immunoprecipitation

SDS–PAGE and immunoblotting were performed according to standard protocols. Lysates were prepared in RIPA buffer, protein concentration was estimated using bicinchoninic acid (BCA) kit (Pierce, 23225), resolved on SDS-PAGE and transferred to Immobilon-P polyvinylidene difluoride (PVDF) membranes (Millipore, IPVH00010) for 90 min at 90 volts. Membranes were blocked with 5% non-fat dried milk in Tris-buffered saline, 0.1% Tween-20 (TBST) for 1h at Room Temperature (RT). Primary and secondary antibodies were diluted in 0.5% non-fat dried milk in 1X TBST. Primary antibodies: anti-Nucleolin (Abcam, ab22758), 1:1000; anti-Actin (Abcam, ab3280), 1:400; anti-histone 2B (Millipore, 07-371, gifted by Sanjeev Galande), 1:1000; anti-Fibrillarin (Abcam, ab4566), 1:1000; anti-Nucleostemin (Abcam, ab70346), 1:2000; anti-Lamin A/C (Epitomics, S2526), 1:5000; anti-Lamin B1 (Abcam, ab16048), 1:1000; anti-Lamin B2 (Abcam, ab8983), 1:400; anti-GFP (Abcam, ab290), 1:1000 for 3h at RT or overnight at 4°C. Secondary antibodies: Sheep anti-Mouse-HRP (Amersham, NA9310V), 1:10,000; Donkey anti-Rabbit-HRP (Amersham, NA9340V), 1:10,000, for 1h at RT. Between incubations, membranes were washed three times in 1X TBST for 10 minutes each at RT. Immunoblots were developed using chemiluminescent substrate ECL Prime (Amersham, 89168-782) and imaged with ImageQuant LAS4000. Relative levels of H2B and Nucleolin were quantified from western blots using Image J (http://imagej.nih.gov/ij/). The intensity of the band was normalized to the respective loading controls.

For co-immunoprecipitation (Co-IP) assays, ~10^7 cells (DLD1) were lysed in co-IP lysis buffer (50 mM Tris [pH 7.4], 150 mM NaCl, 0.5% NP-40, 1× PIC) vortexed and incubated on ice for 15 min, and centrifuged at 12,000 rpm and 4°C for 10 min. The lysate was precleared by incubating with Dynabeads protein A (Invitrogen, 10002D) for 1 h. Anti-Nucleolin antibody (ab22758, 3 µg) or normal rabbit IgG was incubated with lysates overnight at 4°C. Protein A beads, pre-blocked with 0.5% BSA, were incubated with the immunocomplex for ~3 h. Beads were washed 6 times with co-IP lysis buffer to minimize non-specific binding. Bound protein was eluted from the beads by boiling in 2× Laemmli buffer for 15 min at 95°C. Samples were resolved on a 15% SDS-PAGE, followed by western blotting.

qRT-PCR

RNA was prepared by lysing cells in TRIzol (Invitrogen) followed by phenol-chloroform extraction, cDNA was synthesized using the Verso cDNA synthesis kit (Thermo Fisher Scientific). Semi-quantitative real-time PCR (qRT-PCR) was performed using SYBR green (SAF labs). *ACTIN* served as internal control. The primers used for qRT-PCR were:

45S: Forward, 5′-GAACGGTGGTGTGTCGT T-3′; Reverse, 5′-GCGTCTCGTCTCGTCTCACT-3′ and *ACTIN*: Forward, 5′- GATTCCTATGTGG GCGAC-3′, Reverse: 5′-GGTAGTCAGTCAGGTC CCG-3′.

Immunofluorescence assay

Cells grown on coverslips (18 × 18 or 22 × 22 mm^2) were briefly washed twice using 1X Phosphate Buffered Saline (PBS) and fixed for 10 min in 4% Paraformaldehyde (Sigma, P6148) in PBS, pH 7.4 at RT, washed thrice in 1X PBS (5 min each), followed by permeabilization in 0.5% Triton-X-100 (in PBS) for 10 min at RT. Cells were blocked in 1% Bovine serum albumin (BSA) (Sigma, A2153) in 1X PBS, for 30 min, washed thrice with 1X PBS and incubated in primary antibodies for 90 min at RT and secondary antibodies for 60 min at RT, with washes in between using 1X PBS. Primary antibody was diluted in 0.5% BSA (prepared in 1X PBS): anti-Nucleolin (ab13541), 1:300, anti-H2B (Millipore, 07-371), 1:100. Following secondary antibodies were used after diluting in 1X PBS +0.1%Triton X-100 (PBST): anti-mouse IgG-Alexa 568 (Molecular Probes), 1:1000; anti-rabbit IgG Alexa 488 (Molecular Probes) after which cells were washed thrice in 1X PBST. Cells were mounted in Slowfade Gold Antifade (Invitrogen, S36937). Cells were

imaged on a Zeiss LSM710 confocal microscope with 405 nm, 458 nm and 561 nm laser lines at 2% power using a 63X oil immersion objective, NA 1.4 at 2.5X digital zoom. X-Y resolution: 512 pixels X 512 pixels (1 pixel = 0.11 μm). Confocal z-stacks were collected at an interval of 0.32 μm.

Fluorescence Recovery after Photobleaching (FRAP) experiments and analysis

A Zeiss LSM710 confocal microscope equipped with a heated stage at 37°C, was used for all photobleaching experiments and fluorescence image acquisitions. For live imaging, cells were grown on a 22×22 mm^2 coverslip glued onto a 35 mm petridish coated with 100 μg/ml Collagen (BD Biosciences, 354236), CO_2 independent Leibovitz L-15 medium (Gibco, 21083-027) supplemented with 10% FBS (complete L15), was used during microscopy. Images were acquired using a 63X oil immersion objective, NA 1.4 at 2.5X digital zoom, at 2% laser power to avoid photobleaching. The acquisition parameters were adjusted to avoid bleed-through of ECFP and GFP fluorescence. A 10 pixel X 10 pixel square (1 pixel = 0.11 μm) Region of Interest (ROI) was bleached in both nucleoplasmic and nucleolar H2B-ECFP. Photobleaching was performed using the 405 nm laser line at 100% power. Laser iterations of 120 and 150 were used to photobleach labelled H2B in the nucleus and nucleolus respectively. Images were collected every 3.87 s for a total duration of 5 min. Images were analyzed using Zen 2011 FRAP Analysis module and normalized fluorescence intensity (NFI) was calculated as follows:

$$\mathrm{NFI} = [\mathrm{ROI1(t)} - \mathrm{ROI3(t)}]/[\mathrm{ROI2(t)} - \mathrm{ROI3(t)}] \; \mathrm{X}[\mathrm{ROI2(t=0)} - \mathrm{ROI3(t=0)}] \; / \; [\mathrm{ROI1(t=0)} - \mathrm{ROI3(t=0)}] \quad (1)$$

where, *ROI1* is the fluorescence intensity of the 10 px X 10 px ROI that is bleached, *ROI2* is the whole nucleus fluorescence intensity and *ROI3* is the fluorescence intensity of a 10 px X 10 px background region selected outside the nucleus. *ROI1 (t)*: post-bleach fluorescence intensity at time t. *ROI2(t)* and *ROI3(t)*: whole nucleus and background, respectively. *ROI1(t = 0)*: average pre-bleach fluorescence intensity. *ROI2(t = 0)* and *ROI3(t = 0)*: whole nucleus and background, respectively. The NFI was plotted as a function of time to generate double normalized FRAP curves.

Mobile fractions of H2B-ECFP were calculated as follows:

$$\%\text{Mobile fraction} = (Ffinal - Fbleach)/(Fprebleach \times 100 \quad (2)$$

Where, *Ffinal* is the NFI at maximum recovery, *Fbleach* is the NFI at the instant of bleaching and *Fpre-bleach* is the NFI before bleaching.

Actinomycin D treatment

Cells transfected for 24 h were treated with 0.05 μg/ml actinomycin D (Act D) in complete medium for 4 h at 37°C with 5% CO_2 after which they were transferred to complete L-15 medium and imaged live. Equivalent volumes of dimethyl sulfoxide (DMSO) were used as vehicle controls.

Cell cycle analyses

Cells were fixed in 70% ethanol (in 1X PBS) and subjected to RNase treatment and propidium iodide staining for 1 hour at 37°C. Cells were scanned on FACS Calibur (BD Biosciences). Cell cycle analyses was performed by ModFit software.

Statistical analysis and graphs

Two-tailed student's t-test was used to compare the number of cells showing nucleolar H2B-ECFP compartments and mobile fractions of H2B-ECFP, p-value <0.05 was considered significant. Graphs were plotted using GraphPad Prism software.

Acknowledgements

We thank Jennifer Lippincott-Schwartz, Sui Huang, Tom Misteli and Sanjeev Galande for H2B-ECFP, GFP-NCL and NLS-CFP constructs and anti-histone 2B antibody, respectively. We thank the IISER-Pune Microscopy facility. We thank Rupali Jadhav for help with FACS. We thank Richa Rikhy for comments on the manuscript. AS acknowledges CSIR for a PhD fellowship. GJ acknowledges DST-INSPIRE for a scholarship. We thank Wellcome Trust/DBT India alliance (Award No. 500164/Z/09/Z) and IISER, Pune for funding.

Disclosure statement

No potential conflict of interest was reported by the authors.

Funding

This work was funded by an intermediatefellowship from Wellcome Trust/DBT India alliance (Award No. 500164/Z/09/Z) to KS and intramural funds from IISER, Pune.

ORCID

Sumit Pawar http://orcid.org/0000-0003-3161-7524
Kundan Sengupta http://orcid.org/0000-0002-9936-2284

References

[1] Ghamari A, van de Corput MPC, Thongjuea S, et al. In vivo live imaging of RNA polymerase II transcription factories in primary cells. Genes Dev. 2013;27:767–777.
[2] Tripathi V, Song DY, Zong X, et al. SRSF1 regulates the assembly of pre-mRNA processing factors in nuclear speckles. Mol Biol Cell. 2012;23:3694–3706.
[3] Fiserova J, Richards SA, Wente SR, et al. Facilitated transport and diffusion take distinct spatial routes through the nuclear pore complex. J Cell Sci. 2010;123:2773–2780.
[4] Phair RD, Misteli T. High mobility of proteins in the mammalian cell nucleus. Nature. 2000;404:604–609.
[5] Sirri V, Urcuqui-Inchima S, Roussel P, et al. Nucleolus: the fascinating nuclear body. Histochem Cell Biol. 2008;129:13–31.
[6] Guerra-Rebollo M, Mateo F, Franke K, et al. Nucleolar exit of RNF8 and BRCA1 in response to DNA damage. Exp Cell Res. 2012;318:2365–2376.
[7] Boyd MT, Vlatković N, Rubbi CP. The nucleolus directly regulates p53 export and degradation. J Cell Biol. 2011;194:689–703.
[8] Audas TE, Jacob MD, Lee S. Immobilization of proteins in the nucleolus by ribosomal intergenic spacer noncoding RNA. Mol Cell. 2012;45:147–157.
[9] Fankhauser C, Izaurralde E, Adachi Y, et al. Specific complex of human immunodeficiency virus type 1 rev and nucleolar B23 proteins: dissociation by the Rev response element. Mol Cell Biol. 1991;11:2567–2575.
[10] Xue Z, Shan X, Lapeyre B, et al. The amino terminus of mammalian nucleolin specifically recognizes SV40 T-antigen type nuclear localization sequences. Eur J Cell Biol. 1993;62:13–21.
[11] Shaw PJ, Jordan EG. The nucleolus. Annu Rev Cell Dev Biol. 1995;11:93–121.
[12] Emmott E, Hiscox JA. Nucleolar targeting: the hub of the matter. EMBO Rep. 2009;10:231–238.
[13] Leung AKL, Trinkle-Mulcahy L, Lam YW, et al. Nopdb: nucleolar proteome database. Nucl Acids Res. 2006;34:D218–D220.
[14] Thiry M, Lafontaine DLJ. Birth of a nucleolus: the evolution of nucleolar compartments. Trends Cell Biol. 2005;15:194–199.
[15] Feric M, Vaidya N, Harmon TS, et al. Coexisting liquid phases underlie nucleolar subcompartments. Cell. 2016;165:1686–1697.
[16] Shav-Tal Y, Blechman J, Darzacq X, et al. Dynamic sorting of nuclear components into distinct nucleolar caps during transcriptional inhibition. Mol Biol Cell. 2005;16:2395–2413.
[17] Tajrishi MM, Tuteja R, Tuteja N. Nucleolin: the most abundant multifunctional phosphoprotein of nucleolus. Commun Integr Biol. 2011;4:267–275.
[18] Cong R, Das S, Ugrinova I, et al. Interaction of nucleolin with ribosomal RNA genes and its role in RNA polymerase I transcription. Nucl Acids Res. 2012;40:9441–9454.
[19] Goldstein M, Derheimer FA, Tait-Mulder J, et al. Nucleolin mediates nucleosome disruption critical for DNA double-strand break repair. Proc Natl Acad Sci USA. 2013;110:16874–16879.
[20] Srivastava M, Pollard HB. Molecular dissection of nucleolin's role in growth and cell proliferation: new insights. FASEB J. 1999;13:1911–1922.
[21] Angelov D, Bondarenko VA, Almagro S, et al. Nucleolin is a histone chaperone with FACT-like activity and assists remodeling of nucleosomes. EMBO J. 2006;25:1669–1679.
[22] Erard MS, Belenguer P, Caizergues-Ferrer M, et al. A major nucleolar protein, nucleolin, induces chromatin decondensation by binding to histone H1. Eur J Biochem. 1988;175:525–530.
[23] Ghisolfi L, Kharrat A, Joseph G, et al. Concerted activities of the RNA recognition and the glycine-rich C-terminal domains of nucleolin are required for efficient complex formation with pre-ribosomal RNA. Eur J Biochem. 1992;209:541–548.
[24] Serin G, Joseph G, Faucher C, et al. Localization of nucleolin binding sites on human and mouse pre-ribosomal RNA. Biochimie. 1996;78:530–538.
[25] Serin G, Joseph G, Ghisolfi L, et al. Two RNA-binding domains determine the RNA-binding specificity of nucleolin. J Biol Chem. 1997;272:13109–13116.
[26] di Padua Mathieu D, Mura CV, Frado LL, et al. Differing accessibility in chromatin of the antigenic sites of regions 1-58 and 63-125 of histone H2B. J Cell Biol. 1981;91:135–141.
[27] Musinova YR, Lisitsyna OM, Golyshev SA, et al. Nucleolar localization/retention signal is responsible for transient accumulation of histone H2B in the nucleolus through electrostatic interactions. Biochim Biophys Acta. 2011;1813:27–38.
[28] Mélèse T, Xue Z. The nucleolus: an organelle formed by the act of building a ribosome. Curr Opin Cell Biol. 1995;7:319–324.
[29] Melcer S, Hezroni H, Rand E, et al. Histone modifications and lamin A regulate chromatin protein

dynamics in early embryonic stem cell differentiation. Nat Commun. 2012;3:910.
[30] Martin C, Chen S, Maya-Mendoza A, et al. Lamin B1 maintains the functional plasticity of nucleoli. J Cell Sci. 2009;122:1551–1562.
[31] Sen Gupta A, Sengupta K. Lamin B2 modulates nucleolar morphology, dynamics, and function. Mol Cell Biol. 2017;37:e00274-17.
[32] Shimi T, Pfleghaar K, Kojima S, et al. The A- and B-type nuclear lamin networks: microdomains involved in chromatin organization and transcription. Genes Dev. 2008;22:3409–3421.
[33] Taimen P, Pfleghaar K, Shimi T, et al. A progeria mutation reveals functions for lamin A in nuclear assembly, architecture, and chromosome organization. Proc Natl Acad Sci USA. 2009;106:20788–20793.
[34] Cerdido A, Medina FJ. Subnucleolar location of fibrillarin and variation in its levels during the cell cycle and during differentiation of plant cells. Chromosoma. 1995;103:625–634.
[35] Romanova L, Grand A, Zhang L, et al. Critical role of nucleostemin in pre-rRNA processing. J Biol Chem. 2009;284:4968–4977.
[36] Ma N, Matsunaga S, Takata H, et al. Nucleolin functions in nucleolus formation and chromosome congression. J Cell Sci. 2007;120:2091–2105.
[37] Gadad SS, Senapati P, Syed SH, et al. The multifunctional protein nucleophosmin (NPM1) is a human linker histone H1 chaperone. Biochemistry. 2011;50:2780–2789.
[38] Swaminathan V, Kishore AH, Febitha KK, et al. Human histone chaperone nucleophosmin enhances acetylation-dependent chromatin transcription. Mol Cell Biol. 2005;25:7534–7545.
[39] Gaume X, Monier K, Argoul F, et al. In vivo study of the histone chaperone activity of nucleolin by FRAP. Biochem Res Int. 2011;2011:1–15.
[40] Créancier L, Prats H, Zanibellato C, et al. Determination of the functional domains involved in nucleolar targeting of nucleolin. Mol Biol Cell. 1993;4:1239–1250.
[41] Schmidt-Zachmann MS, Nigg EA. Protein localization to the nucleolus: a search for targeting domains in nucleolin. J Cell Sci. 1993;105(Pt 3):799–806.
[42] Heine MA, Rankin ML, DiMario PJ. The Gly/Arg-rich (GAR) domain of Xenopus nucleolin facilitates in vitro nucleic acid binding and in vivo nucleolar localization. Mol Biol Cell. 1993;4:1189–1204.
[43] Weber JD, Taylor LJ, Roussel MF, et al. Nucleolar Arf sequesters Mdm2 and activates p53. Nat Cell Biol. 1999;1:20–26.
[44] Kalashnikova AA, Winkler DD, McBryant SJ, et al. Linker histone H1.0 interacts with an extensive network of proteins found in the nucleolus. Nucl Acids Res. 2013;41:4026–4035.
[45] Szerlong HJ, Herman JA, Krause CM, et al. Proteomic characterization of the nucleolar linker histone H1 interaction network. J Mol Biol. 2015;427:2056–2071.
[46] Cong R, Das S, Douet J, et al. macroH2A1 histone variant represses rDNA transcription. Nucl Acids Res. 2014;42:181–192.
[47] Tessarz P, Santos-Rosa H, Robson SC, et al. Glutamine methylation in histone H2A is an RNA-polymerase-I-dedicated modification. Nature. 2014;505:564–568.
[48] Steger DJ, Workman JL. Transcriptional analysis of purified histone acetyltransferase complexes. Methods. 1999;19:410–416.
[49] Singh RK, Liang D, Gajjalaiahvari UR, et al. Excess histone levels mediate cytotoxicity via multiple mechanisms. Cell Cycle. 2010;9:4236–4244.
[50] Gunjan A, Verreault A. A Rad53 kinase-dependent surveillance mechanism that regulates histone protein levels in S. cerevisiae. Cell. 2003;115:537–549.
[51] Meshorer E, Yellajoshula D, George E, et al. Hyperdynamic plasticity of chromatin proteins in pluripotent embryonic stem cells. Dev Cell. 2006;10:105–116.
[52] Constantinescu D, Gray HL, Sammak PJ, et al. Lamin A/C expression is a marker of mouse and human embryonic stem cell differentiation. Stem Cells. 2006;24:177–185.
[53] Freund A, Laberge R-M, Demaria M, et al. Lamin B1 loss is a senescence-associated biomarker. Mol Biol Cell. 2012;23:2066–2075.
[54] Dixon CR, Platani M, Makarov AA, et al. Microinjection of antibodies targeting the lamin A/C histone-binding site blocks mitotic entry and reveals separate chromatin interactions with HP1, CenpB and PML. Cells. 2017;6:9.
[55] Montes de Oca R, Lee KK, Wilson KL. Binding of barrier to autointegration factor (BAF) to histone H3 and selected linker histones including H1.1. J Biol Chem. 2005;280:42252–42262.
[56] Hirano Y, Hizume K, Kimura H, et al. Lamin B receptor recognizes specific modifications of histone H4 in heterochromatin formation. J Biol Chem. 2012;287:42654–42663.
[57] Tin AS, Park AH, Sundar SN, et al. Essential role of the cancer stem/progenitor cell marker nucleostemin for indole-3-carbinol anti-proliferative responsiveness in human breast cancer cells. BMC Biol. 2014;12:72.
[58] Hardy K, Wu F, Tu W, et al. Identification of chromatin accessibility domains in human breast cancer stem cells. Nucleus. 2016;7:50–67.
[59] Gomez NC, Hepperla AJ, Dumitru R, et al. Widespread chromatin accessibility at repetitive elements links stem cells with human cancer. Cell Rep. 2016;17:1607–1620.
[60] Tollervey D, Lehtonen H, Jansen R, et al. Temperature-sensitive mutations demonstrate roles for yeast fibrillarin in pre-rRNA processing, pre-rRNA methylation, and ribosome assembly. Cell. 1993;72:443–457.
[61] Mongelard F, Bouvet P. Nucleolin: a multiFACeTed protein. Trends Cell Biol. 2007;17:80–86.
[62] Ginisty H, Amalric F, Bouvet P. Nucleolin functions in the first step of ribosomal RNA processing. EMBO J. 1998;17:1476–1486.
[63] Mitrea DM, Cika JA, Guy CS, et al. Nucleophosmin integrates within the nucleolus via multi-modal

interactions with proteins displaying R-rich linear motifs and rRNA. Elife. 2016;5.

[64] Bouvet P, Diaz J-J, Kindbeiter K, et al. Nucleolin interacts with several ribosomal proteins through its RGG domain. J Biol Chem. 1998;273:19025–19029.

[65] Ghisolfi-Nieto L, Joseph G, Puvion-Dutilleul F, et al. Nucleolin is a sequence-specific RNA-binding protein: characterization of targets on pre-ribosomal RNA. J Mol Biol. 1996;260:34–53.

[66] Robbins E, Borun TW. The cytoplasmic synthesis of histones in hela cells and its temporal relationship to DNA replication. Proc Natl Acad Sci USA. 1967;57:409–416.

[67] Mei Q, Huang J, Chen W, et al. Regulation of DNA replication-coupled histone gene expression. Oncotarget. 2017;8:95005–95022.

[68] Morillo-Huesca M, Maya D, Muñoz-Centeno MC, et al. FACT prevents the accumulation of free histones evicted from transcribed chromatin and a subsequent cell cycle delay in G1. PLoS Genet. 2010;6:e1000964.

[69] Meeks-Wagner D, Hartwell LH. Normal stoichiometry of histone dimer sets is necessary for high fidelity of mitotic chromosome transmission. Cell. 1986;44:43–52.

[70] Altan-Bonnet N, Phair RD, Polishchuk RS, et al. A role for Arf1 in mitotic Golgi disassembly, chromosome segregation, and cytokinesis. Proc Natl Acad Sci USA. 2003;100:13314–13319.

[71] Chen D, Huang S. Nucleolar components involved in ribosome biogenesis cycle between the nucleolus and nucleoplasm in interphase cells. J Cell Biol. 2001;153:169–176.